PEGASOS Refinement Project

Volume 4
SP2 - Ground Motion Characterization -

Evaluation Summaries and Hazard Input Documents

by

Philippe L.A. Renault, Norman A. Abrahamson & SP2 Experts

Olten, 20. December 2013
Rev.1: 3. July 2014

Contents

Part I

Master Ground Motion Logic Tree

by Norman A. Abrahamson

Chapter 1

Introduction

In the PEGASOS study, each expert provided a description of his logic tree in his own evaluation summary. The structures of the logic trees used by the five PEGASOS SP2 experts had many similarities. To take advantage of these similarities, the PEGASOS Refinement Project (PRP) SP2 experts agreed to develop a single master logic tree structure that could be used by all of the SP2 experts for their evaluations. Most, but not all, of the elements of the logic tree have been used by all of the SP2 experts, but with their own individual weights and justifications for these weights. Detailed descriptions of the development of the models and parameters are given in a separate set of technical reports. This report provides a brief summary of the information in these references. The structure of the SP2 master logic tree for the horizontal and vertical components is shown in Chapter 9.

1.1 Structure of the Report

Description of SP2 Logic Tree

The structure of the SP2 master logic tree for the horizontal and vertical components is described and shown in chapters 2.1 to 9.

Evaluation Summaries of the SP2 Experts

Part II to V of the report include the evaluation summaries of the SP2 experts. The following chapters contain the expert's individual assessments:

Part II - Chapter 1, Part III - Chapter 1, Part IV - Chapter 1, Part V - Chapter 1.

Hazard Input Documents for SP2

The Hazard Input Documents (HID) are developed to include all of the elements of each expert's assessments of importance to the hazard calculations. Although the HIDs provide the information required for the hazard calculations, they do not include any technical explanation or justification for the models or parameters that comprise the models. Those explanations are given in the Evaluation Summaries. The Chapters 2 in Part II to V include the final HID for each of the SP2 models.

Chapter 2

Selection of GMPEs for Horizontal Motion

The initial selection of candidate ground motion prediction equations (GMPEs) is described by Bommer and Stafford [2010a] (TP2-TB-1039) and is summarized below. This set was later expanded to include additional GMPEs based on a re-evaluation in 2011.

The approach adopted by ground-motion experts in SP2 for the PEGASOS Refinement Project (PRP) was to take advantage of the progress made in the development of GMPEs in the last few years and to begin by selecting a subset of state-of-the-art ground-motion prediction equations (GMPE) from amongst all of those now available. These well-constrained and high-quality ground-motion prediction equations would then, after host-to-target region conversions, populate the branches of the logic-tree. The SP2 experts would individually evaluate the models and assign weights to reflect their degree of belief in these models as being appropriate for the prediction of ground motions from moderate-to-large magnitude earthquakes in Switzerland.

2.1 Selection of GMPEs

The SP2 experts established 10 pre-selection criteria that would exclude any equation that failed to meet any one of these conditions, which included the following as the most important ones: the model did not have an appropriate functional form (including non-linear magnitude scaling and magnitude-dependent attenuation); the model used outmoded parameter definitions (such as epicentral distance or local magnitude); the model did not include predictor variables to account for style-of-faulting and the shear wave velocity at the site (unless the equation was specifically for a single fault rupture mechanism or unique site class); the model was derived using a regression technique that did not take account of correlations between magnitude and distance; or the model was based on an unnecessarily small dataset for the magnitude and distance range covered by the equation, given the size of the global strong-motion databank.

At the PRP SP2 Preparatory Meeting on 27. April 2009, it was decided by the SP2 experts that J. Douglas should apply the first five out of seven exclusion criteria proposed by Cotton et al. [2006] (based on work undertaken in the original PEGASOS Project) plus additional

exclusion criteria to reject models that were published more than 15 years ago (i.e. $\leq$1994). At the meeting, three additional criteria were added, but any rejection based on these, would need a discussion between the SP2 experts. The following exclusion criteria were adopted for the PRP:

1. The model is from a clearly irrelevant tectonic regime
2. The model is not published in an international peer-reviewed journal
3. The documentation of the model and its underlying dataset is insufficient
4. The model has been superseded by more recent publications or is older than 15 years
5. The frequency range of the model is not appropriate for engineering application
6. The model has an inappropriate functional form
7. The regression method or regression coefficients are judged to be inappropriate
8. The equation must use appropriate definitions for predictor variables
9. The model is not appropriate for the required extrapolation in M-R space
10. State-of-the-Art Criterion (SOTAC) - only for empirical equations (e.g. the model is derived from an excessively small strong-motion dataset)

The resource expert J. Douglas then applied these pre-selection criteria to a comprehensive global listing of GMPEs [Douglas 2011b], which resulted in an initial list of 8 equations that satisfied all of the conditions that had been established for retention. The initial selection included the following [Douglas 2009a] (TP2-TB-1015):

- Abrahamson & Silva (2008) - NGA model
- Boore & Atkinson (2008) - NGA model
- Campbell & Bozorgnia (2008) - NGA model
- Chiou & Youngs (2008) - NGA model
- Akkar & Bommer (2007) - European-Middle Eastern model
- Toro (2002) - ENA stochastic model
- Atkinson & Boore (2006) - ENA stochastic model
- Atkinson (2008) - ENA model

The Akkar and Bommer [2007] model was found to have a sigma model with a magnitude dependence that was not well constrained. Therefore, an updated model [Akkar and Bommer 2010] was developed by the authors based on constant sigma rather magnitude dependent sigma. This 2010 model replaced the Akkar and Bommer [2007] model.

The SP2 experts considered whether all of the major strong-motion databases from crustal earthquakes around the world are represented by the models currently in the logic tree. It is immediately apparent that a major omission is the large collection of accelerograms from Japan, the sole Japanese event being represented by the 1995 Kobe earthquake that was included in the NGA database. Looking again at the criteria on which different Japanese GMPEs failed the pre-selection criteria, it was found that the Zhao et al. [2006] model had been excluded because it failed criterion 3 (documentation of the database). While the Zhao et al. [2006] paper did not include the database, the Japanese dataset is well documented in other publications. Therefore, the SP2 experts decided to add the Zhao et al. [2006] model to the set of selected models.

Finally, the SP2 experts reviewed the Atkinson [2008] model. This model was based on a referenced empirical approach and relied on differences in the ground motions from small magnitude earthquakes in the CEUS compared to the predicted small magnitude ground motions from the Boore and Atkinson [2008] NGA model. Given that the NGA models over-predict small magnitudes (see section 4), the approach used to develop the Atkinson [2008] model was questionable. The SP2 experts decided to remove this model from the set of candidates.

2.1.1 Additional GMPEs

In 2011, the composition of the SP2 experts changed with the departure of F. Scherbaum and J. Bommer and the addition of K. Campbell. As part of this change, there was a re-evaluation of the candidate empirical GMPEs. Nine additional GMPEs not considered in the original evaluation were considered (Table I-2.1).

Table I-2.1: Additional candidate models considered in 2011.

Model	Comment
Akkar & Cagnan (2010)	New model based on Turkish strong motion data
Atkinson & Boore (2011)	Update of Boore & Atkinson (2008) NGA model for additional small magnitude data. This also updates the Atkinson & Boore (2006) model.
Chiou et al. (2010)	Update of Chiou & Youngs (2008) NGA model for small magnitudes
Campbell (2003)	Hybrid empirical model for eastern U.S.
Pezeshk et al. (2011)	Hybrid empirical model for eastern U.S.
Cauzzi & Faccioli (2008)	Used by SHARE project [Giardini and Wössner 2013]
Aghabarati and Tehranizadeh (2009a)	New model based on Iranian data plus NGA data at
Aghabarati and Tehranizadeh (2009b)	short distances
Bindi et al. (2011)	Mainly using Italian data

An initial evaluation of these nine models was made by the TFI. This eliminated five of the models for the reasons given below.

The two hybrid models Campbell et al. [2003] and Pezeshk et al. [2011] were excluded because they are based on the Hybrid Empirical Method (HEM). The SP2 experts had previously decided to exclude HEM models because adjusting these models to Swiss conditions would involve applying adjustments to already adjusted models. A single set of adjustments is

preferred (e.g. adjusting the WUS GMPEs to Swiss conditions directly). Up-to-date versions of the WUS GMPEs, represented by the 2008 NGA models, are included in the set of models and these are being adjusted to Swiss $V_S - \kappa$ conditions using the HEM approach.

The Chiou et al. [2010] model only includes an update for four spectral frequencies. Therefore, it was excluded because it does not cover the required frequency range.

The Atkinson and Boore [2011] model updates the Boore and Atkinson [2008] NGA model for magnitudes less than 5.75. Because all of the GMPEs used in the PRP are being adjusted for M<5.5 to be consistent with the observed small magnitude Swiss data, the change to the small magnitudes in the AB11 model will be readjusted to fit the Swiss data. Therefore, this change was not considered to be significant for the PRP.

The Cauzzi and Faccioli [2008] model is based on a linear scaling with magnitude at all spectral frequencies and does not meet the appropriate functional form criteria. For magnitudes 4.5 to 8.0 required for the PRP, the corner frequency will pass through the low frequency range (0.5 to 2 Hz) required for the PRP, so a linear magnitude term will not be adequate. The data used by Cauzzi and Faccioli [2008] are mainly in the M5 to 6.5 range, which is not broad enough to constrain the higher order magnitude terms. While the Cauzzi and Faccioli [2008] functional form is adequate to fit their dataset, it is not adequate for the application needs of the project and this model was therefore rejected.

J. Douglas evaluated the remaining four candidate models using the selection criteria applied to the original set (TP2-TB-1015 [Douglas 2009a], EXT-TN-1200 [Douglas 2011a]). Douglas found that only the Akkar and Cagnan [2010] model passed all of the selection criteria. Aghabarati and Tehranizadeh [2009b] and Aghabarati and Tehranizadeh [2009a] failed because they did not have a sufficiently wide magnitude-distance range. The Bindi et al. [2011] model just failed due to the upper magnitude of M6.9 in the database as compared to the selection criteria lower limit of M7.0. The SP2 experts decided that this small difference in the upper magnitude range of the dataset was not significant, so the Bindi et al. [2011] model was included.

The final ten empirical GMPEs considered for the PRP are listed below:

- Abrahamson & Silva (2008) - NGA model
- Boore & Atkinson (2008) - NGA model
- Campbell & Bozorgnia (2008) - NGA model
- Chiou & Youngs (2008) - NGA model
- Akkar & Bommer (2010) - European-Middle Eastern model
- Toro (2002) - ENA stochastic model
- Atkinson & Boore (2006) - ENA stochastic model
- Zhao et al. (2006) - Japanese model
- Akkar & Cagnan (2010) - Turkish model
- Bindi et al. (2011) - Italian model

2.2 Impact of New Data for the NGA Models

The NGA dataset used by Chiou and Youngs [2008b] to derive the four selected NGA models includes earthquakes up to February 2003. This database is currently being updated to include recordings from recent large magnitude earthquakes worldwide, from small magnitude (M3-M5) data from California and from aftershocks from the 2008 Wenchuan earthquake. The new large magnitude events that have been added to the NGA database are summarized in Table I-2.2.

As a preliminary check of the impact of these additional data on the NGA models, the residuals from the expanded dataset were computed using the Abrahamson & Silva (2008) (termed "AS08" in the following) model with the same data selection criteria used to develop the AS08 model. Using the residuals from the AS08 model based on the expanded dataset, a random effects regression was conducted for only a constant term. The resulting event terms for PGA and spectral acceleration at 1 Hz are shown in Figure I-2.2. In this figure, the constant term is added to the event terms so that the resulting event terms are plotted relative to the original AS08 model. The red line shows the shift due to the constant term. The inclusion of the new earthquakes changes the median by less than 5% at PGA and 1 Hz, respectively. For PGV, there is an indication of a magnitude slope in the residuals for the new data, suggesting that the scaling from M5 to M8 is weaker in the new data than in the AS08 model.

Table I-2.2: New large magnitude (M $\geq$ 6) mainshock data added to the NGA database as part of the NGA-West 2 project.

Year	Earthquake	Magnitude
1978	Basso Tirreno, Italy	6.0
1979	Montenegro, Yugoslavia	7.1
1997	Umbria Marche, Italy	6.0
2000	Totorri, Japan	6.6
2003	San Simeon, CA	6.5
2003	Bam, Iran	6.6
2004	Parkfield, CA	6.0
2004	Niigata, Japan	6.6
2007	Chuetsu-Oki, Japan	6.8
2008	Iwate, Japan	6.9
2008	Wenchuan, China	7.9
2009	L'Aquila, Italy	6.3
2010	Darfield, New Zealand	7.0
2010	El Mayor-Cucapah, Mexico-CA	7.2
2011	Christchurch, New Zealand	6.1

In addition, some comparisons of the selected candidate GMPEs with two recent earthquakes were performed. The technical note PMT-SUP-1063 [Biro 2012] shows the comparison of the recorded ground motion of Christchurch M6.1 on February 22, 2011, Virginia Mineral main shock M5.8 on August 23, and its aftershock M4.5 on August 24, 2011 with the median GMPEs.

The selected NGA models themselves were updated (NGA-West2 project: [PEER Center 2013]) and the expected public availability was mid March 2013. As this was too late to be

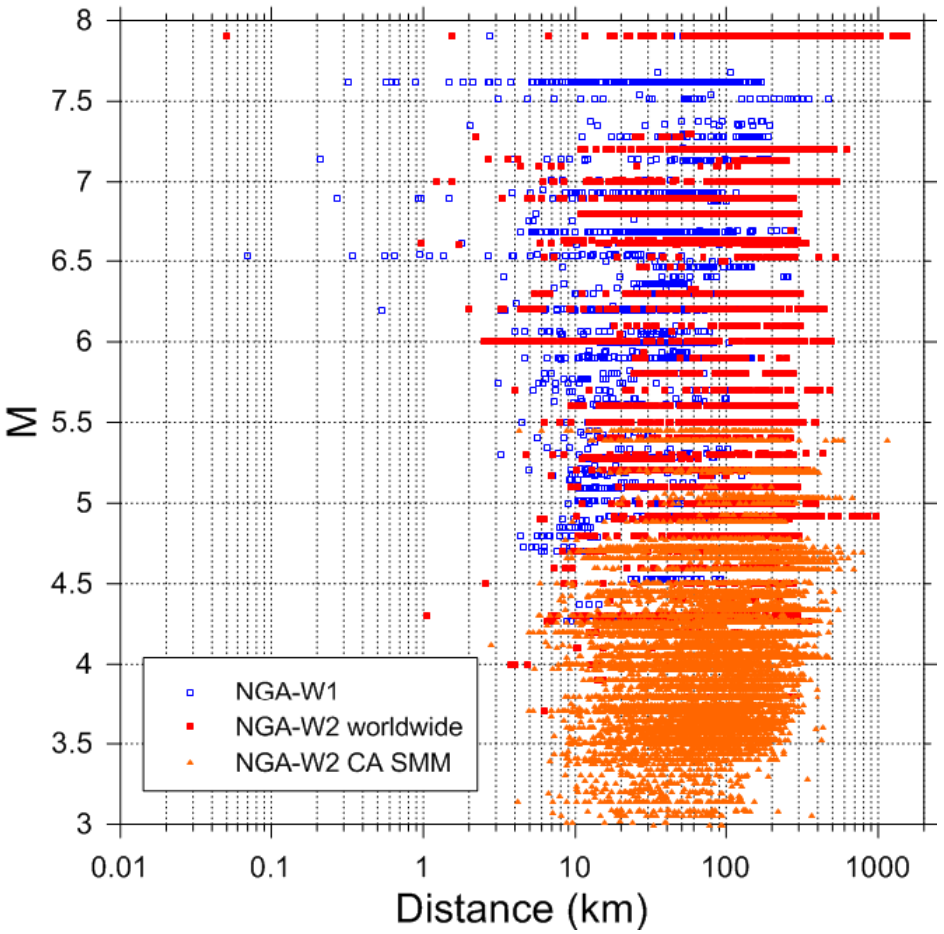

Figure I-2.1: Comparison of the magnitude distance distribution of strong-motion records in the NGA-West2 database (magnitudes 3 to 7.9) and West1 database. Open blue squares are stations included in the NGA-West1. Solid red squares are stations added from worldwide events. Orange triangles are stations added from California only from small to moderate magnitude events (magnitudes 3 to 5.5) [Ancheta et al. 2013]. The new earthquakes below magnitude 6 are mainly from aftershocks from the 2008 Wenchuan earthquake and Italian earthquakes.

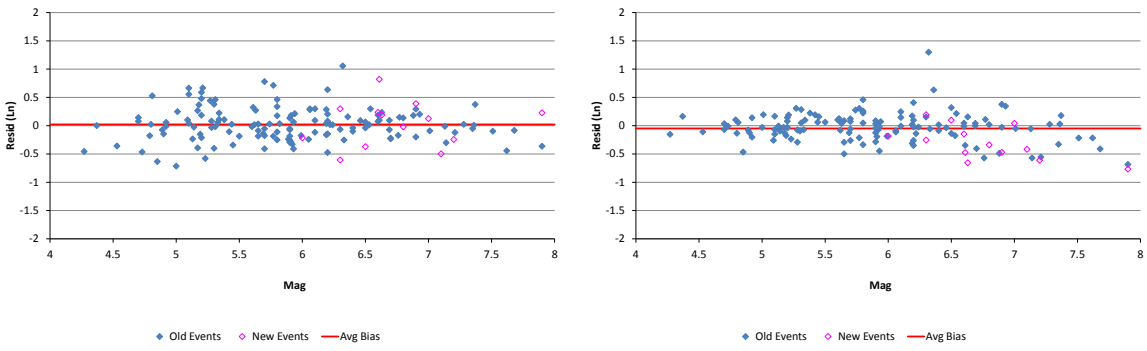

(a) For PGA (b) For 1 Hz

Figure I-2.2: Event terms for the AS08 model using a preliminary version of the NGA-West2 database (release of 11.03.2011). The red line shows the mean value of the event terms from the expanded NGA-West2 dataset as compared to the AS08 model [Al Atik and Abrahamson 2011].

considered as a replacement for the selected NGA 2008 models, the project has performed some comparisons based on the preliminary NGA-West2 models and these were discussed with the experts on the occasion of the WS11/SP2 (TP2-RF-1452 and PMT-TN-1260). This comparison shows that the new NGA models fall well within the range of the PRP models used and the PRP models thus capture the range of available and near-future models.

2.3 Swiss Stochastic Models

As part of the PRP, a new stochastic model for Switzerland was developed by B. Edwards and D. Fäh and is described in Edwards et al. [2010] (TP2-TB-1024) and Edwards and Fäh [2010] (TP2-TB-1052). The model is based on earthquakes recorded by the SED broadband network covering magnitudes between 2.0 and 5.5 and distances between 3 and 300 km.

2.3.1 Magnitude Dependence of Stress-Drop

The analysis of these data shows that there is a strong magnitude dependence of the stress drop increasing from 2 bars for M2.5 to 30 bars for M4.5. A key issue for the application of this model to the larger magnitudes that are relevant to the hazard is the scaling of the stress drop above M4.5. As there is no empirical constraint on the high magnitude stress drop scaling, a suite of alternative models was developed. The magnitude scaling from the ten selected GMPEs described in Section 2.1 does not indicate that there is a strong increase in stress drop with magnitude above M5. Silva (pers. comm.) fitted the NGA GMPEs to a point source model allowing for a magnitude dependent stress drop and he found that the magnitude scaling in the NGA models implied that there is a small decrease in stress drop with magnitude for M<6.5. The Silva results suggest that the strong increase in stress drop with magnitude inferred in the small magnitude Swiss data will not continue at high magnitudes. To capture this trend, a limit on the increase in stress drop at high magnitudes was applied to the Swiss stochastic model as described below.

The models for the magnitude dependence of this stress drop for extrapolating a Swiss stochastic model to high magnitudes have two parameters: the maximum stress drop and the magnitude (M_c) at which the stress drop reaches this maximum level. A suite of values was used for these two parameters. The cutoff magnitude ranges from 4 to 6 and the maximum stress drops range from 30 to 480 bars. An example of the scaling of stress drop with magnitude is shown in Figure I-2.3.

The Swiss stochastic model uses a geometrical spreading term of -1.29 at short distances as compared to a geometrical spreading term of -1.0 typically used in Californian stochastic models, e.g. [Atkinson and Silva 2000]. The stress drop and geometrical spreading are highly correlated, so the steep geometrical spreading should be considered as part of the evaluation of the large magnitude stress drops for the Swiss model. (See technical note of Al Atik and Abrahamson [2012b] (EXT-TN-1233) on comparison of Swiss and WUS stochastic models.)

2.3.2 Effective Point-Source Distance

A second issue for the application of the point-source stochastic model to the PSHA is the effective point-source distance (R_{eff}). The point-source model uses the point-source distance to compute the ground motion. This is similar to the distance metric that is used in empirical

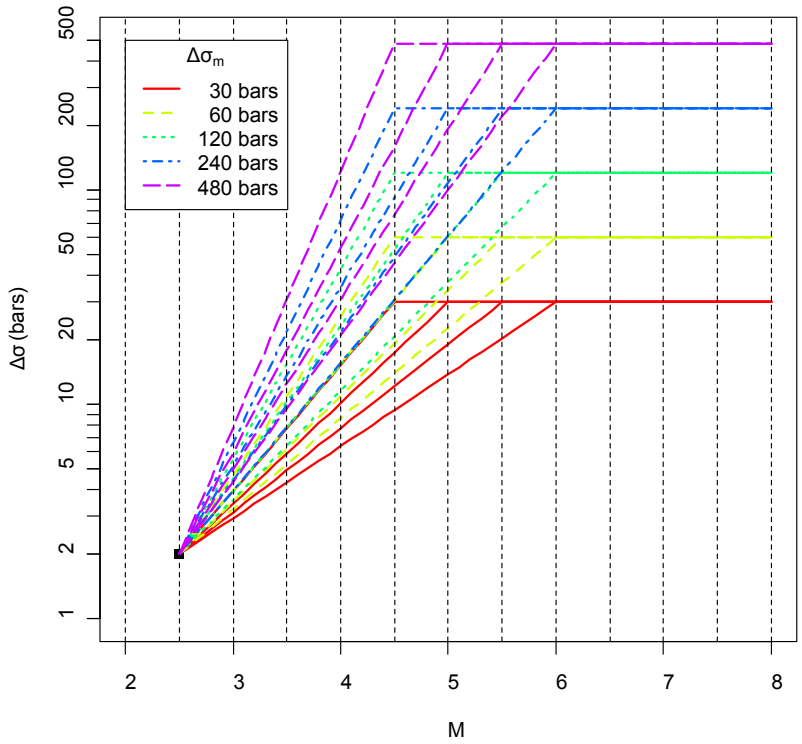

Figure I-2.3: Alternative models of the magnitude dependence of the stress drop for extrapolation of the Swiss stochastic model to high magnitudes.

ground motion models. For example, the rupture distance is the closest point on the site at any point on the rupture plane and is not measured from the same point on the rupture for all site locations. Similarly, for the effective point-source distance, there is not a single point on the fault that is used to compute the effective distance to each site. Rather, an equivalent point-source distance is used for the point-source stochastic model.

For application in the hazard analysis, the point-source model requires a model to convert from the closest distance metric used in the hazard calculation (R_{JB} or R_{rup}) to the effective point-source distance (R_{eff}). Two candidate conversion methods are described below.

Method 1 - Simulation: Edwards and Fäh [2010] (TP2-TB-1052) define the effective point source distance, (R_{eff}, as the distance that, over numerous random simulations of a finite fault with unknown hypocenter, leads to the same attenuation as would be experienced by the RMS summation of unique ray-paths from the discretized finite fault. Their approach is described below:

Normal and strike-slip faults with average dips of 53 and 79 degrees, respectively, are selected as being representative for Switzerland. The Wells and Coppersmith [1994] model is used to estimate the fault dimensions for a given magnitude (above M5) and slip type. For events with magnitude less than 5, the rupture is modeled by a circular rupture with an average stress drop of 50 bars. The 50 bar stress drop is consistent with stress drops of earthquakes in the Wells and Coppersmith [1994] database.

A simple parameterization of the relation between the rupture distance and the effective

distance was developed by Abrahamson [2011a] (TFI-TN-1148) and updated by Al Atik [2011c]. This parameterization is shown in Figure I-2.4 and is given by:

$$R_{eff}[\text{km}] = R_{rup}[\text{km}] + \exp(-1.60 + 1.0(M - 3)) \quad \text{(I-2.1)}$$

This model has the same form as that used to model magnitude saturation effects in some ground motion models (e.g. Chiou and Youngs [2008b]).

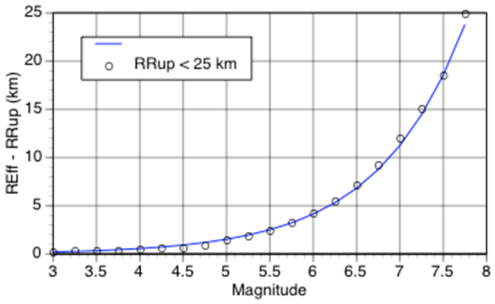

Figure I-2.4: Difference between effective distance and rupture distance based on the simulation model (method 1).

A parameterization for the distance R_{JB} was also developed by Al Atik [2011f] (EXT-TN-1173), but should not be used, as the underlying assumption of the hypocentral depth (8 km) was not appropriate for Switzerland.

It is important to note that the R_{eff}-R_{rup} and R_{eff}-R_{JB} relations described above depend on the fault geometry and depth range used by Edwards and Fäh (2010). These relationships provide an approximate way of relating the distance measures, but they depend on the implicit assumptions made in Edwards and Fäh (2010).

Method 2 - Empirical Calibration: Atkinson and Silva [2000] developed a point-source stochastic model for California. They calibrated the point-source model parameters by fitting the ground motions from large earthquakes in California that had inverted slip models. As part of this calibration, they found that the effective point-source distance could be approximated by the Joyner-Boore distance with a fictitious depth given by the depth of the largest asperity.

$$R_{eff} = \sqrt{R_{JB}^2 + H_{ASP}^2} \quad \text{(I-2.2)}$$

For application in a hazard analysis, the depth of the largest asperity is not known. Silva (personal communication) recommends a value of H_{ASP}=8 km as a default value for California. This model is similar to the distance scaling in GMPEs that use a $\sqrt{R^2 + C^2}$ in the ground motion model. In this model, C=8 km. For comparison, the C term used for AS08 is 4.5 km (note, that for empirical models, the estimate of C is strongly correlated with the distance slope).

These two methods for computing the effective distance for the point-source stochastic model were discussed at the SP2 workshop in March, 2011. Model 1, which converts the rupture distance to the effective distance, was preferred over Model 2, which converts the Joyner-Boore distance to the effective distance, because use of the Joyner-Boore distance does not take the Swiss-specific depth distribution into account and using the depths of the earthquakes

provides a better interface with the SP1 models. Therefore, only model 1 is included in the master logic tree.

Chapter 3

Adjustment to Median Horizontal Motions

3.1 Interpolation for Missing Coefficients

The PEGASOS Refinement Project requires the hazard to be calculated in terms of ordinates of spectral acceleration at 9 response frequencies, listed in the header of Table I-3.1. Not all of the GMPEs provide coefficients for spectral accelerations at all 9 target response frequencies, as indicated in Table I-3.1.

Table I-3.1: Response frequencies for which GMPEs provide coefficients.

GMPE	Response Frequency [Hz]								
	100	**50**	**33**	**20**	**10**	**5**	**2.5**	**1**	**0.5**
Abrahamson & Silva (2008)	✓	✓	✓	✓	✓	✓	✓	✓	✓
Akkar & Bommer (2010)	✓			✓	✓	✓	✓	✓	✓
Atkinson & Boore (2006)	✓			✓	✓	✓	✓	✓	✓
Boore & Atkinson (2008)	✓	✓	✓	✓	✓	✓	✓	✓	✓
Campbell & Bozorgnia (2008)	✓	✓	✓	✓	✓	✓	✓	✓	✓
Chiou & Youngs (2008)	✓	✓	✓	✓	✓	✓	✓	✓	✓
Toro et al. (1997), Toro (2002)	✓				✓	✓	✓	✓	✓
Zhao et al. (2006)	✓			✓	✓	✓	✓	✓	✓
Akkar & Cagnan (2010)	✓		✓	✓	✓	✓	✓	✓	✓
Bindi et. al. (2011)	✓			[ ]*	✓	✓	✓	✓	✓

* 25 Hz is available for Bindi et al. [2011], which is used as part of the interpolation.

For those GMPEs that do not explicitly report coefficients for the spectral acceleration at a response frequency of 100 Hz, those reported for PGA are adopted in their place.

In all, there are 13 cases in which there are missing frequencies for the selected GMPEs. All of the missing frequencies are at the high frequency end. Coefficients for these missing frequencies are estimated by interpolation between the highest frequency at which coefficients are given and PGA.

Although not strictly matching the target response frequencies, some of the models do provide coefficients at other high frequencies: Atkinson [2006] provides coefficients at 31.8 Hz and 40 Hz, and Toro et al. [1997] give coefficients for spectral accelerations at 25 Hz and 35 Hz. The missing coefficients for the four models requiring interpolation are reported in Bommer and Stafford [2010a], (see tables 2.4 to 2.7 in TP2-TB-1039).

3.2 Parameter Compatibility Conversions

In PEGASOS, many of the ground motion models required parameter conversion for magnitude, and definition of the horizontal component. For the selected GMPEs, no parameter conversions are required in PRP.

3.3 Style-of-Faulting Adjustments

Seven of the ten selected models – the four selected NGA models, Akkar and Bommer [2010], Akkar and Cagnan [2010], and Bindi et al. [2011] include coefficients to explicitly model the effects of style-of-faulting, distinguishing between normal, reverse and strike-slip faults. The SP1 seismic source models include all three styles-of-faulting, so every GMPE is required to be applicable to normal, reverse and strike-slip faulting earthquakes. The other three GMPEs [Atkinson 2006]; Toro et al. [1997], Toro [2002]; Zhao et al. [2006] do not provide explicit and separate predictions for all three styles-of-faulting. Therefore, style-of-faulting factors were developed for these three models.

The chosen approach for making the adjustments is that proposed by Bommer et al. [2003]. This method uses the ratio between normal and strike-slip from GMPEs with both types and then applies this ratio to the GMPEs without a normal style-of-faulting factor. To avoid adding a bias to the model, the constant in the model is adjusted to account for the fraction of strike-slip and normal mechanism earthquakes in the dataset used to derive the GMPE.

The SP2 experts selected the Akkar and Bommer [2010] model to provide the basis for the generic ratios between response spectral ordinates from earthquakes of different styles-of-faulting. The Akkar and Bommer [2010] model was selected because it is a recent ground-motion model derived from a dataset in which all three styles-of-faulting are well represented, with 96 records (18%) from reverse-faulting events, 210 (39.5%) from normal-faulting events and 226 (42.5%) from strike-slip events. In addition, this model does not include other complexities, such as depth-to-top and hanging wall effects, that would make estimation of simple style-of-faulting factors more difficult.

Bommer and Stafford [2010a] derived the coefficients for adjusting the three models without complete style-of-faulting factors. These factors are shown in Table I-3.2. The SP2 experts decided (at WS5 in Zurich on 7-8 July 2010) that a single adjustment factor will be sufficient; in other words, it is not necessary to develop a logic-tree approach with branches for multiple alternative options for making the style-of-faulting adjustments to the three GMPEs. Therefore, additional epistemic uncertainty is not added to the adjustment factors given in Bommer and Stafford [2010a].

Table I-3.2: Adjustment factors for the 3 GMPEs not explicitly accounting for all three styles-of-faulting.

Period	Frequency	Toro et al. and Atkinson & Boore			Zhao et al. (FR=0)	
[sec]	[Hz]	Reverse	Normal	Strike-slip	Normal	Strike-slip
0.01	100	1.037	0.783	0.862	0.909	1.002
0.02	50	1.038	0.779	0.856	0.911	1.002
0.03	33.3	1.039	0.776	0.853	0.911	1.002
0.05	20	1.040	0.772	0.852	0.908	1.002
0.1	10	1.036	0.772	0.864	0.895	1.002
0.2	5	1.038	0.814	0.855	0.954	1.001
0.3	3.33	1.042	0.742	0.843	0.882	1.002
0.4	2.5	1.046	0.739	0.832	0.890	1.002
1	1	1.010	0.913	0.962	0.950	1.001

3.4 Host-to-target ($V_S - \kappa$) Adjustments

In PEGASOS and in the PRP, the SP2 experts decided that developing host-to-target region scale factors for the full set of stochastic point source parameters was desirable as the stress drop scaling in Switzerland was not well constrained, but they considered the differences in the shear wave velocity (V_S) and crustal damping (κ) to be important effects that should be considered. Therefore, the objective was to isolate the V_S and κ correction from the full model correction. An important issue identified early on is that there was a high correlation between stress drop and κ, which makes it difficult to isolate the κ correction. To reduce the correction, Scherbaum [2010] (TP2-TB-1036) used normalized spectral shapes in place of the spectral values for the inversion of the point source parameters for the GMPEs. While this method reduced the correlation, the estimation of κ was still not robust. For example, the point source inversion leads to very different estimates of κ values for the four NGA models, even though these models were based on similar datasets.

Significant revisions to the host-to-target ($V_S - \kappa$) adjustment methodology have been developed as part of the PRP. Alternative methods are described below. At the beginning, a preferred method was not selected by the SP2 experts. Therefore, the structure of the logic tree was set to have the individual SP2 experts specify the range of values of the $V_S - \kappa$ scale factors (for each frequency and each GMPE) rather than have them specify the weights on the methods and model parameters. This required more effort by the SP2 evaluators, but the additional effort was justified given the current uncertainty in the $V_S - \kappa$ correction methodologies.

3.4.1 Estimation of Kappa

Estimates of κ are needed for each GMPE (host region) and for Switzerland (target region). Three alternative methods for estimation of κ are considered: 1) κ based on response spectral shapes from the GMPE, 2) κ based on $V_{S30} - \kappa$ correlations, and 3) κ based on the slope of the Fourier amplitude spectrum estimated from the GMPE using inverse RVT (IRVT). These three methods are discussed below.

Kappa based on Response Spectral Shapes

To improve the robustness of the estimation of κ, the expert F. Scherbaum proposed that the κ value be estimated based on the frequency at which the acceleration response spectrum reaches

its peak (called f_{peak}). This approach was implemented by Al Atik [2011e, b] (EXT-TN-1164, EXT-TN-1150). Using the point-source stochastic model, the relation between the f_{peak} and κ can be derived for different magnitudes and distances using only short distances (to avoid large effects of Q).

An example of the relation between f_{peak} and κ is shown in Figure I-3.1. As κ is reduced, the peak of the spectrum shifts to higher frequencies. The relation between κ and f_{peak} is not strongly dependent on the stress drop. The relation is also similar for the WUS and CEUS background models indicating that this correlation is fairly robust. The Swiss stochastic model has larger differences, with lower κ values for the same f_{peak} value. This difference with the Swiss model has been evaluated extensively by the SP2 experts, but without any definitive conclusion.

Using this approach, κ values were estimated for each of the ten GMPEs for M5, M6, and M7 earthquakes at distances of 5, 10, and 20 km. There is a small change in estimated κ for the three different magnitudes. The estimated κ values for M6 are listed in Table I-3.3. With this new approach, the κ values for the four NGA models are similar (0.038 to 0.044 s), indicating that this method is more robust than the spectral shape method.

Based on the different background stochastic models, the coefficient of variation of κ ranges from 0.14 to 0.33. To capture the epistemic uncertainty, a range of host κ values can be considered.

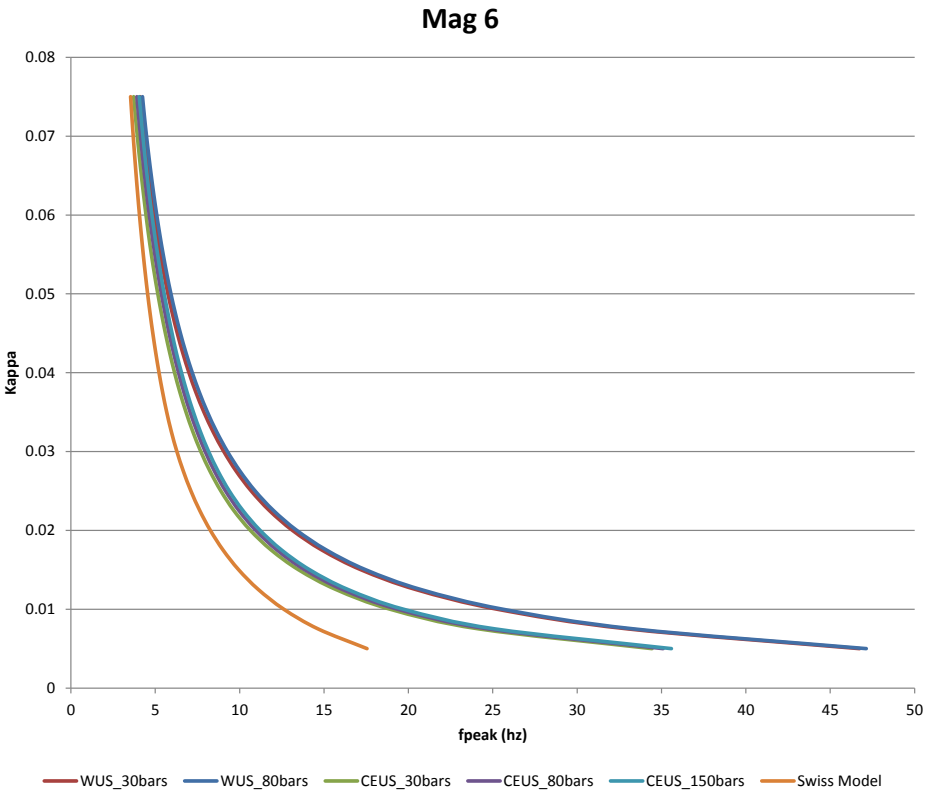

Figure I-3.1: Example of the relation between κ and the frequency at which the acceleration spectrum reaches its peak (f_{peak}) for magnitude 6 earthquakes. The curves are for alternative background stochastic models.

Table I-3.3: Estimates of κ for M6 based on the correlation between κ and f_{peak} shown in Figure I-3.1.

GMPE	Estimated κ [sec]	Coefficient of Variation (based on 6 background stochastic models)
AbSi08	0.044	0.14
BoAt08	0.038	0.16
CaBo08	0.038	0.16
ChYo08	0.038	0.16
Zhao06	0.038	0.16
AkBo10	0.043	0.15
AtBo06	0.0055	0.33
Toro02	0.008	0.3
AkCa10	0.054	0.14
Bind11	0.054	0.14

Kappa based on $V_{S30} - \kappa$ Correlations

κ can be estimated for a GMPE using the V_{S30} for the GMPE and empirical correlations between κ and V_{S30}. Two correlation models are considered: Edwards et al. [2011b] and Silva et al. [1998]. The Edwards et al. model is based on Swiss data using the κ estimated for the Swiss stations as part of the development of the Swiss stochastic model. Edwards et al. are proposing two relationships for the $V_{S30} - \kappa$ correlation; one based on a fit in linear-linear space and the other based on a fit in linear-log space. Through WS9, the SP2 experts considered only the linear-log fit. The Silva model is based on world-wide data (mostly California) using κ values estimated from inversions of the Fourier spectral values. A recent evaluation of the $\kappa - V_{S30}$ relation based on world-wide data using κ values based on measured slopes of Fourier spectra is given by Van Houtte et al. [2011]. They found a $\kappa - V_{S30}$ relation similar to the Silva et al. [1998] model. The alternative $\kappa - V_{S30}$ relations are shown in Figure I-3.2.

In January 2012, Edwards updated his $V_{S30} - \kappa$ correlation and also added a third relationship based on a log-log fit. The update also corrected an error due to using the V_{S40} instead of V_{S30} when deriving the correlation. As a result of the correction, the V_{S30} points were shifted slightly to lower V_{S30} values and the resulting curves in Figure I-3.2 were moved slightly to the left compared to the earlier version.

Kappa based on Fourier Spectra from IRVT

κ can also be estimated for a GMPE based on the slope of the Fourier amplitude spectrum (FAS) estimated from the response spectrum. The method is described by Al Atik and Abrahamson [2012a] (EXT-TB-1087). In this approach, inverse RVT is first used to estimate the FAS for a given response spectral shape for a given magnitude and distance. Given the FAS, κ is estimated from the slope in the FAS. For each GMPE and each reference V_{S30} value, this process is repeated for three magnitudes (M5, M6, and M7) and three distances (R5, R10 and R20). The full set of κ values and fits to the FAS are described in Al Atik and Abrahamson [2012a]. Note that these values are based on an evaluation with a dip of 90° and a hypocentral depth of 5 km. After June 2012, for the final evaluation the target κ values

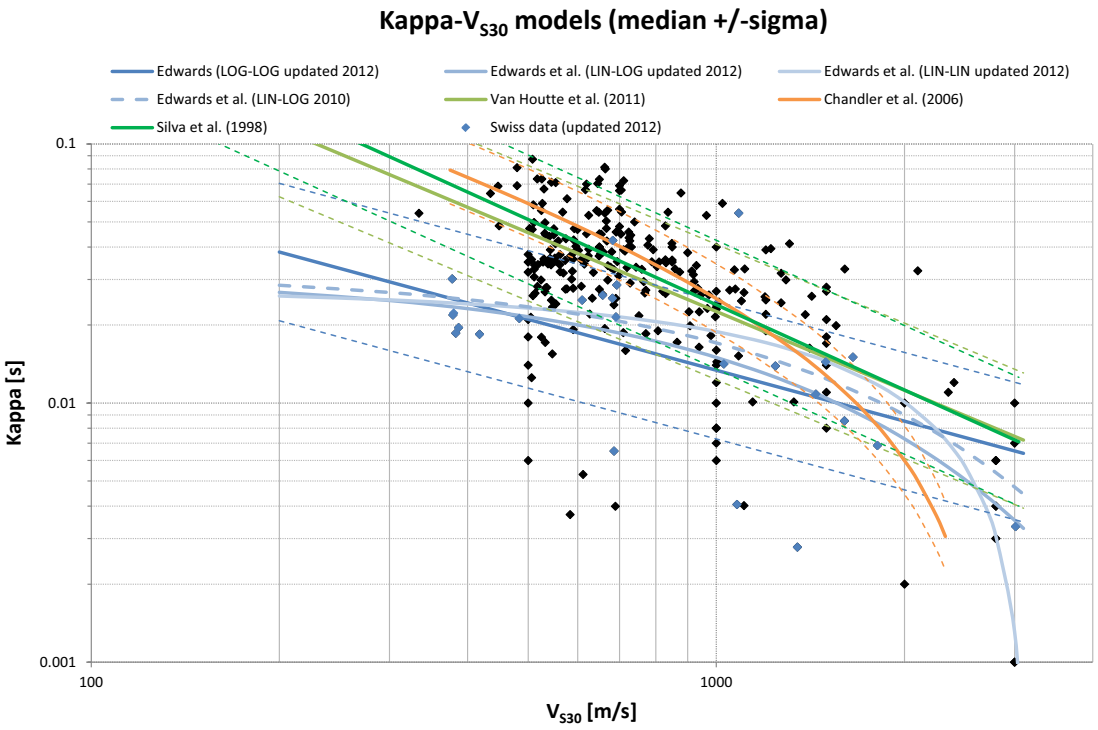

Figure I-3.2: Comparison of different correlations between κ and V_{S30}. The dashed lines indicate one standard deviation about the median model.

were revised using dip and depth with the average source characterization. The resulting κ values for the ten GMPEs are listed in Table I-3.4.

Table I-3.4: Estimates of κ based on Inverse RVT. Revised compared to EXT-TB-1087 to be consistent with the average SP1 depth distribution.

GMPE	V_{S30} [m/s]	κ [sec]	V_{S30} [m/s]	κ [sec]	V_{S30} [m/s]	κ [sec]
AbSi08	620	0.0414	800	0.0409	1000	0.0396
BoAt08	620	0.0404	800	0.0402	1000	0.0400
CaBo08	620	0.0413	800	0.0406	1000	0.0393
ChYo08	620	0.0374	800	0.0349	1000	0.0336
Zhao06	500	0.0383	700	0.0383	900	0.0383
AkBo10	600	0.0344	800	0.0344	1000	0.0344
AtBo06	2000	0.0055	2200	0.0055	2800	0.0055
Toro02	2800	0.0066				
AkCa10	800	0.0445	950	0.0442	1100	0.0440
Bind11	800	0.0424	950	0.0424	1100	0.0424

Kappa for Host GMPEs based on FampXX

As part of the empirical evaluation of κ scaling, Al Atik and Abrahamson [2012b] (EXT-TN-1233) developed correlations between the spectral shape and κ using four GMPEs: AbSi08,

CaBo08, AtBo06, and the Swiss stochastic model. Correlations were developed for four different points on the spectral shape: factors of 1.3, 1.5, 1.7, and 2.0. These correlations were used to estimate κ for the ten GMPEs. The results are listed in Table I-3.5.

Table I-3.5: Estimates of κ for host GMPEs based on the $f_{amp} - \kappa$ correlation.

GMPE	$f_{amp1.3}$	$f_{amp1.5}$	$f_{amp1.7}$	$f_{amp2.0}$
AbSi08	0.047	0.051	0.059	0.064
AkbB10	0.036	0.046	0.054	0.057
AkCa10	0.053	0.049	0.052	0.051
AtBo06	0.011	0.01	0.009	0.008
Bind11	0.046	0.047	0.05	0.051
BoAt08	0.044	0.046	0.044	0.049
CaBo08	0.04	0.044	0.047	0.049
ChYo08	0.044	0.048	0.054	0.06
Toro02	0.014	0.013	0.014	0.013
Zhao06	0.042	0.042	0.043	0.041

3.4.2 Host Region Shear Wave Velocity Profiles

In the previous method, the V_S profile for each GMPE was estimated as part of the point-source model inversion. This led to differences in the gradient of the V_S-profile as well as changes in the shallow velocity (V_{S30}). Again, the issue with the approach is the correlation of the V_S profile with other parameters in the stochastic model. If the host-to-target region adjustment is only applied for V_S and κ, then it is important that the estimate of the V_S profile be robust and not have significant trade-offs with other parameters that are not included in the $V_S - \kappa$ only adjustment.

To improve the robustness of the V_S profile, a revised method was proposed in which a single V_S profile is used for all GMPEs but shifting the profile up or down in depth to match the estimated V_{S30} of the GMPE. In this way, the V_S adjustment captures only the differences in the shallow profile and does not attempt to capture differences in the V_S gradients. This is different to the approach which was adopted for PEGASOS, where the profile was shifted horizontally.

In the application of this method, two alternative generic rock profiles are used: a generic Swiss profile and a generic US profile. The generic US profile consists of the 620 m/s V_{S30} profile for the WUS and the 2800 m/s V_{S30} profile for the EUS [Boore and Joyner 1997]. The V_S profile is interpolated between these two profiles, as shown in Figure I-3.3. For V_{S30} values less than 620 m/s (e.g. for the Zhao06 model), the Silva profile for V_{S30}=270 m/s is used to allow interpolation rather than extrapolation of the profiles. The generic Swiss profile is based on the reference V_S profile shown in Figure I-3.4. For other V_{S30} values, the Swiss reference V_S profile is shifted (vertically) to match the V_{S30} of each GMPEs, as shown in Figure I-3.4. The range of V_{S30} values for each GMPE was selected by the SP2 experts and are given in Table I-3.6.

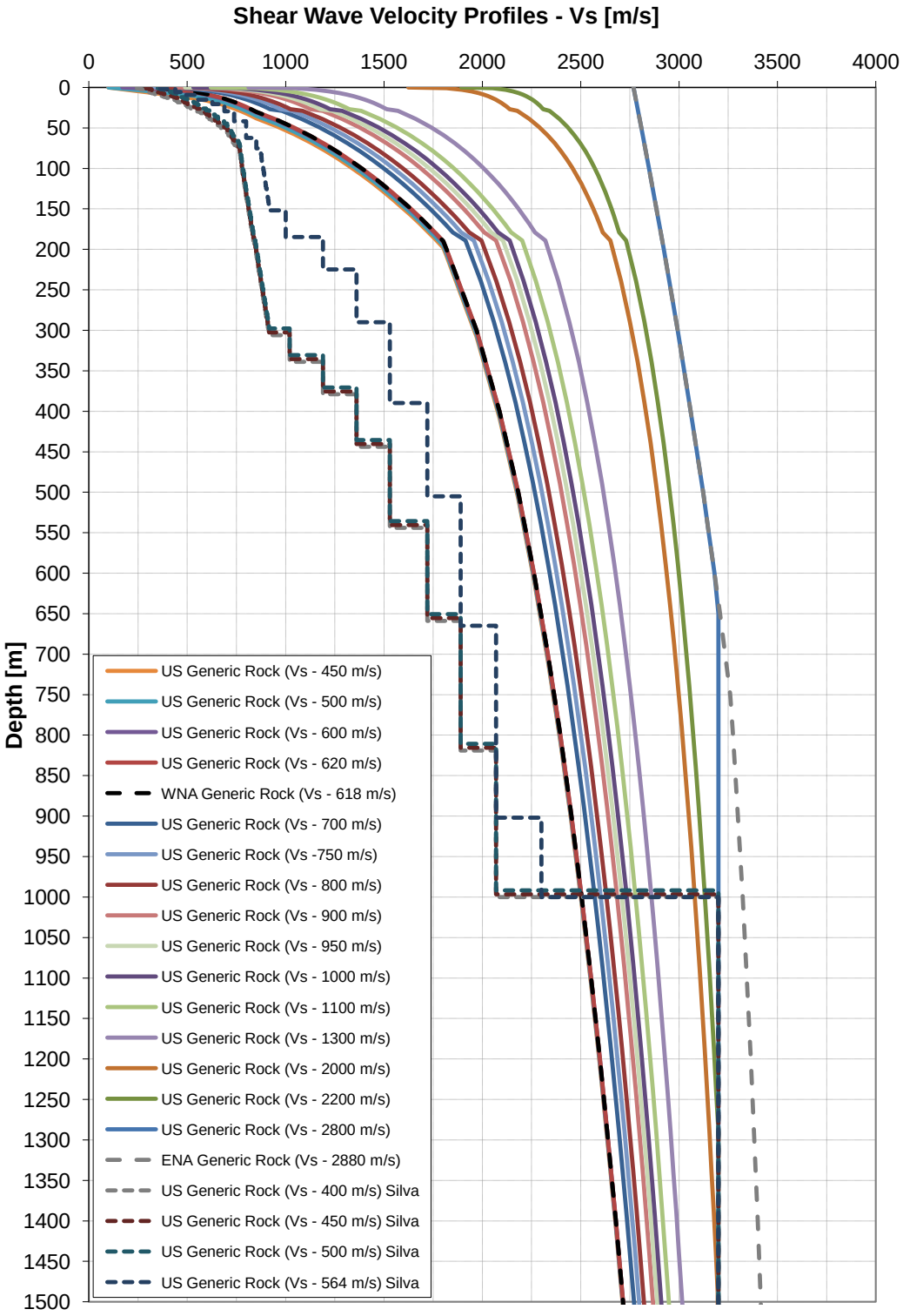

Figure I-3.3: Alternative V_S profiles based on the US reference profiles.

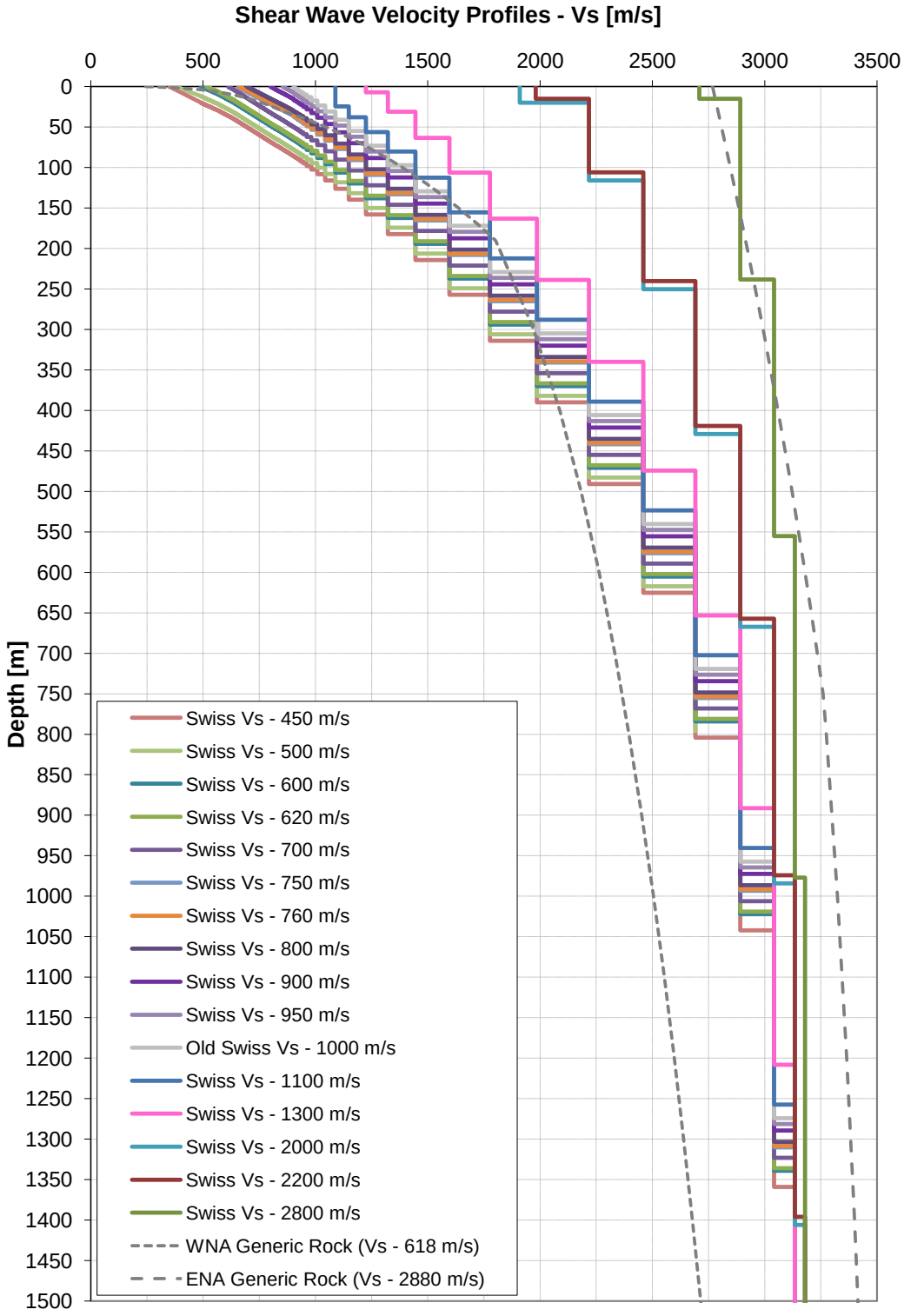

Figure I-3.4: Alternative V_S profiles based on the Swiss reference profile.

Table I-3.6: Alternative reference V_{S30} values to be used for the corrections.

GMPE	$V_{S,Ref1}$	$V_{S,Ref2}$	$V_{S,Ref3}$
AbSi08	620	800	1000
BoAt08	620	800	1000
CaBo08	620	800	1000
ChYo08	620	800	1000
Akka10	600	800	1000
Zhao06	500	700	900
AtBo06	2000	2200	2800
AkCa10	800	950	1100
Bindi11	800	950	1100
Toro02	-	2800	-

3.4.3 Vs-Kappa Correction Methods

Hybrid Model for $V_S - \kappa$ Adjustments

The hybrid model (e.g. Campbell [2003]) uses the point-source stochastic model to correct for differences between the host and target regions. If this approach is used to correct for differences in κ only for rock sites with the same shear wave velocity, the resulting correction factors are shown in Figure I-3.5. As shown in this figure, the κ corrections using this method can be large for high frequencies (10-30 Hz).

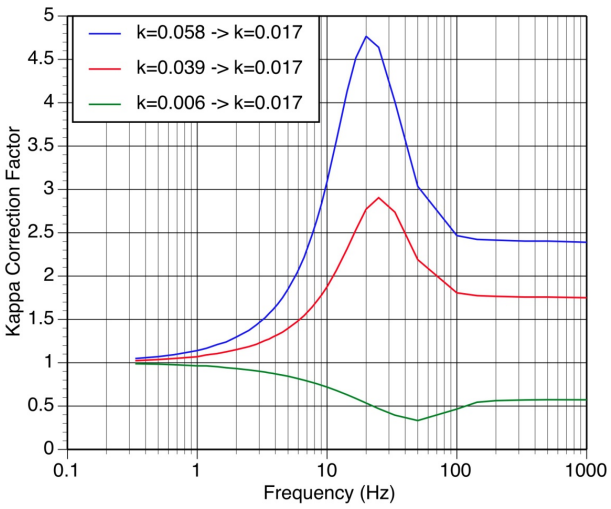

Figure I-3.5: Example of κ only correction factors based on the point source model for a target κ of 0.017 sec and three host κ values.

Iterative Method

The motivation for the iterative method to calculate $V_S - \kappa$ correction factors comes from the fact that the standard method for making host-target adjustments for empirical GMPEs, the hybrid empirical approach by Campbell et al. [2003], is not independent of the stochastic background models. For example, if the Fourier spectrum is assumed to be made up of a source part E, a path part P, a site part S, and an instrument part I, then the full spectrum can be written as

$$Y = E \times P \times S \times I. \tag{I-3.1}$$

Thus, when correcting only site adjustments, the other terms cancel out when dividing the target by the host spectrum. However, this is correct for the Fourier spectrum, but does not hold for the response spectrum, where the other terms do not cancel out. This can lead to unexpected consequences. For example, consider adjustments of a GMPE from its host region to conditions of a Swiss nuclear power plant. This can be done in several ways:

- correct adjustment factors from the GMPE host region with stochastic host model M_{host} to Swiss generic κ and site conditions (all other parameters are as in M_{host})
- correct adjustment factors from the Swiss stochastic model M_{Swiss} to NPP κ and site conditions

- multiply both corrections

Another way would be to directly calculate adjustment factors from M_{host} NPP specific κ and site conditions. The correction factors obtained from the two approaches are not the same, since the background models in the intermediate step of the two-step adjustment do not cancel out (see Figure I-3.6). Here, the GMPE of Campbell & Bozorgnia (2008) is adjusted from its host conditions to target conditions corresponding to $V_{S30,target} = 2500$ m/s and $\kappa_{target} = 0.007$ s. The adjustments are done in one step (blue line) and with an intermediate step via Swiss conditions (red line). In a similar way, there is a difference between correcting $V_S - \kappa$ together and calculating adjustment factors separately for each V_S and κ and multiplying them.

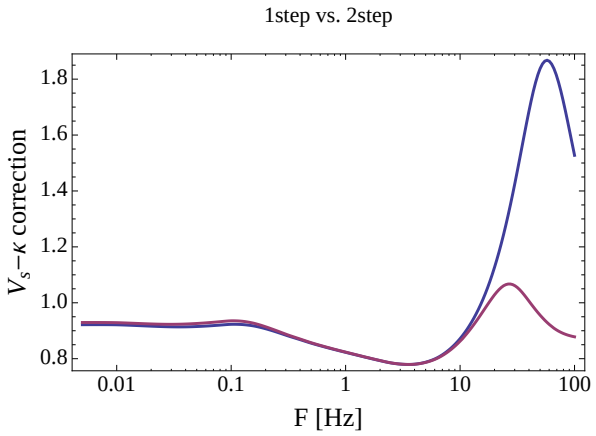

Figure I-3.6: Comparison of 1-step (blue) and 2-step (red) adjustment factors.

The iterative method attempts to avoid the dependence on the stochastic background models - it relies on stochastic simulations only to correct the PGA value. Even this can be avoided if for example a fixed peak-to-PGA ratio is assumed.

The iterative method uses the fact that, for low frequencies (below the peak), the response spectrum behaves like a Fourier spectrum. Thus, in this frequency range corrections can be easily carried out - they are simply the target κ and site amplifications divided by their respective host amplifications. The κ amplification can be calculated by

$$amp_\kappa(f) = \exp^{-\pi\kappa f}, \tag{I-3.2}$$

while the site amplification factors can be computed from a given profile by the quarter-wavelength approximation [Boore and Joyner 1997].

For large frequencies (above the peak), the response spectrum does not behave like a Fourier spectrum. For the case $\kappa_{host} > \kappa_{target}$, this leads to very large adjustment factors - they go to infinity for increasing frequencies, thus leading to a corrected spectrum that also approaches infinity for large frequencies. Therefore, adjustment factors for frequencies above the peak are calculated as follows:

- The input spectrum above the peak is converted into relative frequencies w.r.t. to the peak frequency and relative amplitudes w.r.t. peak amplitude and PGA value.
- Peak and PGA values are corrected.

- The relative amplitudes and frequencies are converted back to absolute values, now w.r.t. the corrected peak and PGA value.

The correction of the peak amplitude is done as described above, by multiplying with the fractions of target/host κ and site amplifications. The PGA value can be corrected as follows:

- Use stochastic host and target model to correct PGA value.
- Use a fixed peak-to-PGA ratio (normally around 2.5).
- Retain input peak-to-PGA value.

The method, described above, needs an estimation of the peak frequency and amplitude, both for the input and the corrected spectrum. If the difference between host and target κ is large, this can pose a problem, because, in this case, the correction factors are very large for frequencies above the peak, which may lead to a corrected spectrum that has no discernible peak. To overcome this issue, the correction factors are calculated iteratively, each time correcting by

$$\delta\kappa = \frac{\kappa_{target} - \kappa_{host}}{n}, \tag{I-3.3}$$

where n denotes the number of iterations.

An example is shown in Figure I-3.7, where the GMPE of Zhao et al. (2006) is corrected from a $\kappa_{host} = 0.044$ s to $\kappa_{target} = 0.017$ s in one step (no site amplification correction is done here). The blue solid and dashed lines describe the corrected spectrum, where the correction is done according to Equation I-3.2. As can bee seen, the shape of the corrected spectrum for large frequencies (above the peak) is not realistic as the amplitudes approach infinity. Figure I-3.7 also shows that there is no real discernible peak for the thus corrected spectrum. This makes it hard to determine the change point between the correction based on the Fourier spectrum and the correction based on bending down to the corrected PGA value. A correction done in four steps is shown in Figure I-3.8.

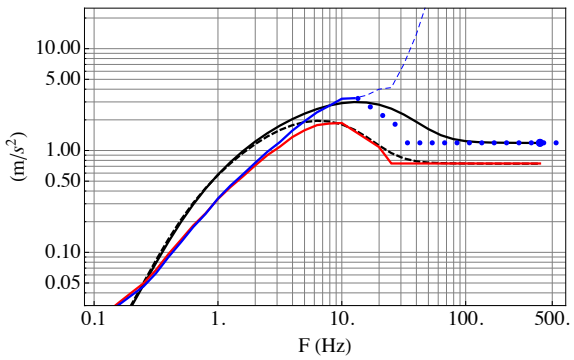

Figure I-3.7: Host, target and intermediate spectra; input empirical spectrum: red; stochastic host spectrum: black dashed; stochastic target spectrum; black solid; corrected spectrum (like Fourier spectrum) below the peak: blue solid; corrected spectrum (like Fourier spectrum) above the peak: blue dashed; corrected (relative/absolute with corrected PGA) spectrum above peak: blue points; corrected PGA value: thick blue point.

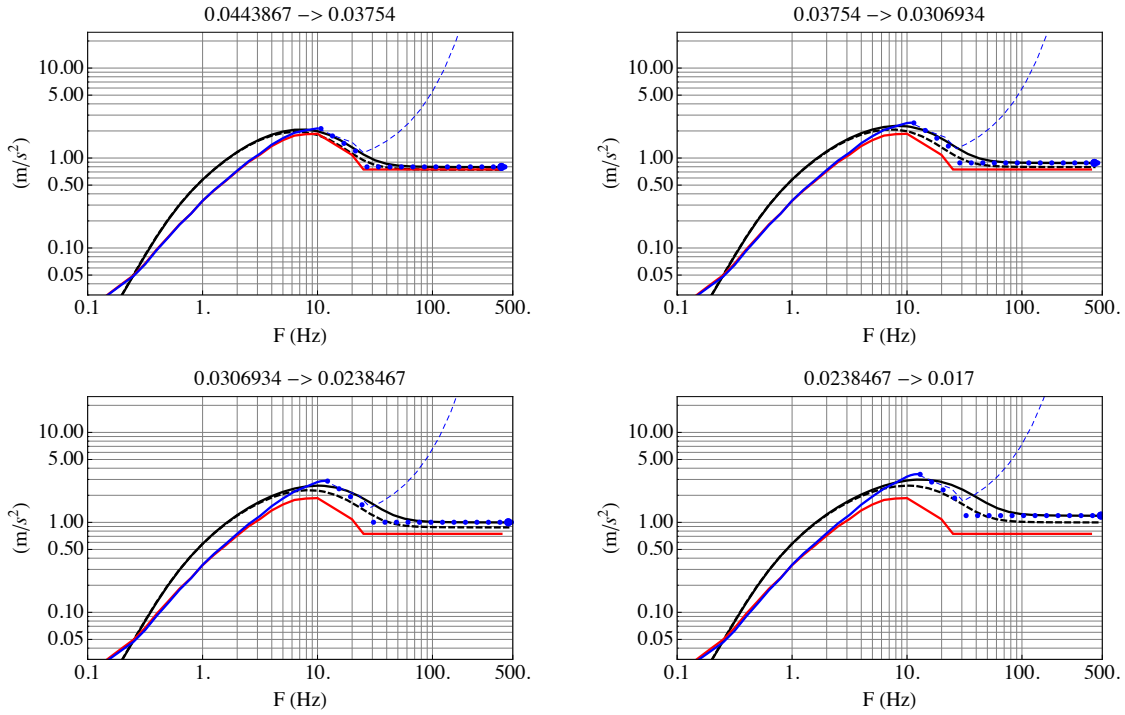

Figure I-3.8: $V_S - \kappa$ correction, done iteratively in four steps. Color schemes are the same as in Figure I-3.7.

IRVT Method

The inverse RVT method is described in Al Atik and Abrahamson [2012a] (EXT-TB-1087) and [Al Atik et al. 2013]. In this method, the κ scaling and the V_{S30} scaling are applied to the FAS estimated using IRVT. Next, RVT is used to transform the FAS back to response spectral values. The ratio of the adjusted response spectrum to the GMPE response spectrum defines the $\kappa - V_{S30}$ scale factor for the GMPE.

Empirical Vs-Kappa Adjustments

As an alternative methodology, empirical strong motion datasets can be used to evaluate the $V_S - \kappa$ adjustments. In this approach, the within-residuals of the GMPEs, which do not explicitly include κ, are evaluated in terms of the κ values estimated for each recording. Three datasets are used: a preliminary version of the NGA-West2 dataset, a preliminary version of the NGA-East data [Goulet et al. 2014], and the Swiss dataset used to derive the Swiss stochastic model.

An issue with this approach is the estimate of κ for each recording. κ values are not yet available for each site in the NGA-West datasets. Therefore, an approximate method was used to estimate κ. Based on the IRVT method, the relation between the spectral shape and κ can be estimated. In particular, there is a relation between κ and the highest frequency at which the spectral shape (Sa/PGA) reaches a specific value (1.5 for NGA-West2 and 2.0 for NGA-East and Swiss data). The κ value for each recording is estimated based on the spectral shape of the recording and this correlation. As noted in Al Atik and Abrahamson [2012b] (EXT-TN-1233), this approach leads to κ values that may not be consistent for

different recordings at the same site. It is expected that this definition will over-estimate the κ scaling because the ground motions with greater high frequency content, and probably higher residuals, will have lower κ estimates.

The results of this method are shown in terms of mean residuals as a function of κ. An example plot is shown in Figure I-3.9. Similar plots for all of the GMPEs and for each of the three datasets are shown in Al Atik and Abrahamson [2012b] (EXT-TN-1233).

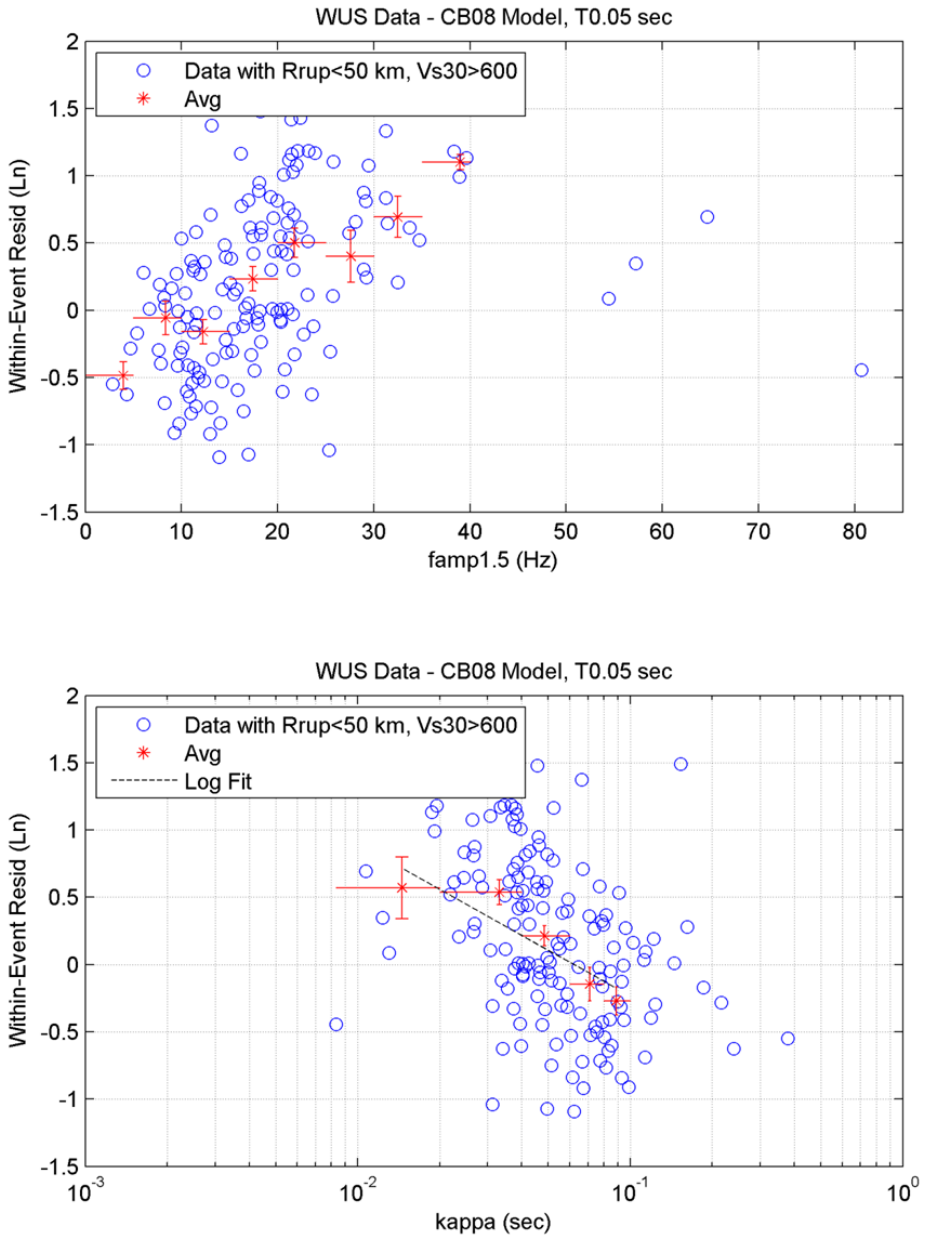

Figure I-3.9: Example of the κ scaling for 20 Hz spectral acceleration based on the empirical method using the NGA-West2 data and the CaBo08 model [Al Atik and Abrahamson 2012b] (EXT-TN-1233).

Table I-3.7: Site specific V_{S30} reference rock conditions

NPP	$V_{S30}rock$
Beznau	1800 m/s
Gösgen	2500 m/s
Leibstadt	2200 m/s
Mühleberg	1100 m/s

3.5 Adjustment to NPP Site Conditions

The initial evaluations of the adjustments of the GMPEs to Swiss site conditions were conducted for a generic reference site condition (V_{S30}=1000 m/s and κ = 0.017 sec). For the hazard application, the SP2 experts developed site-specific models for the reference rock conditions selected for each NPP site. The reference rock was selected based on the V_S-profile at each NPP site. The V_{S30} values, measured from the top of the reference rock, are listed in Table I-3.7. These NPP specific adjustments, which are also expert specific, are marked as red branches in the logic tree in Figure I-3.10.

3.6 Logic Tree Approach to Vs-Kappa Adjustments

The range of alternative methods and data for the $V_S - \kappa$ adjustments are summarized in the logic tree shown in Figure I-3.10. There are three main parts of the tree: a) κ for the host GMPE, b) κ for the target region (Switzerland or NPP site), and c) $V_S - \kappa$ correction method.

In the final master logic tree shown in Chapter 9, this large tree with $V_S - \kappa$ adjustments is reduced to five branches for each GMPE, with the adjustment factors for each branch specified by the SP2 experts. The $V_S - \kappa$ scaling logic tree shown in Figure I-3.10 provides a framework for the SP2 experts to evaluate the $V_S - \kappa$ scaling that they will specify in the final master logic tree.

3.6.1 Kappa for Host GMPE

Four alternative methods are used for the estimation of the host GMPE κ, shown by the four branches on the left hand side of Figure I-3.10.

The first method uses the correlation between κ_0 and the frequency at which the GMPE reaches its peak spectral acceleration value (f_{peak}). The $\kappa_0 - f_{peak}$ correlation is based on the point-source stochastic model. The standard deviation attributed to that branch reflects the variability due to the use of different scenarios (M5, M6, M7 & R5, R10, R20) to derive the correlation.

The second method uses the empirical correlation between κ_0 and V_{S30}. Two alternative empirical correlations are considered. The branch with the $\pm\sigma$ captures the standard deviation of an individual observation of κ. The standard deviation of the aleatory variability of the rock ground motion is the single-station sigma (see Section 6). In principle, the use of single-station sigma account for the site-specific κ at each recording site, as the epistemic uncertainty of the site-specific κ is implicitly considered. The standard deviation of the κ for a given V_{S30} can be

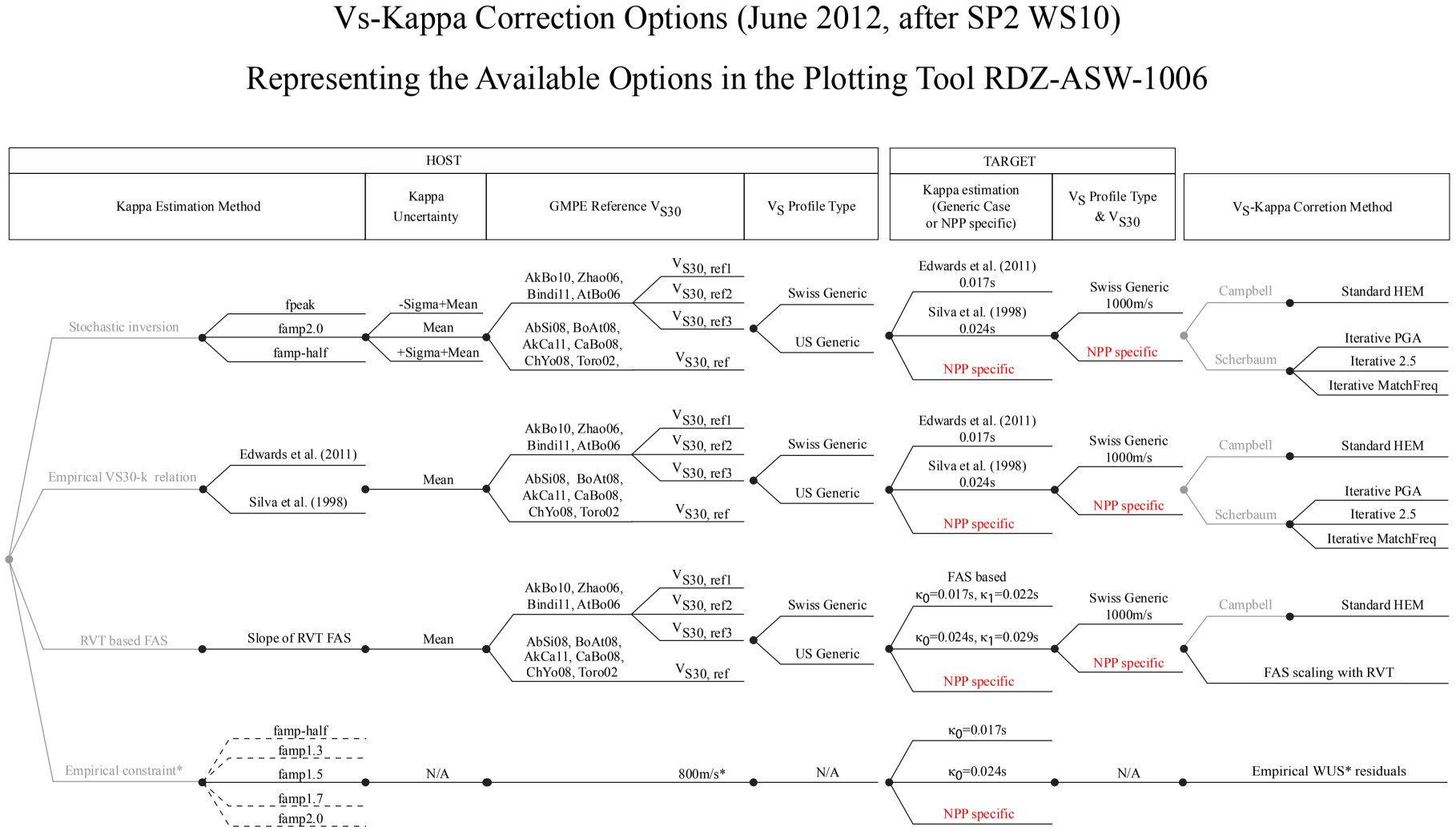

* No empirical CEUS residuals are available at the moment and thus, results of this branch should not be compared to Toro02 and AtBo06

Figure I-3.10: Generic logic tree for the evaluation of $V_S - \kappa$ scaling.

used to estimate the epistemic uncertainty in the site-specific κ; however, if this uncertainty in κ (about 0.5 natural log units) is combined with the κ scaling shown in Figure I-3.5, the standard deviation of the resulting ground motion would be about 0.6 natural log units. The standard deviation due to κ differences is part of the within-event site-to-site standard deviation (ϕ_{S2S}) described in Section 6, but the empirical data show that the total ϕ_{S2S} is about 0.3-0.4 natural log units. Therefore, the range of ground motions from the κ uncertainty given by the standard deviation of κ for a given V_{S30} significantly over-estimates the ground motion uncertainty, suggesting that there are correlated effects that are not being considered. The other methods use a median κ and uncertainty in the median κ.

The third method uses the IRVT method to estimate κ_1 for each GMPE.

The fourth method uses the correlation between κ_1 and the highest frequency at which the spectral shape exceeds a specified value (1.3, 1.5, 1.7, or 2.0).

The κ values estimated for the four different methods are compared in Table I-3.8.

Table I-3.8: Host GMPE κ values from alternative methods (rounded to two significant digits).

GMPE	V_{S30} **[m/s]**	**Stochastic** f_{peak} **Method** κ_0	V_{S30} **Silva et.al. (1998)** κ_0	V_{S30} **Edwards (2010) Lin-Log** κ_0	V_{S30} Edwards **(2012)*** **Log-Log** κ_0	**IRVT Method** κ_1	$f_{amp1.5}$ **Method** κ_1
AbSi08	620	0.044	0.04	0.022	0.017	0.041	0.051
AbSi08	800		0.03	0.019	0.015	0.041	
AbSi08	1000		0.024	0.017	0.013	0.04	
BoAt08	620	0.038	0.04	0.022	0.017	0.04	0.046
BoAt08	800		0.03	0.019	0.015	0.04	
BoAt08	1000		0.024	0.017	0.013	0.04	
CaBo08	620	0.038	0.04	0.022	0.017	0.041	0.058
CaBo08	800		0.03	0.019	0.015	0.041	
CaBo08	1000		0.024	0.017	0.013	0.039	
ChYo08	620	0.038	0.04	0.022	0.017	0.037	0.048
ChYo08	800		0.03	0.019	0.015	0.035	
ChYo08	1000		0.024	0.017	0.013	0.034	
Zhao06	500		0.051	0.024	0.020	0.038	
Zhao06	700	0.038	0.035	0.021	0.016	0.038	0.042
Zhao06	900	0.038	0.027	0.018	0.013	0.038	
AkBo10	600		0.042	0.022	0.017	0.034	
AkBo10	800	0.043	0.03	0.019	0.015	0.034	0.046
AkBo10	1000	0.043	0.024	0.017	0.013	0.034	
AtBo06	2000	0.0055	0.011	0.009	0.0071	0.0055	
AtBo06	2200	0.0055	0.01	0.0079	0.0075	0.0055	0.01
AtBo06	2800	0.0055	0.0077	0.0054	0.0064	0.0055	
Toro02	2800	0.008	0.0077	0.0054	0.0064	0.0066	0.013
AkCa10	800		0.03	0.019	0.015	0.044	
AkCa10	950	0.054	0.025	0.018	0.013	0.044	0.049
AkCa10	1100		0.021	0.016	0.012	0.044	
Bind11	800		0.03	0.019	0.015	0.042	
Bind11	950	0.054	0.025	0.018	0.013	0.042	
Bind11	1100	0.054	0.021	0.016	0.012	0.042	0.047
Swiss κ_0=0.017	1000		0.024	0.017	0.013	0.022	
Swiss κ_0=0.024	1000		0.024	0.017	0.013	0.029	

* The Edwards [2012a] log-log model has not been used so far to derive any correction function, but is shown here for comparison.

3.6.2 Shear Wave Velocity Profile for Host GMPE

For the host GMPE V_S profile, there are two reference profiles: Swiss generic and US generic. The velocity profile for the GMPE is interpolated from the set of reference profiles. For the IRVT approach for estimating the host κ, the NGA and ENA GMPEs only use the US profile as this is consistent with the data used to derive these GMPEs. For the European and Japanese GMPEs, both the Swiss and US profiles are considered because the velocity profiles for these models are not known.

The reference V_{S30} value for the (four) NGA, AkCa10, and Toro02 models are fixed to a single value to be selected by the SP2 expert. A single value is used for these models because the NGA and AkCa10 models include V_{S30} as a parameter in the model and the Toro02 model is based on a fixed VS=2800 m/s. For the other GMPEs, site classes are used so the V_{S30} is not known. Therefore, three values of the median V_{S30} for the site class are considered to capture the epistemic uncertainty in the value of the median V_{S30} appropriate for the site class.

3.6.3 Target Kappa Estimates for NPP Sites

For the target GMPE κ, there are two models based on the empirical correlation between κ and V_{S30}: Edwards et al. [2010] and Silva et al. [1998]. For a V_{S30} of 1000 m/s, these two models lead to κ_0 values of 0.017 and 0.024 s. As mentioned in Section 3.4.1, it should be noted that the Edwards et al. model was updated in 2012 (three versions are now available) and, up to now, has not been used to derive any corrections.

At the end of 2012, the PMT tasked different research groups, besides their own evaluations [Biro and Renault 2012b], to evaluate and investigate target κ estimates for the NPP sites. Based on previous experience in this relatively new area of focus, the first step was a review of current practice in methods for estimating κ [Ktenidou et al. 2014, 2012c, a]. Then, using Swiss specific information, there was an attempt to define ranges of target κ values applicable to the NPP site conditions [Ktenidou [2012] (EXT-RF-1443), Ktenidou and Van Houtte [2013] (EXT-RF-1455), Ktenidou et al. [2013]]. The SED also revisited their earlier evaluations and provided the project with new estimates [Edwards [2012b] (TP2-TN-1236), Edwards and Fäh [2012a, 2013a], Poggi et al. [2012] (TP2-TB-1090), Edwards [2013] (EXT-TN-1261)].

3.6.4 Shear Wave Velocity Profile for the Target

For the target V_S profile, only the Swiss generic model is used because this model was developed for Swiss sites. Three versions of the Swiss stochastic point source model have been developed in the course of the PRP:

- TP2-TB-1024 Stochastic GMM for Switzerland (Ver. 1) - 16. December 2009
- TP2-TB-1024 Stochastic GMM for Switzerland (Ver. 2) - 26. May 2010
- TP2-TB-1051 Extrapolation of Swiss Stochastic GMM - 07. November 2010

The difference between version 1 (December 2009) and version 2 (May 2010) of the stochastic model is mainly the underlying shear wave velocity profile (see Figure I-3.11).

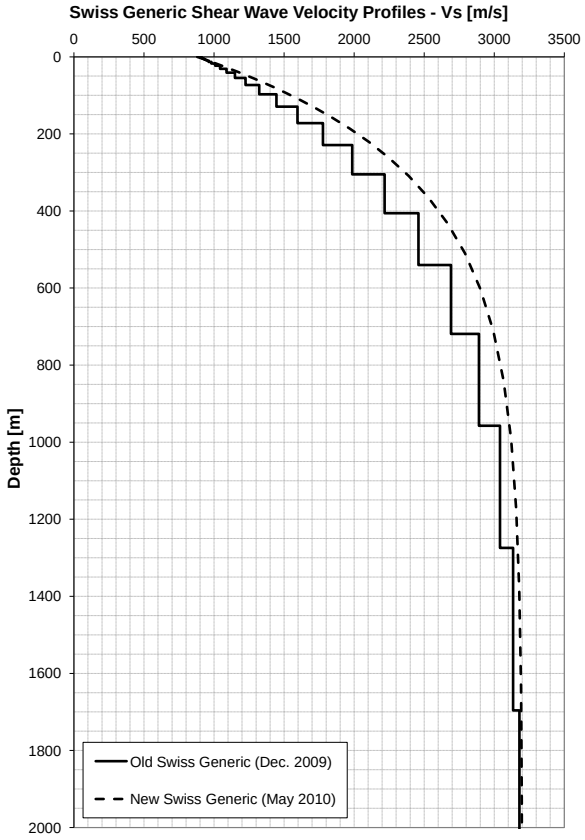

Figure I-3.11: Old and new SGV_{sP} based on Edwards et al. [2009] and Edwards et al. [2010].

The extrapolation of the Swiss stochastic model (November 2010) was performed by Edwards et al. based on the old version 1 of the Swiss Generic Vs Profile (SGVsP). This is due to the fact that when the $V_S - \kappa$ corrections and small magnitude adjustments were performed for the first time in the PRP, they were all based on version 1 of the Swiss stochastic model of December 2009. In order to maintain consistency, the SP2 experts decided during workshop WS5 (7.-8. July 2010) to request the extrapolation to be done on the same basis, even though a new Swiss stochastic model was available (version 2 of May 2010). Following this, the parameterization of the Swiss stochastic model was also based on the old version 1. Furthermore, for the sake of simplicity, the experts decided to use only the constant Q-model proposed by Edwards et al. [2010] and not the layered Q-model. Thus, any computation subsequent to the extrapolated Swiss stochastic model should also be based on the old version 1 shear wave velocity profile and constant Q-model (with Q=1200 m/s for V_S =3500 m/s). This is why it was proposed by the TFI to derive the $V_S - \kappa$ corrections with respect to the old SGVsP and not the new version (PMT-TN-1168). This proposal was accepted by the SP2 experts.

The generic Swiss stochastic model is referenced as having V_{S30} = 1000 m/s. The new SGVsP fits with this V_{S30} if one uses 880 m/s as $V_{S,min}$ at the surface. The old SGVsP in the form documented in the report of Edwards et al. [2010] has a V_{S30} = 978 m/s (with $V_{S,min}$ = 903 m/s at the surface) and was rounded to 1000 m/s for the sake of simplicity in the report (personal communication by B. Edwards, 27. May 2011). This old generic profile has been used for all subsequent evaluations.

3.6.5 $V_S - \kappa$ Adjustment Method

There are four methods for estimating the $V_S - \kappa$ adjustment factor:

1. Standard HEM,
2. Iterative,
3. FAS scaling with RVT, and
4. Empirical scaling based on residuals.

The empirical method only applies κ scaling and should be based on a consistent method for estimating κ (consistent between the κ for the residuals and the κ for the host GMPE and target κ). In principle, the other three methods could be applied to any of the combinations of methods for estimating the host and target κ values and V_S profiles, but there may be some inconsistencies, meaning that the applicability of each method to the different input values should be evaluated. For example, the IRVT method is based on the κ_0 value being consistent with the spectral shape of the GMPE.

Chapter 4

Extrapolation of GMPEs to Small Magnitudes

4.1 Small Magnitude Swiss Ground Motions

As noted in the PEGASOS study, the median ground motions from small magnitude earthquakes in Switzerland are much lower than would be predicted by extrapolating the GMPE to small magnitudes. As an example, Figure I-4.1 illustrates the difference between the extrapolated median ground motions based on the Akkar and Bommer [2010] model and the median Swiss motions for the same magnitude and distance ranges. The extrapolated GMPE significantly over-predicts the observed ground motions.

Table I-4.1 summarizes the minimum magnitudes at which each of the ten selected GMPEs is considered to be applicable, which for six of the ten models is M_W 5.0, while the authors of two of the NGA models suggest that their equations can be used down to M_W 4.0, despite the smallest earthquakes in the dataset being of magnitude M_W 4.3. The ENA model of Atkinson [2006] is applicable down to M_W 3.5.

4.2 Definition of Small Magnitude Target

The Swiss data used to derive the empirical ground-motion model are concentrated in the small magnitude range. Although the bulk of the data are actually in the range M_W 2.0-3.0, the hazard integrations will have a lower limit of M_W 4.5, so there is no particular reason to extend the GMPEs to such small magnitudes. On the basis of these considerations, the SP2 experts selected M_W 3.0 to 3.8 as the magnitude range over which the extended GMPEs should match the Swiss data as represented by the median predictions from the Swiss empirical GMPEs.

4.3 Extrapolation of GMPEs to Small Magnitudes

Recent work by Chiou et al. [2010] has shown that, for small magnitude earthquakes, there are persistent differences in ground-motion amplitudes between northern and southern Cal-

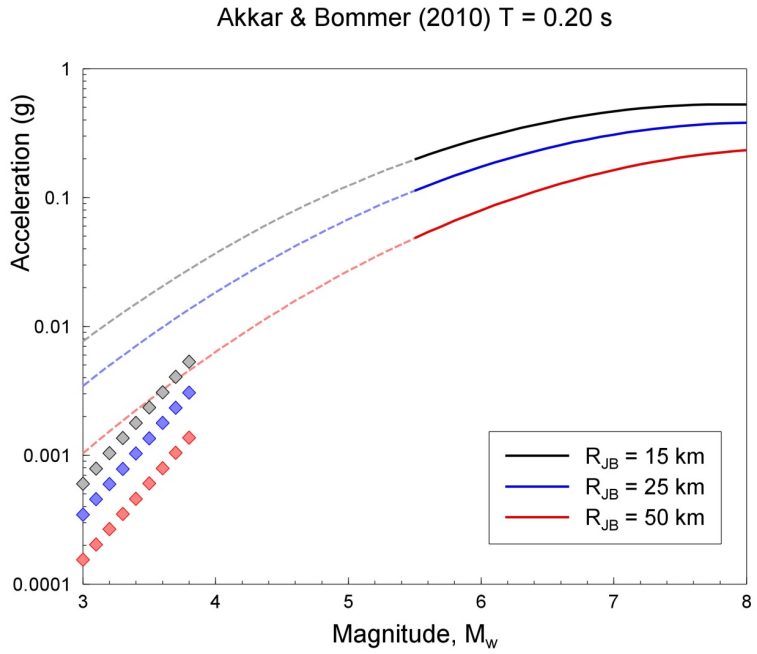

Figure I-4.1: Example comparison of the median predictions of SA(0.2) from the model of Akkar and Bommer [2010], shown as curves, dashed where extrapolated beyond the limit of applicability; and the median predictions from the Swiss empirical model shown as diamonds [Bommer and Stafford 2010a].

Table I-4.1: Minimum magnitudes at which each GMPE is applicable (as suggested by authors).

GMPE	**Minimum mag.** (M_W)
Abrahamson & Silva (2008)	5.0[1]
Akkar & Bommer (2010)	5
Atkinson & Boore (2006)	3.5
Boore & Atkinson (2008)	5.0[1]
Campbell & Bozorgnia (2008)	4.0[2]
Chiou & Youngs (2008)	4.0[2]
Toro et al. (1997), Toro (2002)	5
Zhao et al. (2006)	5
Akkar & Cagnan (2010)	5.0
Bindi et al. (2011)	4.0

[1] Data include M_W 4.27, but authors recommend not extrapolating below 5.0 because of lack of data.
[2] Data include M_W 4.27, but authors believe that equations can be extrapolated to 4.0.

ifornia, which are not encountered for larger magnitude events. This finding leads to two important conclusions: (1) regional differences between ground motions from small-magnitude earthquakes cannot be taken as evidence for regional differences for the moderate-to-large magnitude range that drives hazard estimations, and (2) similarity of ground motions in the small magnitude range cannot be assumed to persist for larger earthquakes. These results indicate that, other than for constraining ground motion models up to a magnitude level of 4 or 4.5, strong-motion recordings of small-magnitude events do not provide strong constraints on ground motions from large magnitude earthquakes.

At the February 2010 workshop (WS4) in Zurich, the SP2 experts agreed that each of the selected and adjusted GMPEs should be retained unaltered in terms of their median predictions for M_W 5.5 and greater. The rationale for selecting this threshold was that recent work has suggested that regional differences in ground motions may become apparent at smaller magnitudes, but even where they have been identified for small-magnitude events they seem not to persist at magnitudes above this level (Table I-4.1).

An example of the adjustment made to small magnitude ground motion is shown in Figure I-4.2 for the Akkar and Bommer [2010] model. This figure shows the magnitude dependence of the adjustment, with a constraint that there is no change at M5.5. Figure I-4.3 shows the adjusted GMPE using the scale factors in Figure I-4.2.

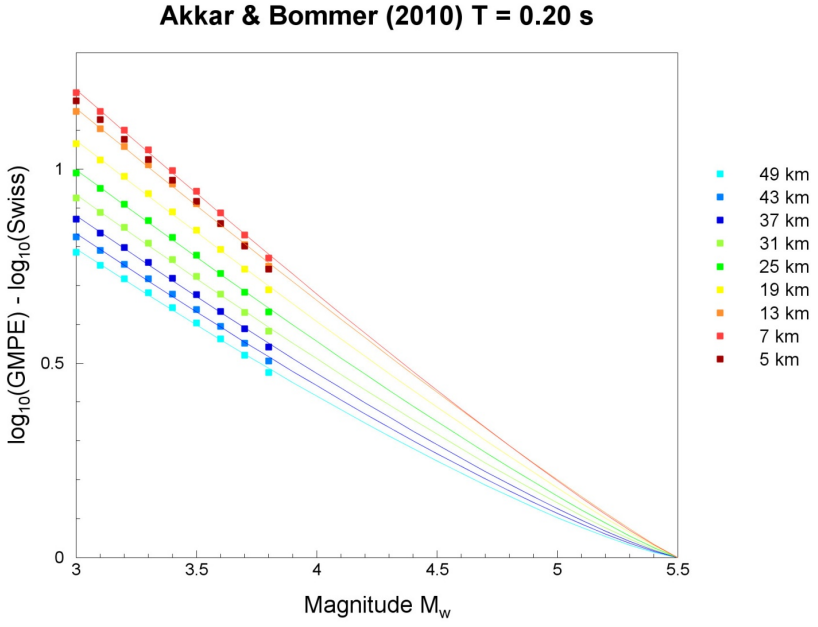

Figure I-4.2: Values of modification for spectral acceleration at T=0.2 second for the model of Akkar and Bommer [2010] at various distances, with a power law fitted to the Swiss small magnitude data at each distance [Bommer and Stafford 2010a].

Earlier in the project, the generic Swiss rock conditions were defined by the SP2 experts to be V_{S30}=1000 m/s and κ=0.017 s, which is the underlying condition of the Swiss stochastic model. In 2013, the method to estimate target κ in Switzerland was tested using ground motions recorded at the SED network stations (see Section 3.6.3). It was found that, on average, the target κ values to be applied to the GMPEs should be higher than initially assumed, in order to be consistent with the recorded data. The small magnitude adjustments

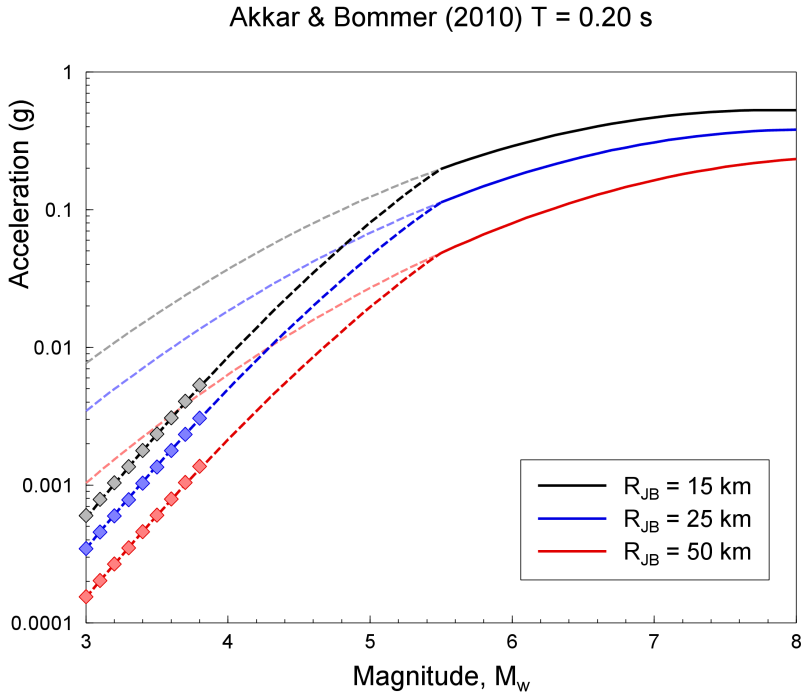

Figure I-4.3: Example comparison of the GMPE extrapolated to small magnitudes (based on the magnitude scaling in the GMPE) and the GMPE modified to be consistent with the Swiss small magnitude data [Bommer and Stafford 2010a].

only need to be applied to the GMPEs, as the PSSM by definition is consistent with the Swiss small magnitudes. The generic rock κ for this adjustment should have been reviewed and potentially revised by the SP2 experts, based on this additional testing. The additional testing occurred late in the project and was not fully incorporated into the SP2 expert evaluation. Thus, the final small magnitude adjustments (of Nov. 2013) were performed with the original κ value of 0.017 s. As the small magnitude adjustments have in the past been shown to be a very minor contributor to the hazard and κ affects only the high frequency content, the project management made the pragmatic decision to not further pursue this issue.

4.4 Alternative Scheme for GMPE Extension to Small Magnitudes

The approach for extending the GMPE to the small magnitude range describe in Section 4.3 is based on developing a power law adjustment function to transition from the GMPE at M5.5 to the Swiss data at M3.5. As an alternative, adjustment functions were developed based on the magnitude dependence of the stress drop with the stress drop fixed at small magnitudes to the median stress drop of small magnitude earthquakes in Switzerland and the stress drops fixed at M6 to be consistent with the high frequency ground motions from the GMPEs. This is described by Al Atik [2010a] (TP2-TB-1059), Al Atik and Abrahamson [2010a] (TP2-TB-1038) and Al Atik [2010b] (TP2-TN-1112).

The advantage of this approach is that it provides a physical interpretation for the adjustment factors in terms of a magnitude dependent stress drop. The adjustment factors developed based on a magnitude dependent stress drop are similar to those from the power law function used by Bommer and Stafford [2010a]. Figure I-4.4 compares the magnitude adjustment

factors for the two approaches. Because the Bommer and Stafford [2010a] method is easier to implement and gives approximately the same results, the SP2 experts agreed to use only the Bommer and Stafford [2010a] model.

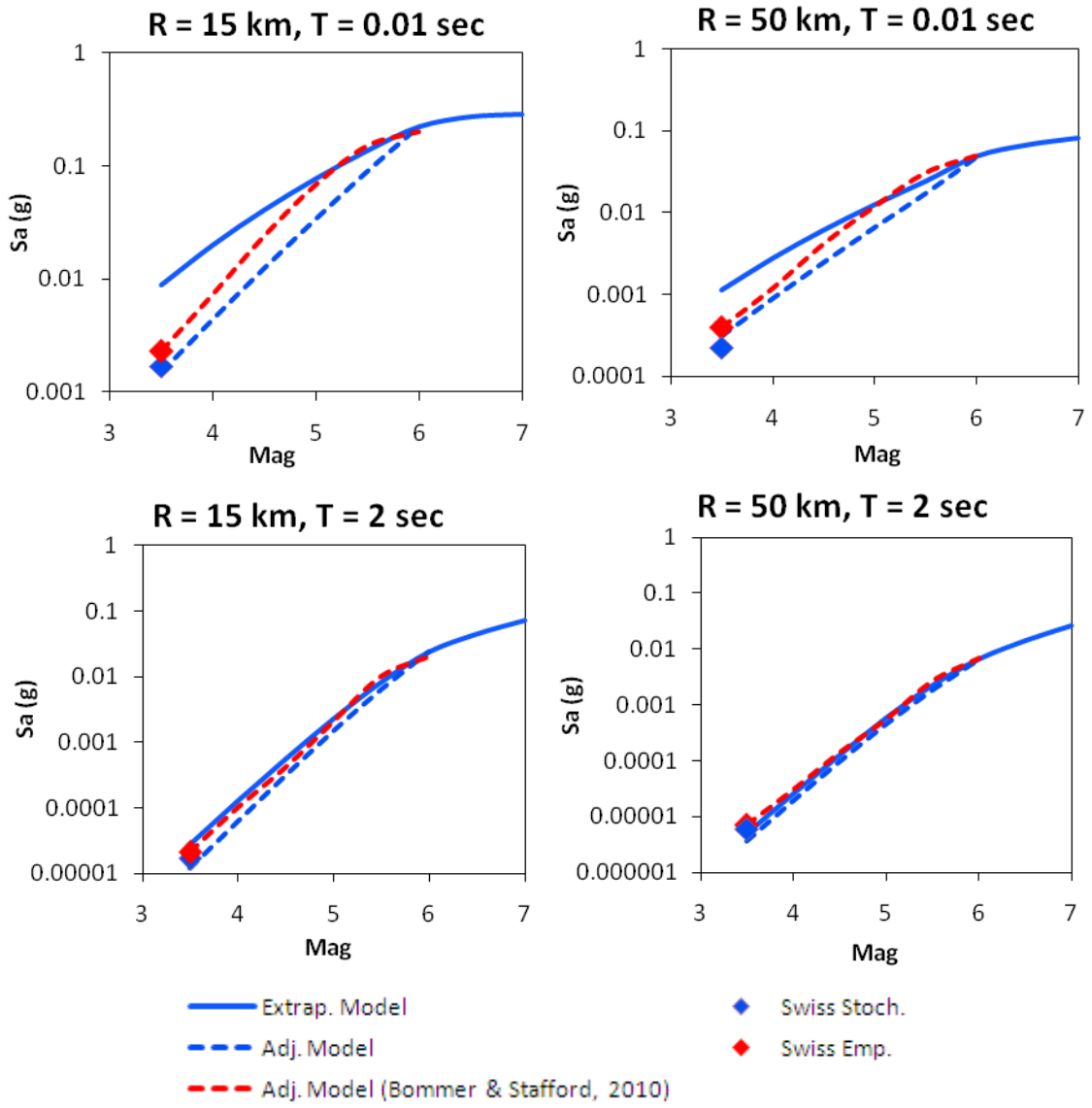

Figure I-4.4: Example comparison of small magnitude adjusted AS08 model based on the stress drop scaling approach with the adjusted AS08 model based on the [Bommer and Stafford 2010a] method. Top frames are for PGA and bottom frames are for T=2 sec [Al Atik and Abrahamson 2010a].

Chapter 5

Comparison of GMPE Median Predictions

5.1 Comparisons of Median Predictions: M4.5-M8.0

The median ground motions from the ten GMPEs and alternative versions of the Swiss stochastic models can be compared using the plotting tool developed by Renault and Kuhlmann [2012] (RDZ-ASW-1005). Example comparisons are shown in this section. The magnitude scaling at short distances is compared in Figures I-5.1, I-5.2, and I-5.3 , for 100 Hz, 5 Hz, and 1 Hz, respectively. The distance scaling for 5 Hz spectral acceleration is compared in Figure I-5.4 and I-5.5 for magnitudes M5 to M7.5. Note that the plots of the median GMPEs shown in this section are based on the original "as published" models and do not include the small PRP magnitude adjustments and $V_S - \kappa$ corrections, described in the previous two chapters.

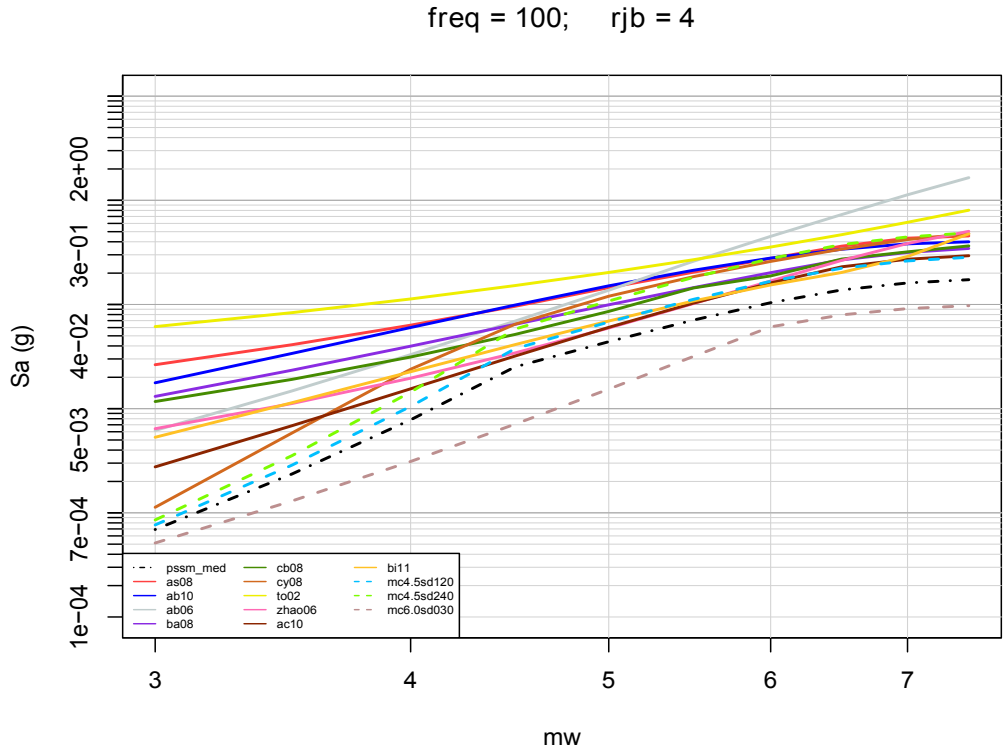

Figure I-5.1: Comparison of the magnitude scaling of the ten empirical GMPEs and the best estimate Swiss stochastic model (pssm_med) and three other alternative Swiss stochastic models (dashed lines) for 100 Hz at short distances (R_{JB}=4km).

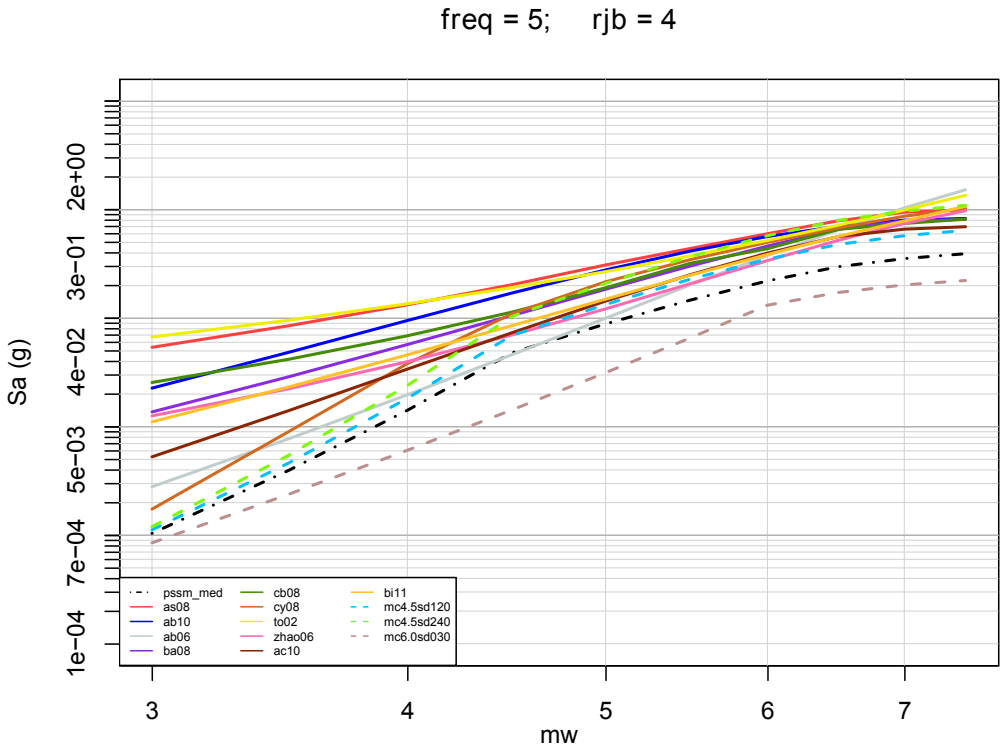

Figure I-5.2: Comparison of the magnitude scaling of the ten empirical GMPEs and the best estimate Swiss stochastic model (pssm_med) and three other alternative Swiss stochastic models (dashed lines) for 5 Hz at short distances (R_{JB}=4km).

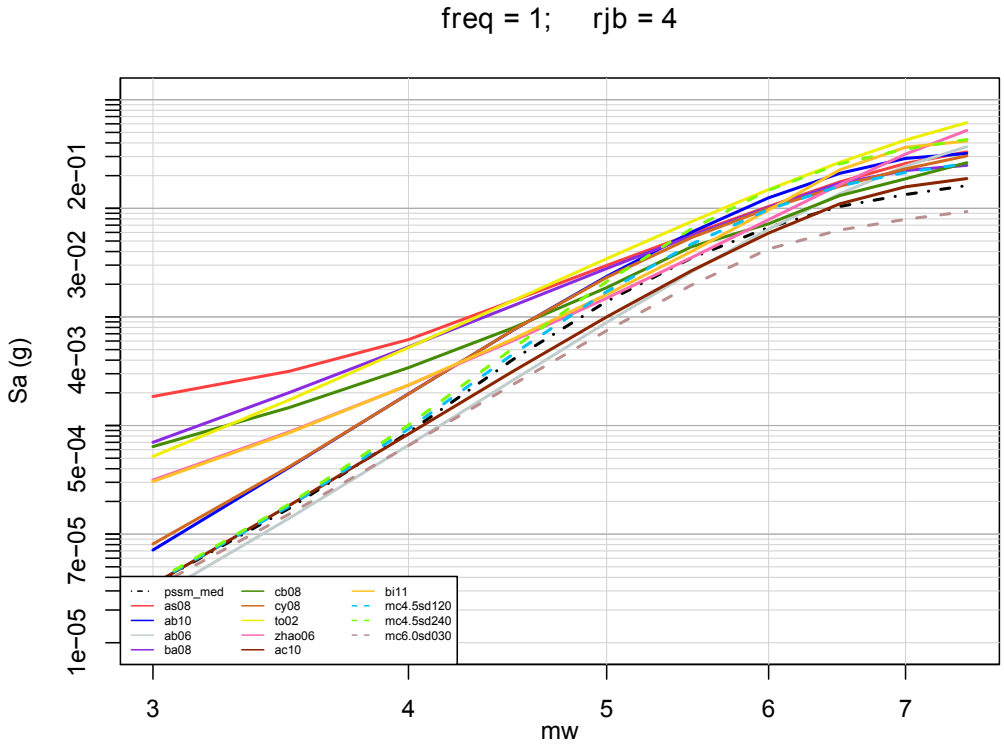

Figure I-5.3: Comparison of the magnitude scaling of the ten empirical GMPEs and the best estimate Swiss stochastic model (pssm_med) and three other alternative Swiss stochastic models (dashed lines) for 1 Hz at short distances (R_{JB}=4km).

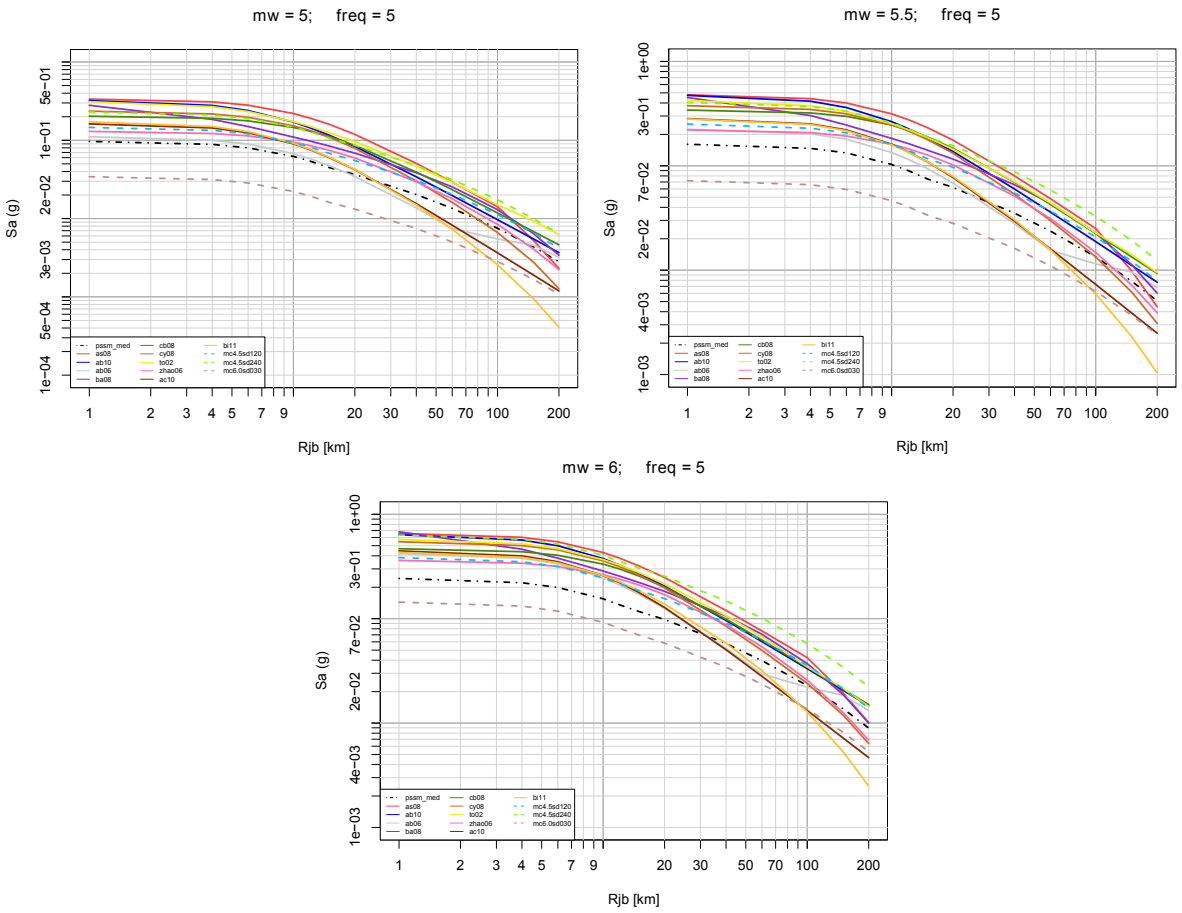

Figure I-5.4: Comparison of the distance scaling of the ten empirical GMPEs and the best estimate Swiss stochastic model (pssm_med) and three other alternative Swiss stochastic models (dashed lines) for 5 Hz spectral acceleration for M5-M6.

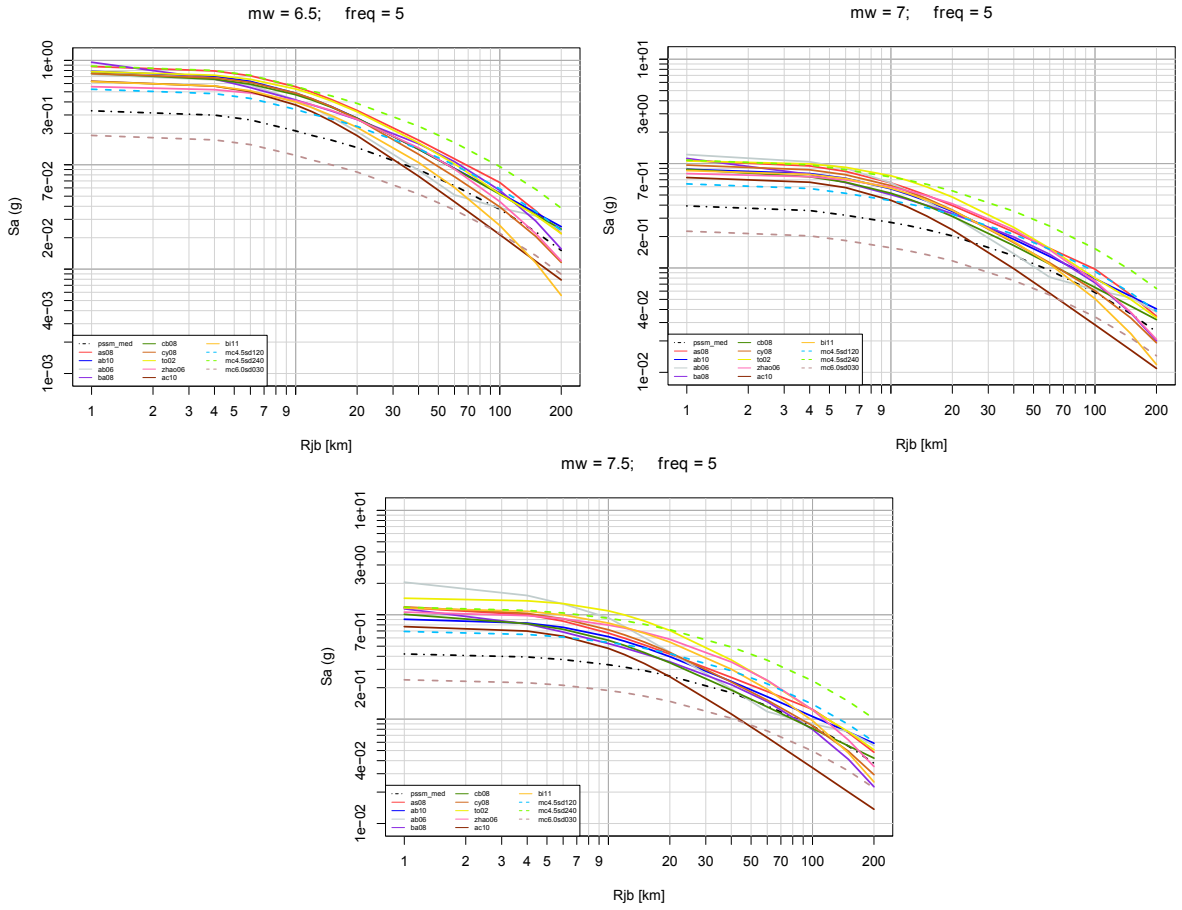

Figure I-5.5: Comparison of the distance scaling of the ten empirical GMPEs and the best estimate Swiss stochastic model (pssm_med) and three other alternative Swiss stochastic models (dashed lines) for 5 Hz spectral acceleration for M6.5-M7.5.

5.2 Comparisons with Swiss Stochastic Models

The parameterized Swiss stochastic model allows the two parameters Mc and stress drop SD to be used to scale the best-estimate model; both are free variables which can accommodate any number. With the suite of alternative models for the magnitude dependence of the stress drop, 20 forms (with Mc= 4.5, 5.0, 5.5, 6.0 and SD= 30, 60, 120, 240, 480 bar) of the Swiss stochastic model for each of the two R_{eff} models were evaluated for illustration. Here, only three of the models are shown for each R_{eff} model: (1) M6.0 cutoff with 30 bars (lowest model), (2) M4.5 cutoff with 240 bars (highest model; the 480 bar model was not considered by the experts), and (3) the best estimate model with M4.5 and 60 bars (which corresponds to "pssm_med").

Figure I-5.6 compares the distance attenuation for M4.5 at 5 Hz for the two R_{eff} models. Figure I-5.7 shows the same comparisons for M7 at 5 Hz. The effects of the differences in the R_{eff} are greatest at the larger magnitudes. Comparing the stochastic models in Figure I-5.7, the 240 bar model differs by about a factor of 2 for the two R_{eff} models at distances of 0 to 20 km.

The spectra for the alternative models for M4 at a distance of R_{JB}= 40 km are compared in Figure I-5.8. The spectra for M5, M6, and M7 are compared in Figures I-5.9, I-5.10, and I-5.11, respectively.

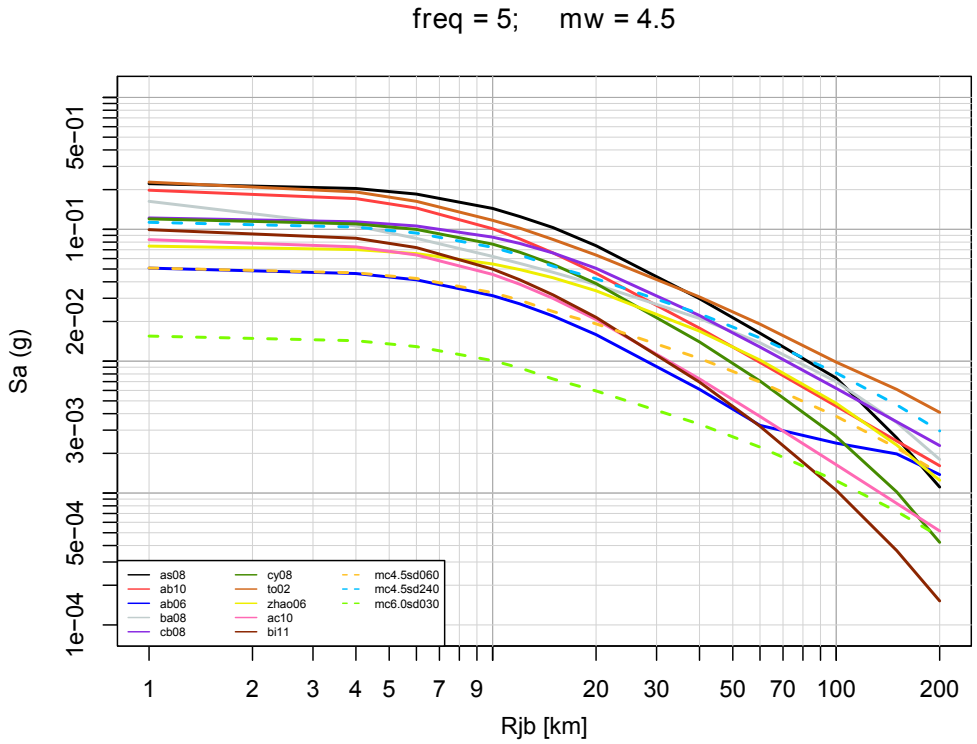

Figure I-5.6: Comparison of the distance scaling for M4.5 earthquakes for the ten empirical GMPEs and low (Mc6.0SD30), high (Mc4.5SD240) and best estimate (Mc4.5SD60) cases from the Swiss stochastic model.

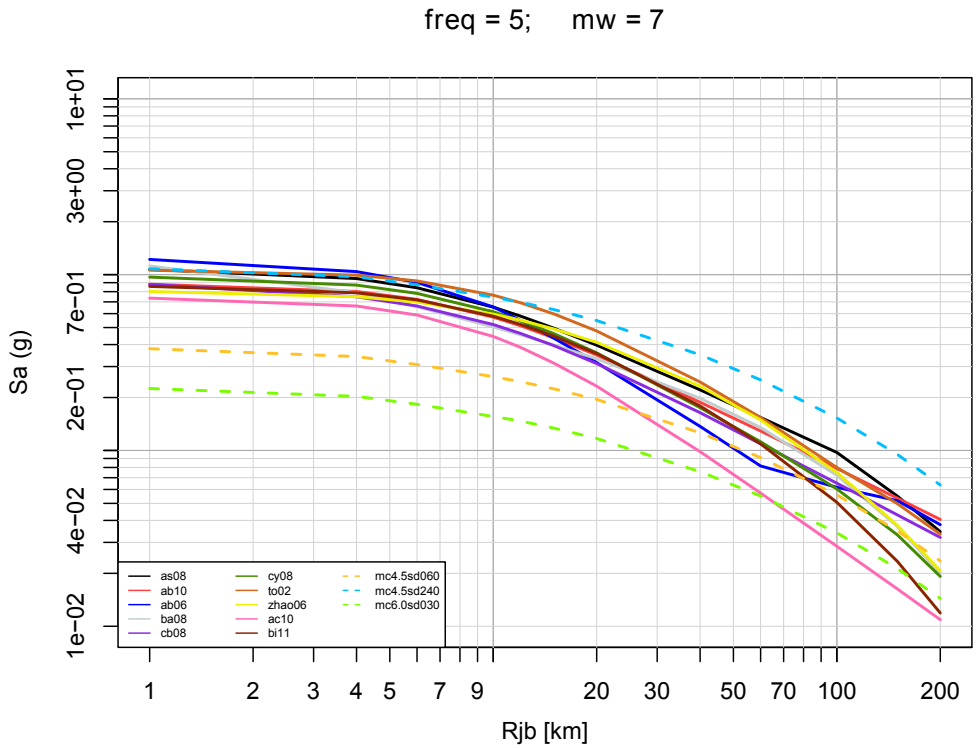

Figure I-5.7: Comparison of the distance scaling for M7 earthquakes for the ten empirical GMPEs and low (Mc6.0SD30), high (Mc4.5SD240) and best estimate (Mc4.5SD60) cases from the Swiss stochastic model.

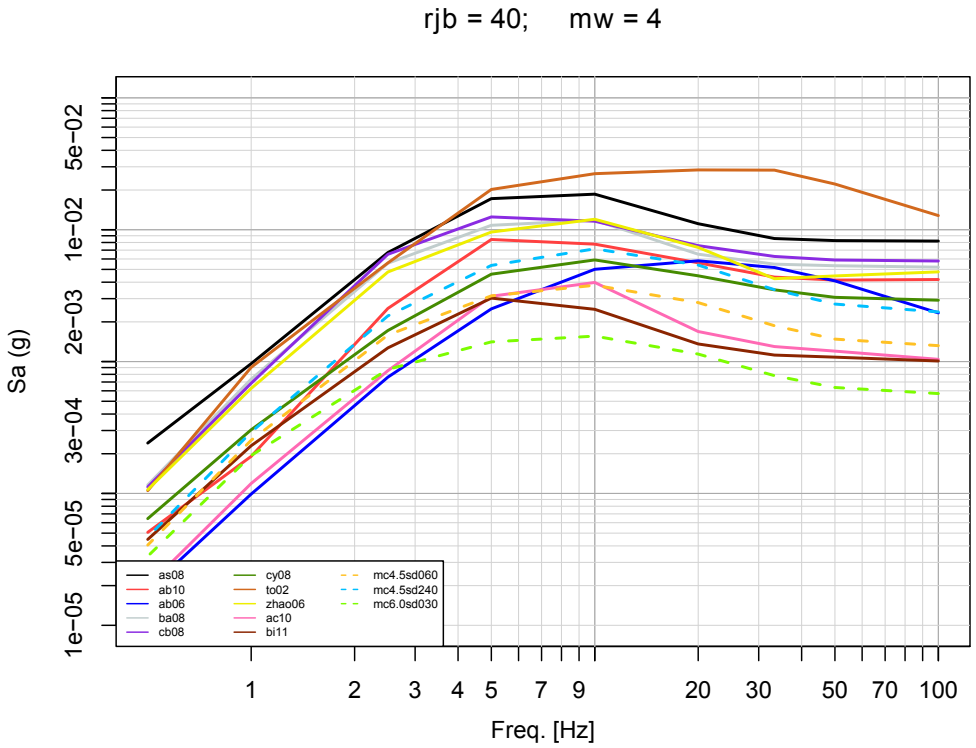

Figure I-5.8: Comparison of the spectra for M4 earthquakes at a distance of 40 km for the ten empirical GMPEs and low (Mc6.0SD30), high (Mc4.5SD240) and best estimate (Mc4.5SD60) cases from the Swiss stochastic model.

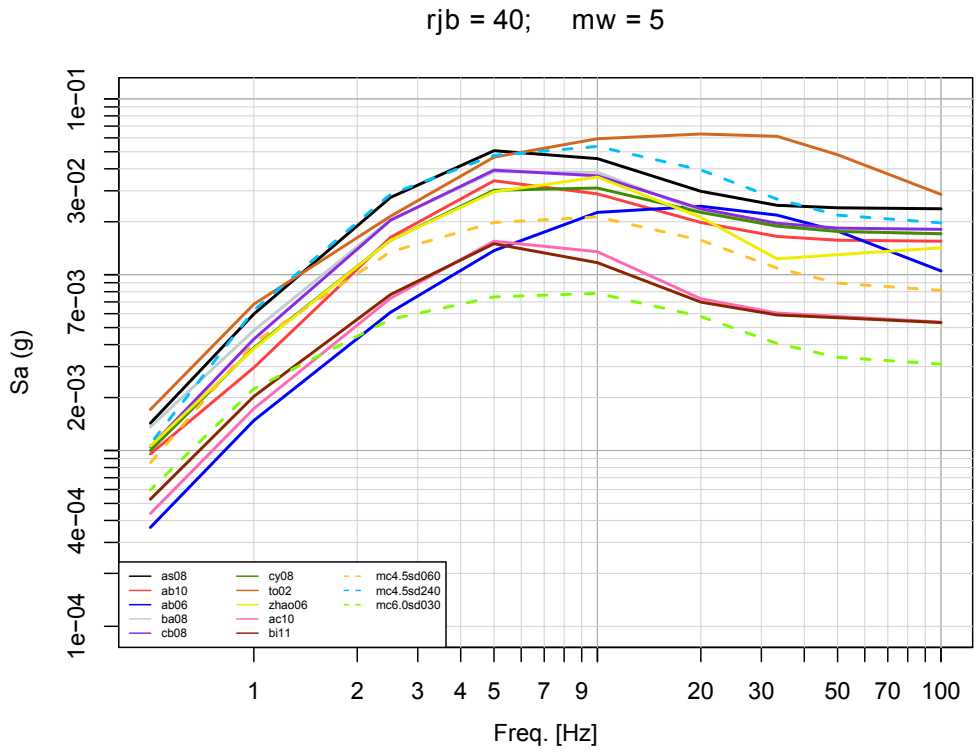

Figure I-5.9: Comparison of the spectra for M5 earthquakes at a distance of 40 km for the ten empirical GMPEs and low (Mc6.0SD30), high (Mc4.5SD240) and best estimate (Mc4.5SD60) cases from the Swiss stochastic model.

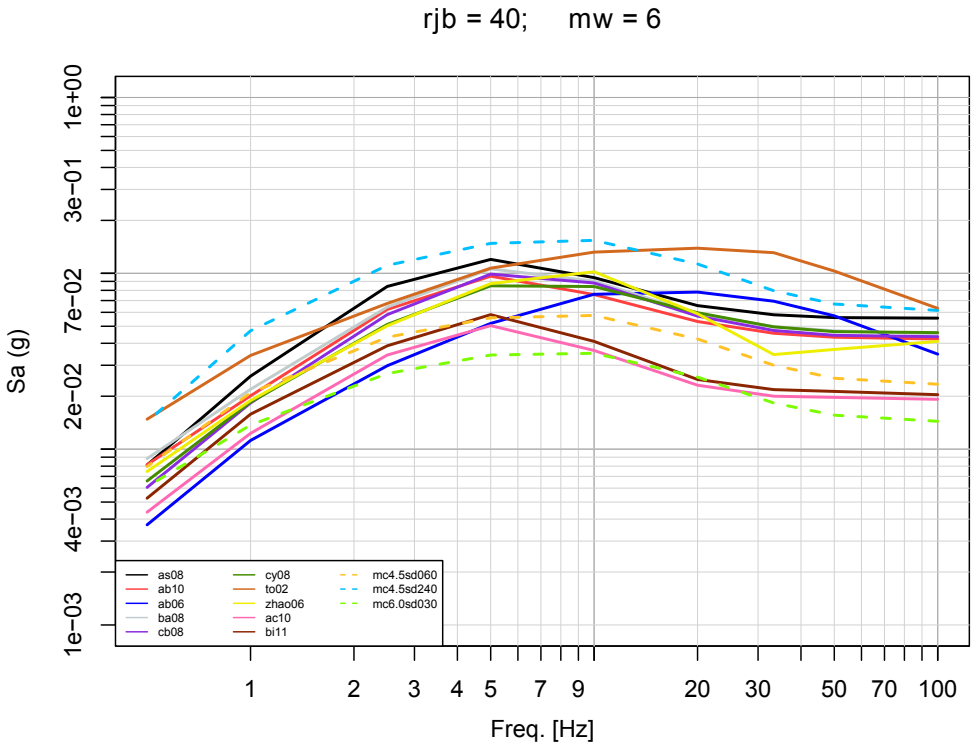

Figure I-5.10: Comparison of the spectra for M6 earthquakes at a distance of 40 km for the ten empirical GMPEs and low (Mc6.0SD30), high (Mc4.5SD240) and best estimate (Mc4.5SD60) cases from the Swiss stochastic model.

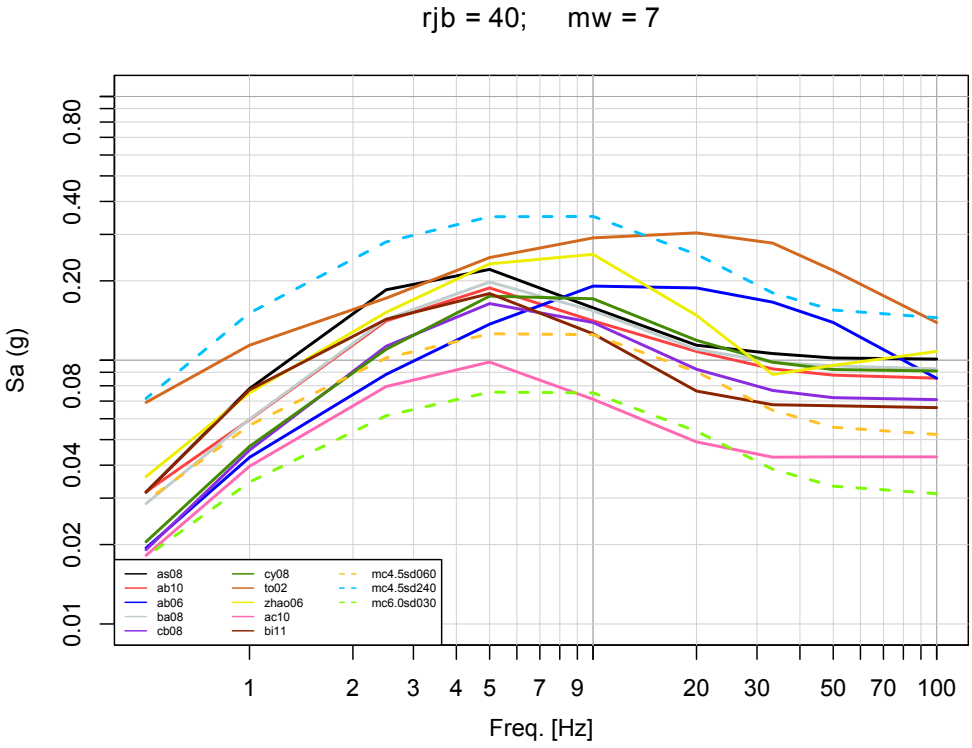

Figure I-5.11: Comparison of the spectra for M7 earthquakes at a distance of 40 km for the ten empirical GMPEs and low (Mc6.0SD30), high (Mc4.5SD240) and best estimate (Mc4.5SD60) cases from the Swiss stochastic model.

5.3 Comparisons of Uncorrected and Corrected Models

Figure I-5.12 compares the effect of the GMPE corrections introduced in the PRP for different magnitudes. The corrections include the small magnitude extrapolation (Section 4.3) and the $V_S - \kappa$ corrections (Section 3.4). The following cases are compared:

(a) No small magnitude adjustments (SMA) and no $V_S - \kappa$ corrections (base case),

(b) SMA and lower bound $V_S - \kappa$ corrections,

(c) SMA and median bound $V_S - \kappa$ corrections,

(d) SMA and upper bound $V_S - \kappa$ corrections.

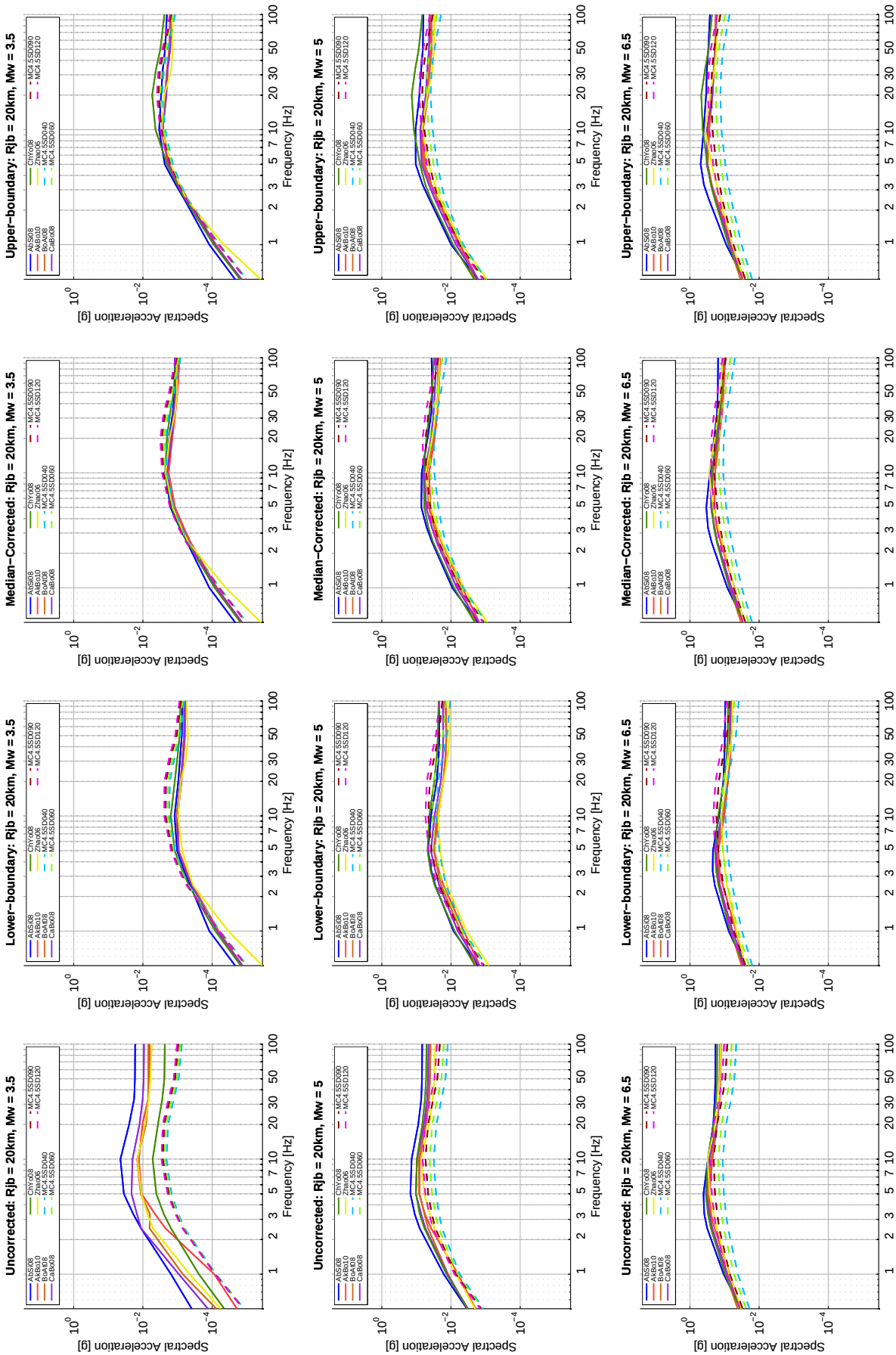

Figure I-5.12: Comparison of response spectra at Beznau for three magnitudes (M3.5, 5 and 6.5) at a distance of 20 km for the GMPEs selected by the expert D. Fäh with, from left to right: a) no small magnitude adjustments (SMA), no $V_S - \kappa$ corrections, b) SMA and lower bound $V_S - \kappa$ corrections, c) SMA and median bound $V_S - \kappa$ corrections, d) SMA and upper bound $V_S - \kappa$ corrections. The three $V_S - \kappa$ correction cases are taken from the 5-point representation of the $V_S - \kappa$ distribution and showing the first, third and fifth correction branch.

Chapter 6

Aleatory Variability for Horizontal Motion

6.1 Components of Ground Motion Variability

Following the notation of Al Atik et al. [2010], the ground motion model can be written as

$$\ln(Sa_{es}) = \hat{S}a(M_e, R_{es}, F_e, V_{S30s}) + \delta B_e + \delta W_{es} \tag{I-6.1}$$

where δB_e is the between-event residual for earthquake e and δW_{es} is the within-event residual for site s and earthquake e. The within-event residual can be separated into a site term, $\delta S2S_s$, and a within-site residual, δWS_{es}:

$$\ln(Sa_{es}) = \hat{S}a(M_e, R_{es}, F_e, V_{S30s}) + \delta B_e + \delta S2S_s + \delta WS_{es} \tag{I-6.2}$$

The site term, $\delta S2S_s$, is the mean difference between the site amplification for a site and the mean site amplification for a site with a given V_{S30}.

Let τ be the standard deviation of the δB_e, ϕ_{S2S} be the standard deviation of $\delta S2S_s$, and ϕ_{SS} be the standard deviation of δWS_{es}. The traditional standard deviation used in ground motion models is given by

$$\sigma = \sqrt{\tau^2 + \phi_{S2S}^2 + \phi_{SS}^2} \tag{I-6.3}$$

The term ϕ_{S2S} is the variability of the systematic differences between the site amplifications for different sites. The single-station σ value is the standard deviation of the ground motion at a single site, after the systematic differences in the site amplification have been removed. Thus, the single-station σ is given by

$$\sigma_{SS} = \sqrt{\tau^2 + \phi_{SS}^2}. \tag{I-6.4}$$

6.2 Ground Motion Variability and the SP2-SP3 Interface

The approach used in the PRP is to develop a model for the input rock motion (SP2) and then combine this input rock motion with the amplification factors (SP3) for the site.

The first issue for the SP2-SP3 interface is the $\delta S2S_s$ term. Each site will have a unique $\delta S2S_s$ term, but there is epistemic uncertainty in the estimation of $\delta S2S_s$. If SP2 uses a single-station σ approach, then the $\delta S2S_s$ values are assumed to be known for each site within the SP2 model. The SP3 models include epistemic uncertainty in the velocity profile and material properties, leading to epistemic uncertainty in the median site amplification. This epistemic uncertainty captures the uncertainty in the $\delta S2S_s$ term for each site. Therefore, using the single-station σ for SP2, which removes the site-to-site variability of $\delta S2S_s$ from the aleatory variability of the rock motion, is consistent with modeling the epistemic uncertainty in the site amplification in SP3.

The second issue is the aleatory variability of the site amplification due to different input rock ground motions (time history and incidence angle). Incorporating the SP2 and SP3 approach into the components of variability, the ground motion model on soil can be written as

$$\ln(SaSoil_{es}) = \hat{S}aRock_{es} + \delta B_e + \hat{S}iteAmp_s + \delta WSRock_{es} + \delta Amp_{es} \qquad \text{(I-6.5)}$$

where the within-event within-site aleatory variability term, δWS, is separated into the within-event variability of the input rock motion at the site (path effects), $\delta WSRock_{es}$, and the within-site variability of site amplification, δAmp_{es}. In this notation, the $\delta S2S_s$ is replaced by the median site amplification from SP3.

The issue for the SP2-SP3 interface is the δAmp_{es} term. Is it part of SP2 or SP3? Because the standard deviations of the GMPEs used for the rock ground motions are based on a combination of soil and rock data, the effects of the aleatory variability of the amplification are part of the single-station σ. It is difficult for SP2 to separate the δWS terms into $\delta WSRock_{es} + \delta Amp_{es}$. For SP3, the site response calculations produce both estimates of the median amplification and the aleatory variability of the amplification. It is much easier for SP3 to isolate the δAmp_{es} term. Therefore, SP2 and SP3 experts agreed to leave the δAmp_{es} term in the SP2 rock model and to remove it from the SP3 site amplification model with the limitation noted below.

The datasets used to derive the GMPEs used by SP2 are dominated by weaker ground motions that are in the linear site response range. Therefore, by including the δAmp term as part of the SP2 model, the aleatory variability of the site response for input ground motions in the linear range are included, but this may not capture the full aleatory variability in the non-linear rage. Therefore, SP3 must consider what additional aleatory variability of the site amplification is needed for high levels of input rock motions.

6.3 Within-Event Single-Station ϕ Values from Global Datasets

The methodology for computing the single-station within-event residuals and standard deviations follows the guidelines outlined in report by Cotton and Abrahamson [2010] (TP2-TN-1080). Single-station σ values were calculated using ground motion data from 5 different tectonic regions: California, Switzerland, Taiwan, Japan, and Turkey. The between-event

residuals and single-station within-event residuals for the different regions were calculated by different developers using only events and stations with a minimum of 5 recordings and following the guidelines outlined in Renault [2010] (TP2-TN-1106).

The data contribution from the different regions is not even. Turkey and Switzerland have the smallest number of recordings and therefore contribute little to the single-station σ models. On the other hand, Taiwan has the largest number of records in the selected magnitude and distance range and therefore, has the largest contribution to the single-station σ models. Because the largest magnitude in the Taiwanese dataset is 6.3, this dataset does not contribute to constraining the magnitude-dependent single-station σ models at large magnitude [Rodriguez-Marek and Cotton 2011].

In their reports Rodriguez-Marek and Cotton [2011] (EXT-TB-1058) and Rodriguez-Marek [2012] (EXT-TN-1225), the authors, proposed nine alternative single-station within-event standard deviations: three alternative forms of the ϕ_{SS} models (constant, distance dependent, and magnitude and distance dependent) with three alternative estimates of the parameters for each model capture epistemic uncertainty.

Three models are proposed for the single-station within-event standard deviation: constant (model 1), distance-dependent (model 2) and magnitude- and distance-dependent (model 3). These models were developed using the data from the different regions together since no significant regional variation in ϕ_{ss} was observed [Rodriguez-Marek and Cotton 2011]. No clear pattern of ϕ_{ss} with respect to V_{S30} was observed. Therefore, the proposed single-station within-event standard deviations are independent of site conditions. The final proposed ϕ values of the models can be found in table 4.2 and 4.3 of Rodriguez-Marek and Cotton [2011], table 4.9 respectively.

Figures I-6.1, I-6.2, and I-6.3 present a comparison of the three proponent ϕ_{ss} models with the single-station within-event standard deviations calculated using the same dataset for selected magnitude and distance bins for periods of 0.01, 0.2 and 1.0 sec.

Figures I-6.4, I-6.5, and I-6.6 present examples of comparisons of the proposed ϕ_{ss} models with the ergodic within-event standard deviations using the Abrahamson and Silva [2008] residuals. These plots show that ϕ_{ss} at short distance for model 2 (distance-dependent model) exceeds ergodic ϕ calculated using the Abrahamson and Silva [2008] residuals. This is likely due to the different magnitude sampling of the two datasets with the NGA dataset having mainly large magnitude events [Rodriguez-Marek and Cotton 2011]. Similarly, ϕ_{ss} for model 3 exceeds ergodic ϕ calculated using the Abrahamson and Silva [2008] residuals in the small magnitude and short distance bin.

6.4 Between-Event Values (τ)

Only events and stations with a minimum of 5 recordings were used in the analysis. The between-event and within-event standard deviations versus period for the ten selected PRP GMPEs (not adjusted for Swiss conditions or small magnitude extension) and for the Swiss stochastic model are shown in Figures I-6.7 and I-6.8, respectively. The initial τ values for the Swiss data were calculated as part of the single-station σ ("SigmaSS") computations that were done for the different regions and following the guidelines for σ_{SS} calculations in terms of number of recordings per station and per event and methodology used. The computation

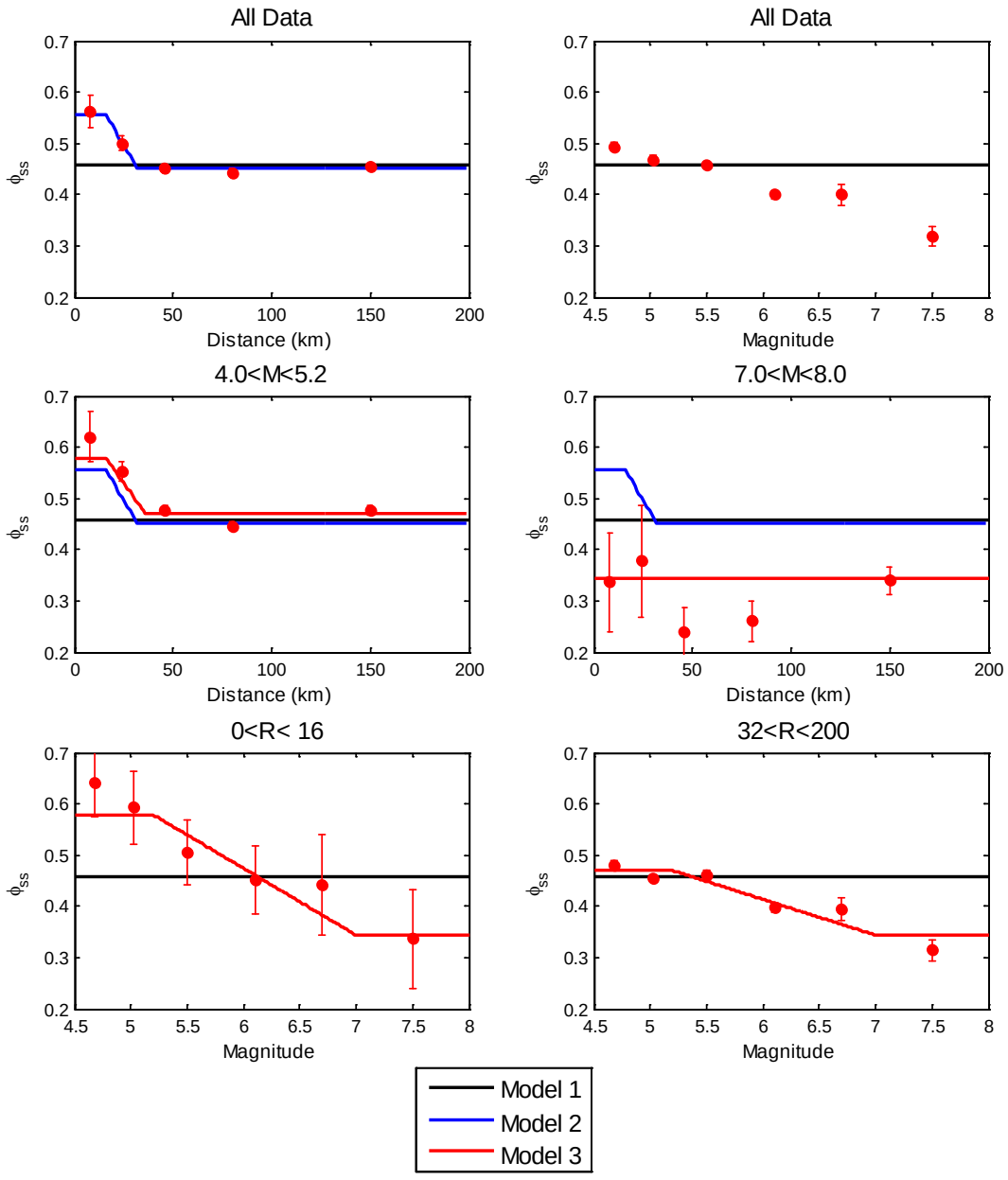

Figure I-6.1: Standard deviations for selected magnitude and distance bins compared with the proposed ϕ_{SS} models at PGA [Rodriguez-Marek and Cotton 2011].

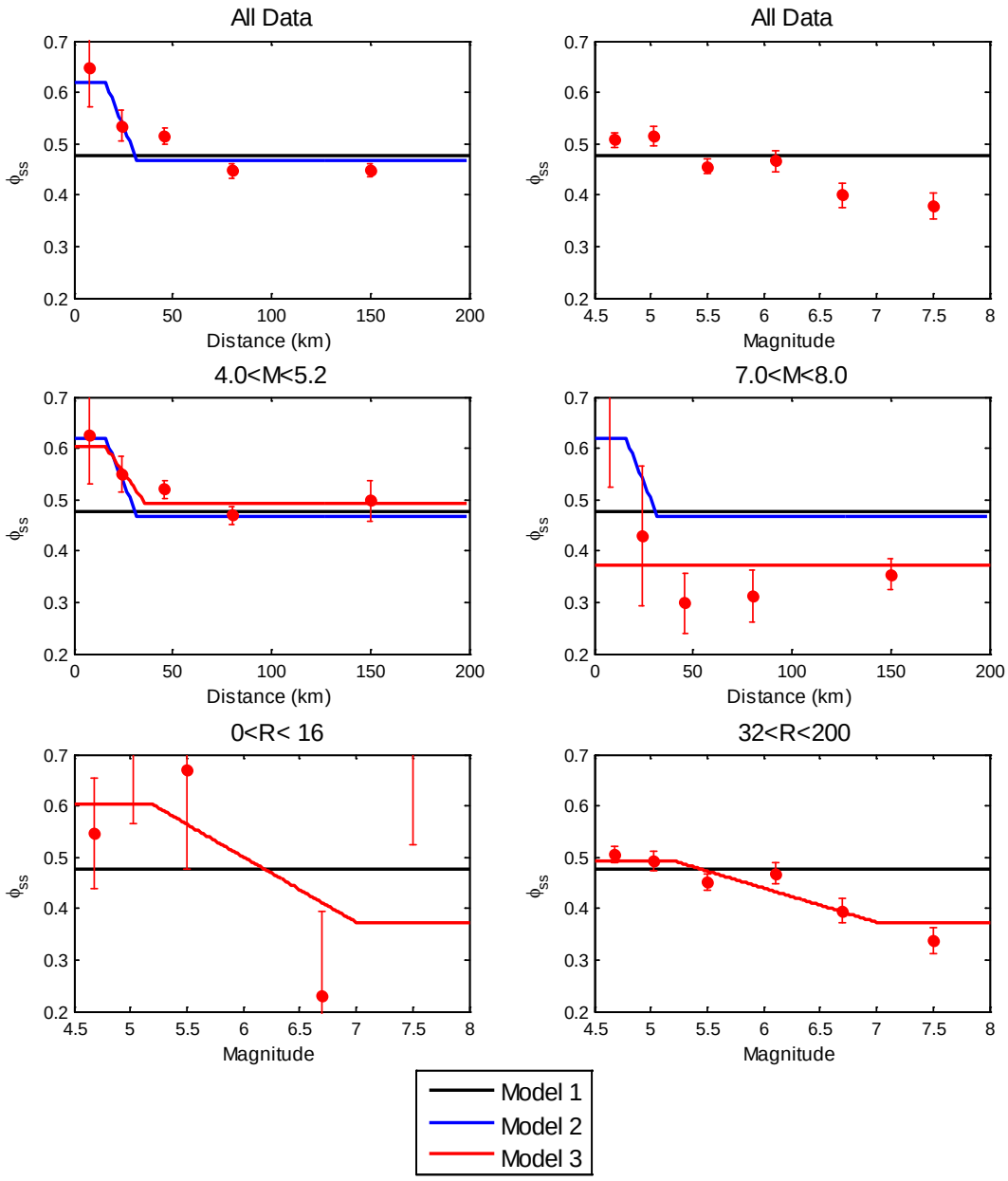

Figure I-6.2: Standard deviations for selected magnitude and distance bins compared with the proposed ϕ_{SS} models at period of 0.2 sec [Rodriguez-Marek and Cotton 2011].

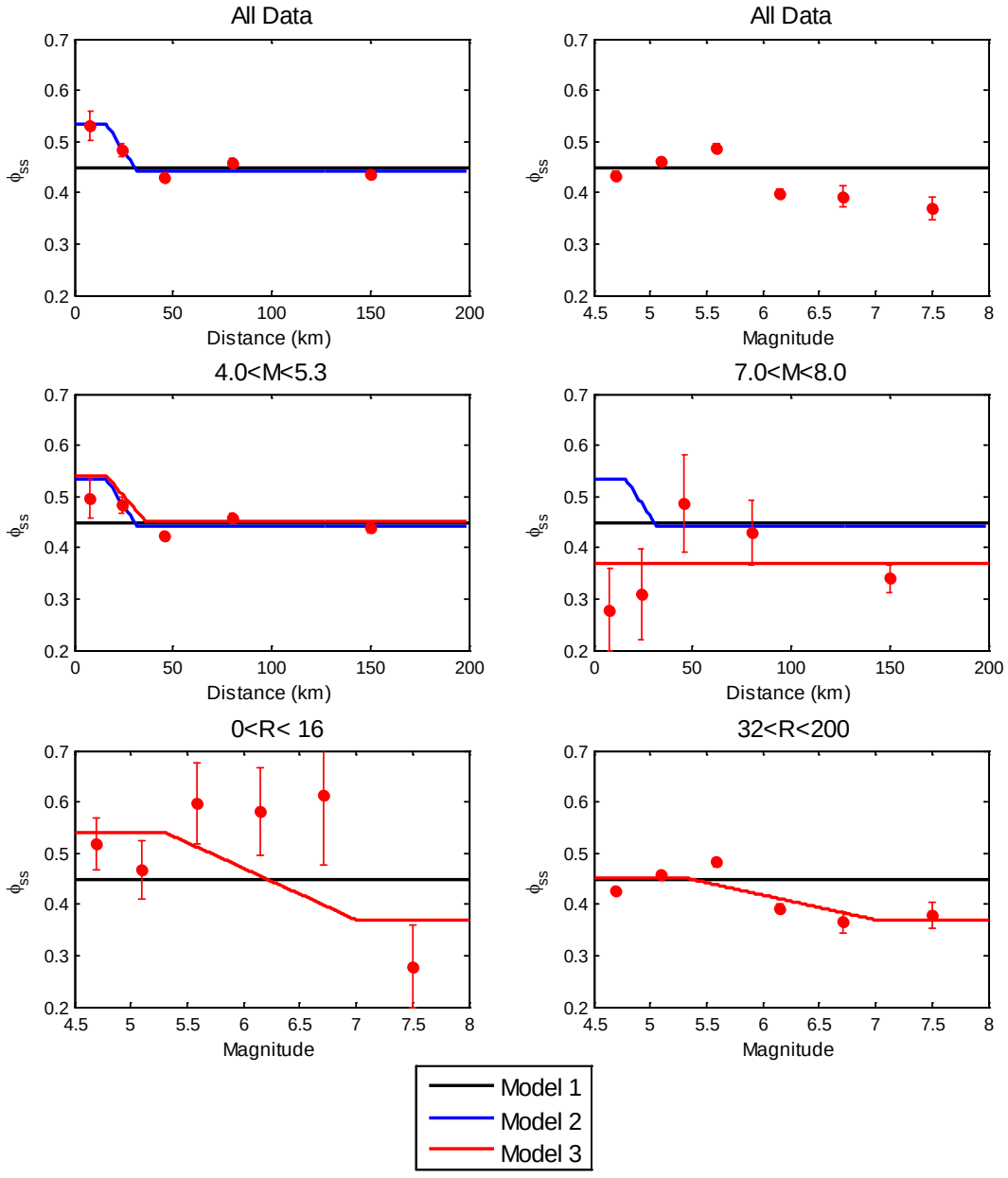

Figure I-6.3: Standard deviations for selected magnitude and distance bins compared with the proposed ϕ_{SS} models at period of 1 sec [Rodriguez-Marek and Cotton 2011].

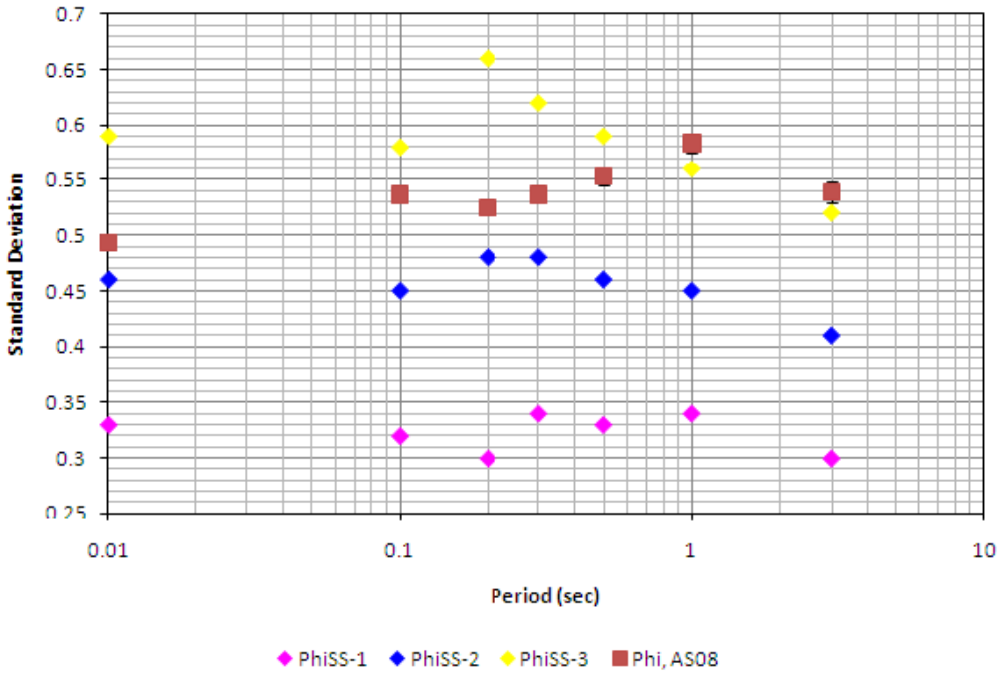

Figure I-6.4: Comparison of ϕ_{SS} model 1 (constant ϕ_{SS}) versus period to ergodic ϕ evaluated using the Abrahamson and Silva [2008] residuals [Al Atik 2011a].

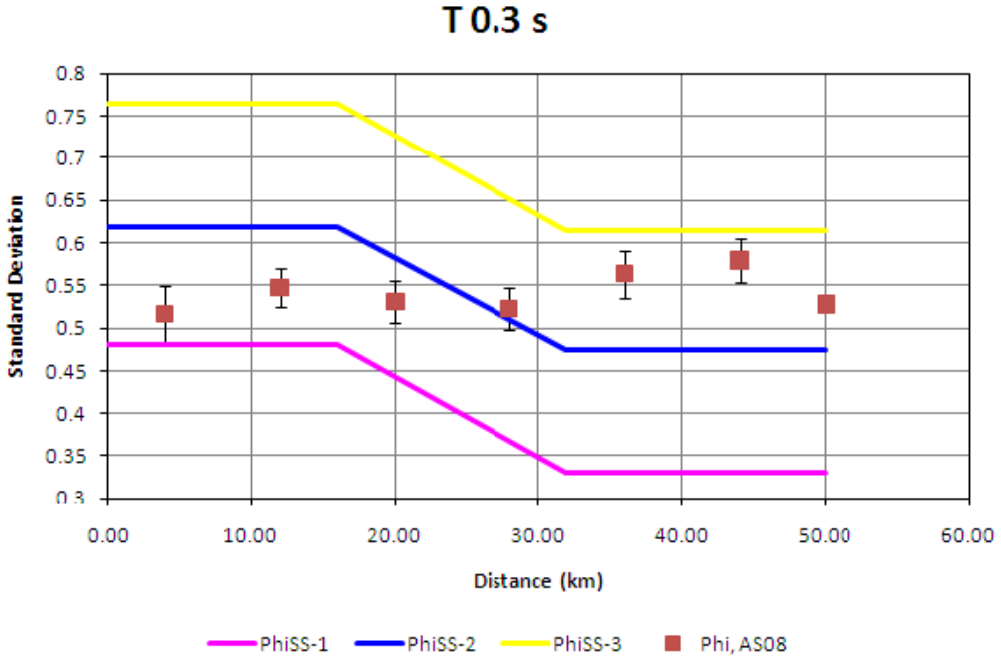

Figure I-6.5: Comparison of ϕ_{SS} model 2 (distance-dependent) versus period with ergodic ϕ evaluated using the Abrahamson and Silva [2008] residuals at a period of 0.3 sec [Al Atik 2011a].

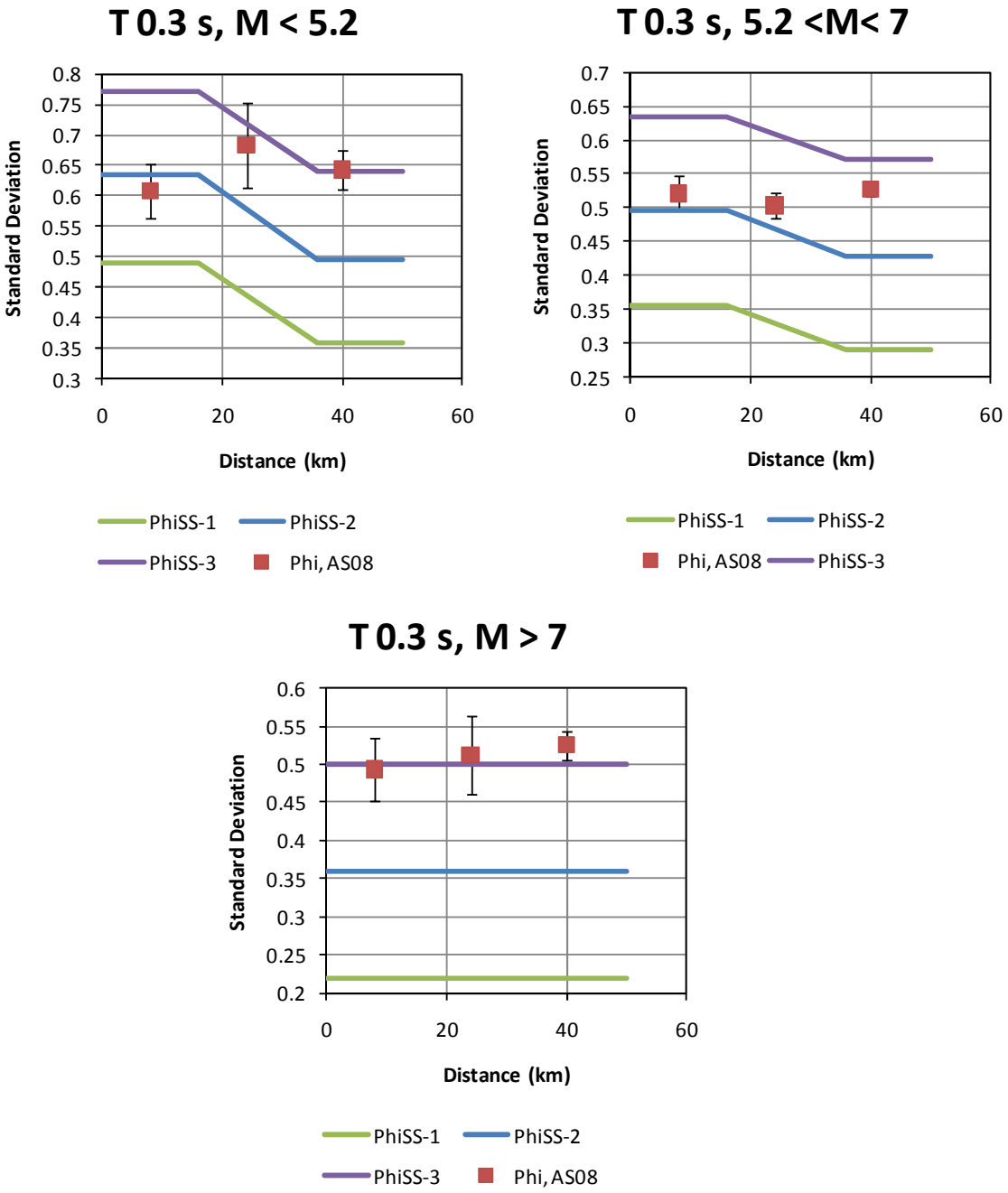

Figure I-6.6: Comparison of ϕ_{SS} model 3 (magnitude- and distance-dependent) versus period with ergodic ϕ evaluated using the Abrahamson and Silva [2008] residuals at a period of 0.3 sec [Al Atik 2011a].

of the within-event and between-event residuals was done using the Swiss dataset that B. Edwards used for developing the Swiss stochastic model and then fitting an empirical ground motion model to the data (basic empirical model based on the form used by J. Douglas [Al Atik 2010d]). The τ values for the Swiss stochastic model by L. Al Atik (April 2011) are based on the total residuals of the Swiss data with respect to the Swiss stochastic model (residuals provided by B. Edwards) and computation of the within-event and between-event residuals using a random effects algorithm. The difference between the two sets of values in Rodriguez-Marek and Cotton [2011] is due to the different models (Swiss stochastic model versus empirical Swiss model) and also the use of different criteria for the number of recordings per event and per station. For the sake of consistency with the implemented Swiss model, the τ values for the Swiss stochastic model based on Edwards et al. [2010], table 16 were used for the GMPE branch of the τ model. The authors of Rodriguez-Marek and Cotton [2011] decided not to update the period dependent τ model (model 1) based on the new Swiss stochastic model, as this would have artificially increased the weight of the Swiss data if introduced as an additional dataset. A compilation of all the τ values for all models is reproduced in Table I-6.1 (originally based on Al Atik [2010c] (TP2-TN-1122)).

Standard deviations for Abrahamson and Silva [2008] and Campbell and Bozorgnia [2008] were calculated for linear site conditions in Figures I-6.7 and I-6.8. Standard deviations for the Swiss stochastic model were evaluated using a random effects algorithm. Between-event and within-event standard deviations for GMPEs based on stochastic models [Toro 2002; Atkinson 2006] were not reported.

Table I-6.1: Overview of τ values for GMPE dependent model for τ. Extended table based on table 5.4 of Rodriguez-Marek and Cotton [2011].

Freq. (Hz)	AbSi08 M5	AbSi08 M6	AbSi08 M7	AkBo10	BoAt08	CaBo08	ChYo08 M5	ChYo08 M6	ChYo08 M7	Toro02	Zhao06	Swiss10 Stoch.	AkC10	Bind11
100	0.42	0.36	0.3	0.229	0.262	0.219	0.344	0.304	0.264	0.46	0.398	0.380	0.5163	0.3546
50	0.42	0.36	0.3	0.244	0.262	0.219	0.347	0.307	0.267	0.463	0.418	0.415	0.5154	0.3546
33.33	0.462	0.384	0.305	0.252	0.274	0.235	0.36	0.32	0.28	0.463	0.429	0.435	0.5148	0.3546
25	0.492	0.401	0.309	0.258	0.281	0.248	0.372	0.332	0.292	0.463	0.438	0.405	0.5092	0.3546
20	0.515	0.414	0.312	0.263	0.286	0.258	0.385	0.345	0.305	0.463	0.444	0.419	0.5049	0.3528
10	0.55	0.436	0.321	0.269	0.318	0.286	0.384	0.349	0.315	0.461	0.49	0.417	0.5182	0.3546
5	0.52	0.425	0.329	0.249	0.288	0.249	0.36	0.334	0.308	0.457	0.423	0.372	0.5562	0.4812
2.5	0.449	0.394	0.338	0.254	0.267	0.217	0.335	0.317	0.298	0.446	0.39	0.344	0.5857	0.4835
1	0.35	0.35	0.35	0.341	0.302	0.255	0.358	0.35	0.342	0.393	0.41	0.355	0.6407	0.5112
0.5	0.35	0.35	0.35	0.382	0.389	0.296	0.402	0.402	0.402	0.291	0.414	0.353	0.6574	0.4858

Between-event standard deviations of the Toro [2002] model were back-calculated using the corresponding stochastic model and the aleatory variability of the *stressdrop* of the model.

A total of four between-event standard deviation models are proposed: two alternative τ models, with one of the models having three branches that capture epistemic uncertainty.

6.5 Epistemic Uncertainty for Within-Event Single-Station ϕ

Epistemic uncertainty in ϕ_{ss} was estimated using stations with a minimum of 20 recordings whereby the mean and the standard deviation of the ϕ_{ss} values at the different stations ($\phi_{ss,s}$) were calculated. The epistemic uncertainty in ϕ_{ss} was assumed to follow a normal distribution. The standard deviations of ϕ_{ss} calculated using this approach strictly apply to ϕ_{SS} model 1. Due to insufficient data in the distance and magnitude bins of ϕ_{SS} models 2 and 3, the

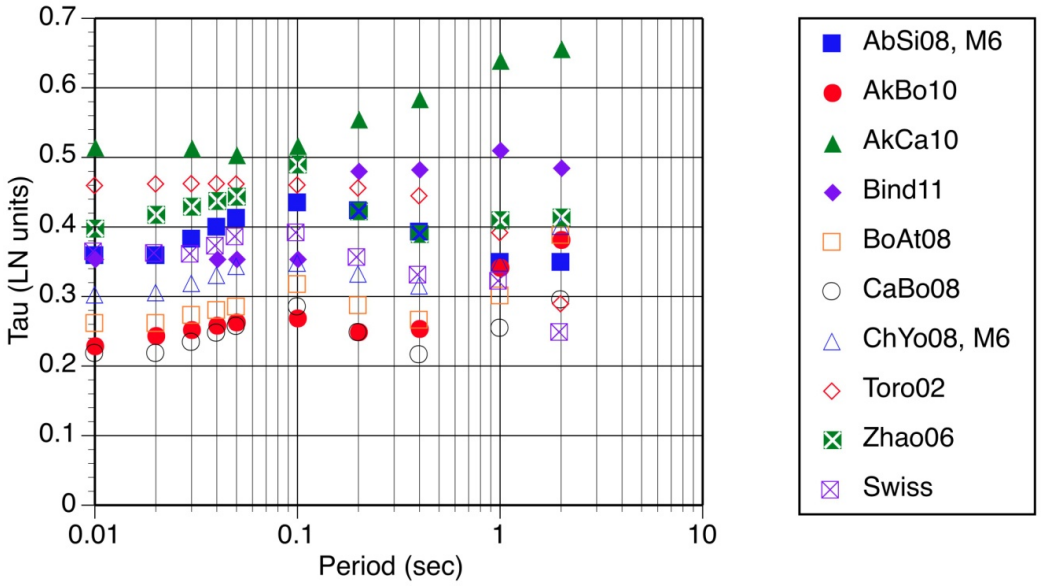

Figure I-6.7: Comparison of the between-event standard deviations of the PRP selected GMPEs and the Swiss stochastic model at different periods. τ values for AbSi08 and ChYo08 are calculated for a magnitude 6 earthquake (Update of figure 5.3 in Rodriguez-Marek and Cotton [2011]).

same standard deviation values of ϕ_{ss} were assumed to apply to all three ϕ_{SS} models. Three branches are proposed to model the epistemic uncertainty in ϕ_{ss} shown in Table I-6.2.

Table I-6.2: Alternative models for ϕ_{SS} [Rodriguez-Marek et al. 2011].

Level 3: ϕ Model	**Level 4: ϕ Model branches for epistemic uncertainty**
ϕ Model 1 (constant)	Mean – 1.6 standard deviation Mean Mean + 1.6 standard deviation
ϕ Model 2 (distance dependent)	Mean – 1.6 standard deviation Mean Mean + 1.6 standard deviation
ϕ Model 3 (distance- and magnitude dependent)	Mean – 1.6 standard deviation Mean Mean + 1.6 standard deviation

Rodriguez-Marek and Cotton [2011] compared the single-station within-event standard deviations of each of the different regions to the ones calculated using data from all regions together. These single-station within-event standard deviations were calculated using only small magnitude events (magnitude between 3 and 4.8). Figure I-6.8 shows the results of this comparison. Rodriguez-Marek and Cotton [2011] found that, with the exception of PGA, the ϕ_{ss} values from the individual regions agree well with the ones calculated using the Swiss dataset, which suggests that the derived ϕ_{ss} models are applicable to Switzerland [Rodriguez-Marek and Cotton 2011] (EXT-TB-1058). In the amendment to the single-station σ report of Rodriguez-Marek [2012] (EXT-TN-1225), some additional assessments are documented as

a response to the requests from workshop WS9. The evaluation of the standard deviation on the ϕ model is one of the items addressed to support the evaluation of the appropriate values to put in the logic tree.

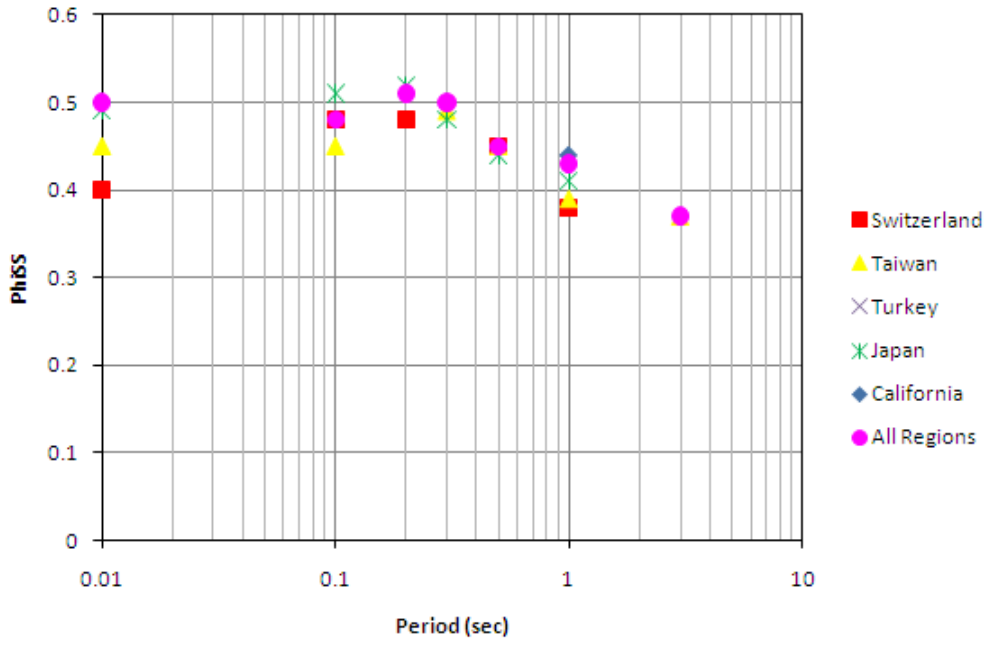

Figure I-6.8: Comparison of single-station within-event standard deviations calculated for different regions using only events with magnitude ranging from 3 to 4.8.

6.6 Between-Event Standard Deviation for τ Models

Two (period-dependent) τ models are proposed: (1) a global average τ model and (2) a GMPE specific τ model. The latter values are based on the original published τ values of the GMPEs selected for the PRP. The global average τ model was obtained by calculating the mean of the between-event variability of the ten GMPEs and the Swiss stochastic model. The values are reported in table 5.3 and figure 5.2 of Rodriguez-Marek and Cotton [2011] (EXT-TB-1058) and amended with standard deviation values by Rodriguez-Marek [2012] (EXT-TN-1225, see last page). Three branches are proposed to capture the epistemic uncertainty for τ model 1 (period-dependent τ model):

- Mean τ – 0.1
- Mean τ
- Mean τ + 0.1

The second τ model consists of the between-event standard deviations of the original GMPEs. The values are reported in Table I-6.1. Figure I-6.9 presents a comparison of τ model 1 with its three epistemic branches with τ values for the GMPEs as well as τ calculated for the different datasets available to the PRP. Rodriguez-Marek and Cotton [2011] noted that the between-event variability generally decreases as magnitude increases and that the variability is generally smaller for datasets with events from the same tectonic region.

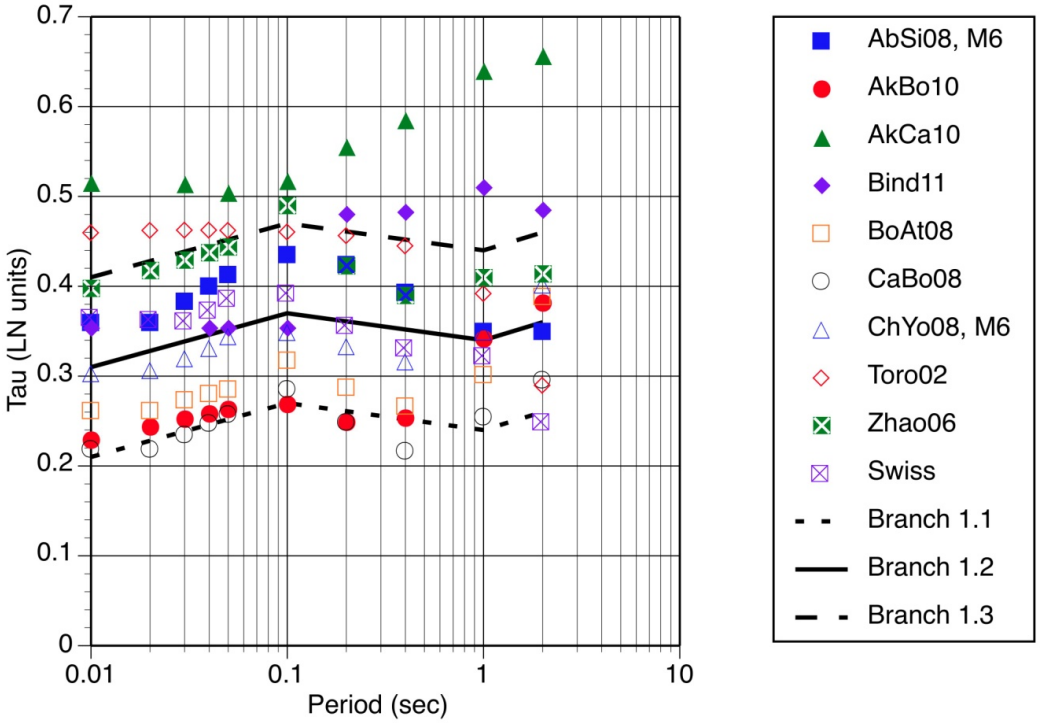

Figure I-6.9: Comparison of proposed τ model 1 to between-event standard deviations calculated for the different datasets. τ values for the GMPEs are also shown.

6.7 Smoothed Models for Missing Coefficients of τ and ϕ

Based on the feedback and review at the workshop WS10/SP2 (10. May 2012), the decision was made to use simplified smoothed models to interpolate for the missing coefficients at the given PRP frequencies for τ and ϕ (see TFI-RF-1440 and TFI-RF-1453). Figures I-6.10 to I-6.12 show the discussed and selected models on top of the data for the τ and ϕ_{ss} models, respectively. The Tables I-6.3 and I-6.4 list the derived smoothed model values.

Table I-6.3: Finally used smoothed τ model values (in natural logarithmic units). The other frequencies can be linearly interpolated.

Freq. [Hz]	τ-0.1	τ	τ+0.1
0.5	0.257	0.357	0.457
30	0.257	0.357	0.457
100	0.210	0.310	0.410

Table I-6.4: Finally used smoothed ϕ model values (in natural logarithmic units). The other frequencies can be linearly interpolated.

	Model 1	Model 3		
Freq. [Hz]	ϕ_{SS}	ϕ_{11}	ϕ_{21}	C_2
0.333	0.456	0.440	0.370	0.371
2	0.456	0.588	0.476	0.371
100	0.456	0.588	0.476	0.371

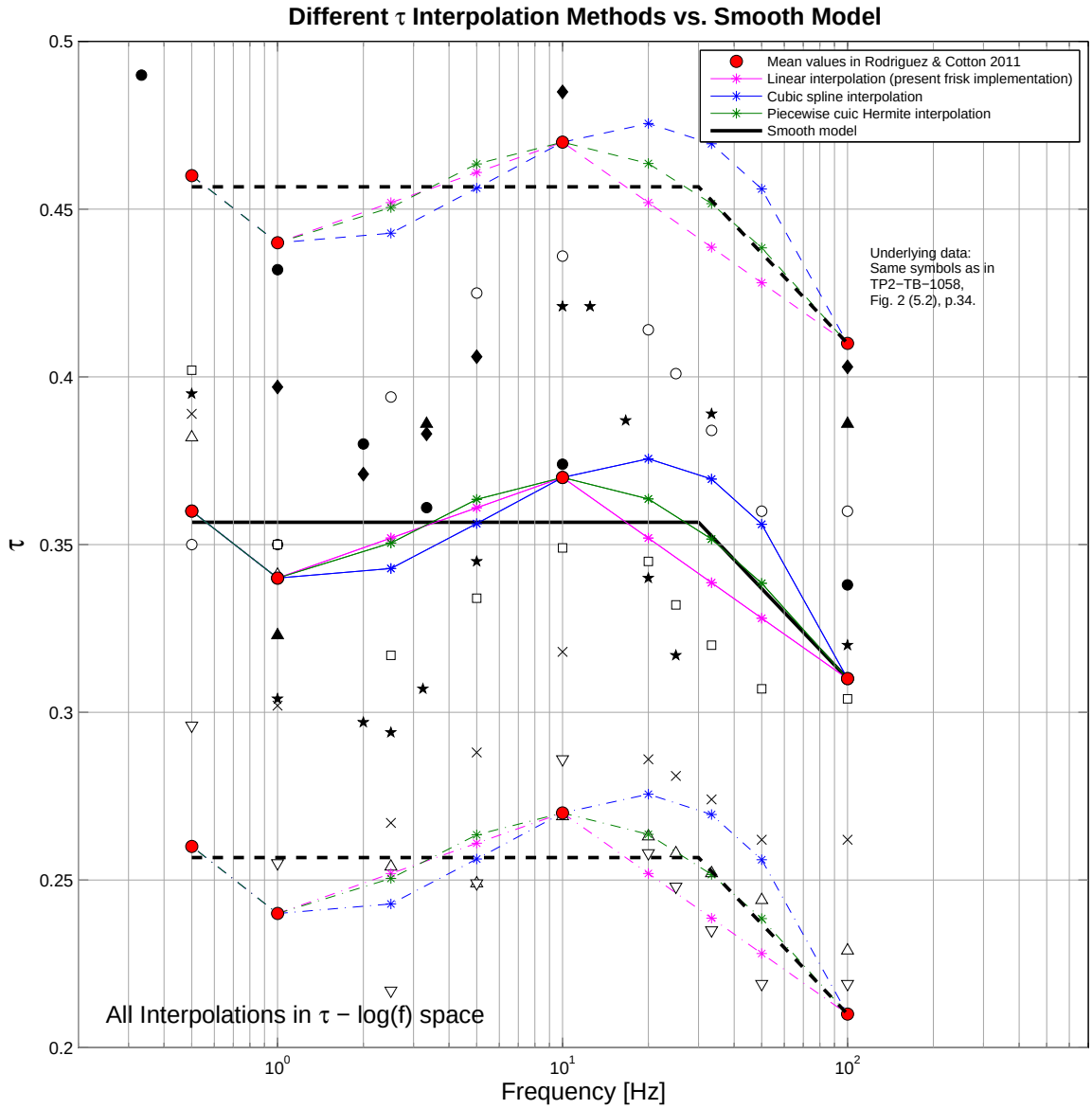

Figure I-6.10: Data points vs. different τ interpolation models and smoothed model.

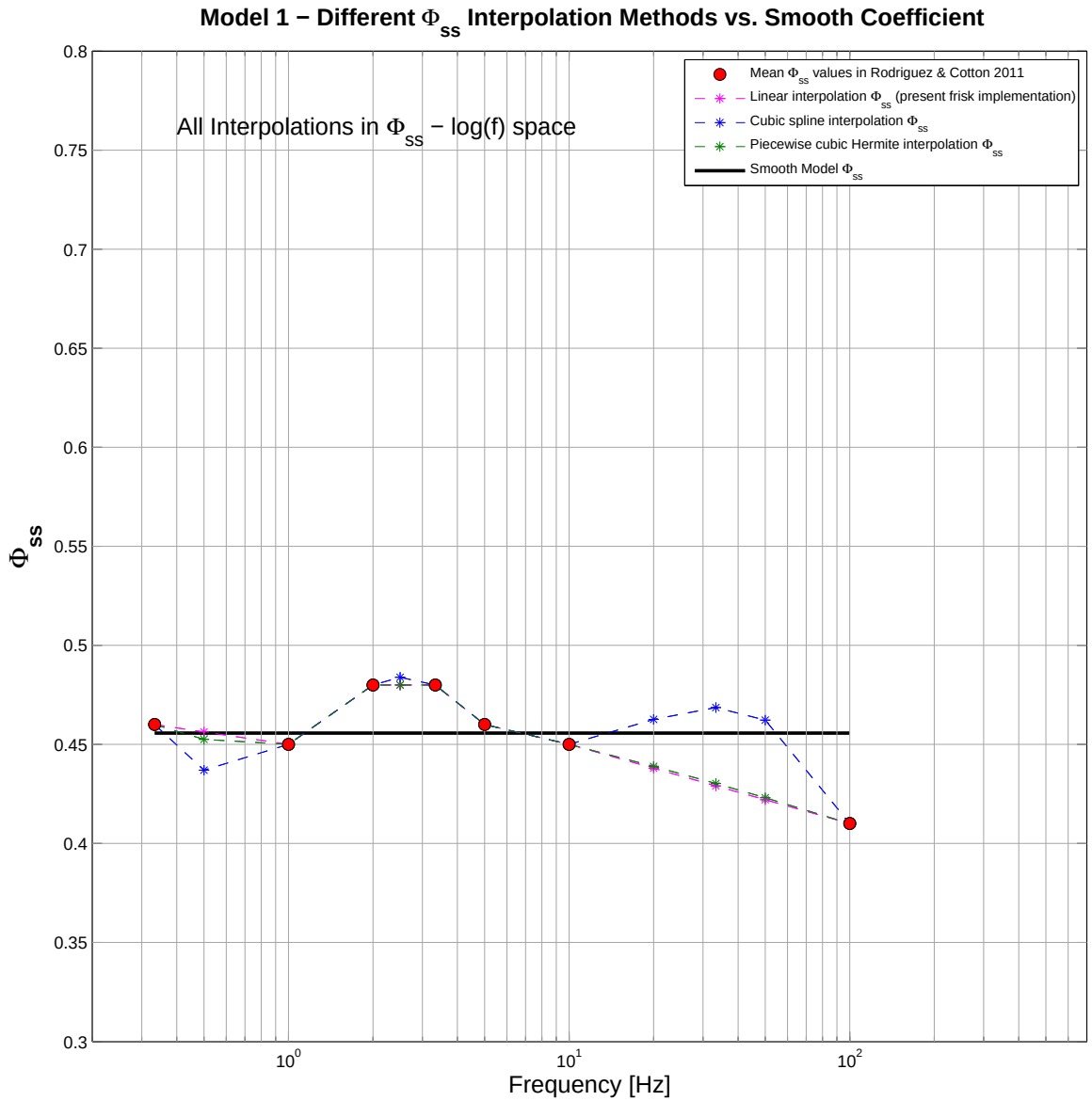

Figure I-6.11: Data points vs. different ϕ_{ss} interpolations and smoothed model for model 1.

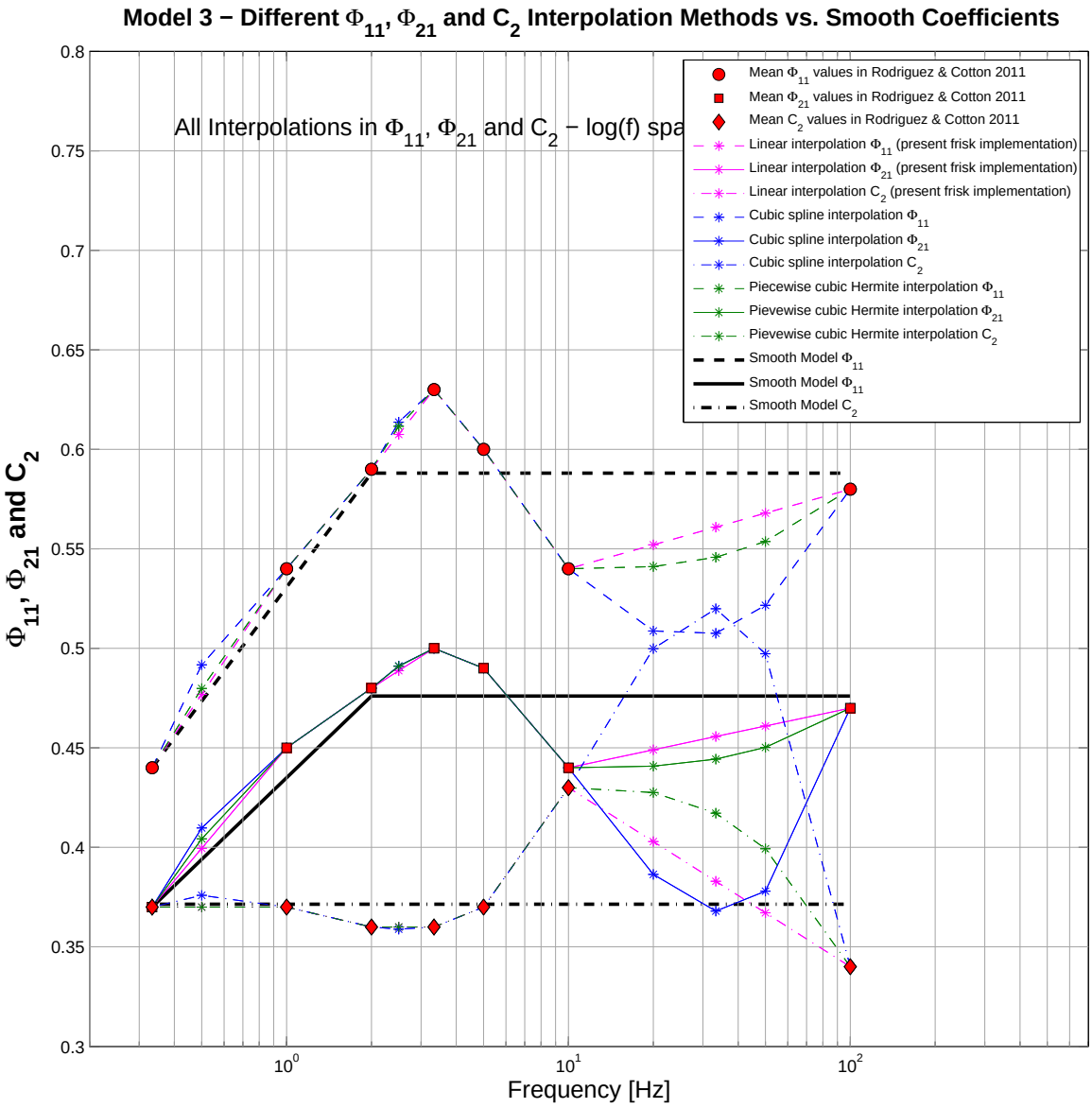

Figure I-6.12: Data points vs. different ϕ interpolations and smoothed model for model 3.

Chapter 7

Vertical Ground Motion

7.1 SP2 Position on Vertical Motions and V/H Ratios

There are two main approaches for estimating the seismic hazard for the vertical component: (1) conduct an independent hazard calculation using vertical GMPEs in place of horizontal GMPEs, or (2) scale the horizontal UHS resulting from the PSHA by a V/H ratio.

A key weakness of the independent vertical approach in a PSHA is that the horizontal and vertical spectral values will often be controlled by different earthquakes, so the vertical and horizontal components estimated using this approach will not occur during a single earthquake. This raises problems as to how to combine the vertical and horizontal loads. The SP2 experts have agreed that the preferred method is to specify the V/H ratio and, not a completely separate vertical model.

Thus, the SP2 expert's preferred approach is to develop models for the vertical-to-horizontal ratios of response spectral ordinates, which can then be used to scale the ordinates of a horizontal scenario response spectrum to obtain the vertical spectrum. The horizontal response spectrum will correspond to a particular earthquake scenario obtained from disaggregation, for this reason the V/H ratio should be defined in terms of the same explanatory variables that define the scenario (i.e., magnitude, style-of-faulting, distance, and site class).

7.2 Selected V/H Models

The following criteria were considered for selecting the V/H models:

1. Applicable to the PRP response periods, namely from 0.01 second (or PGA) to 2.0 seconds,

2. Applicable to site conditions corresponding to the SP2 target profile, namely a hard rock site (V_{S30} value of 1000 m/s to 2000 m/s),

3. As well as providing estimates of the median V/H response spectral ratios for the target response periods as a function of magnitude, style-of-faulting, distance, and site class, the models must provide a consistent measure of the associated aleatory variability.

Three models were found that met these criteria: Campbell and Bozorgnia [2003], Gülerce and Abrahamson [2010], and Akkar and Bommer [2010] (later published as Bommer et al. [2011]). The first model is for the horizontal and vertical GMPEs separately, so it combines the two GMPEs to estimate the V/H, but Campbell and Bozorgnia [2003] also provides the standard deviation of the aleatory variability of the V/H ratio. The other two models are for the V/H ratio directly.

Campbell and Bozorgnia [2003] provided coefficients for PGA and for spectral ordinates at 0.05 second and higher, so use of this model would require interpolation in order to obtain coefficients at 0.02 and 0.03 second in order to satisfy criterion 1 above. At SP2/WS6, held in Zurich (7.-8. October 2010), it was decided that if this model is included in the logic-tree for V/H ratios, then rather than interpolate for the missing coefficients, the approach would be to interpolate to find the actual missing ordinates for the specific earthquake scenarios under consideration.

At the beginning, due to the lack of hard rock V/H ratios, an attempt was made to use the V/H ratios for CEUS and WUS provided in NUREG/CR 6728 [McGuire et al. 2001] and to interpolate for the necessary V_{S30} conditions. After further evaluations by the experts, this model was dropped from the list of candidates.

An issue which arose in discussions of the V/H models was the impact of hard-rock site conditions. For some of the plant sites, it would be necessary to perform the transformation from horizontal to vertical spectra in rock with very high V_{S30} values, in some cases in excess of 2000 m/s. To address the effect of a hard-rock site, Edwards et al. [2011b] developed a model for the V/H ratio for hard-rock site conditions which meets all three selection criteria. This led to a fourth model (see Figure I-7.1): The Edwards et al. [2011b] model is site specific and depends on the underlying QWL profile. During the evaluation of this model, it was proposed to also have the option to use the version of the model which does not have a high frequency correction (>7Hz).

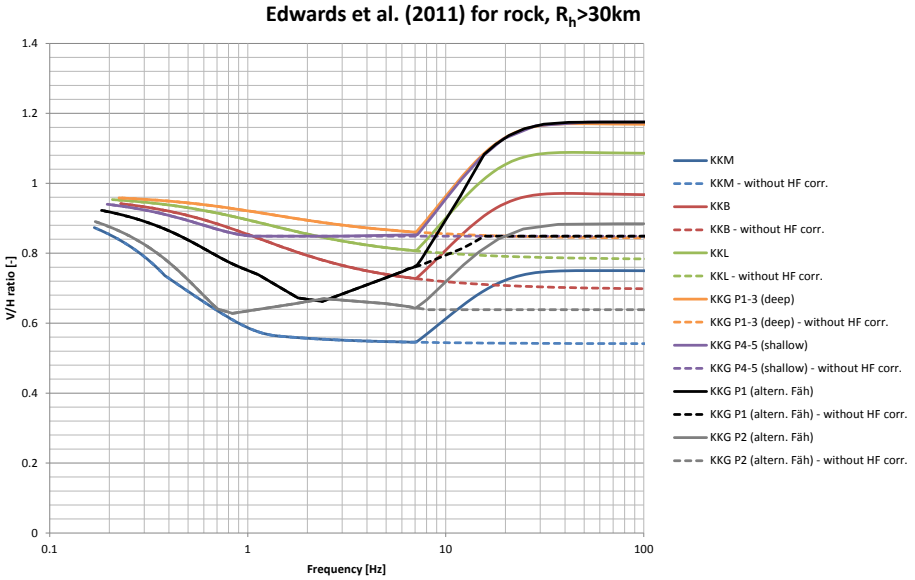

Figure I-7.1: Comparison of the site specific V/H ratios for the Edwards et al. [2011b] model.

Furthermore, in the course of 2012 empirical models based on the East and West US data were introduced in order to provide some reference for comparison [Biro and Renault 2012a] (PMT-TN-1257). These models have been included in the set of candidate models by the SP2 experts. A smoothed version of the raw US East and West median models was developed for the workshop WS11/SP2 (16.-18. January 2013) and approved by the experts to be used for the final assessment (Figure I-7.2). The values are presented in Tables I-7.1 and I-7.2 compared in Figure I-7.2.

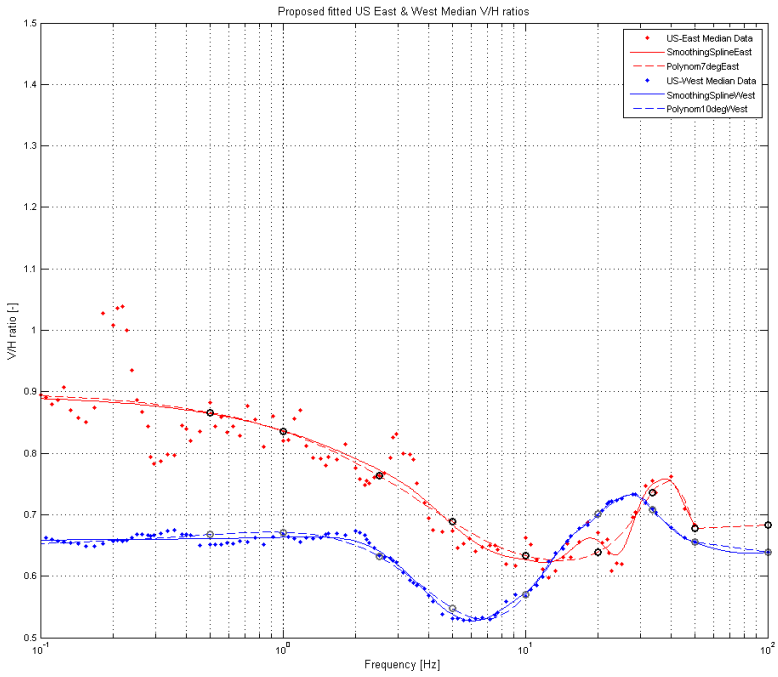

Figure I-7.2: US East and West V/H data and alternative smoothed versions. The polynomial fits were used for the final model.

Table I-7.1: Values of the smoothed V/H US East model compared to the data for the nine PRP frequencies.

Freq. [Hz]	Data	Spline Fit	Poly Fit	Spline Error [%]	Poly Error [%]
0.5	0.883	0.865	0.866	-2.093	-1.892
1	0.820	0.839	0.836	2.230	1.885
2.5	0.763	0.773	0.763	1.272	-0.036
5	0.673	0.686	0.689	1.863	2.188
10	0.662	0.625	0.633	-5.942	-4.618
20	0.671	0.652	0.639	-2.976	-4.983
33	0.755	0.746	0.737	-1.208	-2.559
50	0.684	0.684	0.684	0.085	-0.873
100	NaN	0.683	0.684		

The final set of candidate V/H models is as follows:

- Bommer et al. (2011)

Table I-7.2: Values of the smoothed V/H US West model compared to the data for the nine PRP frequencies.

Freq. [Hz]	Data	Spline Fit	Poly Fit	Spline Error [%]	Poly Error [%]
0.5	0.651	0.661	0.668	1.504	2.451
1	0.668	0.663	0.671	-0.705	0.490
2.5	0.634	0.640	0.632	0.996	-0.346
5	0.531	0.538	0.548	1.222	3.010
10	0.567	0.572	0.570	0.999	0.536
20	0.697	0.700	0.701	0.405	0.674
33	0.710	0.710	0.709	-0.042	-0.199
50	0.655	0.655	0.655	-0.009	0.008
100	0.639	0.639	0.639	-0.0002	0

- Campbell and Bozorgnia (2003)
- Gülerce and Abrahamson (2011)
- Edwards et al. (2011) without correction above 7 Hz
- Edwards et al. (2011) with correction above 7 Hz
- US West Median (PMT-TN-1257)
- US East Median (PMT-TN-1257)

These median V/H ratios for the models are shown in Figures I-7.3 and I-7.4 for M6 earthquakes at distances of 30 and 10 km, respectively. The Akkar and Bommer [2010] (or Bommer et al. [2011]) and Gülerce and Abrahamson [2010] models are both based on updated datasets and lead to similar V/H ratios for rock sites. The Edwards et al. [2011a] model is flatter with amplification only above 10 Hz.

There is epistemic uncertainty in the V/H ratio, but, the approach used here to estimate the vertical component ground motion is to scale the horizontal ground motion by the V/H ratio. There is already significant epistemic uncertainty in the horizontal ground motion so scaling a single V/H by the full range of horizontal spectral will lead to a wide range of vertical spectra. Incorporating epistemic uncertainty into the V/H ratio and scaling the range of horizontal spectra by the full range of V/H ratios would over-predict the total uncertainty in the vertical component. Therefore, only a few V/H models are used. That is, combining a single V/H ratio model with all of the alternative horizontal results will lead to a large range of vertical ground motions due to the wide range of horizontal models. The range of V/H models used should consider the total range of the results for vertical ground motions after combination with the range of horizontal ground motions and avoid double counting uncertainty.

7.3 Aleatory Variability of V/H Ratios

Figure I-7.5 compares the standard deviation of the ln(V/H ratio) from these four models. For frequencies above 1 Hz, the models, standard deviations are similar, but they differ significantly for frequencies less than 0.5 Hz.

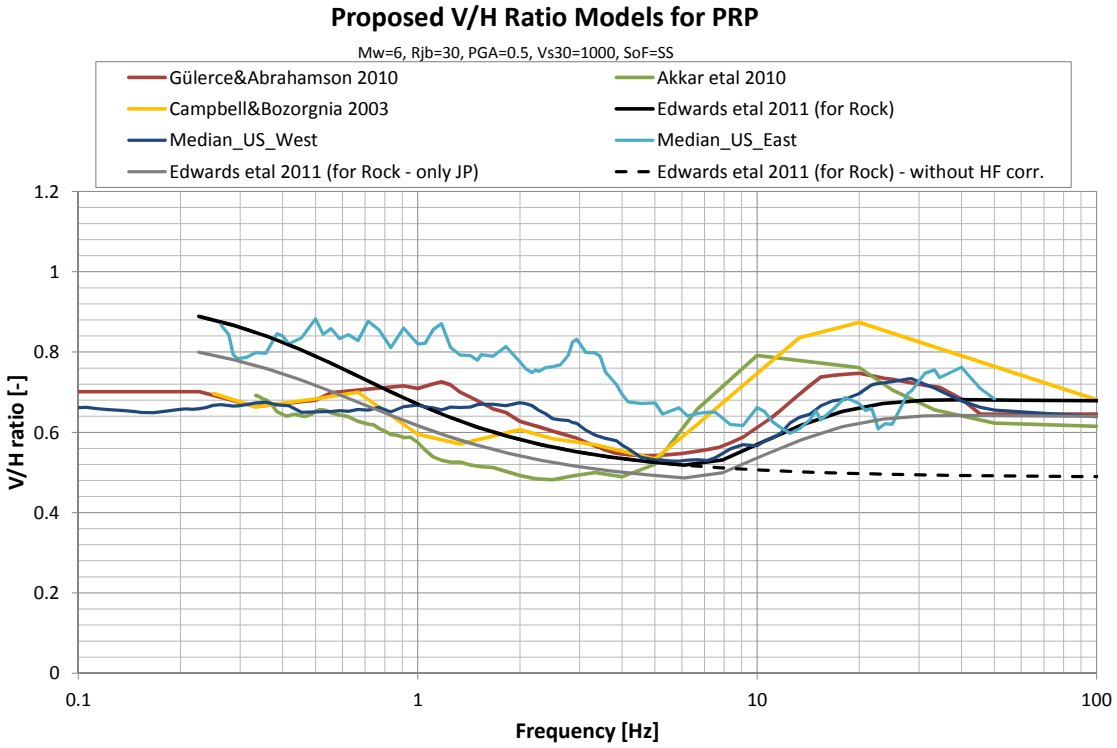

Figure I-7.3: Comparison of median V/H ratio for the candidate models for M=6 and R=30 km for Swiss generic hard-rock site condition.

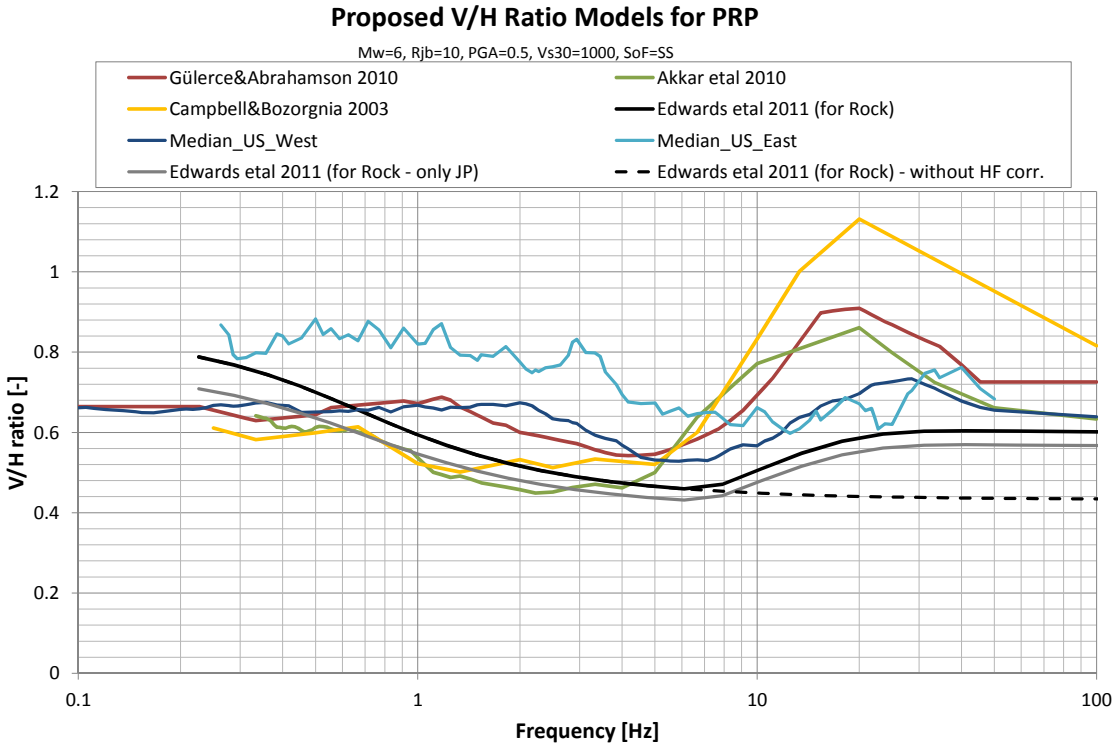

Figure I-7.4: Comparison of median V/H ratio for the candidate models for M=6 and R=10 km for Swiss generic hard-rock site condition.

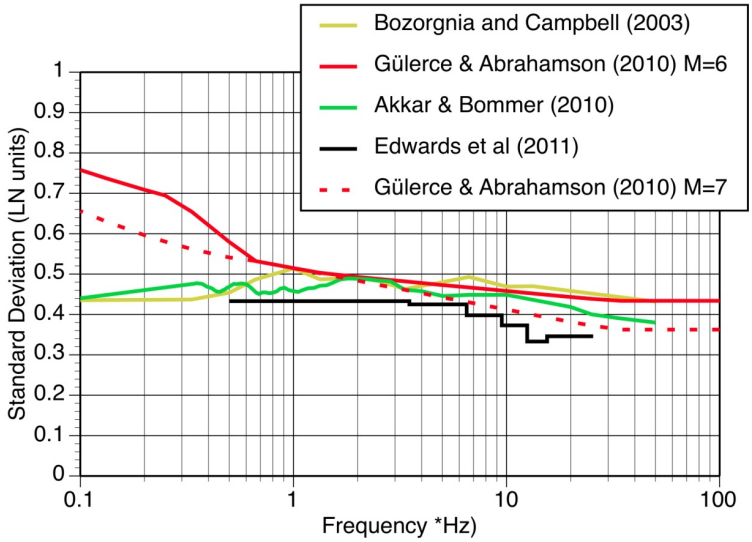

Figure I-7.5: Comparison of the standard deviation of ln(V/H) for spectral ordinates for the four empirical models.

The initial V/H logic tree included the median and aleatory variability of the V/H ratio with four alternative models. This initial form of the V/H logic tree did not properly account for the aleatory variability of the V/H ratio in the hazard calculation. This issue is discussed below. The V/H ratio model is combined with the horizontal hazard to estimate the vertical hazard. The V/H ratio has a median and an aleatory variability. The aleatory variability of the V/H ratio is correlated with the aleatory variability of the horizontal, which is included in the horizontal hazard. To estimate the vertical hazard, the correlation needs to be considered. Accounting for the correlation, the total single-station aleatory variability of the vertical component can be written as:

$$\sigma_{SS_{Vert}} = \sqrt{\phi^2_{SS_{Horiz}} + \phi^2_{SS_{V/H}} + 2\rho_{\phi:H,V/H} \cdot \phi_H \cdot \phi_{V/H} + \tau^2_H + \tau^2_{V/H} + 2\rho_{\tau:H,V/H} \cdot \tau_H \cdot \tau_{V/H}} \quad \text{(I-7.1)}$$

These terms are described in Table I-7.3.

The objective of the V/H model is to estimate the hazard for the vertical component. For the aleatory variability part of this model, the difference in the aleatory variability for the V/H and horizontal components can be added to the horizontal hazard. That is, the additional variability given by the difference in the vertical and horizontal variability can be added:

$$\sigma_{V_{ADD}} = \sqrt{\sigma^2_{SS_{Vert}} - \sigma^2_{SS_{Horiz}}} \quad \text{(I-7.2)}$$

Two approaches for estimating the $\sigma_{V_{ADD}}$ term are given here:

1. Using the V/H GMPEs including the correlations, the additional sigma is given by:

$$\sigma_{V_{ADD}} = \sqrt{\phi^2_{SS_{V/H}} + 2\rho_{\phi:H,V/H} \cdot \phi_H \cdot \phi_{V/H} + \tau^2_{V/H} + 2\rho_{\tau:H,V/H} \cdot \tau_H \cdot \tau_{V/H}} \quad \text{(I-7.3)}$$

2. Using the GMPEs with both H and V models, the additional sigma is given by:

$$\sigma_{V_{ADD}} = \sigma_{SS_{Horiz}} \sqrt{\frac{\sigma^2_{SS_{Vert}}}{\sigma^2_{SS_{Horiz}}} - 1} \approx \sigma_{SS_{Horiz}} \sqrt{\frac{\sigma^2_V}{\sigma^2_H} - 1} \quad \text{(I-7.4)}$$

Table I-7.3: Notation and terms for σ_{SS} of the vertical component.

	Term	Estimates
$\phi_{SS_{Horiz}}$	Single-station within-event standard deviation for the horizontal component	Horizontal GMPE logic tree
$\phi_{SS_{V/H}}$	Single-station within-event standard deviation for the V/H ratio	Traditional (not single-station) $\phi_{V/H}$ is available in GüAb11 and BoEtal11. Can be used to approximate $\phi_{SSV/H}$
$\rho_{\phi:H,V/H}$	Correlation of the within-event residuals of the horizontal and V/H ratio	Available in GüAb11 (not single-station)
τ_H	Between event standard deviation for the horizontal	Horizontal GMPE logic tree
$\tau_{V/H}$	Between event standard deviation for the V/H ratio	Available in GüAb11 and BoEtal11
$\rho_{\tau:H,V/H}$	Correlation of the between-event residuals of the horizontal and V/H ratio	Available in GüAb11

With GüAB11: Gülerce and Abrahamson [2011] and BoEtal11: Bommer et al. [2011]

The ratio of the ergodic standard deviations for the H and V components can therefore be used. These two approaches are estimated in Tables I-7.4 and I-7.5.

For approach 1, four cases are considered based on different models for the horizontal component aleatory terms (ϕ_H and τ_H) and the V/H aleatory terms ($\phi_{v/H}$ and $\tau_{v/H}$). The additional variability required is small, ranging from 0 to 0.3 natural log units.

For approach 2, two GMPEs with both horizontal and vertical models are used to compute the $\sigma_{V_{ADD}}$ term: the Abrahamson and Silva [1997] and Campbell and Bozorgnia [2003] models. These two models both show a significantly larger standard deviation on the vertical component than on the horizontal component in the short period range ($\sigma_{V_{ADD}}$ ranging from 0.21 to 0.37). These two models are based on broad site categories and so the standard deviations include a wide range of sites within each category. Currently, the σ_{SSH} used in Table I-7.5 was evaluated based on the average single station sigma models of all SP2 experts as presented and revised during the SP2 workshop on May 9-10, 2012.

7.4 Application of the V/H Model

There are two approaches that can be used. The first approach is to estimate the vertical ground motion by scaling the horizontal UHS by the median V/H ratio using the mean magnitude and distance that control the UHS as determined by disaggregation and adding the additional aleatory variability (V_{ADD}). This approach is straight-forward and leads to a vertical spectrum that is similar to the UHS in that the correlation between the horizontal and vertical is not directly used. Figure I-7.6 shows the correlation of the residuals of the V/H ratio with the residuals from the horizontal component (for the same data). The key feature of this figure is that the correlation is negative. That is, if the horizontal ground motion for a given return period corresponds to a high epsilon value, then the V/H ratio for that case is

Table I-7.4: Estimation of $\sigma_{V_{ADD}}$ using Method 1.

ϕ_H:	AbSi08	global ϕ_{SS}	AbSi08	global ϕ_{SS}
τ_H:	AbSi08	global avg.	AbSi08	global avg.
$\phi_{V/H}$:	Akkar et.al. 2010	Akkar et.al. 2010	GüAb10	GüAb10
$\tau_{V/H}$:	Akkar et.al. 2010	Akkar et.al. 2010	GüAb10	GüAb10
$\rho_{V/H,H}$:	GüAb10	GüAb10	GüAb10	GüAb10
Freq. [Hz]	σV_{ADD} [LN units]	σV_{ADD} [LN units]	σV_{ADD} [LN units]	σV_{ADD} [LN units]
100	0*	0*	0.08	0.14
50	0.07	0.12	0.17	0.20
33.3	0.16	0.19	0.21	0.24
20	0.21	0.25	0.23	0.27
10	0.13	0.21	0.14	0.22
5.0	0*	0*	0*	0*
2.5	0*	0*	0*	0*
1.0	0*	0.12	0*	0.2
0.5	0.16	0.25	0.23	0.3

* Negative value under the square-root

Table I-7.5: Estimation of $\sigma_{V_{ADD}}$ using Method 2.

Freq. [Hz]	σ_{SS_H}	CaBo03	AbSi97
100	0.543	0.21	0.35
50	0.559		
33.3	0.569		0.37
20	0.572	0.35	0.34
10	0.572	0.31	0.29
5.0	0.572	0.25	0.10
2.5	0.572	0.23	0*
1.0	0.563	0.10	0*
0.5	0.554	0.10	0*

* Negative value under the square-root

expected to be lower than average. This indicates that the standard practice of applying the median V/H ratio to the horizontal UHS will over-estimate the vertical ground motions for return periods corresponding to high epsilon values on the horizontal hazard.

An alternative approach is to estimate the vertical spectrum in a manner that is similar to developing the CMS for horizontal ground motions. The best estimate of the vertical, given a horizontal UHS, is given by

$$Sa_Z(T) = Sa_H(T)\frac{V}{H}(T)\exp\left(\rho_{H,V/H}(T,T)\cdot\sigma_{V/H}(T)\cdot\varepsilon_H(T)\right) \quad \text{(I-7.5)}$$

where $\rho_{H,V/H}(T)$ is the correlation coefficient of the residuals between the horizontal and the V/H at the same spectral period (Figure I-7.6).

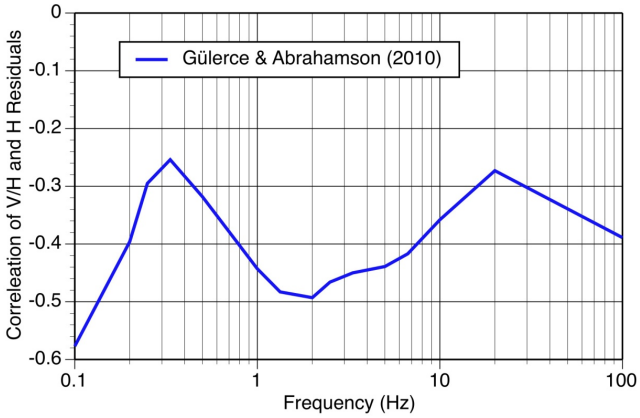

Figure I-7.6: Correlation of the spectral acceleration residuals between the horizontal and the V/H ratio at the same spectral period.

From the beginning, the project decision was to use available V/H models for the vertical hazard calculation.

7.5 Consideration of Kappa Effects on the Vertical Component

Section 3.4 described the κ adjustments that have been made for the horizontal component GMPEs. The approach for the vertical ground motion, described in Section 7, is to use the V/H ratio to scale the horizontal rock ground motion based on empirical V/H ratios. The empirical V/H ratios are based on datasets similar to those used for the candidate GMPEs, but V/H ratios have not been adjusted for κ. This raises the question as to the applicability of published V/H ratios to the κ adjusted horizontal GMPEs at high frequencies.

At high frequencies, the peak vertical ground motion is generally controlled by P-waves [Beresnev et al. 2002], so the V/H ratio represents the ratio of vertical component P-waves to horizontal component S-waves. The effect of κ on the horizontal S-waves is addressed in the κ scaling in Section 3.4 and the denominator V/H ratio can be adjusted for κ, but there is also the issue of the κ effects on the P-waves. W. Silva (pers. comm.) has estimated κ values for the vertical component and finds that they are about 1/2 of the horizontal component κ. Including the effects of κ on both components would shift the peak in the V/H ratio to higher frequencies.

The three candidate empirical GMPEs for the V/H ratio described in Section 7.2 do not specifically include κ. The data used to derive these models are similar to the data used to derive the horizontal GMPEs. Given the large effect of κ on the horizontal component, it is not clear that the V/H ratio would not also be strongly affected by the κ. As an alternative, four additional models for the V/H ratio for rock sites were developed: two models by Edwards et al. (2011) and two statistical models based on the NGA-West2 and NGA-East datasets. The Edwards et al. models are based on V/H ratios from the QWL method using an average of hard-rock sites in Japan and Switzerland. They have a strong dependence on the shear-wave velocity. The resolution of the QWL method is limited to frequencies below 7 Hz. The two versions of the model reflect different assumptions for the V/H ratio at high frequencies (> 7 Hz). In one model, there is no change in the V/H ratio above 7 Hz. In the second model, the V/H ratio above 7 Hz increases, similar to empirical models. The two statistical models are

based on the median V/H for sites with V_{S30} >700 m/s for the NGA-East data and V_{S30} >800 m/s for the NGA-West2 data. By using the rock site data, these two statistical models for the V/H ratio will reflect the kappa that is represented by these rock sites.

Chapter 8

Maximum Ground Motions

Traditionally, the ground motion distribution used in PSHAs has been truncated based on a maximum number of standard deviations of the log-normal distribution based on the concept that the upper tail of the lognormal distribution is too broad and does not predict the distribution of ground motions. Several recent papers have suggested that there is evidence of such a truncation [Rhoades et al. 2008; Huyse et al. 2010] based on evaluations of residuals, but these evaluations failed to account for the correlations in the residuals through the event term. If these correlations are considered, then there is no evidence for truncation of the log normal distribution [Abrahamson and Wooddell 2009; Al Atik and Abrahamson 2010b].

The SP2 experts agreed that there is no statistical basis for such a truncation and that the truncation should be based only on physical limits.

The PEGASOS Project explicitly included models for the maximum ground motion based on a number of datasets provided to the experts. These datasets included the results of numerical simulations performed specifically to capture the most extreme ground motions resulting from the distributions assumed for the seismological input parameters [Pitarka et al. 2002; Priolo et al. 2002], and the largest ground motions for selected magnitude-distance bins found in the strong-motion database compiled for the PEGASOS Project.

8.1 Maximum Ground Motions from Numerical Simulations

The numerical simulations for extreme ground motions conducted for PEGASOS have not been updated, but they were developed for a reference site condition of V_S=2000 m/s and the reference site condition has now been changed to 1000 m/s. If these simulations are used to guide the selection of the maximum ground motion, then the change in the reference V_{S30} value should be considered.

8.2 Maximum Ground Motions from Empirical Data

The global database of strong-motion recordings with large amplitudes has considerably expanded, essentially as a result of the operation and densification of recording networks. Additionally, a number of studies have been published dealing specifically with the compilation

of such recordings and the analysis of their characteristics [Strasser and Bommer 2009; Anderson 2008, 2010]. The work summarized here seeks to update the empirical information used in the PEGASOS Project with this newly available information.

The datasets used to define the largest empirical ground motions are described in Strasser and Zulu [2010] (EXT-TB-1067). Eight main databases and six individual networks were searched for extreme ground motions:

Databases:

1. Waveform database (TP2-WAF-0008) developed for PEGASOS
2. Strasser & Bommer (2009): Database developed to understand causes of extreme ground motions
3. Anderson (2008, 2010): Database developed for the ExGM project (Hanks et al. 2011)
4. Imperial College strong motion archive (ICSMA)
5. Internet Site for European Strong-Motion Data (ISESD)
6. COSMOS VDC
7. Centre for Engineering Strong-Motion Data (CESMD)
8. Italian Accelerometric Databank

Individual Networks:

1. Kyoshin Net (K-Net)
2. Kiban-Kyoshin Net (KiK-net)
3. Japanese Meteorological Agency
4. Iranian Strong-Motion Network
5. Turkish Strong-Motion Network
6. National Observatory of Athens, Greece

Strasser and Zulu [2010] applied a number of exclusion criteria to exclude recordings which do not reflect free-field conditions, as well as those exhibiting quality problems that would affect the value of the ground motion amplitudes calculated. These criteria include:

- Record cannot be considered free-field (recorded at higher level of structure, or in basement or at ground level in structure of 3 or more storeys); recordings from dam abutments that are routinely included in GMPE datasets (e.g., Pacoima Dam) are not excluded.
- Instrument malfunction (loss of damping, or stalling of the recording medium). In some cases, the PGA value can still be used, but spectral response ordinates are considered unreliable.

- Foundation condition is likely to have influenced recorded ground motions; this is the case, for example, for the UCSC recordings from the 1989 Loma Prieta earthquake included in the NGA database, which were recorded on instruments that were not bolted to a concrete pier (K. McNally, D.M. Boore, personal communications, May 2010).
- Data were only used up to a meaningful frequency varying with the instrument characteristics. In particular, recordings from analogue instruments were only used for frequencies below the natural frequency of the instrument (typically of the order of 25 Hz).

The selected empirical data were put into 1-unit wide magnitude bins (M5-6, M6-7, M7-8) and into distance bins shown by the dashed lines in Figures I-8.1,I-8.2, and I-8.3. Based on the trends in the empirical data, Bungum [2010b] proposed two models: a distance-independent model and a distance-dependent model. The distance-independent model set a maximum ground motion applicable to all distances for a given magnitude based on scaling of the Boore and Atkinson [2008] model evaluated at a distance of 1 km. This corresponds to physical limits on ground motion. The distance-dependent model set a maximum based on a scaling of the Boore and Atkinson [2008] median ground motion at a given magnitude and distance. This second model corresponds to a limit on the energy generated at the source and then attenuated to the site distance.

For both models, Bungum [2010b] recommended a set of alternative scale factors that range from 7.5 to 100, equally spaced on the log scale. The six alternative factors are: 7.5, 13, 21, 35, 60 and 100.

For the vertical component, two alternative approaches considered for the reference ground motion are proposed: (1) use the Boore and Atkinson [2008] horizontal model and adjust the scale factors for the vertical component, and (2) scale the Boore and Atkinson [2008] horizontal model by the V/H ratio using one of the models from Chapter 7.

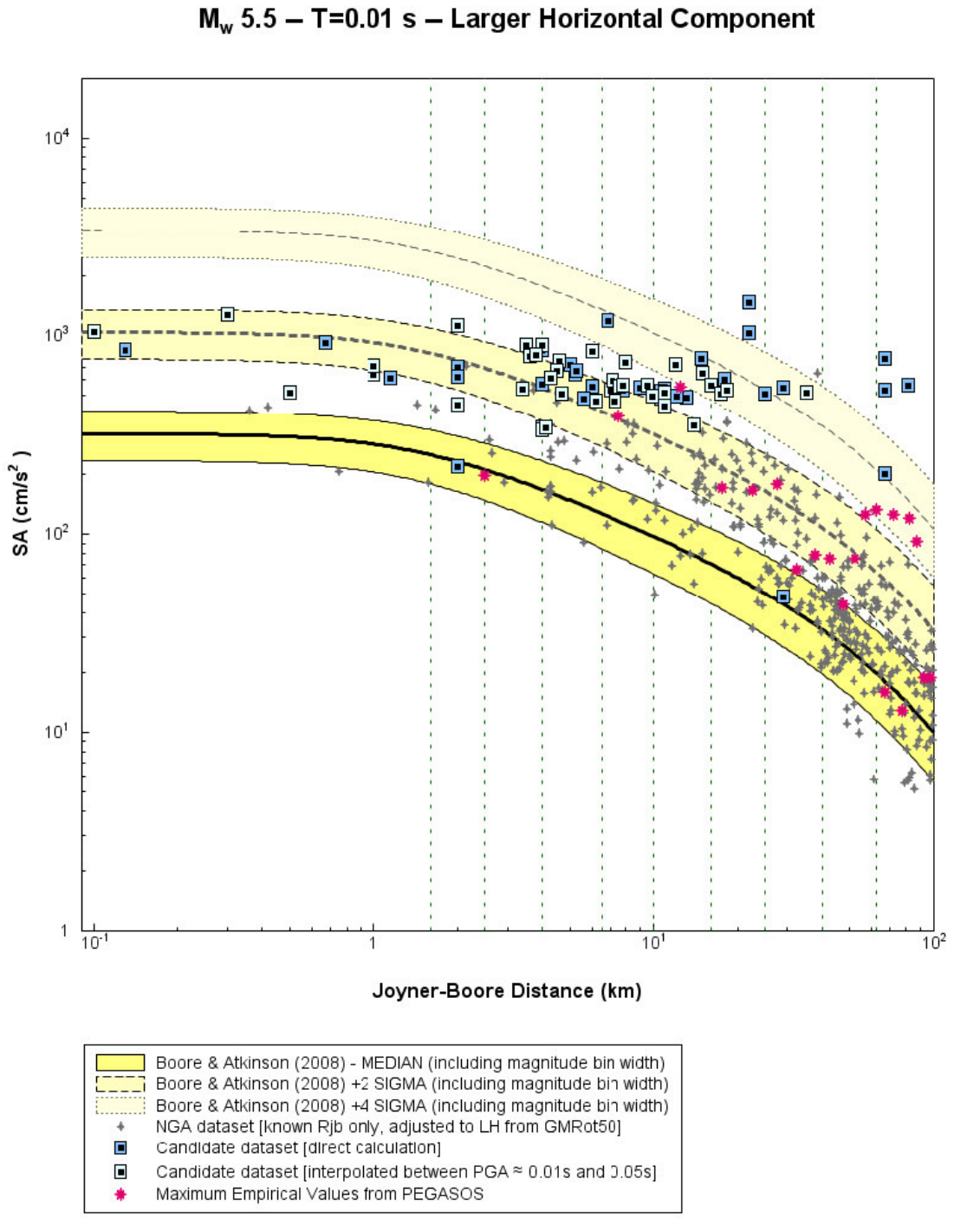

Figure I-8.1: Maximum ground motions for M4.5-5.5 bin [Strasser and Zulu 2010].

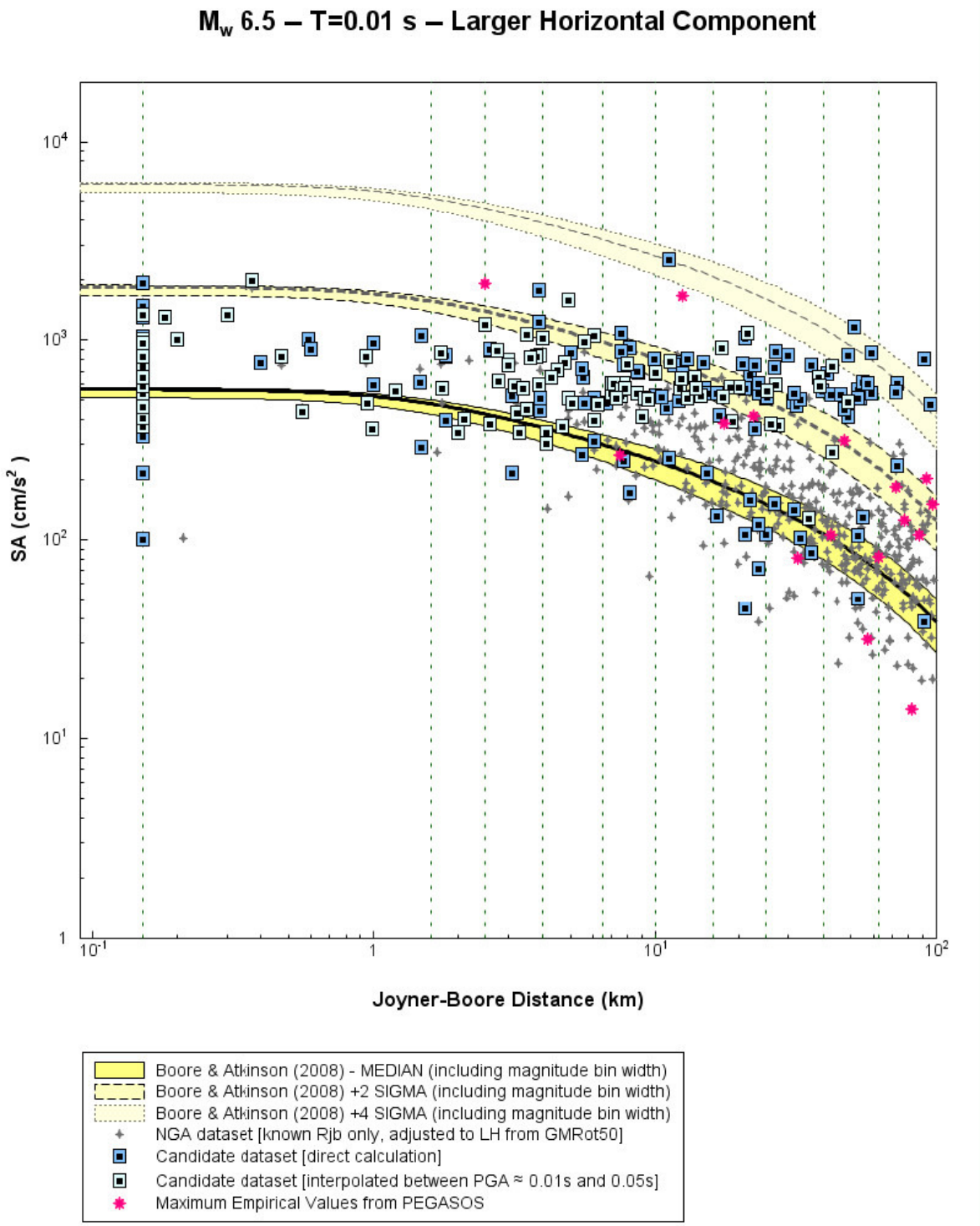

Figure I-8.2: Maximum ground motions for M5.5-6.5 bin [Strasser and Zulu 2010].

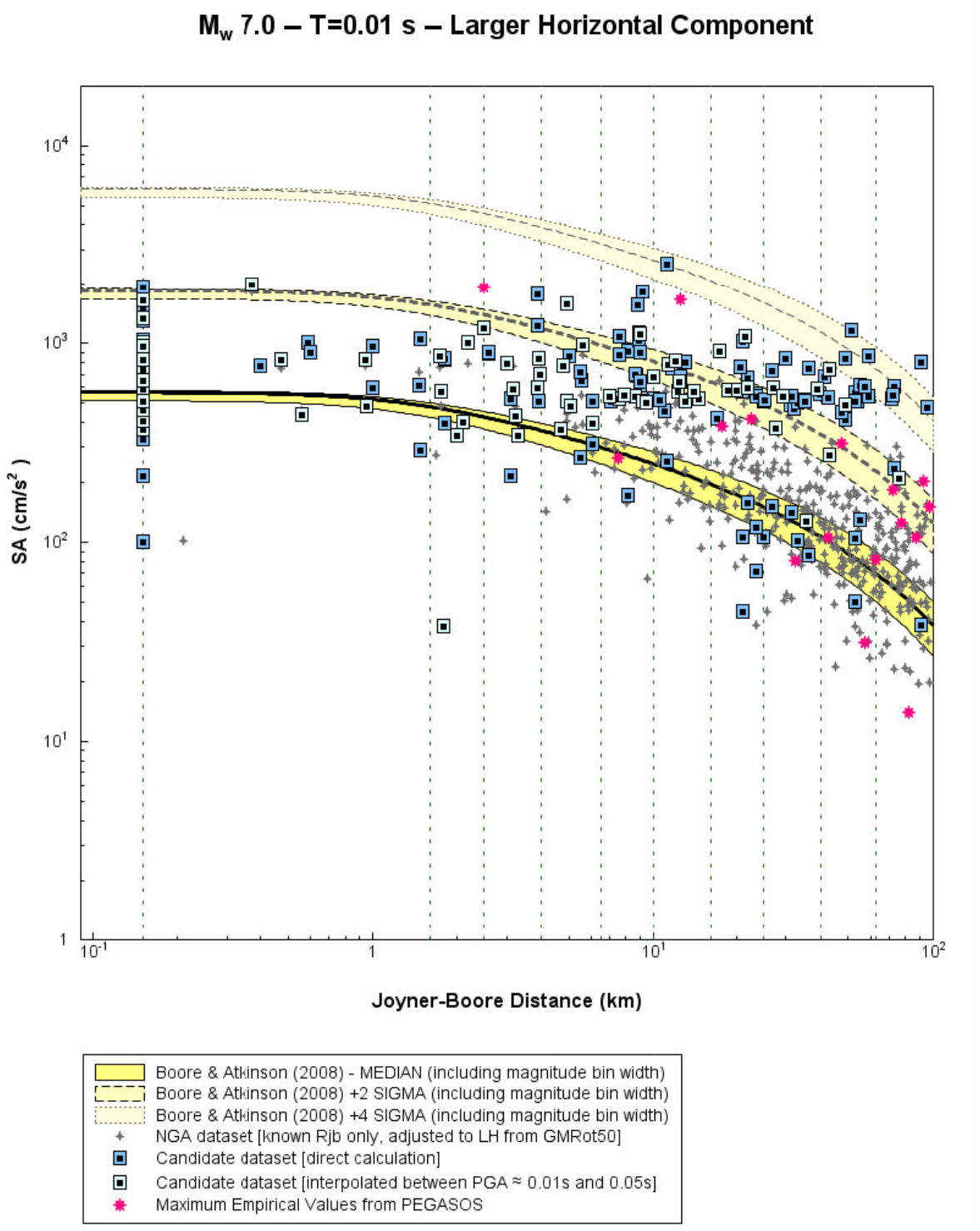

Figure I-8.3: Maximum ground motions for M6.5-7.5 bin [Strasser and Zulu 2010].

Chapter 9

SP2 Master Logic Tree Figures

The master logic trees for the horizontal component ground motion are shown in Figures I-9.1, I-9.2, and I-9.3 for the median, aleatory variability, and maximum ground motion, respectively.

The master logic trees for the vertical component ground motion are shown in Figure I-9.4 for the median and aleatory variability (together).

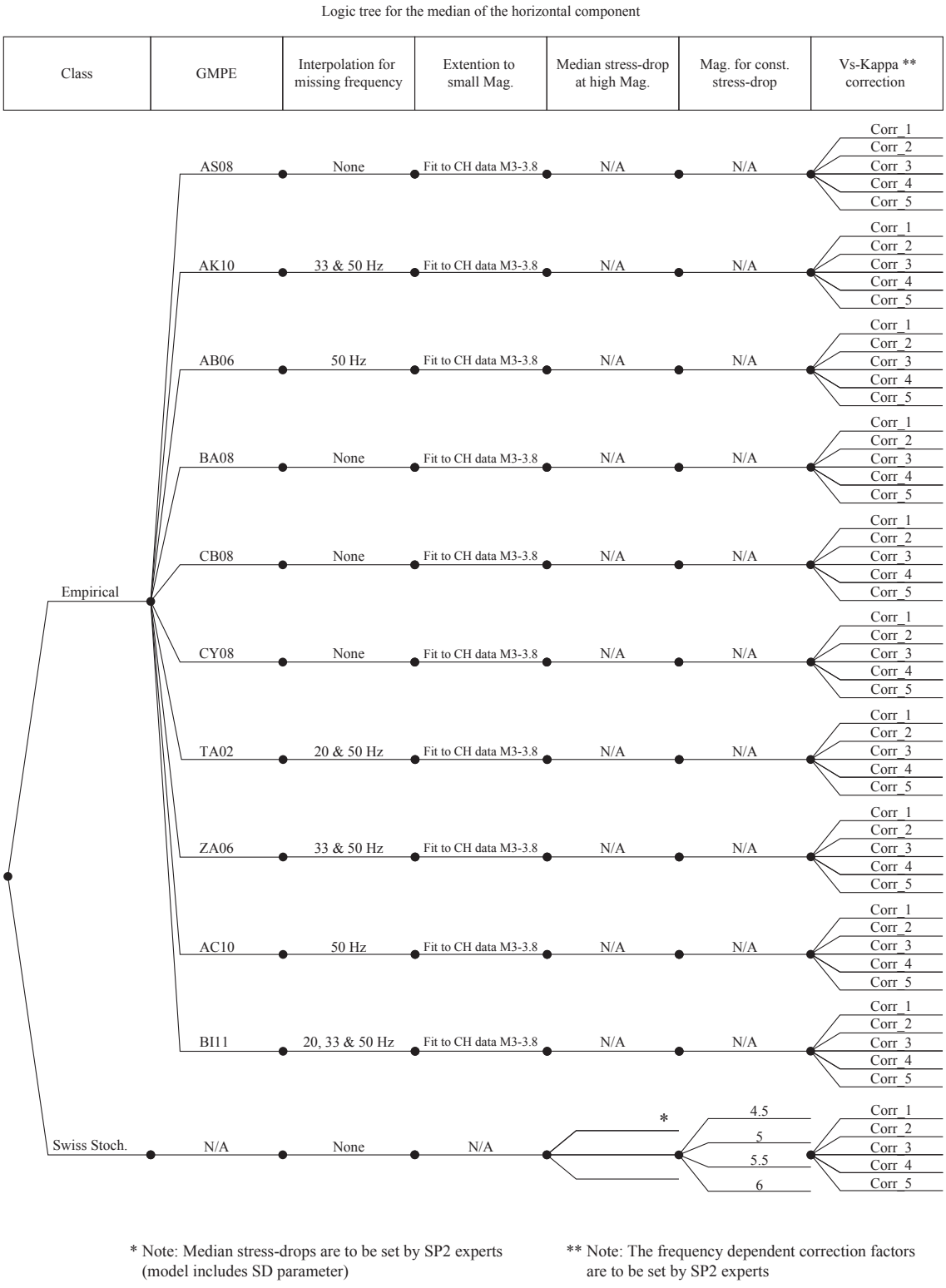

Figure I-9.1: Logic tree for the median of the horizontal component.

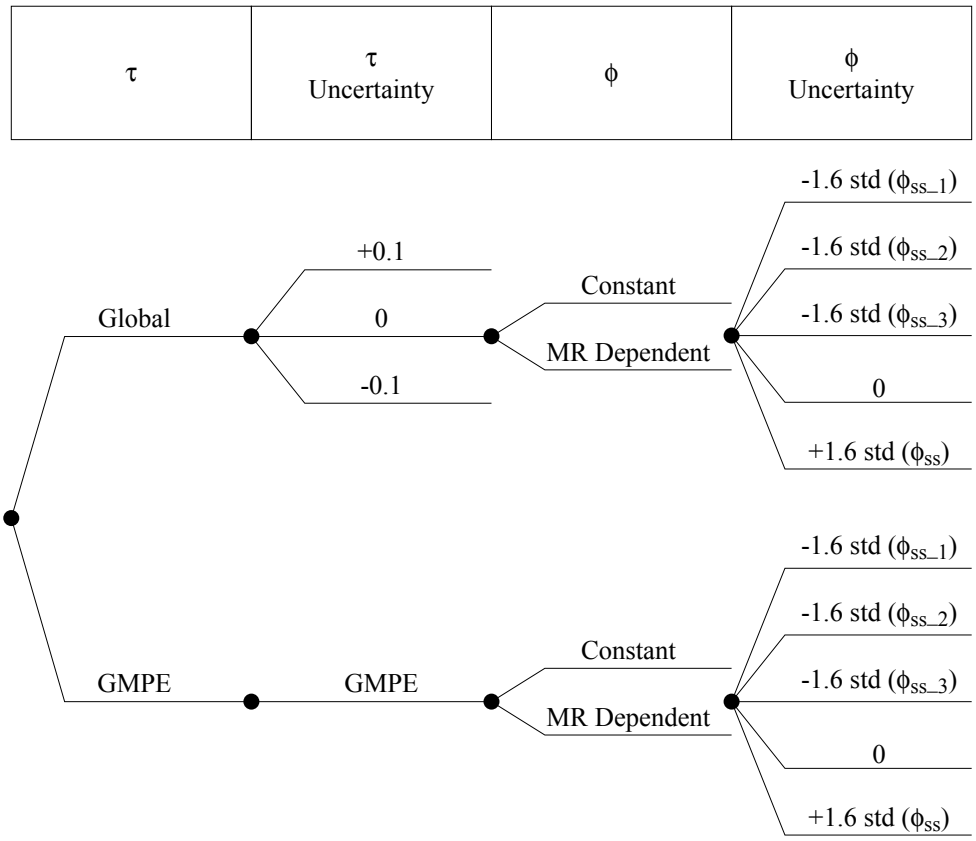

Figure I-9.2: Logic tree for the aleatory variability of the horizontal component (post WS9).

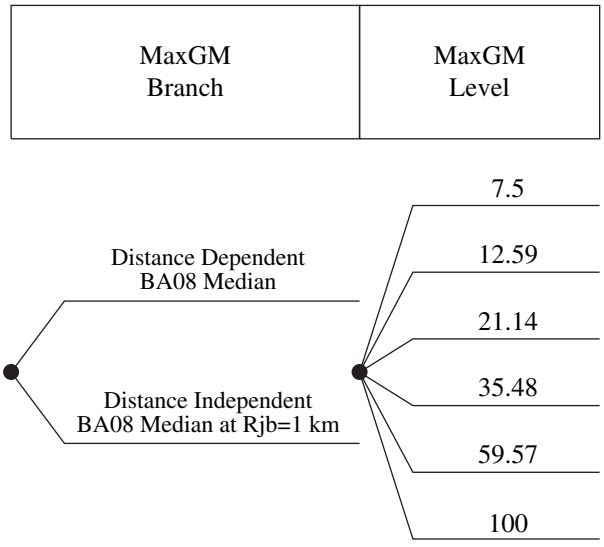

Figure I-9.3: Logic tree for maximum horizontal component.

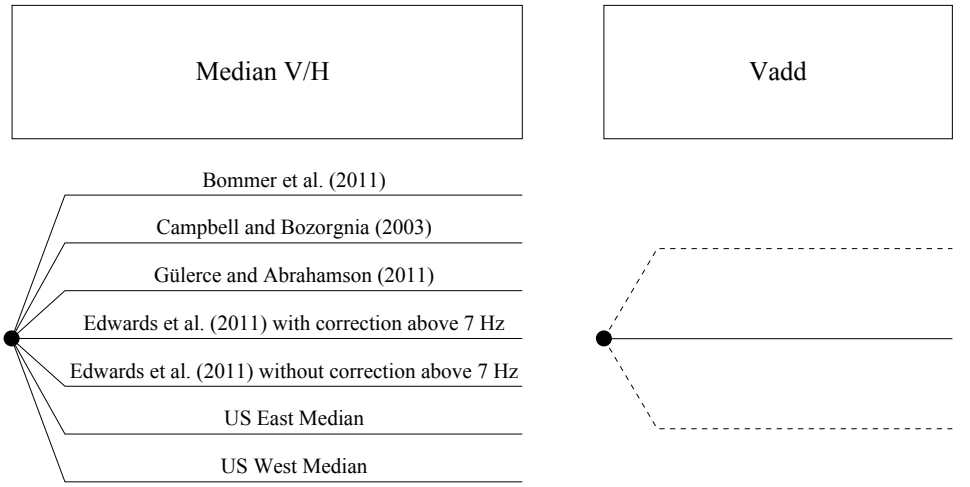

Figure I-9.4: Logic tree for the V/H models and generic additional variability (σ_{VADD}). Note: The final σ_{VADD} model of the experts only consists of a single branch.

Part II

Assessments of H. Bungum

Chapter 1

Evaluation Summary (EG2-ES-1018) of H. Bungum

1.1 Introduction

The present document comprises the author's evaluation summary in his capacity as SP2 expert in the PEGASOS Refinement Project (PRP). As agreed upon between the experts, the expert models will all be based on a single and common master ground motion logic tree [Abrahamson 2012a]. Most, but not necessarily all, of the elements of this master logic tree will be used by all of the experts, but with their own individual weights and justifications for the weights.

While the master ground motion logic tree report provides a fairly detailed summary of the work done and the underlying documentation within the different parts of the model, the details are given in a large number of separate technical project reports issued throughout the PRP, which have been the basis for extensive discussions at workshops and working meetings between and within the expert panel, with extensive participation also from a large number of resource and proponent experts, and specialty contractors. To the extent possible and feasible reference will be made to these reports as part of the justification expert model and weights.

The present evaluation summary is resulting from extensive evaluations and discussions performed throughout the PRP, providing the underlying reasoning for the final models and weights. During this evaluation process the complete set of data, models, and methods proposed by the larger technical community that are relevant to the hazard analysis have been considered. The integration of the available information into the proposed models and weights are furthermore aimed so as to represent the centre, body, and range of the technically defensible interpretations that the larger informed technical community would have if they were to conduct the study [Kammerer and Ake 2012].

In II-1.1 my logic tree is shown (reproduced from a preliminary HID), relating to the entire model presented and justified in this document. The first level in the logic tree, "Model Category" is not explicitly specified by me but is used by SP4 to allow for an easier treatment of those subsequent global variables (or logic tree levels) like $V_S - \kappa$, which are dependent

on whether a GMPE (ground motion prediction equation) or a PSSM (Swiss stochastic) model is considered. The logic tree is frequency dependent as the weights associated with the maximum ground motion truncation models vary with frequency. This logic tree has in total 7104 branches.

The structure of this evaluation summary will largely follow the structure of the master ground motion logic tree report [Abrahamson 2012a], and in the following I will fill in the details of my logic tree and justify my decisions in each particular case.

1.2 Selection of GMPEs for Horizontal Motion

1.2.1 Approach to be used

The approach chosen in this elicitation for selection of relations and determination of weights is as follows:

- Start with the pre-selected relations as the results of application of detailed and strict selection criteria; review briefly the behaviour of the medians.
- Review the testing done (higher order properties, comparisons with ground motions derived from Swiss intensities) and separate the relations that will not be used from those that will be used. The number of relations should be limited in order to avoid a situation where logic-tree weights are becoming less important.
- Determine weights based on degree-of-belief principles (weights as probabilities) where tectonic criteria are used together with a general consideration of CBR (centre, body and range) and MECE (mutually exclusive and collectively exhaustive) criteria, aided by median distributions for different magnitudes, distances and periods.

In using this approach, there is a principle difference between the way in which ground-motion prediction models are selected and the way in which those selected are assigned weights.

1.2.2 Overview of Relations and their Properties

The GMPEs selected by the SP2 experts, after some recent changes [Abrahamson 2012a] are the first ten in this list, where the Swiss stochastic model is added as No.11, actually comprising a suite of models:

1. Abrahamson and Silva (2008), NGA: AS08
2. Boore and Atkinson (2008), NGA: BA08
3. Campbell and Bozorgnia (2008), NGA: CB08
4. Chiou and Youngs (2008), NGA: CY08
5. Atkinson and Boore (2008), ENA stochastic: AB06
6. Toro (2002), ENA stochastic, based on Toro et al. (1997): To02

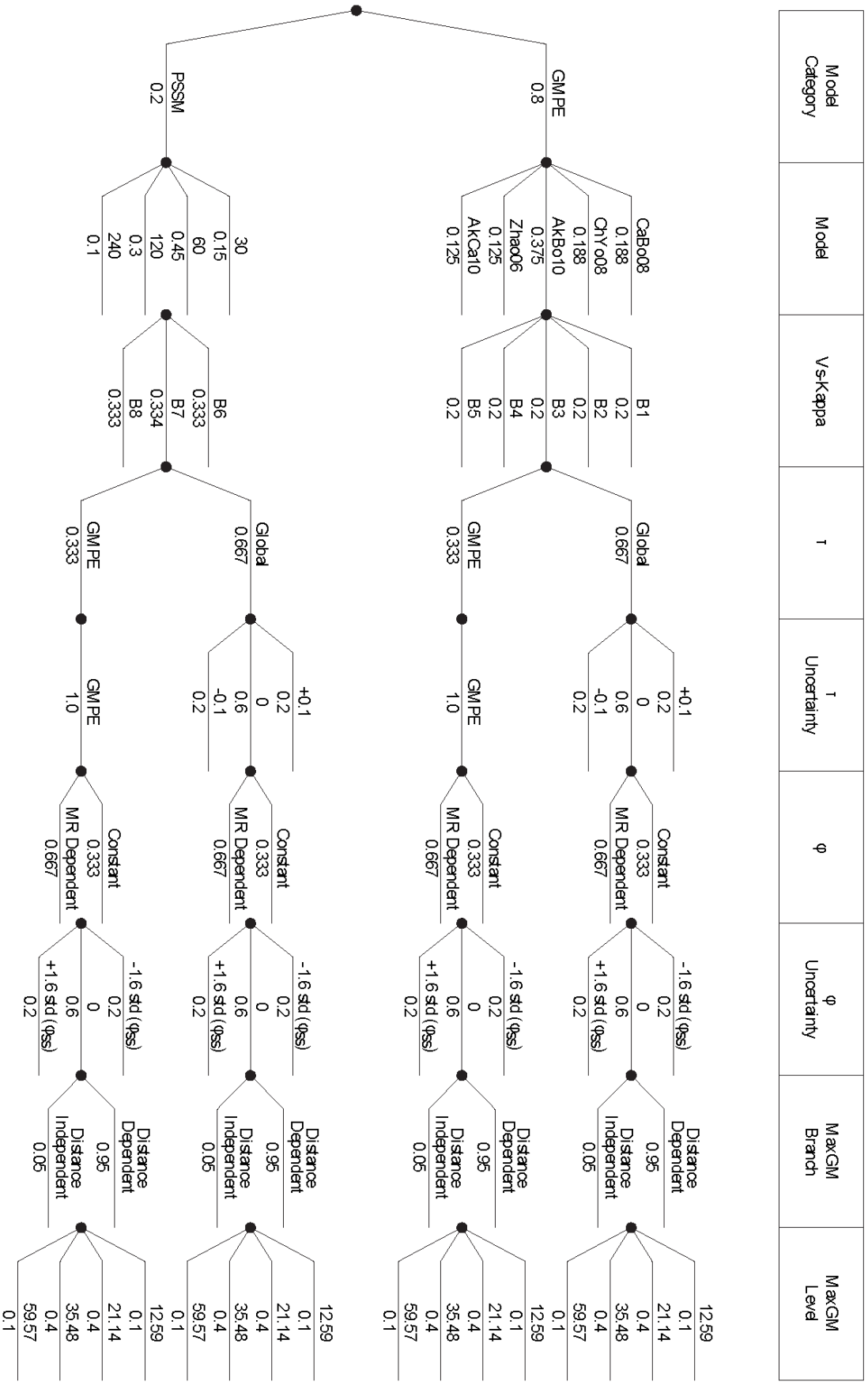

Figure II-1.1: Logic tree for horizontal ground motion, here for 5 Hz (HID Figure 1.1).

7. Zhao et al. (2006), Japan: Zh06
8. Akkar and Bommer (2010), Europe-Middle East: AB10
9. Akkar and Cagnan (2010), Turkey: AC10
10. Bindi et al. (2011), Italy: Bi11
11. Edwards et al. (2010) Swiss stochastic, based also on Edwards and Fäh (2010): Ed10

All of these ten models have been adjusted to observed Swiss ground-motions for lower magnitudes, so all of them should fit that target equally well.

The NGA (Next Generation Attenuation Relationships; http://peer.berkeley.edu/ngawest/) models include data only up to 2003, and it is in this case noteworthy that when the more extensive NGA West 2 (http://peer.berkeley.edu/ngawest2/) dataset is used, the median is changed by less than 5% [Abrahamson 2012a].

The Swiss stochastic model (see Abrahamson [2012a]) is described in detail by Edwards et al. [2009] and by Edwards et al. [2010]. The parameterized Swiss stochastic model (PSSM) model includes different stress drop models (between 30 and 480 bars) and different related cutoff (saturation) magnitudes (between 4 and 6), and in addition there are two candidate models for effective point source distance. The SP2 experts came to a consensus that the simulation model (Model 1) for the effective point source distance was the appropriate model.

In the following I will justify a subset of these relations to be used in the present model along with their corresponding weights.

There are strong indications that while regional differences are often significant at smaller magnitudes, the effects of which will be removed through the low-magnitude adjustments, such differences are becoming much less for larger magnitudes. The main question is therefore, which of the relations satisfy Swiss conditions in the best possible way, for magnitudes which are greater than the largest instrumentally recorded earthquakes in Switzerland?

Two key questions here are:

- Are there any tectonically based differences between the selected relations?
- If so, to which extent can those tectonic characteristics be related to those of Switzerland?

This in turn triggers two more questions:

- Are there any common characteristics within the four NGA (1-4) and the two (5-6) ENA (Eastern North America) relations such that they are providing redundant information?
- Are there any differences between the different groups of relations (NGA, ENA (stochastic), Europe/Middle East, Japan) which are larger than the differences within each group?

If the answers are negative on the tectonics question I could then concentrate on more quality-related arguments, such as magnitude-distance-frequency coverage, etc. However, such criteria should be largely covered through the strict selection criteria that have been applied

in the pre-selection process. In that case, the main task will be to cover "the centre, body and range (CBR) of the informed technical community (ITC)"

The selected relations show us, in terms of median levels, that:

- The four NGA relations are all quite close, for all periods and magnitudes.
- The two ENA relations are very different: To02 is consistently much higher than all of the others for $M \geq 5.5$, while AB06 has a more "erratic" behaviour, and for large magnitudes and short distances it is even significantly higher than TO02. The two ENA relations differ much more than the four NGA relations.
- AB10 is always reasonably close to the others.
- AC10 (the new Turkish relation) has lower PGA levels for all magnitudes, but for longer periods this difference is less for large than for small magnitudes. The authors indicate that the relatively larger number of deeper events in Turkey may explain the smaller ground motions there, which is likely to be related to their use of the RJB (Joyner-Boore) distance metric.
- Bi11 (the new Italian relation) is based on a significantly updated dataset, and also shows generally low levels (as seen for AC10), except for higher magnitudes.
- Zh06 is also largely in the range of the other models, except for $M > 7$, where it is higher than for the NGA relations, but lower than the ENAs.
- For the Swiss stochastic model(s) (Ed10) which by definition fits perfectly to the low-magnitude data, the main challenge is to define the stress drop scaling for the large-magnitude earthquakes. The extrapolated models in Ed10 are guided by comparisons with Swiss intensity data.

The pre-selection work of Douglas [2009a] showed that:

- Relations from active regions (NGA + Europe) are similar, especially outside the near-source region, as supported also by Stafford et al. [2008].
- SCR (Stable Continental Region) relations, in this case the two from ENA, show a wider variation and are generally higher, in particular for short distances, due to higher V_{S30} values, lower κs, higher Qs and higher stress drops.
- The Kullback-Leibler (KL) distances again show that the relations from active regions are similar. However, for small and large magnitudes, the models diverge significantly due to lack of data and different choices made by the modelers.
- The SCR models show larger KL-distances, indicating greater variations in the predicted GMs and the associated aleatory variabilities between these models. Surprisingly, the KL distances decrease with increasing magnitude, indicating that epistemic uncertainties for the large magnitude earthquakes may have been underestimated.

Scherbaum et al. [2010] found that:

- In the Sammon's maps (Scherbaum's Fig. 4), the NGA models organize in two clusters, BA08+CB08 and AS08+CY08, but between these I find both AB07 (AB10; Europe) and Zh06 (Japan). The two ENA models separate from all but also between themselves.
- The SOMs (Scherbaum's Figs. 9-11) show that most relations have a lowland position, including To02, but not AB06, but the two ENAs are still widely separated. The NGAs are quite separated but all in lowland positions.
- In the Sammon's map from SOM weights (Scherbaum's Fig. 12), all of the NGAs except CB08 are quite close, while the ENAs again are different from all and also between themselves. The European AB07 (AB10) is in the middle of all.

The SOM analysis of Kühn [2011b], including the new relations (plus some of those recently considered, but not used), can be summarized as follows:

- The median levels show a spread of about a factor of five for most magnitudes, with a bit more for low magnitudes. For PGA, AC10 is (as already noted) generally low, but not an outlier. This spread suggests a range for the epistemic uncertainty, even if I will not be using all of these relations in my model.
- Sammon's maps are quite sensitive to frequency and magnitude range, and essentially confirm earlier results. The new relations do not deviate significantly from the old ones.
- The SOMs also generally confirm earlier results, with mostly lowland positions, but with individual locations which again are quite sensitive to both frequency and magnitude range. However, the new AC10 has a tendency to be located at the edges of the map.
- Sammon's maps from SOMs also generally confirm earlier results, including a lack of magnitude-frequency stability, and again with AC10 often at the edge of the maps.

Kühn [2011b] has also repeated the analyses with the original eight relations, added only the two new ones, AC10 and Bi11. For all of the tests (Sammon's maps, SOMs, Sammon's maps from SOMs), the two new GMPEs tend to be located at the outer parts of the maps (but not always), but well inside of what could be called outlier space. Therefore, they fill in the map, and they are moreover reasonably well separated from each other. In a CBR context, this is positive.

Kühn [2011b] has also reanalysed the ten selected GMPEs against the Swiss intensity data, including also eight versions of the stress drop scaling of the Swiss stochastic model (PSSMs). First, residual plots are shown for each of the tested models. Then, mixture weights are calculated, based on a mixture model rather than a partition view, with different values for the prior distribution, different period combinations and different data ranges. Regarding the prior weight distributions, two distinct cases are considered: uniform and non-uniform priors.

The results can be summarized briefly as follows:

- For the ten GMPEs, it is difficult to see any conclusive and significant differences based on the residual distributions alone.

- For the eight PSSM relations, however, combining Mc 4.5 and 5.5 with $\Delta\sigma = 30, 60, 90 and 120 bars$, there are some interesting differences in that 120 bars shows a fairly consistent overprediction, with a similar underprediction for 30 bars, often with as much as a full intensity unit. The best fit is usually found for about 60 bars (for Mc 4.5) or in the range 60-90 (for Mc 5.5). This indicated that 30 and 120 bars are outlier values which should carry less weight, judging from the intensity testing alone.

- With uniform weights, the derived weights show a fairly erratic behaviour for low precision values, with different GMPEs "winning" dependent on magnitude and distance ranges. For the PSSMs, these get generally low weights except for the Mc 4.5 and $\Delta\sigma 60 bars$ (sometimes also 90). This is consistent with the previous bullet point.

- When using highly non-uniform weights (0.8 weight assigned to one relation) it is interesting to see that some GMPEs still manage to grab a significant weight (again for low precision values), including actually most of the GMPEs, but also the M4.5-60 bar PSSM (in some cases also 30 and 90 bars). When the 0.8 weight is moved to another relation, the results are quite similar.

A detailed review of the testing results of Kühn [2011b] shows that there is also a considerable instability, but still some trends, and the goal here is to find which relations that are "required" by the data (red in Table II-1.1), which are consistent with the data but not required (green in Table II-1.1), and which are less consistent (or inconsistent) with the data. The tests with uniform priors are not easy to interpret, but the relations that most often occur with positive weights are CY08, CB08, AB06 and AC10 (> 4 scores), while AS08, TO02 and BI11 never get any score. AB10 gets only one score and BA08 and Zh06 gets two each.

For non-uniform weights, I have reviewed results for three different combinations of spectral periods: NOPGA, PGA and $T = 2s$ as seen in Table II-1.1. The results in Table II-1.1 show the ten cases where each one of the relations start with a weight of 0.8, looping over four combinations of magnitudes and distances, and considering only the low precision ones ($beta = 1$) where there is more leverage for change.

Table II-1.1 shows a significant instability, in particular in magnitude-distance space; all of the relations have problems with "surviving" some of the time. For example, I find that in only two of 12 cases, AS08, To02 and Bi11 are able to come out of the test with a weight ≥ 0.1 and that they almost never (only once for To02) are able to get any weight if they do not start with a high weight. The relations with the highest scores (CB08, CY08, AB06) are able to maintain a high weight only in at most 7 of the 12 test cases.

Table II-1.1: Summary of non-uniform prior tests from Kühn [2011b], where the parenthesis indicates the relation which is given weight 0.8 as prior and the number in the parenthesis indicates the final number of scores ≥ 0.1 for that relation. The other numbers indicate number of scores ≥ 0.1 for the other relations in the same test. Each test includes four combinations of magnitudes ($M4-6.6, R10-200; M4-5.5, R10-100; M5.5-6.6, R10-100; M5.5-6.6, R100-200$), each one for NOPGA, PGA and $T = 2s$, all for a precision (β) of 1.0 only. This gives a maximum score of $4x3 = 12$ in each bin.

Non-uniform priors; No of scores ≥ 0.1										
Test	as08	ba08	cb08	cy08	ab06	to02	zh06	ab10	ac10	bi11
1		2	3	4	(6)			2		
2			3	2	4	1	2	(6)	2	
3		1	3	2	2		2		(3)	
4	(2)	1	3	3	4			2	1	
5		(3)	2	4	2		3	2	1	
6		1	5	3	4			1	2	(2)
7		2	(7)	3	3		1		2	
8		1	3	(7)	3		2		3	
9			4	4	1	(2)	2		2	
10		1	1	4	4		(7)	2	2	
Sum	0	9	27	29	27	1	12	9	15	0

In spite of this apparent instability, there are still some trends in Table II-1.1:

- The relations with consistently poorest scores are AS08 (NGA), TO02 (ENA) and Bi11 (Italy), which are the same that got the lowest scores with uniform weights. These are largely inconsistent with the intensity data.
- The relations which seem to be more or less required by the data are CB08, CY08 (both NGA) and AB06 (ENA).
- Relations which are largely consistent with the data but less required include BA08 (ENA), Zh06 (Japan) and AB10 (Europe) and AC10 (Turkey).

These results are quite different from the earlier test results from 2010 based on the original eight relations, since what was found then was that

1. BA08 and CB08 seemed to be often "required" by the data
2. AB10 were consistent with the data but less required
3. To02 were largely inconsistent with the data
4. AS08 and CY08 got occasional good scores
5. Zh06 and AB06 got consistently low scores

This instability indicates that one should be careful with relying too heavily on these tests, and I see two possible reasons for this:

- The intensity target is weakly defined, particularly with respect to the intensity-GM conversion.
- The present tests also include, together with the ten GMPEs, eight PSSMs for which the scores also (surprisingly) are somewhat instable (but also with some consistent trends, as discussed below).

A very useful supplement to these tests is the report by Kühn [2012], comparing Sammon's maps and SOMS between uncorrected and $V_S - \kappa$ corrected GMPEs, based on mean correction factors specified by the experts (except for AC10 and Bi11, which came in later). After corrections are applied the differences between the relations tend to become smaller, as expected.

I read these maps as follows:

- Generally, the Sammon's maps, the SOMs and the Sammon's maps from the SOMs confirm earlier results; the ten GMPEs are reasonably well separated but without outliers, indicating that CBR and thereby the epistemic uncertainties are quite well covered.
- The high-dimensional (HD) distance matrices, reflecting differences in means and standard deviations between pairs of relations, are particularly useful here, indicating the following:
- The four NGA relations are more similar than the others, but still quite close to both AB10 and Zh06. These differences are, as expected, reduced after $V_S - \kappa$ corrections.
- AB06 and To02 (both ENA) are quite different from most others, but least different from AB10 and Zh06. However, the $V_S - \kappa$ corrections also here reduce the differences significantly, especially for PGA and M 6-7.
- Bi11 (Italy) is closer to AB10 (Europe-ME) than to AC10 (Turkey), especially for the lower magnitudes, which may reflect the lower medians for the latter. The differences here are also larger for the lower magnitudes, however.

It could have been useful to be able to revisit these maps when AC10 and Bi11 have been $V_S - \kappa$ corrected.

1.3 Selection of GMPEs and PSSMs and Assignment of Weights

The testing as reviewed above has been very extensive, including both higher order properties (beyond medians) and the extent to which the GMPEs are compatible with observed Swiss earthquake intensities.

There are two important points to be noted initially here:

- Much of the differences between the relations are at low and intermediate magnitudes, which largely are removed as a result of the low-magnitude corrections, targeting Swiss ground motions.

- The $V_S - \kappa$ corrections are further significantly reducing the differences, in particular for the ENA relations.

Following the above review and testing there are some important questions to be asked before I assign weights to the GMPEs:

- What does the locations and differences in KL, Sammons maps, SOMs, Sammons maps from SOMs, and HD distance matrices mean in terms of the relation's attractiveness in a Swiss PSHA? Clearly, if they are very close they will be similar in most ways, and therefore largely redundant.
- Therefore, to be included with a positive weight, a relation should be located somewhat separated from others, to help span the range and cover the epistemic uncertainties. While this helps to secure that the relations are mutual exclusive (ME) it does not necessarily tell us that they are collectively exhaustive (CE), which in combination gives the important MECE criterion.
- Also, if a relation is widely separated from the others, when does it stop covering the desired range and start to become an (not applicable) outlier?

As discussed above, the relations are quite evenly distributed, and without outliers, in the various test spaces, in particular when also considering variations in magnitude, frequency and distance. This is likely to be largely a result of the strict selection criteria that have been applied.

Even so, I do not want to include all of the relations, to avoid the situation which occurs when a large number of relations are included, namely that the weights become of less value and influence and one might as well just give them uniform weight (e.g.,Sabetta et al. [2005]).

Instead, I choose to follow the approach of Scherbaum and Kühn [2011] who convincingly advocates for treating weights as probabilities and using a sequential weighting strategy in which they start with the relation(s) for which they have the highest degree-of-belief, followed by the next highest, etc., until the commutative probability reaches unity. The (traditional) alternative to this is to start with all of the more or less strictly selected relations and then just distribute weights that add up to one, which, as just stated, is more or less the same as giving uniform (non-informative) weights.

After the first selection of relations, and the corresponding testing, two additional European relations (AC10, Bi11) have been added. The new PSSMs also became available during this project, offering new and viable alternatives to the problematic ENA relations.

My basis for my present weights is as follows (see Table II-1.2):

- The selected relations are largely based on the documented test results, while weights are given more on the basis of regional and tectonic criteria. Firstly there is an overall 0.8-0.2 weight balance between GMPEs and PSSMS, justified below.
- The European models score highest on the degree-of belief scale, distributed with 30% on AB10, 10% on AC10 and 20% on the PSSMs, which now fully replace the ENA relations. The PSSM weight is distributed on three branches with stress drops of 30,

60 and 90 bars, respectively, and when these are included the European models receive altogether a weight of 60%.

- The NGA models are given a weight of 30%, equally distributed between CB08 and CY08, while the one Japanese model (Zh06) is given the remaining weight of 10%.

The overall weight balance of 0.8 and 0.2 between GMPEs and PSSMs is based on the fact that the GMPEs provide a solid empirical backbone of the model, using screened and tested relations which have been shown largely to be applicable to European conditions Stafford et al. [2008], at least outside of the near field. While the PSSMs have been judged to be of sufficient quality to replace the available ENA relations, consistent with Swiss weak motions, they do have a significant challenge related to the stress drop scaling which determine the larger motions. For these reasons I limit my overall PSSM weight to 0.2.

The way in which the overall PSSM weight is distributed among the different stress drops models is based, but only in part, on a detailed scrutiny of the test results, in particular Kühn [2011a] where eight PSSMs are tested together with the ten GMPEs (see the above review of this). A recent mixture model comparison [Kühn and Renault 2012] has also been important here, however. I have already noted the test result instabilities also for the PSSMs (it would have been better if these had been tested separately from the GMPEs), but there are still some trends to be seen:

- For the Mc 4.5 and 120 bars stress drop model, the residual plots show a fairly consistent overprediction, and also, to some extent, for the 90 bars model. The 60 bars model matches quite well while the 30 bars model underpredicts.
- For the Mc 5.5 and 120 bars model, there is also an overprediction, and an underprediction for the 30 bars model. In this case, however the 90 bars model matches a bit better than the 60 bars model, which underpredicts a little.
- These results are largely confirmed by the subsequent tests in the same report, providing intensity-based support for a model which centres on Mc 4.5 and 60 bars, branching at least between 30 to 90 bars.
- It follows from this that models based on 120 bars and higher span outside the range which is fully consistent with the ground motions inferred from intensities.

These conclusions from the PSSM test results are, however, not fully compatible with what one finds when comparing medians. The Mc 4.5 and stress drops 30 to 90 bars models plots consistently on the low side of the GMPEs, indicating a systematic shift. It is reasonable that the explanation for this can be found in Faenza and Michelini [2011] Faenza & Michelini (2010, 2011) intensity to ground motion conversion (for PGA, 0.3, 1 and 2 sec) and/or in the large uncertainty in the stress drop scaling. In any case, this shift has to be included in the discussion of how to cover the range as well as the centre.

My first approach in response to the difference between the GMPEs and the PSSMs was to extend the range of PSSM stress drops so that the range defined by the already selected GMPEs would be covered also by the PSSMs, which is demonstrated in II-1.2; II-1.3 and II-1.4

where the stress drops range all the way between 30 and 240 bars. Even in that case, however, the overlap is not very good, especially since the PSSM still are generally below the GMPEs for large magnitudes and short distances, which is the most important magnitude-distance range. So a full overlap between GMPEs and PSSMs is not possible, and neither is it desirable, since that would imply that the PSSMs are not considered to be an independent alternative, and they would only serve to reiterate the GMPE ground-motion levels.

It is important to keep in mind here that stress drop levels in a stochastic model are not necessarily mirrored well in observed stress drops from individual earthquakes; the stress drops are simply what is needed parameter-wise for the PSSM models to cover an acceptable and reasonable CBR. In a stochastic model, all parameters are strongly connected and it has been known for a long time (e.g., Atkinson and Beresnev [1997]) that one cannot isolate and interpret single stochastic-model parameters physically. This means that one should not be too controlled by what would be reasonable single-earthquake stress drops, but even so it will still be important to be informed by the intensity testing referred to above [Kühn 2011a].

A new and important testing in line with this has now been made available, namely a mixture-model test [Kühn and Renault 2012] aimed to check to what degree the observed macroseismic intensity data are consistent with the set of candidate ground motion models from each of the experts. The mixture model and the intensity testing is based on the generic Swiss rock conditions ($V_s = 1000m/s$, $\kappa = 0.017s$). The combination of $V_S - \kappa$ correction branches used to derive the expert GMPE specific Swiss generic corrections are based on the earlier (September 2012) weights, and only the median expert specific $V_S - \kappa$ correction has been used for the final comparisons. Four magnitude-distance combinations are used.

The mixture-model testing [Kühn and Renault 2012] of my preliminary model showed a reasonably good consistency between the weighted average and the intensity data. When tested individually against my preliminary GMPE model the results are still reasonable stable and therefore did not call for any adjustments in weights at this stage. This is not the case, however, with the PSSMs, where my preliminary model included 30, 60, 120 and 240 bars (with skew weights), in line with what is plotted in Figures II-1.2, II-1.3 and II-1.4, plotted for magnitudes of 4.5, 6.0 and 7.5 and frequencies of 1 and 100 Hz (PGA), thereby covering the entire magnitude-frequency range of interest.

Some examples from this latest mixture model testing are shown in Figures II-1.5, II-1.6 and II-1.7 where II-1.5 shows the GMPE and PSSM averages, indicating that the latter are quite high for large magnitudes, at least for periods of 1 and 2s. Some individual curves given in II-1.6 are more instructive, showing two important things:
(1) the GMPEs behave quite well for all of the periods tested in that they never deviate much from the mixture model;
(2) the PSSMs have a much larger spread, where the 240 bars curve is consistently much higher and the 30 bars curve is lower, at least for PGA and 0.3 s. This is even more clearly seen with a logarithmic Y-axis (not reproduced here).

The test results reproduced in Figure 2.2c are also important in that they indicate what the spread would look like when the GMPEs are combined with the lower and upper bounds for the $V_S - \kappa$ corrections. The spread from these combinations are not too great, however, and they are also centred in a reasonable way. If the PSSMs were tested similarly, however, one should expect quite extreme effects of 240 bars stress drop combined with the lowest

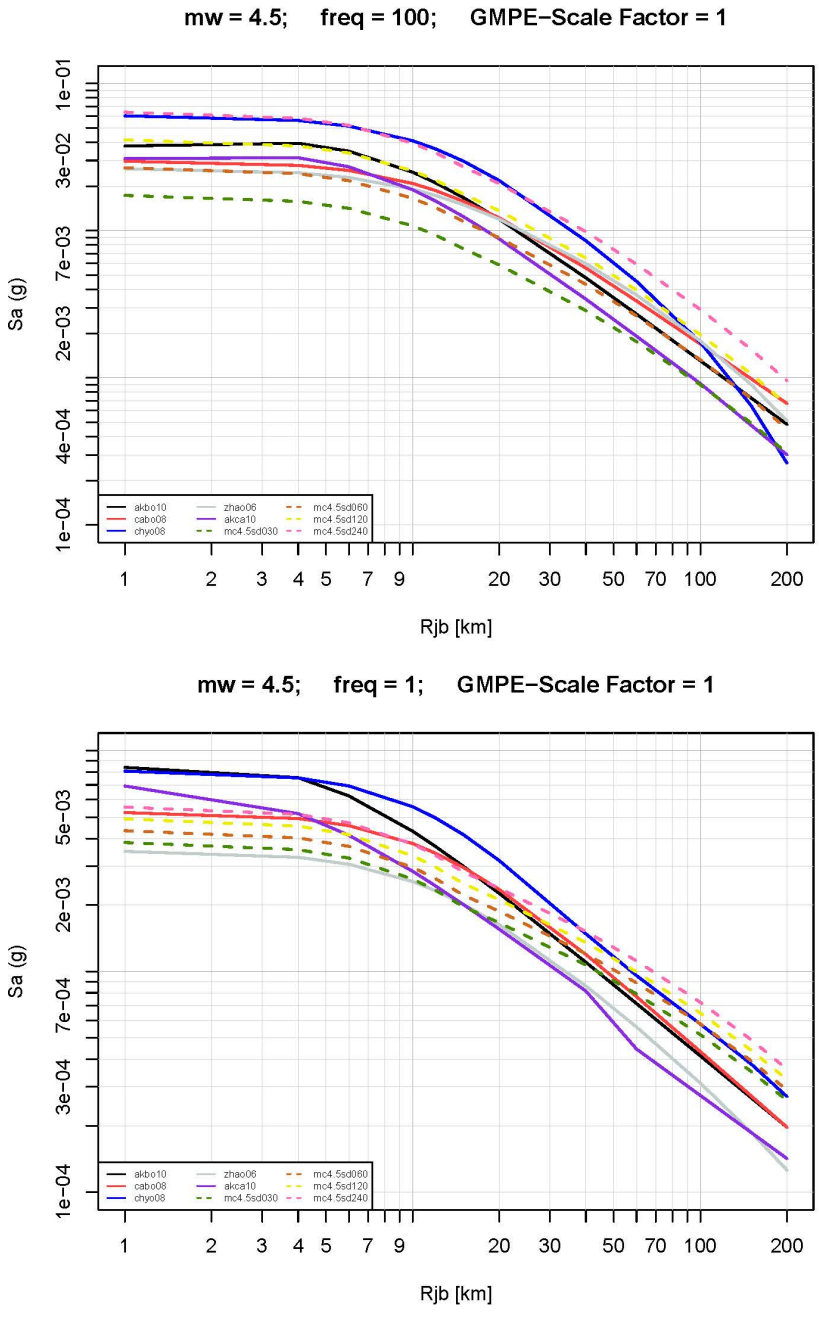

Figure II-1.2: Ground-motion prediction relations with positive weight in Table II-1.2, for M 4.5, PGA and 1s. The GMPEs are RVT FAS $V_S - \kappa$ corrected. Note that the 30 and the 240 bars stress drop PSSM models are not used in my model.

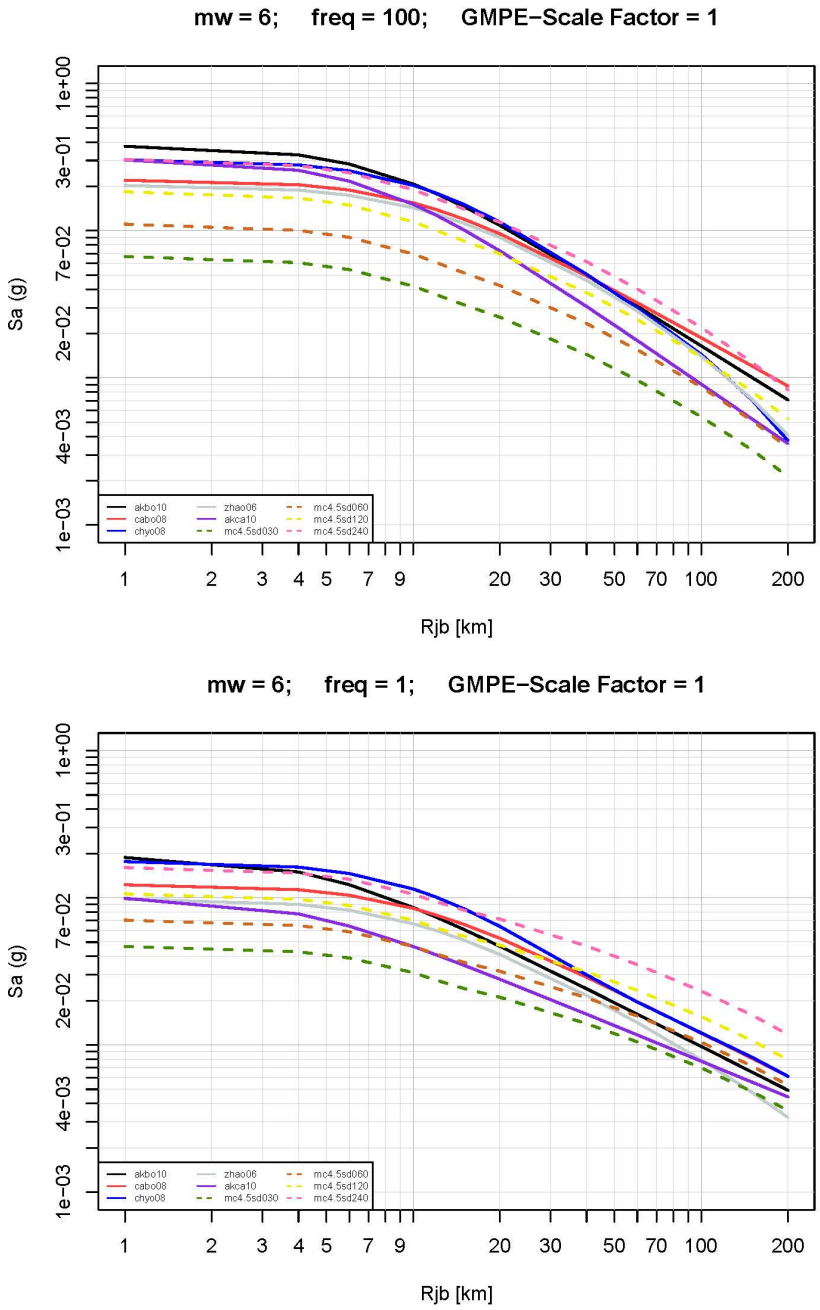

Figure II-1.3: Ground-motion prediction relations with positive weight in Table II-1.2, for M 6.0, PGA and 1s. The GMPEs are RVT FAS $V_S - \kappa$ corrected. Note that the 30 and the 240 bars stress drop PSSM models are not used in my model.

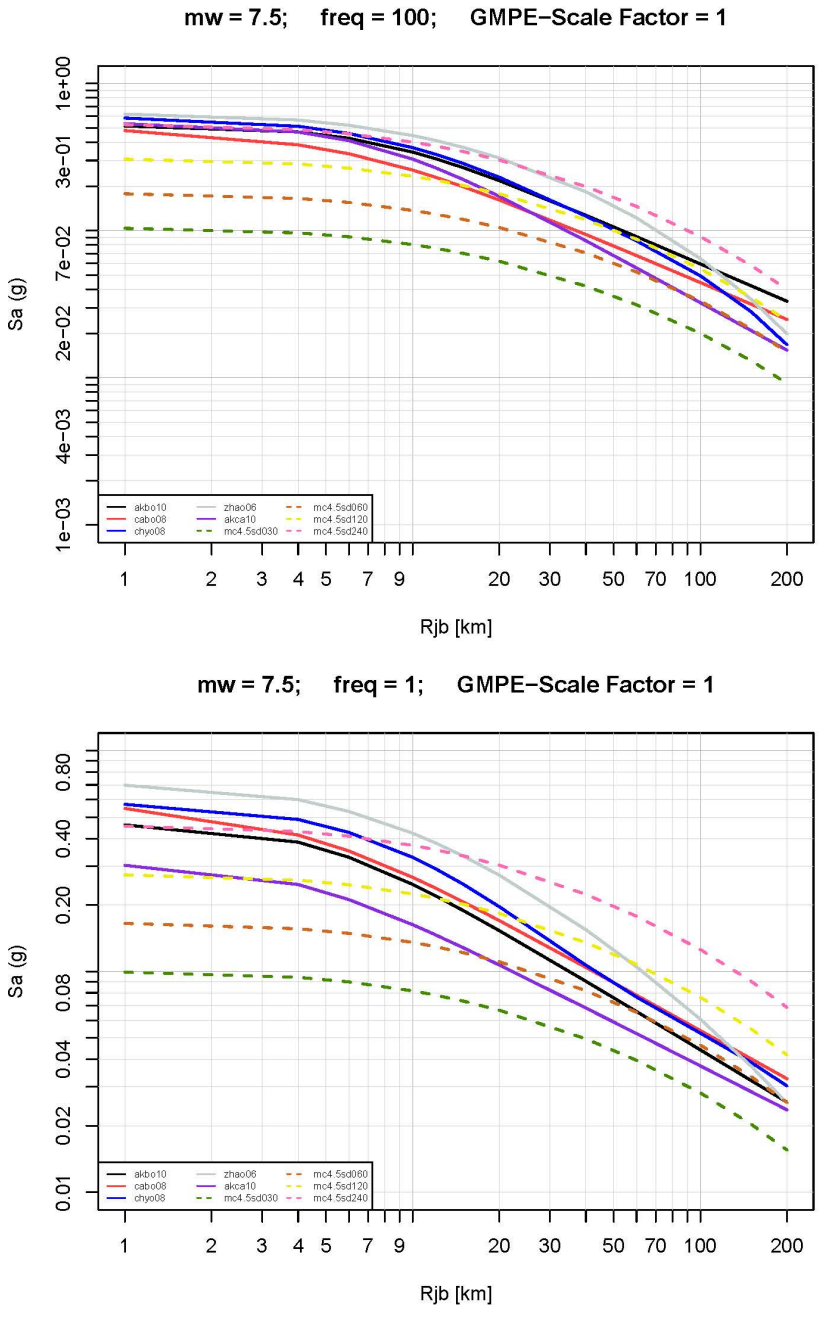

Figure II-1.4: Ground-motion prediction relations with positive weight in Table II-1.2, for M 7.5, PGA and 1s. The GMPEs are RVT FAS $V_S - \kappa$ corrected. Note that the 30 and the 240 bars stress drop PSSM models are not used in my model.

κs, and may be also for 30 bars combined with the highest κs, given the large spread in the uncorrected curves. This has convinced me to exclude both the 240 bars and the 30 bars PSSMs from my model, keeping only 60, 90 and 120 bars as shown in Table 2.2, with weights skewed towards the lower values (0.40, 0.40, 0.20) which have been shown earlier to correspond better to the intensity data.

Table II-1.2: Assigned GMPE and PSSM weight. See the main text for justification.

No	Ground-motion relations	Weights	Comments
1	AS08		
2	BA08		NGA = 0.30
3	CB08	0.15	
4	CY08	0.15	
5	AB06		ENA replaced
6	To02		by PSSMs
7	Zh06	0.1	Japan = 0.10
8	AB10	0.3	Europe-Middle East = 0.40
9	AC10	0.1	
10	Bi11		
11	PSSMs	0.2	Three branches:
			Mc =4.5, $\Delta\sigma$= 60 bars, weight= 0.40
			Mc =4.5, $\Delta\sigma$=90 bars, weight= 0.40
			Mc =4.5, $\Delta\sigma$= 120 bars, weight= 0.20

1.3.1 Centre, Body and Range

The question of how this model is satisfying the SSHAC regulatory requirements on covering centre, body and range (CBR) of the technically-defensible interpretations has been kept in mind during all of the preceding discussions, and it has also been referred to on several occasions. The very careful selection process for the GMPEs, and the subsequent extensive testing (e.g., Sammon's maps, SOMs, distance matrices, and in particular the intensities where a suite of tests have been done), have been a very important part of this. This applies in particular to the mixture-model testing presented in Figures II-1.5, II-1.6 and II-1.7 and Figure II-1.8, which provides particular support for the centring of my model. An indication to the same is given in Figure II-1.8 [Baltay and Hanks 2013] which shows a well-centred consistency between NGA and Swiss ground motions, even if the magnitude overlap is small. The GMPE range, however, is more of a challenge, referring back to the earlier discussion about the problems in defining outliers. Even so, the range given by the selected GMPEs is quite large (see Figures II-1.2, II-1.3 and II-1.4), and considered to be well justified, given our limitations.

The mixture-model test results (Figures II-1.5, II-1.6, II-1.7 and II-1.8) and the Swiss-NGA-West2 comparisons in Figure II-1.9 can also be seen as an indication for the centring of my PSSM model. Except for that, however, the PSSM model is more difficult to assess in a CBR context, which is a contributing reason for giving them a weight of only 0.20. When the weights are not lower, however, it is because they were needed in order to replace the even

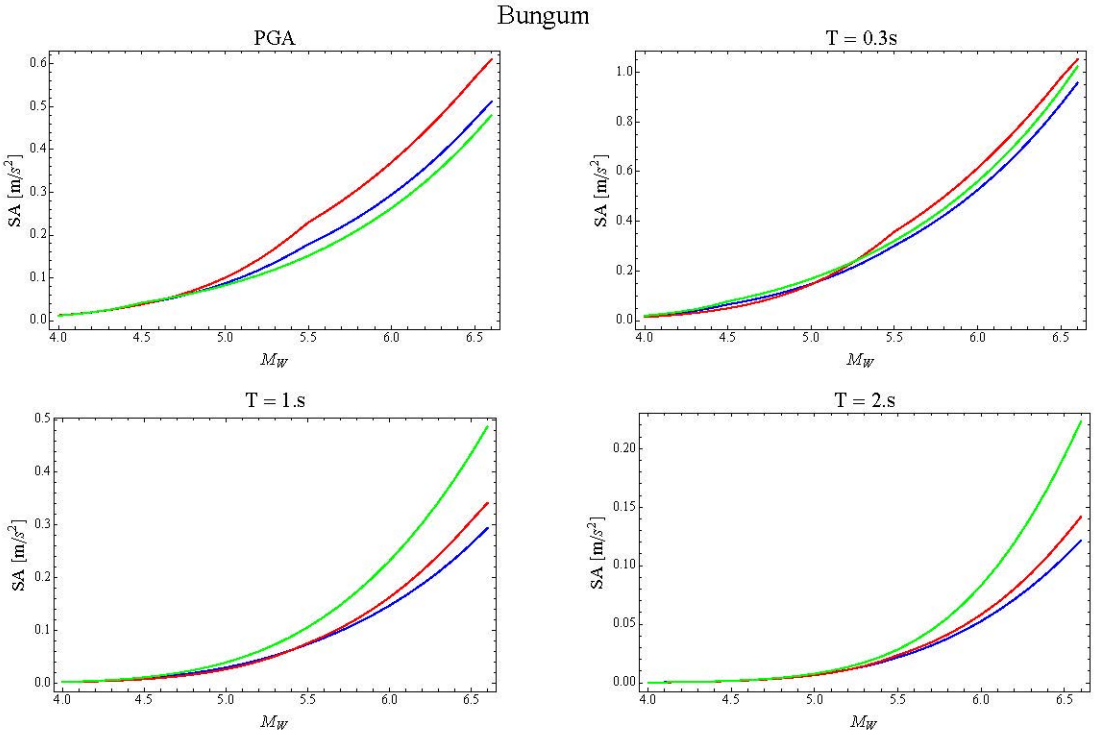

Figure II-1.5: Comparison of the mixture model (blue) with the expert's average GMPE (red) and average PSSM (green) at PGA and periods 0.3s, 1s and 2s as spectral acceleration versus magnitude. From Kühn and Renault (2012).

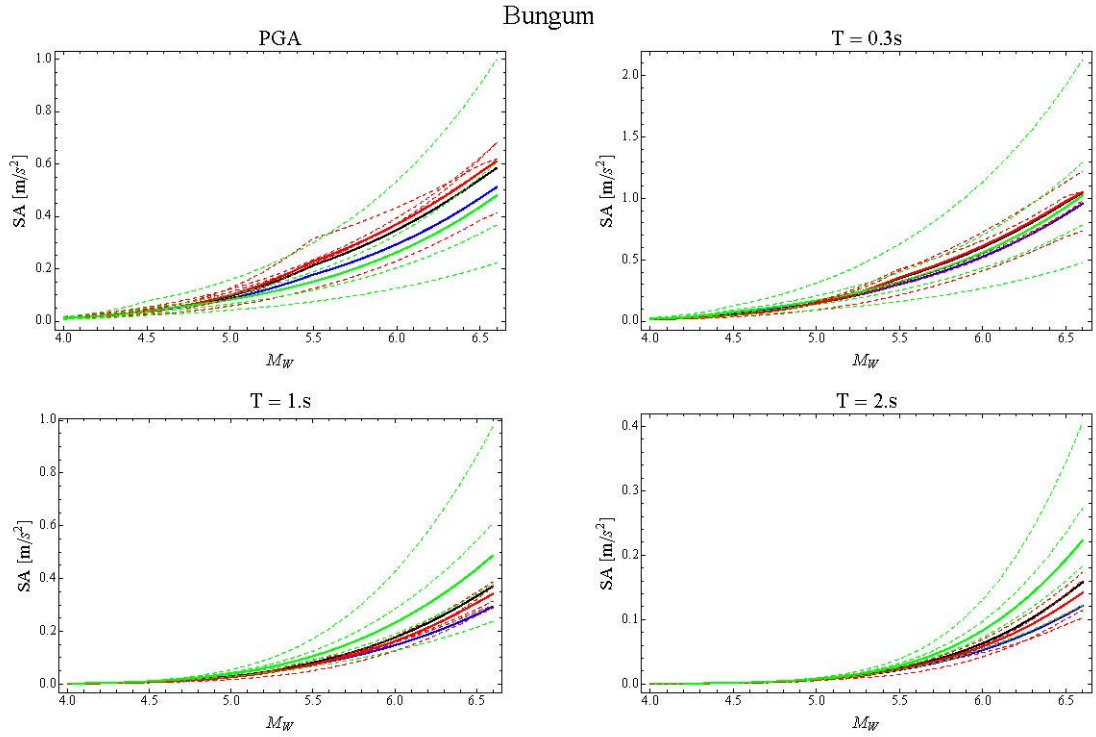

Figure II-1.6: Comparison of the mixture model (blue) with the expert's average (black) and the different GMPEs (red) and PSSMs (green) at PGA and periods 0.3s, 1s and 2s as spectral acceleration versus magnitude. From Kühn and Renault (2012).

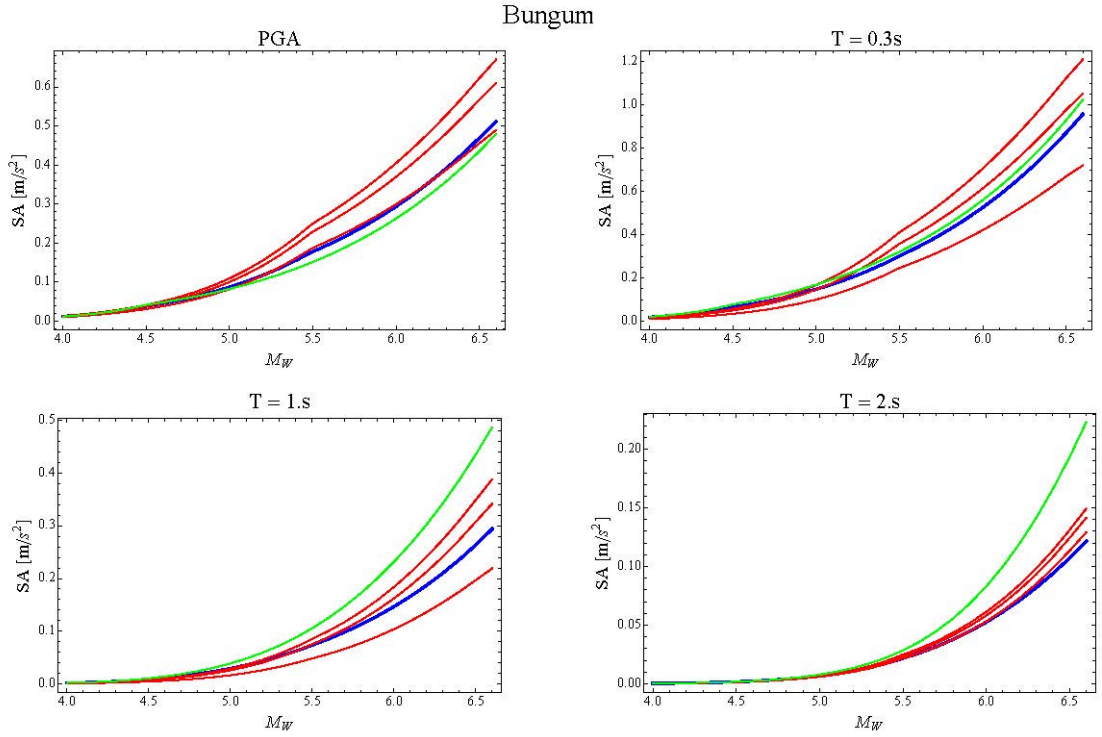

Figure II-1.7: Comparison of the mixture model (blue) with the expert's average GMPE based on the median, lower and upper bound $V_S - \kappa$ corrections (red) and average PSSM (green) at PGA and periods 0.3s, 1s and 2s as spectral acceleration versus magnitude. From Kühn and Renault (2012).

more uncertain ENA models. I concluded in Section 1.3 that the PSSMs cannot be stress drop scaled so as to cover the same range as the GPMEs since they in that case would not represent an independent alternative. The relations chosen (60, 90 and 120 bars) are therefore generally centred lower than the GMPEs, which I consider to be well justified given that they thereby are consistent with the available regional intensity data. Like for the GPMEs the range of the PSSMs is more difficult to assess, but in this case we have been well supported by the latest mixture model testing, showing that the 30 bars and even more so the 240 bars model ranges farther than can be justified. This is even more the case when combined with the $V_S - \kappa$ corrections, where some extreme combinations would be even harder to justify. So on this basis the more limited range of 60 to 120 bars seem well justified also for the range.

It is seen also (Figures II-1.2, II-1.3 and II-1.4) that the balance between the GMPEs and the PSSMs is frequency dependent, with an apparent PSSM overprediction at high frequencies and a similar underprediction at low frequencies. This could have been balanced by introducing frequency-dependent weights, but that would in turn be allowing the GMPE model to determine both the centre and the range of the PSSM model, which I have already aimed to avoid.

It is important to note also that it would not be correct if the CBR requirement were imposed individually on both the GMPEs and the PSSMs, since it is the combination of the two which counts in this case. This supports in turn that the CBR is well covered by my model.

There is also an additional study that can be referred to in support of the Swiss stochastic

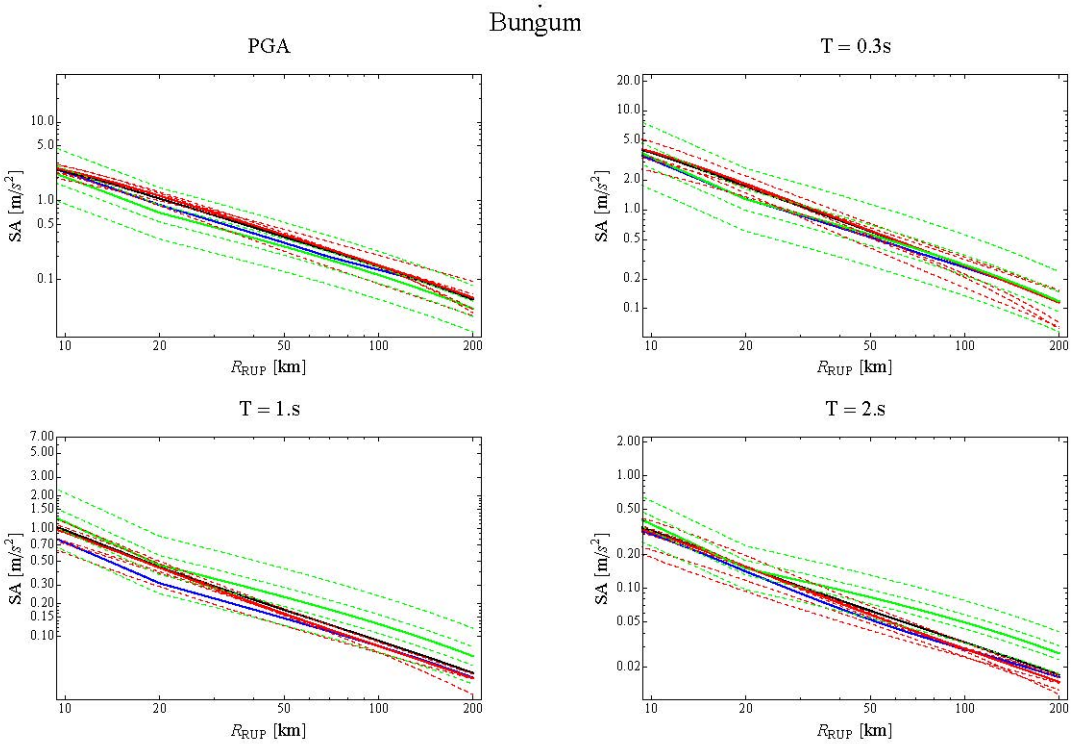

Figure II-1.8: Comparison of the mixture model (blue) with the expert's average (black) and the different GMPEs (red) and PSSMs (green) at PGA and periods 0.3s, 1s and 2s as spectral acceleration versus distance. From Kühn and Renault [2012]. Note that the outer green lines for 30 and 240 bars PSSM are not used in my final model.

model, by Edwards and Fäh [2013b], comparing simulations from the model with Japanese strong-motion data up to M 7.3. The results indicate show good agreement across a range of frequencies, which in turn supports the centring of the PSSM model.

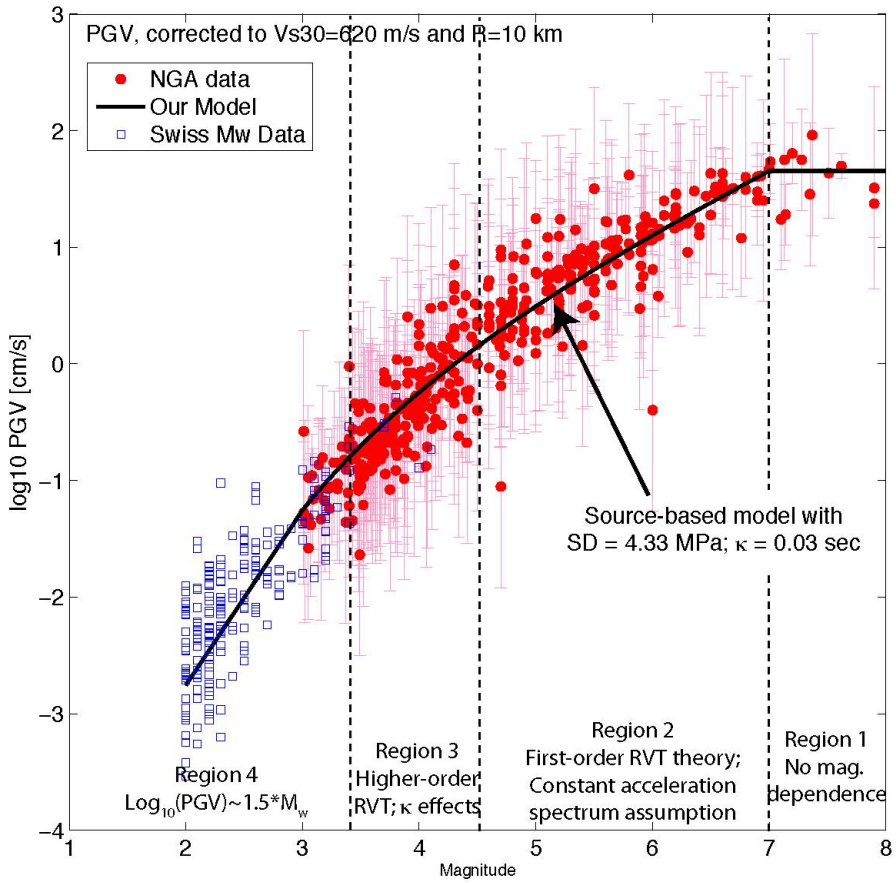

Figure II-1.9: PGV of NGA-West2 data (red dots) and Swiss data (blue squares) for data within 20 km. All data are corrected to 10 km with 1/R geometrical spreading, and to $V_{s30} = 620m/s$. The black line shows the source-based model developed for NGA-West2 with a stress drop of 4.3 MPa and a κ of 0.03s. From Baltay and Hanks [2013].

1.4 Adjustments to Median Horizontal Motions

1.4.1 Interpolation for Missing Coefficients

Interpolation for missing coefficients will be based on Stafford and Bommer [2010] and needs no further discussion here.

1.4.2 Parameter Compatibility Conversions

Parameter compatibility conversions are not needed with the present selection of ground-motion prediction equations.

1.4.3 Style-of-faulting Adjustments

Style-of-faulting adjustments will be based on Bommer et al. [2003], with details as outlined by Abrahamson [2012a].

1.4.4 Host-to-Target $V_S - \kappa$ Adjustments

The issues related to the derivation of host-to-target region scale factors for the selected GMPEs has been extensively discussed by the SP2 experts, as reviewed in detail by Abrahamson [2012a]. It was agreed that a conversion based on a full set of stochastic parameters would not be stable and therefore less attractive, in particular because the most important parameters are V_S and κ, which need to be considered together because they are correlated. Consequently it was decided to limit the host-to-target correction to a $V_S - \kappa$ correction, which is addressed in the following.

The $V_S - \kappa$ correction options that have been developed are shown in Figure II-1.10. The options are discussed in detail by Abrahamson [2012a], so only a brief review will be given here, focusing on the delivered model.

There are four main branches in Figure II-1.10, based on: (1) stochastic inversion, (2) empirical $V_{S30} - \kappa$ relations, (3) RVT based FAS, and (4) empirical constraints. I will return to each of these, but would like to note first that the following elements need to be defined for each branch:

- Host kappa estimation method, with options between deriving kappa from GMPE response spectral shape using fpeak1-3 [Al Atik 2011b] and [Laurendeau and Cotton 2012] or from observed response spectral shape using famp (e.g.Al Atik and Abrahamson [2012a]), from empirical $V_S - \kappa$ relations [Edwards 2012b]; Silva et al. [1998]; see also Edwards et al. [2011a], and from the shape of RVT-inverted Fourier amplitude spectra (RVT FAS).
- Host kappa uncertainty, based on mean and standard deviations.
- Host V_S profile type, choosing between Swiss Generic and US Generic.
- Host reference V_{s30}, with a range of three values (ref1-3) for most (but not all) GMPEs.
- Target κ, based on Edwards [2012b] and Silva et al. [1998], later to be replaced by NPP specific κs.

- Kappa correction method, with a choice of four: Standard HEM, Hybrid Empirical Method, [Campbell 2003]; Three iterative methods (PGA, 2.5, constant), Scherbaum et al. [2011]; Empirical, Al Atik and Abrahamson [2012b]; FAS scaling with RVT, Al Atik and Abrahamson [2012a].

The main decision to be taken here is which correction method to use. I did not use the standard HEM because that would reverse the earlier consensus decision by the SP2 experts to use a limited $V_S - \kappa$ correction, with two parameters (albeit correlated), instead of full stochastic correction with a large number of highly inter-dependent parameters. Also, the factors from the standard HEM approach can be very high (up to a factor of five) for high frequencies (10-30 Hz).

I also decided not to use Scherbaum et al. [2011] iterative method, which initially appeared as quite attractive theoretically but, when implemented, turned out to have some significant instabilities (as seen for example in my 24 Nov 2011 delivery). Another reason why I decided not to use the iterative approach was the fact that two new a viable correction methods now have been developed, namely the inverse RVT [Rathje et al. 2005] method which offers a scaling of FAS (Fourier amplitude) instead of response spectra, and an empirical method. The iRVT approach is documented by Al Atik and Abrahamson [2012a]; Al Atik et al. [2013] and appears as a stable and attractive approach to $V_S - \kappa$ scaling.

The new empirical approach, developed and documented by Al Atik and Abrahamson [2012b], is also showing interesting results even if it is based on a database which has potentials to be improved. In this approach Kappas are estimated from individual records using the iRVT approach, based on famp1.5 and/or famp2.0, where my preferred value is famp2.0 since that one appears to be both representative and stable [Al Atik and Abrahamson 2012b] and [Abrahamson 2012a].

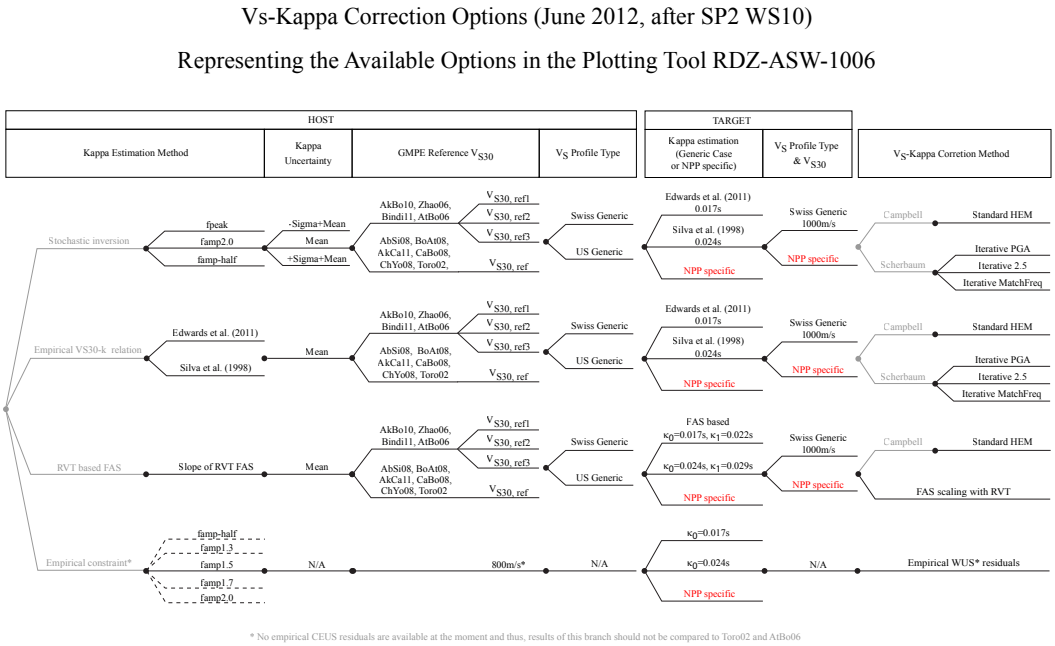

Figure II-1.10: Logic tree for $V_S - \kappa$ correction options as mirrored in the available plotting tool.

I have consequently used only the i_{RVT} approach and the empirical approach, weighting them 0.80 and 0.20, respectively, based on a degree-of-belief reasoning but also because the i_{RVT} approach has been found to be quite robust while the empirical method suffers from being derived on the basis of a limited and weakly documented database. An additional limitation for this method is that the estimated κ as based on f_{amp} 2.0 is really only a crude proxy.

I consider the empirical method as applicable to all GMPEs, with different V_{s30} and κ, on the basis that the GMPE specific f_{amp} measures capture the differences in scaling. The 0.8 RVT weight will apply to all cases and the 0.2 weight for the empirical model will apply to all of the GMPEs.

The setup for the $V_S - \kappa$ amplification factor calculations are shown in Table II-1.3. It is seen there that for the two NGA relations, only the US Generic profile is used and only a central V_{s30} reference (Ref2), given that V_{s30} is built into these relations, and therefore will provide similar κs for different V_{s30} levels (which is a short-coming of the model). The latter is the case also for AC10 where I also use Ref2 only. For the remaining two site-class based models I centre on Ref2 with a weight of 0.6, with a weight of 0.2 for each of Ref1 and Ref3. The three Ref (V_{s30}) levels used here were selected by the SP2 experts [Abrahamson 2012a], with values of 600, 800 and 1000 for AB10 and 500, 700 and 900 for Zh06. These values are admittedly uncertain, reflecting also on the weights. I do not consider Ref1 and Ref3 to be upper and lower bounds (in the strict sense), in fact, they may not necessarily be outside of $\pm 1.6\sigma$, which will justify a weight of 0.2. In Table II-1.3 the second column provides the central reference V_{s30} value for each of the GMPEs used in the model [Abrahamson 2012b].

For the resulting amplification factors, I will use a 5-point distribution with weights of 1/12, 1/6, 1/2, 1/6 and 1/12, corresponding to -2σ, -1σ, median, $+1\sigma$ and $+2\sigma$, respectively. Note that for the two site-class based models (Zh06, AB10) and for AC10 the host V_S profile is weighted 50/50 between US and SW (CH), essentially because none of these profiles apply specifically to the three relations in question (Zh06, AB10 and AC10).

Table II-1.3: Models for $V_S - \kappa$ correction factor derivation. The 0.8 RVT weight will apply to all cases and the 0.2 weight for the empirical model will apply to all of the GMPEs. See main text for details.

GMPE	Host					Target		Method	Weight
	Ref. V_{s30}	κ est.	κ unc.	V_S prof.	Ref. V_{s30}	κ est.	V_S prof.	$V_S - \kappa$ corr.	
CB08	800	RVT FAS	BE	US	Ref2	NPP	SW	RVT FAS	0.8
CY08	800	RVT FAS	BE	US	Ref2	specific	profile type	RVT FAS	0.8
Zh06	700	RVT FAS	BE	US+SW	Ref1,2,3	κs	(shape)	RVT FAS	0.8
AB10	800	RVT FAS	BE	US+SW	Ref1,2,3	as		RVT FAS	0.8
AC10	950	RVT FAS	BE	US+SW (50/50)	Ref2	defined in		RVT FAS	0.8
PSSM		famp2.0				Table II-1.7		Emp WUS	0.2

1.4.5 Kappa Estimates for NPP Hard-Rock Conditions

The four NPP sites are all on hard rock with V_{s30} values of $1100m/s$ for KKM, $1800m/s$ for KKB, $2200m/s$ for KKL and $2500m/s$ for KKG, ranging considerably also in the character of

their velocity profiles. The goal here will be to provide specific κ values for each of the NPPs, with uncertainties, so that corresponding (5-point) $V_S - \kappa$ corrections can be developed in a consistent way for each NPP site.

Ideally, κ is estimated from ground motion data recorded at the NPP sites, however, there are only limited records available that could be used for inferring κ values. Firstly, Al Atik [2011b] addressed this using a PSA approach (comparing empirical with simulated response spectra) based on five events between M 2.5 and 3.9. Unfortunately, the resolution is quite poor and it is difficult to conclude clearly from this study. A later study by Biro and Renault [2012b]; (see also Renault [2012b]), using a FAS approach [Anderson and Hough 1984], is more extensive and also more promising. The number of records is still small, but with magnitudes up to 4.2 the records have reasonably good SNRs, and the results show kappas averaging at 0.015 for KKG ($2500m/s$) and 0.025 for KKB ($1800m/s$), as also presented earlier by Renault [2012b]. These values are reasonably consistent with earlier results for the SED network [Edwards et al. 2010] and [Edwards et al. 2011a].

A summary plot from Biro and Renault [2012b] is shown in Figure II-1.11, giving values in the same range as the estimated κ values from recordings at the NPP sites. There are also indications of a significant difference between FAS and PSA derived values, for the same sites (linked by vertical lines in the plot). If this difference between FAS and OSA is sustainable it could indicate either that one of them is more reliable (e.g., Edwards [2012b], prefers FAS over PSA), but it could also indicate a method-related difference (measuring different properties of the spectrum). I will return to this below.

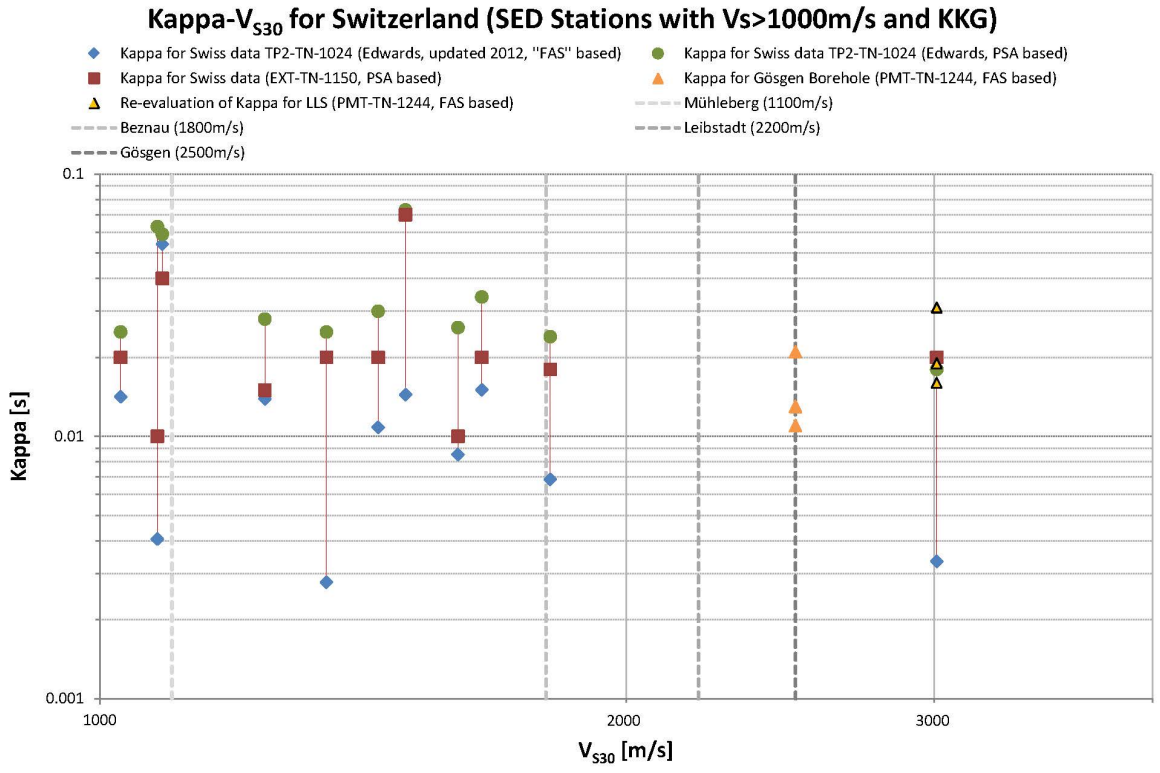

Figure II-1.11: Kappa vs. V_{s30}(log-log) for SED and some NPP sites, where the legend and the text provides more details. From Biro and Renault [2012b].

Given the uncertainty of these specific NPP κ values and the importance of the issue it is necessary to look elsewhere in order to gather additional support for these values, including relations between κ and V_{S30}. Besides Biro and Renault [2012b] several other efforts to this end have been done within this project, and in the following I will review these, and derive my model on that basis.

The most comprehensive effort towards NPP κs is that of Edwards [2012b] who has collated and summarized a large database, including Swiss (Edwards et al. [2010] and Edwards et al. [2011a]), Japanese (including Van Houtte et al. [2011]), NGA (Van Houtte et al. [2011]), French (Drouet et al. [2010]; Douglas et al. [2010]) and global sites [Silva et al. 1998]. The data are combined, regressed and presented in various ways. The main problem is again the sparsity of data for high V_{s30} values and shorter distances.

Edwards [2012b] has combined the available datasets in a number of ways, one of which is shown in Figure II-1.12, with preference to the Van Houtte et al. [2011] data, mostly from KiK and NGA. Even if the data coverage now is much improved it is seen that it is still quite poor for V_{S30} values above $1700m/s$. Edwards [2012b] routinely uses both lin-log and log-log domains, whereas I prefer to use the former, like in Figure II-1.12. Unfortunately there is no physical model that could support this, but since κ is proportional to log amplitude but less likely similarly related to V_{S30}, a lin-log relation appears to be reasonable. The distribution of the data (see subsequent figures) also seems to support this.

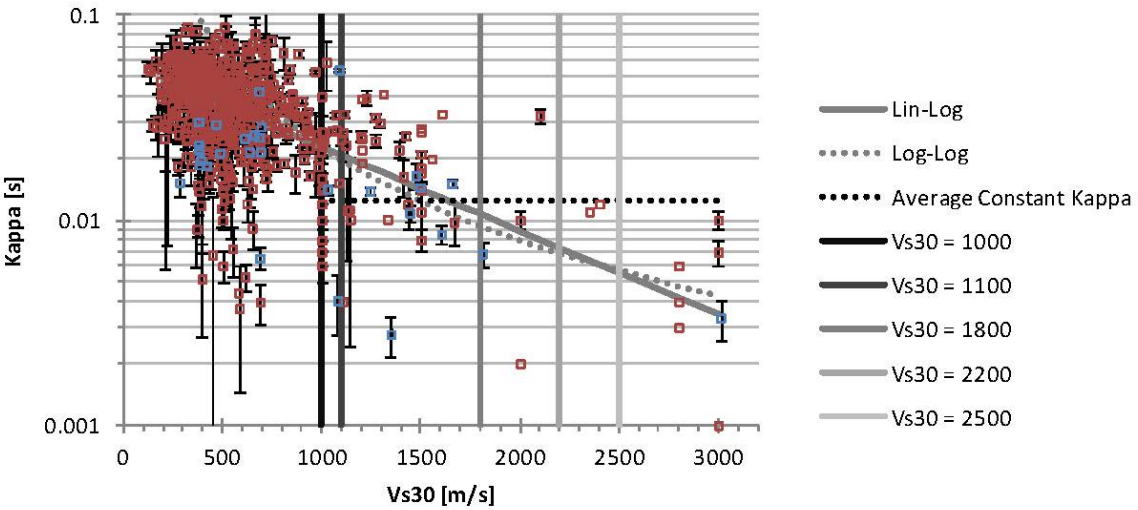

Figure II-1.12: Kappa vs $V_{S30}$for all datasets and all distances, with Van Houtte et al. [2011] preference over Edwards [2012b]. The lin-log fit is for $V_{S30} > 800m/s$ and is shown along with the V_{S30} values of the NPPs (vertical bars). The constant average kappa is computed over $V_s30 > 1000m/s$. The blue boxes were added 13 Jun 2012 (included in the original regressions, but not plotted).

A regression done by Edwards [2012b] on the basis of the data shown in Figure II-1.12, for data above $800m/s$, leads to a κ of 0.022 (see Table II-1.4), which is a typical SED value, for $Vs_{30}1100m/s$ (KKM). For $2500m/s$ (KKG), however, the value is as low as 0.005. It is indicated that the values for $V_s30 > 1700m/s$ are largely controlled by the data at lower V_{s30}values and therefore they reflect an extrapolation more than a regression. Table II-1.4 also shows average and weighted average κs above different threshold velocities, limited to

1500m/s, also reflecting the amount of limited data for higher V_{S30}values.

An overview of the different lin-log kappa predictions, based on different datasets, is given in Figure II-1.13, which shows the results from Figure II-1.12 and Table II-1.4 but also include also some RVT-based estimates. Figure II-1.14 finally provides some weighted averages for the same databases as also seen in Table II-1.4, but only for V_{s30}values up to 1500m/s.

Given that the underlying databases are quite different this may appear as being reasonably encouraging because the goal here is to be able to specify κ values for each of the NPP sites, which range in V_{s30} from 1100 to 2500 m/s (the range covered in Figure II-1.13). However, if keeping in mind that both Figures II-1.13 and II-1.14 are regressed for $V_{S30} > 600m/s$ it appears that the extrapolation problem is even larger than what it was for Figure II-1.12, where the threshold was $V_{S30} > 800m/s$.

Table II-1.4: Predicted κ at the V_{S30} values of the rock reference and the NPP sites.

(a) Log-average κ values given a minimum V_{S30} threshold, with standard deviations.

V_{S30} [m/s]	κ [s]	
	lin-log	log-log
1000	0,024	0,021
1100	0,022	0,019
1800	0,011	0,010
2200	0,007	0,008
2500	0,005	0,006

(b) Log-average κ values given a minimum V_{S30} threshold, with standard deviations.

$V_{S30,min}$ [m/s]	Average κ [s]	$-\sigma$	$+\sigma$
800	0,0169	0,0012	0,0013
1000	0,0125	0,0010	0,0010
1200	0,0106	0,0008	0,0009
1500	0,0064	0,0005	0,0006

(c) Weighted log-average κ values given a minimum V_{S30} threshold.

$V_{S30,min}$ [m/s]	Weighted Avg. κ [s]
800	0,0220
1000	0,0175
1200	0,0144
1500	0,0101

Another useful summary of all of this is given in Figure II-1.15 where most of the data and regressions discussed in the above are shown, including some KKG (Goesgen) borehole values (see also Figure II-1.11). This figure illustrates quite well the dilemma one is facing here, with quite dispersive values for higher V_{S30} values and with regressions that are largely extrapolations in that range.

Before I reach a conclusion here, however, it could be useful to revisit some more of the results that have only briefly referred to. The French data, used also by Edwards [2012b], are certainly of importance here because of its proximity to Switzerland. One figure from Drouet et al. [2010] is reproduced here in Figure II-1.16 and one from Douglas et al. [2010] in Figure II-1.17, both showing generally consistent values with those presented already. This consistence is of course expected since these French data also are used by Edwards [2012b]. The global relation of Silva et al. [1998] in Figure II-1.16 is plotted also in Figure II-1.15.

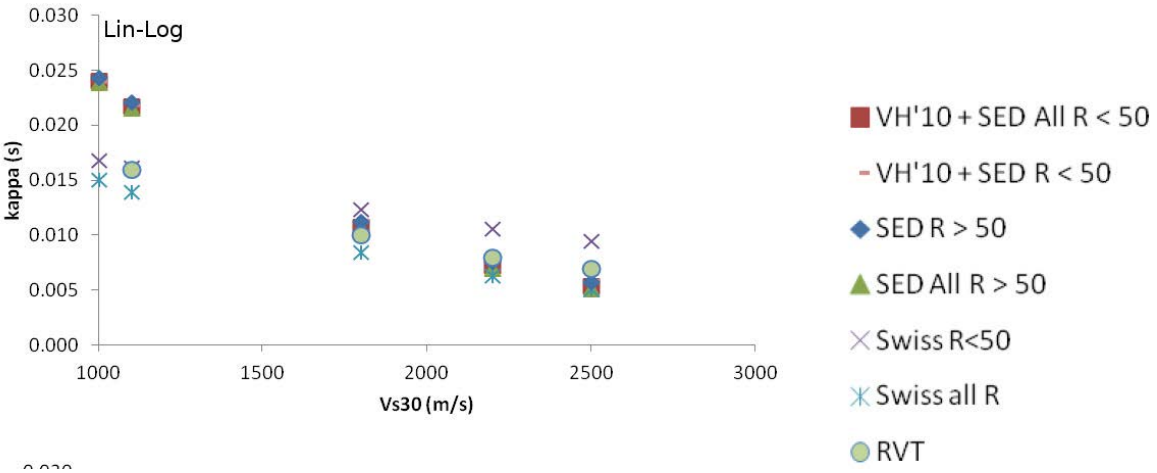

Figure II-1.13: Overview of lin-log κ predictions for different dataset combinations, for $V_{S30} > 600m/s$. [Edwards and Fäh 2012b].

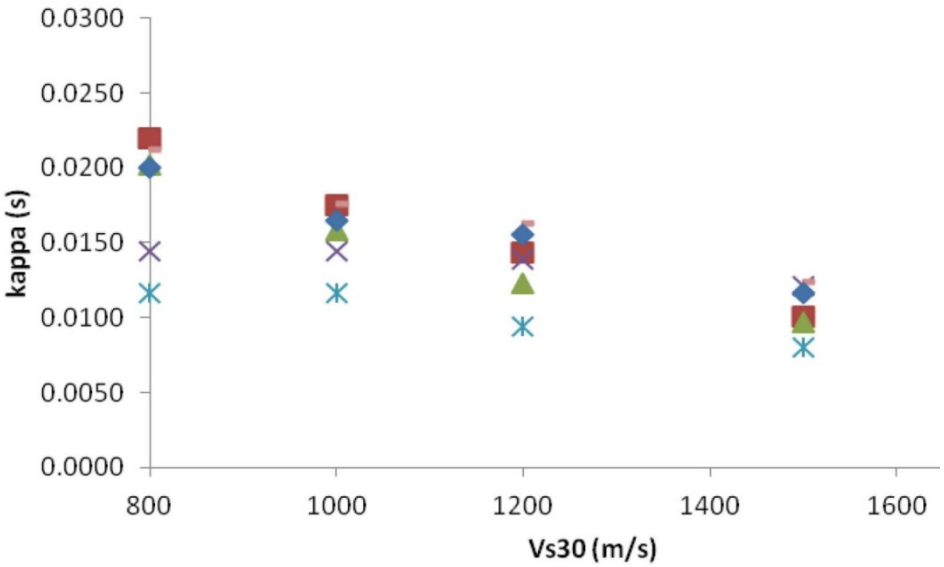

Figure II-1.14: Overview of weighted average κ for different dataset combinations, for $V_s30 > 600m/s$ [Edwards and Fäh 2012b]. Legend as for Figure II-1.13.

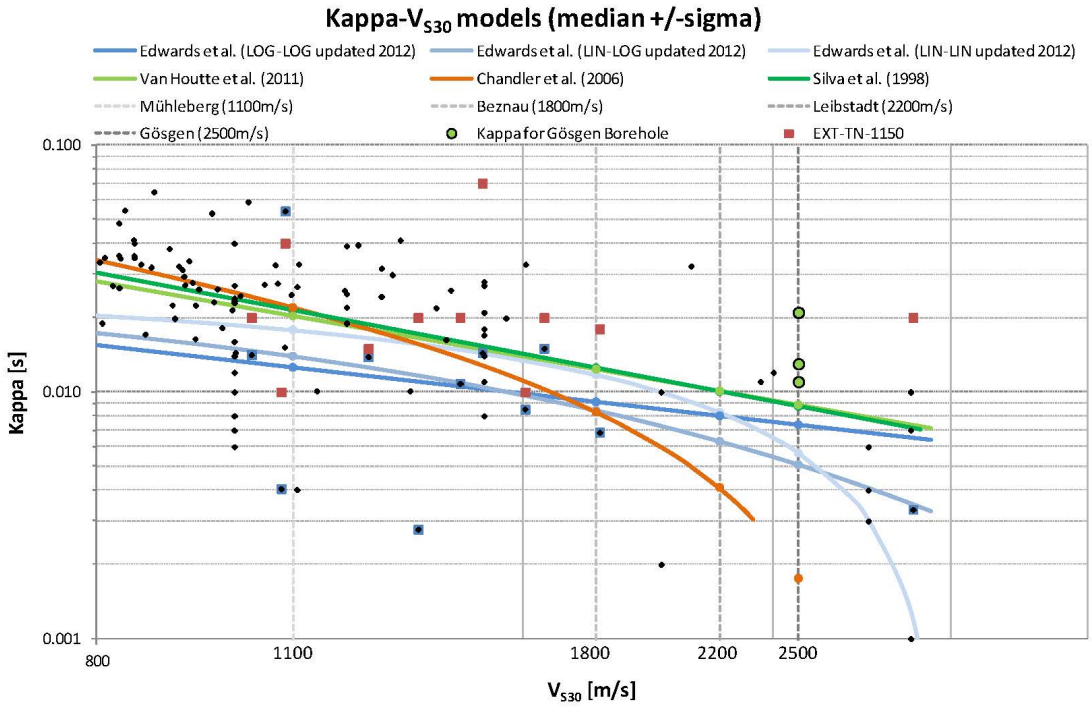

Figure II-1.15: Summary of $\kappa - V_{S30}$ data points and empirical equations discussed earlier, together with some KKG borehole values. [Abrahamson 2012b]. A similar version is used by Renault [2012b].

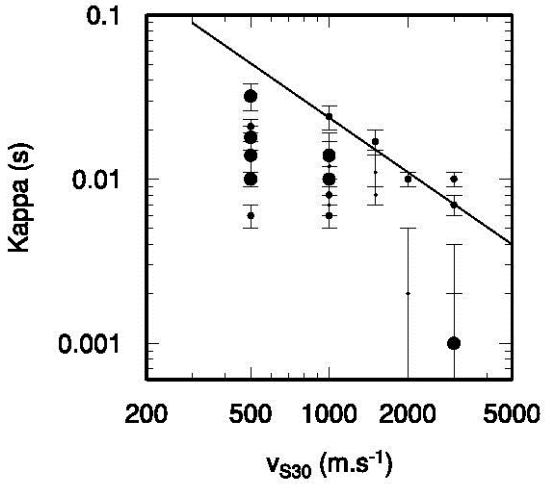

Figure II-1.16: Plot of the V_{S30} versus the κ-values (circles) compared with the relationship derived by Silva et al. [1998]. The size of the symbol refers to the quality of the V_{S30}. From Drouet et al. [2010].

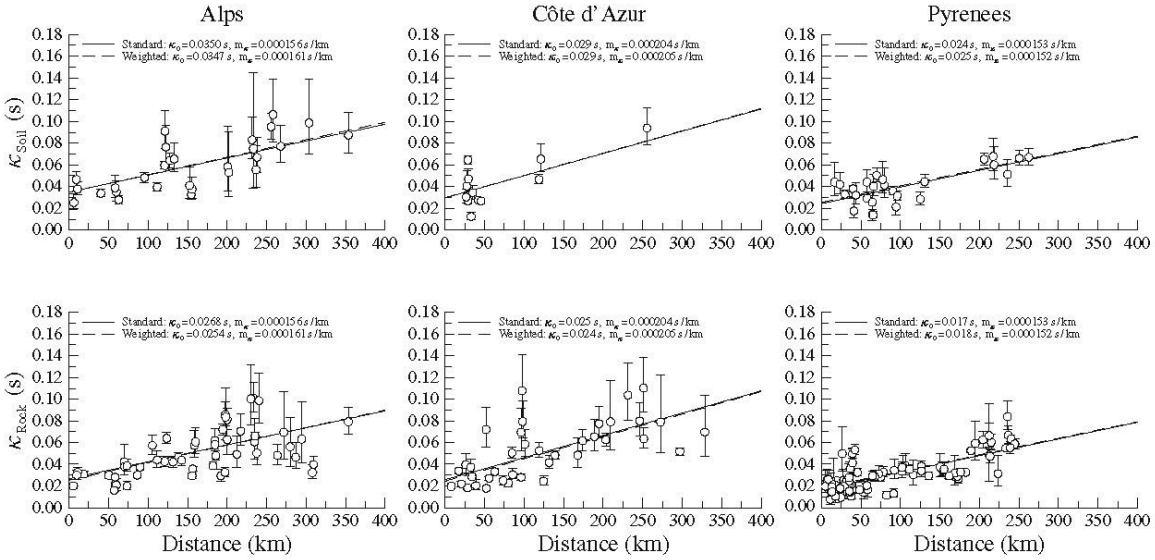

Figure II-1.17: Distance dependence of κ-values for three regions in mainland France. The top plots present the results for stations located on soil. The bottom plots show the results for stations located on rock. From Douglas et al. [2010].

Another important study is that of Van Houtte et al. [2011], from which a figure is reproduced in figure II-1.18, where again data and models from a number of studies, most of them reported on already, are plotted together.

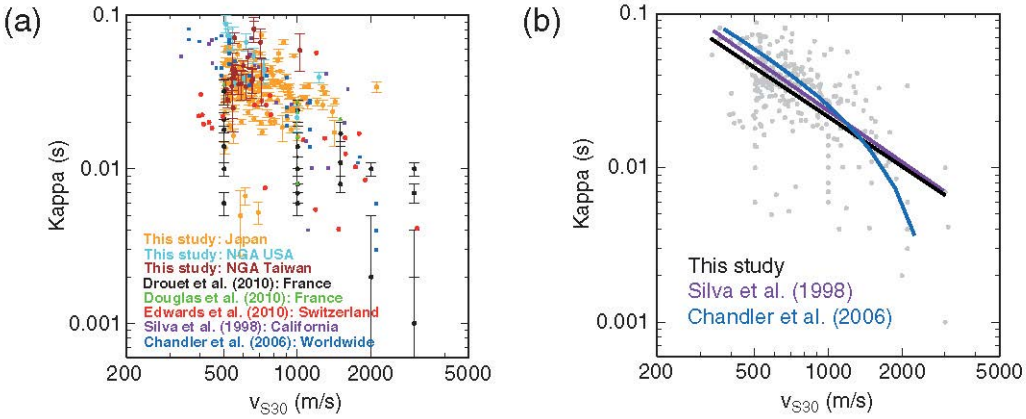

Figure II-1.18: (a) $\kappa_0 - V_{S30}$ data from various papers (see legend). (b) The same data are plotted together with the correlations from Silva et al. [1998], Chandler et al. [2006], and the present [Van Houtte et al. 2011] study. From Van Houtte et al. [2011].

A new study from Silva and Darragh [2012] should also be included in this review, and here the data are plotted in Figure II-1.19 together with Silva et al. [1998]. The data used there show no relation at all to V_{S30} and therefore does not provide much guidance, except to indicate that κ for hard rock conditions may be relating very poorly to V_{S30}. In this figure, an eyeball kappa average for $V_{S30} > 1000m/s$ is about 0.020s.

During the last phase of this work yet another analysis of Swiss data was conducted by Ktenidou et al. [2012a] and discussed at a web-meeting on July 4, 2012, between the SP2 experts [Abrahamson and PMT 2012]. The main purpose of this reanalysis was quality

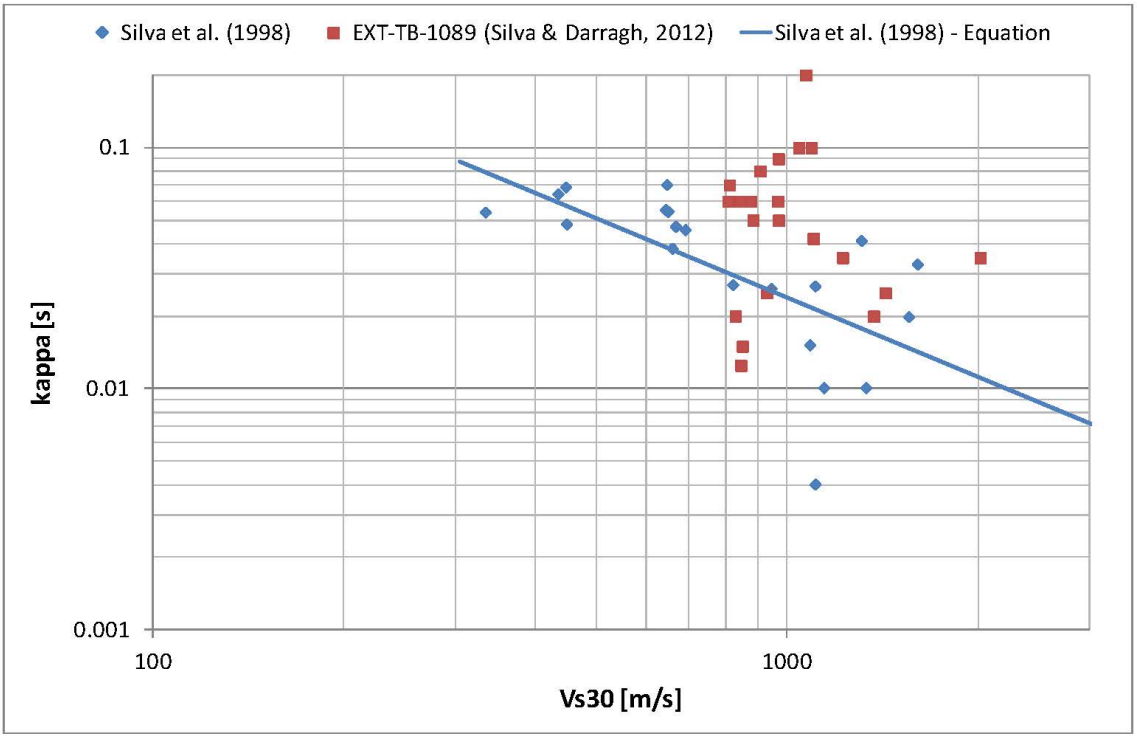

Figure II-1.19: Data and model from Silva et al. [1998] and data from Silva and Darragh [2012]. From Abrahamson [2012b].

control, related to the results from NPP stations and the SED hard-rock station LLS, earlier analysed by Edwards [2012b] and later in more detail by Biro and Renault [2012b]. The LLS station is important since it has been assigned a V_{s30} of 3000 m/s and thereby is an end member on the rock hardness scale.

The approaches used in these three studies has been shown by Abrahamson and PMT [2012] to have some important differences, such as with respect to selection of data (noise ranges, distance range), to the way the fit was done (whole spectrum or only part of it) and to acceptance of results (negative kappas or not). This clearly explains many of the differences between the results and helps to understand the associated uncertainties.

A summary of Ktenidou et al. [2012a] results for LLS is given in Figure II-1.20, accepting only data with less than 17% difference between components (an additional requirement to use data only up to 30 Hz, because of system response problems, further increased κs). The heavy green line is a regression under the restriction of $Q \approx 1300$, while the thin line is a free regression implying a much higher Q. The scatter in these data is, however, so large that it is obviously problematic to derive an acceptable κ_0 based on any distance regression. To me it is equally important to look also at the close-distance data in Figure 3.12, which are from $M \leq 4$ events with κs ranging between 0 and 0.040 s, averaging at around 0.025 s. Ktenidou et al. [2012a] preferred value is 0.020 s, but she does not say to which extent this is influenced by the regression and by the close-distance data, respectively. The way the re-evaluated data compare with earlier results is summarized by Ktenidou et al. [2012a] in Figure II-1.21.

It seems to me that Ktenidou et al. [2012a] results in Figure II-1.21 largely corroborates Biro

κ_0=0.025 s : average/upper bound (high Q)
κ_0=0.012 s : lower value (for fixed slope with average Q~1300 based on previous results at HG,HH)

κ_0=0.020 s : preferred value

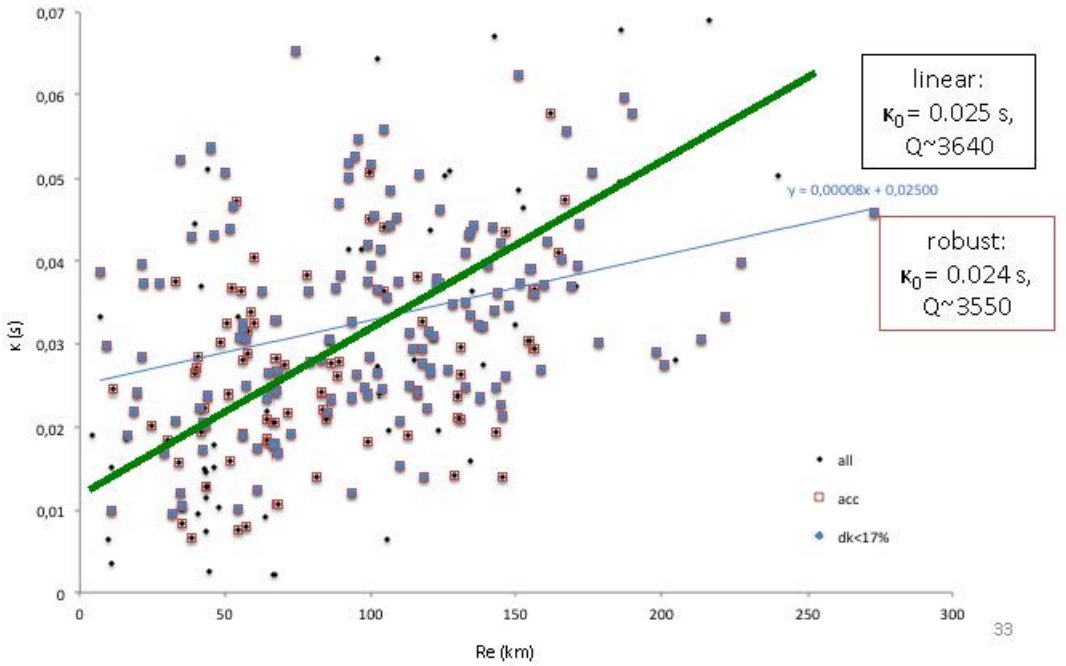

Figure II-1.20: FSA-based κ vs. distance for station LLS (from Ktenidou et al. [2012a]). See main text for details.

and Renault [2012b] earlier results (see Figure II-1.11) in that none of them can clearly confirm a kappa decrease with increasing V_{S30} claimed by Edwards [2012b] and shown in the same figures. In addition, Ktenidou et al. [2012a] has shed important lights on the uncertainties in κ estimation. It also seems to me that the differences between these three studies largely may be related to the way in which the analyses have been conducted, as summarized by Abrahamson and PMT [2012]. Edwards [2012b] use of the entire spectrum and his acceptance also of negative values may be important here.

At the SP2 WS11 in Zürich on January 16-18, 2013, a new kappa evaluation report was presented by Olga Ktenidou [Ktenidou and Van Houtte 2013] in which another reanalysis of SED rack station data are conducted aimed at resolving epistemic uncertainties pertaining to κ, in particular the influence of data used and Q constraints. A good summary of both is given in Figure II-1.22, with a modest sensitivity to database scenario but with a great sensitivity to Q, where the preferred one for this inversion is 1900 as compared to the established value of 1200 [Edwards et al. 2011a]. For the two cases the κ-values range between 0.016 and 0.036 s and between 0.007 and 0.026 s, respectively.

In order to demonstrate how these κ-values compare to earlier ones an important summary figure from Ktenidou and Van Houtte [2013] is reproduced in Figure II-1.23, showing very high values as compared to earlier ones. The only way to "lower" the new κ-values would be to impose a lower Q, which is not consistent with what the inversion provides. This sensitivity to Q is well known, of course, but this study demonstrates better that earlier ones the nature

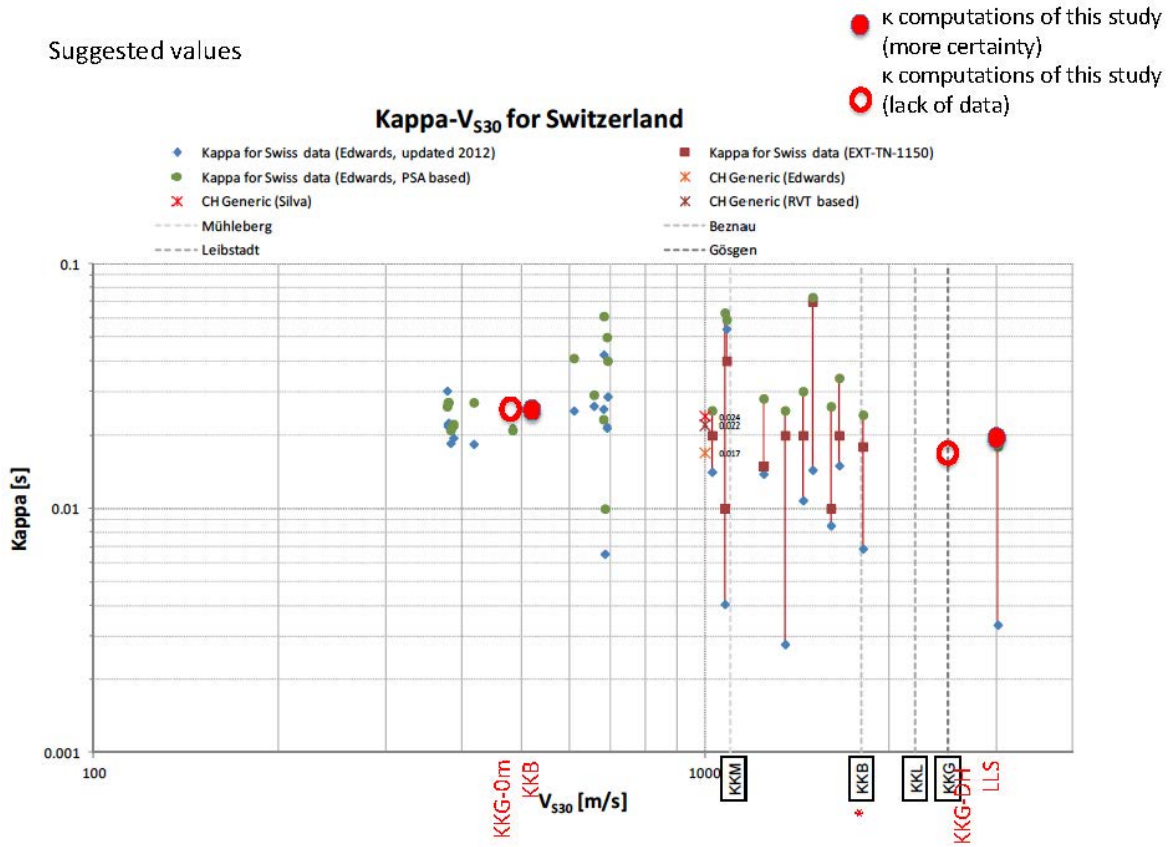

Figure II-1.21: Summary of $\kappa - V_{S30}$ results for Switzerland, including reevaluated data for NPP stations and the LLS station (see also Figure II-1.11). From Ktenidou et al. [2012a].

and importance of this sensitivity. The average κ for Q=1200 is 0.015, for a free Q (scenario 6) it is 0.025, and for Re<40 km (scenario 2) it is 0.033 s. This clearly poses an additional challenge in determining justifiable κs and uncertainty ranges.

I should also refer to a new study from SED [Edwards et al. 2013b] in which Japanese and Swiss data are used based on a quarter-wavelength representation of velocity profiles. In this case (see Figure II-1.24) the κ-values taper off at about 0.020s for higher velocities. The authors emphasize, however, that these values are upper bounds and that there are extrapolation problems and limited resolution. I therefore cannot trust these values even if this is the first time that a functional relationship between V_{S30} and κ has been developed.

What has been seen in this extensive review is not uncommon in science, namely a mixture of consistency and inconsistency, and a large scatter. Given this uncertainty an important limitation is that we do not have a theoretical model for the relation between κ and V_{S30}, except for the general understanding that the near-site attenuation should be decreasing with increasing rock hardness. The fact that V_{S30} is a crude proxy of the site conditions combined with the uncertainty with respect to which parts of the local site conditions that influence κ the most, are additional problems here.

Before I conclude I can summarize my main findings as follows:

- The NPP records are important but they are not by themselves sufficient as a basis for a κ model for the NPP sites. The local NPP values are on the high side of those often

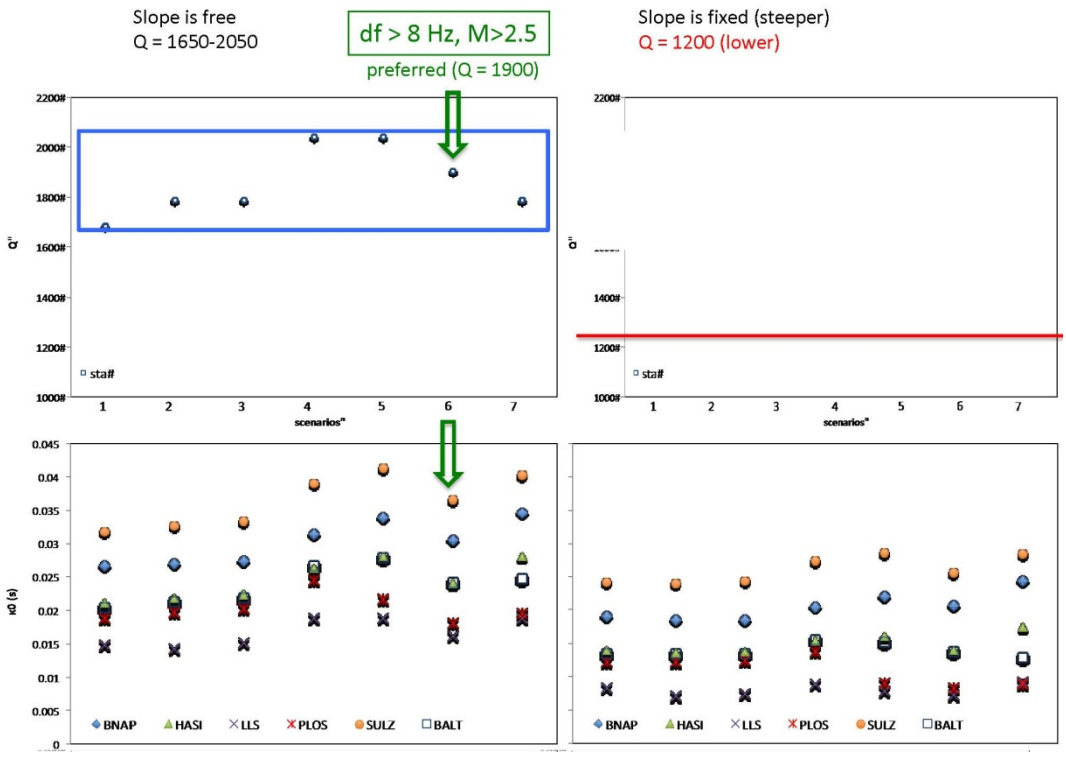

Figure II-1.22: Summary of κ inversion results from Ktenidou and Van Houtte [2013] where the left frame is with a free Q and the right one with a Q fixed at 1200 [Edwards et al. 2011a], which is also the value used for the Swiss stochastic model [Edwards and Fäh 2013b]. For each frame seven data selection scenarios are used, the preferred one (no 6) being indicated with an arrow.

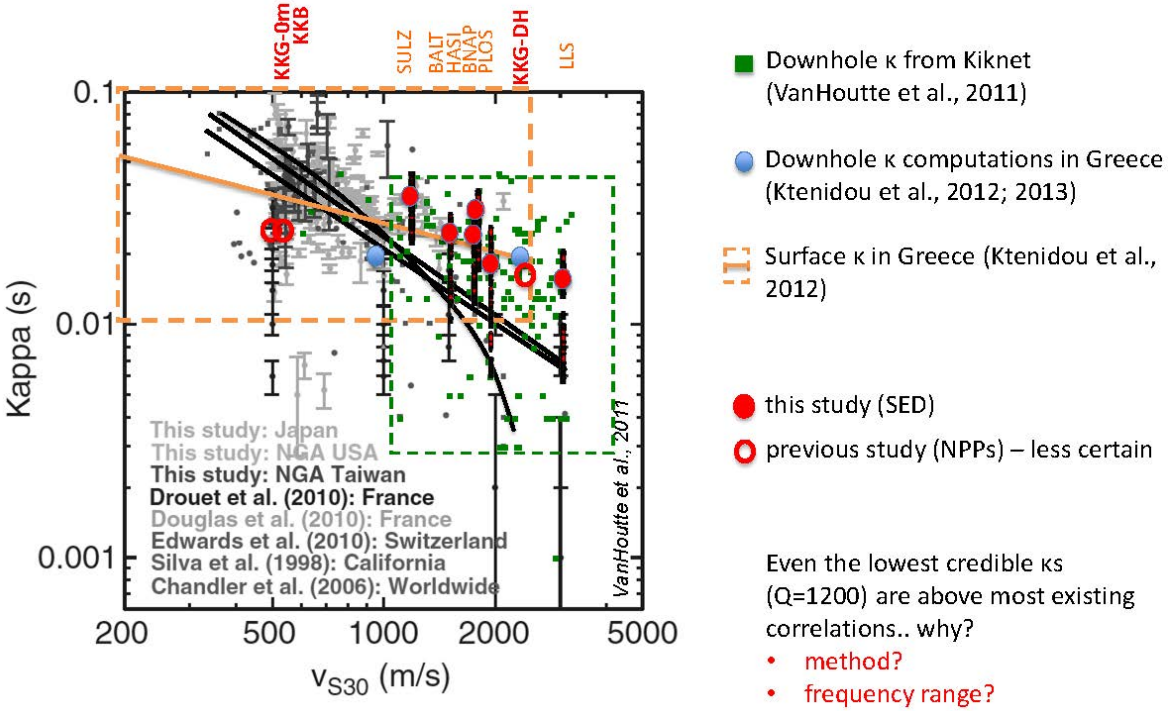

Figure II-1.23: The new κ preferred inversion values of Ktenidou and Van Houtte [2013] together with a suite of earlier results, many of which are shown also earlier in this evaluation summary.

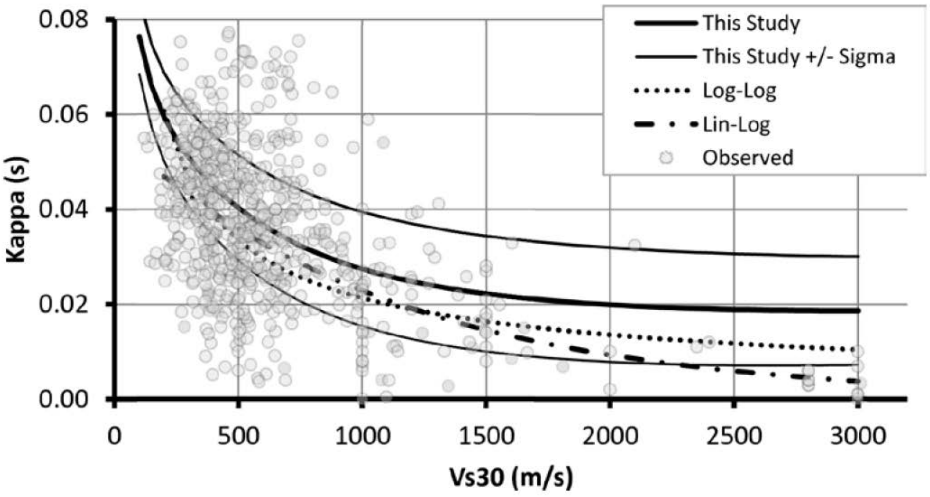

Figure 13. *Comparison of the relation developed in this study with Vs30 – kappa data pairs from Japan, Switzerland and worldwide (Edwards et al., 2011; Van Houtte et al., 2011; Silva et al., 1998; Drouet et al. 2010) and with a log-log and log-lin fit of data.*

Figure II-1.24: $V_S - \kappa$ relation developed by Edwards and Fäh [2013b] plotted on top of data from Japan, Switzerland and worldwide [Edwards et al. 2011a; Van Houtte et al. 2011; Silva 2008; Drouet et al. 2010].

obtained for the same V_{S30} values in other studies.

- The records from the additional Swiss (SED) stations are also important since they are more numerous and cover a wider distance and magnitude range, even if the latter also here is limited as compared to global data. The main problem here, however, is the sensitivity to Q restraints that was so clearly emphasized by Ktenidou and Van Houtte [2013].

- Observations from other studies for the range of NPP V_{s30} values (1100 to 2500 m/s) are relatively few, and more important, they show a great scatter.

- When a large V_{s30} range is considered kappa is found to decrease with increasing V_s30, as expected theoretically, but the scatter is large. We do not, however, have a theoretical model for kappa vs. V_{s30} and the scatter is such that it is difficult to judge whether a least squares fit should be in lin-log, log-log or lin-lin space. All these models are used (mostly the first two), and this adds an additional uncertainty to values that largely are based on extrapolations.

- As already indicated, κs are estimated either from Fourier amplitude spectra (FAS) or from response spectra (PSA), with quite varying results. Since the latter is an indirect method which requires stochastic simulation this is likely to yield additional uncertainty as compared to FAS-based methods, even if host κs have to be PSA-derived.

- I could note in passing also that there (in some of the studied reviewed) not always seems to be a clear distinction between k and $k0$ (the influence of distance), but this is well covered by Ktenidou et al. [2012a] and Ktenidou and Van Houtte [2013] and not believed to have any noticeable effect on my use of the results from the different studies.

The conclusion that I draw from this is that the predictive equations for κ vs. V_{S30} are of limited value, and that we essentially have to revert to assessment of individual data points. Initially the SP2 experts discussed deriving NPP kappa values from a regression like the one in Figure II-1.12, which includes all available data at that time, and all distances, and which resulted with a regressed κ of 0.05 s at 2500 m/s. An alternative here could be to use only distances less than say 50 km, but in that case one would not be able to take advantage of the distance dependence of κ for establishing the intercept value $k0$ (note that Ktenidou and Van Houtte [2013], found an average kappa of 0.033 s when limiting the distance to 40 km).

The problem with this, however, is that this model significantly underpredicts the local NPP values and also a number of other individual observations, such as in Figures II-1.11, II-1.15 and II-1.21. There are also important relations such as Silva et al. [1998] and Van Houtte et al. [2011] that give a κ of about 0.01 s at 2000 m/s. The French data also seem to have few observations with κ below 0.01 s.

In a previous version of this evaluation summary I therefore concluded with a lin-log relation defined by a κ of 0.021s for V_{s30} = 1100 m/s (KKM) and a κ of 0.010s at 2500m/s (KKG), which is reasonably close to the Silva et al. [1998] model. These values are also reasonably close to those suggested about a year ago by Abrahamson [2011b] and Abrahamson [2011c], based on some of the same studies.

However, after the latest re-evaluation by Ktenidou et al. [2012a] I can no longer justify properly a model which has a V_{s30} dependent kappa within this fairly narrow range of hard-rock velocities (1100-2500 m/s), in spite of the fact that Ktenidou [2012] brings back such a dependence, albeit with a new quantitative understanding of the great sensitivity to Q. My conclusion is therefore to us a single kappa value for all of the four NPP sites, independent of V_{s30}. This is reasonably consistent with the data in Figure II-1.21 (and other similar plots) and a lack of significant distance dependence is also what is seen in Figure II-1.19, developed by Silva and Darragh [2012].

I also need to note that this review has revealed also another important property of kappa, namely that it now seems to evolve more as a parameter for a method than as a physical parameter. As pointed out by Abrahamson and PMT [2012], when fitting full spectrum, κ is correlated with other parameters, but when fitting the slope within a limited frequency band the correlation will be reduced, but at the expense of spectral amplitude. A question that derives from this is if different κ values may be needed for the GMPEs and the PSSMs, related in turn to PSA and FAS based κ inversions.

The classical FAS approach [Anderson and Hough 1984] uses only the high-frequency part of the spectrum. This is the approach used also by Biro and Renault [2012b], Figure II-1.11, and by Ktenidou [2012], Figure II-1.21. In the analysis of Edwards [2012b], on the other hand, the FAS-derived κs for the Swiss stations are derived from the entire spectrum (above the noise), including also potentially negative slopes. These are the values most applicable to PSSM corrections, shown in Edwards [2012b] Fig. 6, also shown here in Figure II-1.11 Biro and Renault [2012b] and in Figure II-1.21 [Ktenidou 2012]. Edwards [2012b] is not giving the actual values and there are some unclear differences between his Figure 6 (all data) and Figure 7 (<50 km), and in terms of averages there will also be differences depending on using linear or logarithmic domain. A good average, however, seems to be around 0.012 s. For

GMPE applications the amount of data are much larger and more diverse, as reviewed in the above, and here I find that a good average at this stage will be of the order od 0.020 s.

More recently a report became available [Renault and Biro 2013] which addressed specifically the centring of the $V_{S-\kappa}$ corrections by studying within-event residuals for recordings at Swiss stations for which κ-values are available, discussed also at an SP2 web meeting on 01 Feb 2013 and with an example shown in Figure II-1.25. A negative slope on the left side (no correction) is consistent with the need for a $V_{S-\kappa}$ correction while a positive slope on the right side (after correction) indicates that the correction is too strong. This is what we see (in Figure II-1.25 the correlation changes from -0.293 to +0.656), and a similar behaviour is seen also for the PSSMs. A pure V_S-correction does not change the slope at all.

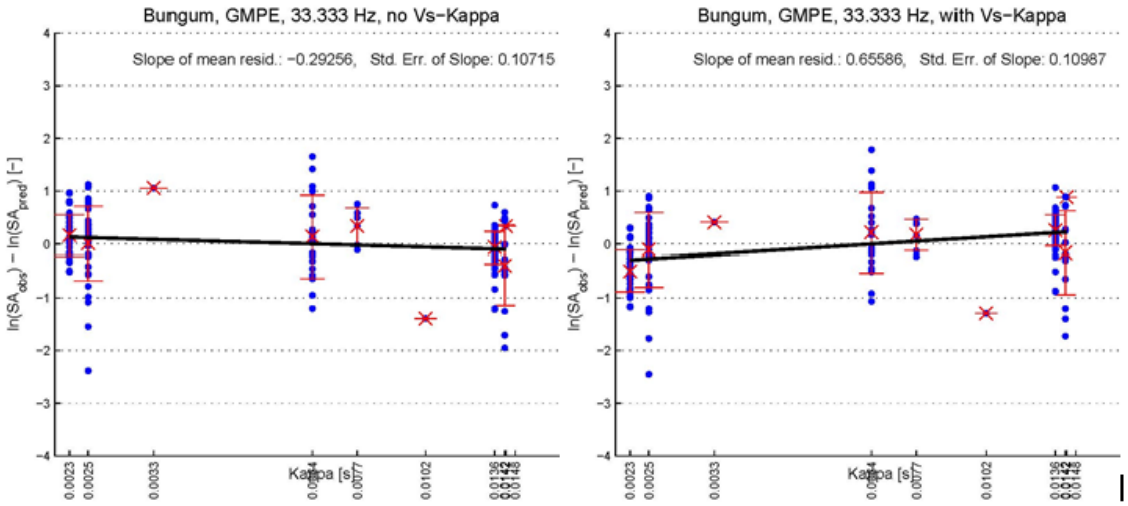

Figure II-1.25: Residual plots vs. κ with a without $V_S - \kappa$ corrections for GMPE and 33 Hz. From Renault and Biro [2013].

The analysis of Renault and Biro [2013] was done for 1, 10 and 33 Hz, and PGA, and as expected the slope is unchanged for 1 Hz while the effect is weaker for 10 Hz and PGA than for 33 Hz. This evaluation can be used and interpreted to a certain extent in the same way as the mixture model comparison, except that this one is based on recordings while the mixture model is based on intensities.

Figure II-1.25 indicates that my $V_S - \kappa$-correction, based on an initial κ value of 0.020 s, is a bit stronger than what is needed to achieve a balanced centring, and there are two ways in which this could be explained, namely the correction methodology and the κ values on which the correction is based. Changing the target κs alone while keeping the rest unchanged is not a safe way to solve this since it that case it would take (at least) one subsequent iterative testing in order to check the effects of an adjustment on the centring. A better solution could be to introduce an additional branching between a V_S-correction only and a full $V_S - \kappa$-correction. Judging from Figure II-1.25 and the more complete information in Renault and Biro [2013] I found that a weight of about 3/4 for a full $V_S - \kappa$-correction should give a more balanced adjustment, leaving the remaining for a pure V_S correction. This model was, however, also used only as a preliminary model, since a later update of kappa values and centring tests

provided more stable estimates, as documented in the following.

Following this, another study has been conducted [Abrahamson 2013a], comprising a new assessment of observed κs for hard-rock Swiss stations and with a careful attention of quality, as discussed also at a PRP SP2 workshop 19-20 Sep 2013. The study also contains a scaling exercise, in which the $V_S - \kappa$-correction method is applied to small-magnitude NGA-West2 GMPEs and subsequently compared to the new observations from Swiss stations. The analysis is based on an iterative i_{RVT} method [Al Atik and Youngs 2013] in which a target/host κ ratio is derived which gives zero residuals, resulting in a "fictitious" κ which could also contain source effects. Since the exercise also is based on the assumption of similarities between small (NGA West2, used in comparing with Swiss data) and large magnitudes (NGA West 1, providing the applied GMPEs) it is clear that the fictitious κs can only be used as an indication for the κ range for which centring (zero residuals) is obtained.

The hard-rock station κs are shown in Table 3.3, where the eight "low" (FAS) κs average at 0.009 s, the "high" (PSA) κs at 0.026 s, and the Ktenidou [2012] κs at 0.027 s.

Table II-1.5: Summary of SED hard-rock station κs, including also those of Ktenidou [2012]. The "low" κs are based on FAS estimation and "high" κs are based on PSA estimation, applicable to PSSM and GMPE relations, respectively. From Renault and Biro [2013].

Station	V_{S30} [m/s]	"low" κ [s]	"high" κ [s]	*Std. Dev.*	κ [s] by Ktenidou	*Std. Dev.*
BRANT	1079	0.00333	0.063	*0.00113*	N.A.	N.A.
SLUB*	1094	0.0257	0.017	N.A.	N.A.	N.A.
SVIO*	1124	0	0.024	N.A.	N.A.	N.A.
SULZ	1168	0.01361	0.025	*0.00077*	0.03643	*0.00186*
AIGLE	1228	0.01425	0.028	*0.00082*	N.A.	N.A.
BALST	1332	0.00235	0.025	*0.00081*	0.02414	*0.00139*
WIMS	1440	0.01021	0.03	*0.00095*	N.A.	N.A.
SIOV	1453	0.0162	0.017	*0.00302*	N.A.	N.A.
GIMEL	1496	0.01481	0.073	*0.00094*	N.A.	N.A.
BNALP	1601	0.01419	0.034	*0.00069*	0.03057	*0.00114*
HASLI	1603	0.00769	0.026	*0.00078*	0.02401	*0.00142*
PLONS	1794	0.00638	0.024	*0.00097*	0.01819	*0.0016*
LLS	2925	0.00254	0.018	*0.00076*	0.01627	*0.00115*

The resulting centred (fictitious) κs, based on the same eight stations, are shown in Table II-1.6 , where the average of the κ 0 values is about 0.025 s, but with a noticeable GMPE-related spread from 0.020 to 0.029. If all 12 stations are used the κ-values are a little higher, with an average of 0.027.

The individual data points are shown in Figure II-1.26, plotted against V_{S30} for each of the 12 stations in Table II-1.5 and classified by GMPE. The values are centred in the sense that the values will yield zero residuals for the NGA West2 models at low magnitude.

The results of the centring are shown in Figure II-1.27, with uncorrected residuals, V_{S-only}-corrected residuals and κ-corrected residuals for the ASK13 model. What is seen there is that the "high" (PSA) κs give a very good match (zero residuals) for frequencies above 10 Hz, while for low frequencies there is a systematic overestimation.

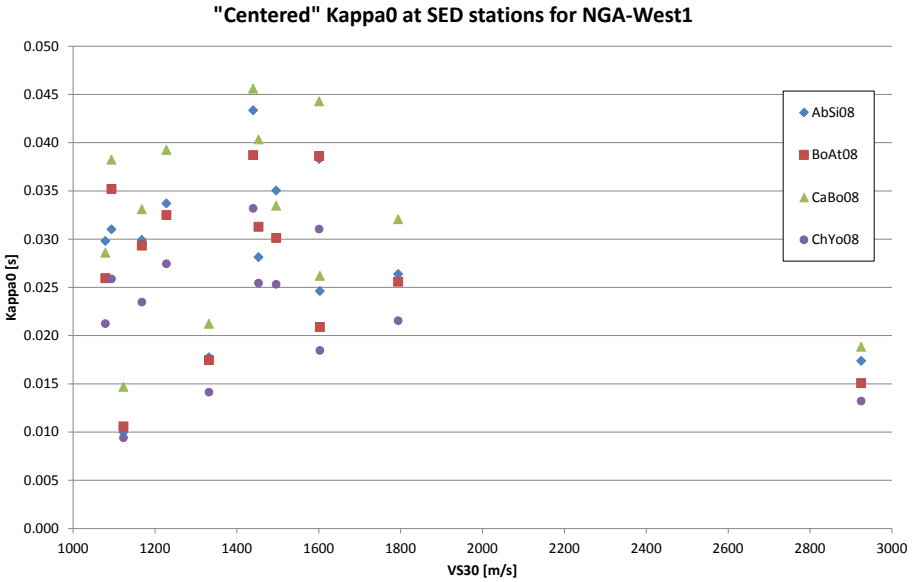

Figure II-1.26: Centred κ 0 values shown against V_{S30} for each of the SED stations. From Renault and Biro [2013].

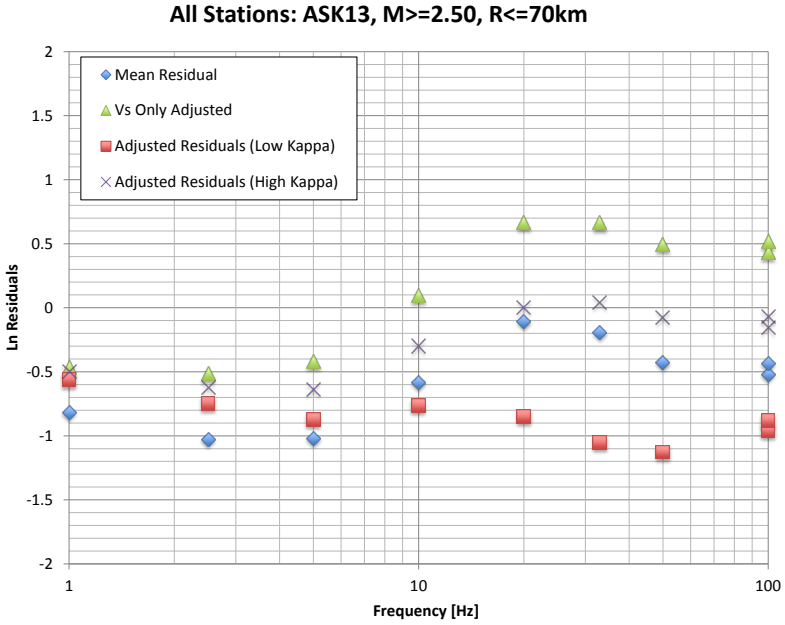

Figure II-1.27: Example plot of residuals (Obs.-Pred.) for ASK13 against frequency. From Renault and Biro [2013].

Table II-1.6: Centred κ_1 and κ_0 values for the NGA-West1 models at large magnitude, as weighted averaged over the SED stations, compared to the host κ_1 of each model. From Renault and Biro [2013].

	Avg. without (BRA,GIM,) SIO, SLU, SVI		
GMPE	Host κ 1 [s]	Target κ 1 [s]	Target κ 0 [s]
AbSi08	0.047	0.034	0.026
BoAt08	0.04	0.032	0.024
CaBo08	0.039	0.038	0.029
ChYo08	0.031	0.027	0.02

The overestimation at low frequencies was investigated by Poggi and Fäh [2013] in order to see if it could be removed through an adjustment of the V_S-profiles. While it was possible to find a velocity profile that resulted in near zero low frequency residuals, the inverted profiles gave too large reductions in the shallow velocity profile, leading to unrealistic values. So other factors seem to contribute here, such as source effects.

This latest study has given me a valuable additional basis for the κ assessment, and in two ways. Firstly it provides a new assessment of Swiss hard-rock κs, centred on about 0.025 s but with a considerable spread (cf. Figure II-1.26, and secondly it provides a centring for about the same values of κ (cf. Figure II-1.27, last column). This gives me a sufficient justification for adjusting my target GMPE (PSA based) κs from 0.020 to 0.024 s, while the PSSM (FAS based) κs are kept at 0.012 s. Proper centring is now achieved without the use of a V_S-only branch.

The estimation of uncertainty bounds on these κ values, as also included in Table II-1.7, is also quite difficult, because they essentially cover epistemic uncertainties which to a large extent have to be based on expert judgments. The σ values from the regressions of Edwards [2012b] are ranging from 0.0005 for 1500 m/s to 0.0013 at 800 m/s (Table II-1.4), while Abrahamson [2011b] and Abrahamson [2011c] indicates total uncertainties which are significantly higher than this. The scatter in the $\kappa - V_{s30}$ plots naturally reflect an unknown combination of real variation due to physical effects not picked up by the simple V_{s30} parameter, and the uncertainty in the measurements. There are also uncertainty estimates available for individual data points for most of the studies as seen in the plots above, varying considerably.

There is only limited uncertainty guidance from both the regressional scatter and the single point uncertainty, except that these estimates should be lower bounds. In defining the uncertainty model, an important question is if the uncertainty changes with V_{s30} (like for the regressions), but I see no reason why this should be so, unless it can be found that hard-rock recordings systematically come from lower magnitude earthquakes (which could be the case).

The uncertainty model will, therefore, have to be based on expert judgment guided by empirical data. I have concluded that the uncertainty can be best justified if it is symmetric in log domain, corresponding to a $\kappa - V_{S30}$ representation in lin-log domain. Also, since κ (in the present definition) is required to be non-negative it will be bounded on the low side, also supporting a log-linear symmetry.

The implication of this is that lower and upper bounds are obtained by dividing and multiplying

by a given factor. It is useful to note here that Abrahamson [2011b] has used a factor of 1.3 on both sides (not claiming to cover epistemic uncertainties) while Abrahamson [2011c], claiming to cover epistemic uncertainties, has a factor of about 1.8 (on both sides) for Silva et al. [1998] and a factor of about 1.3 on the low side and 2.3 on the high side for Edwards et al. [2010]. It is not stated, however, what lower and upper bounds means in terms of standard deviations.

My approach is to use weights on the three values of 0.2, 0.6 and 0.2, respectively, corresponding to $\pm 1.6\sigma$. After testing a number of uncertainty factors in the range between one and two I ended up with a factor on the order of 1.5, which would have given a range from 0.016 to 0.036, resulting in a kappa uncertainty range between 0.013 and 0.030 when centred on 0.020 (for GMPEs), and between 0.008 and 0.018 when centred on 0.012 (for PSSMs). When comparing this range with the individual data points shown in Figures II-1.11 to II-1.21 there are several (but not too many) values both below and above, thereby justifying, for each of the NPPs, my central value as well as my range.it seems like a reasonable range, while the new data points just discussed indicate that both the low and the high value could have been a bit higher. I have therefore settled on a factor of 1.4 for the lower value and a factor of 1.6 for the higher value, as shown in Table II-1.7. A similar range is given for the PSSM κs. The previous arguments for a site (V_{S30}) independence of κ are still valid.

When applied to the PSSMs this requires another clarification about how to convert to correction values, because the PSSMs were all developed for a κ value of 0.017 s and $V_{S30} = 1000m/s$. This should be done by developing scaling functions by evaluation of response spectral ratios between a κ of 0.017 s and the NPP target κ values, to be done for each of the three values. This will imply $4 \times 3 = 12$ versions.

Given the fairly wide uncertainty range for the target κs it could happen that some of the higher values would be found to exceed one or more of the host (GMPE) κs, implying that one would have a deamplification situation. In order to be methodologically consistent this would have to be acceptable.

For the PSSMs there is an additional issue related to the possible correlation between target κ and stress drop, such that a higher stress drop would give a higher κ. Abrahamson [2013b] has referred to this briefly with an indication that the western US data gives correlations on the order of 0.2-0.7, and that a reduction in kappa range coming from this correlation would be $\sqrt{1-r^2}$. For $r = 0.5$ the reduction factor would be 0.87, which is not much given the large uncertainties in kappa, but the main problem here is the uncertainty in the correlation coefficient. Also, I have not access to the underlying study, and for both of these reasons it is problematic to base my model on these numbers.

Independently of this a similar study has been done by Edwards [2013], comparing kappa residuals with stress drop residuals based on two different approaches. In both cases no correlation has been found, even if there is a significant scatter, concluding that the SED site specific $k0$ values are robust. This helps me to conclude not to include the effects of such a correlation in my model, assisted also by the fact that my range of stress drops (60 to 120 bars) is fairly limited, thereby avoiding extreme combinations of high stress drops and low kappas.

With the final κ model finished I now have the complete model so that also the resulting 5-point distributions of the $V_S - kappa$ correction factors can be computed, as shown in Figures II-1.28 and II-1.29, for GMPEs and PSSMs, respectively.

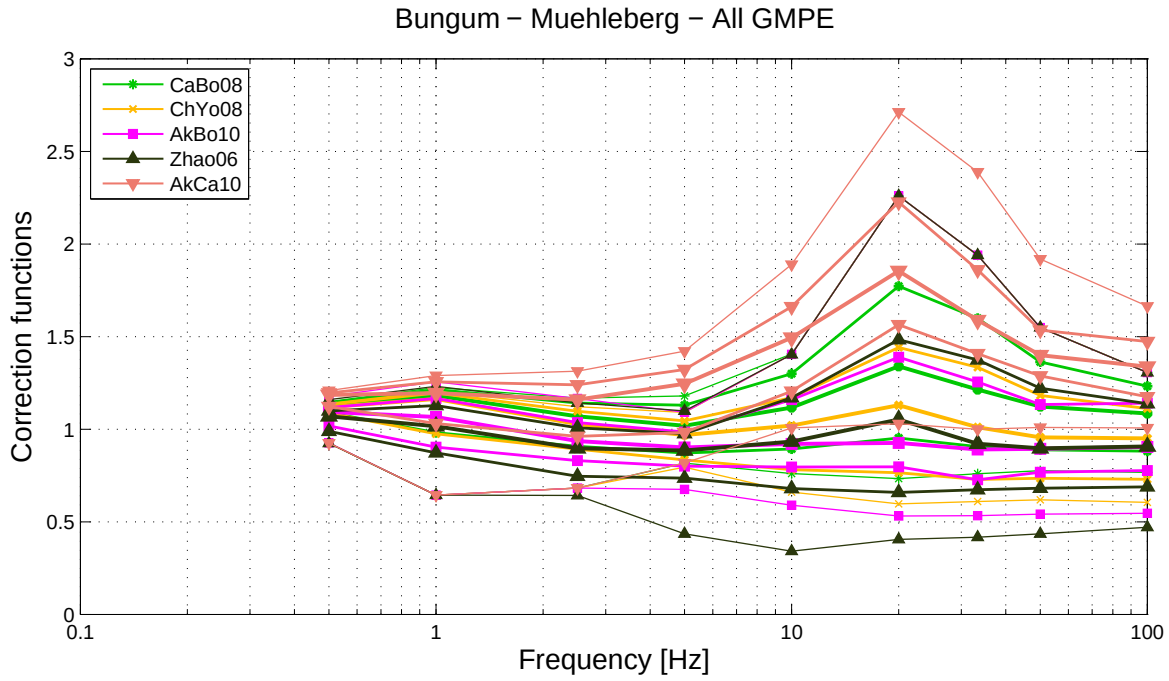

Figure II-1.28: V_S-correction factors as applied to the GMPEs for Mühleberg NPP.

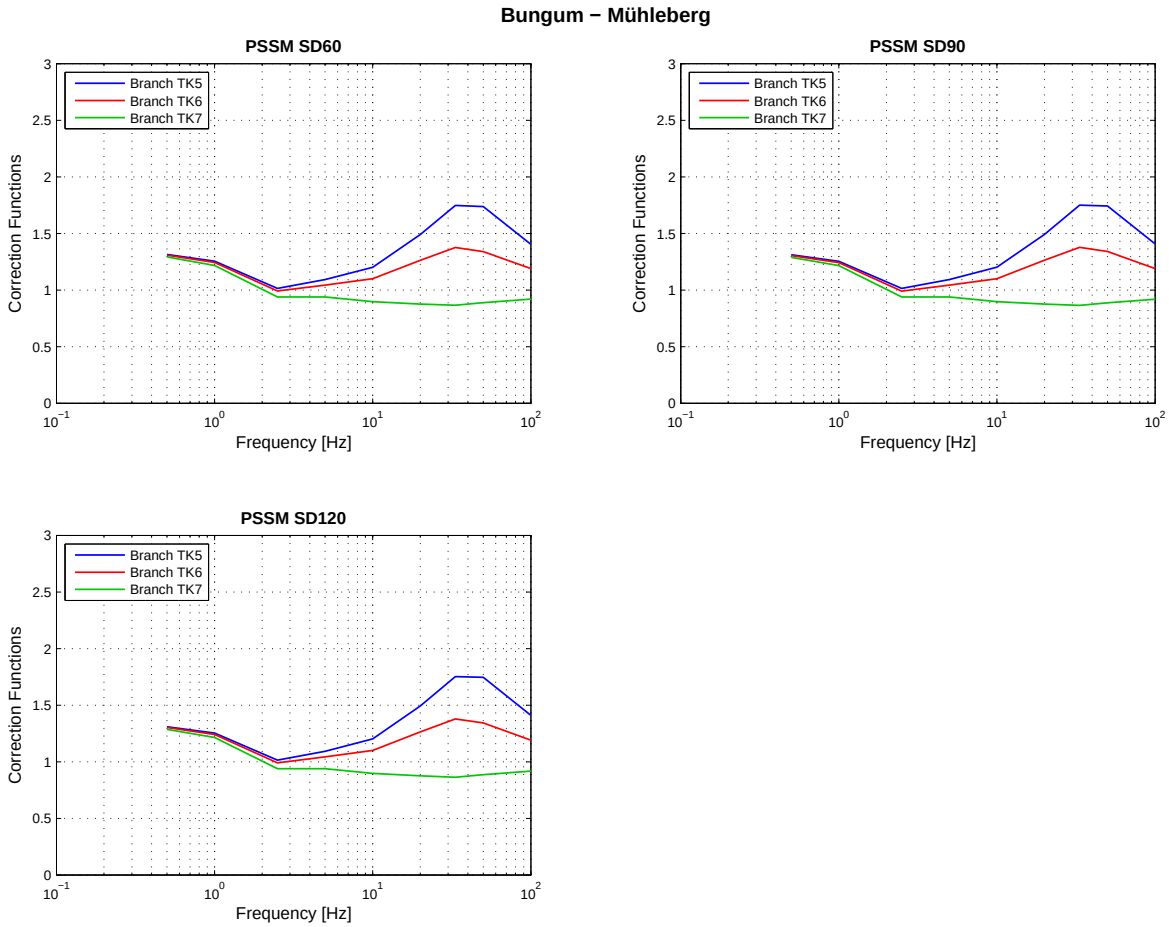

Figure II-1.29: $V_S - \kappa$ correction factors as applied to the PSSMs for Mühleberg.

Table II-1.7: NPP target κ best estimates for GMPE and PSSM applications, respectively. The values are given with lower and upper bounds, where the lower is obtained by dividing a factor of 1.4, and a higher by multiplying by a factor of 1.6. The best estimate should be given a weight of 0.6, with a weight of 0.2 for each of the two flank values, corresponding to $\pm 1.6\sigma$.

	Target V_S [m/s]	-1.6 σ	Best estimate	± 1.6 σ
Weight		0.20	0.60	0.20
GMPE	All 4 sites	0.017	0.024	0.038
PSSM	All 4 sites	0.0085	0.012	0.019

1.5 Extrapolation of GMPEs to Small Magnitudes

This is covered by decisions already taken by the SP2 experts [Abrahamson 2012a], adopting the Bommer and Stafford [2010b] extrapolation methodology. For more details see Bommer et al. [2009] and Bommer and Stafford [2010b], Stafford [2011] and Stafford [2012].

1.6 Comparison of Extended GMPE Median Predictions

In Section 1.3, Figures II-1.2, II-1.3 and II-1.4 the selected relations are plotted, including a suite of PSSMs, all RVT FAS $V_S - \kappa$ corrected. In comparison, in Figure II-1.30, II-1.31 and II-1.32 the full suite of prediction relations corrected the same way are shown. The magnitudes in Figures II-1.30, II-1.31 and II-1.32 are the same as those used in Figures II-1.2, II-1.3 and II-1.4, but only for 1Hz. In it interesting to see how the spread is increasing with magnitude, which mainly is due to the low-magnitude adjustments for all of the GMPEs, where the target is observed Swiss ground motions.

For M 7.5 the spread in Figure II-1.32 is considerable, but mostly caused by relations not included in my model (cf. Figure II-1.4). It is interesting that the difference between the models increase so strongly with magnitude in spite of the fact that regional differences generally decrease with magnitude (cf. Section 1.2.2). It should be kept in mind that the 30 and 240 bars PSSMs as shown in Figures II-1.30 and II-1.31 and II-1.32 are not used in my final model.

Comparisons with observed data from Christchurch and Virginia [Biro 2012] show a good fit to the Christchurch event but a significant underprediction of the Virginia 2011 main shock. Possible explanations here could be relating to stress drop, directivity and site response, or a combination of all of those.

1.7 Aleatory Variability for Horizontal Motion

The issue of aleatory variability for horizontal motion has been receiving a considerable attention in the PRP project and is also well documented, representing a major state-of-the-art improvement. The work is summarized also in the Master Ground Motion Logic Tree report [Abrahamson 2012a], yielding a final model which is reasonably simple and a lot less complicated than the underlying data analyses, which in turn vouches for an efficient data reduction process. Given that Abrahamson [2012a] is quite detailed on the model I see no

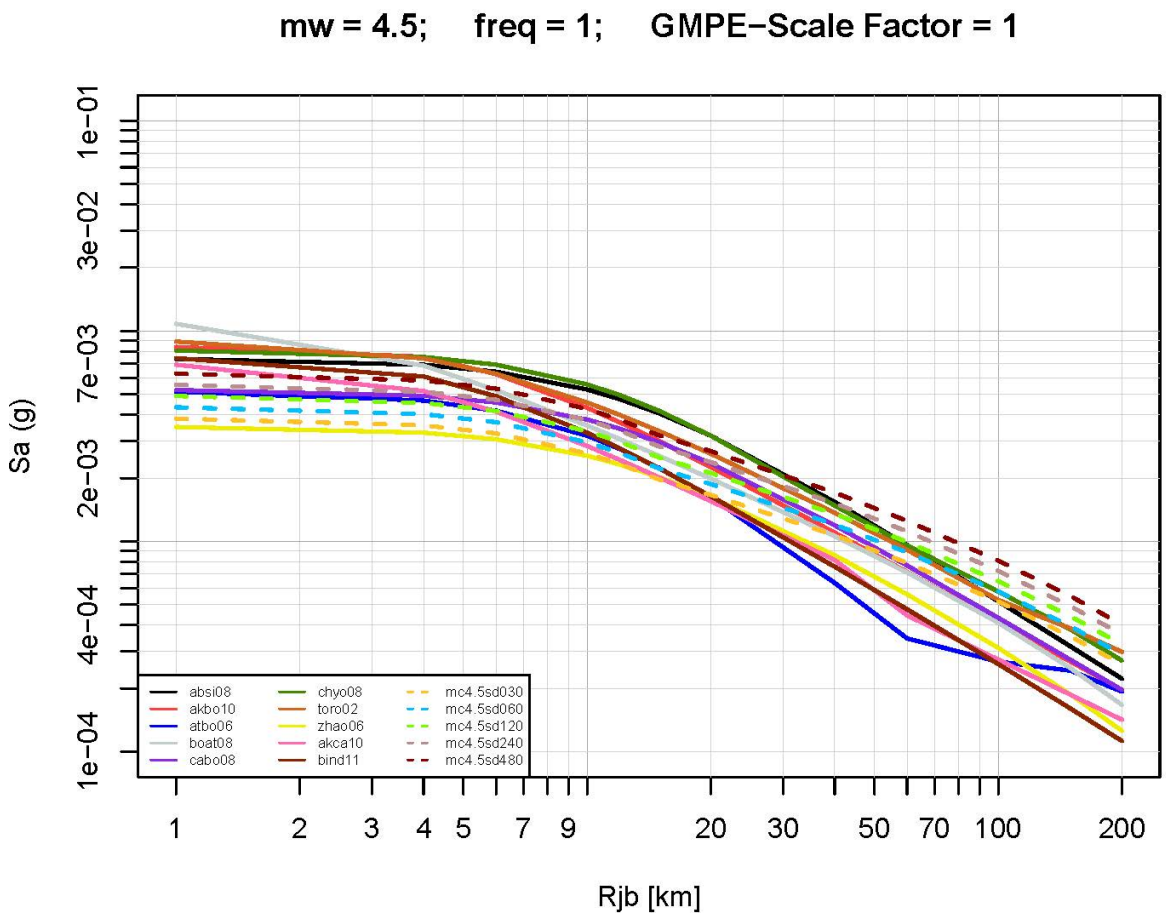

Figure II-1.30: Ground-motion prediction relations for all ten GMPEs plus five PSSMs (30-240 bars), for M 4.5 and 1 Hz. The GMPEs are RVT FAS $V_S - \kappa$ corrected.

reason to overlap too much with that report, which reflects the SP2 expert consensus model. Therefore, only my expert weights, with justification, are provided here.

1.7.1 Tau (Between Event) Model

The first part of the model (following the logic tree) consists of GMPE specific tau (between event) values, with uncertainties. There are as seen in Figure II-1.33 two branches, a period-dependent (global) model (Tau Model 1) which in turn bifurcates into three models aimed at capturing uncertainties, and a model based on the original (selected) GMPEs (Tau Model 2).

The question of how to balance between the two main tau branches is concerned with how much the original GMPE tau values, derived from different, often regional, databases, can be trusted to be representative of the between-event variation expected to be experienced in Switzerland. In the global model the mean is seen to be between 0.31 and 0.37 [Rodriguez-Marek and Cotton 2011], while the two branches at ±0.10 more or less envelope the values from the different relations as seen in Figure II-1.34.

My judgment here is that I have a higher confidence in the global model which I consider as being both more robust and I am also more confident that the global model more reliably covers the CBR of the between-event variability. Consequently I give the global branch a weight of 2/3 and the GMPE branch a weight of 1/3. Rodriguez-Marek [2012] has shown that

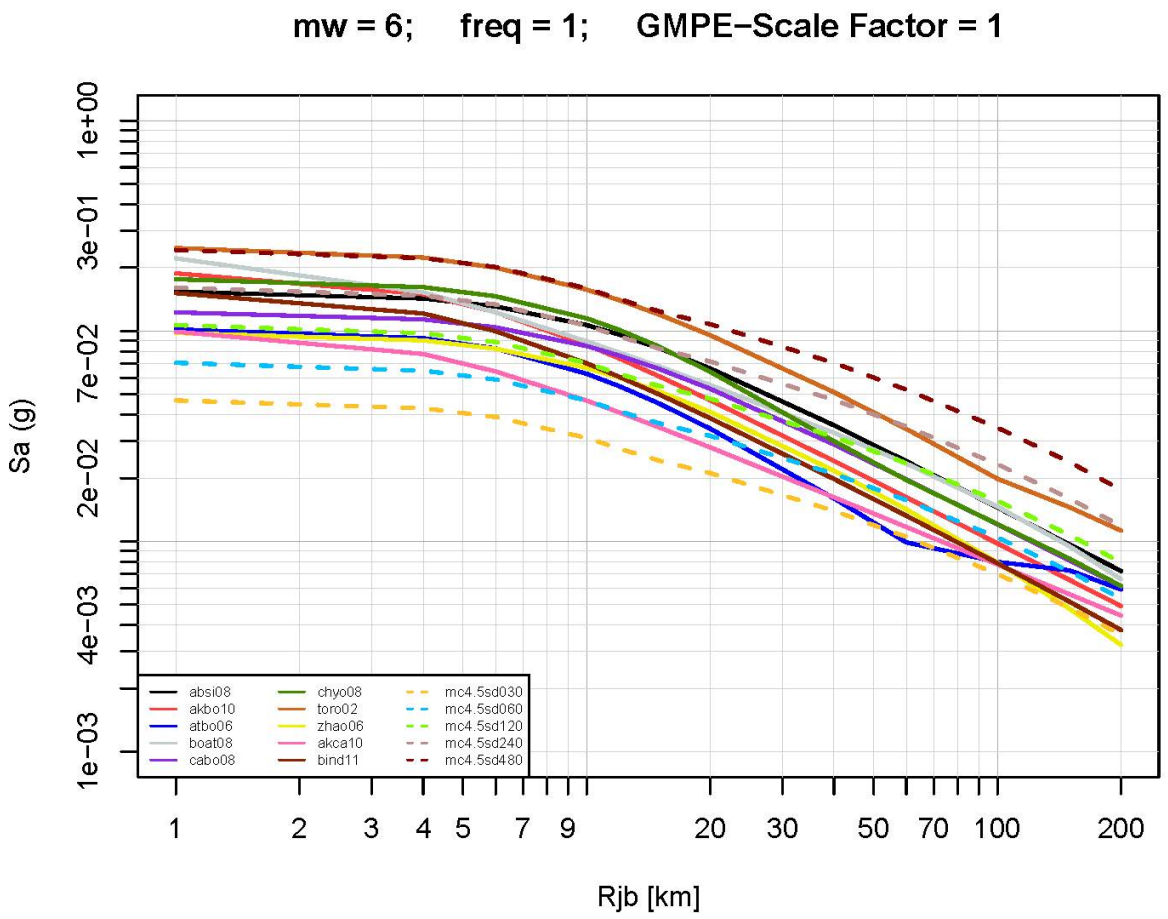

Figure II-1.31: Ground-motion prediction relations for all ten GMPEs plus five PSSMs (30-240 bars), for M 6.0 and 1 Hz. The GMPEs are RVT FAS $V_S - \kappa$ corrected.

1σ in Figure II-1.34 ranges between 0.04 and 0.08, making it reasonable that the range of ± 0.10 corresponds roughly to $\pm 1.6\sigma$, which in turn supports that the mean ± 0.10 branches be weighted with 0.2, 0.6 and 0.2, respectively.

1.7.2 Phi (Within-Event) Model

The second part of the model (see Figure II-1.33) consists of within-event single station phi values, with uncertainties, as outlined in detail by Rodriguez-Marek and Cotton [2011] and Rodriguez-Marek [2012]; see also Rodriguez-Marek et al. [2011]. There are three phi models (branches): constant, R-dependent and MR-dependent. According to Rodriguez-Marek and Cotton [2011], the epistemic uncertainty in single-station phi can be assumed to follow a normal distribution.

It appears from Rodriguez-Marek and Cotton [2011] that none of the main models is particularly good in terms of fit to the data, which of course is a good reason why they have offered three different models for evaluation. Between the three models, however, Model 2 (the R-dependent one) appears to be the most problematic one, and the authors in fact recommend specifically not using that model. The reason for this is that standard deviations are well constrained only for large distances and small magnitudes, and that both Model 1 and 2 generally give values of ϕss larger than the standard deviation of the residuals. At

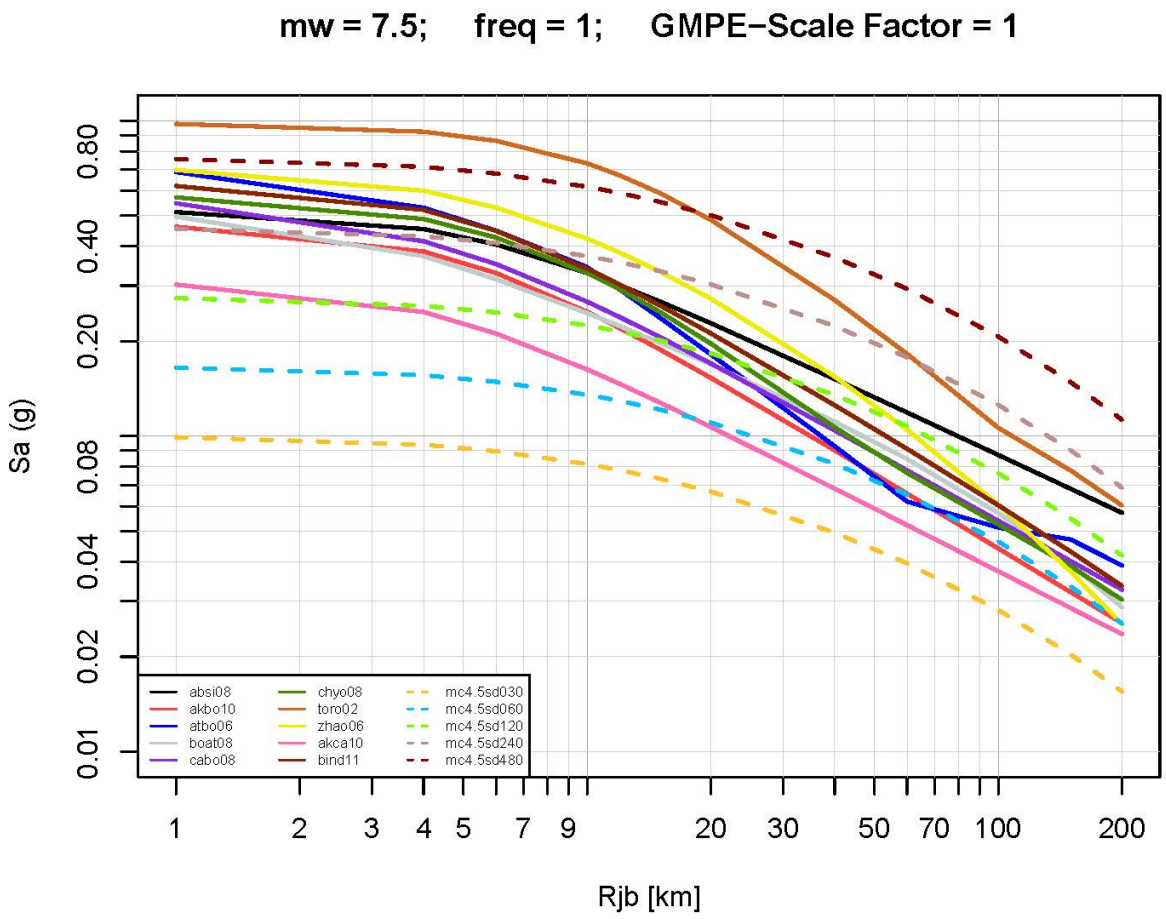

Figure II-1.32: Ground-motion prediction relations for all ten GMPEs plus five PSSMs (30-240 bars), for M 7.5 and 1 Hz. The GMPEs are RVT FAS $V_S - \kappa$ corrected.

short distances, the overprediction can be high.

Consequently I have decided not to use Model 2 and to retain Model 1 with a weight of 1/3 and Model 3 with a weight of 2/3, given that Model 3 has a better overall fit to the data while still appearing to be reasonably robust and stable.

For the uncertainty in ϕ the SP2 experts have earlier reached a consensus to use mean $\pm 1.6\sigma$ with weights of 0.2, 0.6 and 0.2, respectively, assuming a normal distribution (see Figure II-1.33). The standard deviations to be used should be reconsidered by the individual experts, however. Rodriguez-Marek and Cotton [2011] have in their Table 4.9, used standard deviations as taken from Table 4.6, for $N \geq 20$, with values ranging between 0.07 and 0.11. When reviewing the standard deviations also for $N \geq 10$ and $N \geq 15$ it appears that there is some variation which suggests that a period-independent value of Ïf would be well justified, in which case a value of 0.08 seems reasonable (as the average for $N \geq 20$).

Consequently my uncertainty model for ϕss is based on a standard error of 0.08. Using $\pm 1.6 * 0.08$ for the uncertainty, the three uncertainty values are -0.13, 0.0, and 0.13, with weights of 0.2, 0.6 and 0.2, respectively.

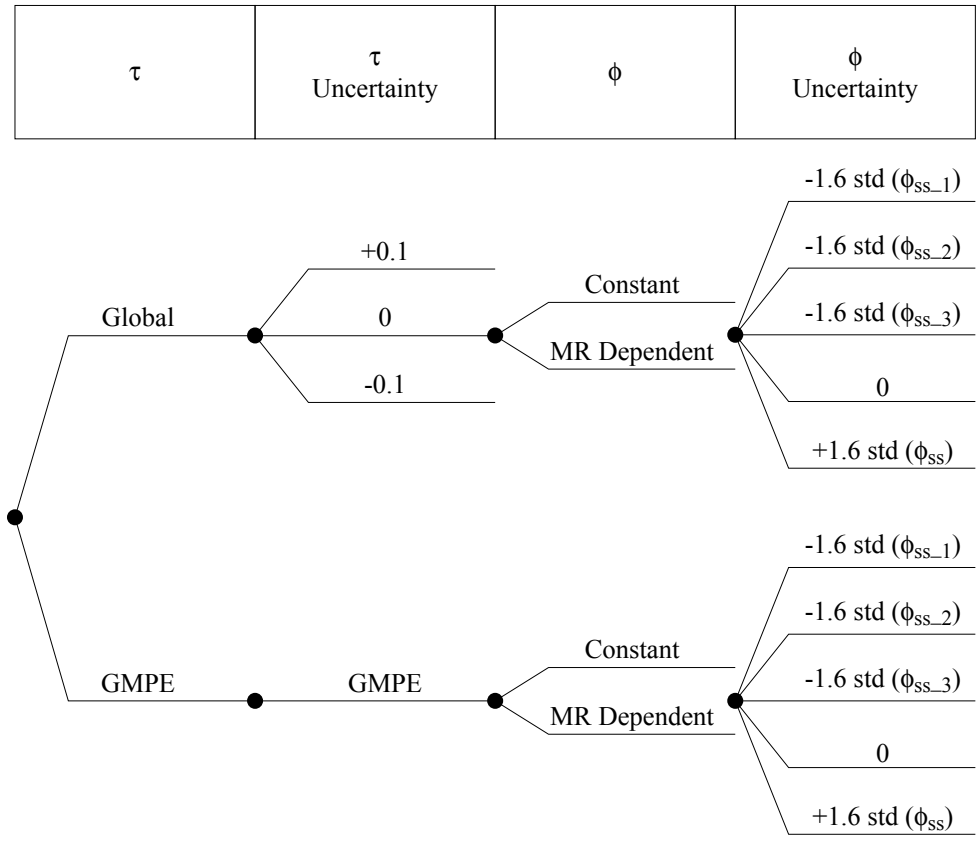

Figure II-1.33: Logic tree for the aleatory variability of the horizontal component.

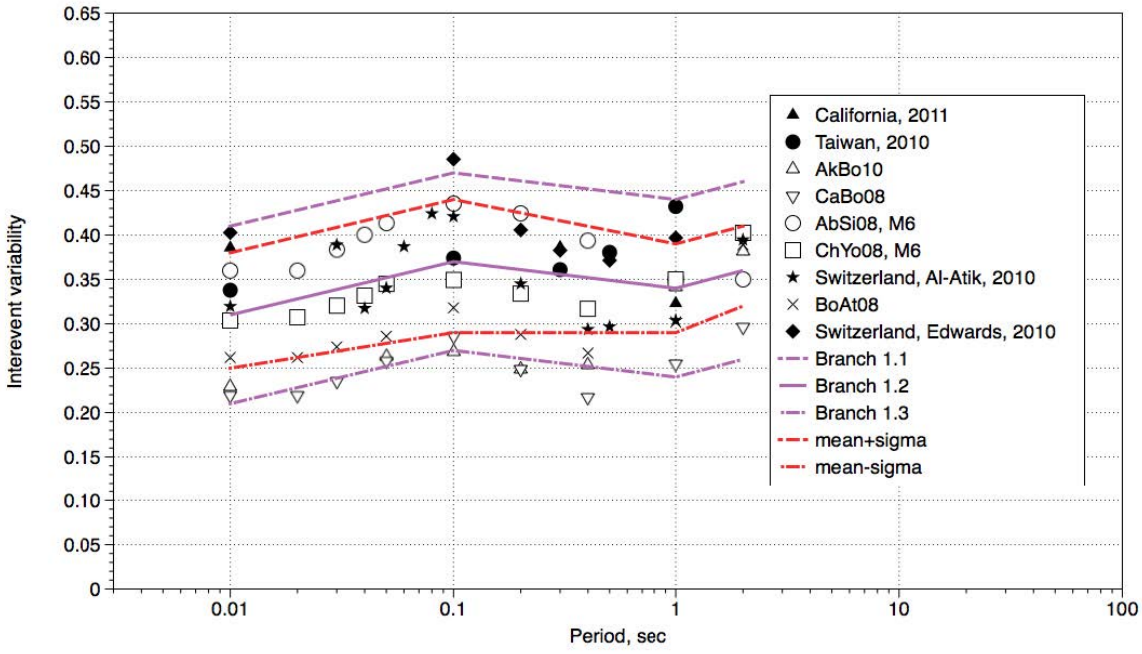

Figure II-1.34: Between-event variability: Tau model 1 (three branches). From Rodriguez-Marek [2012].

1.8 Vertical Ground Motions

For vertical ground motions the SP2 experts have decided [Abrahamson 2012a] to base these on conversions from horizontal response spectral ordinates. In the selection process for acceptable relations the following main requirements have been applied:

- Applicable to the PRP response periods
- Applicable to PRP site conditions
- Providing estimates of median V/H ratios as a function of magnitude, style-of-faulting and site class, with a consistent measure of aleatory variability

Three acceptable models were initially identified that satisfy these criteria (Bommer and Akkar [2010b] and Bommer and Akkar [2010a]: namely Campbell and Bozorgnia [2003], Gülerce and Abrahamson [2010], and Bommer [2011].)

In addition, a fourth model, Edwards et al. [2011b] subsequently became available, based on data from Switzerland and Japan. This model characterizes the V/H ratio at rock sites in terms of the recording site's average quarter-wavelength velocity. The model is frequency independent, in quite some contrast to the other models, and they also find no systematic dependence on either magnitude or distance.

Bommer [2011] based their analysis on data from Europe and the Middle East, Gülerce and Abrahamson [2011] used the PEER NGA database, while Campbell [2003] use pre-1995 data, also mostly from Californian, but supplemented by a number of global earthquakes. The four relations as plotted in Figures II-1.35 and II-1.36are therefore based on quite different and thereby complementary data, so in that sense they all qualify, even if Edwards et al. [2011b], with its non-traditional approach, is quite different.

In terms of developing the weights for the four models, I note that the first three relations, passing the initial criteria, are quite similar and comparable, except for the data used, the range of V_S values and the use of site classes, as discussed below. Another question is related to the use of Edwards et al. [2011a] because that one has a very different approach to the problem, invoking quarter-wavelength velocities instead of site conditions, and moreover not being able to resolve V/H differences as a function of magnitude, distance and period. The other models show, in contrast, significant differences particularly in terms of period. While this is a potential problem with the Edwards et al. [2011a] model, its advantage is that it is using available Swiss data (even if all of the larger-magnitude data are from Japan) and that it is also tuned to the site conditions of the Swiss NPP sites.

There are some important differences, however, in terms of the range of V_S for the data used in the empirical models. Campbell and Bozorgnia [2003] is predating the NGA development and is, therefore, based only on generic site classes, which is the case also for Bommer [2011] since that one is largely based on older Mediterranean-Middle East data. Gülerce and Abrahamson [2011] on the other hand is based on continuous $V_s - dependent$ functions (up to a 1500 m/s), but as pointed out by Bommer [2011] that one may have stronger site effects than the other models for soil sites because it is based on non-linear site response. The fourth model, [Edwards et al. 2011b], is exclusively a hard-rock ($> 800m/s$) model.

As seen in Table II-1.8 I decided in the end not to include the Edwards et al. [2011b] model, even if it is specifically developed for hard-rock conditions applicable to the sites in question. The problem here is twofold:

- (1) that the relation, as shown in Figures II-1.35 and II-1.36, is very sensitive to the site conditions, over the entire frequency range, and
- (2) that I have not been getting a satisfactory assessment from the authors with respect to the balance between the HF corrected version and the one without corrections.

The two models are very different, and in the lack of convincing reasons why one of them is more reliable that the other I find that solving this by giving equal weight cannot really be justified.

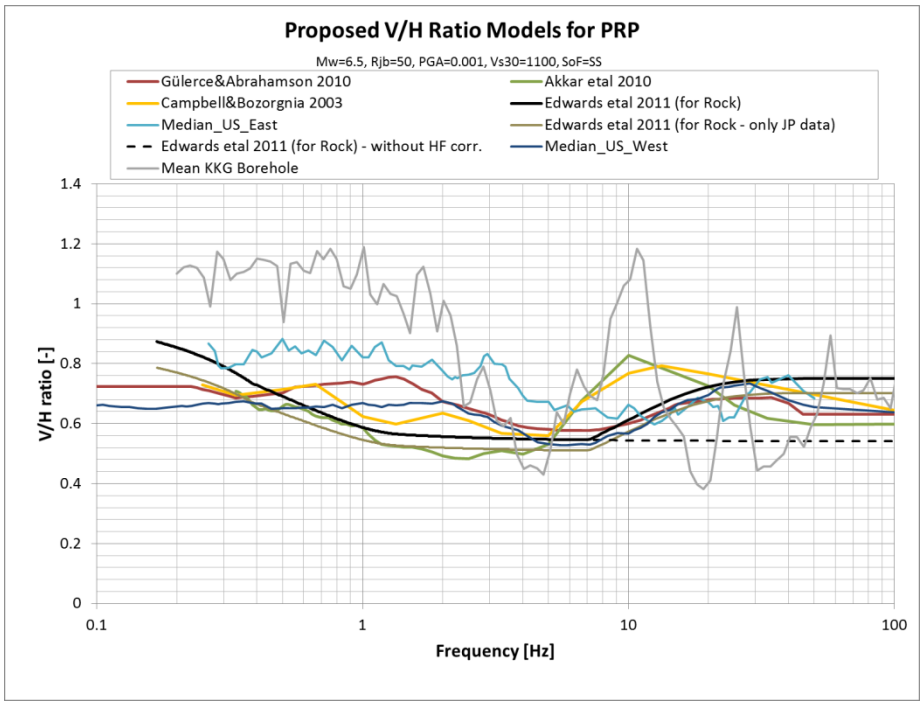

Figure II-1.35: Median V/H ratios for the four candidate models, for M=6.5 and $R_{jb} = 50km$ for $V - S30 = 1000m/s$ corresponding to the KKM (Mühleberg) site. Also shown are median US West and US East data, as well as mean KKG (Gösgen) data (3 events).

Since I am not able to justify using the Edwards et al. [2011b] model I find it useful instead to include the empirical US West and East data, also shown in Figures II-1.35 and II-1.36, in smoothed versions. The eastern US data are recorded at site conditions comparable to the NPP sites, while the advantage with the western US data is that it is abundant and of high quality.

The differences between the V_S levels for the four relations, even if the quality otherwise is comparable, makes me conclude that the two site-class based relations are less applicable to the NPP sites than the other two. Consequently I give higher weights to the latter ones and lower weights to the site-class based relations, as shown in Table II-1.8. Most of the weight (0.4) is given to the V_{s30} based Gülerce and Abrahamson [2011] relation, developed with NGA data, with a weight 0.10 both to Bommer et al. [2011] and to Campbell et al. [2003].

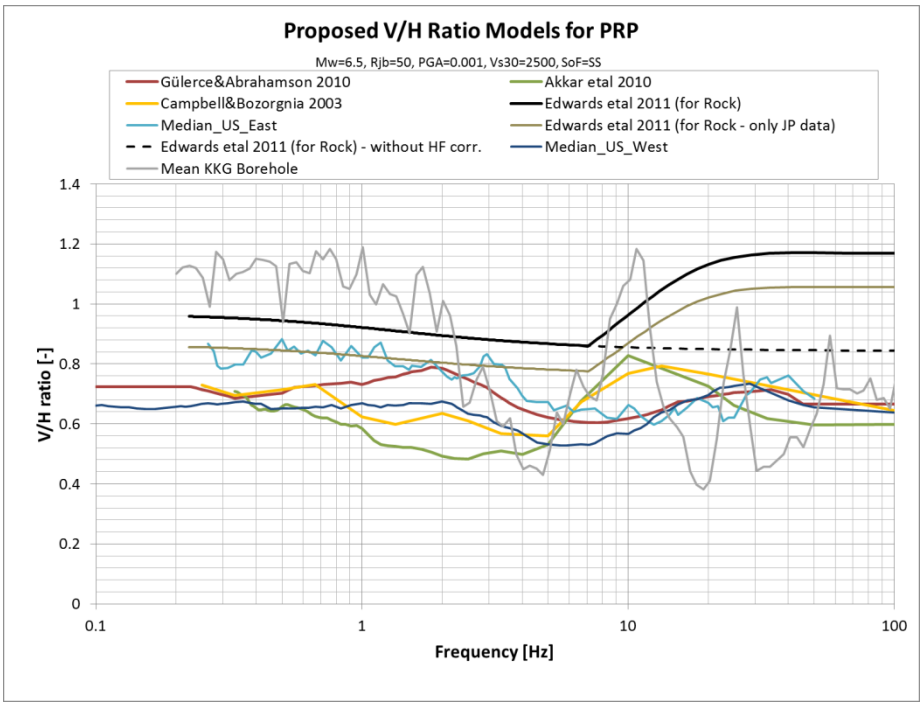

Figure II-1.36: Median V/H ratios for the four candidate models for M=6.5 and $R_{jb} = 50km$ for $V - S30 = 2500m/s$, corresponding to the KKG (Gösgen) site. Also shown are median US West and US East data, as well as mean KKG (Gösgen) data (3 events).

Table II-1.8: Weights for the four candidate V/H models, to be applied to all of the NPP sites.

V/H Model	Weight
Gülerce and Abrahamson [2011]	0.4
Median US West	0.2
Median US East	0.2
Campbell et al. [2003]	0.1
Bommer et al. [2011]	0.1

There is also an issue related to the difference between the NPP sites in terms of V_{S30}, which is 1100 m/s for Mühleberg (KKM), 1800 m/s for Beznau (KKB), 2200 m/s for Leibstadt (KKL), and 2500 m/s for Gösgen (KKG) [Roth 2010b]; [Renault 2012b]. This difference makes it relevant to consider a V/H model which is also site specific. Not using the Edwards et al. [2011b] model, which was highly sensitive to V_{S30}, the only one with some site dependence now is Gülerce and Abrahamson [2011]. On this basis it is difficult to justify any additional site specific effect by also changing the weights.

The V/H ratios also have potential implications related to the $V_S - \kappa$ corrections. It was shown by Ktenidou et al. [2012c], based on data from hard-rock sites in Switzerland, that horizontal surface kappas are about half (0.5-0.6) of the vertical ones, as shown also by Abrahamson [2013b] (average of 0.55, possibly based on the same data). My solution for κ correcting the verticals will therefore be to do this on the basis of uncorrected horizontals, using the horizontal κ model scaled by a constant factor of 0.55, without any additional uncertainty related to the V/H scaling. The same scaling should apply to the host kappas.

Models for the aleatory variability of the V/H ratio is discussed in some detail by Abrahamson [2012a] who points out the fact that the V/H ratio is correlated with the aleatory variability of the horizontal, which is already included in the horizontal hazard. This correlation needs to be considered in order to avoid double counting.

Abrahamson [2012a] has outlined two different approaches for how to estimate the additional σ_{VADD}, Approach 1 for the case when V/H models are used and Approach 2 for the case when independent H and V models are used. Approach 1 yields somewhat lower σ_{VADD} values (≤ 0.30) than Approach 2 (≤ 0.37), where the two models (Abrahamson and Silva [1997] and Campbell and Bozorgnia [2003]) also have significantly larger standard deviations on the vertical than on the horizontal component. These two models are also based on broad site categories which should be expected to add to the scatter, which is a problem for Approach 2.

Approach 1 is based on two of the V/H ratio models used here (Bommer [2011] and Gülerce and Abrahamson [2011]), with horizontal values either from Abrahamson and Silva [2008] or from global averages. Four different combinations are tested in this case, with reasonably stable σ_{VADD} values in the range between 0.07 and 0.30. My approach here is, therefore, to use an average of the four Approach 1 estimates, as shown in Table II-1.9, where the values for 5 and 2.5 Hz are interpolated linearly in log(freq)–σ_{VADD} space.

Table II-1.9: σ_{VADD} values computed as an average of the four combinations under Approach 1 of Abrahamson [2012a]. The values for 5 and 2.5 Hz are interpolated.

Freq. [Hz]	100	50	33.3	20	10	5	2.5	1	0.5
σ_{VADD} [LN units]	0.11	0.14	0.2	0.24	0.175	0.171	0.166	0.16	0.235

1.9 Maximum Ground Motions

A model for maximum ground motions has also been agreed upon by the SP2 experts, as outlined by Abrahamson [2012a], based on an extensive data collection and analysis effort as documented by Strasser and Zulu [2010]. It was resolved at an early stage of this work [Bungum 2010f] that there was no basis for a statistical truncation of extreme ground motions and that a truncation therefore needs to be based on physical limits. Earlier work was reviewed in parallel with the acquisition and analysis of new data and a new upper bounds model was developed over the summer and fall of 2010 (Bungum [2010a]; Bungum [2010e] and Bungum [2010c]). An example of some of the data analysed by Strasser and Zulu [2010] is shown in Figure II-1.37, using a plotting tool developed by F. Strasser in connection with the data.

In Figure II-1.38 data for the magnitude bin 5-0 are shown, for frequencies of 10 and 1 Hz, where also the lower and upper levels of the proposed model are shown, corresponding to scale factors of 7.5 and 100, respectively.

A detailed review of earlier upper bounds studies and the analysis done by Strasser and Zulu [2010] showed that the extreme ground motions come from a variety of regions, sources, magnitudes, distances, frequencies and site conditions. Large stress drops, high rupture speeds and directivity effects are important, but also focusing/defocusing effects which can vary greatly over short distances on the surface. The increased sampling density is therefore a key reason why the largest observed ground motions have been steadily increasing, and a model

has to allow for even further increases. For more details I refer to Abrahamson [2012a] and to Strasser and Zulu [2010]

Based on these reviews and the new database a simple model for maximum horizontal ground motion was developed, with a distance-independent branch, corresponding to physical limits on ground motion, and a distance-dependent branch, corresponding to a source-related energy limit, with attenuation. The distance-independent model defines a maximum ground motion applicable to all distances for a given magnitude based on scaling of the Boore and Atkinson [2008] model, a distance of 1 km. A set of six scale factors between 7.5 and 100 are given, corresponding to sigma levels ranging between 3.54 and 8.08, and the weighting will specify the distribution of weights for these factors. This model is shown in Figure II-1.39.

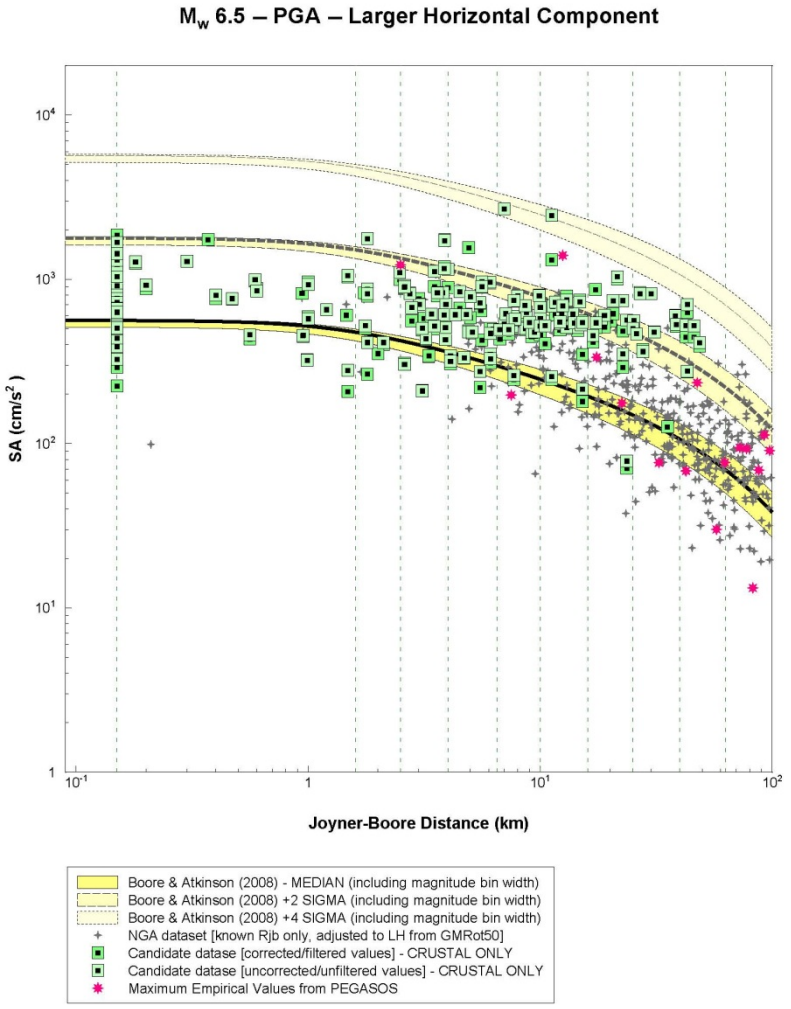

Figure II-1.37: Maximum ground motions (PGA) for the M6-7 bin.

Initial weights for this model was provided by all of the SP2 experts as early as on 07 Oct 2010 (including Bungum [2010d]), and hazard sensitivity feedback was provided a couple of months later (Roth [2010a] and Roth [2011]). This has the advantage that the final weights given here are real updates, following hazard sensitivity analyses from the initial weights.

One important limitation with the database established is that most of the collected ground motions collected are for site conditions softer than hard rock, so that when only hard rock

data are plotted there is an obvious sampling problem. Even so, there is a clear trend, as expected, in that the hard-rock amplitudes are lower than those for softer site conditions. This means that if the model is defined on the basis of all of the collected data, like it is here, it will contribute on the conservative side. I have kept this in mind when defining my model in the following

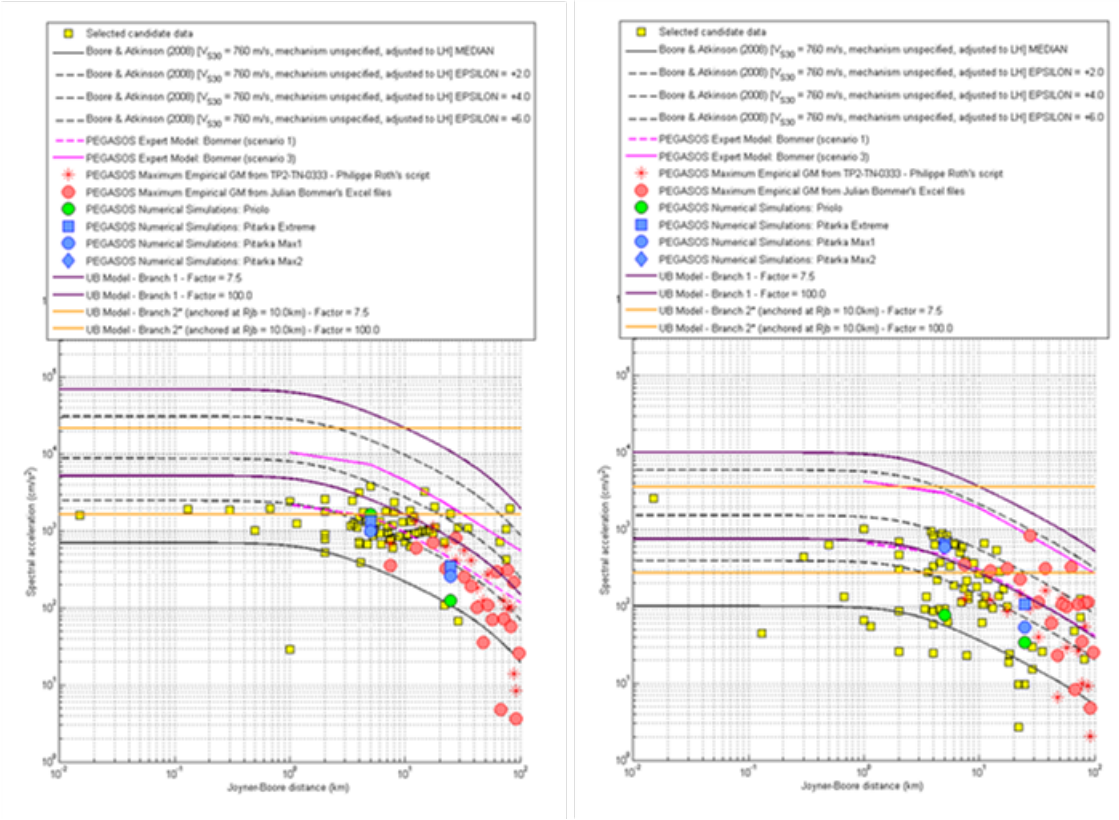

Figure II-1.38: Maximum ground motions for the M5-6 bin, for 10 Hz (left) and 1 Hz (right). All available data and models are used. From Bungum [2010c].

1.9.1 Horizontal Motions

Branch weights are given in Table II-1.10. The reason for the different weights for different frequencies is that a distance-independent structure is seen first of all at 100 Hz while at 5 Hz it is almost gone.

Table II-1.10: Branch weights for upper bounds model, horizontal motions.

Branch / Freq. [Hz]	PGA	50	33	20	10	5	2.5	1.0	0.5
1. Distance dependent (Relative to BA08 median)	0.7	0.75	0.8	0.85	0.9	0.95	1	1	1
2. Distance independent (BA08 anchored at 1 km)	0.3	0.25	0.2	0.15	0.1	0.05	0	0	0

Amplitude factor weights are then given in Table II-1.11. There are some data points exceeding the lowest value and a few also on the level of the second one, for both branches.

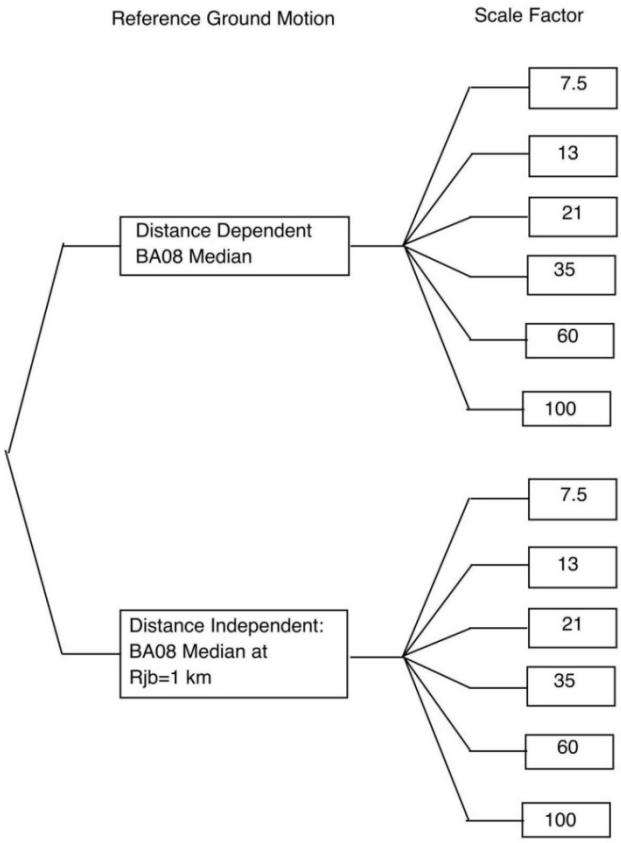

Figure II-1.39: Logic tree for maximum horizontal motion.

Table II-1.11: Branch weights for upper bounds model, horizontal motions.

Scale factor:	7.50	12.59	21.14	35.48	59.57	100.00
Branch 1	0.0	0.1	0.4	0.4	0.1	0.0
Branch 2	0.0	0.1	0.4	0.4	0.1	0.0

1.9.2 Vertical Motions

For vertical motions I keep the same weights as for the horizontal motions. Even though this may not be justifiable based on the V/H ratios for ordinary ground motions (see Chapter 1.8) it has not been possible, when using the present extreme motion database, to document any significant difference between horizontal and vertical extreme motions even though it is a bit more common to observe V/H values below 1.0 than above 1.0.

Chapter 2

Hazard Input Document for H. Bungum (EG2-HID-1009)

Written by the PMT, SP4 and TFI

This document describes the implementation and parametrization of Hilmar Bungums's expert model EG2-EXM-1009, as described in the evaluation summary EG2-ES-1018 (see Chapter 1) and delivered on 06.02.2013, with an update for the target κ estimates on 16.11.2013. The purpose of this document is to translate the expert's evaluation of ground motion into an input usable by the hazard software. For PRP a consensus master logic tree for the median, the aleatory variability, the maximum and the V/H ratio of the ground motion was developed by the SP2 experts and is described in part I. The basic elements of those trees and models are not repeated here. This document only summarizes the parameters and model weights assigned by the expert H. Bungum. By this the master logic tree becomes expert specific and reflects the individual evaluations.

2.1 Model Implementation

Based on the evaluation summary, the logic trees for the median horizontal ground motion, the vertical/horizontal ratio, the maximum ground motion and the aleatory variability of the horizontal and vertical component were implemented. The key elements in the model are given below. Figure II-2.1 shows the logic tree. The first level in the logic tree, "Model Category" is not explicitly specified by the expert but is used by SP4 to allow for an easier treatment of those subsequent global variables (or logic tree levels) like "$V_S - \kappa$", which are dependent on whether a GMPE or a PSSM model is considered. The logic tree is frequency dependent as the weights associated with the maximum ground motion truncation models vary with frequency, see Section 2.5. The logic tree has in total 6528 branches.

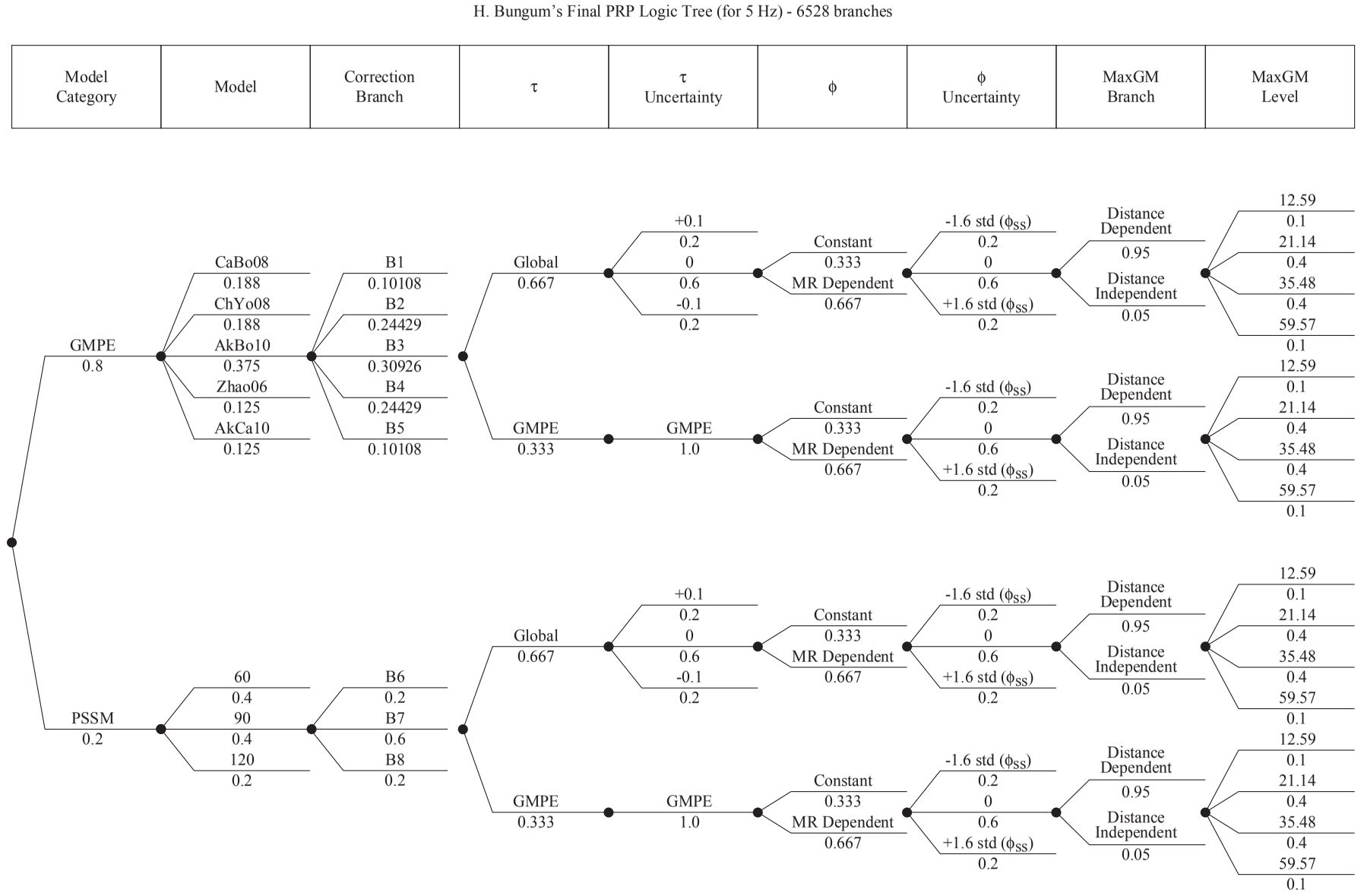

Figure II-2.1: Logic tree for the horizontal ground motion, here for 5 Hz PSA.

2.2 Median Horizontal Ground Motion

Five of the ten candidate models by SP2 get non-zero weights in H. Bungum's model. The empirical GMPEs have a total weight of 80% and the Swiss stochastic model a total weight of 20%. For the parameterized Swiss stochastic model (PSSM) the versions with a M_C=4.5 and stress drop values of 60, 90 and 120 bars have been selected.

Table II-2.1: Weights assigned to the GMPEs.

GMPE	Abbrv.	Weight	Weight by category
Abrahamson & Silva (2008)	AbSi08	-	-
Boore & Atkinson (2008)	BoAt08	-	-
Campbell & Bozorgnia (2008)	CaBo08	0.15	0.1875
Chiou & Youngs (2008)	ChYo08	0.15	0.1875
Atkinson & Boore (2006)	AtBo06	-	-
Toro et al. (2002)	Toro02	-	-
Akkar & Bommer (2010)	AkBo10	0.30	0.3750
Akkar & Cagnan (2010)	AkCa10	0.10	0.1250
Bindi et al. (2011)	Bind11	-	-
Zhao et al. (2006)	Zhao06	0.10	0.1250
PSSM30		-	-
PSSM60		0.08	0.40
PSSM90		0.08	0.40
PSSM120		0.04	0.20
Sum GMPE		0.80	1.00
Sum PSSM		0.20	1.00

Table II-2.2 specifies the reference shear wave velocity ($V_{S30,rock}$) to be used for the NGA models and the site category for the models which have only a category, respectively. The host-to-target correction is applied to those reference models to account for the hard rock conditions at the Swiss NPP sites.

For the depth to sediment layer with V_S=1.0 km/s and 2.5 km/s at the site, the sediment thickness is defined as the depth to a material (bedrock) with a given shear-wave velocity or greater, starting at the top of the rock, as defined in the site response and not the ground surface. For ChYo08 the parameter $Z_{1.0}$=0 m for rock sites, as the reference $V_{S,30}$ values of all four NPP sites is greater than 1000 m/s after application of the $V_S - \kappa$ corrections. For CaBo08 $Z_{2.5}$=0.800 km, based on assumed generic conditions of the Swiss region. The GMPE is evaluated with respect to the generic rock condition of 620 m/s and the value for $Z_{2.5}$ needs to be consistent, as the host-to-target correction towards the Swiss conditions (based on a full V_S profile) is applied afterwards.

Table II-2.2: GMPE specific reference shear wave velocity or site category.

GMPE	Ref. V_{S30} [m/s]
CaBo08, ChYo08	800
AkCa10	950
AkBo10	Rock Cat. (=800)
Zhao06	Rock Cat. (=700)

2.3 Host-to-target Correction

2.3.1 Host-to-target Correction

The host and target κ values were evaluated according to the PRP reports EXT-TB-1087 [Al Atik and Abrahamson 2012a] and EXT-TN-1233 [Al Atik and Abrahamson 2012b], where the average of different evaluated scenarios is taken. The scenarios are based on M=5, 6, 7 and R_{JB}=5, 10 , 20 km with an average depth of 12 km (which is consistent with the average depth in Switzerland).

The expert specific target κ values are summarized together with their weights in Table II-2.3. The Figure I-3.10 depicts the generic logic tree which was developed in the course of the PRP and Figure II-2.2 shows the expert specific version. The finally selected parameters and weights are summarized in Tables II-2.4 to II-2.7. Applying the given combinations leads to 252 discrete correction functions for the combined $V_S - \kappa$ cases. The resulting 5-point distribution of $V_S - \kappa$ corrections for each of the used GMPEs is reported in Tables II-2.8 to II-2.11. As the resulting distribution is not a known distribution, the evaluated 5 point distribution is based on the approach of Miller and Rice [1983] with the 0.034893, 0.211702, 0.50, 0.788298 and 0.965107 fractiles. The corresponding probabilities/weights for this given discretization are: 0.10108, 0.24429, 0.30926, 0.24429, 0.10108. Tables II-2.12 and II-2.13 have the correction functions to be applied to the different versions of the parameterized Swiss stochastic model, depending on the defined target κ per site. The scaling of the response spectrum depends on the shape of the Fourier spectrum. Changes in the frequency content of the Fourier spectrum due to different stress drops leads to differences in the $V_S - \kappa$ scale factors for different stress drops. The Tables II-2.12 and II-2.13 illustrate the small numerical differences, but the figures show almost no visible difference between the stress drops.

Table II-2.3: Target Kappa values for GMPE and PSSM with weights for all sites.

		GMPE	PSSM
	Weight	κ_0 [s]	κ_0 [s]
TK5	0.20	0.017	0.0085
TK6	0.60	0.024	0.012
TK7	0.20	0.038	0.019

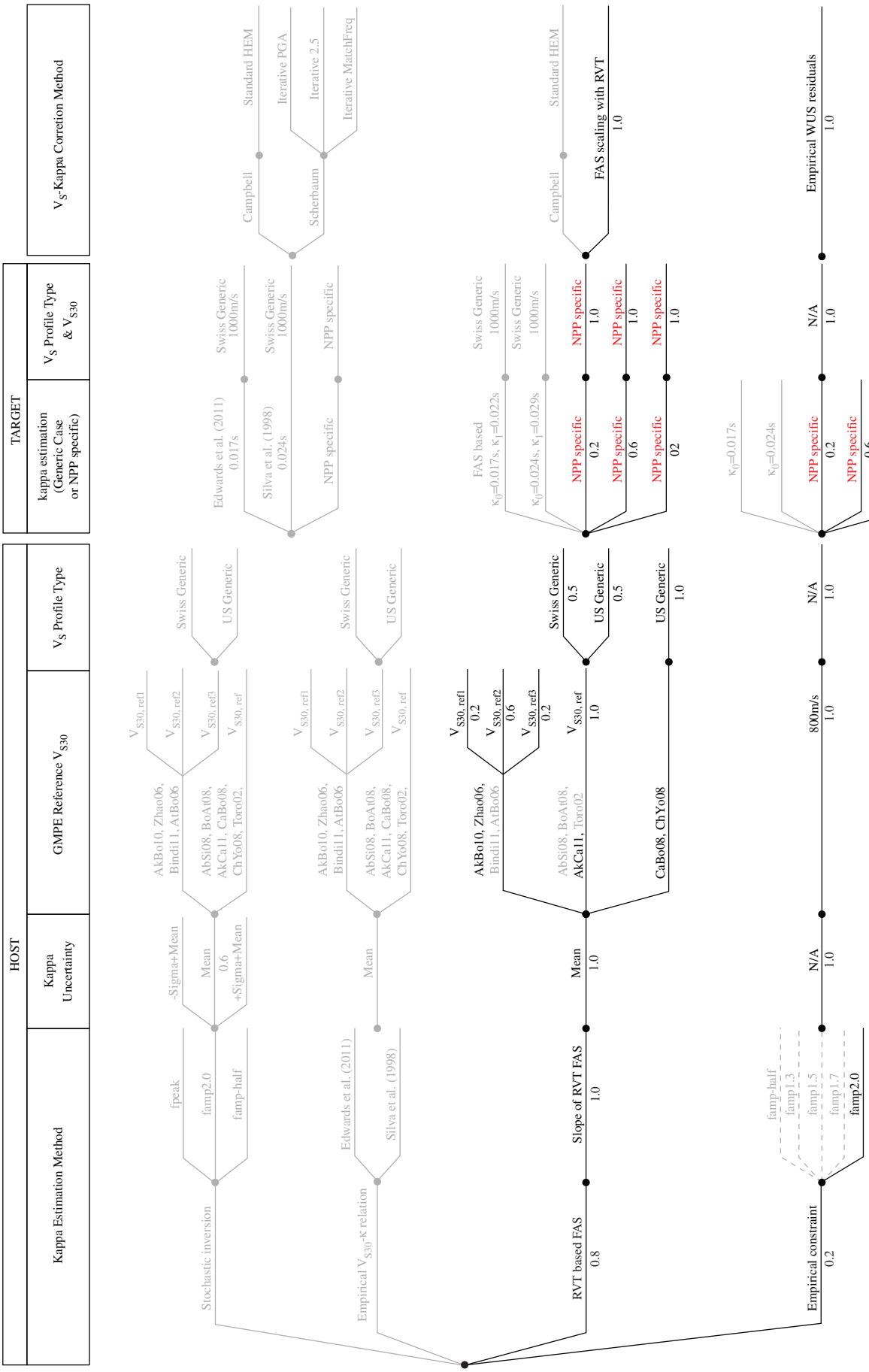

Figure II-2.2: Logic tree for the evaluation of $V_S - \kappa$ scaling for GMPEs.

Table II-2.4: Overview of parameters and weights assigned to the $V_S - \kappa$ logic tree for the NGA models.

Estimation Method emethod	**wt.**	**Host** hkest & emethod	**Host** κ_1 hostk	**wt.**	**GMPE**	**HostVS** vs30est	**wt.**	**Profile** vstypestr	**wt.**	**TargetVS** (npp) targetp	**Target** target TK	**Targ.** κ_0	**Targ.** κ_1 targetk	**wt.**	**Correction Method** cmethod	**wt.**
iRVT	0.80	kBE6	0.0396	1.00	CaBo08	800	1.00	US	1.00	KKB1800	TK5	0.017	0.022	0.20	FAS scaling w. iRVT	1.00
Emp. Constr. f_{amp2}	0.20	kBE9		1.00							TK6	0.024	0.029	0.60	Empirical WUS resid.	1.00
		kBE6	0.0345	1.00	ChYo08	800	1.00	US	1.00	KKG2500	TK7	0.038	0.043	0.20		
		kBE9		1.00							TK5	0.017	0.022	0.20		
											TK6	0.024	0.029	0.60		
											TK7	0.038	0.043	0.20		
										KKL2200	TK5	0.017	0.022	0.20		
											TK6	0.024	0.029	0.60		
											TK7	0.038	0.043	0.20		
										KKM1100	TK5	0.017	0.022	0.20		
											TK6	0.024	0.029	0.60		
											TK7	0.038	0.043	0.20		

Table II-2.5: Overview of parameters and weights assigned to the $V_S - \kappa$ logic tree for the Akkar & Bommer (2010) model.

Estimation Method emethod	**wt.**	**Host** hkest & emethod	**Host κ_1** hostk	**wt.**	**GMPE**	**HostVS** vs30est	**wt.**	**Profile** vstypestr	**wt.**	**TargetVS** (npp) targetp	**Target Targ. κ_0** target TK	**Targ. κ_1** targetk	**wt.**	**Correction Method** cmethod	**wt.**
iRVT	0.80	kBE6	0.0290	1.00	AkBo10	600	0.20	CH	0.50	KKB1800	TK5	0.017	0.022	0.20	FAS scaling w. iRVT	1.00
Emp. Constr. f_{amp2}	0.20	kBE9	0.0346	1.00			0.20	US	0.50		TK6	0.024	0.029	0.60	Empirical WUS resid.	1.00
			0.0290		AkBo10	800	0.60	CH	0.50		TK7	0.038	0.043	0.20		
			0.0314				0.60	US	0.50	KKG2500	TK5	0.017	0.022	0.20		
			0.0290		AkBo10	1000	0.20	CH	0.50		TK6	0.024	0.029	0.60		
			0.0307				0.20	US	0.50		TK7	0.038	0.043	0.20		
										KKL2200	TK5	0.017	0.022	0.20		
											TK6	0.024	0.029	0.60		
											TK7	0.038	0.043	0.20		
										KKM1100	TK5	0.017	0.022	0.20		
											TK6	0.024	0.029	0.60		
											TK7	0.038	0.043	0.20		

Table II-2.6: Overview of parameters and weights assigned to the $V_S - \kappa$ logic tree for the Akkar & Cagnan (2010) model.

Estimation Method emethod	**wt.**	**Host** hkest & emethod	**Host** κ_1 hostk	**wt.**	**GMPE**	**HostVS** vs30est	**wt.**	**Profile** vstypestr	**wt.**	**TargetVS** (npp) targetp	**Target** target TK	**Targ.** κ_0	**Targ.** κ_1 targetk	**wt.**	**Correction Method** cmethod	**wt.**
iRVT	0.80	kBE6	0.0444	1.00	AkCa10	950	1.00	CH	0.50	KKB1800	TK5	0.017	0.022	0.20	FAS scaling w. iRVT	1.00
Emp. Constr. f_{amp2}	0.20	kBE9	0.0467	1.00				US	0.50		TK6	0.024	0.029	0.60	Empirical WUS resid.	1.00
										KKG2500	TK7	0.038	0.043	0.20		
											TK5	0.017	0.022	0.20		
											TK6	0.024	0.029	0.60		
											TK7	0.038	0.043	0.20		
										KKL2200	TK5	0.017	0.022	0.20		
											TK6	0.024	0.029	0.60		
											TK7	0.038	0.043	0.20		
										KKM1100	TK5	0.017	0.022	0.20		
											TK6	0.024	0.029	0.60		
											TK7	0.038	0.043	0.20		

Table II-2.7: Overview of parameters and weights assigned to the $V_S - \kappa$ logic tree for the Zhao et al. (2006) model.

Estimation Method emethod	**wt.**	hkest & emethod	**Host** **Host** κ_1 hostk	**wt.**	**GMPE**	**HostVS** vs30est	**wt.**	**Profile** vstypestr	**wt.**	**TargetVS** (npp) targetp	target TK	**Target** **Targ.** κ_0	**Targ.** κ_1 targetk	**wt.**	**Correction Method** cmethod	**wt.**
iRVT	0.80	kBE6	0.00.0329	1.00	Zhao06	500	0.20	CH	0.50	KKB1800	TK5	0.017	0.022	0.20	FAS scaling w. iRVT	1.00
Emp. Constr. f_{amp2}	0.20	kBE9	0.0322	1.00				US	0.50		TK6	0.029	0.024	0.60	Empirical WUS resid.	1.00
			0.0326		Zhao06	700	0.60	CH	0.50		TK7	0.038	0.043	0.20		
			0.0353					US	0.50	KKG2500	TK5	0.017	0.022	0.20		
			0.0327		Zhao06	900	0.20	CH	0.50		TK6	0.024	0.029	0.60		
			0.0346					US	0.50		TK7	0.038	0.043	0.20		
										KKL2200	TK5	0.017	0.022	0.20		
											TK6	0.024	0.029	0.60		
											TK7	0.038	0.043	0.20		
										KKM1100	TK5	0.017	0.022	0.20		
											TK6	0.024	0.029	0.60		
											TK7	0.038	0.043	0.20		

Table II-2.8: Frequency dependent resulting $V_S - \kappa$ correction 5-point distributions for used GMPEs at Beznau.

GMPE	Frequency [Hz]									Weight
	0.5	1	2.5	5	10	20	33.3	50	100	
CaBo08	0.8407	0.6444	0.6804	0.6376	0.5754	0.5507	0.5656	0.5761	0.5680	0.1011
	0.8483	0.7963	0.7409	0.6998	0.6770	0.7202	0.6787	0.6623	0.6555	0.2443
	0.8622	0.8294	0.7886	0.7989	0.8792	1.0853	0.9583	0.8618	0.8278	0.3093
	0.9015	0.8480	0.8278	0.8785	1.1077	1.4237	1.3190	1.1623	1.0663	0.2443
	1.0748	0.8727	0.8520	0.9472	1.4045	2.2598	1.9393	1.5486	1.3060	0.1011
ChYo08	0.8353	0.6444	0.6800	0.5909	0.4999	0.4473	0.4529	0.4578	0.4468	0.1011
	0.8425	0.7844	0.6984	0.6480	0.5922	0.5778	0.5450	0.5473	0.5420	0.2443
	0.8556	0.8164	0.7613	0.7554	0.7741	0.8601	0.7641	0.7184	0.7117	0.3093
	0.8987	0.8345	0.7809	0.8146	1.0599	1.3105	1.2151	1.0764	1.0083	0.2443
	1.0748	0.8726	0.8515	0.9472	1.4045	2.2598	1.9393	1.5486	1.3060	0.1011
AkBo10	0.7633	0.6365	0.5602	0.5018	0.4454	0.3983	0.3966	0.4013	0.4038	0.1011
	0.8224	0.7101	0.6593	0.5954	0.6026	0.6049	0.5471	0.5752	0.5797	0.2443
	0.8461	0.7554	0.7096	0.6960	0.6975	0.7035	0.6720	0.6732	0.6773	0.3093
	0.9012	0.8126	0.7719	0.8106	0.9236	1.0605	0.9523	0.8529	0.8543	0.2443
	1.0748	0.8794	0.8603	0.9472	1.4045	2.2598	1.9393	1.5486	1.3060	0.1011
Zhao06	0.7364	0.6022	0.4600	0.3226	0.2579	0.3033	0.3090	0.3211	0.3322	0.1011
	0.7993	0.6533	0.6125	0.5471	0.5163	0.4953	0.5056	0.5090	0.5126	0.2443
	0.8254	0.7498	0.6806	0.6765	0.7098	0.8031	0.6978	0.6754	0.6809	0.3093
	0.8857	0.7932	0.7560	0.8101	0.9831	1.2595	1.1301	0.9536	0.9114	0.2443
	1.0748	0.8730	0.8537	0.9472	1.4045	2.2598	1.9393	1.5486	1.3060	0.1011
AkCa10	0.8622	0.6444	0.6812	0.7469	0.7633	0.7761	0.7463	0.7524	0.7492	0.1011
	0.8776	0.7949	0.7781	0.8345	0.9843	1.1372	1.0021	0.9237	0.8978	0.2443
	0.8901	0.8374	0.8407	0.9388	1.1676	1.4477	1.2115	1.0604	1.0194	0.3093
	0.9116	0.8764	0.8894	0.9856	1.3528	1.9241	1.7160	1.4103	1.2266	0.2443
	1.0748	0.8977	0.9420	1.0595	1.4386	2.2665	1.9441	1.5505	1.3068	0.1011

Table II-2.9: Frequency dependent resulting $V_S - \kappa$ correction 5-point distributions for used GMPEs at Gösgen.

GMPE	Frequency [Hz]									Weight
	0.5	1	2.5	5	10	20	33.3	50	100	
CaBo08	0.8512	0.6444	0.6534	0.5583	0.4936	0.4787	0.4978	0.5095	0.5036	0.1011
	0.8585	0.7944	0.6832	0.6124	0.5794	0.6193	0.5919	0.5819	0.5774	0.2443
	0.8718	0.8271	0.7327	0.7142	0.7503	0.9226	0.8235	0.7485	0.7223	0.3093
	0.9052	0.8454	0.7662	0.7971	1.0488	1.3411	1.2472	1.1059	1.0176	0.2443
	1.0748	0.8727	0.8510	0.9472	1.4045	2.2598	1.9393	1.5486	1.3060	0.1011
ChYo08	0.8463	0.6444	0.6281	0.5180	0.4294	0.3901	0.4006	0.4069	0.3982	0.1011
	0.8534	0.7830	0.6813	0.5677	0.5073	0.4983	0.4771	0.4816	0.4786	0.2443
	0.8660	0.8147	0.7040	0.6611	0.6610	0.7326	0.6584	0.6243	0.6214	0.3093
	0.9027	0.8326	0.7396	0.7743	1.0082	1.2458	1.1596	1.0326	0.9675	0.2443
	1.0748	0.8725	0.8501	0.9472	1.4045	2.2598	1.9393	1.5486	1.3060	0.1011
AkBo10	0.7728	0.6359	0.5155	0.4402	0.3842	0.3485	0.3514	0.3575	0.3609	0.1011
	0.8325	0.7080	0.6065	0.5218	0.5177	0.5189	0.4759	0.5039	0.5106	0.2443
	0.8553	0.7529	0.6801	0.6100	0.5975	0.6021	0.5817	0.5851	0.5926	0.3093
	0.9098	0.8092	0.7293	0.7582	0.7900	0.9012	0.8173	0.7405	0.7462	0.2443
	1.0748	0.8781	0.8504	0.9472	1.4045	2.2598	1.9393	1.5486	1.3060	0.1011
Zhao06	0.7474	0.6016	0.4247	0.2847	0.2234	0.2670	0.2773	0.2899	0.3127	0.1011
	0.8111	0.6528	0.5644	0.4802	0.4408	0.4316	0.4422	0.4488	0.4537	0.2443
	0.8369	0.7488	0.6436	0.5927	0.6048	0.6833	0.6010	0.5867	0.5943	0.3093
	0.8971	0.7918	0.7064	0.7589	0.8367	1.0657	0.9615	0.8210	0.7899	0.2443
	1.0748	0.8729	0.8498	0.9472	1.4045	2.2598	1.9393	1.5486	1.3060	0.1011
AkCa10	0.8702	0.6444	0.6783	0.6530	0.6533	0.6701	0.6530	0.6602	0.6581	0.1011
	0.8845	0.7917	0.7360	0.7502	0.8397	0.9697	0.8648	0.8031	0.7823	0.2443
	0.8961	0.8341	0.7638	0.8228	0.9943	1.2275	1.0378	0.9166	0.8833	0.3093
	0.9146	0.8726	0.8300	0.8947	1.2038	1.7159	1.5204	1.2473	1.1101	0.2443
	1.0748	0.8927	0.8646	0.9483	1.4045	2.2598	1.9393	1.5486	1.3060	0.1011

Table II-2.10: Frequency dependent resulting $V_S - \kappa$ correction 5-point distributions for used GMPEs at Leibstadt.

GMPE	Frequency [Hz]									Weight
	0.5	1	2.5	5	10	20	33.3	50	100	
CaBo08	0.8184	0.6444	0.6559	0.5793	0.5196	0.4994	0.5151	0.5255	0.5185	0.1011
	0.8256	0.7590	0.6835	0.6358	0.6110	0.6511	0.6163	0.6029	0.5971	0.2443
	0.8388	0.7899	0.7354	0.7419	0.7929	0.9778	0.8663	0.7817	0.7519	0.3093
	0.8920	0.8075	0.7677	0.8090	1.0684	1.3698	1.2714	1.1235	1.0319	0.2443
	1.0748	0.8722	0.8511	0.9472	1.4045	2.2598	1.9393	1.5486	1.3060	0.1011
ChYo08	0.8135	0.6432	0.6304	0.5371	0.4516	0.4061	0.4131	0.4183	0.4086	0.1011
	0.8203	0.7502	0.6815	0.5889	0.5346	0.5228	0.4955	0.4985	0.4942	0.2443
	0.8327	0.7777	0.7070	0.6863	0.6982	0.7754	0.6914	0.6517	0.6466	0.3093
	0.8895	0.7949	0.7428	0.7851	1.0253	1.2681	1.1780	1.0459	0.9793	0.2443
	1.0748	0.8720	0.8501	0.9472	1.4045	2.2598	1.9393	1.5486	1.3060	0.1011
AkBo10	0.7435	0.6198	0.5175	0.4563	0.4030	0.3622	0.3621	0.3672	0.3698	0.1011
	0.8010	0.6765	0.6090	0.5413	0.5446	0.5466	0.4966	0.5234	0.5284	0.2443
	0.8234	0.7359	0.6802	0.6327	0.6298	0.6353	0.6091	0.6109	0.6160	0.3093
	0.8764	0.7736	0.7311	0.7870	0.8336	0.9555	0.8608	0.7737	0.7764	0.2443
	1.0748	0.8721	0.8505	0.9472	1.4045	2.2598	1.9393	1.5486	1.3060	0.1011
Zhao06	0.7182	0.5741	0.4255	0.2940	0.2337	0.2766	0.2836	0.2954	0.3194	0.1011
	0.7794	0.6422	0.5661	0.4975	0.4657	0.4495	0.4614	0.4641	0.4680	0.2443
	0.8044	0.7146	0.6459	0.6149	0.6398	0.7238	0.6314	0.6128	0.6187	0.3093
	0.8626	0.7559	0.7092	0.7880	0.8859	1.1333	1.0187	0.8628	0.8263	0.2443
	1.0748	0.8715	0.8499	0.9472	1.4045	2.2598	1.9393	1.5486	1.3060	0.1011
AkCa10	0.8367	0.6440	0.6800	0.6783	0.6888	0.7023	0.6783	0.6844	0.6818	0.1011
	0.8510	0.7585	0.7397	0.8193	0.8874	1.0253	0.9069	0.8378	0.8149	0.2443
	0.8626	0.7971	0.7638	0.8554	1.0522	1.3031	1.0939	0.9601	0.9237	0.3093
	0.8941	0.8410	0.8328	0.9183	1.2694	1.8001	1.6121	1.3005	1.1438	0.2443
	1.0748	0.8726	0.8694	0.9621	1.4050	2.2620	1.9402	1.5486	1.3060	0.1011

Table II-2.11: Frequency dependent resulting $V_S - \kappa$ correction 5-point distributions for used GMPEs at Mühleberg.

GMPE	Frequency [Hz]									Weight
	0.5	1	2.5	5	10	20	33.3	50	100	
CaBo08	0.9249	0.6444	0.6820	0.8170	0.7601	0.7333	0.7596	0.7764	0.7668	0.1011
	1.0899	0.9815	0.9074	0.8713	0.8931	0.9520	0.9058	0.8887	0.8812	0.2443
	1.1274	1.1817	1.0695	1.0189	1.1171	1.3394	1.2140	1.1226	1.0852	0.3093
	1.1430	1.2137	1.1418	1.1298	1.2993	1.7722	1.5984	1.3636	1.2326	0.2443
	1.1483	1.2247	1.1674	1.1791	1.4062	2.2598	1.9393	1.5486	1.3069	0.1011
ChYo08	0.9249	0.6444	0.6820	0.7946	0.6609	0.5967	0.6099	0.6186	0.6049	0.1011
	1.0873	0.9746	0.8920	0.8345	0.7816	0.7651	0.7289	0.7346	0.7293	0.2443
	1.1197	1.1634	1.0277	0.9689	1.0195	1.1291	1.0108	0.9562	0.9505	0.3093
	1.1343	1.1946	1.0970	1.0451	1.1708	1.4417	1.3345	1.1818	1.1118	0.2443
	1.1394	1.2053	1.1215	1.0904	1.4045	2.2598	1.9393	1.5486	1.3060	0.1011
AkBo10	0.9258	0.6444	0.6820	0.6748	0.5898	0.5313	0.5328	0.5412	0.5458	0.1011
	1.0181	0.9034	0.8304	0.8004	0.7963	0.7970	0.7270	0.7681	0.7772	0.2443
	1.0936	1.0655	0.9357	0.9014	0.9202	0.9257	0.8906	0.8942	0.9041	0.3093
	1.1170	1.1655	1.0357	0.9854	1.1592	1.3891	1.2553	1.1335	1.1404	0.2443
	1.1778	1.2555	1.1660	1.0911	1.4045	2.2598	1.9393	1.5486	1.3060	0.1011
Zhao06	0.9245	0.6444	0.6424	0.4349	0.3418	0.4047	0.4168	0.4346	0.4703	0.1011
	0.9883	0.8720	0.7462	0.7359	0.6794	0.6591	0.6733	0.6818	0.6885	0.2443
	1.0698	1.0157	0.8965	0.8848	0.9331	1.0527	0.9213	0.8967	0.9070	0.3093
	1.0984	1.1276	1.0074	0.9763	1.1692	1.4830	1.3739	1.2213	1.1373	0.2443
	1.1599	1.2313	1.1421	1.0986	1.4031	2.2598	1.9393	1.5486	1.3060	0.1011
AkCa10	0.9249	0.6444	0.6820	0.8180	1.0071	1.0295	0.9996	1.0099	1.0064	0.1011
	1.1224	1.0303	0.9612	0.9820	1.2053	1.5640	1.4076	1.2880	1.1750	0.2443
	1.1849	1.1951	1.1593	1.2454	1.4942	1.8542	1.5890	1.3994	1.3375	0.3093
	1.1956	1.2559	1.2398	1.3226	1.6614	2.2264	1.8605	1.5354	1.4729	0.2443
	1.2090	1.2893	1.3129	1.4216	1.8895	2.7120	2.3885	1.9187	1.6637	0.1011

Table II-2.12: Frequency dependent $V_S - \kappa$ correction for PSSMs at the sites Beznau and Gösgen.

	Beznau			Gösgen		
Weight Branch	0.20	0.60	0.20	0.20	0.60	0.20
Freq. [Hz]	B6 (TK5)	B7 (TK6)	B8 (TK7)	B6 (TK5)	B7 (TK6)	B8 (TK7)
Mc4.5 SD60						
0.5	0.8371	0.8328	0.8229	0.8922	0.8880	0.8782
1	0.7774	0.7700	0.7531	0.7686	0.7615	0.7450
2.5	0.7931	0.7748	0.7337	0.6712	0.6558	0.6212
5	0.8558	0.8175	0.7351	0.7097	0.6781	0.6100
10	0.9624	0.8806	0.7179	0.7976	0.7299	0.5955
20	1.1720	0.9922	0.6871	0.9736	0.8248	0.5723
33.33	1.3695	1.0772	0.6737	1.1387	0.8969	0.5638
50	1.3601	1.0454	0.6889	1.1329	0.8730	0.5790
100	1.0943	0.9243	0.7111	0.9149	0.7746	0.5989
Mc4.5 SD90						
0.5	0.8362	0.8317	0.8213	0.8892	0.8849	0.8747
1	0.7771	0.7697	0.7526	0.7675	0.7604	0.7439
2.5	0.7932	0.7749	0.7337	0.6712	0.6557	0.6210
5	0.8560	0.8176	0.7351	0.7098	0.6780	0.6099
10	0.9627	0.8807	0.7178	0.7977	0.7300	0.5954
20	1.1731	0.9928	0.6867	0.9745	0.8251	0.5718
33.33	1.3724	1.0785	0.6734	1.1409	0.8977	0.5632
50	1.3649	1.0478	0.6882	1.1366	0.8744	0.5779
100	1.0977	0.9260	0.7105	0.9172	0.7753	0.5978
Mc4.5 SD120						
0.5	0.8357	0.8310	0.8202	0.8871	0.8827	0.8721
1	0.7770	0.7695	0.7524	0.7667	0.7596	0.7430
2.5	0.7933	0.7749	0.7337	0.6712	0.6556	0.6209
5	0.8561	0.8177	0.7351	0.7098	0.6780	0.6098
10	0.9630	0.8809	0.7178	0.7978	0.7300	0.5952
20	1.1736	0.9936	0.6866	0.9749	0.8257	0.5717
33.33	1.3747	1.0798	0.6729	1.1427	0.8987	0.5625
50	1.3686	1.0499	0.6878	1.1395	0.8760	0.5772
100	1.1008	0.9273	0.7102	0.9194	0.7760	0.5970

Table II-2.13: Frequency dependent $V_S - \kappa$ correction for PSSMs at the sites Leibstadt and Mühleberg.

	Leibstadt			Mühleberg		
Weight Branch	0.20	0.60	0.20	0.20	0.60	0.20
Freq. [Hz]	B6 (TK5)	B7 (TK6)	B8 (TK7)	B6 (TK5)	B7 (TK6)	B8 (TK7)
Mc4.5 SD60						
0.5	0.8079	0.8038	0.7946	1.3137	1.3074	1.2927
1	0.7226	0.7159	0.7001	1.2556	1.2439	1.2167
2.5	0.7117	0.6953	0.6585	1.0148	0.9914	0.9393
5	0.7644	0.7302	0.6567	1.0926	1.0437	0.9387
10	0.8592	0.7862	0.6411	1.2015	1.0996	0.8972
20	1.0472	0.8869	0.6145	1.4906	1.2628	0.8764
33.33	1.2235	0.9629	0.6032	1.7469	1.3763	0.8656
50	1.2165	0.9355	0.6178	1.7369	1.3388	0.8890
100	0.9797	0.8281	0.6381	1.4039	1.1890	0.9199
Mc4.5 SD90						
0.5	0.8063	0.8021	0.7924	1.3111	1.3045	1.2892
1	0.7222	0.7153	0.6996	1.2544	1.2426	1.2156
2.5	0.7118	0.6953	0.6584	1.0146	0.9911	0.9389
5	0.7646	0.7303	0.6567	1.0927	1.0437	0.9386
10	0.8594	0.7864	0.6410	1.2016	1.0996	0.8971
20	1.0482	0.8872	0.6141	1.4919	1.2632	0.8757
33.33	1.2260	0.9639	0.6028	1.7501	1.3775	0.8647
50	1.2205	0.9376	0.6170	1.7424	1.3412	0.8873
100	0.9826	0.8294	0.6374	1.4074	1.1901	0.9183
Mc4.5 SD120						
0.5	0.8053	0.8009	0.7908	1.3091	1.3024	1.2865
1	0.7220	0.7151	0.6992	1.2534	1.2417	1.2144
2.5	0.7117	0.6953	0.6583	1.0144	0.9910	0.9386
5	0.7646	0.7303	0.6566	1.0927	1.0437	0.9384
10	0.8597	0.7864	0.6409	1.2017	1.0996	0.8967
20	1.0488	0.8879	0.6140	1.4925	1.2642	0.8755
33.33	1.2280	0.9651	0.6023	1.7529	1.3789	0.8637
50	1.2238	0.9394	0.6165	1.7468	1.3433	0.8861
100	0.9852	0.8305	0.6370	1.4105	1.1913	0.9172

Figures II-2.3 to II-2.6 show the five discrete correction functions versus frequency for all GMPEs per site. Figures with all individual correction functions resulting from all combinations and color coded by their weight can be found in the appendix to the HID (Chapter 3). Furthermore, the individual histograms, selected 5-point distributions and a theoretically fitted distribution are also shown in the appendix. Figures II-2.7 to II-2.10 shows the different $V_S - \kappa$ corrections to be applied to the generic parameterized Swiss stochastic model in order to be applicable for the given site specific NPP conditions.

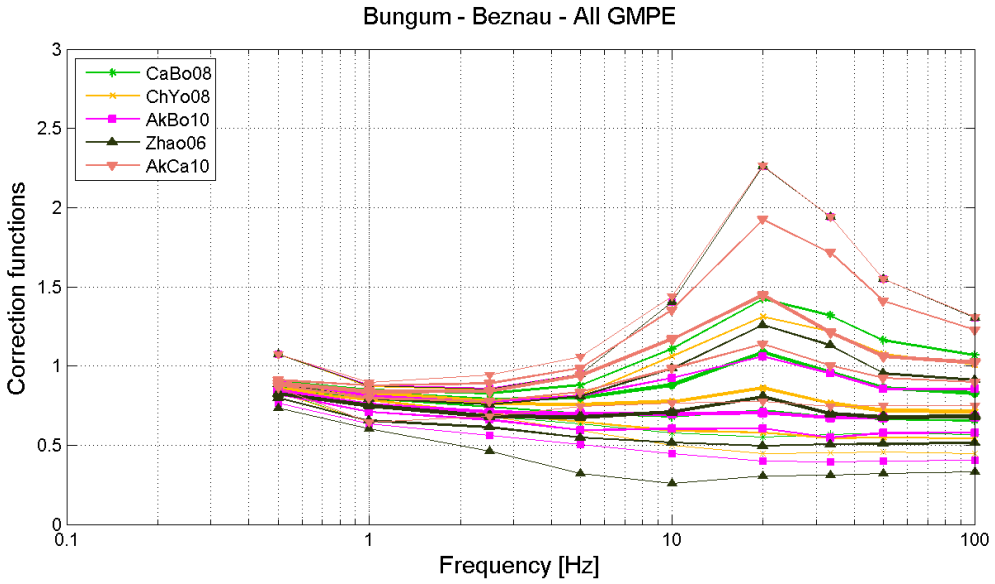

Figure II-2.3: $V_S - \kappa$ corrections to be applied to the GMPEs for Beznau.

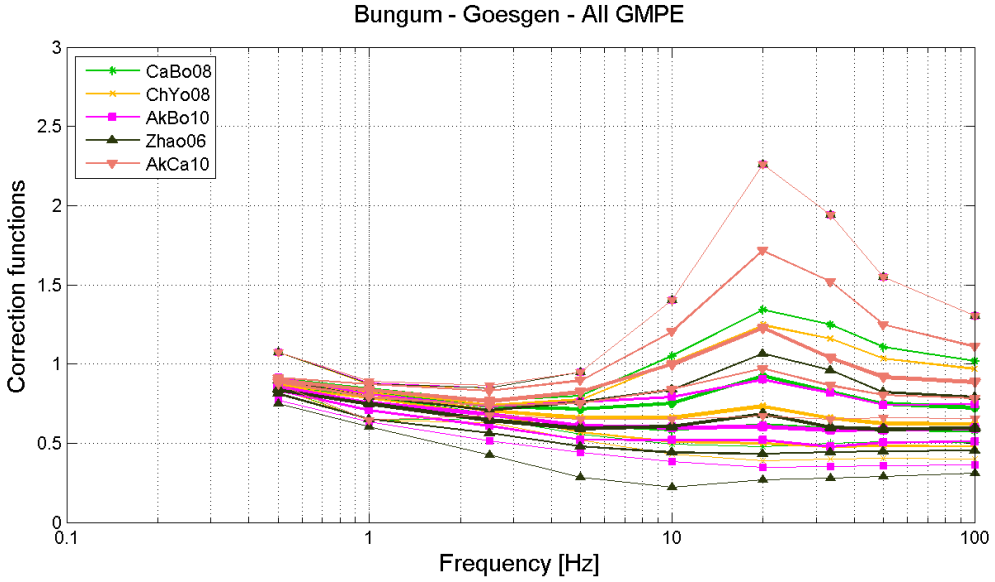

Figure II-2.4: $V_S - \kappa$ corrections to be applied to the GMPEs for Gösgen.

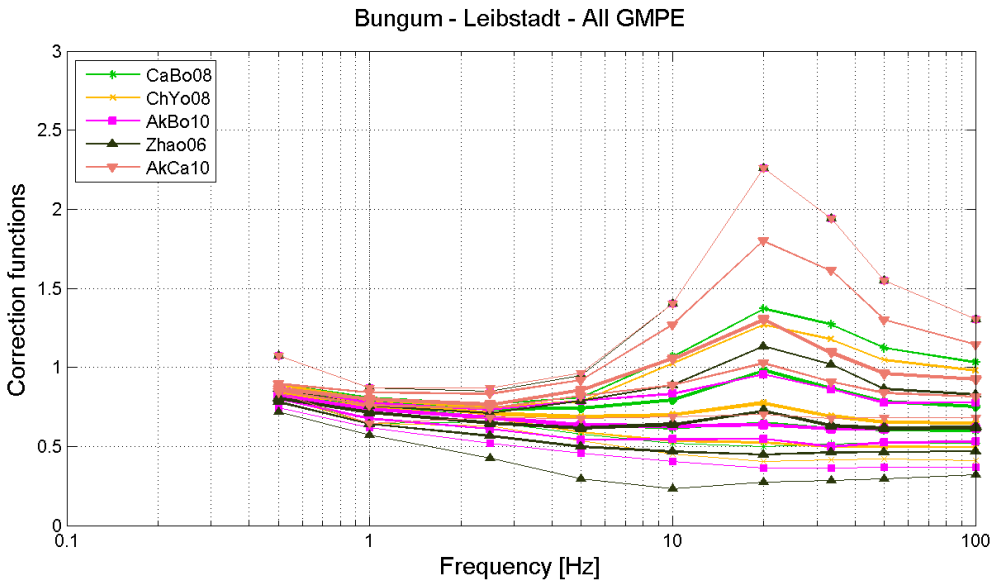

Figure II-2.5: $V_S - \kappa$ corrections to be applied to the GMPEs for Leibstadt.

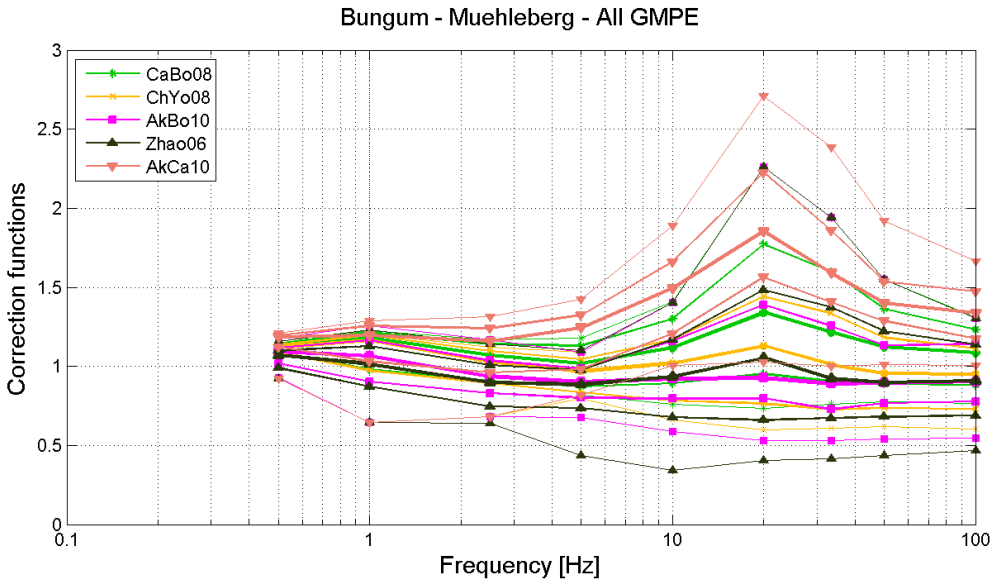

Figure II-2.6: $V_S - \kappa$ corrections to be applied to the GMPEs for Mühleberg.

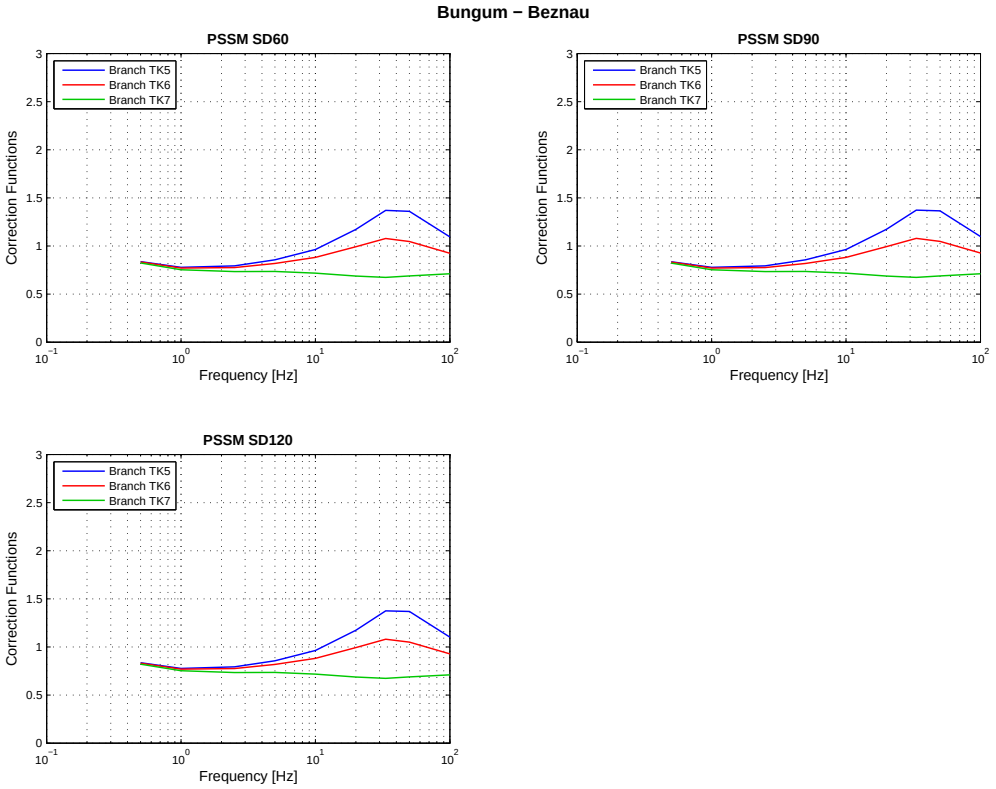

Figure II-2.7: $V_S - \kappa$ corrections to be applied to the PSSMs for Beznau.

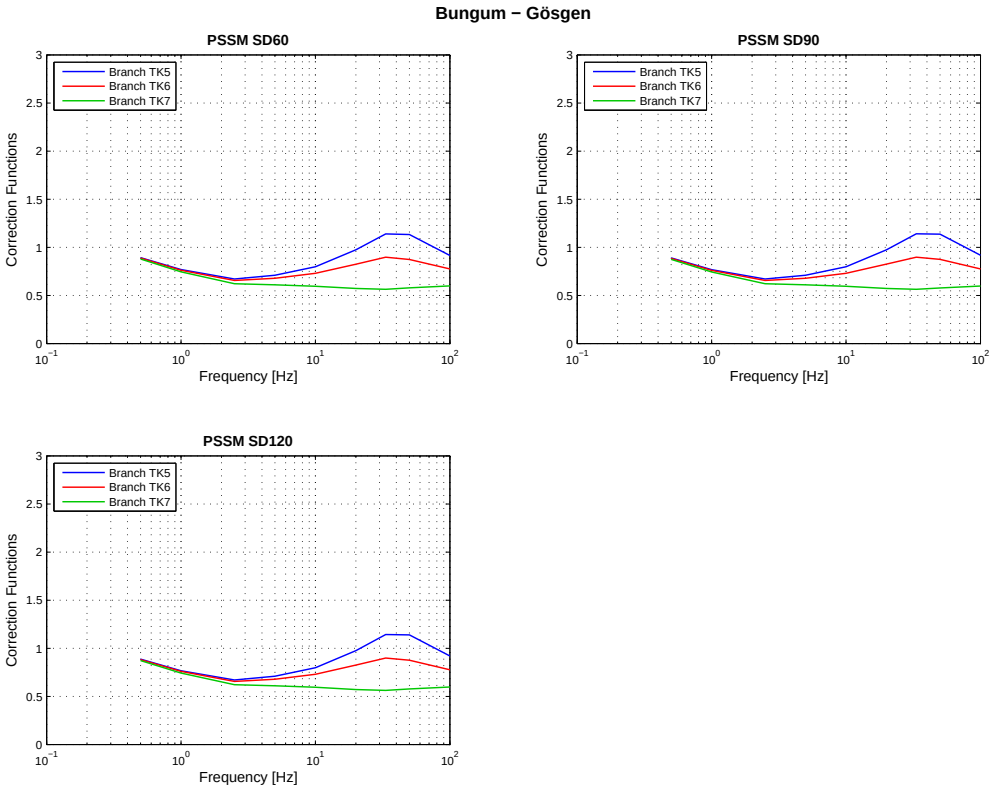

Figure II-2.8: $V_S - \kappa$ corrections to be applied to the PSSMs for Gösgen.

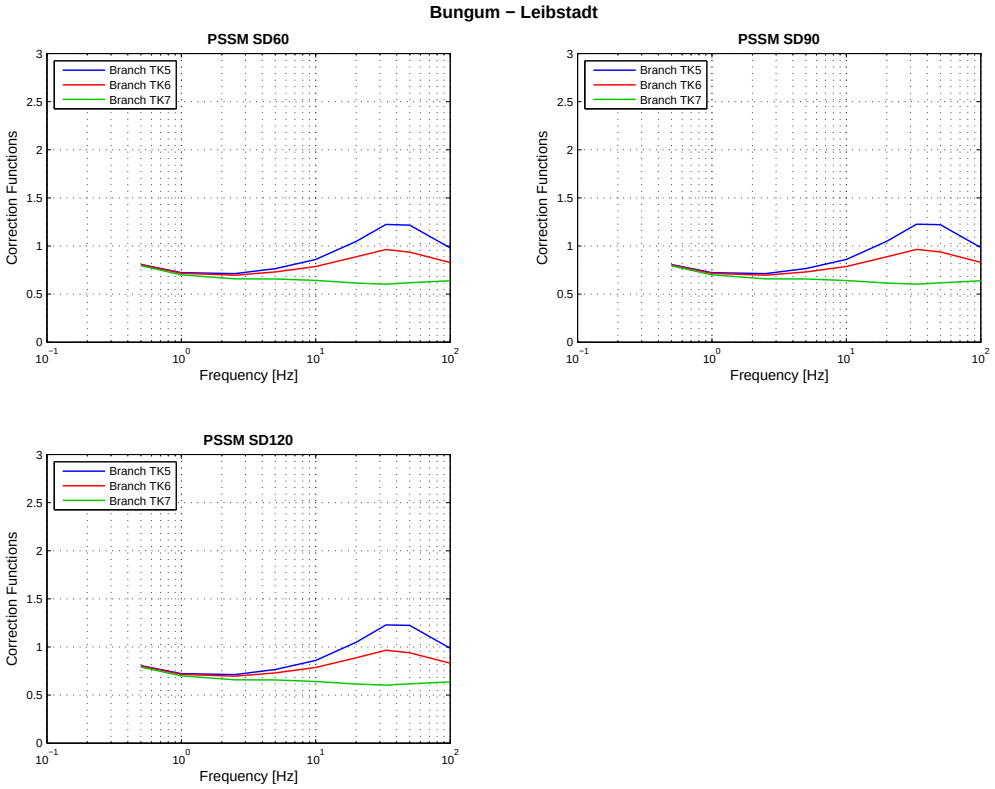

Figure II-2.9: $V_S - \kappa$ corrections to be applied to the PSSMs for Leibstadt.

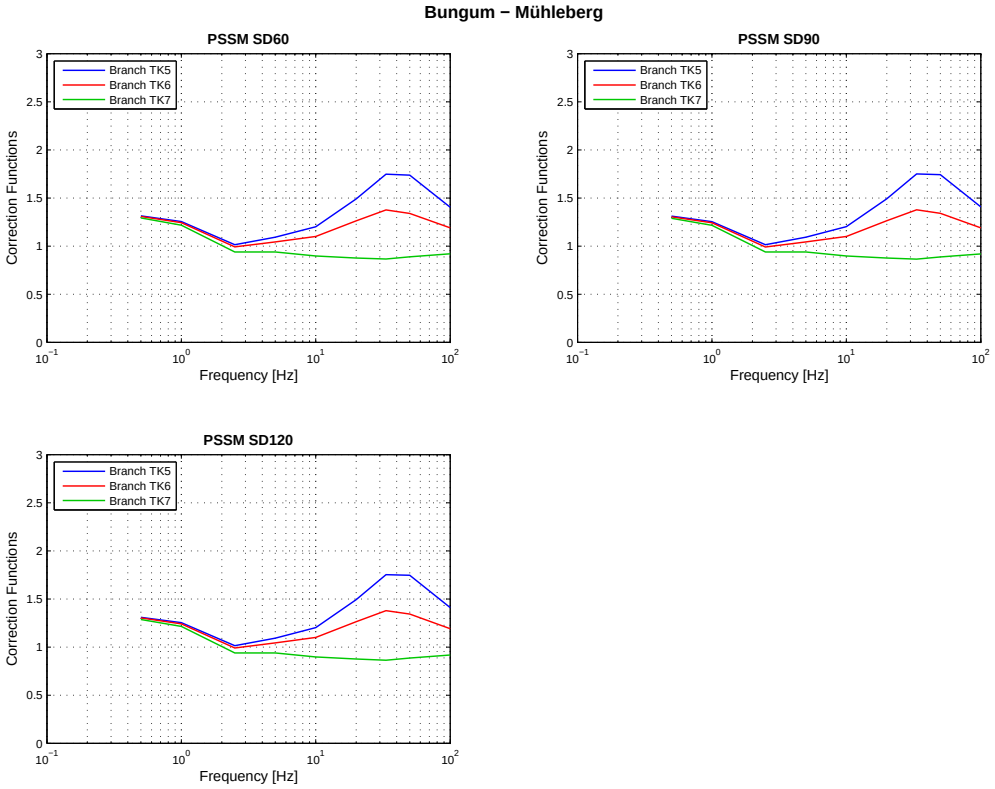

Figure II-2.10: $V_S - \kappa$ corrections to be applied to the PSSMs for Mühleberg.

2.3.2 Small Magnitude Adjustments

For the evaluation of the GMPE specific small magnitude adjustments only the median $V_S - \kappa$ correction factors of all the provided 5-point distributions are used, as it was decided that the small magnitude adjustments will only be developed for the average case and not for each individual correction function (PMT-TN-1238). Thus, the small magnitude adjustments are the same for all experts, but repeated here in Table II-2.14 for the sake of completeness and illustrated in Figure II-2.11 and II-2.12.

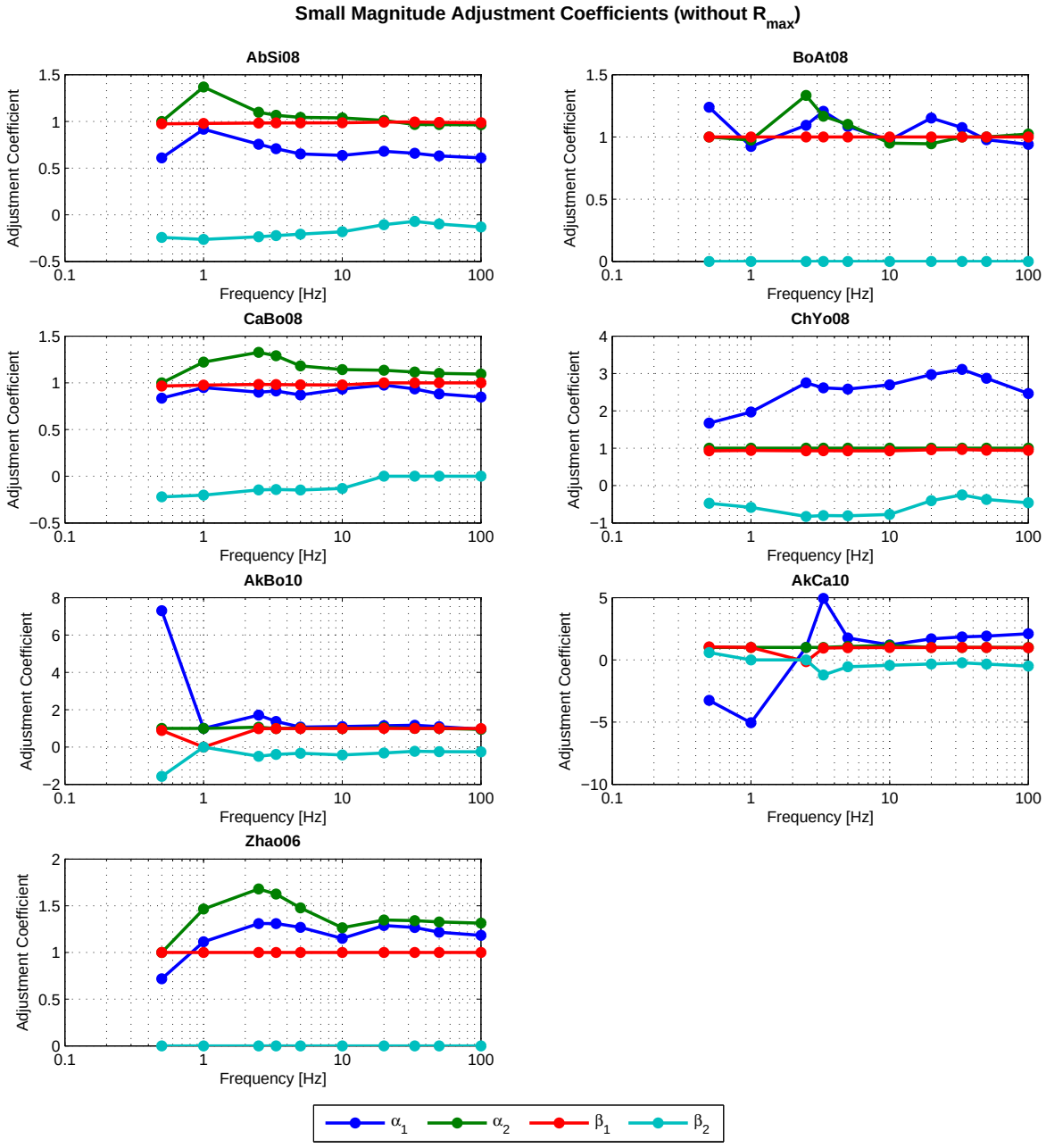

Figure II-2.11: Small magnitude adjustments coefficients as function of frequency for the all GMPEs.

Table II-2.14: Small magnitude adjustments coefficients.

	Abrahamson & Silva (2008)					Boore & Atkinson (2008)				
T [s]	α_1	α_2	β_1	β_2	R_{max}	α_1	α_2	β_1	β_2	R_{max}
0.01	0.609036	0.964257	0.986605	-0.131781	3.57E+04	0.940502	1.022616	1.000000	0.000000	1.00E+09
0.02	0.629604	0.965329	0.988756	-0.099660	4.07E+05	0.977300	1.000000	1.000000	0.000000	1.00E+09
0.03	0.657761	0.967357	0.993601	-0.071271	2.27E+07	1.074586	1.000000	1.000000	0.000000	1.00E+09
0.05	0.679706	1.010904	0.991680	-0.106456	2.22E+05	1.151448	0.945013	1.000000	0.000000	1.00E+09
0.1	0.635927	1.037980	0.984796	-0.182620	4.40E+03	0.974222	0.950274	1.000000	0.000000	1.00E+09
0.2	0.651637	1.043100	0.984107	-0.207141	2.31E+03	1.084848	1.101550	1.000000	0.000000	1.00E+09
0.3	0.707216	1.065147	0.983422	-0.222960	1.65E+03	1.205896	1.166359	1.000000	0.000000	1.00E+09
0.4	0.755898	1.097644	0.982712	-0.236174	1.28E+03	1.093478	1.334035	1.000000	0.000000	1.00E+09
1	0.915893	1.367623	0.978436	-0.263900	8.15E+02	0.924116	0.974715	1.000000	0.000000	1.00E+09
2	0.608779	1.000000	0.974376	-0.242967	1.10E+03	1.238186	1.000000	1.000000	0.000000	1.00E+09

	Campbell & Bozorgnia (2008)					Chiou & Youngs (2008)				
T [s]	α_1	α_2	β_1	β_2	R_{max}	α_1	α_2	β_1	β_2	R_{max}
0.01	0.847179	1.094261	1.000000	0.000000	1.00E+09	2.462946	1.000000	0.944935	-0.458418	1.57E+02
0.02	0.881357	1.100586	1.000000	0.000000	1.00E+09	2.873730	1.000000	0.946856	-0.372663	2.54E+02
0.03	0.934893	1.114376	1.000000	0.000000	1.00E+09	3.109735	1.000000	0.966292	-0.248344	9.79E+02
0.05	0.976058	1.135405	1.000000	0.000000	1.00E+09	2.969316	1.000000	0.959155	-0.402534	2.17E+02
0.1	0.932945	1.141482	0.977278	-0.130765	3.52E+04	2.695695	1.000000	0.930247	-0.772189	6.67E+01
0.2	0.870681	1.181271	0.979148	-0.147509	1.53E+04	2.584716	1.000000	0.931449	-0.809059	6.32E+01
0.3	0.912008	1.289225	0.981219	-0.142015	2.00E+04	2.614341	1.000000	0.932936	-0.801818	6.40E+01
0.4	0.899165	1.326194	0.982502	-0.145844	1.69E+04	2.750116	1.000000	0.930586	-0.824968	6.18E+01
1	0.949262	1.221818	0.975229	-0.202856	2.45E+03	1.966745	1.000000	0.939658	-0.583454	1.00E+02
2	0.835687	1.000000	0.965445	-0.220424	1.60E+03	1.671214	1.000000	0.931415	-0.473294	1.43E+02

	Akkar & Bommer (2010)					Akkar & Cagnan (2010)				
T [s]	α_1	α_2	β_1	β_2	R_{max}	α_1	α_2	β_1	β_2	R_{max}
0.01	0.956934	0.949129	0.992409	-0.258327	9.32E+02	2.098964	1.000000	0.985549	-0.499646	1.44E+02
0.02	1.090919	1.000000	0.994584	-0.253021	1.02E+03	1.913122	1.000000	0.990459	-0.335515	3.83E+02
0.03	1.164927	1.000000	0.998788	-0.230673	1.52E+03	1.851248	1.000000	0.997570	-0.236164	1.37E+03
0.05	1.134080	1.040216	0.995602	-0.321814	4.41E+02	1.689890	1.000000	0.995553	-0.333705	3.95E+02
0.1	1.093536	0.986668	0.988564	-0.425342	2.04E+02	1.204350	1.157951	0.987542	-0.431630	1.97E+02
0.2	1.068203	1.007264	0.988710	-0.334035	3.86E+02	1.759524	1.071974	0.978784	-0.546911	1.20E+02
0.3	1.369695	0.988071	0.987967	-0.400250	2.36E+02	4.937988	1.000000	0.951557	-1.213879	4.38E+01
0.4	1.710275	1.062132	0.984888	-0.499538	1.44E+02	1.000000	1.000000	-0.142956	0.000000	1.99E+01
1	1.000000	1.000000	0.000000	0.000000	1.00E+09	-5.048030	1.000000	1.000000	0.000000	1.99E+01
2	7.299540	1.000000	0.881761	-1.575579	3.50E+01	-3.254365	1.000000	1.044931	0.593817	1.00E+09

	Zhao et al. (2006)				
T [s]	α_1	α_2	β_1	β_2	R_{max}
0.01	1.182482	1.313722	1.000000	0.000000	1.00E+09
0.02	1.217249	1.326714	1.000000	0.000000	1.00E+09
0.03	1.267071	1.340177	1.000000	0.000000	1.00E+09
0.05	1.288501	1.347281	1.000000	0.000000	1.00E+09
0.1	1.150978	1.265212	1.000000	0.000000	1.00E+09
0.2	1.268576	1.476775	1.000000	0.000000	1.00E+09
0.3	1.310229	1.625552	1.000000	0.000000	1.00E+09
0.4	1.308962	1.679158	1.000000	0.000000	1.00E+09
1	1.113543	1.465133	1.000000	0.000000	1.00E+09
2	0.718525	1.000000	1.000000	0.000000	1.00E+09

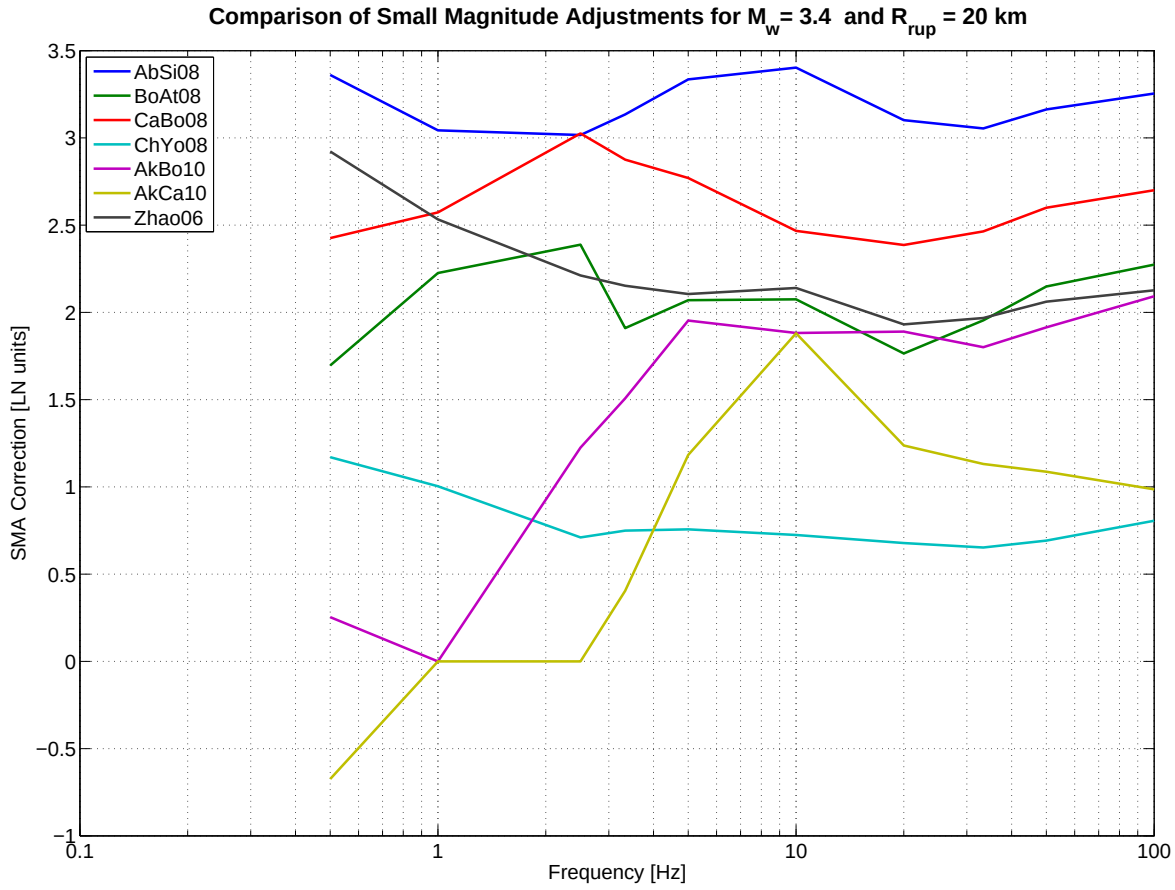

Figure II-2.12: Comparison of the resulting small magnitude adjustments functions as function of frequency for M=3.4 and R=20 km.

2.4 Aleatory Variability for the Horizontal Component

Section 6.7 in Part I, provides the final τ and ϕ models used for the PRP, which supersede the model of Rodriguez-Marek and Cotton [2011] (equations 4.1, 4.2 and table 5.3 and 5.4 in EXT-TB-1058) and Rodriguez-Marek [2012] (EXT-TN-1225). In Table II-2.15 the different weights for the aleatory variability logic tree branches are shown. The selected values for the ϕ_{SS} uncertainty are given in the second column at the bottom. The generic σ logic tree is represented in Figure I-9.2.

Table II-2.15: Weights and parameters assigned to the aleatory variability.

Model	Branch / Value for $\sigma(\phi_{SS})$	Weight
τ Model	Global	0.667
	Original GMPE	0.333
τ Uncert.	+0.1	0.20
	0	0.60
	-0.1	0.20
ϕ_{SS}	Model 1 (Constant)	0.333
	Model 2 (Distance Dependent)	-
	Model 3 (Dist. and Mag. Dependent)	0.667
ϕ_{SS} Uncert.	$-1.6 \cdot \sigma(\phi_{SS})$	0.20
	$0 \cdot \sigma(\phi_{SS})$	0.60
	$+1.6 \cdot \sigma(\phi_{SS})$	0.20
$\sigma(\phi_{SS})$	0.08	1.00

2.5 Maximum Ground Motion

Table II-2.16 shows the frequency dependent weights assigned to the horizontal maximum ground motion logic tree (see generic Figure I-9.3). The weights assigned to the six scaling factors for the six branches are given in Table II-2.17.

Table II-2.16: Weights for the horizontal maximum ground motion model.

Model	Frequency [Hz]								
	0.5	1	2.5	5	10	20	33.3	50	100
R-dependent	1.00	1.00	1.00	0.95	0.90	0.85	0.80	0.75	0.70
R-independent	0.00	0.00	0.00	0.05	0.10	0.15	0.20	0.25	0.30

The vertical maximum ground motion model is the same as the horizontal (see Figure I-9.3). Thus, the same weights and scale factors apply for the vertical hazard.

Based on the hazard feedback, which showed very little impact of the maximum ground motion truncation for rock, the project has decided to trim the maximum ground motion

Table II-2.17: Weights for the scaling factors for the maximum ground motion model (both horizontal and vertical).

Model	Scale Factors [LN units]					
	7.50	12.59	21.14	35.48	59.57	100
R-dependent	0	0.10	0.40	0.40	0.10	0
R-independent	0	0.10	0.40	0.40	0.10	0

branches for the practical implementation. Thus, the hazard will be computed based on untruncated ground motions for rock.

2.6 V/H Ratio

Table II-2.18 shows the weights of the candidate V/H models. No NPP site specific weights were assigned. This implies for the site of Gösgen to use the "shallow" case defined by the ratio based on the merged profiles 4-5 (see TP3-ASW-1004). The basic logic tree for the V/H models can be found in Figure I-9.4.

Table II-2.18: Weights for median V/H models.

Model	Weight
Bommer et al. (2011)	0.10
Campbell and Bozorgnia (2003)	0.10
Gülerce and Abrahamson (2011)	0.40
Edwards et al. (2011) without correction above 7 Hz	-
Edwards et al. (2011) with correction above 7 Hz	-
US West Median	0.20
US East Median	0.20

2.7 Aleatory Variability for the Vertical Component

The additional aleatory variability to be added to the median V/H models is shown in Table II-2.19 (see Figure I-9.2 for the generic logic tree). The missing values for 2.5 and 5 Hz were obtained through linear interpolation in the log(frequency) – σ_{VADD} space.

Table II-2.19: Additional vertical variability (σ_{VADD} in LN units).

Frequency [Hz]								
0.5	1	2.5	5	10	20	33.3	50	100
0.235	0.16	0.166*	0.171*	0.175	0.24	0.20	0.14	0.11

* Based on interpolated values. σ_{VADD} values of zero are discarded for the averaging.

Figure II-2.13 shows the additional aleatory variability for the vertical component over frequency.

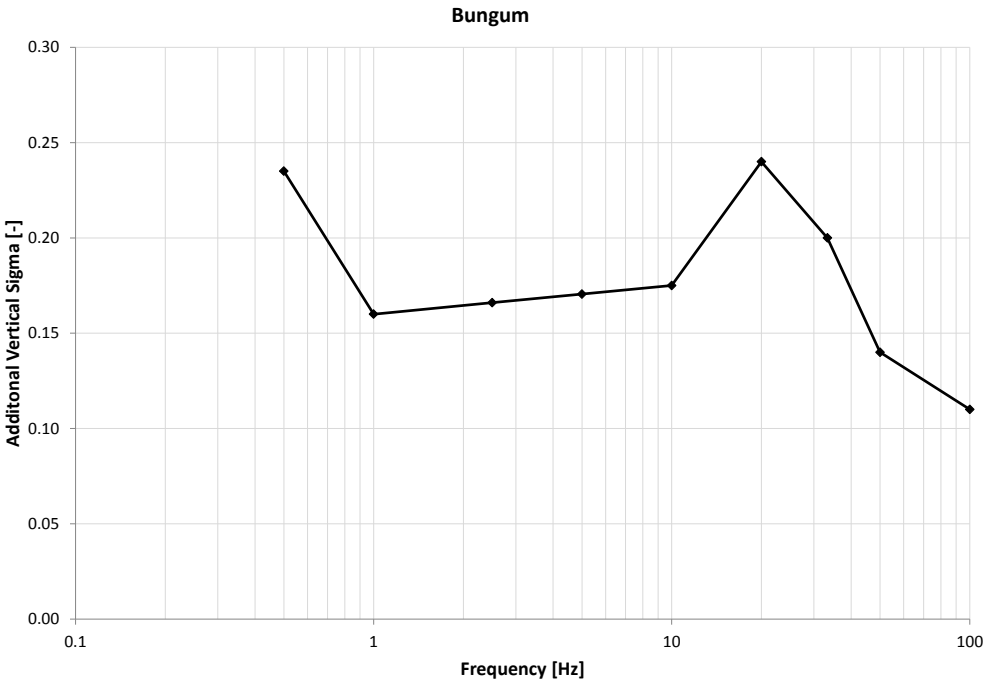

Figure II-2.13: Additional aleatory variability for the vertical component

2.8 Implementation of Hazard Logic Tree

The total number of logic tree branches amounts to 6528 (see Figure II-2.1). Each individual combination of zonation alternatives and source parameters in each individual SP1 source has to be combined with these 6528 alternative ground motion models. Among other such measures, the project decided to reduce the huge number of combinations and thus, the CPU time necessary to obtain the rock hazard results by removing the maximum ground motion truncation from the SP2 models. This section documents the effect of this project management decision.

To be in the position to run the untrimmed case, we reduce the model for the aleatory variability (single-station sigma) from 24 to four branches. NB: This is only done for the demonstration that the project management's decision has only a little effect on the final results. The final calculations will be performed with the entire, 24-branch sigma tree (but without the maximum ground motion part, thus reducing the total number of branches from 6528 to 816).

Figure II-2.14 shows the four selected sigma branches. The weights are the original weights for these branches, renormalized to sum up to unity. Figure II-2.15 shows the difference in the sigma domain between the entire and the simplified tree. Since the sigma value is magnitude (M) and distance (R) dependent the comparison in Figure II-2.15 is performed for the mean of the nine M-R bins. The calculation of the effect of the project management's decision to cap the maximum ground motion part of the logic tree is performed at 5 Hz spectral acceleration since the effect of the maximum ground motion truncation has been shown to be the highest for this frequency (see TP4-RF-1441). At 5 Hz the total single-station sigma amounts to 0.583 before and to 0.580 after the simplification.

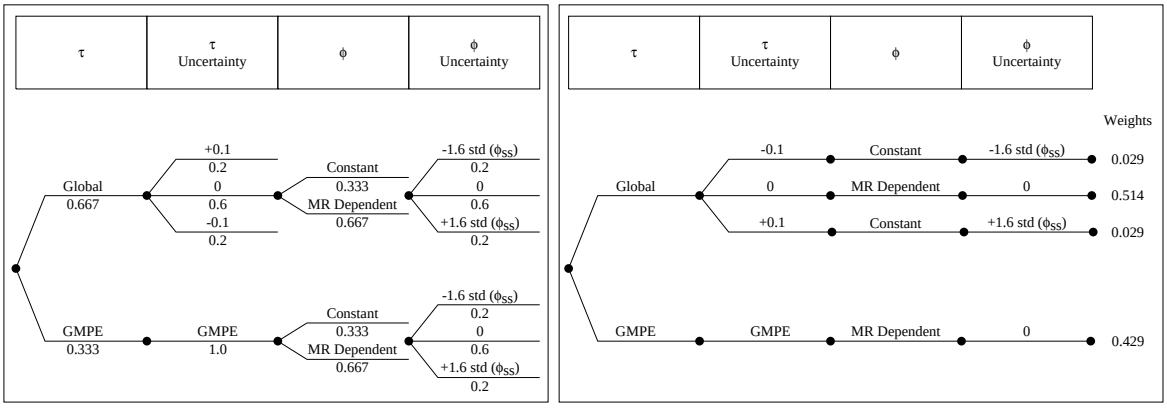

Figure II-2.14: Simplification made to the sigma logic tree. The four branches (on the right hand side) are used to quantify the effect of the removal of the maximum ground motion part in the logic tree of Figure I-9.3.

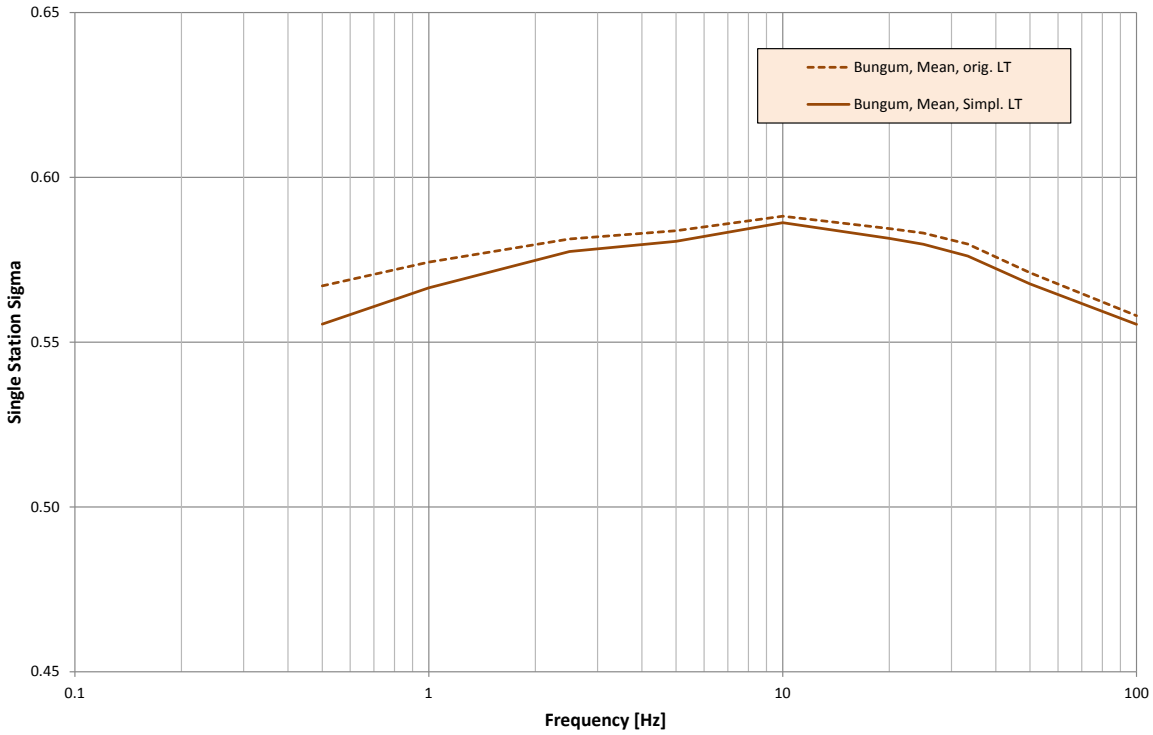

Figure II-2.15: Comparison of the overall σ before and after the simplification documented in Figure II-2.14.

For the hazard computation we used one of the four SP1 Expert Group models, EG1c, with its entire complexity. We performed the calculation for one site only, Beznau, as we know the effect of the maximum ground motion truncation to be largely site independent. Figure II-2.16 shows the comparison for the mean hazard and four fractiles.

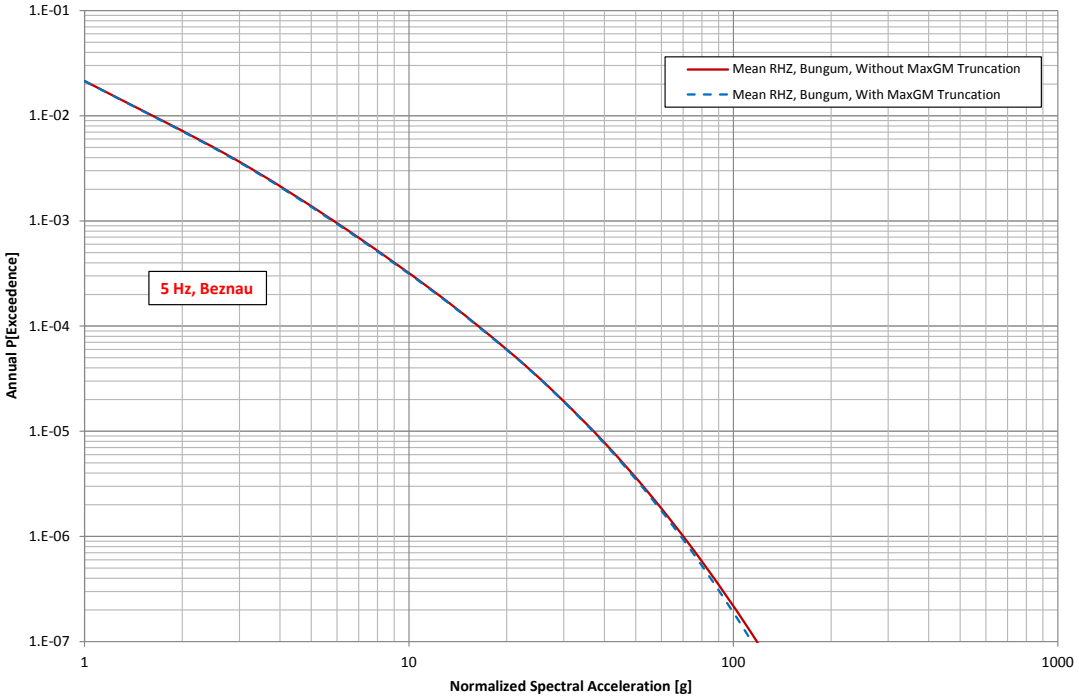

Figure II-2.16: Effect of the removal of the maximum ground motion truncation in the logic tree on the rock hazard for Beznau, 5 Hz.

This conversion of the original "scientific logic tree" to a dealable "hazard logic tree" has been introduced in the framework of the PRP in order to allow for efficient computation without tradeoffs for the overall model in key elements of the initial logic tree.

Chapter 3

Appendix to EG1-HID-1009

The procedure to retrieve the discrete 5-point distributions for the $V_S - \kappa$ corrections is visualized by means of 3 figure types:

- XY graph showing all correction function versus frequency with curve colors indicating the curve weights (see example Figure II-3.1)
- Plot of the probability distributions (cumulative weights) of $V_S - \kappa$ corrections at the 9 PRP frequencies (see example Figure II-3.2)
- Corresponding plot of the probability density of $V_S\kappa$ at the 9 analysis frequencies (see example Figure II-3.3)

which are attached as an electronic appendix to this HID and contains folders/files (or ZIP files), which correspond to the above listed figure types. Figures within above folders are provided as individual PNG and/or EPS files, where the individual files are named according to the convention and example as follows:
<expert>_<site>_<gmpe>_<figure-type>.<graphic-format>
Bungum_Beznau_AbSi08_fig1.png

A direct link to files containing a compilation of all figures per site is given here:

- Open external file: $V_S - \kappa$ correction functions for Beznau and associated cumulative probability functions and probability density functions.
- Open external file: $V_S - \kappa$ correction functions for Gösgen and associated cumulative probability functions and probability density functions.
- Open external file: $V_S - \kappa$ correction functions for Leibstadt and associated cumulative probability functions and probability density functions.
- Open external file: $V_S - \kappa$ correction functions for Mühleberg and associated cumulative probability functions and probability density functions.

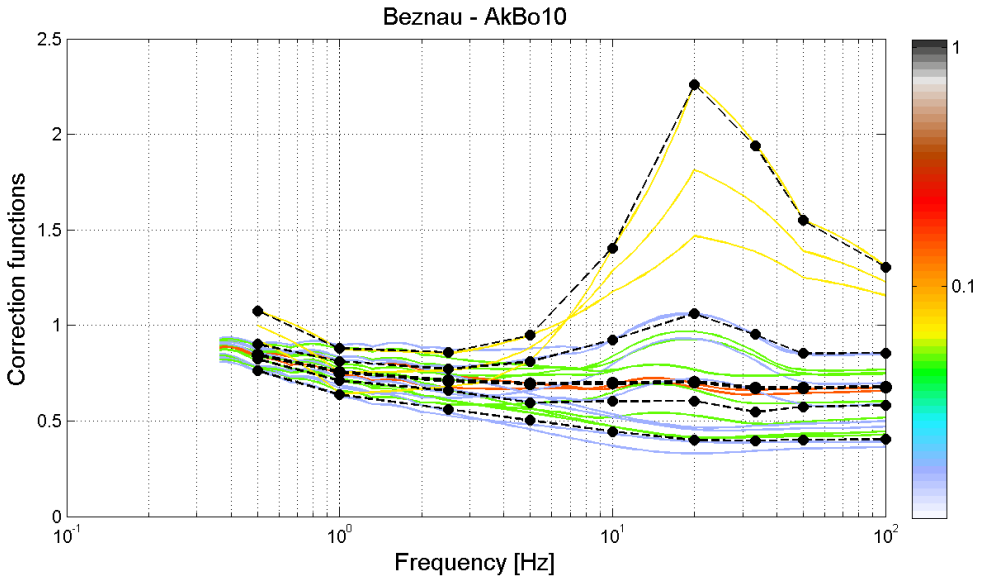

Figure II-3.1: Evaluated $V_S - \kappa$ correction functions for Akkar & Bommer (2010) at the site of Beznau and the final 5 discrete correction functions in black dashed lines. The weights of the individual correction functions are color coded according to the scale on the right.

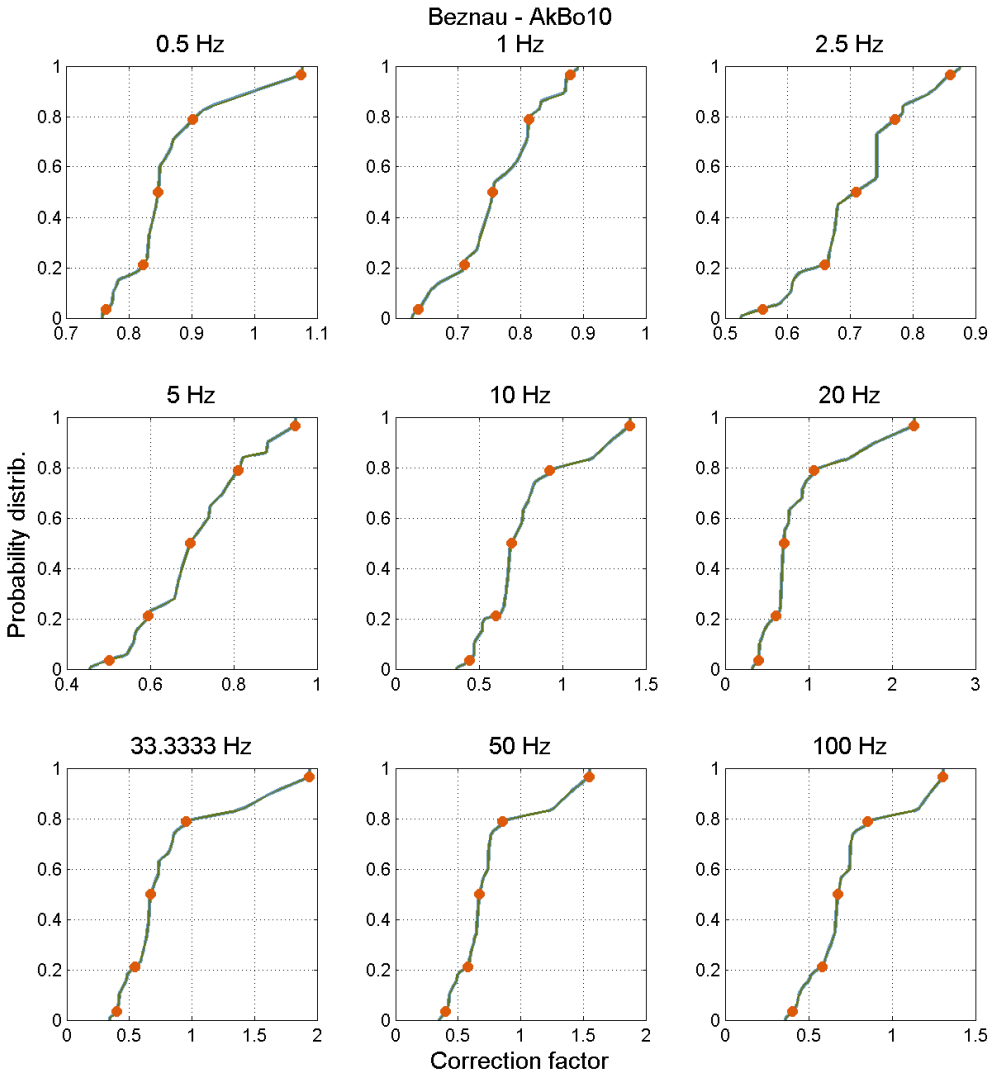

Figure II-3.2: Probability distributions (cumulative weights) of $V_S - \kappa$ corrections at the 9 PRP frequencies for Akkar & Bommer (2010) at the site of Beznau. The blue line represents the data by means of 105 fractiles. The thin green line is a smoothed version of above blue line (just for display, not used for further processing). The orange dots are the 3.4893, 21.1702, 50, 78.8298 and 96.5107 % percentiles used for the 5-point distribution.

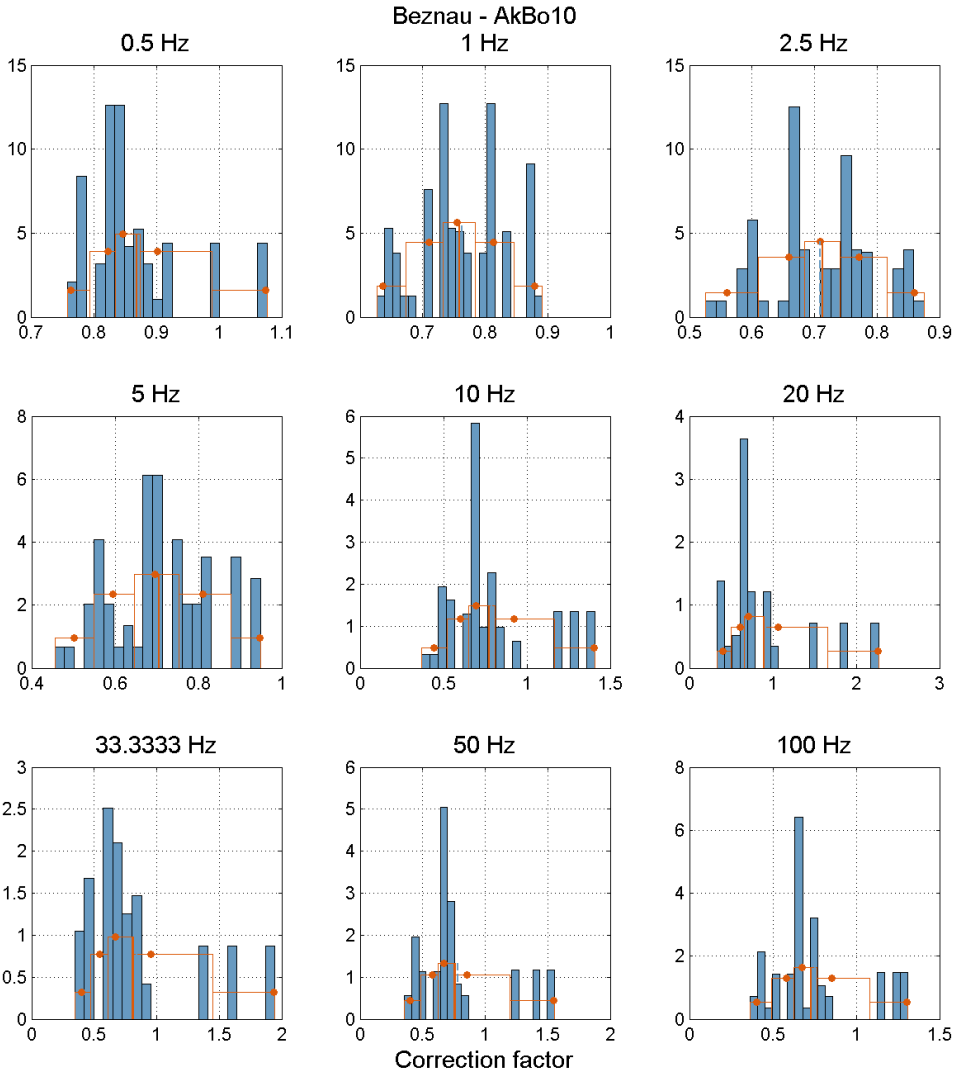

Figure II-3.3: Probability density functions of $V_S - \kappa$ corrections at the 9 PRP frequencies for Akkar & Bommer (2010) at the site of Beznau. The blue bars represent the weighted histogram of the data partitioned into 21 bins. The orange dots are the corresponding discrete 5 distribution points for the 3.4893, 21.1702, 50, 78.8298 and 96.5107 % percentiles, as in Figure II-3.2. The corresponding probabilities/weights are for the given discretization: 0.10108, 0.24429, 0.30926, 0.24429, 0.10108. The thin red and thin dashed blue line in the middle show the mean value of the data and the approximation with the 5-point distribution, respectively. Note that in the case of the thin dashed blue and red line being identical, only the red line is seen as it is on top of the blue line.

Chapter 4

QA-Certificate EG2-QC-1060

QA Certificate	PEGASOS REFINEMENT PROJECT
EG2-QC-1060	

Hazard Input Document (HID)

Expert group: EG2 ***HID designation:*** **EG2-HID-1009**

Expert: H. Bungum ***Expert Model (EXM)*** EG2-EXM-1009

HID parameterisation of Expert Model:

TFI: N. A. Abrahamson ***Hazard Input Specialist of TFI-team:*** Ph. Roth

HID based on Elicitation Documents: ☒ EG2-ES-1009

HID based on Exp. Assessments (EXA): ☒ EG2-EXA-1017 to 1029

Remarks on the HID model parameterisation in terms of hazard computation input:

The undersigned Hazard Input Specialist confirms that this HID includes all required (subproject specific) input information for hazard computations. No further interpretations of this input will be required and no simplifications except Algorithmic Pinching according to paragraph 2.9 of the QA-Guidelines will be applied to convert this HID into hazard software Input Files.

Signature:

HID acceptance by the Expert / Expert Group:

Date of HID review by the Expert / Expert group: 20.11.2013

HID accepted: ☒ ***HID not accepted:*** ☐

Reasons for non-acceptance of HID / Recommendations:

The undersigned Expert(s) accept(s) the parameterisation proposed in this HID as a faithful and adequate representation of his/their Expert Model. He/they confirm(s) that this HID is free of errors and agree(s) to its use as hazard computation input.

Signature Expert 1 / Expert:

Signature Expert 2:

Signature Expert 3:

Part III

Assessments of K. Campbell

Chapter 1

Evaluation Summary (EG2-ES-1019) of K. Campbell

1.1 Introduction

In the PEGASOS study, the Subproject 2 (SP2) experts developed individual ground motion logic trees and provided a description of these logic trees in their elicitation summaries. The structures of the individual logic trees used by the five SP2 experts had many similarities. To take advantage of these similarities, the SP2 PEGASOS Refinement Project (PRP) experts agreed to develop a single master ground motion logic-tree structure that could be used by all of the SP2 experts for their evaluations. This logic-tree structure is presented by Abrahamson [2012a] and in Part I, Section 9, of the PRP SP2 Subproject report Abrahamson and SP2 Experts [2013]. This latter report, which incorporates this evaluation summary as Part III, will be referenced simply as Part I in the remainder of this report. Most, but not all, of the elements of the logic tree were used by all of the SP2 experts, but with their own individual weights and justifications for these weights. Detailed descriptions of the development of the SP2 expert weights and justifications are given in a set of separate evaluation reports and hazard input documents (HIDs) that are included as Parts II through V of the SP2 Subproject report Abrahamson and SP2 Experts [2013].

Although the master ground motion logic-tree in Part I provides a fairly detailed summary of the work performed and the underlying documentation that supports the structure of the logic tree, the bases for the logic tree are given in a large number of separate technical project reports and presentations that were provided throughout the PRP. This information formed the basis for extensive discussions among the SP2 experts at a series of workshops and physical and Internet ("web") working meetings that included extensive interaction with resource and proponent experts, speciality contractors, and SP2 experts. All of this information was evaluated by the SP2 experts in order to justify the development of their individual models and weights for each branch of the master ground motion logic tree.

This report (Part III of the SP2 Subproject report; Abrahamson and SP2 Experts [2013]) presents my evaluation summary as one of the four PRP SP2 experts. I joined the project just prior to SP2 Workshop No. 9 (SP2/WS9), which was held in Zurich, Switzerland on

August 30 - September 1, 2011. At this point, the project had already been underway for three years. I was invited to join the SP2 expert panel after SP2 experts Julian Bommer and Frank Scherbaum resigned from the project. Shortly after joining the project, I was given a list of reading materials to review [Renault 2011] in order to catch up with what had already been done on the project to date. These materials included the final PEGASOS Project report NAGRA [2004], the review panel comments of the [HSK 2004], and the PRP Project plan [swissnuclear 2011].

Much of the description of the background and technical support information developed for the PRP, especially concerning the SP2 master ground motion logic tree, is available in Part I of this report [Abrahamson and SP2 Experts 2013]. In order to avoid redundancy, I will not repeat this information but will instead include it by reference. I encourage the reader to become familiar with this material prior to reading my elicitation report. I provide a description of the decision process I went through to develop my specific ground motion logic tree and reference Part I when appropriate. As appropriate for a SSHAC Level 4 study, my elicitation integrates all of the available information in order to represent the center, body, and range (CBR) of the technically defensible interpretations (TDI) that the larger informed technical community would have arrived at if they were to evaluate the same information [Kammerer and Ake 2012].

1.2 Selection of GMPEs for Horizontal Motion

The general selection of GMPEs for horizontal ground motion is described in Part I, Section 2 of this report. My specific selection and weighting of the GMPEs is described in the following sections.

1.2.1 Preselection of GMPEs

There were originally eight ground motion prediction equations (GMPEs) that were considered for use in the PRP. These GMPEs were preselected using a set of criteria agreed to by the SP2 experts and applied by Douglas [2009a] (Part I, Section 2.1). After I joined the project, Workshop No. 1 (data needs) was repeated to allow me the opportunity to participate in the discussions regarding the selection of the GMPEs. During this workshop, it was decided that new GMPEs that were not available at the time of the original preselection process should be compiled and put through this same preselection process. As a result, the SP2 experts selected the following final set of 10 GMPES for possible inclusion in their logic trees [Douglas 2011a] (Part I, Section 2.1.1):

The new GMPEs that were added are Akkar and Cagnan [2010], based on Turkey strong motion data, and Bindi et al. [2011], based on Italian strong motion data. It was also decided to replace the originally selected GMPE of Akkar and Bommer [2007] [AkBo07] with the updated relation by Akkar and Bommer [2010], the difference being that the later uses a standard deviation ("σ") that is independent of magnitude.

1.2.2 Adjustments to GMPEs

The SP2 experts considered several adjustments to the GMPEs as described in Part I, Sections 3 to 4. Some of these adjustments were developed prior to my joining the project. I reviewed

Table III-1.1: Candidate GMPEs.

Authors	Region	Abbrev.
Abrahamson and Silva (2008)	NGA	[AbSi08]
Boore and Atkinson (2008)	NGA	[BoAt08]
Campbell and Bozorgnia (2008)	NGA	[CaBo08]
Chiou and Youngs (2008)	NGA	[ChYo08]
Atkinson and Boore (2008)	ENA stochastic	[AtBo06]
Toro (2002), based on Toro et al. (1997)	ENA stochastic	[Toro02]
Zhao et al. (2006)	Japan	[Zhao06]
Akkar and Bommer (2010)	Europe and Middle East	[AkBo10]
Akkar and Cagnan (2010)	Turkey	[AkCa10]
Bindi et al. (2011)	Italy	[Bind11]

the basis for these adjustments and found them acceptable. For all of the adjustments, except for the those regarding site κ (κ_0) and shear-wave velocity (V_S) profiles, or so-called $V_S - \kappa$ adjustments, the SP2 experts reached consensus evaluations and were not subject to individual evaluation. These included adjustments for interpolation to determine missing model coefficients (Part I, Section 3.1), conversions for parameter compatibility (Part I, Section 3.2), style-of-faulting (Part I, Section 3.3), and extrapolation to small magnitudes (Part I, Section 4). My selection of methods for developing and applying $V_S - \kappa$ adjustments is given in Section 1.5 of this report.

1.2.3 Tests Performed on GMPEs

There were several tests that were conducted to help the SP2 experts decide on the selection and weighting of the preselected GMPEs. These included observations and Kullback-Leibler divergence tests performed during the preselection process [Douglas 2009a, 2011a], evaluation of self-organized maps (SOMs) and Sammon's maps [Scherbaum 2010; Kühn 2011b], and comparison with Swiss intensity observations [Kühn 2011a].

1.2.4 Kullback-Leibler Divergence

Douglas [2009a] compared the original eight selected GMPEs and found that the stochastic models for eastern North America (ENA), representative of stable continental regions (SCR), predicted generally higher ground motions, especially at short periods and short distances, than the empirical relations from active tectonic regions (ACRs). He attributed this to generally higher values for V_{S30}, lower values of κ_0, higher values of crustal damping (Q), and higher values of stress drop ($\Delta\sigma$) than inferred by the ACR models. He also applied a Kullback-Leibler (KL) divergence test to the GMPEs and found that KL-distances implied that the GMPEs from ACRs are generally similar, except at small and large magnitudes, where they differ significantly due to lack of data and differences in the way their functional forms extrapolate. This latter observation is an intrinsic feature of empirical GMPEs. Douglas [2009a] also found that the KL-distances were larger for SCR models than ACR models as a result of greater differences in predicted ground motions and aleatory variabilities. This latter observation is an intrinsic feature of stochastic GMPEs.

1.2.5 Sammon's and Self-Organizing Maps

To aid in the selection and quantitative comparison of ground-motion models for seismic hazard analysis, Scherbaum et al. [2010] proposed the use of Sammon's maps and self-organizing maps (SOMs) from the field of high-dimensional information visualization to evaluate the original eight preselected GMPEs. Both techniques allow the projection of high-dimensional vectors onto two-dimensional maps such that the mutual distances between these vectors and even their topological neighborhood can be preserved. The Sammon's map indicates that the eight GMPEs exhibit a good distribution along the vertical axis but a somewhat skewed distribution along the horizontal axis. The models loosely form three clusters with AbSi08 + CaBo08 + AtBo06 located towards the top of the map, AkBo07 + BoAt08 + Zhao06 located towards the middle of the map, and CaBo08 + Toro02 located towards the bottom of the map, although I would argue that CaBo08 could be included with the middle cluster, falling almost equidistant between this cluster and Toro02. Two observations can be drawn from these observations. First, the NGA models are relatively spread out despite having been derived from a common database and subject to a large degree of developer interaction. Second, the two ENA models plot far from one another despite them having been developed from similar seismological data. Other GMPEs considered by Scherbaum et al. [2010] occupy parts of the Sammon's map not occupied by the eight preselected PRP models, but these differences are likely caused by the same limitations that prevented them from being selected in the first place. This brings up an interesting conundrum. The fact that a GMPE occupies a part of the Sammon's map that is not occupied by other models is not sufficient by itself to justify its selection if it does not have characteristics that are believed to represent the tectonics of the region in which they are applied and the range of earthquake parameters that are of greatest interest in the project.

The SOMs show that the NGA models all occupy "low-altitude" positions, but are separated spatially. The exceptions are AbSi08 and ChYo08, which fall next to each other. AkBo07 (and presumably AkBo10) occupies a mid-altitude position away from all of the other models except for BoAt08, but this latter model occupies a lower altitude and is separated from AkBo07 by cells that have higher altitudes than either model. Zhao06 and Toro02 occupy positions near one another but away from the other models, but they also have higher-altitude grids between them. CaBo08 is located away from all of the other models except for Zhao06 and Toro02, but these latter two models occupy higher altitudes that make up for the shorter distance. AtBo06 occupies a high-altitude position away from all of the other models. Three observations can be drawn from the Sammon's map. First, the NGA models, except for AbSi08 and ChYo08, are spread out spatially, which makes up for their occupation of similarly low altitudes. Second, the two ENA models are spatially spread out and occupy relatively high altitudes, setting them apart from each other and the other models. Third, AkBo07 is separated from all of the other models. Fourth, the remaining models are either spatially separated or separated by high-altitude cells from the other GMPEs. These conclusions are similar to those derived from the Sammon's maps.

Kühn [2011b] repeated the Sammon's and SOM analysis of Scherbaum et al. [2010] using the original eight PRP GMPEs, the two new preselected GMPEs, and some models that had been recently considered but eventually not preselected. Of interest is his Section 3 that performs the analysis for the original eight PRP preselected GMPEs plus the two new ones.

Unlike Scherbaum et al. [2010], Kühn produced separate Sammon's maps and SOMs for peak ground acceleration (PGA) and psuedo-acceleration response-spectral acclerations (PSA) for 10, 1 and 0.5 Hz (0.1, 1 and 2 sec). For PGA, he produced a Sammon's map for both the entire (4.5-7.0) and large (6.0-7.0) magnitude ranges. The large-magnitude Sammon's map for PGA showed that the eight ACR models were relatively tightly clustered but separated from the two SCR models. Since the full-magnitude range is more appropriate for the PRP study and because it is available for all four frequencies, I concentrated on those results. In this case, the Kühn [2011b] Sammon's maps for PGA and 10 Hz show similar results to those of Scherbaum et al. [2010], except that AtBo06 and Toro02 plot closer together. The two new models plot relatively close to AbSi08 and ChYo08 and do not occupy new space on the map. The Sammon's maps for 1 and 0.5 Hz indicate that all of the GMPEs tend to cluster together, except for Toro02 and AkCa10, which separate from the other models in opposite directions (i.e., they are far apart). The SOM for PGA shows that the two new models are spatially close, but are walled-off from each other as well as from other nearby GMPEs by relatively high-altitude cells. The 10 Hz SOM map shows results that are more similar to the high-frequency Sammon's maps, with AbSi08 + AkCa10 + Bind11 + ChYo08 clustering together. For the lower frequencies, AkCa10 occupies one corner of the map walled-off by high-altitude cells consistent with the results of the Sammon's maps.

1.2.6 Comparison with Swiss Intensity Observations

Kühn [2011a] tested the ten PRP preselected GMPEs against the Swiss macroseismic intensity observations documented in Fäh et al. [2009a, 2011] and SED [2011]. The tests were performed on intensity data because there are insufficient ground motion recordings at the moment magnitudes (M_W), fault-rupture distances (R_{RUP}), and horizontal fault-rupture distances, also known as Joyner-Boore distances (R_{JB}), of interest in this study to directly test the GMPEs using these recordings. Therefore, intensities are the only "strong ground motion" data that are available. Two types of tests were performed. The first was to compare the residuals predicted from the GMPEs with the observed intensities. The second was to compare the relative weights between the GMPEs assuming that the intensity data are generated by a "Mixture Model" in which the GMPEs are considered to be mixture components with weights that can be determined from Bayesian inference (e.g., Spiegelhalter and Rice [2009]). All of the GMPEs were adjusted to agree with the Swiss small-magnitude recordings and the original eight PRP preselected GMPEs were additionally adjusted using the average $V_S - \kappa$ corrections proposed by the SP2 experts at that time (December 19, 2011). Later all GMPEs were adjusted, see e.g. Kühn [2011a].

Residuals

Although it would seem that comparisons with Swiss intensity observations are the best way of judging the validity of a GMPE, there are issues with interpreting the intensity data as well as with estimating intensities from the GMPEs that makes such comparisons difficult to interpret. Some of the issues related to the intensity database are as follows:

- Most of the intensity data, especially for the larger earthquakes and closer distances of interest in this study, are from Italian earthquakes, with the majority of the remaining

data coming from earthquakes in neighboring Austria, France and Germany (e.g., Figure 7-1 of Fäh et al. [2011]). There are very few earthquakes of $M_W \geq 4$ that have occurred in Switzerland.

- The Italian intensities were reduced by -0.38 [Fäh et al. 2009b] to correct them from an average Italian reference site condition of approximately $V_{S30} = 600$ m/sec to a Swiss generic rock site condition of $V_{S30} = 1000$ m/sec. This reduction was based on an estimated PGA de-amplification of about 1.46 calculated from the Swiss stochastic reference rock ground motion model of Edwards et al. [2010], which was converted to an intensity decrement using the PGA versus intensity relationship of Kästli and Fäh [2006]. Note that V_{S30} is the time-averaged shear-wave velocity over the top 30 m of the site V_S profile.

Conversions between PGA or PSA and intensities were done using the relationships of Faenza and Michelini [2011]; Faenza [2010]. These relationships were developed using Italian intensity observations based on the MCS intensity scale, which for purposes of comparison was assumed to be consistent with the EMS intensity scale used in Switzerland and the MSK intensity scale used in France. Some of the issues related to these conversions are as follows:

- Although the MCS and EMS (and by proxy the MMI and MSK) intensity scales are expected to be nominally similar, Musson et al. [2010] suggest that *"experience seems to show that MCS intensity assignments are frequently higher than those in EMS for the same data"*. This bias in intensity assignments was also suggested by Douglas [2009b] after comparing various intensity conversion relationships with Italian intensity data.

- There is a systematic trend in the residuals for earthquakes with $M_W < 5$, even though the GMPEs were corrected to agree with the Swiss stochastic model and, therefore, the Swiss recordings, at small magnitudes. This bias could possibly be related to the first bullet item, to a tendency to assign smaller intensities in regions outside of Italy for similar shaking effects, or to biases in the GMPEs that are not accounted for in the small-magnitude correction.

- Many of the Italian earthquakes used in the Faenza and Michelini [2011]; Faenza [2010] conversion relationships have normal focal mechanisms and, therefore, represent a different tectonic environment than the tectonic regime in Switzerland, which results in strike slip and normal focal mechanisms.

- Different conversion relationships can lead to differences in estimated intensities of as much as one or more intensity units [Douglas 2009b].

These issues suggest that the absolute bias in the residuals must be viewed with caution. Nonetheless, there are still some general observations that can be derived from these residuals. These observations are based on those comparisons of greatest interest in this study (i.e. $M_W \geq 5.0, R_{RUP}/R_{JB} \leq 50$km). I also limit my observations to natural spectral frequencies (f_0) of 0.5 and 1.0 Hz, corresponding to natural periods (T_0) of 1.0 and 2.0 sec, since PGA and high-frequency PSA ordinates do not correlate as well with the larger intensity values of interest in this study (e.g., Kästli and Fäh [2006]) or with damage [Boatwright et al. 2001].

On the other hand, the mid-period PSA ordinates, centered on a spectral period of about 1.5 sec, have been found to have the strongest correlation with damage [Boatwright et al. 2001].

My first observation from the mid-period PSA residuals of Kühn [2011a] is that the residuals of Bind11 do not indicate any significant biases or trends for $M_W \geq 5.0$ and $R_{JB} \leq 50$km. Since the Bind11 GMPE is based on Italian strong motion data, this consistency would seem to imply that there are no significant biases (i.e., intensity residuals larger than ± 0.5) in the Italian intensity data or the intensity conversion relationships. Similarly good comparisons were found for AtBo06 + AkBo10 + AbSi08 + BoAt08 + CaBo08 + ChYo08 + Zhao06. AkCa10 exhibited a strong trend of increasing bias towards under-prediction with decreasing magnitude for $M_W < 6.0$ and a greater than +1 intensity unit under-prediction for $R_{JB} \leq$ 50km. Toro02 exhibited a larger than (in a negative sense) -1 intensity unit over-prediction. It is interesting to note that one of the ENA GMPEs (AtBo06) is relatively unbiased, whereas the other (Toro02) is strongly biased.

Mixture Model

The Mixture Model analysis of Kühn [2011a] was conducted for multiple magnitude-distance ranges, precision parameters (β), and prior weighting schemes. The two weighting schemes for the priors were to treat them either as uniform (equal prior weights for all GMPEs) or to give each GMPE in turn a prior weight of 0.8. I concentrated on the $M_W = 5.5 - 6.5$ and $R_{RUP}/R_{JB} = 10 - 100$km magnitude and distances ranges, which are the closest to the magnitude and distance ranges of most interest in this study, and on the nonuniform weighting scheme. The results show that the mixture components are relatively unstable. At high precision values the priors always dominate the mixture weights. At low precision parameters, the GMPEs with the highest weights will vary depending on which one is given the high prior weight. Since the analysis was done with both the GMPEs and the PSSMs, often the PSSMs were the models with the highest mixture weights. I consider these results too unstable to be used to select or weight individual GMPEs.

1.2.7 Comparison of Predicted Values

I compared predicted values of PGA and PSA for both adjusted and unadjusted versions of the GMPEs to see how they differed in terms of magnitude, distance, and spectral scaling. The adjustments included the small-magnitude correction to the Swiss stochastic model (i.e., Swiss recordings) and a preliminary set of $V_S - \kappa$ adjustments (version of 16.08.2012). Illustrative comparisons for M_W=6.0, R_{JB}=20 km, and f_0 =10 Hz (T_0=0.1 sec) are given in terms of distance attenuation characteristics (Figure III-1.1), magnitude scaling characteristics (Figure III-1.2 and III-1.3), and response spectral scaling characteristics (Figure III-1.4). The magnitude and distance used in the comparisons were chosen to be similar to those that dominate the seismic hazard at the Swiss nuclear power plants for the selected spectral frequency and the exceedance frequencies of interest [Roth 2012]. The spectral frequency was chosen to be near the peak in the adjusted response spectra. It is clear from the comparison of the unadjusted and adjusted predictions that the adjustments significantly reduced the differences between the GMPEs, especially for the ENA stochastic relationships that were developed using a very different set of seismological data and models than the empirical GMPEs. This demonstrates that the $V_S - \kappa$ adjustments are generally in the right direction.

Note that the small-magnitude correction applied to the GMPEs does not modify their scaling characteristics at $M_W > 5.5$.

The comparison in Figure III-1.1 indicates that AtBo06, AkCa10 and Bind11 attenuate much faster than the other GMPEs and the PSSMs, which causes them to have lower predictions than the other GMPEs at R_{JB} >10 km. AtBo06 also demonstrates a strong "Moho bounce" that is not seen in the other GMPEs or the PSSMs. AkCa10 (Turkey) and Bind11 (Italy) have much stronger attenuation then AkBo10, which was derived from European and Middle Eastern strong motion recordings. A possible reason for this will be discussed in the next section. Note that the adjustments do not modify the attenuation characteristics of the relationships, but does signicantly reduce their variability. The attenuation characteristics of the other GMPEs are generally similar to one another but somewhat stronger than those of the PSSMs.

The obvious observation in Figure III-1.2 is that Bind11 has an upward kink in its magnitude scaling characteristics at $M_W = 6.5$ when all of the other GMPEs show that magnitude scaling should be decreasing. All of the GMPEs except AtBo06 and Toro02, the two ENA models, predict decreasing magnitude scaling as magnitude increases (i.e., magnitude saturation). This difference becomes much stronger at smaller distances (Figure III-1.3), where the lack of magnitude saturation in these models rivals that of Bind11.

Figure III-1.4 (top) demonstrates the large difference in the spectral shapes of the uncorrected GMPEs, which largely disappears after the $V_S - \kappa$ adjustment (bottom). There are two adjusted spectral shapes that stand out from the others. The Toro02 spectrum falls virtually on top of the 240-bar PSSM spectrum and predicts higher PSA ordinates at f_0 <2 Hz than the other GMPEs. The AtBo06 spectrum is more peaked than the other spectra which causes it to predict lower PSA ordinates at f_0 >20 Hz. The other GMPEs have generally similar spectral shapes with approximate amplitude differences of a factor or 2 across the entire frequency range.

1.3 Selection and Weighting of GMPEs

Although the test results presented in the previous sections are useful, they are not sufficient for determining which GMPEs are appropriate for the intended use and how those that are should be weighted. The preselection criteria applied by Douglas [2009a, 2011a] eliminated most GMPEs that were not clearly applicable based on their general properties and characteristics but did not look at other more site-specific criteria. Therefore, I apply additional screening of the preselected GMPEs in terms of their applicability to the tectonic environment of Switzerland and their appropriateness for the magnitude and distance range of most interest in the PRP seismic hazard analysis. This additional screening is intended to eliminate those GMPEs that should not be considered to contribute to the Center, Body and Range of the technically defensible interpretations.

1.3.1 Additional Screening Based on Tectonic Environment

Switzerland is classified as an Active Shallow Continental Region (ASCR) according to the seismotectonic map of the Euro-Mediterranean area developed for the Seismic Hazard Harmonization in Europe (SHARE) project (Figure III-1.5) [Delavaud et al. 2012a]. This

classification is reinforced by the moderately high level of seismicity in the region (Figure III-1.6) that includes the Swiss Foreland, the location of the nuclear power plants. The Swiss Foreland is part of the North Alpine Foreland Basin (NAFB) that has formed as a result of the flexural depression of the European tectonic plate that developed in front of the migrating thrust load of the Alps (e.g., Sinclair et al. [1991]). This thrust load is caused by the indentation of the Adrian block as it pushes northward and collides with central Europe. In Switzerland the NAFB is represented by the Molasse Basin. This flexure and other tectonic processes have deformed and weakened the European plate (e.g., Carminati et al. [2009]). The NAFB is currently being uplifted and laterally extruded due to continued, albeit reduced, compression within the central Alps [Selverstone 2005] and results in earthquakes with primarily strike-slip focal mechanisms with some normal faulting (e.g., Kastrup et al. [2004]).

It is clear from the above description that the Swiss Foreland is not located in a Stable Continental Region (SCR) similar to the tectoinc environment of ENA. Therefore, the two preselected ENA GMPEs that passed the initial screening, which did not consider screening for tectonic environment, are not considered to be appropriate for estimating ground motions in Switzerland and were not considered in the selection of GMPEs for my SP2 ground motion logic tree. All of the remaining GMPEs are from ASCRs and were retained based on this criterion.

One could argue that the transtensional tectonic environment of western Turkey and the extensional environment of most of Italy could possibly make these GMPEs inappropriate for site-specific application in the compressional environment of Switzerland. However, since these models come from regions classified as ASCRs, I did not exclude them for this reason. As I indicate below, there are other reasons why these models were not selected.

1.3.2 Additional Screening Based on Magnitude and Distance

The attenuation and magnitude scaling characteristics of ground motion have been shown to vary substantially with the size of the earthquake (e.g., Chiou et al. [2010]; Campbell and Bozorgnia [2013]). Therefore, it is important that the selected GMPE appropriately represent these characteristics as they apply to their specific application. The magnitudes and distances of greatest interest in the PRP range from about 5.8-6.8 and 7-37 km, respectively [Roth 2012]. Although all of the preselected GMPEs include recordings in these ranges, some of these models are strongly biased towards smaller earthquakes. This is particularly a problem with GMPEs that are based on strong motion data that come solely from a single, relatively small country. The two preselected GMPEs that meet these criteria are AkCa10 based only on data from Turkey and Bind11 based only on data from Italy. Note that Zhao06, which is based primarily on data from Japan, used large earthquakes outside of Japan to help guide the near-source scaling of moderate-to-large shallow crustal earthquakes and does not have the same limitations that the other country-specific GMPEs have.

Some issues related to AkCa10 that makes it inappropriate for site-specific application to the Swiss nuclear power plants are as follows:

- It includes a high percentage of singly recorded earthquakes, especially for the smaller events, which increases uncertainty in both distance attenuation and magnitude scaling.

This can also lead to biased estimates of magnitude scaling and distance attenuation because of the trade-off between source scaling and distance scaling characteristics for such events.

- It includes only two earthquakes with $M_W > 6.5$, which adds uncertainty to the moderate-to-large magnitude scaling, making it unreliable. Furthermore, these two earthquakes (M_W 7.4 1999 Kocaeli and M_W 7.1 1999 Duzce events) have been shown to predict lower than average ground motion, possibly as a result of their location on a major plate boundary located in a transtensional tectonic environment [Campbell and Bozorgnia 2008].

- It includes a significant number of aftershocks, which have been shown to exhibit lower high-frequency ground motion amplitudes than mainshocks (e.g., Abrahamson and Silva [2008]). Furthermore, the strong bias towards small earthquakes and the lack of a significant number of larger earthquakes can lead to an overestimation of near-source attenuation because of the steeper distance attenuation exhibited by such events [Douglas 2007; Chiou et al. 2010].

- The between-earthquake (τ), within-earthquake (ϕ), and total standard deviation (σ) ranges from 0.52-0.68, 0.62-0.71, and 0.81-0.92, respectively, for T_0 =0.04-2.0sec, all of which are significantly larger than found for the NGA models [Abrahamson and Silva 2008] and the other more globally based GMPEs [Douglas 2011b]. This is caused by including a large number of small-magnitude earthquakes in the model without accounting for a magnitude-dependent standard deviation.

The bias towards small-to-moderate earthquakes, the inclusion of aftershocks, and the location of most of the events in a transtensional tectonic environment might be the reason that predictions from AkCa10 are observed to exhibit generally smaller amplitudes and steeper distance attenuation than the more globally based GMPEs or the PSSMs (Figure 2-1). As a result, I conclude that this model is not appropriate for site-specific application in the PRP and, therefore, does not pass my additional screening criteria. In addition, use of the inappropriately large σs would lead to an overestimation of the hazard at small exceedance frequencies.

Some issues related to Bind11 that makes it inappropriate for site-specific application to Swiss nuclear power plants are as follows:

- The vast majority of the recordings are from normal-faulting earthquakes, which have been shown to exhibit lower high-frequency amplitudes than other styles-of-faulting (e.g. Douglas [2007]), possibly because of predominantly lower stress drops in extensional tectonic regimes.

- It includes only three earthquakes with $M_W > 6.0$, which adds uncertainty to the moderate-to-large magnitude scaling making it unreliable. Furthermore, one of these earthquakes (M_w6.3 2009 L'Aquila event) has been shown to have high-frequency ground motions that are weaker than expected for normal-faulting earthquakes of this magnitude and ground motions that attenuate more steeply than the NGA models and consistent with other earthquakes in Italy [Stewart et al. 2012].

- It includes a significant number of aftershocks and swarms that have been shown to exhibit lower high-frequency ground motion amplitudes than mainshocks (e.g., Abrahamson and Silva [2008]; Chiou and Youngs [2008b]). Furthermore, the strong bias towards small earthquakes and the lack of a signficant number of larger earthquakes can lead to an overestimation of near-source attenuation because of the steeper distance attenuation exhibited by such events [Douglas 2007; Chiou et al. 2010].
- The between-earthquake (τ), within-earthquake (ϕ), and total standard deviation (σ) ranges from 0.35-0.52, 0.65-0.76, and 0.79-0.87, respectively, for $T_0 = 0.04 - 2.0$sec, all of which are significantly larger than found for the NGA models [Abrahamson et al. 2008] and the other more globally based GMPEs [Douglas 2011b]. This is caused by including a large number of small-magnitude earthquakes in the model without accounting for a magnitude-dependent standard deviation.

The bias towards small-to-moderate earthquakes, the inclusion of aftershocks and swarms, and the location of most of the events in an extensional tectonic environment might be the reason that predictions from Bind11 are observed to exhibit generally smaller amplitudes and steeper distance attenuation than the more globally based GMPEs or the PSSMs (Figure III-1.1). As a result, this model is not appropriate for site-specific application in the PRP and does not pass my additional screening criteria. In addition, use of the inappropriately large σs would lead to an overestimation of the hazard at small exceedance frequencies.

1.3.3 Final Selected GMPEs and Weights

After applying the additional selection criteria discussed in the previous sections, I selected the following six GMPEs and corresponding weights as the final set of empirical ground motion models to use in the ground motion logic tree:

- AbSi08 (weight = 1/12)
- BoAt08 (weight = 1/12)
- CaBo08 (weight = 1/12)
- ChYo08 (weight = 1/12)
- AkBo10 (weight = 1/3)
- Zhao06 (weight = 1/3)

I retained all four NGA models in my final selection because of their non-clustering behavior when evaluated frequency by frequency in the SOM's and Sammon's maps. However, because they were developed from a common database and with a large degree of developer interaction, I believe that the informed technical community would not give them as much weight as the other independently developed GMPEs. Therefore, I decided to give the four NGA models (AtSi08, BoAt08, CaBo08, ChYo08) the equivalent weight of a single GMPE. Since no one final selected GMPE was clearly better than the other, I also decided to weight the four NGA models as a group equally with AkBo10 and Zhao06. Figures III-1.7 to III-1.10 compare the final selected and adjusted models (based on final corrections of 23.04.2013) to their uncorrected versions.

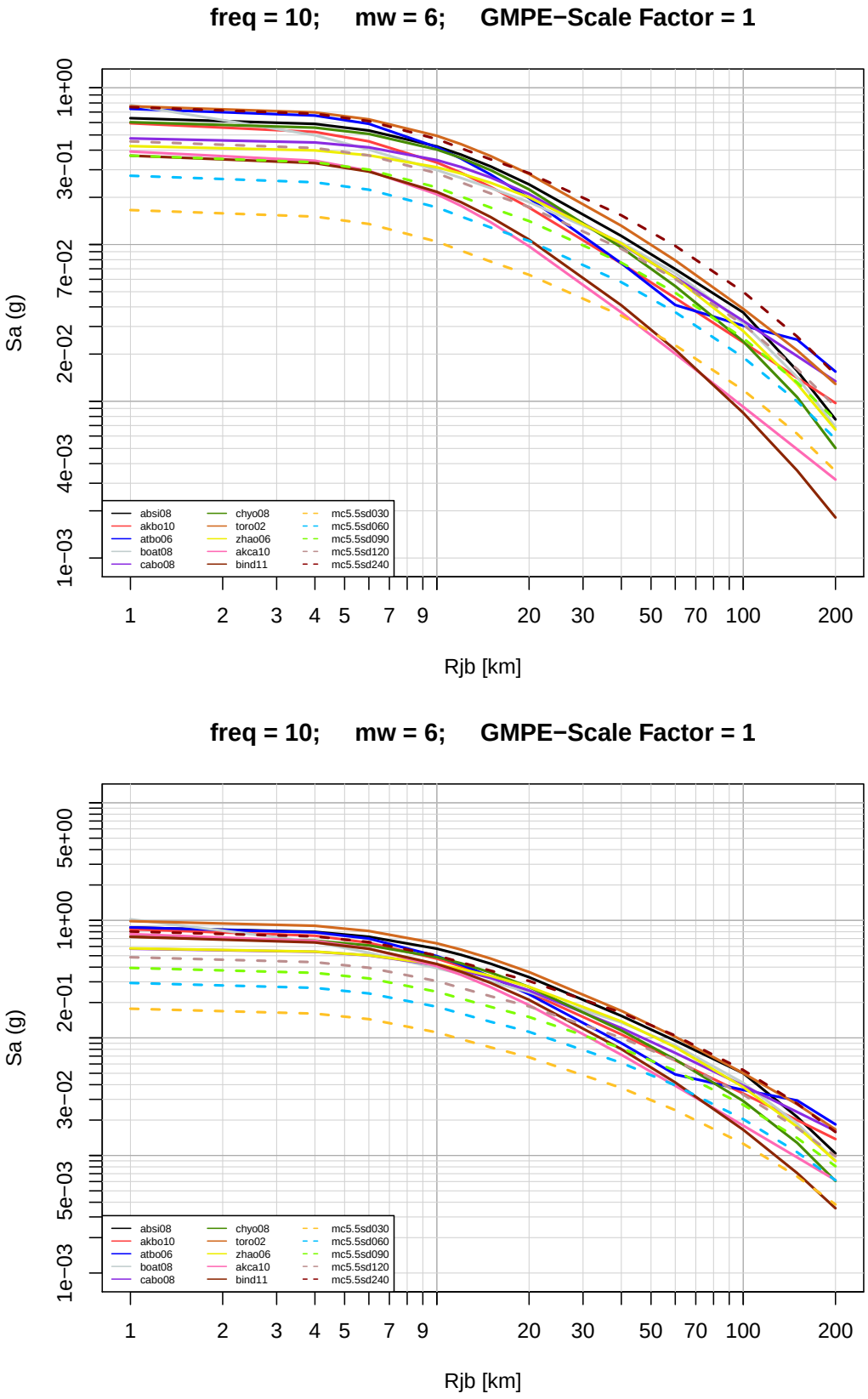

Figure III-1.1: Illustrative comparison of distance attenuation characteristics between unadjusted (top) and adjusted (bottom) PRP preselected GMPEs and PSSMs.

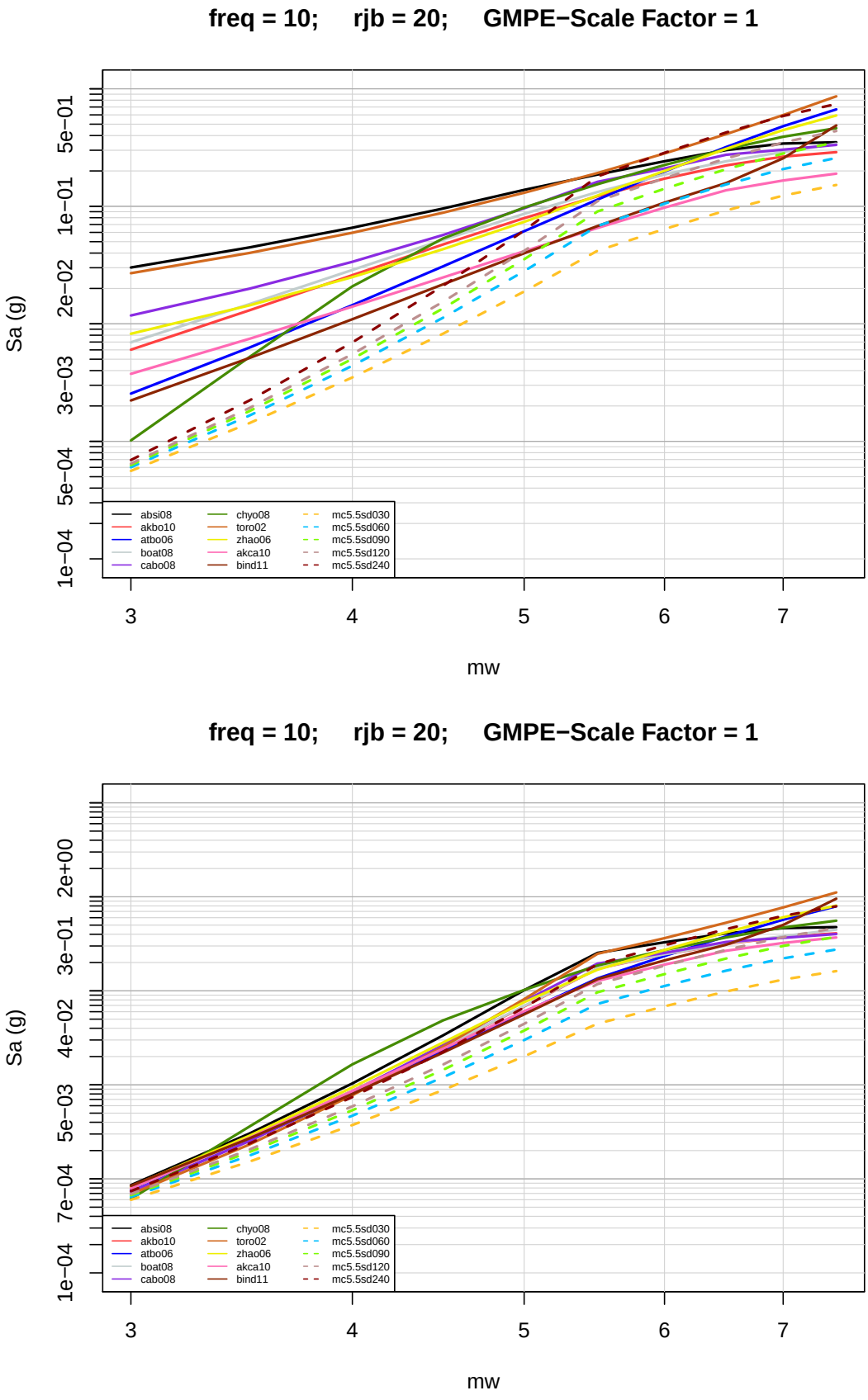

Figure III-1.2: Illustrative comparison of magnitude scaling characteristics between unadjusted (top) and adjusted (bottom) PRP preselected GMPEs and PSSMs.

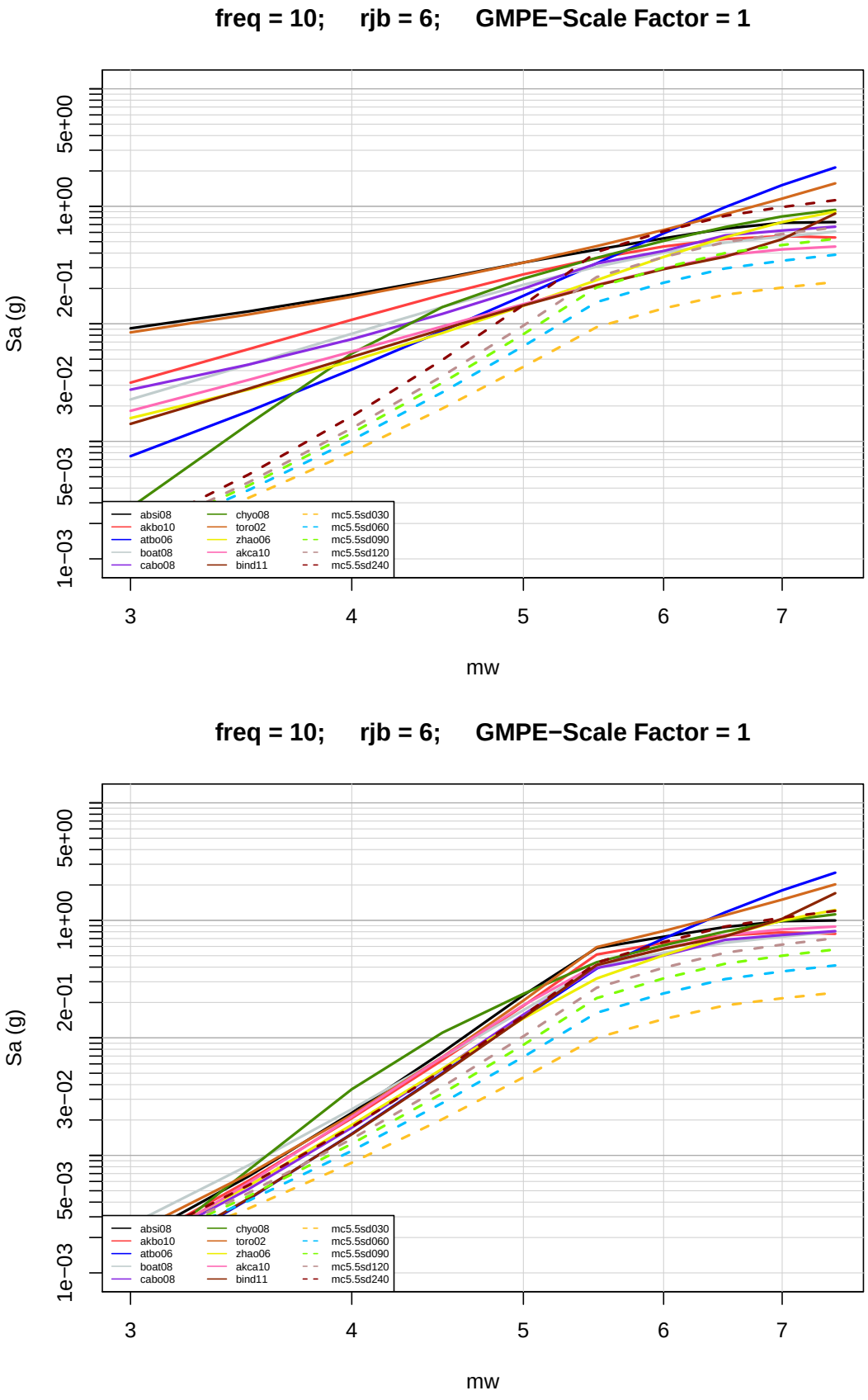

Figure III-1.3: Illustrative comparison of near-source magnitude scaling characteristics between unadjusted (top) and adjusted (bottom) PRP preselected GMPEs and PSSMs.

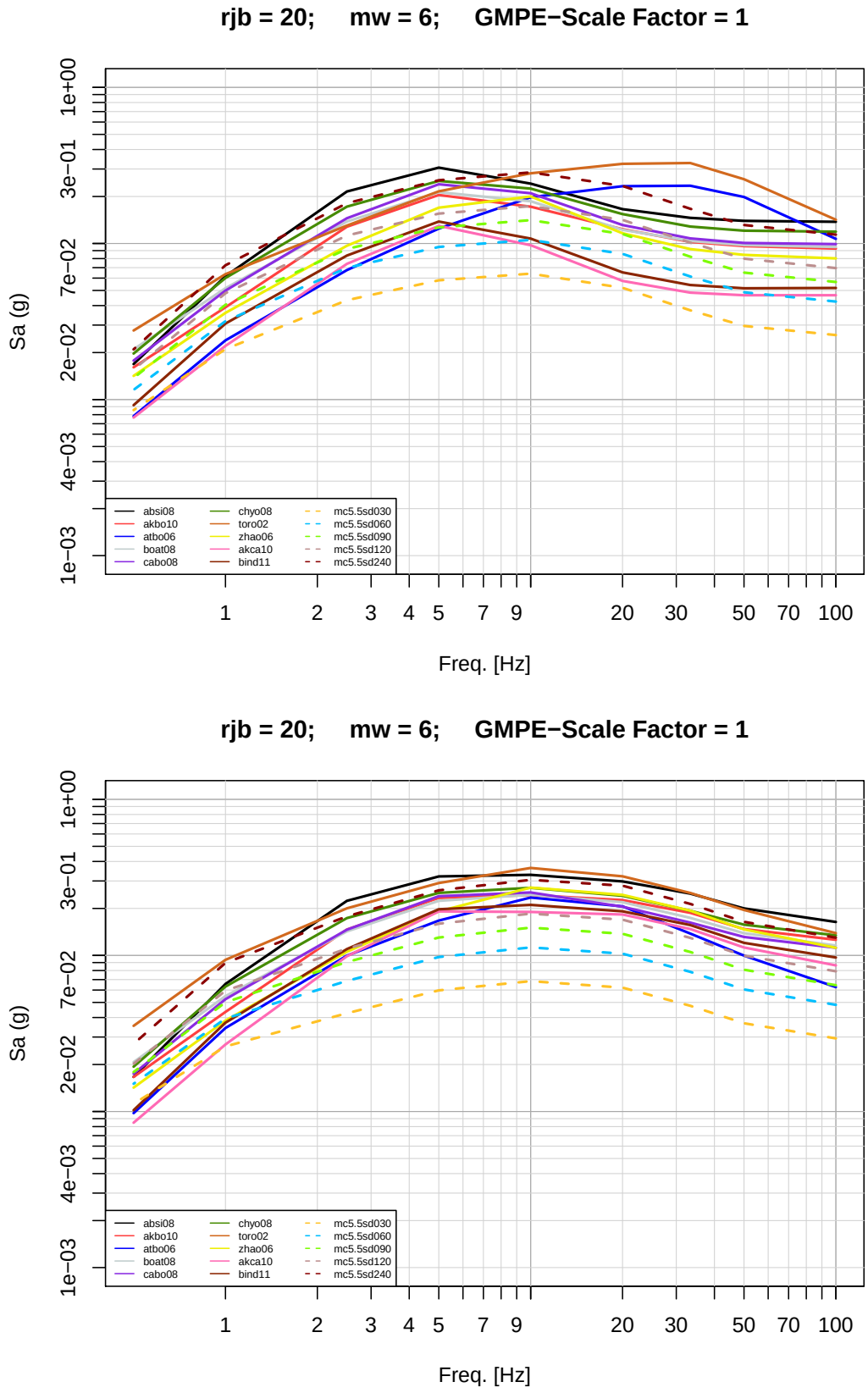

Figure III-1.4: Illustrative comparison of response spectral scaling characteristics between unadjusted (top) and adjusted (bottom) PRP preselected GMPEs and PSSMs.

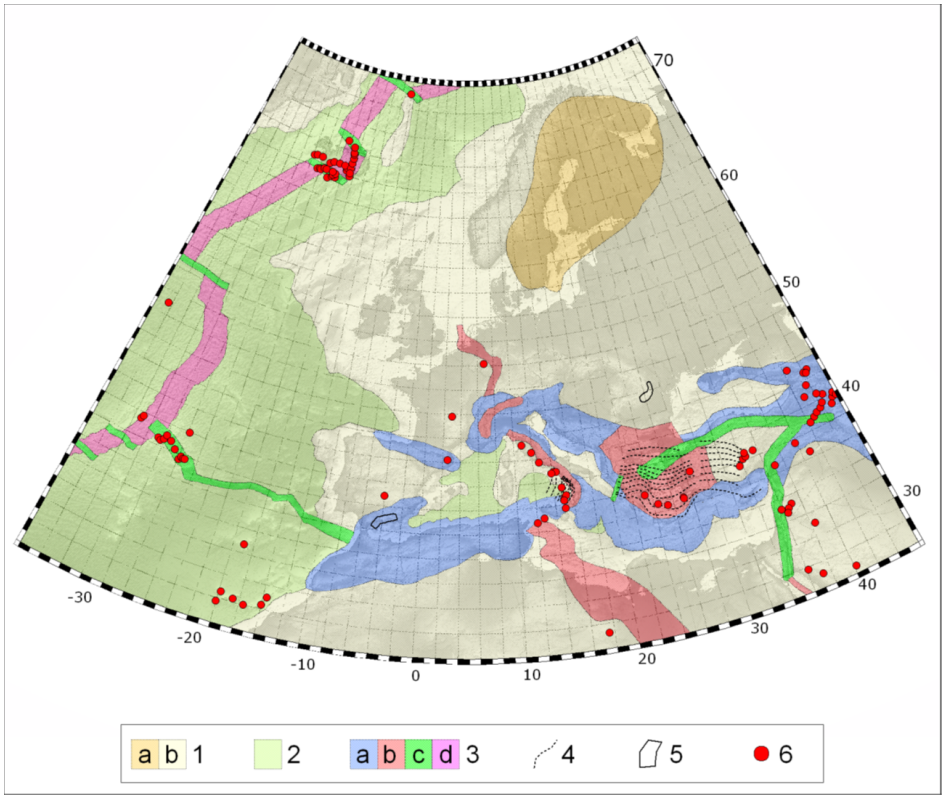

Figure III-1.5: Seismotectonic map of the Euro-Mediterranean area developed for the SHARE project by WP3.2 [Delavaud et al. 2012a].

1. SCR, shield (a)
   and continental crust (b);

2. oceanic crust;

3. ASCR, compression-dominated areas (a)
   including thrust or reverse faulting, associated transcurrent faulting (e.g. tear faults), and contractional structures in the upper plate of subduction zones (e.g. accretionary wedges), extension-dominated areas (b)
   including associated transcurrent faulting, major strikeslip faults and transforms (c), and mid oceanic ridges (d);

4. subduction zones shown by contours at 50 km depth interval of the dipping slab;

5. areas of deep-focus non-subduction earthquakes;

6. active volcanoes and other thermal/magmatic features.

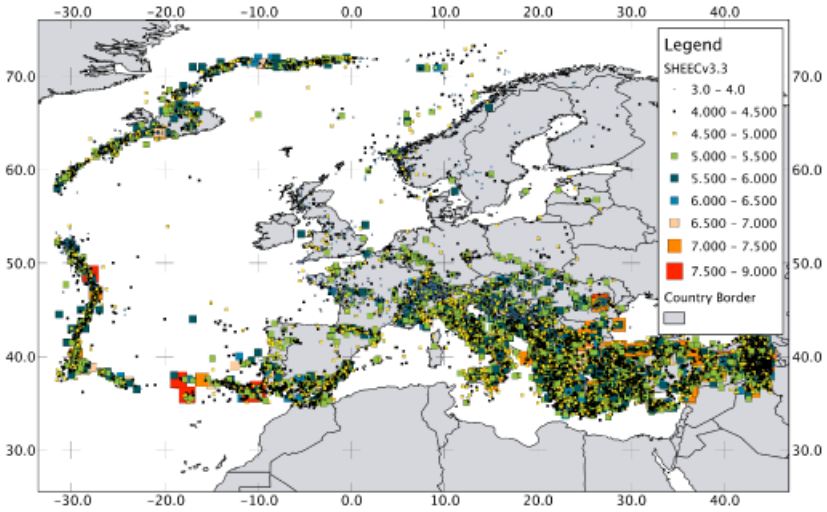

Figure III-1.6: Seismicity map of the Euro-Mediterranean area developed for the SHARE project by WP3.2.1. From http://www.share-eu.org/ (2013).

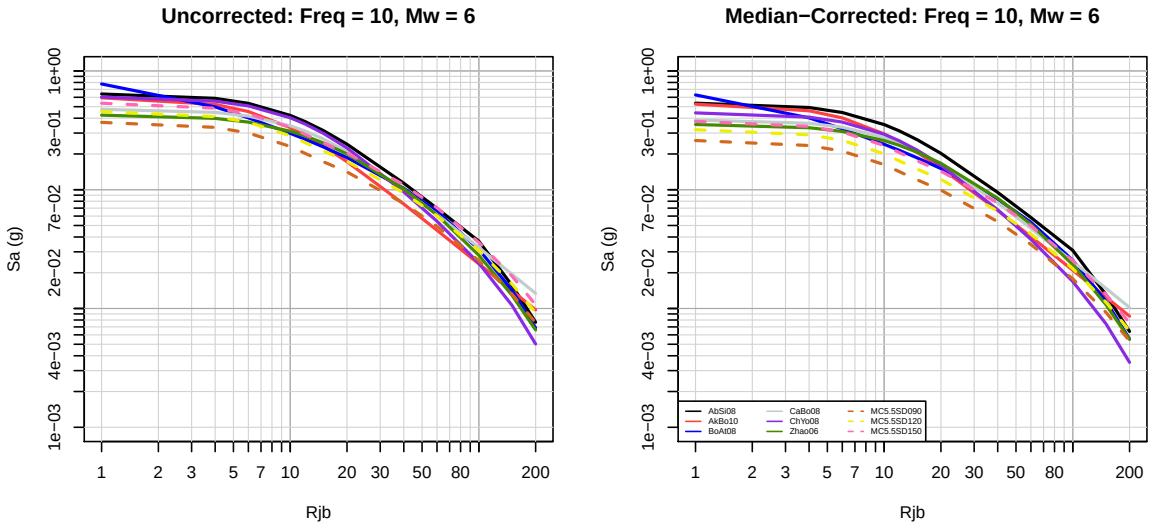

Figure III-1.7: Comparison of distance attenuation characteristics between unadjusted (left) and adjusted (right) PRP finally selected GMPEs and PSSMs.

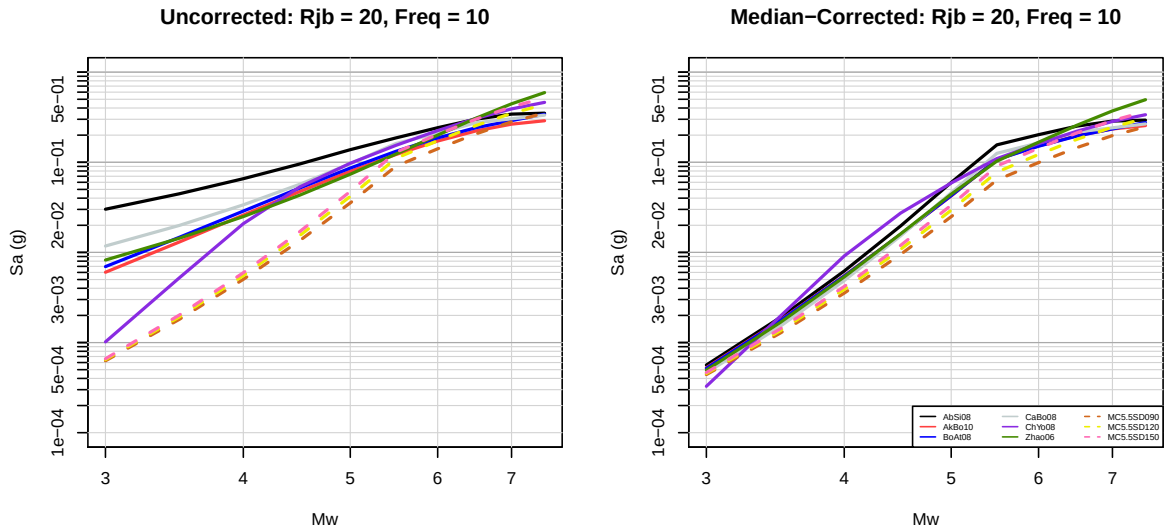

Figure III-1.8: Comparison of magnitude scaling characteristics between unadjusted (left) and adjusted (right) PRP finally selected GMPEs and PSSMs.

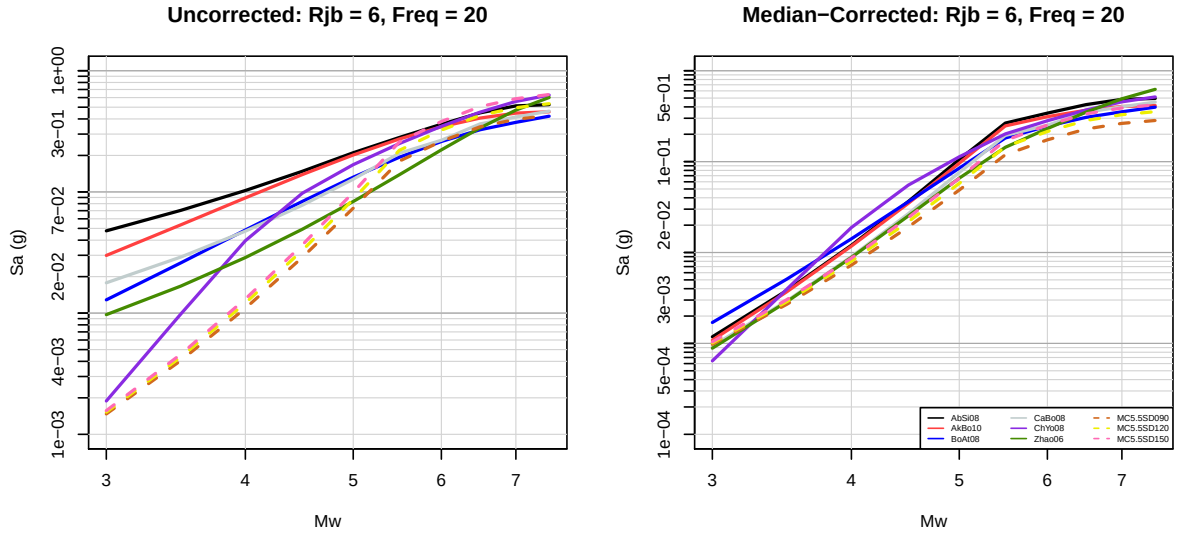

Figure III-1.9: Comparison of near-source magnitude scaling characteristics between unadjusted (left) and adjusted (right) PRP finally selected GMPEs and PSSMs.

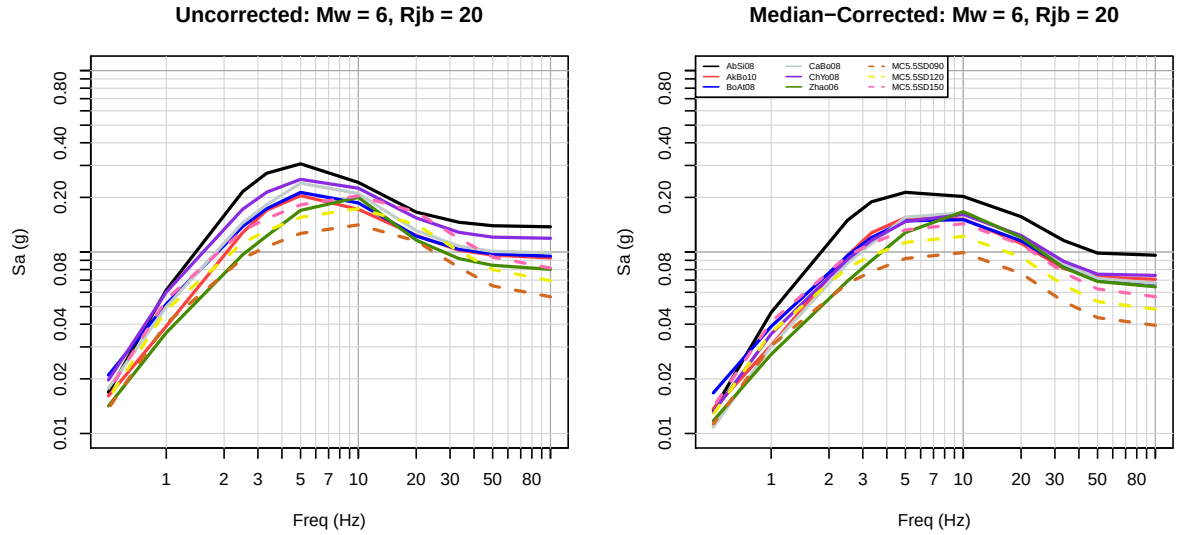

Figure III-1.10: Comparison of response spectral scaling characteristics between unadjusted (left) and adjusted (right) PRP finally selected GMPEs and PSSMs.

1.4 Selection of PSSMs for Horizontal Motion

As part of the PRP, a new parameterized Swiss stochastic model (PSSM) was developed by Edwards et al. [2010]; Edwards and Fäh [2010]. The model is based on earthquakes recorded by the SED broadband network with magnitudes ranging between 2.0 and 5.5 and distances ranging between 3 and 300 km. It is briefly described in Part I, Section 1.2.3 of this report. The basis for my specific selection and weighting of the various adjusted versions of the PSSM is described in the following sections.

1.4.1 Magnitude-Dependent Stress Drop

The analysis of the Swiss earthquake data showed that there is a strong magnitude-dependence of the stress drop increasing from 2 bars for $M2.5$ to 30 bars for $M4.5$. A key issue for the application of this model to the larger magnitudes of importance to the hazard at the Swiss nuclear power plants is the scaling of the stress drop for $M > 4.5$. Since there is no empirical constraint on stress drop scaling above this magnitude, a suite of alternative models were developed based on other information. The magnitude-scaling from the ten selected GMPEs described in Part I, Section 1.3 of this report do not indicate that there is a strong increase in stress drop for $M > 5$. Walt Silva (personal communication) fit the NGA models to a point-source stochastic model allowing for a magnitude-dependent stress drop and found that the magnitude-scaling in the NGA models implied that there is only a small decrease in stress drop with magnitude for $M < 6.5$. These results suggest that the strong increase in stress drop with magnitude seen in the small-magnitude Swiss data will not continue at high magnitudes. To capture this trend, a limit on the increase in stress drop at high magnitudes was applied to the PSSM as described below.

The models for the magnitude-dependence of stress drop for extrapolating a PSSM to larger magnitudes have two parameters. The first is the maximum stress drop and the second is the magnitude (M_C) at which the stress drop reaches this maximum value. A suite of values was used for these two parameters in which M_C was allowed to range from 4 to 6 and the maximum stress drop was allowed to range from 30 to 480 bars. An example of this scaling model is shown in Figure I-2.3 of Part I, Section 2.1.

1.4.2 Effective Point-Source Distance

A second issue for the application of the point-source PSSM in the hazad model is the effective point-source distance (R_{EFF}). The PSSM uses the point-source distance to compute the ground motion. This is similar to the distance metric that is used in empirical ground motion models. For example, the rupture distance (R_{RUP}) is the distance to the site from the closest point on the rupture plane and is not measured from the same point on the rupture for every site location. Similarly, there is not a single point on the fault that is used to compute the value of R_{RUP} to each site. Instead, an equivalent point-source distance is used in the PSSM.

For application in the hazard analysis, the point-source model requires a model to convert from the closest distance metric used in the hazard calculation (e.g., R_{JB} or R_{RUP}) to the effective point-source distance R_{EFF}. Two candidate conversion methods were proposed for use in the PRP: one based on stochastic simulation and one based on empirical calibration.

These two methods are described in Part I, Section 2.3.2. I decided to use the stochastic simulation method because it allowed for Swiss-specific earthquake depths. It uses a simple parameterization of the relation between the rupture distance and the effective point-source distance measure developed by Abrahamson [2011a] based on the stochastic calculations of Edwards and Fäh [2010] that defined R_{EFF} as the distance that, over numerous random simulations of a finite fault with unknown hypocenter, leads to the same attenuation as would be experienced by the RMS summation of unique ray-paths from the discretized finite fault.

1.4.3 Selection and Weighting of PSSMs

A paucity of moderate-to-large magnitude data in Switzerland means that ground motion predictions from the PSSMs at these magnitudes are unconstrained by instrumental recordings. They were, however, calibrated to agree with Swiss macroseismic intensity data in the moderate-magnitude range [Edwards et al. 2010; Edwards and Fäh 2010]. There were two evaluations required to select and weight the PSSMS. The first was the selection of one or more appropriate values of M_C and the second was the selection of one or more values of maximum stress drop.

Selection of M_C

The value of magnitude above which stress drop is considered to be constant (M_C) was determined by comparing the moderate-to-large magnitude scaling characteristics of the PSSMs with M_C values of 4.5, 5.0, 5.5 and 6.0 with the magnitude-scaling characteristics of the GMPEs after applying the small-magnitude adjustment. The GMPEs were used as the benchmark because of their empirical constraint at the larger magnitudes of interest. It was clear from this comparison that the smallest value of M_C caused the magnitude-scaling of the PSSMs to become flatter (i.e., less magnitude scaling) at too small of a magnitude, compared to the GMPEs, whereas the largest value caused them to become flatter at too large of a magnitude. I selected $M_C = 5.5$ as an appropriate value based on this comarison. All of the other SP2 experts selected $M_C = 4.5$. Figure III-1.11 shows the comparison of magnitude-scaling characteristics of the PSSMs and the GMPEs for M_C values if 4.5 and 5.5 to support my selection of 5.5.

Selection of Maximum Stress Drop

The choice of a maximum stress drop to use with the selected value of $M_C(\Delta\sigma_{max})$ was more problematic. There are only two studies that can be used to determine an appropriate value for this stress drop. This first study is a comparison of the PSSMs with the Swiss intensity database that was compiled by Fäh et al. [2009b]. Figure III-1.12 shows this comparison for $\Delta\sigma_{max} = 30$, 60, 90, 120 and 240 bars and spectral periods of 0.01 (PGA), 0.3, 1 and 2 sec. The PSSM predictions were converted to intensity using relationships developed by Faenza [2010]; Faenza and Michelini [2011]. The Figures show the average difference (residual) between the PSSM prediction and the intensity observations (N. Kühn, written communication). This Figure shows that $\Delta\sigma_{max} = 120$ bars gives the best comparison for $T_0 = 0.3$ sec but that $\Delta\sigma_{max} = 240$ bars gives the best comparison for PGA, both with residuals near -0.05. The best comparison for $T_0 = 1$ and 2 sec is with $\Delta\sigma_{max} = 30$ bars with a residual of around -0.1 with 60 bars having a residual of around -0.25. Note that 60 (actually 62.5) bars is the average stress drop associated with the PSSM [Edwards et al. 2010; Edwards and Fäh 2010;

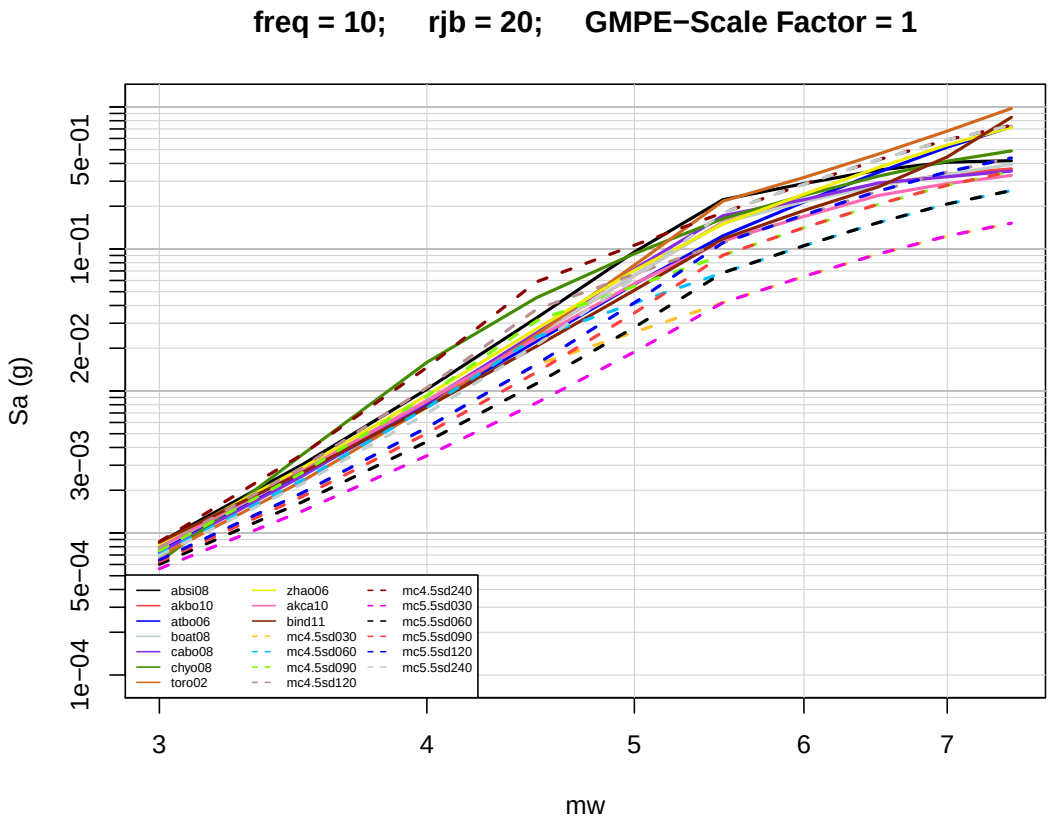

Figure III-1.11: Comparison of magnitude-scaling characteristics of the PSSMs and GMPEs

Edwards et al. 2013a]. This stress drop was calibrated through comparison of the stochastic model simulations with the macroseismic intensity model used to determine M_W of large historical earthquakes in Switzerland.

The second study is a comparison of the PSSM with moderate-to-large magnitude data from Japan [Edwards et al. 2012]. In this case the Swiss model is that published in the Bulletin of the Seismological Society of America, which is slightly different from the PSSM developed by Edwards et al. [2010]; Edwards and Fäh [2010]. However, these differences do not affect the conclusions regarding the PSSM. The authors use strong-motion data from surface accelerometers of the Japanese Kik-Net network. Each network station has a corresponding shear-wave velocity profile down to 100-200 m, which was used to correct for site effects (both amplification and site attenuation). All of the earthquakes were crustal with focal depths less than 25 km and magnitudes (Japan Meteorological Agency, M_{JMA}) that range from 5.5 to 7.3. The comparison indicated that ground motion attenuation was stronger in Japan than in Switzerland. After correcting for this attenuation, the data within a distance of 50 km were compared to the Swiss stochastic model using a stress drop of 62.5 bars, the best estimate for Switzerland (Figure III-1.13). This comparison showed that there was a negative bias (over-prediction) at spectral frequencies of 0.5-1 Hz (spectral periods of 1-2 sec) and a positive bias (under-prediction) at spectral frequencies of 3.3-20 Hz (spectral periods of 0.05-0.3 sec).

Because of the biases observed for the 62.5-bar stress drop, Edwards et al. [2012] performed the same comparison for stress drops of 30, 90 and 120 bars (Figure III-1.14). The 30-bar stress drop comparison results in nearly unbiased residuals for the low frequencies consistent with the Swiss intensity comparisons for these same frequencies. However, if one concentrates

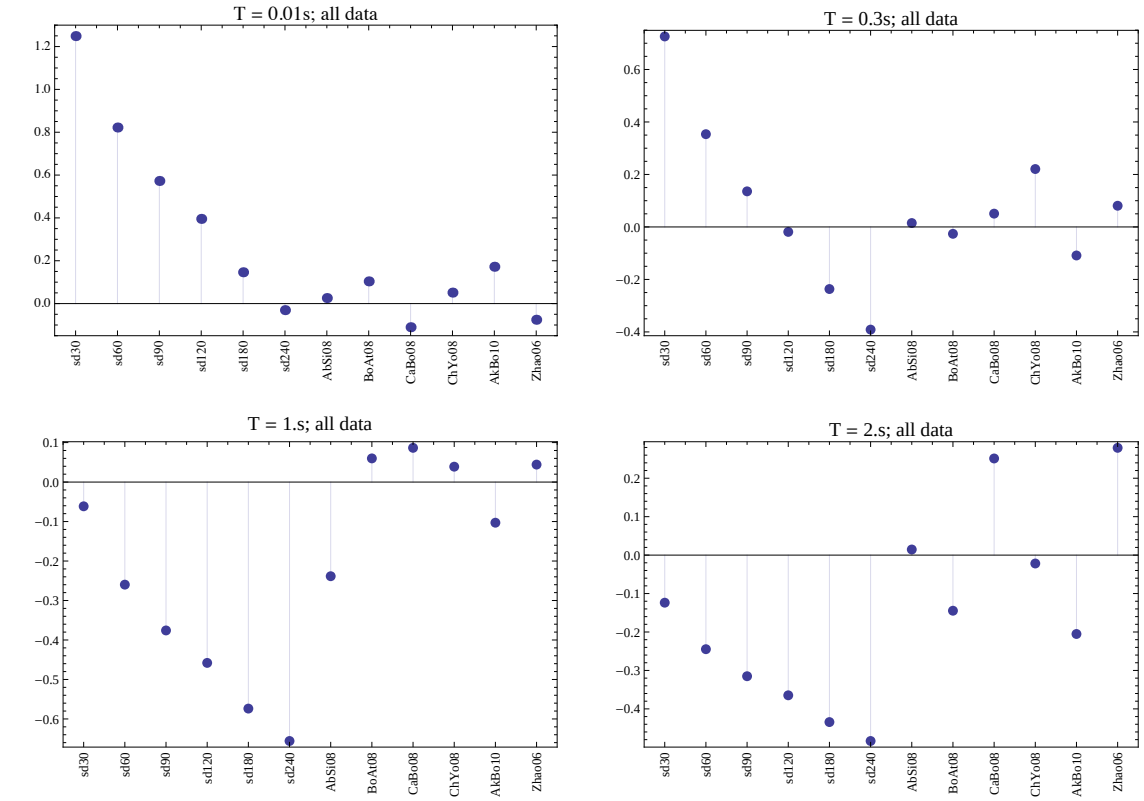

Figure III-1.12: PSSM with various stress drops compared to Swiss intensity data at the spectral periods of 0.01, 0.3, 1 and 2sec.

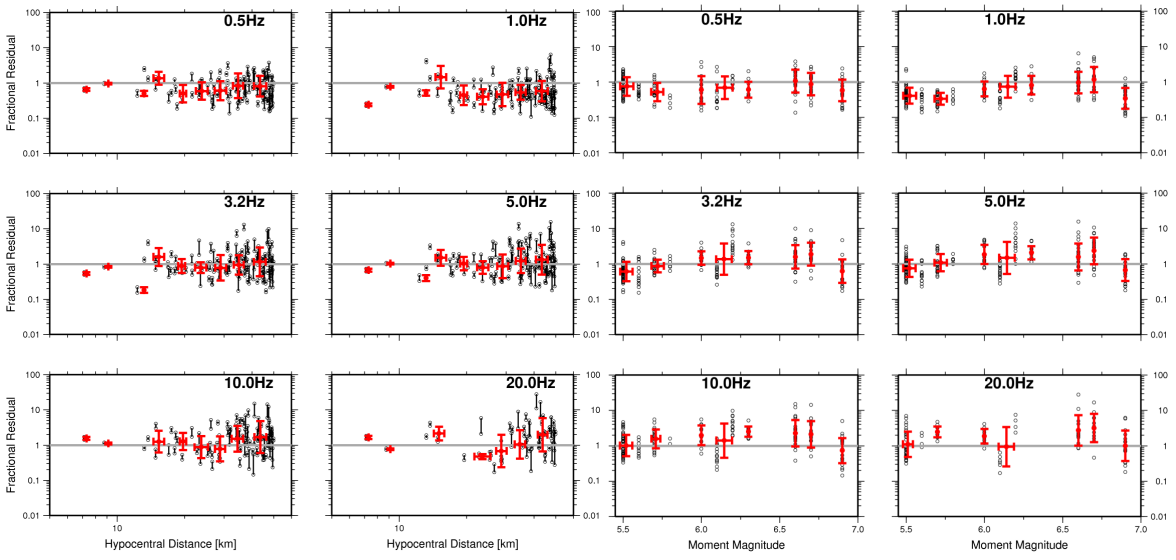

Figure 8: residual misfit (observed/model) of simulated ground motion using the 6.25 MPa Swiss model (adapted to the Japanese attenuation model of Edwards and Rietbrock (2009)) versus the site corrected Japanese strong motion data for distances up to 50km. The lines joining the circles indicate the range of possible predictions between the estimated R_{JB}^{min} and R_{JB}^{max} for each observation. The red symbols indicate the mean and standard deviation of residuals at given distances.

Figure III-1.13: Comparison of Japanese Strong Ground-Motion Recordings with the Swiss Stochastic Model for a stress drop of 62.5 bars [Edwards et al. 2012].

only on those events with $M_{JMA} > 6.0$, the best fit is for stress drops ranging between 30

and 60 bars. The 120-bar stress drop comparison results in nearly unbiased residuals for the high frequencies consistent with the Swiss intensity comparison for $T_0 = 0.3$ sec. Another observation made by Edwards et al. [2012] is that there is no apparent trend in the residuals with M_{JMA} indicating that a constant stress drop model is appropriate for magnitudes greater than 5.5 in Japan.

In a related study, Edwards et al. [2012] analyzed acceleration time-series data from the European Strong Motion Database using the same methodology they used to develop the Swiss stochastic model. After selecting high-quality recordings, suitable for Fourier analysis, they estimated crustal and site attenuation properties, Q_0 and κ_0 respectively, using two methods: a broadband spectral modeling approach and a high-frequency linear fit (i.e., the approach developed by Anderson and Hough [1984]). They found that κ_0 varies strongly from site to site but that both approaches resulted in virtually the same average value of κ_0, although I note that the smaller values of κ (<0.02-0.03 sec) for the broadband approach were approximately 0.01 sec smaller than those determined from the high-frequency linear fit. The large variability in κ estimates is consistent with the wide variety of recording-site conditions from hard rock to very soft soil. Using the attenuation model, they determined site-class amplification, seismic moments, and ω^2 [Brune 1970, 1971] stress drops for several events with moment magnitudes ranging between 5.0 and 7.6. They show that seismic moments determined from Fourier spectra are consistent with M_W determinations from moment tensor analysis of the database. The resulting average stress drop from the inversions was 88 bars with a common logarithmic standard deviation of 0.23 corresponding to a range of 50 to 150 bars. This range is consistent with the range of period-specific stress drops found in the comparisons of the PSSM with the Swiss intensity data and the Japanese recordings discussed above. Another observation was that the resulting stress drops are independent of magnitude or focal depth.

Based on the studies discussed above, I selected the following PSSMs and corresponding weights as the final set of stochastic ground motion models to use in the ground motion logic tree:

Spectral Frequencies of 0.5 and 1 Hz ($T_0 = 1$ and 2 sec):

- PSSM, $M_C = 5.5$, $\Delta\sigma_{max} = 30$ bars (weight = 0.5)
- PSSM, $M_C = 5.5$, $\Delta\sigma_{max} = 60$ bars (weight = 0.5)

Spectral Frequencies of 2.5, 5, 10, 20, 33, 50 and 100 Hz ($T_0 = 0.01$ (PGA), 0.02, 0.03, 0.05, 0.1, 0.2 and 0.4 sec):

- PSSM, $M_C = 5.5$, $\Delta\sigma_{max} = 90$ bars (weight = 0.2)
- PSSM, $M_C = 5.5$, $\Delta\sigma_{max} = 120$ bars (weight = 0.6)
- PSSM, $M_C = 5.5$, $\Delta\sigma_{max} = 150$ bars (weight = 0.2)

The different values of stress drop represent an estimate of the epistemic uncertainty associated with this parameter. This range represents a bias in the range -0.25 to 0.15 bias with respect to the Swiss intensity data, which is relatively small compared to the uncertainty in the

intensity assignments and in the conversion of ground motion values to intensity. The only exception is PGA for which the bias ranges from 0.25 to 0.6, which is still relatively small. The different values of stress drop with frequency represent the differences between low and high frequencies observed in the comparison studies. The 240-bar stress drop found to be the best average value for PGA based on the comparison with the Swiss intensity data was not used consistent with the findings of Kästli and Fäh [2006] who found a weak correlation between PGA and macroseismic intensity. Furthermore, the adjusted spectral shapes are grossly distorted if a stress drop of 240 bars is used for PGA and a lower value is used for the high-frequency spectral ordinates. The jump in the selected stress drop between frequencies of 0.5 and 2.5 Hz (periods of 0.4 and 1 sec) does not lead to a discontinuity in the adjusted spectral shape and was retained. The magnitude threshold of 5.5 above which stress drop is considered to be constant is supported by the empirical GMPEs as well as the comparisons with the Swiss intensity data and the Japanese strong-motion data.

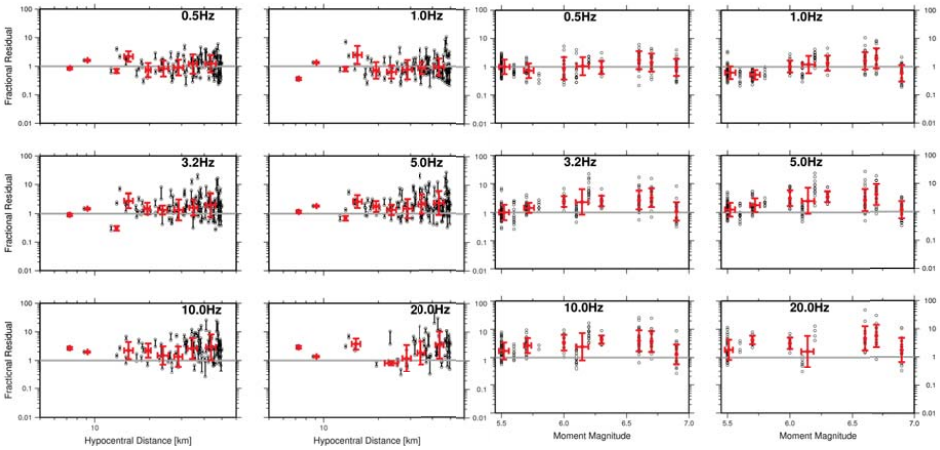

Figure 9: residual misfit (observed/model) of simulated ground motion using the modified 3 MPa Swiss model (adapted to the Japanese attenuation model of Edwards and Rietbrock (2009)) versus the site corrected Japanese strong motion data for distances up to 50km. The lines joining the circles indicate the range of possible predictions between the estimated R_{JB}^{min} and R_{JB}^{max} for each observation. The red symbols indicate the mean and standard deviation of residuals at given distances.

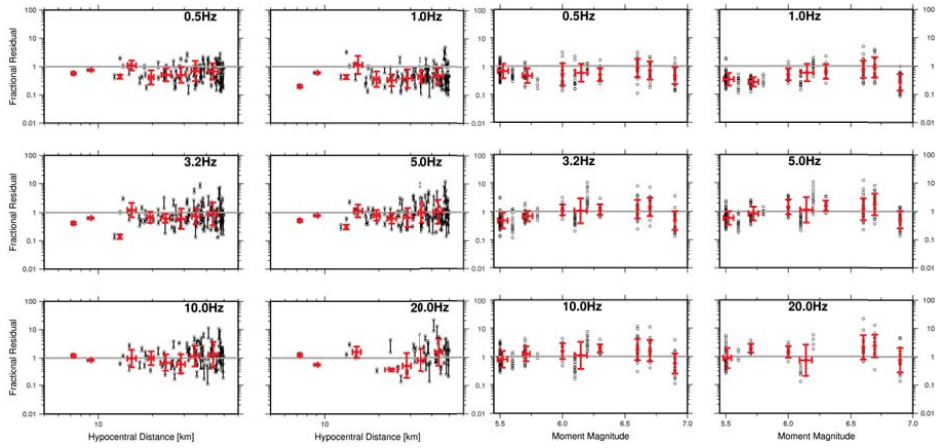

Figure 10: residual misfit (observed/model) of simulated ground motion using the modified 9 MPa Swiss model (adapted to the Japanese attenuation model of Edwards and Rietbrock (2009)) versus the site corrected Japanese strong motion data for distances up to 50km. The lines joining the circles indicate the range of possible predictions between the estimated R_{JB}^{min} and R_{JB}^{max} for each observation. The red symbols indicate the mean and standard deviation of residuals at given distances.

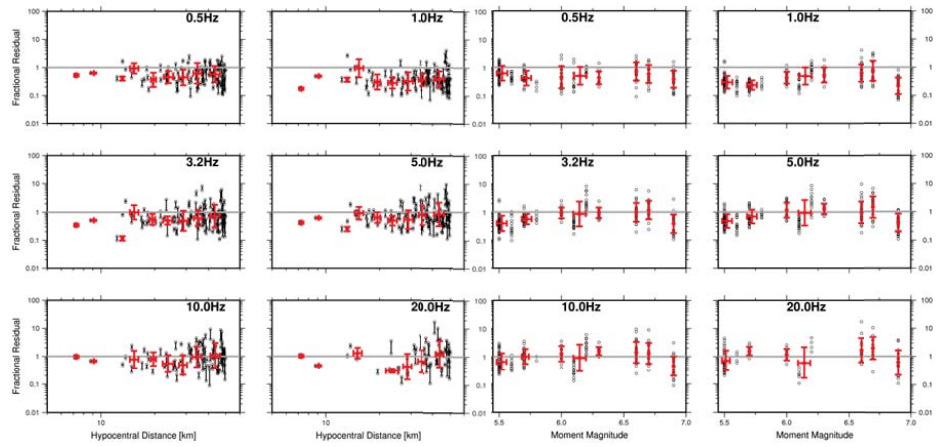

Figure 11: residual misfit (observed/model) of simulated ground motion using the modified 12 MPa Swiss model (adapted to the Japanese attenuation model of Edwards and Rietbrock (2009)) versus the site corrected Japanese strong motion data for distances up to 50km. The lines joining the circles indicate the range of possible predictions between the estimated R_{JB}^{min} and R_{JB}^{max} for each observation. The red symbols indicate the mean and standard deviation of residuals at given distances.

Figure III-1.14: Comparison of Japanese Strong Ground-Motion Recordings with the Swiss Stochastic Model [Edwards et al. 2012].

1.4.4 Relative Weighting Between GMPEs and PSSMs

Having selected the models and weights for the GMPEs and PSSMs, the last step was to evaluate the relative weights between these two model groups. There is uncertainty in importing GMPEs to the Swiss Foreland region that indicates they should not be given 100% weight. However, they are constrained empirically by data in the magnitude range that has the largest contribution to the hazard. On the other hand, the PSSMs are derived from Swiss recordings but must be extrapolated by several magnitude units beyond the range of the available Swiss data in order to represent the magnitude range that has the largest contribution to the hazard. Both the GMPEs and the PSSMs have large uncertainty associated with the $V_S - \kappa$ adjustments. Because of the large uncertainty in extrapolating the PSSMs to the magnitude range of interest, I consider them to have a considerably lower relative probability compared to the GMPEs. As a result, I decided to assign the GMPEs 80% weight and the PSSMs 20% weight.

1.5 Host-to-Target $V_S - \kappa$ Adjustments

In PEGASOS and in the PRP before I joined the project, the SP2 experts decided that developing host-to-target region adjustment factors for the full set of stochastic point-source parameters was problematic because the stress drop scaling in Switzerland was not well constrained. However, they also considered the differences in the shear-wave velocity (V_S) profile and the site attenuation (κ_0) to be important effects that should be considered. Therefore, the objective of the adjustment methodology was to isolate the adjustment for these latter parameters from the full model correction. This latter correction came to be known as the $V_S - \kappa$ adjustment, where κ refers to the site attenuation parameter κ_0. After joining the PRP, I reviewed the basis for this decision and found it to be acceptable.

An important issue identified early on was that there was a relatively strong correlation between stress drop and κ that made it difficult to isolate the $V_S - \kappa$ adjustment. To reduce this correlation, Scherbaum [2010] used normalized spectral shapes in place of the spectral values for the inversion of the point-source parameters associated with the GMPEs. Although this method reduced the correlation, the estimation of κ was still not robust. For example, the point-source inversion lead to very different estimates of κ values for the four NGA ground motion models even though these models were based on similar datasets.

Because of the issues encountered by Scherbaum [2010], significant revisions to the host-to-target $V_S - \kappa$ adjustment methodology were developed as part of the PRP. These alternative methods are described in Part I, Section 1.5. A preferred method was not selected by the SP2 experts. Therefore, the structure of the $V_S - \kappa$ logic tree is set up to have the individual SP2 experts specify the range of values of the $V_S - \kappa$ adjustment factors for each spectral frequency and each GMPE or PSSM rather than to specify weights on the methods and model parameters. This requires more effort by the SP2 evaluators but this additional effort was considered to be justified given the current uncertainty in the $V_S - \kappa$ adjustment methodologies.

1.5.1 V_S Profiles

In the inversion method of Scherbaum [2010], the V_S profile for each GMPE was estimated as part of the point-source model inversion. This lead to differences in the gradient of the

V_S profile as well as changes in the shallow shear-wave velocity defined as the time-averaged shear-wave velocity in the top 30 m of the site (V_{S30}). Again, the issue with the approach is the correlation of the V_S profile with other parameters in the stochastic model. If the host-to-target region adjustment is only applied for V_S and κ, then it is important that the estimate of the V_S profile be robust and not have significant trade-offs with other parameters that are not included in the $V_S - \kappa$ adjustment. In order to improve the robustness of the V_S profile, a revised method was proposed in which a single V_S profile is used for all GMPEs but shifting the profile up or down in depth to match the V_{S30} of the GMPE. In this way, the V_S adjustment captures only the differences in the shallow profile and does not attempt to capture differences in the V_S gradients.

In the application of this method, two alternative generic profiles were used: a generic Swiss rock profile and a generic U.S. rock profile. The generic U.S. profile consists of the V_{S30} = 620 m/sec generic soft-rock profile for the western U.S. and the V_{S30} = 2800 m/sec generic hard-rock profile for the eastern U.S. (Boore and Joyner, 1997). The given shear-wave velocity profile is interpolated between these two profiles as shown in Part I, Section 3.4.3. For $V_{S30} < 620$ m/sec, a generic V_S profile provided by Walt Silva (written communication) for V_{S30} = 270 m/sec is used to allow interpolation rather than extrapolation of the profiles. The generic Swiss rock profile corresponding to V_{S30} = 1000 m/sec is based on the reference V_S profile shown in Part I, Section 3.4.3. For other values of V_{S30}, the Swiss reference profile is shifted (vertically) to match the V_{S30} value of each GMPEs.

The range of V_{S30} values for each GMPE was selected by consensus of the SP2 experts and are given in Part I, Section 3.4.3. Table III-1.2 lists the values used for the GMPEs that passed my selection criteria.

Table III-1.2: Alternative reference V_{S30} values used for the $V_S - \kappa$ adjustments.

GMPE	Reference V_{S30} Values [m/sec]			Reference V_{S30} Weight		
AbSi08	620	-	-	1	-	-
BoAt08	620	-	-	1	-	-
CaBo08	620	-	-	1	-	-
ChYo08	620	-	-	1	-	-
AkBo10	600	800	1000	0.3	0.4	0.3
Zhao06	500	700	900	0.3	0.4	0.3

The SP2 experts agreed that the reference V_{S30} value for the NGA ground motion models, which include V_{S30} as a parameter, should be the value of 620 m/sec associated with the generic western U.S. soft-rock profile. The range of reference V_{S30} values for the other ground motion models are based on the estimated range of values representing the softest rock site category. These ranges were provided by the authors. The softest rock category was used because it has a larger number of recordings and, therefore, is more representative of the value of κ derived from the GMPE. I assigned a higher weight to the central value because it represents the authors' best estimate for the site category. However, I also assigned significant weight to the lower and higher values because of the relatively large uncertainty associated with these estimates.

1.5.2 Host κ Values

After the Scherbaum [2010] stochastic inversion method was found to give unstable values of κ for the GMPEs, there was a considerable effort to develop and test different methods as described in Part I, Section 1.5. These included so-called stochastic inversion methods (f_{peak}, $f_{amp2.0}$, $f_{amp-half}$) proposed by Scherbaum [2010], empirical $V_S - \kappa$ correlations, empirical constraints ($f_{amp-half}$, $f_{amp1.3}$, $f_{amp1.5}$, $f_{amp1.7}$, $f_{amp2.0}$), and inverse radom vibration theory (IRVT). In the stochastic inversion and empirical constraint methods, f_{peak} refers to the spectral frequency at the peak of the acceleration response spectrum, $f_{amp-half}$ refers to the spectral frequency at a point on the response spectrum that is half way between the value of PGA and the value at the spectral ordinate at the peak, and f_{ampXX} refers to a point on the response spectrum that is a specified factor between the value of PGA and the value at the spectral ordinate at the peak.

I rejected the empirical $V_S - \kappa$ correlations because of the large uncertainty associated with extrapolating them beyond $V_{S30} > 1000$ m/sec representative of the Swiss NPP sites. This extrapolation is based on very few data and is strongly dependent on the assumed functional forms used to develop the relationships. The methods based on f_{ampXX} resulted in reasonable stable results among the NGA ground motion models that are expected to have similar κ values but very different results depending on the factor used to define the term. The method based on f_{peak} also gave consistent results for the NGA models and was associated with a relatively small standard deviation that makes it one of the more viable methods. However, it tended to give relatively high values of κ, more consistent with those associated with soil, for some of the European models for rock.

After reviewing all of the methods, I found that the IRVT method [Al Atik and Abrahamson 2012a; Al Atik et al. 2013] was the most accurate and stable. It estimates the Fourier amplitude spectrum (FAS) corresponding to the predicted response spectrum from the GMPE using inverse random vibration theory [Rathje et al. 2005] and uses this FAS to estimate κ using the method of Anderson and Hough [1984]. The range of spectral frequencies used for this purpose is from a point past the spectral peak to about 20 Hz in order to avoid contaminations of the high-frequency shape of the response spectrum with broadband response as noted by Scherbaum et al. [2010]. Thus, this method provides a direct estimate of the value of κ associated with the GMPE. In order to get a robust estimate of κ, the inversion is done for $M_W = 5$, 6 and 7 and $R_{JB} = 5$, 10 and 20 km. Because these distances are larger than those usually associated with κ_0, the IRVT-based κ is referred to as κ_1 so as not to be confused with the former.

I assigned 100% weight to the IRVT approach of estimating κ for several reasons:

1. it gives the lowest standard deviation (less than 0.003 sec) of all of the methods for which a standard deviation was calculated,
2. it provides a direct estimate from the high-frequency slope of the FAS based on the original definition of κ by Anderson and Hough [1984],
3. it is the only method that almost exactly recovers the value of κ used to derive the AtBo06 and Toro02 stochastic simulation models,
4. it gives consistent results among the NGA models,

5. it gives similar values of κ for the U.S., European and Japanese GMPEs for similar values of V_{S30}, and

6. it is consistent with how κ is determined from actual recordings.

This last point is important since the $V_S - \kappa$ adjustments described later are based on κ values that are estimated from recordings in Switzerland. Table III-1.3 lists the host values of κ_1 corresponding to the PSSM and the GMPEs that I selected [Al Atik and Abrahamson 2012a, b].

Table III-1.3: Host V_{S30} values used for the $V_S - \kappa$ adjustments.

GMPE	Reference V_{S30} Values (m/sec)			Host κ_1 Values (sec)		
AbSi08	620	-	-	0.0412	-	-
BoAt08	620	-	-	0.0404	-	-
CaBo08	620	-	-	0.0405	-	-
ChYo08	620	-	-	0.0379	-	-
AkBo10	600	800	1000	0.0424	0.0367	0.0367
Zhao06	500	700	900	0.0425	0.0376	0.0376
PSSM	1000	-	-	0.0216	-	-

The value of κ_1 for the PSSM corresponds to the Swiss generic rock profile with $V_{S30} = 1000$ m/sec and $\kappa_1 = 0.017$ sec used to develop the PSSM used by the SP2 experts [Edwards et al. 2010].

1.5.3 Target κ Values

The Swiss NPP sites have V_S profiles with V_{S30} values that range from 1100 to 2500 m/sec. Because of the small number of recordings on Swiss rock sites with V_{S30} values in this range, the SP2 experts were concerned whether the values of κ derived from the simultaneous broadband inversion approach used to derive the PSSM were robust and consistent enough to use in the $V_S - \kappa$ adjustments. Sensitivity studies showed that the value of target κ has a large impact on these adjustments, emphasizing the importance of the target κ values. As a result of this concern, a variety of methods and resource experts were used in an attempt to find a stable set of κ values.

Stochastic Broadband Inversion of Swiss Recordings

One of the major issues was the apparent discrepancy between the κ values derived for the Swiss rock sites ($V_{S30} > 1000$ m/sec) from the PSSM broadband inversion of FAS and those derived by fitting the high-frequency shapes of the corresponding acceleration response spectra (SA) [Edwards et al. 2010]. In that study, the κ values for the 11 rock sites (excluding MUO based on the advice of D. Fäh, written communication) obtained from the simultaneous FAS broadband inversion were found to range between 0.0024-0.016 sec, whereas the κ values using the same stochastic model but fitting the high-frequency part of the acceleration response spectra were found to range between 0.017-0.073 sec. These two sets of values are mutually exclusive, although the authors suggest that the values based on the SA approach should

be considered to be an upper bound. This apparent discrepancy in κ values could be due to the different subsets of the database that were used in each approach. In the broadband inversion earthquakes with $M_W \geq 2$ and recordings with $R_{epi} \leq 250$ km were used, where R_{epi} is epicentral distance. In the SA approach earthquakes with $M_W \geq 3.5$ and recordings with $R_{epi} \leq 30$ km were used in order to have sufficient high-frequency content and neglect path effects.

Edwards et al. [2010] tested whether the use of larger magnitudes in the SA method might have caused the κ discrepancy by fitting the high-frequency slope of the FAS using the method of Anderson and Hough [1984] for those events with $M_W \geq 3.5$. They found that the κ values were similar to those derived from the broadband inversion approach. This led the authors to suggest that there is a fundamental difference between the FAS and SA methods. Another difference between the two approaches is the constraint in the simultaneous broadband inversion that the total path and site attenuation parameters should be greater than zero (i.e., that $t* + \kappa_0 > 0$), meaning that κ_0 could be negative. On the other hand, the SA approach always resulted in positive values of κ_0. The authors also tested whether the magnitude-dependent stress drop that came from the inversion could have impacted κ. Assuming that stress drop is constant, they found that a f_{max} [Hanks 1982] of 6 Hz was consistent with a magnitude-independent stress drop based on how the source corner frequency interacts with κ for small-magnitude earthquakes with short corner frequencies. This value of f_{max} is consistent with $\kappa_0 = 0.027$ sec based on the relationship

$$\kappa_0 = \frac{1}{2\pi f_{max}}. \tag{III-1.1}$$

which is consistent with the median κ estimate of 0.028 sec for the 11 rock stations obtained using the SA approach. In a related study, Baltay and Hanks [2013] show that it is very difficult to recover both κ and source corner frequency (i.e., stress drop) for small-magnitude recordings in which f_{max} is smaller than the corner frequency (FiguresIII-1.15 and III-1.17). These authors note that "For a constant stress drop, the effect of κ is to decrease the "apparent" stress drop because the apparent corner frequency is always underestimating the true corner frequency. This effect is worse at small magnitudes and large values of κ. The stress drop values given in Figure 73 [of the PEGASOS report; i.e., Edwards and Fäh [2010]] would actually be consistent with a constant stress drop and a kappa of 0.02-0.03 sec." This conclusion is demonstrated in Figure III-1.17.

The concept of constant stress drop is further supported by the study of Baltay and Hanks [2013] who found that PGA from near-source recordings ($R_{JB} < 20$ km) of $M_W = 3.0$-7.9 earthquakes compiled by the Pacific Earthquake Engineering Research Center (PEER) for the NGA-West2 Project [Bozorgnia et al. 2012] could be modeled using a simple seismological model with a constant κ of 0.035 sec and a constant stress drop of 75.6 bars (Figure III-1.18), except at large magnitudes where PGA was found to be constant at approximately 0.31 g for M_W>6.6. They also found that the near-source NGA-West2 PGV data could be fit using the same constant κ value and simple seismological model with a constant stress drop of 57.2 bars (Figure III-1.19), except for M_W>6.9 where PGV was found to be approximately constant.

These figures show that the Swiss data are generally consistent with both the proposed simple seismological model and the NGA-West2 data in the limited region where the two databases overlap. Baltay and Hanks [2013] also show that the consistency between the near-source

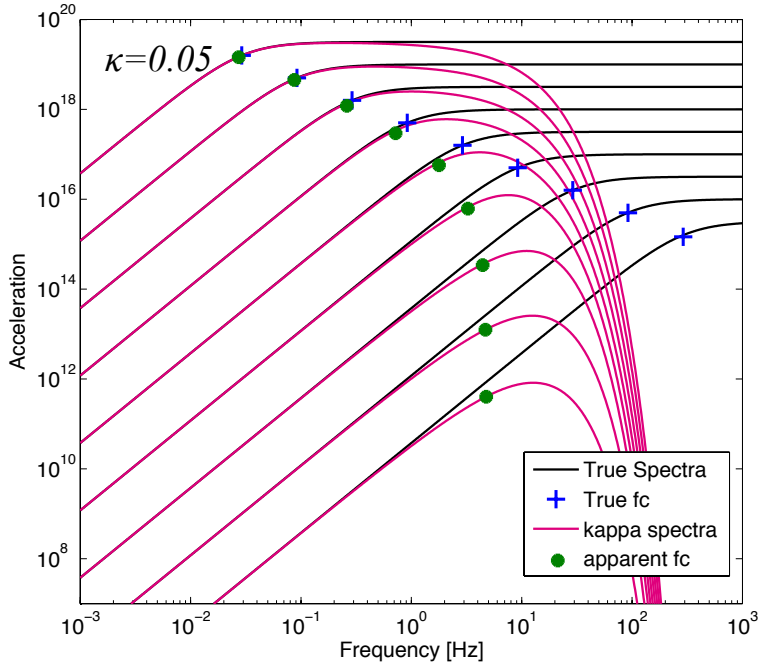

Figure III-1.15: Black lines are the true Brune spectra for Mw 0 (bottom) to Mw 8 (top). True corner frequency shown by the blue plus signs. Magenta spectra show the effect of κ on the spectra and corner frequency, with the measured, or apparent, corner frequency shown by green dots. The apparent corner frequency reaches a maximum at about magnitude 4. The smaller events have artificially small corner frequencies (Baltay and Hanks [2013] after Figure 4 from Anderson and Hough [1984]).

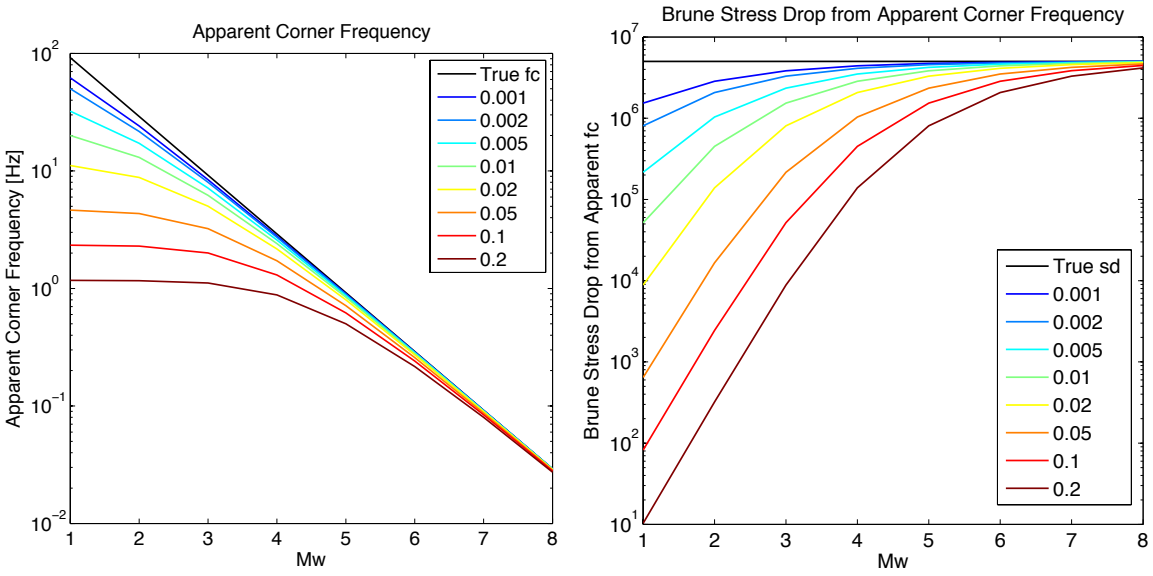

Figure III-1.16: Figures 6 (left) and 7 (right) from Anderson and Hough [1984], reproduced here, showing apparent corner frequencies measured from the spectra shown in Figures 2 and 4 of Anderson and Hough [1984] (above), and inferred stress drop from that apparent corner frequency, with given κ values. Models were run with input 100 bar stress drop. [Baltay and Hanks 2013].

NGA-West2 and Swiss data extend to SA at periods of 1 and 0.1 sec (Figure III-1.20) and

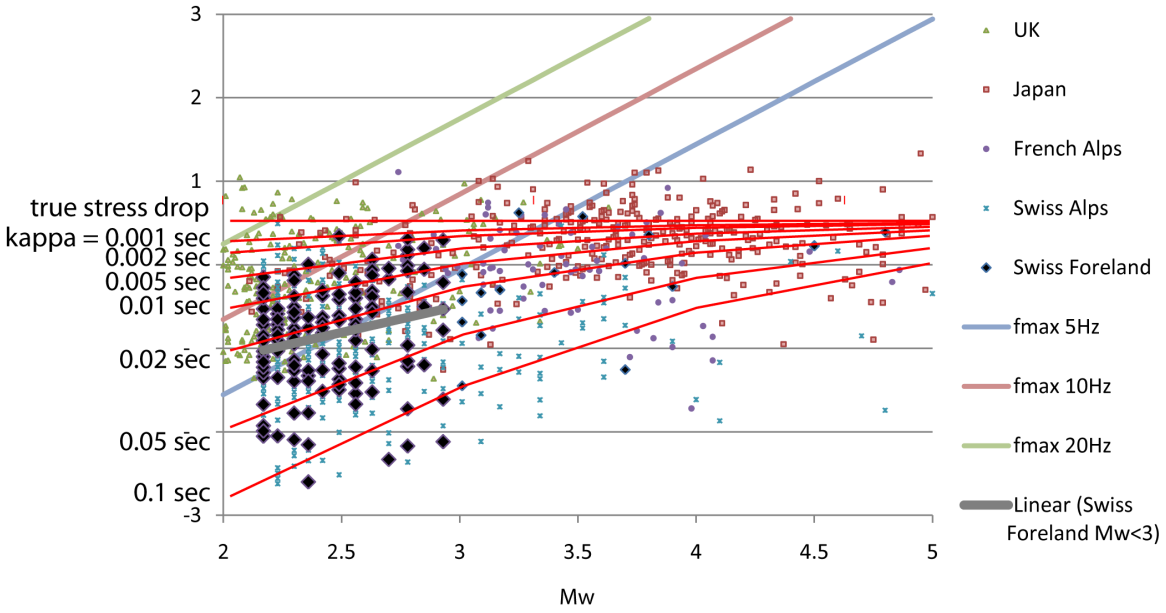

Figure III-1.17: Combination of Figure 7 from Anderson and Hough [1984] overlain on Figure 73 from the PEGASOS report TP2-TB-1024 [Edwards et al. 2010] showing the strong effect of κ on estimated stress drop, especially on the smaller magnitude data. [Baltay and Hanks 2013].

that the near-source NGA-West2 and Swiss PGA data are consistent with small-magnitude Japanese data (Figure III-1.21). Based on these results, Baltay and Hanks [2013] conclude that" ...we see no reason that the Swiss GM [ground motion] data should not be modeled with a constant stress drop. The strongly magnitude dependent stress drop model proposed in the PEGASOS report (i.e., Edwards and Fäh [2010]) either extrapolates wildly into the larger magnitudes, or is arbitrarily cut off to a constant stress drop at some magnitude (M 5). This variable stress drop model is [not] consistent with our seismological perspective or many other global studies. The strong motion Swiss data is not inconsistent with either the NGA-West2 data or Japan Kik-Net data. From a first pass, our simple source-based, constant stress drop model would describe all these data well."

Edwards et al. [2010] estimated κ values for three of the NPP sites from the high-frequency slope of the FAS [Anderson and Hough 1984]. They used only recordings with signal-to-noise ratios that allowed fitting the slope between 10 and 40 Hz. In addition, they only used earthquakes of $M_W > 2.6$ in order to ensure that the source corner frequency was less than 10 Hz and assumed a constant crustal attenuation of Q = 1216 obtained from the broadband inversion. They used 28 horizontal traces for both the surface and buried recordings at Beznau (KKB) and 2 traces each for the surface recordings at Gösgen (KKG) and Leibstadt (KKL). All of the κ estimates for the surface sites were found to be 0.02 sec or greater. The buried site at KKB had a slightly lower κ estimate of 0.017 sec. The relatively shallow soil at these sites is not expected to reduce the κ values very much assuming reasonable estimates of Q for the shallow surface layers [Edwards et al. 2010]. Even if the difference in κ between the surface and buried sites at KKB of 0.003 sec is applied to the other sites, the κ estimates at these sites are still larger than 0.02 sec, much larger than the κ values obtained for the SED sites with the FAS approach, but similar to the values obtained with the SA approach.

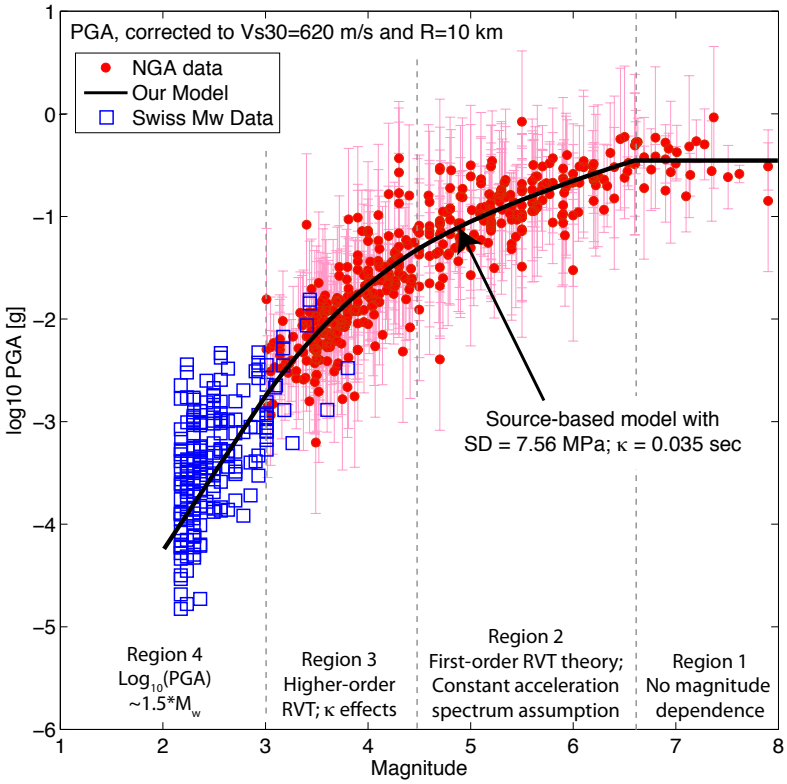

Figure III-1.18: PGA of NGA-West2 data (red dots) and Swiss data (blue squares) for data within 20 km. NGA data are corrected to 10 km with 1/R geometrical spreading and to V_{S30}=620 m/s using Boore and Atkinson [2008]; Swiss data with $1/R^{1.29}$ and amplification factors provided. Black line shows the source-based model developed for NGA-West2 with a stress drop of 7.56 MPa and a κ of 0.035 s. The four regions of the model, based on different source behavior at close recording distances, are indicated with the dashed grey lines. [Baltay and Hanks 2013].

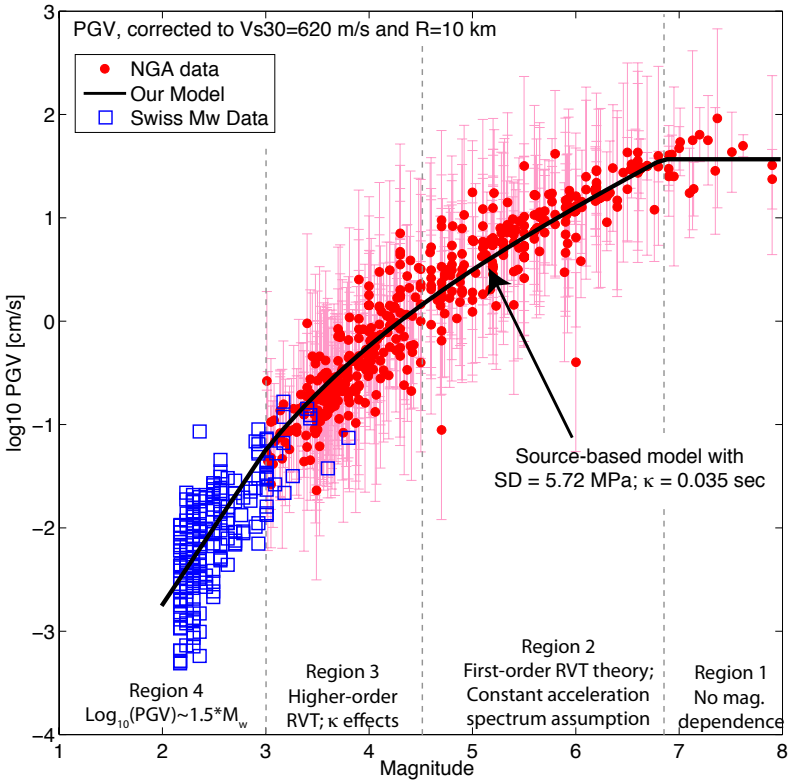

Figure III-1.19: PGV of NGA-West2 data (red dots) and Swiss data (blue squares) for data within 20 km. All data are corrected to 10 km with 1/R geometrical spreading, and to V_{S30}=620 m/s using Boore and Atkinson [2008]. Black line shows the source–based model developed for NGA-West2 with a stress drop of 5.72 MPa and a κ of 0.035s. (Note: the difference in stress drop for the model between PGA and PGV is still an artifact of the model parameters and constants which is being investigated. Thus, only relative values of stress drop should be considered.) The four regions of the model, based on different source behavior at close recording distances, are indicated with the dashed grey lines. [Baltay and Hanks 2013].

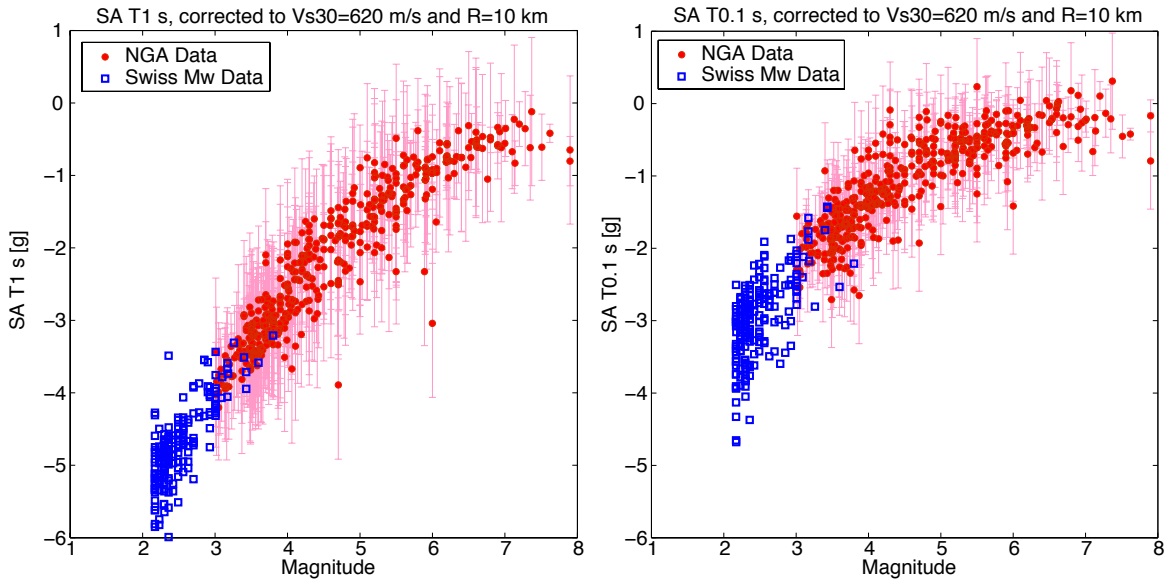

Figure III-1.20: Comparison of NGA and Swiss SA data at 0.1 s (10 Hz) and 1 s (1 Hz). All data are corrected in the same manner as in previous plots. The data are in fairly good agreement. [Baltay and Hanks 2013].

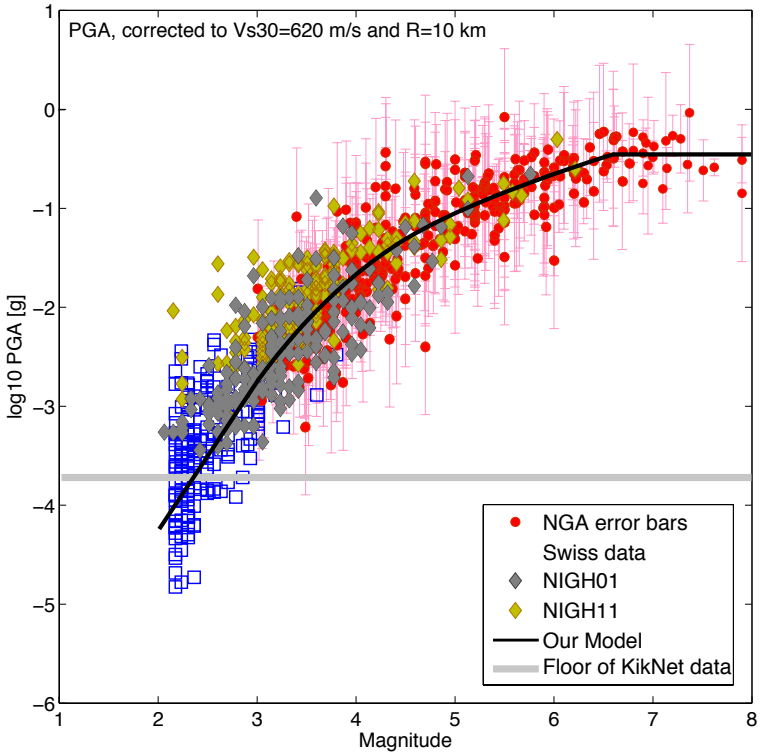

Figure III-1.21: Same as Figure III-1.18, but adding Japanese strong motion Kik-Net data from 6 stations in the northern Honshu, Japan area. [Baltay and Hanks 2013].

A summary of the κ values determined by Edwards et al. [2010] for the SED rock sites and the three NPP sites is given in Table III-1.4.

Table III-1.4: Summary of κ estimates from the Swiss Stochastic Model and recordings at the Swiss NPP sites.

Site	V_{S30} *(m/sec)*	Site κ (κ_0, sec)	
		FAS Approach	SA Approach
AIGE	1243	0.0142	0.028
BALT	1348	0.0024	0.025
BNAP	1654	0.0142	0.034
BRAT	1079	0.0033	0.063
GIML	1496	0.0148	0.073*
HASI	1603	0.0077	0.026
LLS	3011	0.0025	0.018
MUO**	1086	0.0533	0.058
PLOS	1810	0.0064	0.024
SIOV	1473	0.0162	0.017
SULZ	1028	0.0136	0.025
WIMS	1443	0.0102	0.03
KKB (Surface)	600 - 800	0.02	-
KKB (Buried)	-	0.0165	-
KKG	500	0.0276	-
KKL	550	0.0391	-

* Value was poorly constrained.
** On a slope and not considered reliable (D. Fäh, personal communication)

FAS-Based Studies

Because of the widely varying κ estimates derived for the SED seismic stations by Edwards et al. [2010] using the FAS and SA approaches, several other estimates using FAS approaches were done to help the SP2 experts decide what an appropriate set of target κ values should be. These studies are briefly reviewed in this section.

Biro and Renault [2012b] used recordings obtained from 2004 to 2012 at the SED seismic station LLS and the NPP sites KKG and KKB (both at depth and at the surface) to derive κ estimates using the high-frequency slope of the FAS [Anderson and Hough 1984]. They used the same values of crustal velocity and attenuation used to develop the PSSM [Edwards et al. 2010; Edwards and Fäh 2010] in an attempt to be consistent with that study. They used both acceleration and velocity (corrected to acceleration) FAS to see if there was a bias if velocity FAS were used. When all 22 recordings obtained at LLS were used, they found an average κ of 0.008 (-0.009 to 0.026) sec, where the values in brackets represent the range. This would seem to support the relatively small values obtained by Edwards et al. [2010] for this station, although the value they obtained was only 0.003 sec. However, the authors noticed that some of the FAS did not represent what they called "useful" recordings. Such recordings resulted in negative κ values and the seismic moment (M_0) does not fit with the selected frequency band used to derive κ. As a result, there was no clear decay to observe or fit. If the frequency

band used to derive κ was adjusted to fit a smaller frequency range that gives a reasonable (positive) κ then the M_0 fit was unreasonable. As a result, the authors decided to use only what was considered to be "useful" recordings. This decision is consistent with the plots of the FAS spectral fits used to develop the PSSM, which show that negative values of κ tend to be associated with high-frequency FAS shapes that either flatten at high frequencies or begin to roll over at a relative high frequency [Edwards et al. 2012]. In this case, the nine useful acceleration FAS recordings resulted in an average κ value of 0.019 (0.013-0.026) sec and the nine useful velocity FAS recordings resulted in an average κ value of 0.019 (0.012-0.031) sec, consistent with the value of 0.018 sec obtained by Edwards et al. [2010] using the SA approach. κ values for the NPP sites were based on three recordings at KKG and six recordings at KKB. A summary of the κ values calculated by Biro and Renault [2012b] is given in Table III-1.5. Figure III-1.22 compares these values to those derived by Edwards et al. [2010] using both the FAS and SA approaches and Al Atik [2011b] using the SA approach.

Table III-1.5: Summary of κ values obtained by Biro (PMT-TN-1244).

Site	V_{S30} *(m/sec)*	Site Kappa (κ_0, sec)
LLS	3011	0.019
KKG (0 m)	467	0.015
KKG (-27 m)	2500	0.014
KKB (0 m)	516	0.025
KKB (-7 m)	-	0.023

There is little difference in the κ values determined from the surface recordings compared to those obtained at depth. The values for KKB are slightly larger than found by Edwards et al. [2010], whereas the values for KKG are considerable smaller.

Ktenidou and Van Houtte [2013] used the same data used to develop the PSSM [Edwards et al. 2010] to estimate κ values at six SED seismic stations. Two were in the Swiss Foreland and four were in the Swiss Alps. Of the two in the Swiss Foreland, the BALT station was near KKG and the SULZ station was near KKB and KKL. The four stations in the Alps were PLOS, BNAP, HASI and LLS. They used the high-frequency spectral decay method of Anderson and Hough [1984]. The authors applied various selection criteria to the databased on distance, magnitude, Q, whether κ was allowed to be negative, and the consistency between the two horizontal components. They found Q to be similar for both regions and used a single slope with distance (i.e., Q value) to fit them. This was equivalent to assuming a single Q value that is independent of frequency.

When allowing both Q and κ_0 to be determined by the data, Ktenidou and Van Houtte [2013] found κ values that were consistent with those found by the SA approaches. However, they also found that Q ranged from 1650-2050, substantially larger than the nominal value of 1200 found by Edwards et al. [2010]. When Q was constrained to be 1200, κ values were found to be significantly lower. The κ values are summarized in Table III-1.6.

In Table III-1.6 the minimum and maximum values are those obtained from the different data selection scenarios, the preferred value is the authors best-estimate, and the median is the geometric mean of the minimum and maximum values. The authors also note that the estimates show a slight trend of decreasing values of κ with V_{S30} that is consistent with Greek

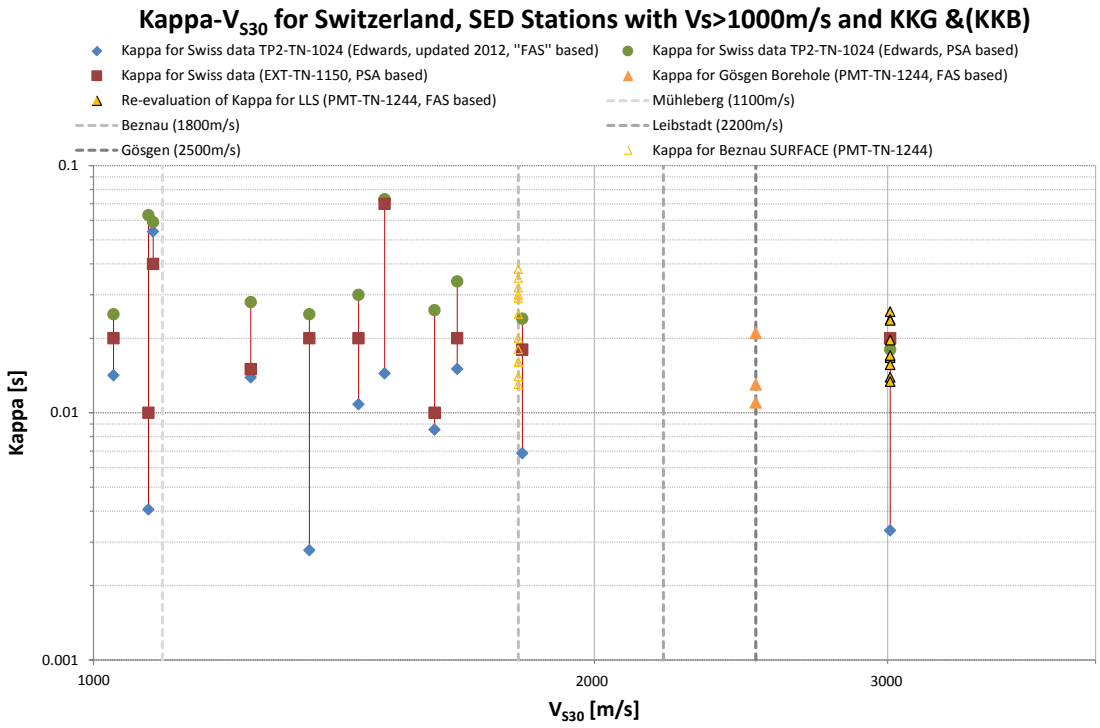

Figure III-1.22: $\kappa - V_{S30}$ for Switzerland SED Stations with $V_S > 1000$ m/sec and KKG and KKB [PMT-TN-1244].

Table III-1.6: Summary of κ Values obtained by Ktenidou and Van Houtte (EXT-RF-1448).

Site	*VS30 (m/sec)*	Site Kappa (k0, sec)			
		Minimum	Maximum	Preferred	Median
SULZ	1030	0.024	0.041	0.036	0.031
BALT	1650	0.013	0.028	0.024	0.019
HASI	1600	0.014	0.028	0.024	0.02
BNAP	1650	0.019	0.035	0.031	0.026
PLOS	1800	0.008	0.024	0.018	0.014
LLS	3000	0.007	0.019	0.016	0.011

estimates from surface recordings, but that two down-hole estimates of κ in Greece for sites with V_{S30} values of about 950 and 2300 m/sec are approximately 0.02 sec.

Figure III-1.23 compares the κ values derived for the selected SED rock stations by Ktenidou and Van Houtte [2013] to those derived by Edwards et al. [2010] and several other studies and sets of data that were used to developed $\kappa_0 - V_{S30}$ relationships. Also included in this Figure is the $\kappa_0 - V_{S30}$ relationship developed for Greece by Ktenidou et al. [2012a, b] and the two borehole estimates of κ in Greece by Ktenidou et al. [2012a, b, c] and the down-hole κ estimates from the Japan KiK-Net recordings by Van Houtte et al. [2011]. The open red circles are the preferred values given in Table III-1.6 and the small solid red circles are the individual estimates, where the higher set of values were estimated by allowing Q to be determined by the data and the lower set of values were estimated by forcing $Q = 1200$.

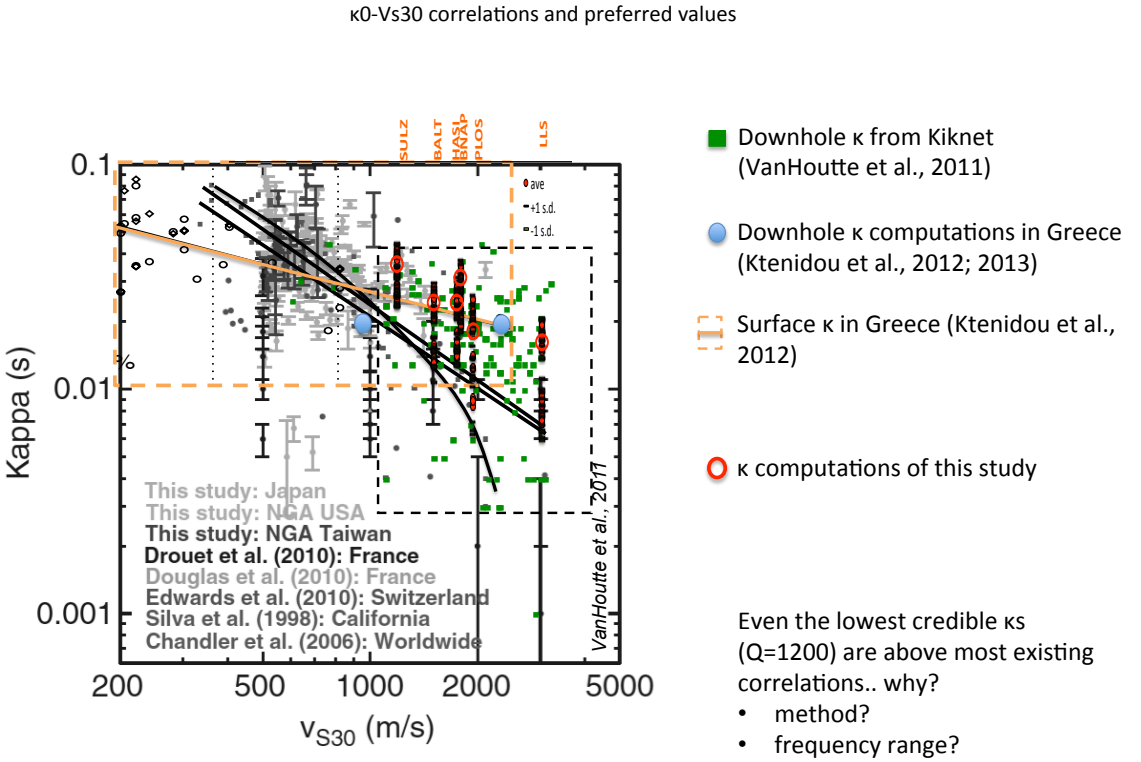

Figure III-1.23: $\kappa - V_{S30}$ for Selected Switzerland SED Stations with $V_S > 1000$ m/sec [EXT-RF-1448].

Figure III-1.24 compares the estimates of Ktenidou and Van Houtte [2013] with those compiled by Biro and Renault [2012b].

If one focuses on the κ estimates for rock with $V_S > 1000$ m/sec in Figures III-1.23 and III-1.24, it becomes obvious that there is no clear trend between κ_0 and V_{S30}. Any apparent trend is based primarily on the extrapolation of the higher κ values for the lower V_{S30} sites to the cloud of lower κ estimates for the higher V_{S30} sites. The other observation by Ktenidou and Van Houtte [2013] is that most estimates of κ on rock sites based on the high-frequency decay method are higher than those derived from the broadband inversion of FAS by Edwards et al. [2010].

SA-Based Studies

Al Atik [2011b] used acceleration response spectra (SA) normalized by PGA from recordings at the eleven SED rock seismic stations and the four NPP sites to derive κ values using spectral templates derived from stochastic simulation. The values determined in this way are not very precise, but the results are useful for comparison purposes. Excluding MUO and GIML (the latter gave a very large κ value that was not reliable), the author obtained an average κ value of 0.017 sec for the 9 remaining SED rock stations. The author calculated approximate average values of 0.035 sec for both surface and buried recordings at KKB, 0.01 sec for KKL, and 0.02 sec for KKG. The five recordings at LLS resulted in an average κ

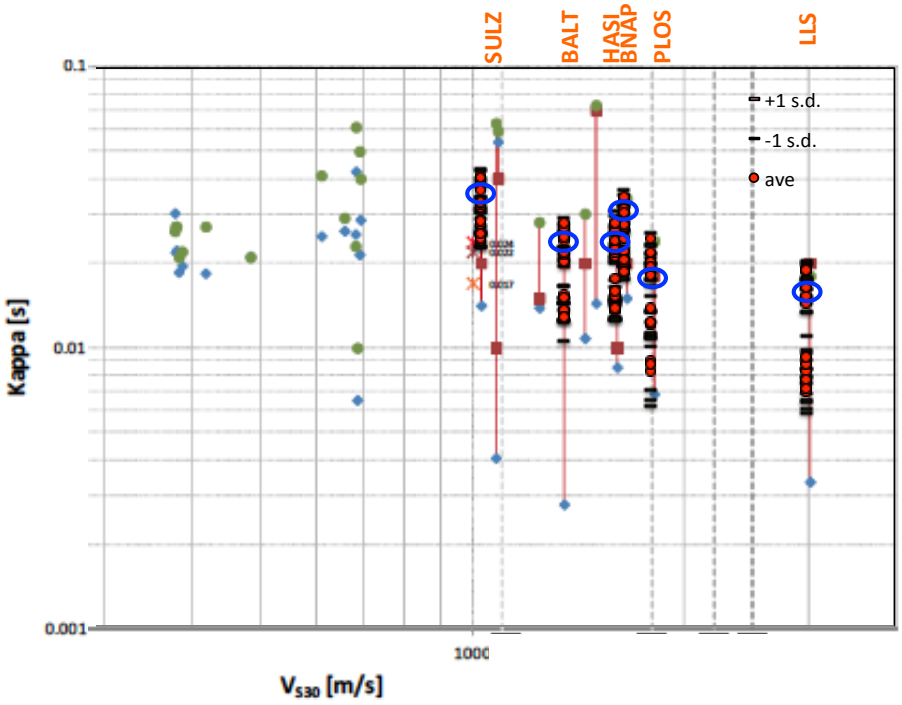

Figure III-1.24: κ estimates for SED stations based on entire Range of Q and preferred values [EXT-RF-1448].

value of 0.020 sec. This latter value is consistent with the value obtained by Edwards et al. [2010] using the SA approach and by Biro and Renault [2012b] using the FAS approach but restricting the calculations to only what was considered to be useful values.

Quarter-Wavelength Studies

The Swiss Seismological Service developed a method to obtain the attenuation characteristics of reference rock from a regional seismic network through the definition of a reference κ operator [Poggi et al. 2013]. The method is an extension of the procedure introduce by Poggi et al. [2011] for Switzerland and was subsequently applied to 38 selected rock site stations of the Japanese KiK-Net network.

The method is based on the comparison between attenuation factors derived from direct spectral modeling of observed earthquakes and those derived from the quarter-wavelength representation of measured velocity profiles over a range of discrete frequencies. The results were used to develop a relationship between site attenuation and the average quarter-wavelength velocity. This approach allows one to estimate κ for rock sites for which a velocity profile and/or an average quarter-wavelength velocity is available. These same results also were used to develop a simplified approach to predict κ from V_{S30}.

The Swiss Seismological Service [Poggi et al. 2012; Edwards et al. 2013a] applied this method to the rock profiles developed in the PRP for the Swiss NPP sites using two approaches:

1. the whole quarter-wavelength (Q_{WL}) profile of the site and
2. the value of V_{S30}.

The results for both of these approaches are given in Table III-1.7.

Table III-1.7: Estimated site κ using the Q_{WL} method for the rock profiles of the Swiss NPP sites.

NPP Site	κ_0 *from* Q_{WL} *(sec)*		κ_0 *from* V_{S30} *(sec)*	
	Mean	Standard Error	Mean	Standard Error
KKB	0.02378	0.01072	0.02038	0.01214
KKG	0.02161	0.01072	0.01843	0.01180
KKL	0.02243	0.01072	0.01902	0.01197
KKM	0.02727	0.01072	0.02610	0.01211

The κ values estimated using this method range between 0.020 and 0.027 sec for the Q_{WL} approach and between 0.018 and 0.026 sec for the V_{S30} approach. As suggested by Poggi et al. [2013], these κ values should be considered as an upper-bound of possible values because of the high average velocities of the NPP sites.

Selected Values and Weights

The large discrepancies between the κ values obtained from the broadband inversion results of the Swiss recordings by Edwards et al. [2010] and practically every other estimate of κ for the SED rock sites or the Swiss NPP sites estimated by others triggered a great deal of discussion amongst the SP2 experts. D. Fäh, one of the authors of the Swiss stochastic ground motion model and one of the SP2 experts, suggested that the target κ should be estimated using an approach (FAS-based or SA-based) that is consistent with that used to develop the ground motion model being adjusted. That would imply that the low κ estimates obtained from the broadband inversion used to develop the PSSM [Edwards et al. 2010] should be used to correct the PSSM from Swiss average rock site conditions ($\kappa_0 = 0.017$ sec, $V_{S30} = 1000$ m/sec) to target reference rock site conditions using $V_S - \kappa$ adjustment factors.

I reviewed this approach and eventually rejected it for three major reasons:

1. the approach does not consider that it is the PSSM acceleration response spectral model that is being used to estimate ground motion and not the FAS model,
2. the high-frequency part of the near-source stochastic response spectra used to develop the PSSM is consistent with larger κ values [Edwards et al. 2010], and
3. all other κ estimates, whether FAS-based or SA-based, for the SED rock stations and the Swiss NPPs consistently indicate much larger κ values.

Another decision was whether to use $\kappa_0 - V_{S30}$ relationships to estimate κ at the NPP sites. Figures III-1.22, III-1.23 and III-1.24 indicate that there is no real evidence to support such a relationship for the 11 Swiss seismic stations with $V_{S30} > 1000$ m/sec or, for that matter, the other data plotted by Ktenidou and Van Houtte [2013] for this same velocity range. Although these authors suggest that there might be a slight trend in their preferred values, this observation is based on only five Swiss rock sites and cannot be justified statistically. The same is true for the κ estimates of all 11 Swiss rock sites derived by Edwards et al. [2010] and for the Japanese KiK-Net sites. The trend predicted by the $\kappa_0 - V_{S30}$ relationships

can only be statistically justified if soil sites are included in the relationship because of the large uncertainty in the derived values. Based on these observations, I rejected the use of predictions from the $\kappa_0 - V_{S30}$ relationships. If a lognormal distribution of κ is assumed, the κ values derived from the 11 Swiss rock sites from the broadband simulation are consistent with a median of 0.00781 sec, a natural logarithmic standard deviation of 0.743, and a natural logarithmic standard error of 0.224. The median estimate of the SA-based values was about three times larger.

Considering the κ estimates from the SED rock sites and the Swiss NPP sites presented in the previous sections, I developed weights based on the lognormal distribution of target κ values given in Table III-1.8 to use with the V_S profiles at the NPP sites to develop $V_{S30} - \kappa$ adjustment factors for both the GMPEs and the PSSMs. I selected a lognormal distribution to be consistent with:

1. my evaluation of κ as a site attenuation parameter that cannot be negative and, therefore, must be truncated at zero at its lower end, and
2. use of a lognormal distribution to characterize site κ for reference hard-rock site conditions in ENA [Campbell et al. 2013; Hashash et al. 2013].

Table III-1.8: Target κ values recommended for making $V_{S30} - \kappa$ adjustments at the Swiss NPP sites for the GMPEs and PSSMs.

κ_0 *(sec)*	Weight
0.0126	0.057
0.0158	0.256
0.0197	0.374
0.0248	0.256
0.031	0.057

This distribution is assumed to have the same standard error determined from the 11 SED rock stations, since there is insufficient information to independently derive this epistemic uncertainty. I excluded some of the κ estimates in deriving the median of the distribution because they were obtained from sites that were either located on a slope (MUO), unreliable because of too few recordings (GIML), or exhibited strong high-frequency resonance (BRAT).

Ktenidou et al. [2012c] point out that κ estimates can vary considerably depending on the person, method, and database used to calculate them and suggested that the most reliable estimates are those derived from the same general region as the site of interest. I have attempted to capture this uncertainty by using κ values estimated by different people using different approaches. I attempted to mitigate any potential regional differences by using estimates only from SED and the NPP rock sites. The biggest uncertainty is the assumption that the same distribution of target κ values can be used for all four Swiss NPP sites, even though their V_{S30} values range from 1100 to 2500 m/sec. More data and additional studies will be needed in order to reduce this uncertainty.

1.5.4 Adjustment Method

There are four methods that could be used to estimate the $V_S - \kappa$ adjustment factor:

1. the standard hybrid empirical method (HEM),
2. the iterative method,
3. FAS scaling with random vibration theory (RVT) referred to as the inverse RVT or IRVT method, and
4. empirical scaling based on residuals.

These methods are described in Part I, Section 3.4.3

The empirical method only applies κ scaling and should be based on a consistent method for estimating κ (i.e., consistent between the κ value for the residuals and the κ value for the host GMPE and target κ value). In principle, the other three methods could be applied to any of the combinations of methods for estimating the host and target κ values and V_S profiles, but there may be some inconsistencies so the applicability of each method to the different input values need to be evaluated. For example, the IRVT method is based on the assumption that κ_0 is consistent with the spectral shape of the GMPE or PSSM.

The iterative method was originally proposed by F. Scherbaum for use in the PRP. However, he is no longer a proponent of the method and, as a result, it was never fully developed or documented by him. Therefore, I rejected it as a viable and defensible method. The empirical method [Al Atik and Abrahamson 2012b] was performed using residuals of two of the 2008 NGA ground motion models using preliminary NGA-West2 and NGA-East project datasets. It is important to note that these datasets as well as the data selections of the NGA-West2 GMPE developers were subject to change at the time this analysis was performed and might not be stable. The adopted criteria for selecting ground motion data to be used for the regression and the evaluation of the $V_S - \kappa$ scaling (recordings with distances less than 50 to 70 km and V_{S30} greater than 600 m/sec) significantly reduced the size of available data for the analysis and required that sites with V_{S30} values outside of the range of interest (i.e., $V_{S30} < 1100$ m/sec) be included in the analysis. Furthermore, a limited number of recordings were available in the κ range of interest for the PRP ($\kappa_0 \leq 0.02$ sec). Another limitation of the empirical method includes the use of $\kappa_0 - f_{amp}$ relationships to estimate κ, which results in recordings at the same station having different κ values. Because of these limitations, I rejected the empirical method as being too preliminary for estimating $V_S - \kappa$ adjustments at the Swiss NPP sites.

After rejecting the iterative and empirical methods, only the HEM and IRVT were left as viable methods. At first, I proposed using both methods. When I first joined the PRP, I had no scientific basis for preferring one method over the other. However, when I compared the resulting adjustment factors from the two methods (Figure III-1.25). I noted that the HEM gave significantly higher adjustment factors. I found that the other SP2 experts had found the same when using relatively small κ values ($\kappa_0 < 0.01$ sec) and that Scherbaum [2011a, b] had discovered that this was because of the difference in the spectral shapes between the GMPEs and the stochastically simulated response spectra at high frequencies ($f_0 > 15$ Hz). This is not an issue for more moderate values of κ where the spectral shapes are more similar and the peak adjustments do not occur at such high spectral frequencies. This inconsistency between stochastic and empirical estimates of response spectra are likely because the high-frequency shapes of the GMPE predictions are not well constrained empirically and do not adequately

represent the high-frequency shape of small-to-moderate magnitude ground motions. This apparent bias at high frequencies in the GMPEs will lead to an overestimate of $V_S - \kappa$ adjustment factors by the HEM at these frequencies (e.g., Campbell [2013]).

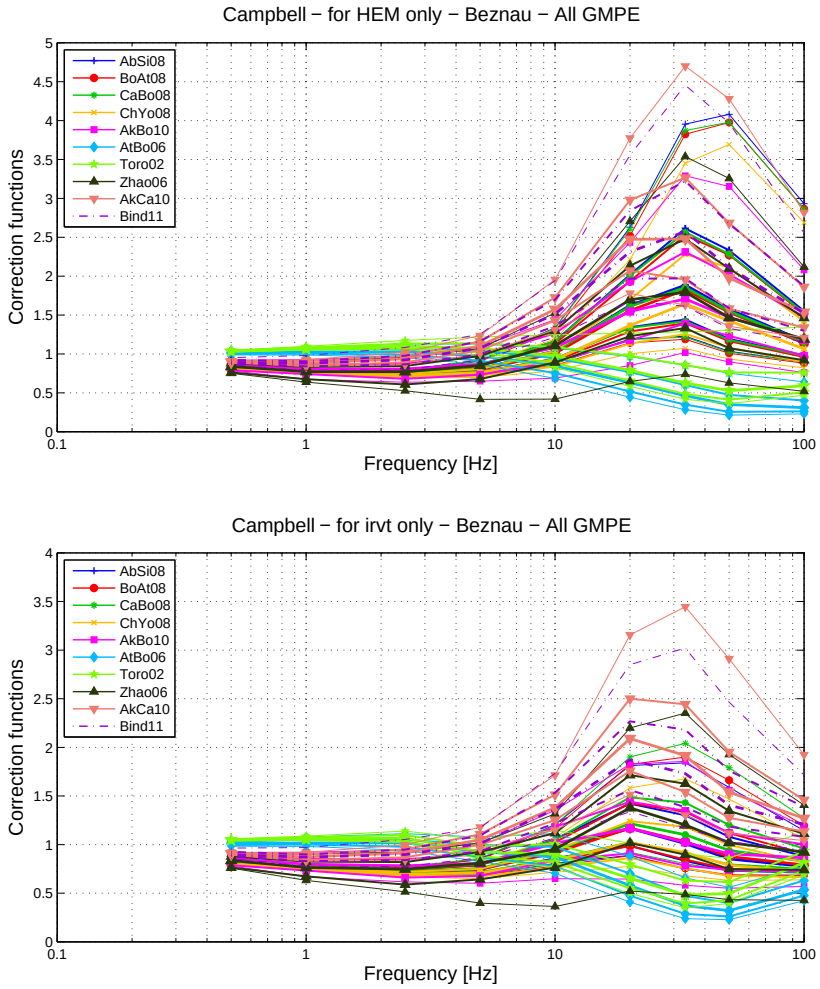

Figure III-1.25: Comparison of $V_S - \kappa$ scaling functions for the HEM and IRVT approach shown as example for Beznau and all GMPEs.

Because of the HEM bias at high frequencies and my original selection of Target κ values less than 0.01 sec, I assigned 100% weight to the IRVT approach. Not only did this avoid the HEM bias, it also is consistent with my selection of the IRVT approach as the sole method to use in determining the host κ values from the GMPEs and PSSMs. This decision should not be interpreted to infer that the HEM is invalid. It remains a valid approach for larger values of κ and for calculating adjustment factors for other seismological parameters. In fact, it is still being used in the PRP to calculate adjustment factors for differences in V_S profiles. In my final evaluation, I decided to give zero weight to Target κ values less than 0.01 sec, which reinstated the HEM as a viable method for calculating $V_S - \kappa$ adjustment factors. However, the IRVT and HEM methods give similar adjustment factors for the larger Target κ values and, therefore, only one of these methods, the IRVT, was used in the final evaluation in order to be consistent with the use of this method to develop the Host κ values.

1.5.5 Adjustment Factors

My final logic tree for calculating the $V_S - \kappa$ adjustment factors is given in Figure III-1.26. It incorporates branches and branch weights for the method for estimating host κ, the host κ values, the target κ values, and the method for calculating the adjustment factors as described in the preceding sections. These adjustment factors are presented in Figures III-2.3 to III-2.10.

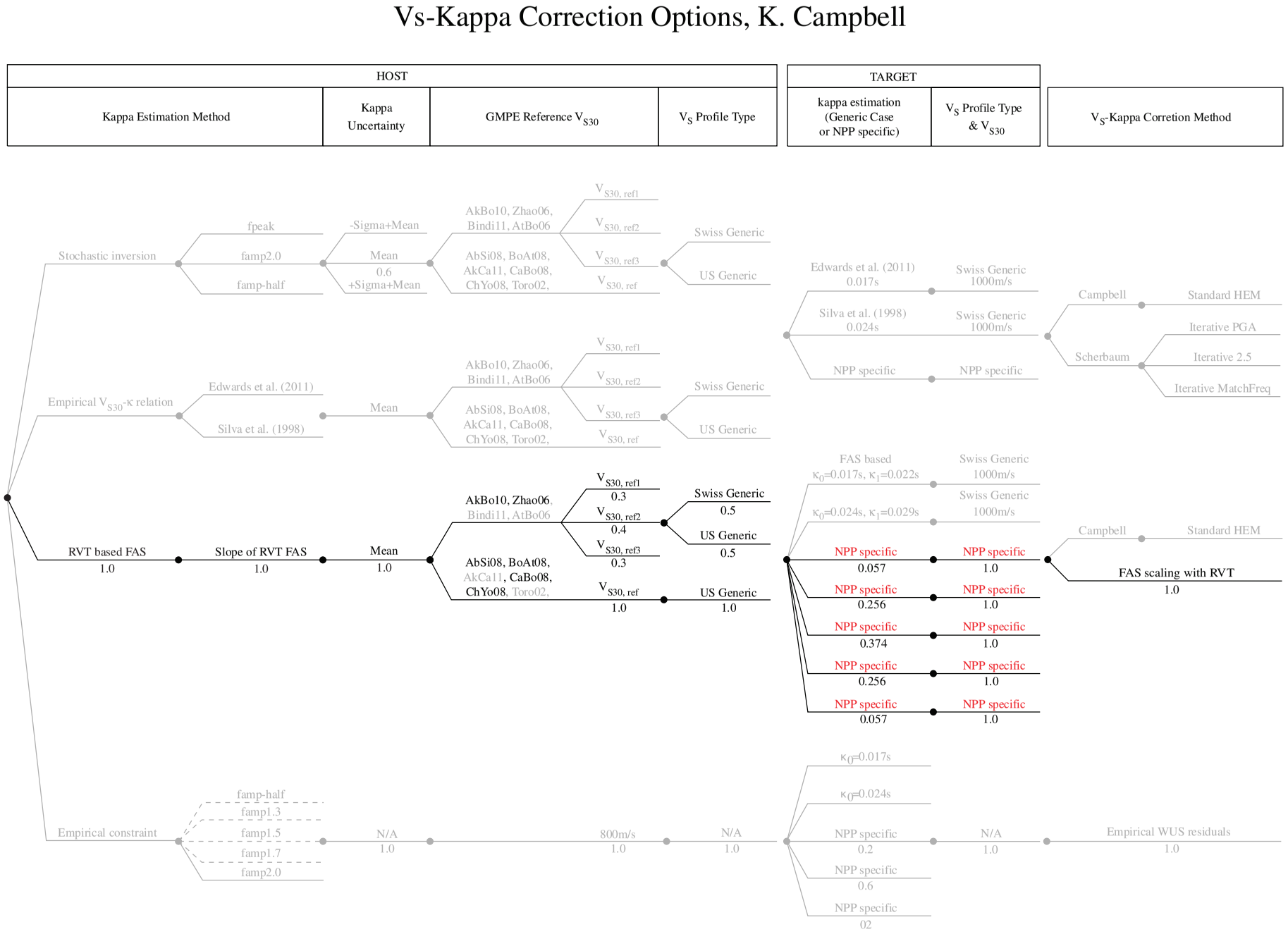

Figure III-1.26: Logic tree for the evaluation of $V_S - \kappa$ scaling for GMPEs.

1.6 Aleatory Variability for Horizontal Motion

The approach used to account for site amplification in the PRP is to use a model for the input rock motion developed by SP2 and then combine this input rock motion with the amplification factors developed for each of the Swiss NPP sites by SP3. The SP3 NPP site models include epistemic uncertainty in the V_S profile and material properties which directly translates to epistemic uncertainty in the median site amplification. This epistemic uncertainty captures the uncertainty in the site-to-site variability term for each site. Therefore, the SP2 used a single-station σ model (i.e., within-site standard deviation ϕ_{SS}) rather than an ergodic σ model in order to remove the site-to-site (between-site) epistemic uncertainty of the within-event standard deviation from the aleatory variability of the rock motion and avoid double-counting epistemic uncertainty in the within-event standard deviation.

Another issue related to the SP2-SP3 interface is which group should model aleatory within-site variability in site amplification. Because the standard deviations of the GMPEs used for the rock ground motions are based on a combination of soil and rock data, the effects of the aleatory variability of site amplification are part of the single-station σ model. Therefore, it is difficult for SP2 to separate the aleatory variability of rock motion from that of the soil motion. For SP3 the site-response calculations produce both estimates of the median amplification and the aleatory variability of the amplification. As a result it is much easier for SP3 to isolate these two terms. Therefore, SP2 and SP3 experts agreed to leave the aleatory site amplification variability term in the SP2 rock model and to remove it from the SP3 site amplification model with the limitation noted below. The site amplification variability in the GMPEs represents that associated with linear site response because the vast majority of data used in the development of the GMPEs is from recordings that are not subject to nonlinear site behavior. Therefore, SP3 must still consider what additional aleatory variability of the site amplification is needed for high levels of input rock motions.

SP2 was required to provide standard deviations or weights to model the aleatory variability for the horizontal ground motion. This aleatory variability was divided into its between-event standard deviation (τ) and within-event standard deviation (ϕ) components. For the within-event component of variability, SP2 was asked to provide an estimate of single-station $\sigma(\phi_{SS})$, the median standard deviation of ϕ_{SS} (ϕ_{SS_S}), and the weight associated with the epistemic distribution on ϕ_{SS_S} associated with the median $\pm$ 1.6 ϕ_{SS_S}. For the between-event component of variability, SP2 was asked to provide a τ model and the weight associated with the epistemic distribution on τ represented by adding 0 $\pm$ 0.1. All standard deviations are defined in terms of natural logarithms.

1.6.1 Within-Event Variability

The methodology developed in the PRP for computing the single-station within-event residuals and standard deviations follows the guidelines outlined in Cotton and Abrahamson [2010]. Values of ϕ_{SS} were calculated using ground motion data from California, Switzerland, Taiwan, Japan, and Turkey. The between-event residuals and single-station within-event residuals for the different regions were calculated by different developers using only events and stations with a minimum of five recordings and following the guidelines outlined in Renault et al. [2010]. Because the largest magnitude in the Taiwanese dataset is 6.3, this dataset does not contribute to the magnitude-dependent ϕ_{SS} models at large magnitude. A summary of ϕ_{SS}

and ϕ values compiled for the PRP by Rodriguez-Marek and Cotton [2011] is shown in Figure III-1.28.

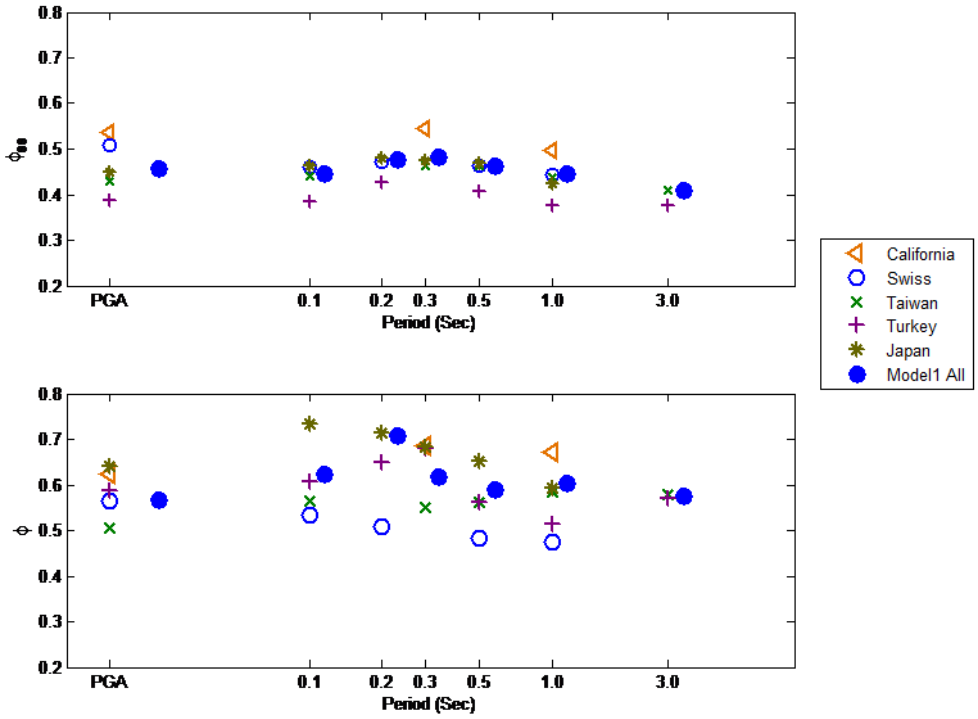

Figure III-1.27: Comparison of single station within-event standard deviations (ϕ_{SS}) and ergodic within-event standard deviations (ϕ) [Rodriguez-Marek and Cotton 2011]. Standard deviations are computed for records with M≥4.5 and R≤200. The solid circle shows the values for the entire dataset. The point is offset only for clarity, but it corresponds to the same periods as the region-by-region data.

Mean Single-Station σ

Based on the studies of Rodriguez-Marek and Cotton [2011]; Rodriguez-Marek [2012], three models were proposed for estimating the mean value of ϕ_{SS}:

- constant (Model 1),
- distance-dependent (Model 2)
- and magnitude- and distance-dependent (Model 3).

These models (shown in Figure III-1.28 for PGA) were developed using the combined data from the different regions since no significant regional variation in ϕ_{SS} was observed. Furthermore, no significant dependence on V_{S30} was observed so that the proposed estimates of ϕ_{SS} are considered to be independent of site conditions. Rodriguez-Marek and Cotton [2011] found the overall average of ϕ_{SS} over all regions to be generally independent of spectral period with a value of around 0.45 (see their Table 4.1). It was found to exhibit much less variability than the ergodic value (Figure III-1.28). It was also found to be consistent with the values

from the Swiss recordings, indicating that combining the regional datasets does not bias the estimates for Switzerland.

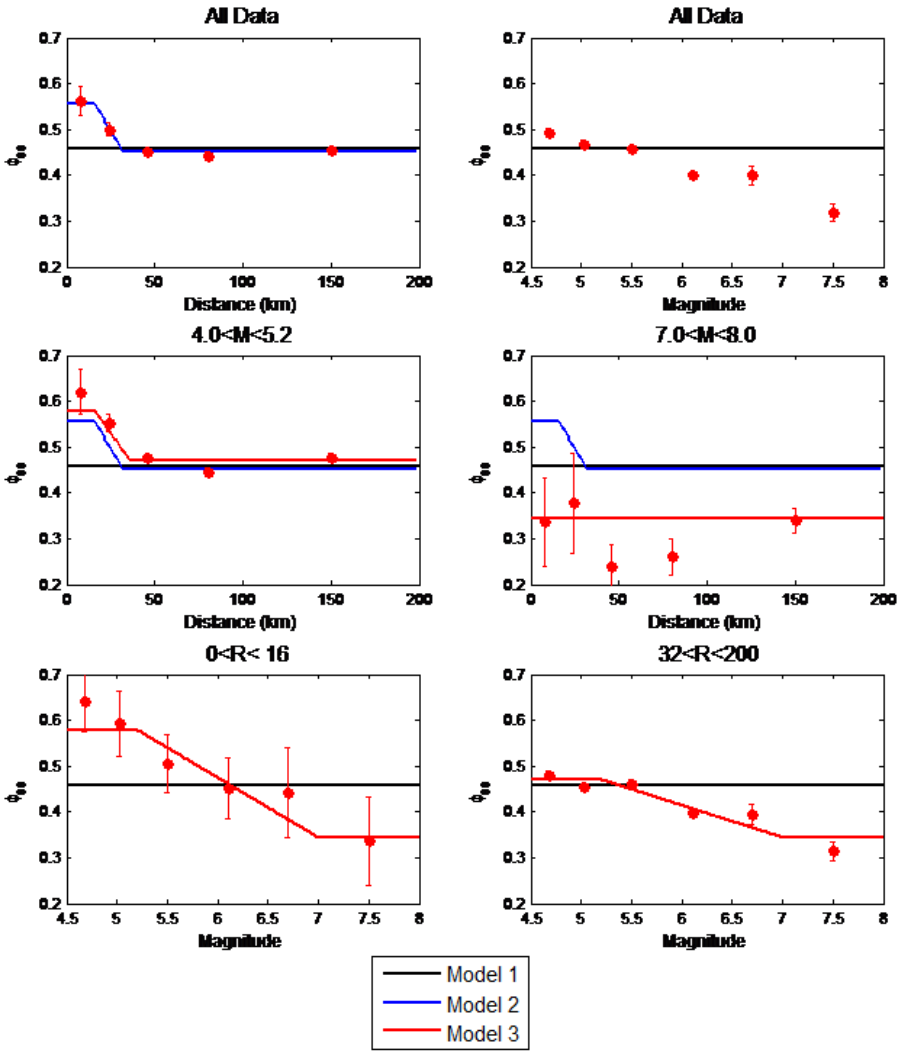

Figure III-1.28: Standard deviations for selected magnitude and distance bins compared with the proposed models [Rodriguez-Marek and Cotton 2011]. Plots are for PGA. The error bars indicate a one-standard deviation error of the sample standard deviations.

The three single-station σ models were included in the SP2 master logic tree. In my evaluation of these models, I was concerned that the increase in ϕ_{SS} at close-in distance incorporated into Models 2 and 3 was caused by uncertainty in earthquake hypocentral depths and not an inherent property of single-station sigma. As a result I gave Model 2 zero weight. I thought that there was merit to a magnitude-dependence in ϕ_{SS} based on several studies that have shown similar behaviour in the ergodic estimate of ϕ [Abrahamson and Silva 2008; Chiou and Youngs 2008b]. However, there was no model that included only magnitude dependence in ϕ_{SS}. Nonetheless, I thought it was important to include a model with magnitude dependence in order to incorporate the view of the informed technical community. Therefore, I assigned a weight of 0.2 to Model 3. I would have assigned a higher weight had the model not included a distance-dependent component as well. The remaining probability of 0.8 was assigned to Model 1 (constant).

Standard Deviation of Single-Station σ

The SP2 experts were asked to provide an evaluation of the standard deviation of the median value of ϕ_{SS} in order to capture the between-site component of epistemic uncertainty in this standard deviation (ϕ_{SS_S}). Rodriguez-Marek [2012] estimated this standard deviation using different criteria on how many recordings were required at a given site to calculate it (their Table 4.6). There was a trade-off on this number and the number of sites available to determine the between-site component of the uncertainty. The required number of recordings per site (N) varied from at least 10 to at least 20. It was found that the mean value of ϕ_{SS} was quite stable, but the value of ϕ_{SS_S} decreased as the number of recordings increased.

After reviewing the results of Rodriguez-Marek [2012], I selected the results for $N \geq 20$ for several reasons. First, the mean value of ϕ_{SS} was generally independent of this number so that the reduced number of stations does not have an impact on the mean estimate of ϕ_{SS}. Second, the value of ϕ_{SS_S} for those spectral periods with at least 16 sites varies between 0.07 and 0.09 with a mean of 0.08. This value is about 20% smaller than the standard deviation of the total value of ϕ from four GMPEs used by Campbell and Bozorgnia [2003] to develop a GMPE for CEUS using the HEM. I would expect to see a somewhat smaller value considering that the values of ϕ_{SS} are themselves smaller. The estimates for a fewer number of stations resulted in values of ϕ_{SS_S} that were equal to or larger than this value. Finally, the smaller values are expected to be closer to the population standard deviations.

Epistemic Uncertainty of Single-Station σ

Rodriguez-Marek and Cotton [2011] assumed the epistemic uncertainty in ϕ_{SS} to follow a normal distribution. The standard deviations of ϕ_{SS} calculated using this approach strictly apply to Model 1 (constant ϕ_{SS}). Due to insufficient data in the distance and magnitude bins used to develop Models 2 and 3, the values of ϕ_{SS_S} were assumed to apply to all three single-station σ models. Rodriguez-Marek and Cotton [2011] proposed three branches to model epistemic uncertainty in ϕ_{SS}: 0, +1.6 ϕ_{SS_S}, and -1.6 ϕ_{SS_S} which the SP2 experts adopted for the PRP. Since this represents an optimum three-point distribution for characterizing a normal distribution, I assigned the 0 (mean) branch a weight of 0.6 and each of the other branches a weight of 0.2.

1.6.2 Between-Event Variability

Rodriguez-Marek and Cotton [2011] summarize all of the between-event standard deviations that were compiled and reviewed as part of the PRP. This summary is shown in Figure III-1.29. Based on these results, they suggested two models for estimating τ and its epistemic uncertainty: a period-dependent model based on the global collection of estimates (Model 1) and a model based on the between-event standard deviations of the GMPEs and PSSMs (Model 2). The SP2 experts adopted this two-model approach for the PRP.

Mean Between-Event Standard Deviation

The GMPE approach to estimating τ (Model 2) is straightforward. The idea is to use the value of τ reported for a given ground motion model when using that model to estimate ground motion in the hazard analysis (Rodriguez-Marek and Cotton [2011], Table 5.4). The

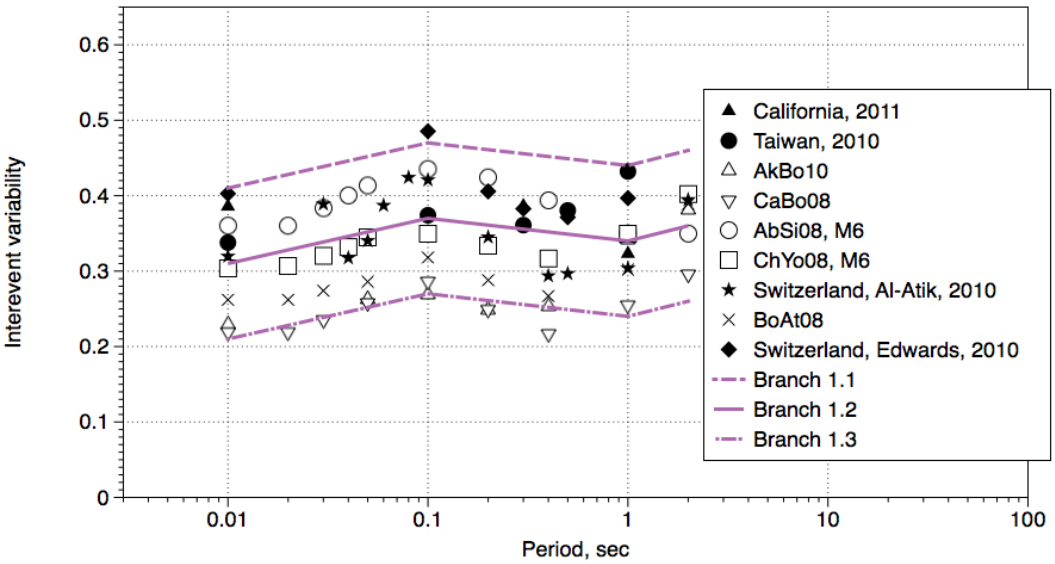

Figure III-1.29: Between event variability: Tau Model 1 (Branch 1.1, Branch 1.2, Branch 1.3).

global approach to estimating τ (Model 1) is somewhat more complicated but still reasonably simple. In Model 1, Rodriguez-Marek and Cotton [2011] eliminated those estimates of τ that were considered to be unreliable and used the remainder to propose a period-dependent mean estimate of τ. These estimates are shown in Figure III-1.29. The mean estimates are 0.31, 0.37, 0.34 and 0.36 for spectral periods of 0.01 (PGA), 0.1, 1 and 2 sec, respectively. Note that two additional GMPEs (AkCa10 and Bind11) were included in the PRP after the study of Rodriguez-Marek et al. [2011] was conducted and exhibit τ values that are much higher than the other GMPEs at some spectral periods. Since I rejected these two GMPEs, partly because of their large aleatory variability, their omission in the study by Rodriguez-Marek and Cotton [2011] is not an issue in my evaluation of between event standard deviation.

Epistemic Uncertainty of Between-Event Standard Deviation

The epistemic uncertainty in τ from Model 2 is explicitly represented by the different values from the ground motion models and, therefore, assigned the same weight as the selected GMPEs and PSSMs. These values were compiled by Al Atik et al. [2010] and are listed in Table 5.4 of Rodriguez-Marek and Cotton [2011]. Based on Figure III-1.29 of Rodriguez-Marek and Cotton [2011], these authors proposed that a reasonable estimate of epistemic uncertainty in τ using the global approach of Model 1 was ± 0.1.

Selected Models and Weights

The SP2 master logic tree includes both the global (Model 1) and GMPE (Model 2) approaches to estimating τ. In my judgment both approaches are reasonable, but I believe that the informed technical community would prefer using the value of τ associated with the selected GMPE based on my knowledge of the scientific literature that overwhelmingly uses the standard deviation associated with the GMPE when conducting seismic hazard studies. As a result, I assign the majority of the weight (0.8) to the GMPE approach and the remainder (0.2) to the global approach.

The SP2 experts were also asked to assign weights (i.e., a probability distribution) to the three values of τ representing epistemic uncertainty. After reviewing the scatter in the values presented in Rodriguez-Marek and Cotton [2011], I decided that a reasonable probability distribution was to assume that the ± 0.1 values of τ represented ± 1.6 times the standard deviation assuming a normal distribution. This corresponds to weights of 0.6 for the mean and 0.2 for the ± 0.1 values. The corresponding standard deviation of the mean value of τ is 0.1/1.6 or about 0.063. This value is smaller than that selected for ϕ_{SS} (0.08) but corresponds to the same coefficient of variation (COV) of 0.18, assuming a mean value of approximately 0.35 for τ and 0.45 for ϕ_{SS} which I consider to be reasonable.

1.6.3 Summary of Aleatory Variability Model

The aleatory variability models for τ and ϕ_{SS} are summarized in Table III-2.15 of the Hazard Input Document (EG2-HID-1010) provided in the next chapter.

1.7 Vertical Ground Motion

There are two main approaches for estimating the seismic hazard for the vertical component:

1. conduct an independent hazard calculation using vertical GMPEs in place of horizontal GMPEs, or
2. scale the horizontal Uniform Hazard Spectrum (UHS) resulting from the PSHA using a vertical-to-horizontal (V/H) ratio.

Prior to me joining the PRP, the SP2 experts selected approach 2 and decided to use available models for the V/H ratios of response spectral ordinates to scale the ordinates of horizontal scenario response spectra derived from deaggregation analyses to obtain a vertical response spectrum. I evaluated the bases for this decision and accepted it as the most reasonable approach for estimating vertical ground motion.

1.7.1 Mean Estimate of V/H Ratios

As summarized in Part I, Section 7, a set of criteria were developed to select a set of candidate V/H ratio models. Three available empirical models met these criteria. The model by Gülerce and Abrahamson [2010] directly predicts the V/H ratio in the same way that a GMPE is used to predict either the vertical or horizontal response spectra. They include site conditions by including V_{S30} as a parameter. Campbell and Bozorgnia [2003] and Akkar and Bommer [2010] provide separate GMPEs for the horizontal and vertical components of response spectra from which a V/H ratio can be computed. These latter two studies characterize site effects using site categories, in which their hardest rock category was used to estimate the V/H ratios. A different approach was used by Edwards et al. [2011b, a], who developed models that predict V/H ratios for hard-rock site conditions based on calibration of the quarter wave-length (Q_{WL}) method using data from Japan and Switzerland. However, since the data they used was only valid up to around 10 Hz, they proposed two versions of the model: one that assumes that there is no amplification in the upper layers that would increase the V/H ratio and one that

assumes there is. The model that assumes no amplification predicts that there is no peak or increase in the V/H ratio at high frequencies as do the three empirical models.

Issues for Hard-Rock Sites

The SP2 experts struggled with the concept of whether there should or should not be a peak in the V/H ratio at higher spectral frequencies for hard-rock sites. One of the experts (D. Fäh, personal communication) argued that perhaps there should not be an increase at high frequencies at the foundation levels of the Swiss NPPs, which are sited on hard rock in which the uppermost layers have been removed. To help with this, the Technical Facilitator Integrator (TFI) N. Abrahamson provided pure empirical estimates of V/H ratios for rock sites using a preliminary version of the NGA-West2 project database (U.S. West Median Model) and the NGA-East project database (U.S. East Median Model). Biro and Renault [2012a] summarize these V/H ratios and compare them to borehole recordings at the KKG NPP. The latter is expected to represent harder sites than the NGA-West2 database, but since most of the sites did not yet have estimates of V_{S30} it was not known what range of values were represented. Both of these empirical databases exhibited peaks or rises in V/H ratios at high frequencies.

Silva and Darragh [2012] provided estimates of κ_0 for vertical and horizontal components of selected recordings on rock sites with V_{S30} values between 800 and 2000 m/sec in order to see if there is a systematic difference between the two that would infer that the V/H ratio should increase at high frequencies. For V_{S30} values up to about 1500 m/sec, they found that the horizontal κ was about twice the vertical κ. This implies a systematic shift in the peak of the vertical response spectrum compared to the horizontal response spectrum by a factor of two. Considering that the horizontal response spectra of the selected GMPEs and PSSMs have a peak at around 10 Hz, one would then expect the corresponding vertical response spectra to peak at around 20 Hz.

It is interesting to note that the one site investigated by Silva and Darragh [2012] that had the highest V_{S30} of 2000 m/sec had vertical and horizontal κ values that were similar to one another, thus adding to the uncertainty of whether there should be a peak in the V/H ratio at high frequencies. When the SP2 experts quizzed SP2 expert D. Fäh as to which of the Edwards et al. [2011a, b] models that he had coauthored he preferred, he said that he had no basis for preferring one over the other.

Selected Models and Weights

Because of the large uncertainty in estimating V/H ratios at hard rock sites, I concluded that the informed technical community would likely select a large number of models to use. The only model that I dropped from consideration was that of Akkar and Bommer [2010] that had a peak V/H ratio at around 10 Hz when evaluated for magnitudes and distances representing the expected controlling hazard at the Swiss NPP sites. This peak occurs at a lower frequency than any other model and would not result in a higher peak frequency in the vertical response spectrum. Based on the discussion in the previous section, I favored those V/H ratio models that exhibited a peak at around 20 Hz. I retained the Campbell and Bozorgnia [2003] model, although some of the SP2 experts suggested that it was superseded by Gülerce and Abrahamson [2010], because it provides an alternative to the empirical parametric

model of Gülerce and Abrahamson [2010] and is still used by the engineering community (one element of the informed technical community) as a means of estimating V/H ratios for design ground motions [Bozorgnia and Campbell 2004]. However, I assigned it less weight (0.3) than the Gülerce and Abrahamson model (0.4).

Because the U.S. West Median model was based on the more recent NGA-West2 rock database, I decided to give it about half the weight of the Campbell and Bozorgnia [2003] model (0.15). Because of all of the uncertainty associated with the U.S. East Median model and its reliance on small-magnitude earthquakes, I dropped it from consideration as a model. However, I used it to help justify why I am giving most of the weight to those models that predict increased V/H ratios at high frequencies. I gave the Edwards et al. [2011a, b] models the same weight as the U.S. West Median model (0.15) because their dependence on the Q_{WL} approach is new and not yet vetted sufficiently in the technical community. However, it was developed using Swiss and Japanese hard-rock data and is considered a viable approach for the Swiss NPP sites. The V/H ratio for this model changes from site-to-site because of its dependence on the velocity profile and gives the largest V/H ratios of any of the models at the Gösgen NPP site. I split this weight between the two Edwards et al. [2011a, b] models (0.075 each) after D. Fäh said that he was not sure which one was more valid during one of the SP2 working meetings. Example V/H ratios estimated from the models I selected for my evaluation are shown in Figure III-1.30.

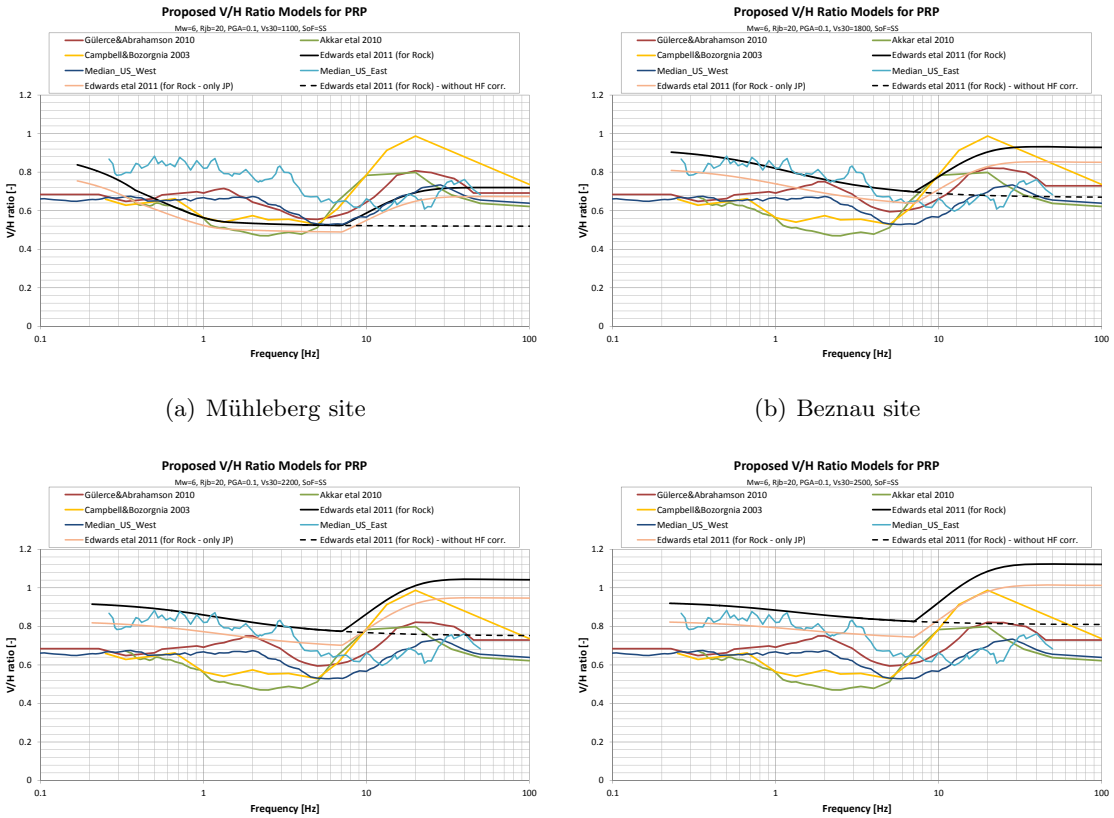

(a) Mühleberg site

(b) Beznau site

(c) Leibstadt site

(d) Gösgen site

Figure III-1.30: Comparison of V/H ratios at all four NPP sites for magnitude 6 and distance=20km.

1.7.2 Aleatory Variability in Vertical Ground Motion

Studies that have developed both horizontal and vertical GMPEs have found that the aleatory variability in the vertical component is higher than that in the horizontal component. As a result there needs to be an additional component of aleatory variability that is added to the horizontal aleatory variability to take this increased aleatory variability into account. SP2 addressed this by providing the value of standard deviation (V_{ADD}) that should be arithmetically added to the horizontal single-station σ to obtain the vertical single-station σ.

Part I, Section 7.3, and Renault and Biro [2012] provides two methods for estimating V_{ADD}:

1. Propagation of uncertainty and,
2. GMPEs.

The propagation of uncertainty methods were highly variable, predicting V_{ADD} to be zero at some frequencies and differing greatly at others. Furthermore, these estimates were provided with virtually no documentation. Therefore, I decided to use them as additional guidance but not to use them to directly estimate the standard deviation of ln(V/H) standard deviations or V_{ADD}. The V/H model of Gülerce and Abrahamson [2010] predicts very large ln(V/H) standard deviations at spectral frequencies below about 1 Hz (Part I, Figure I-7.4) that is not supported by Campbell and Bozorgnia [2003]; Akkar and Bommer [2010], or Edwards et al. [2011a, b]. At high frequencies it gives similar ln(V/H) standard deviations to these models. Therefore, I dropped that model from consideration. The model of Akkar and Bommer [2010] gives similar ln(V/H) standard deviations to Campbell and Bozorgnia [2003], but since their V/H ratio model was not selected I also dropped it from consideration. The Edwards et al. [2011a, b] model predicts ln(V/H) standard deviations that are about 0.05 smaller than the other models at moderate-to-high frequencies. Because this difference is so small and because this Q_{WL} model has not yet been fully vetted by the technical community, I also dropped it from consideration.

This left only Campbell and Bozorgnia [2003] with which to estimate V_{ADD}. However, because of their similarity, the other models are incorporated by proxy. This is especially true of the Gülerce and Abrahamson [2010] model for M = 6 and frequencies above 1 Hz, which represents the predictions of greatest concern in the PRP. The values of the ln(V/H) standard deviations of Campbell and Bozorgnia [2003] are for the combined total between-event and within-event standard deviations. If it is assumed that the ratios of the total vertical and horizontal standard deviations are the same as single-station standard deviations, then V_{ADD} can be calculated from the equation

$$V_{ADD} = \frac{\phi_{SS}}{\sigma_H}\sqrt{\sigma_V^2 - \sigma_H^2} \tag{III-1.2}$$

where ϕ_{SS} is the single-station σ of the horizontal component, σ_H^2 is the total standard deviation of the horizontal component, and σ_V^2 is the total standard deviation of the vertical component.

The values of the median V/H ratios and their weights and the values of V_{ADD} calculated from the Campbell and Bozorgnia [2003] horizontal and vertical GMPEs are summarized in

Tables III-2.18 and III-2.19 of the Hazard Input Document (EG2-HID-1010) provided in the next chapter.

1.8 Maximum Ground Motions

The SP2 master logic tree includes two methods for estimating maximum horizontal ground motions (Part I, Section 9, Figure I-9.3):

1. BA08 distant-dependent median estimate and
2. BA08 distant-independent median estimate at $R_{JB} = 1$ km.

Each method is associated with a vector of levels corresponding to factors to be applied to the median estimate that range from 7.5 to 100. An alternative set of maximum horizontal ground motions based on numerical ground motion simulations was also provided (Part I, Section 8.2), but based on consensus of the SP2 experts this approach was not included in the final logic tree. An extensive database of recordings was compiled to compare with the median estimates of BA08 (Part I, Section 8.2, Figures I-8.1, I-8.2 and I-8.3) to aid the SP2 experts in their evaluation of maximum horizontal ground motions.

1.8.1 Maximum Horizontal Ground Motion

Ground motions must have a physical limit based on the material properties of the deposits that they propagate through. For hard rock this limit is expected to be very large (e.g. as found in the Extreme Ground Motion Project, done as part of the Yucca Mountain high-level nuclear waste repository investigations), well beyond the level that impacts the seismic hazard results at probabilities of concern in the PRP. Sensitivity studies indicated that the PRP seismic hazard results were not significantly impacted when no limit on the maximum ground motion was used in the PSHA. After evaluating all of the information provided to the SP2 experts, I gave 100% weight to the BA08 distant-independent approach with a maximum level defined by a factor of 12.59 for all spectral periods of interest (Part II, Section 2.5, Tables II-2.16 and II-2.17). This allows for the possibility of a physical limit of ground motion while not impacting the hazard results. In fact for practical application, the PRP hazard analysts decided not to impose a maximum limit on the calculated ground motions based on the sensitivity studies that indicated that limits on ground motion imposed by the SP2 experts did not give hazard results that were different from those that did not impose a limit on ground motion.

1.8.2 Maximum Vertical Ground Motion

For the same reasons stated in Section 1.8.1 for the horizontal ground motions, I selected the same logic tree branch and level to assess the maximum vertical ground motion.

Chapter 2

Hazard Input Document for K. Campbell (EG2-HID-1010)

Written by the PMT, SP4 and TFI

This document describes the implementation and parametrization of Kenneth W. Campbell's expert model EG2-EXM-1010, as described in the evaluation summary EG2-ES-1019 (see Chapter 1) and delivered on 16.02.2013. The target κ values were not revised by K. Campbell after the SP2 working meeting in November 2013. The purpose of this document is to translate the expert's evaluation of ground motion into an input usable by the hazard software. For PRP a consensus master logic tree for the median, the aleatory variability, the maximum and the V/H ratio of the ground motions was developed by the SP2 experts and is described in part I. The basic elements of those trees and models are not repeated here. This document only summarizes the parameters and model weights assigned by the expert K. Campbell. By this the master logic tree becomes expert specific and reflects the individual evaluations.

2.1 Model Implementation

Based on the evaluation summary, the logic trees for the median horizontal ground motion, the vertical/horizontal ratio, the maximum ground motion and the aleatory variability of the horizontal and vertical component were implemented. The key elements in the model are given below. Figure III-2.1 shows the logic tree. The first level in the logic tree, "Model Category" is not explicitly specified by the expert but is used by SP4 to allow for an easier treatment of those subsequent global variables (or logic tree levels) like "Vs-Kappa", which are dependent on whether a GMPE or a PSSM model is considered. The logic tree is frequency dependent as the weights associated with the maximum ground motion truncation models vary with frequency, see Section 2.5. The logic tree has in total 1080 branches.

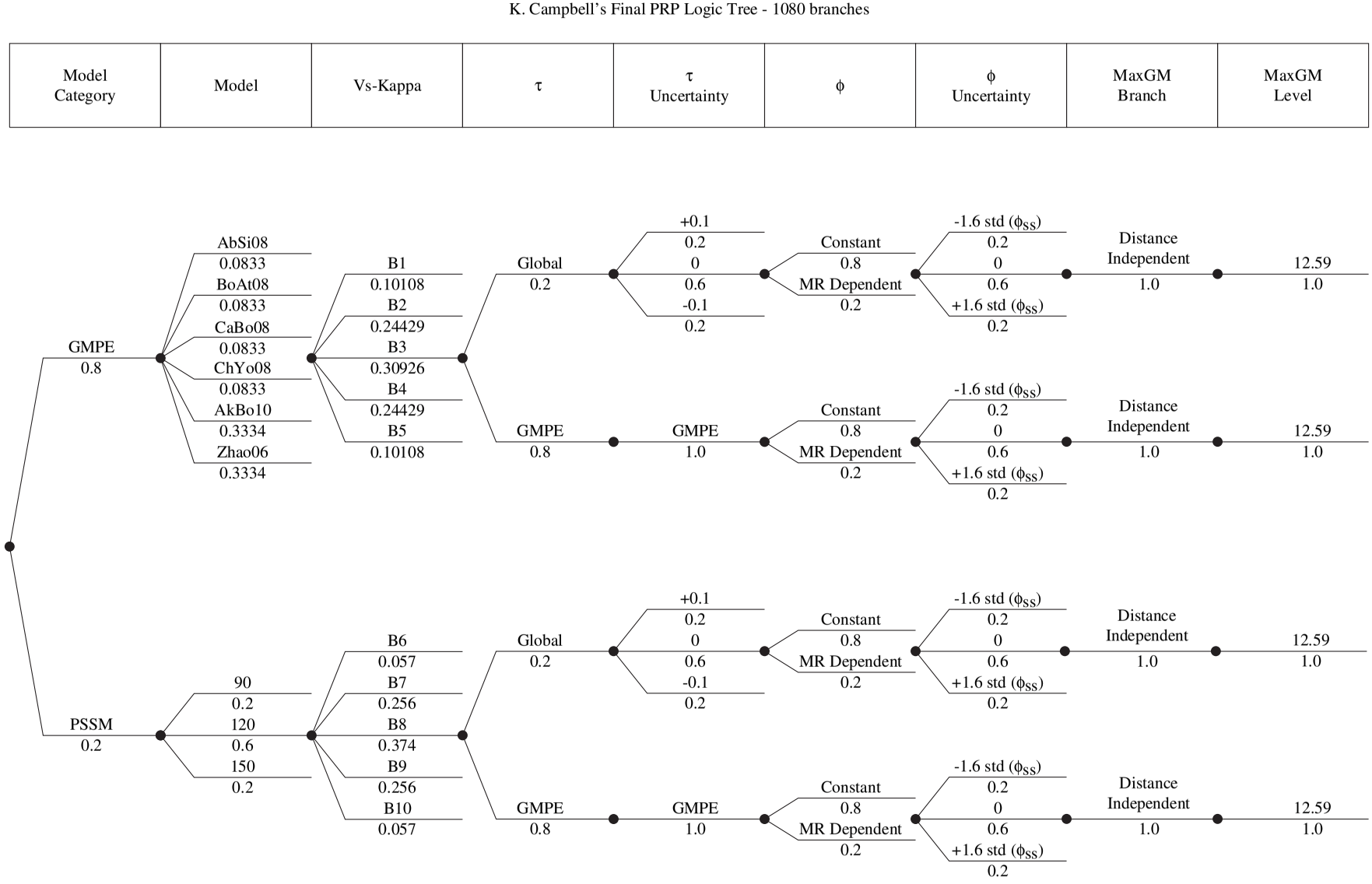

Figure III-2.1: Logic tree for the horizontal ground motion, here for 5 Hz PSA.

2.2 Median Horizontal Ground Motion

Six of the ten candidate models by SP2 get non-zero weights in K. Campbell's model. The empirical GMPEs have a total weight of 80% and the Swiss stochastic model a total weight of 20%. For the parameterized Swiss stochastic model (PSSM) the versions with a M_C=5.5 and frequency dependant stress drop values ranging from 30 to 150 bars have been selected (see Table III-2.2).

Table III-2.1: Weights assigned to the GMPEs.

GMPE	Abbrv.	Weight	Weight by category
Abrahamson & Silva (2008)	AbSi08	0.0667	0.0833
Boore & Atkinson (2008)	BoAt08	0.0667	0.0833
Campbell & Bozorgnia (2008)	CaBo08	0.0667	0.0833
Chiou & Youngs (2008)	ChYo08	0.0667	0.0833
Atkinson & Boore (2006)	AtBo06	-	-
Toro et al. (2002)	Toro02	-	-
Akkar & Bommer (2010)	AkBo10	0.2666	0.3334
Akkar & Cagnan (2010)	AkCa10	-	-
Bindi et al. (2011)	Bind11	-	-
Zhao et al. (2006)	Zhao06	0.2666	0.3334
PSSM* (see tab. III-2.2)		0.20	1.00
Sum GMPE		0.80	1.00
Sum PSSM		0.20	1.00

Table III-2.2: Frequency dependant weights assigned to the PSSMs.

Freq. [Hz]	0.5	1	2.5	5	10	20	33	50	100
PSSM	Weight								
PSSM30	0.50	0.50	-	-	-	-	-	-	-
PSSM60	0.50	0.50	-	-	-	-	-	-	-
PSSM90	-	-	0.20	0.20	0.20	0.20	0.20	0.20	0.20
PSSM120	-	-	0.60	0.60	0.60	0.60	0.60	0.60	0.60
PSSM150	-	-	0.20	0.20	0.20	0.20	0.20	0.20	0.20

Table III-2.3 specifies the reference shear wave velocity ($V_{S30,rock}$) to be used for the NGA models and the site category for the models which have only a category, respectively. The host-to-target correction is applied to those reference models to account for the hard rock conditions at the Swiss NPP sites.

For the depth to sediment layer with V_S=1.0 km/s and 2.5 km/s at the site, the sediment thickness is defined as the depth to a material (bedrock) with a given shear-wave velocity or greater, starting at the top of the rock, as defined in the site response and not the ground surface. For AbSi08 and ChYo08 the parameter $Z_{1.0}$=0 m for rock sites, as the reference $V_{S,30}$ values of all four NPP sites is greater than 1000 m/s after application of the $V_S - \kappa$ corrections. For CaBo08 $Z_{2.5}$=0.800 km, based on assumed generic conditions of the Swiss

region. The GMPE is evaluated with respect to the generic rock condition of 620 m/s and the value for $Z_{2.5}$ needs to be consistent, as the host-to-target correction towards the Swiss conditions (based on a full V_S profile) is applied afterwards.

Table III-2.3: GMPE specific reference shear wave velocity or site category.

GMPE	Ref. V_{S30} [m/s]
AbSi08, BoAt08, CaBo08, ChYo08	620
AkBo10	Rock Cat. (=800)
Zhao06	Rock Cat. (=700)

2.3 Host-to-target Correction

2.3.1 Host-to-target Correction

The host and target κ values were evaluated according to the PRP reports EXT-TB-1087 [Al Atik and Abrahamson 2012a] and EXT-TN-1233 [Al Atik and Abrahamson 2012b], where the average of different evaluated scenarios is taken. The scenarios are based on M=5, 6, 7 and R_{JB}=5, 10 , 20 km with an average depth of 12 km (which is consistent with the average depth in Switzerland). Remark: In 2013 the IRVT method was slightly improved by introducing a dynamic frequency range to pick the high frequency slope of the FAS and the removal of the crustal amplification before calculation of the κ for each spectrum. K. Campbell evaluated these methodological improvements, but maintained his $V_S - \kappa$ corrections from May 2013 for the final hazard computations, because of the complex relationship between these revised corrections and the assessment of weights used to evaluate the GMPEs and PSSMs in the logic tree, which were not easily re-evaluated using the revised corrections.

The expert specific target κ values are summarized together with their weights in Table III-2.4. The Figure I-3.10 depicts the generic logic tree which was developed in the course of the PRP and Figure III-2.2 shows the expert specific version. The finally selected parameters and weights are summarized in Tables III-2.5 to III-2.7. Applying the given combinations leads to 252 discrete correction functions. The resulting 5-point distribution of $V_S - \kappa$ corrections for each of the used GMPEs is reported in Tables III-2.8 to III-2.11. As the resulting distribution is not a known distribution, the evaluated 5 point distribution is based on the approach of Miller and Rice [1983] with the 0.034893, 0.211702, 0.50, 0.788298 and 0.965107 fractiles. The corresponding probabilities/weights for this given discretization are: 0.10108, 0.24429, 0.30926, 0.24429, 0.10108. Tables III-2.12 and III-2.13 have the correction functions to be applied to the different versions of the parameterized Swiss stochastic model, depending on the defined target κ per site. The scaling of the response spectrum depends on the shape of the Fourier spectrum. Changes in the frequency content of the Fourier spectrum due to different stress drops leads to differences in the $V_S - \kappa$ scale factors for different stress drops. The Tables III-2.12 and III-2.13 illustrate the small numerical differences, but the figures show almost no visible difference between the stress drops.

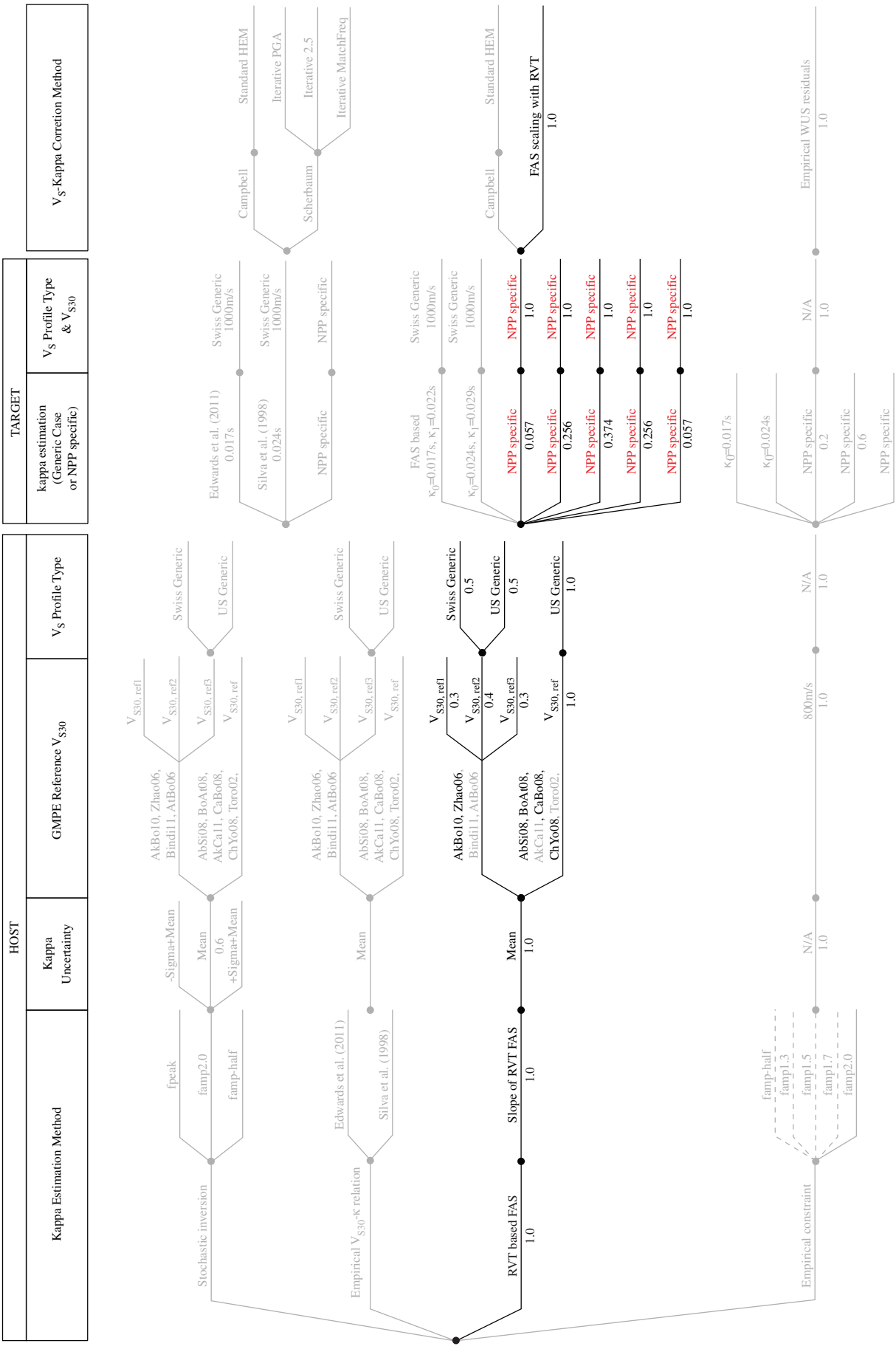

Figure III-2.2: Logic tree for the evaluation of $V_S - \kappa$ scaling for GMPEs.

Table III-2.4: Target Kappa values for GMPE and PSSM with weights for all sites.

	Weight	GMPE κ_0 [s]	PSSM κ_0 [s]
TK5	0.057	0.0126	0.0126
TK6	0.256	0.0158	0.0158
TK7	0.374	0.0197	0.0197
TK8	0.256	0.0248	0.0248
TK9	0.057	0.0310	0.0310

Table III-2.5: Overview of parameters and weights assigned to the $V_S - \kappa$ logic tree for the NGA models.

Estimation Method emethod	**wt.**	**Host** hkest & emethod	**Host** κ hostk	**wt.**	**GMPE**	**HostVS** vs30est	**wt.**	**Profile** vstypestr	**wt.**	**TargetVS** (npp) targetp	**Target** target TK	**Targ.** κ_0	**Targ.** κ_1 targetk	**wt.**	**Correction Method** cmethod	**wt.**
iRVT	1.00	kBE6	0.0414	1.00	AbSi08	620	1.00	US	1.00	KKB1800	TK5	0.0126	0.016	0.057	FAS scaling with iRVT	1.00
		kBE6	0.0404	1.00	BoAt08	620	1.00	US	1.00		TK6	0.0158	0.020	0.256		
		kBE6	0.0413	1.00	CaBo08	620	1.00	US	1.00		TK7	0.0197	0.024	0.374		
		kBE6	0.0374	1.00	ChYo08	620	1.00	US	1.00		TK8	0.0248	0.029	0.256		
											TK9	0.031	0.035	0.057		
										KKG2500	TK5	0.0126	0.017	0.057		
											TK6	0.0158	0.020	0.256		
											TK7	0.0197	0.024	0.374		
											TK8	0.0248	0.029	0.256		
											TK9	0.031	0.035	0.057		
										KKL2200	TK5	0.0126	0.017	0.057		
											TK6	0.0158	0.020	0.256		
											TK7	0.0197	0.024	0.374		
											TK8	0.0248	0.029	0.256		
											TK9	0.031	0.035	0.057		
										KKM1100	TK5	0.0126	0.017	0.057		
											TK6	0.0158	0.020	0.256		
											TK7	0.0197	0.024	0.374		
											TK8	0.0248	0.029	0.256		
											TK9	0.031	0.035	0.057		

Table III-2.6: Overview of parameters and weights assigned to the $Vs - \kappa$ logic tree for the Akkar & Bommer (2010) model.

Estimation Method emethod	**wt.** 1.00	**Host** hkest & emethod kBE6	**Host** κ hostk 0.0344	**Host wt.** 1.00	**GMPE** AkBo10	**HostVS** vs30est 600	**wt.** 0.30	**Profile** vstypestr CH	**wt.** 0.50	**TargetVS** (npp) targetp KKB1800	**Target** target TK TK5	**Target Targ.** κ_0 0.0126	**Targ.** κ_1 0.016	**wt.** 0.057	**Correction Method** cmethod FAS scaling with iRVT	**wt.** 1.00
iRVT								US	0.50		TK6	0.0158	0.020	0.256		
					AkBo10	800	0.40	CH	0.50		TK7	0.0197	0.024	0.374		
								US	0.50		TK8	0.0248	0.029	0.256		
					AkBo10	1000	0.30	CH	0.50		TK9	0.031	0.035	0.057		
								US	0.50	KKG2500	TK5	0.0126	0.017	0.057		
											TK6	0.0158	0.020	0.256		
											TK7	0.0197	0.024	0.374		
											TK8	0.0248	0.029	0.256		
											TK9	0.031	0.035	0.057		
										KKL2200	TK5	0.0126	0.017	0.057		
											TK6	0.0158	0.020	0.256		
											TK7	0.0197	0.024	0.374		
											TK8	0.0248	0.029	0.256		
											TK9	0.031	0.035	0.057		
										KKM1100	TK5	0.0126	0.017	0.057		
											TK6	0.0158	0.020	0.256		
											TK7	0.0197	0.024	0.374		
											TK8	0.0248	0.029	0.256		
											TK9	0.031	0.035	0.057		

Table III-2.7: Overview of parameters and weights assigned to the $V_S - \kappa$ logic tree for the Zhao et al. (2006) model.

Estimation Method emethod	**wt.**	**Host** hkest & emethod	**Host κ** hostk	**wt.**	**GMPE**	**HostVS** vs30est	**wt.**	**Profile** vstypestr	**wt.**	**TargetVS** (npp) targetp	target TK	**Target Targ. κ_0**	**Targ. κ_1** targetk	**wt.**	**Correction Method** cmethod	**wt.**
iRVT	1.00	kBE6	0.0383	1.00	Zhao06	500	0.30	CH	0.50	KKB1800	TK5	0.0126	0.016	0.057	FAS scaling with iRVT	1.00
								US	0.50		TK6	0.0158	0.020	0.256		
					Zhao06	700	0.40	CH	0.50		TK7	0.0197	0.024	0.374		
								US	0.50		TK8	0.0248	0.029	0.256		
					Zhao06	900	0.30	CH	0.50		TK9	0.031	0.035	0.057		
								US	0.50	KKG2500	TK5	0.0126	0.017	0.057		
											TK6	0.0158	0.020	0.256		
											TK7	0.0197	0.024	0.374		
											TK8	0.0248	0.029	0.256		
											TK9	0.031	0.035	0.057		
										KKL2200	TK5	0.0126	0.017	0.057		
											TK6	0.0158	0.020	0.256		
											TK7	0.0197	0.024	0.374		
											TK8	0.0248	0.029	0.256		
											TK9	0.031	0.035	0.057		
										KKM1100	TK5	0.0126	0.017	0.057		
											TK6	0.0158	0.020	0.256		
											TK7	0.0197	0.024	0.374		
											TK8	0.0248	0.029	0.256		
											TK9	0.031	0.035	0.057		

Table III-2.8: Frequency dependent resulting $V_S - \kappa$ correction 5-point distributions for used GMPEs at Beznau.

GMPE	Frequency [Hz]									Weight
	0.5	1	2.5	5	10	20	33.3	50	100	
AbSi08	0.7780	0.7256	0.6380	0.5923	0.6181	0.6009	0.5588	0.5652	0.5748	0.1011
	0.7869	0.7407	0.6707	0.6497	0.7355	0.7707	0.6556	0.6318	0.6375	0.2443
	0.7935	0.7519	0.6957	0.6965	0.8369	0.9441	0.7930	0.7065	0.6974	0.3093
	0.7987	0.7605	0.7156	0.7351	0.9265	1.1217	0.9601	0.8165	0.7588	0.2443
	0.8037	0.7688	0.7350	0.7738	1.0212	1.3307	1.1858	0.9820	0.8363	0.1011
BoAt08	0.7875	0.7268	0.6346	0.5920	0.5954	0.5936	0.5562	0.5661	0.5764	0.1011
	0.7938	0.7412	0.6666	0.6498	0.7098	0.7659	0.6596	0.6362	0.6422	0.2443
	0.7983	0.7518	0.6911	0.6971	0.8086	0.9420	0.8040	0.7195	0.7062	0.3093
	0.8016	0.7599	0.7106	0.7360	0.8960	1.1224	0.9789	0.8382	0.7729	0.2443
	0.8047	0.7677	0.7296	0.7751	0.9883	1.3346	1.2153	1.0148	0.8582	0.1011
CaBo08	0.7856	0.7275	0.6386	0.5979	0.6076	0.6107	0.5724	0.5827	0.5891	0.1011
	0.7928	0.7422	0.6712	0.6584	0.7257	0.7924	0.6986	0.6640	0.6621	0.2443
	0.7980	0.7531	0.6960	0.7066	0.8277	0.9776	0.8563	0.7650	0.7333	0.3093
	0.8020	0.7615	0.7157	0.7462	0.9177	1.1669	1.0455	0.8976	0.8075	0.2443
	0.8057	0.7695	0.7350	0.7861	1.0129	1.3893	1.3010	1.0897	0.9030	0.1011
ChYo08	0.7782	0.7179	0.6191	0.5633	0.5478	0.5237	0.5222	0.5328	0.5428	0.1011
	0.7858	0.7325	0.6506	0.6183	0.6523	0.6714	0.5966	0.5908	0.5992	0.2443
	0.7913	0.7433	0.6746	0.6630	0.7427	0.8232	0.7205	0.6537	0.6533	0.3093
	0.7955	0.7517	0.6937	0.6998	0.8225	0.9787	0.8724	0.7542	0.7088	0.2443
	0.7995	0.7596	0.7124	0.7367	0.9070	1.1618	1.0780	0.9069	0.7787	0.1011
AkBo10	0.7725	0.6566	0.5860	0.5496	0.5449	0.5048	0.4885	0.5009	0.5170	0.1011
	0.7830	0.7211	0.6329	0.6258	0.7053	0.7221	0.6628	0.6294	0.6415	0.2443
	0.8502	0.7835	0.7490	0.7564	0.8839	0.9042	0.7914	0.7567	0.7629	0.3093
	0.8828	0.8385	0.8182	0.8267	1.0120	1.1046	0.9759	0.8647	0.8675	0.2443
	0.9112	0.9070	0.9124	0.9338	1.1579	1.3814	1.2124	1.0203	0.9658	0.1011
Zhao06	0.7520	0.6214	0.4931	0.3674	0.3121	0.4082	0.3802	0.3731	0.3836	0.1011
	0.7603	0.6641	0.5673	0.5968	0.6135	0.7322	0.6424	0.6262	0.6331	0.2443
	0.8286	0.7596	0.7163	0.7550	0.8343	1.0381	0.8900	0.8146	0.8017	0.3093
	0.8735	0.8144	0.7933	0.8552	0.9797	1.3283	1.1462	0.9667	0.9321	0.2443
	0.8972	0.8892	0.8925	0.9580	1.1161	1.6819	1.5845	1.2781	1.0762	0.1011

Table III-2.9: Frequency dependent resulting $V_S - \kappa$ correction 5-point distributions for used GMPEs at Gösgen.

GMPE	Frequency [Hz]									Weight
	0.5	1	2.5	5	10	20	33.3	50	100	
AbSi08	0.7848	0.7217	0.5831	0.5142	0.5202	0.5078	0.4853	0.4935	0.5034	0.1011
	0.7932	0.7365	0.6129	0.5630	0.6168	0.6417	0.5583	0.5469	0.5543	0.2443
	0.7995	0.7475	0.6356	0.6033	0.7004	0.7787	0.6624	0.6042	0.6024	0.3093
	0.8044	0.7560	0.6537	0.6365	0.7742	0.9190	0.7891	0.6852	0.6508	0.2443
	0.8091	0.7641	0.6713	0.6697	0.8522	1.0840	0.9593	0.8070	0.7105	0.1011
BoAt08	0.7984	0.7243	0.5811	0.5140	0.5011	0.5023	0.4853	0.4969	0.5077	0.1011
	0.8048	0.7386	0.6103	0.5632	0.5951	0.6376	0.5620	0.5524	0.5604	0.2443
	0.8093	0.7492	0.6325	0.6038	0.6765	0.7766	0.6717	0.6151	0.6114	0.3093
	0.8126	0.7573	0.6502	0.6372	0.7485	0.9190	0.8039	0.7034	0.6636	0.2443
	0.8156	0.7650	0.6675	0.6707	0.8244	1.0865	0.9820	0.8331	0.7288	0.1011
CaBo08	0.7953	0.7244	0.5844	0.5179	0.5101	0.5140	0.4968	0.5090	0.5160	0.1011
	0.8023	0.7389	0.6139	0.5699	0.6073	0.6572	0.5915	0.5734	0.5748	0.2443
	0.8074	0.7497	0.6365	0.6114	0.6914	0.8036	0.7122	0.6496	0.6316	0.3093
	0.8112	0.7580	0.6544	0.6454	0.7656	0.9532	0.8556	0.7498	0.6899	0.2443
	0.8148	0.7659	0.6720	0.6796	0.8440	1.1291	1.0484	0.8914	0.7630	0.1011
ChYo08	0.7872	0.7147	0.5665	0.4899	0.4612	0.4445	0.4553	0.4671	0.4776	0.1011
	0.7947	0.7292	0.5951	0.5360	0.5470	0.5594	0.5102	0.5132	0.5227	0.2443
	0.8001	0.7399	0.6170	0.5744	0.6215	0.6792	0.6030	0.5616	0.5660	0.3093
	0.8041	0.7482	0.6343	0.6060	0.6872	0.8019	0.7179	0.6344	0.6096	0.2443
	0.8079	0.7560	0.6513	0.6377	0.7567	0.9465	0.8727	0.7465	0.6633	0.1011
AkBo10	0.7808	0.6527	0.5356	0.4774	0.4587	0.4238	0.4193	0.4323	0.4486	0.1011
	0.7907	0.7170	0.5786	0.5421	0.5921	0.6016	0.5589	0.5295	0.5464	0.2443
	0.8579	0.7783	0.6842	0.6552	0.7394	0.7444	0.6616	0.6430	0.6562	0.3093
	0.8902	0.8324	0.7474	0.7159	0.8445	0.9027	0.7990	0.7370	0.7408	0.2443
	0.9180	0.9004	0.8333	0.8079	0.9661	1.1206	0.9770	0.8349	0.8229	0.1011
Zhao06	0.7623	0.6192	0.4524	0.3200	0.2636	0.3427	0.3277	0.3289	0.3405	0.1011
	0.7709	0.6619	0.5193	0.5162	0.5147	0.6050	0.5576	0.5396	0.5482	0.2443
	0.8388	0.7564	0.6554	0.6534	0.6956	0.8484	0.7342	0.6907	0.6800	0.3093
	0.8838	0.8109	0.7259	0.7392	0.8156	1.0796	0.9306	0.8066	0.7909	0.2443
	0.9072	0.8851	0.8161	0.8278	0.9277	1.3585	1.2600	1.0262	0.9023	0.1011

Table III-2.10: Frequency dependent resulting $V_S - \kappa$ correction 5-point distributions for used GMPEs at Leibstadt.

GMPE	Frequency [Hz]									Weight
	0.5	1	2.5	5	10	20	33.3	50	100	
AbSi08	0.7559	0.6904	0.5881	0.5369	0.5551	0.5404	0.5069	0.5136	0.5228	0.1011
	0.7643	0.7047	0.6183	0.5886	0.6598	0.6900	0.5910	0.5725	0.5785	0.2443
	0.7705	0.7153	0.6413	0.6310	0.7504	0.8429	0.7107	0.6377	0.6315	0.3093
	0.7754	0.7234	0.6596	0.6658	0.8303	0.9995	0.8562	0.7327	0.6856	0.2443
	0.7800	0.7313	0.6774	0.7007	0.9148	1.1835	1.0523	0.8754	0.7532	0.1011
BoAt08	0.7677	0.6924	0.5855	0.5367	0.5349	0.5343	0.5056	0.5156	0.5257	0.1011
	0.7737	0.7061	0.6150	0.5888	0.6368	0.6859	0.5950	0.5774	0.5838	0.2443
	0.7780	0.7161	0.6375	0.6315	0.7250	0.8411	0.7208	0.6497	0.6403	0.3093
	0.7812	0.7239	0.6554	0.6667	0.8030	1.0001	0.8730	0.7525	0.6989	0.2443
	0.7842	0.7312	0.6729	0.7019	0.8853	1.1869	1.0783	0.9046	0.7731	0.1011
CaBo08	0.7652	0.6927	0.5890	0.5416	0.5454	0.5487	0.5193	0.5298	0.5361	0.1011
	0.7720	0.7067	0.6189	0.5964	0.6507	0.7087	0.6288	0.6014	0.6008	0.2443
	0.7770	0.7170	0.6418	0.6399	0.7417	0.8720	0.7665	0.6892	0.6636	0.3093
	0.7807	0.7250	0.6599	0.6757	0.8221	1.0389	0.9313	0.8045	0.7289	0.2443
	0.7842	0.7326	0.6777	0.7117	0.9069	1.2349	1.1533	0.9702	0.8121	0.1011
ChYo08	0.7574	0.6834	0.5710	0.5108	0.4920	0.4716	0.4743	0.4848	0.4946	0.1011
	0.7646	0.6973	0.6000	0.5603	0.5852	0.6013	0.5385	0.5361	0.5444	0.2443
	0.7699	0.7076	0.6221	0.6007	0.6659	0.7350	0.6461	0.5909	0.5922	0.3093
	0.7739	0.7155	0.6396	0.6339	0.7372	0.8721	0.7783	0.6773	0.6411	0.2443
	0.7776	0.7230	0.6568	0.6672	0.8124	1.0334	0.9569	0.8089	0.7020	0.1011
AkBo10	0.7521	0.6249	0.5402	0.4983	0.4895	0.4532	0.4417	0.4537	0.4688	0.1011
	0.7619	0.6864	0.5836	0.5670	0.6330	0.6464	0.5958	0.5654	0.5784	0.2443
	0.8269	0.7454	0.6904	0.6852	0.7924	0.8069	0.7090	0.6773	0.6901	0.3093
	0.8583	0.7975	0.7542	0.7486	0.9066	0.9836	0.8694	0.7791	0.7829	0.2443
	0.8854	0.8626	0.8409	0.8456	1.0373	1.2273	1.0748	0.9085	0.8705	0.1011
Zhao06	0.7332	0.5920	0.4553	0.3335	0.2807	0.3667	0.3445	0.3406	0.3510	0.1011
	0.7413	0.6328	0.5234	0.5404	0.5504	0.6541	0.6034	0.5669	0.5741	0.2443
	0.8072	0.7234	0.6607	0.6838	0.7472	0.9244	0.7947	0.7352	0.7197	0.3093
	0.8506	0.7755	0.7317	0.7742	0.8771	1.1808	1.0186	0.8659	0.8389	0.2443
	0.8733	0.8466	0.8230	0.8672	0.9987	1.4924	1.3994	1.1317	0.9657	0.1011

Table III-2.11: Frequency dependent resulting $V_S - \kappa$ correction 5-point distributions for used GMPEs at Mühleberg.

GMPE	Frequency [Hz]									Weight
	0.5	1	2.5	5	10	20	33.3	50	100	
AbSi08	1.0292	1.0418	0.8858	0.7903	0.8037	0.7820	0.7427	0.7541	0.7686	0.1011
	1.0413	1.0634	0.9312	0.8656	0.9539	0.9919	0.8580	0.8377	0.8482	0.2443
	1.0503	1.0795	0.9658	0.9278	1.0838	1.2065	1.0223	0.9279	0.9234	0.3093
	1.0573	1.0918	0.9933	0.9788	1.1986	1.4262	1.2221	1.0562	0.9993	0.2443
	1.0641	1.1037	1.0202	1.0301	1.3199	1.6850	1.4913	1.2496	1.0933	0.1011
BoAt08	1.0359	1.0416	0.8814	0.7892	0.7731	0.7705	0.7381	0.7541	0.7696	0.1011
	1.0446	1.0624	0.9258	0.8652	0.9195	0.9834	0.8600	0.8416	0.8526	0.2443
	1.0508	1.0777	0.9597	0.9279	1.0461	1.2015	1.0334	0.9408	0.9327	0.3093
	1.0554	1.0894	0.9866	0.9794	1.1580	1.4247	1.2425	1.0808	1.0149	0.2443
	1.0597	1.1006	1.0130	1.0312	1.2764	1.6877	1.5246	1.2870	1.1180	0.1011
CaBo08	1.0341	1.0432	0.8869	0.7960	0.7881	0.7910	0.7582	0.7754	0.7854	0.1011
	1.0439	1.0643	0.9319	0.8763	0.9394	1.0159	0.9083	0.8765	0.8777	0.2443
	1.0510	1.0800	0.9663	0.9401	1.0701	1.2452	1.0986	0.9969	0.9667	0.3093
	1.0564	1.0920	0.9936	0.9926	1.1854	1.4796	1.3250	1.1551	1.0583	0.2443
	1.0616	1.1036	1.0203	1.0454	1.3074	1.7555	1.6301	1.3801	1.1736	0.1011
ChYo08	1.0273	1.0303	0.8600	0.7524	0.7122	0.6830	0.6950	0.7118	0.7270	0.1011
	1.0377	1.0513	0.9036	0.8238	0.8457	0.8640	0.7822	0.7842	0.7979	0.2443
	1.0453	1.0669	0.9369	0.8830	0.9615	1.0517	0.9292	0.8604	0.8657	0.3093
	1.0510	1.0789	0.9633	0.9317	1.0637	1.2440	1.1106	0.9762	0.9342	0.2443
	1.0564	1.0903	0.9892	0.9807	1.1719	1.4708	1.3556	1.1544	1.0190	0.1011
AkBo10	1.0149	0.9395	0.8130	0.7332	0.7079	0.6521	0.6410	0.6596	0.6825	0.1011
	1.0292	1.0330	0.8784	0.8332	0.9149	0.9308	0.8592	0.8129	0.8369	0.2443
	1.1188	1.1217	1.0391	1.0072	1.1438	1.1529	1.0170	0.9864	1.0050	0.3093
	1.1617	1.2005	1.1352	1.0999	1.3074	1.4010	1.2372	1.1315	1.1370	0.2443
	1.2004	1.2993	1.2659	1.2425	1.4959	1.7428	1.5190	1.2925	1.2640	0.1011
Zhao06	0.9870	0.8895	0.6850	0.4902	0.4056	0.5255	0.4970	0.4958	0.5121	0.1011
	0.9985	0.9513	0.7872	0.7934	0.7956	0.9355	0.8599	0.8243	0.8360	0.2443
	1.0895	1.0881	0.9942	1.0044	1.0771	1.3165	1.1343	1.0650	1.0428	0.3093
	1.1489	1.1673	1.1013	1.1369	1.2636	1.6780	1.4439	1.2434	1.2147	0.2443
	1.1814	1.2749	1.2388	1.2733	1.4379	2.1152	1.9650	1.5953	1.3907	0.1011

Table III-2.12: Frequency dependent $V_S - \kappa$ correction for PSSMs at the sites Beznau and Gösgen.

	Beznau					Gösgen				
Weight	0.057	0.256	0.374	0.256	0.057	0.057	0.256	0.374	0.256	0.057
Freq. [Hz]	B6 (TK5)	B7 (TK6)	B8 (TK7)	B9 (TK8)	B10 (TK9)	B6 (TK5)	B7 (TK6)	B8 (TK7)	B9 (TK8)	B10 (TK9)
Mc5.5 SD30										
0.5	0.8345	0.8303	0.8253	0.8187	0.8107	0.8936	0.8895	0.8843	0.8774	0.8690
1	0.7691	0.7613	0.7520	0.7400	0.7255	0.7622	0.7546	0.7456	0.7338	0.7198
Mc5.5 SD60										
0.5	0.8328	0.8287	0.8234	0.8166	0.8084	0.8904	0.8861	0.8808	0.8739	0.8655
1	0.7686	0.7609	0.7515	0.7395	0.7250	0.7609	0.7534	0.7443	0.7325	0.7184
Mc5.5 SD90										
2.5	0.7711	0.7521	0.7297	0.7015	0.6687	0.6527	0.6367	0.6178	0.5940	0.5663
5	0.8100	0.7716	0.7274	0.6736	0.6141	0.6719	0.6401	0.6036	0.5593	0.5100
10	0.8651	0.7877	0.7035	0.6083	0.5117	0.7171	0.6531	0.5836	0.5050	0.4253
20	0.9602	0.8094	0.6632	0.5203	0.3997	0.7982	0.6734	0.5526	0.4346	0.3353
33.33	1.0290	0.8207	0.6478	0.5058	0.4041	0.8571	0.6848	0.5423	0.4254	0.3419
50	0.9985	0.8097	0.6682	0.5553	0.4701	0.8339	0.6783	0.5616	0.4688	0.3987
100	0.8986	0.7899	0.6962	0.6079	0.5299	0.7532	0.6635	0.5864	0.5138	0.4498
Mc5.5 SD120										
2.5	0.7711	0.7521	0.7297	0.7013	0.6685	0.6526	0.6365	0.6176	0.5938	0.5661
5	0.8101	0.7716	0.7274	0.6735	0.6139	0.6718	0.6400	0.6035	0.5591	0.5099
10	0.8652	0.7877	0.7035	0.6081	0.5114	0.7171	0.6531	0.5835	0.5048	0.4250
20	0.9609	0.8096	0.6631	0.5199	0.3990	0.7986	0.6734	0.5523	0.4341	0.3345
33.33	1.0299	0.8209	0.6474	0.5047	0.4027	0.8575	0.6848	0.5415	0.4243	0.3404
50	0.9998	0.8100	0.6675	0.5541	0.4686	0.8348	0.6782	0.5609	0.4674	0.3969
100	0.8996	0.7902	0.6958	0.6070	0.5286	0.7537	0.6632	0.5856	0.5128	0.4481
Mc5.5 SD150										
2.5	0.7711	0.7521	0.7296	0.7013	0.6684	0.6525	0.6365	0.6175	0.5936	0.5660
5	0.8101	0.7716	0.7273	0.6735	0.6138	0.6718	0.6400	0.6035	0.5590	0.5097
10	0.8652	0.7877	0.7034	0.6080	0.5113	0.7171	0.6530	0.5834	0.5046	0.4248
20	0.9609	0.8096	0.6630	0.5196	0.3985	0.7986	0.6733	0.5521	0.4338	0.3338
33.33	1.0305	0.8211	0.6470	0.5040	0.4016	0.8579	0.6847	0.5410	0.4233	0.3391
50	1.0008	0.8102	0.6671	0.5532	0.4674	0.8356	0.6780	0.5601	0.4663	0.3955
100	0.9002	0.7902	0.6955	0.6062	0.5275	0.7537	0.6629	0.5848	0.5114	0.4467

Table III-2.13: Frequency dependent $V_S - \kappa$ correction for PSSMs at the sites Leibstadt and Mühleberg.

	Leibstadt					Mühleberg				
Weight	0.057	0.256	0.374	0.256	0.057	0.057	0.256	0.374	0.256	0.057
Freq. [Hz]	B6 (TK5)	B7 (TK6)	B8 (TK7)	B9 (TK8)	B10 (TK9)	B6 (TK5)	B7 (TK6)	B8 (TK7)	B9 (TK8)	B10 (TK9)
Mc5.5 SD30										
0.5	0.8070	0.8031	0.7983	0.7920	0.7843	1.3120	1.3056	1.2978	1.2875	1.2750
1	0.7153	0.7082	0.6995	0.6884	0.6751	1.2434	1.2310	1.2161	1.1967	1.1736
Mc5.5 SD60										
0.5	0.8048	0.8007	0.7958	0.7893	0.7815	1.3096	1.3031	1.2952	1.2848	1.2721
1	0.7147	0.7076	0.6989	0.6877	0.6744	1.2424	1.2301	1.2150	1.1957	1.1725
Mc5.5 SD90										
2.5	0.6920	0.6751	0.6549	0.6296	0.6002	0.9867	0.9626	0.9341	0.8982	0.8566
5	0.7235	0.6893	0.6498	0.6019	0.5487	1.0342	0.9851	0.9288	0.8603	0.7845
10	0.7724	0.7034	0.6283	0.5434	0.4572	1.0803	0.9839	0.8794	0.7612	0.6414
20	0.8582	0.7236	0.5931	0.4657	0.3582	1.2222	1.0312	0.8463	0.6659	0.5142
33.33	0.9199	0.7341	0.5800	0.4535	0.3630	1.3152	1.0513	0.8328	0.6536	0.5258
50	0.8937	0.7253	0.5992	0.4986	0.4227	1.2794	1.0411	0.8626	0.7205	0.6133
100	0.8052	0.7082	0.6247	0.5460	0.4765	1.1564	1.0190	0.9010	0.7898	0.6920
Mc5.5 SD120										
2.5	0.6920	0.6749	0.6548	0.6295	0.6000	0.9865	0.9624	0.9338	0.8979	0.8562
5	0.7236	0.6892	0.6498	0.6018	0.5486	1.0341	0.9850	0.9287	0.8601	0.7841
10	0.7724	0.7033	0.6282	0.5432	0.4570	1.0803	0.9838	0.8792	0.7608	0.6409
20	0.8588	0.7237	0.5931	0.4653	0.3575	1.2227	1.0312	0.8460	0.6653	0.5130
33.33	0.9206	0.7343	0.5795	0.4526	0.3617	1.3159	1.0512	0.8317	0.6521	0.5235
50	0.8947	0.7255	0.5986	0.4975	0.4212	1.2805	1.0410	0.8612	0.7183	0.6106
100	0.8059	0.7083	0.6242	0.5450	0.4752	1.1573	1.0187	0.8999	0.7883	0.6894
Mc5.5 SD150										
2.5	0.6919	0.6749	0.6548	0.6294	0.5999	0.9864	0.9622	0.9336	0.8977	0.8559
5	0.7236	0.6892	0.6497	0.6017	0.5485	1.0341	0.9850	0.9285	0.8600	0.7839
10	0.7725	0.7033	0.6282	0.5431	0.4568	1.0803	0.9838	0.8790	0.7605	0.6406
20	0.8588	0.7237	0.5929	0.4650	0.3570	1.2228	1.0311	0.8457	0.6646	0.5121
33.33	0.9211	0.7344	0.5791	0.4518	0.3606	1.3165	1.0512	0.8311	0.6507	0.5216
50	0.8955	0.7256	0.5981	0.4966	0.4200	1.2815	1.0409	0.8603	0.7168	0.6085
100	0.8064	0.7083	0.6238	0.5443	0.4741	1.1574	1.0184	0.8989	0.7867	0.6874

Figures III-2.3 to III-2.6 show the five discrete correction functions versus frequency for all GMPEs per site. Figures with all individual correction functions resulting from all combinations and color coded by their weight can be found in the appendix to the HID (Chapter 3). Furthermore, the individual histograms, selected 5-point distributions and a theoretically fitted distribution are also shown in the appendix. Figures III-2.7 to III-2.10 shows the different $V_S - \kappa$ corrections to be applied to the generic parameterized Swiss stochastic model in order to be applicable for the given site specific NPP conditions.

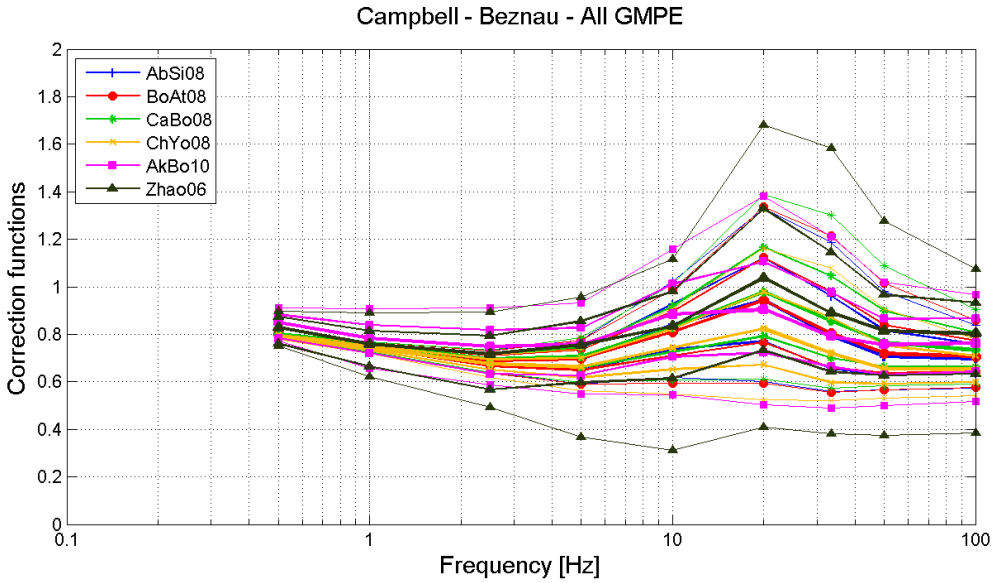

Figure III-2.3: $V_S - \kappa$ corrections to be applied to the GMPEs for Beznau.

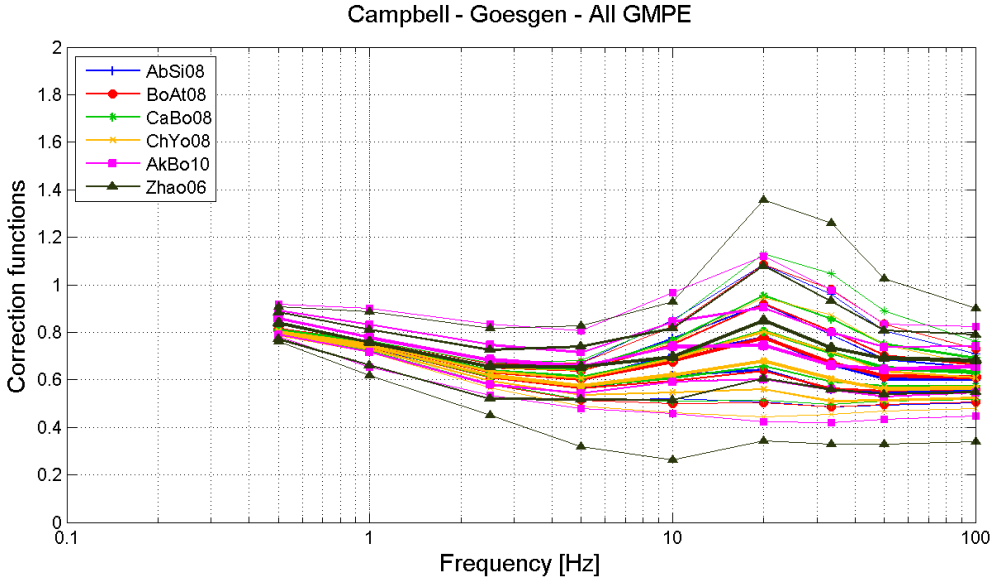

Figure III-2.4: $V_S - \kappa$ corrections to be applied to the GMPEs for Gösgen.

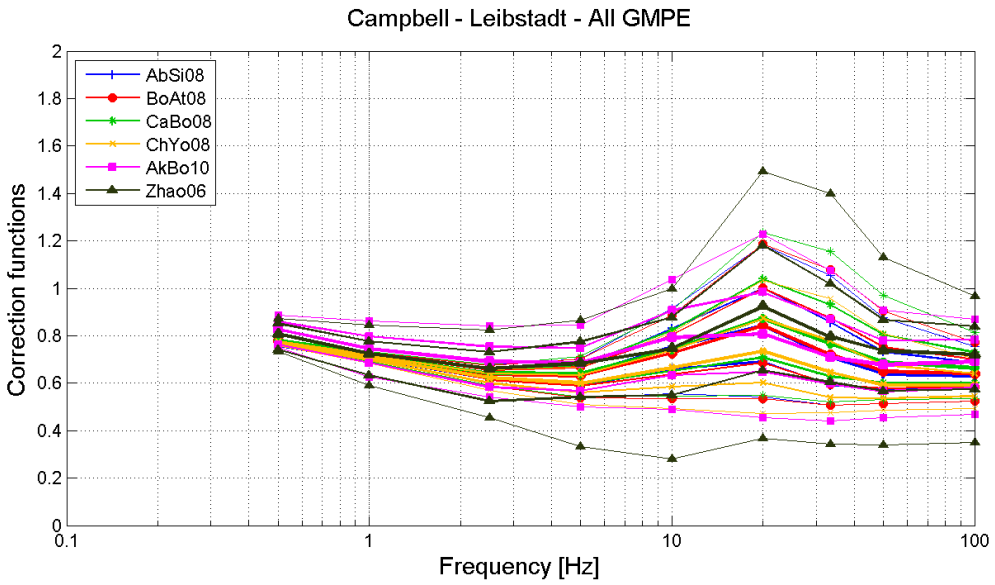

Figure III-2.5: $V_S - \kappa$ corrections to be applied to the GMPEs for Leibstadt.

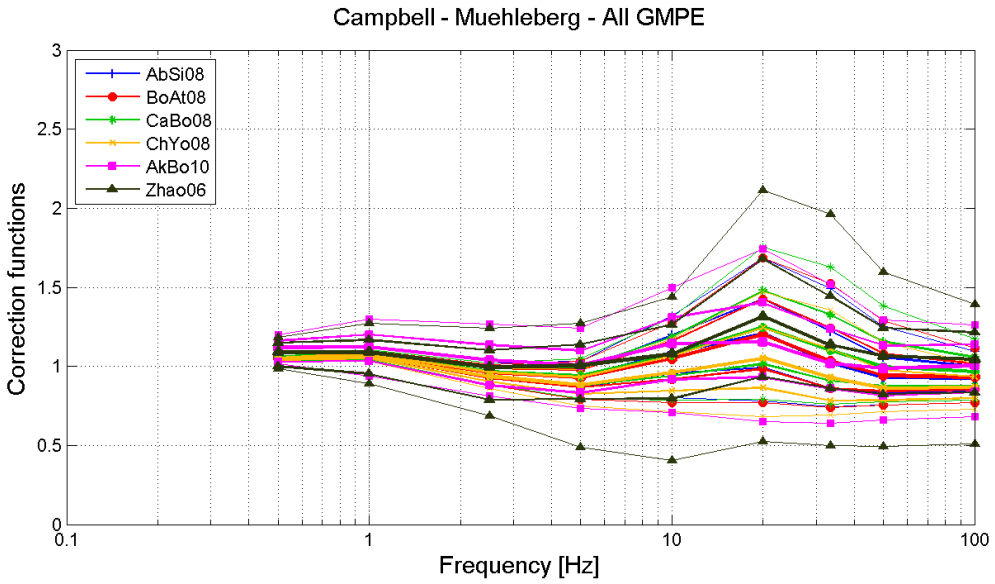

Figure III-2.6: $V_S - \kappa$ corrections to be applied to the GMPEs for Mühleberg.

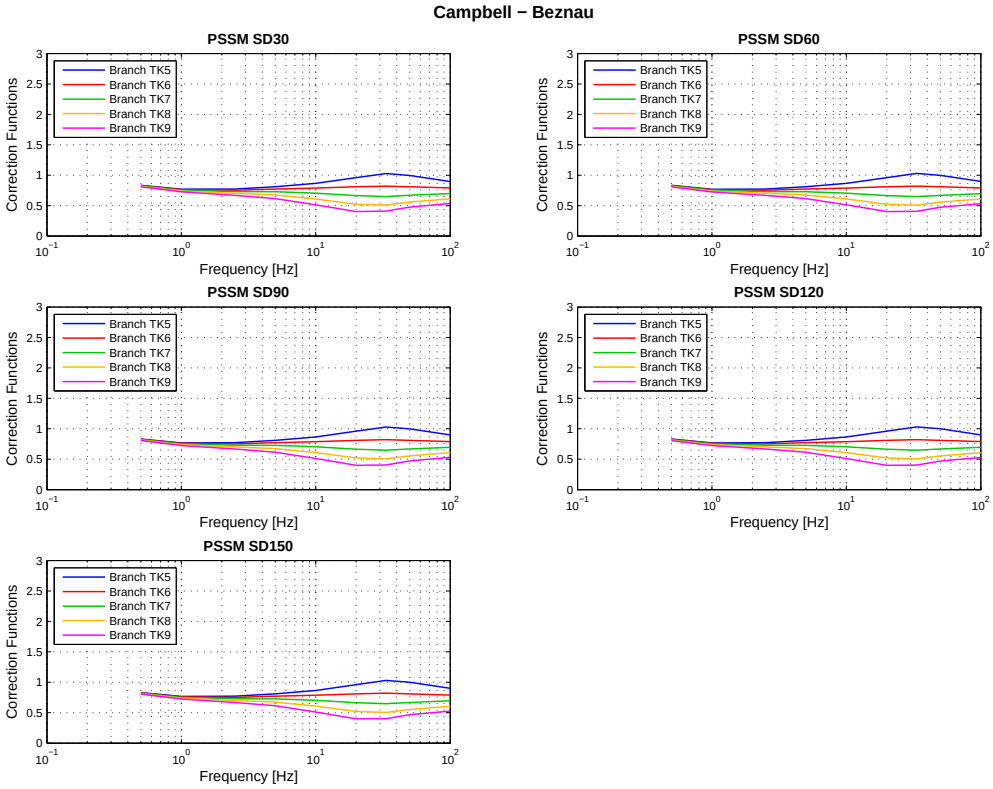

Figure III-2.7: $V_S - \kappa$ corrections to be applied to the PSSMs for Beznau.

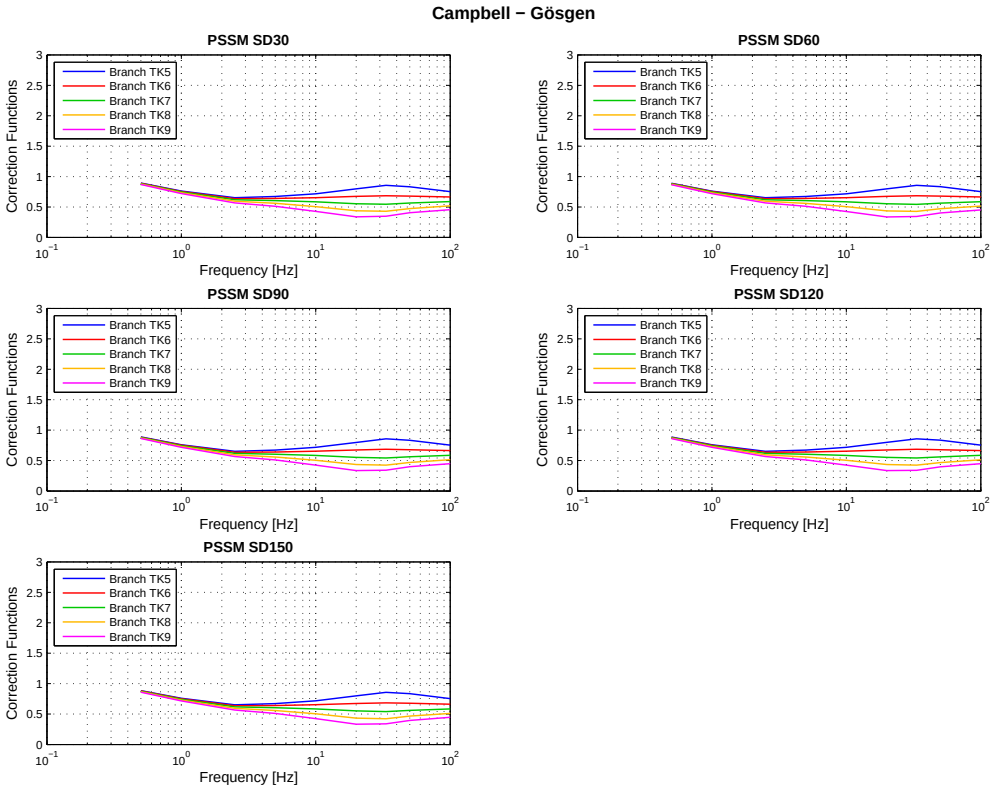

Figure III-2.8: $V_S - \kappa$ corrections to be applied to the PSSMs for Gösgen.

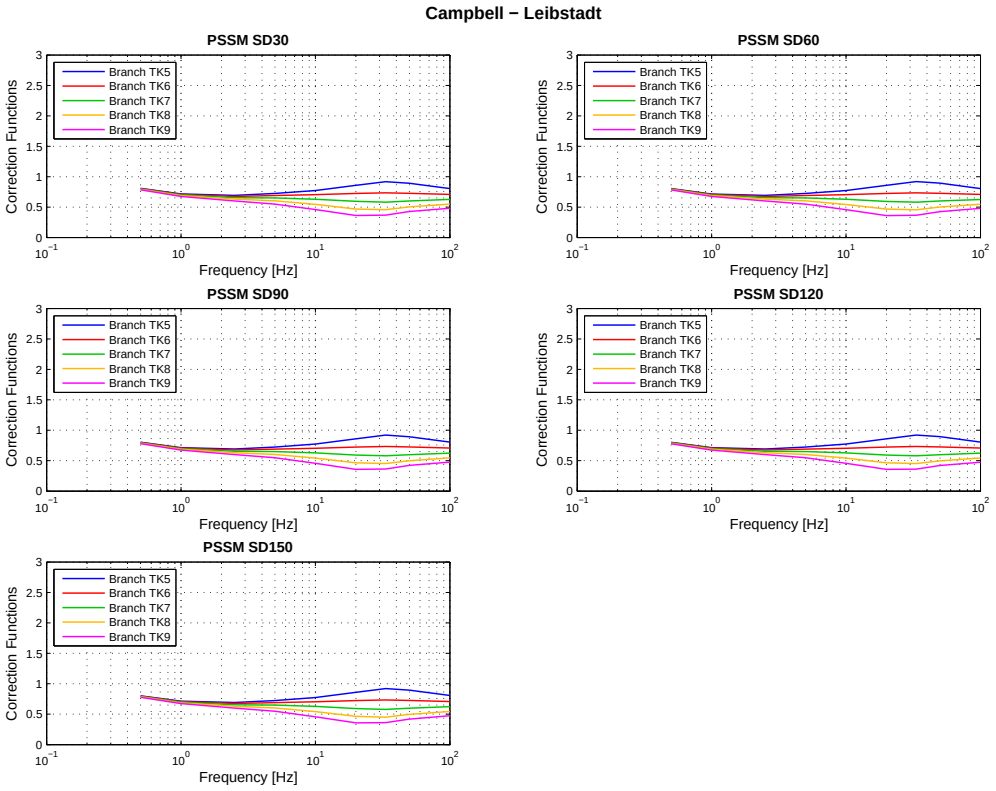

Figure III-2.9: $V_S - \kappa$ corrections to be applied to the PSSMs for Leibstadt.

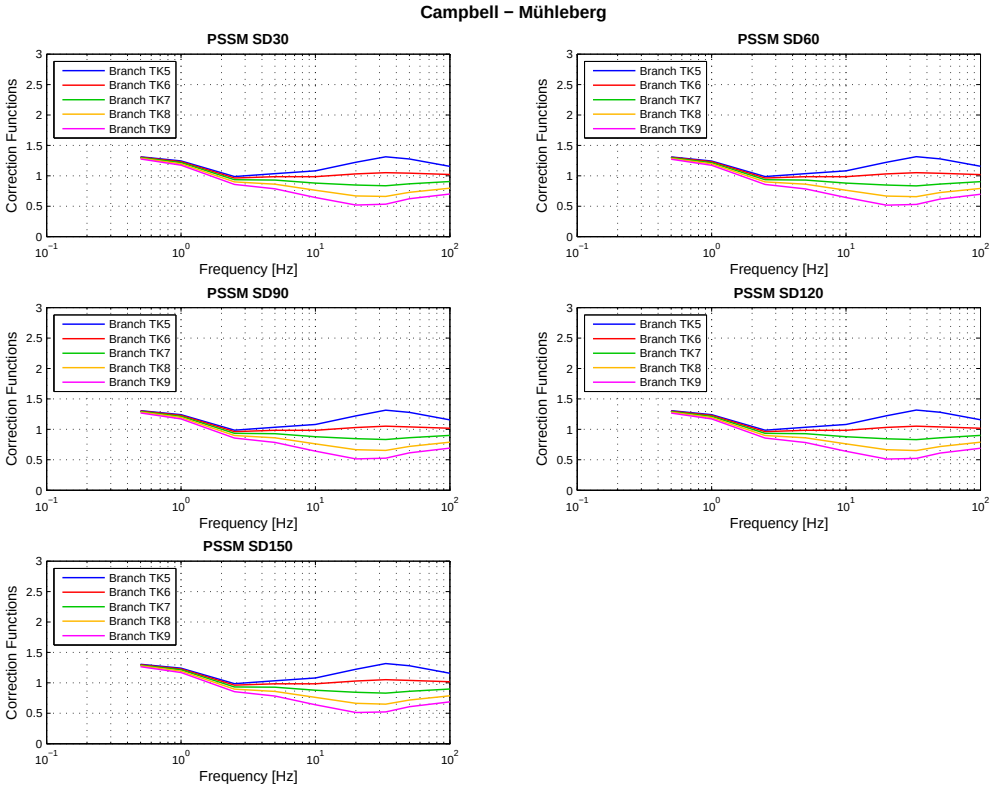

Figure III-2.10: $V_S - \kappa$ corrections to be applied to the PSSMs for Mühleberg.

2.3.2 Small Magnitude Adjustments

For the evaluation of the GMPE specific small magnitude adjustments only the median $V_S - \kappa$ correction factors of all the provided 5-point distributions are used, as it was decided that the small magnitude adjustments will only be developed for the average case and not for each individual correction function (PMT-TN-1238). Thus, the small magnitude adjustments are the same for all experts, but repeated here in Table III-2.14 for the sake of completeness and illustrated in Figure III-2.11 and III-2.12.

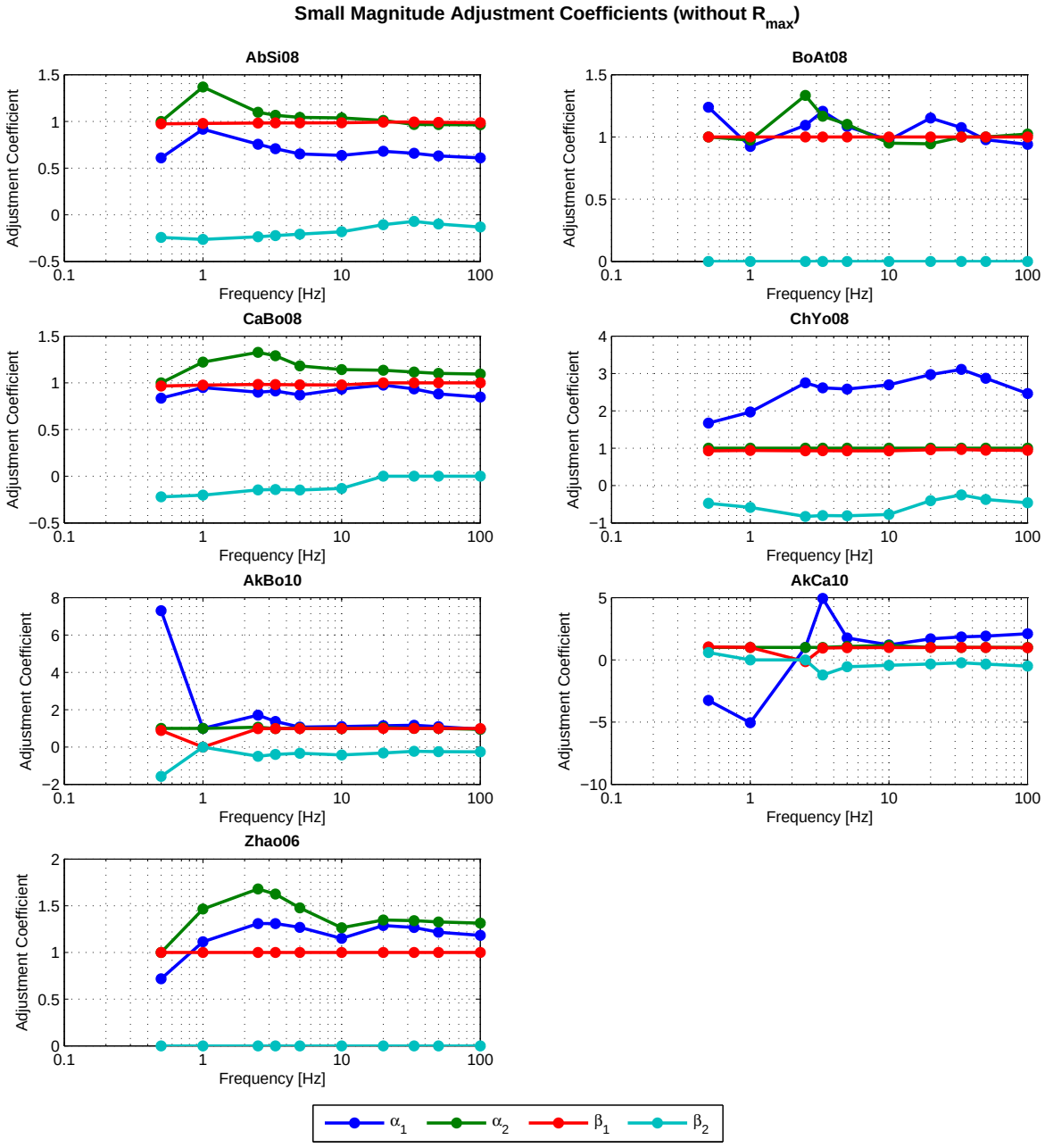

Figure III-2.11: Small magnitude adjustments coefficients as function of frequency for the all GMPEs.

Table III-2.14: Small magnitude adjustments coefficients.

	Abrahamson & Silva (2008)					Boore & Atkinson (2008)				
T [s]	α_1	α_2	β_1	β_2	R_{max}	α_1	α_2	β_1	β_2	R_{max}
0.01	0.609036	0.964257	0.986605	-0.131781	3.57E+04	0.940502	1.022616	1.000000	0.000000	1.00E+09
0.02	0.629604	0.965329	0.988756	-0.099660	4.07E+05	0.977300	1.000000	1.000000	0.000000	1.00E+09
0.03	0.657761	0.967357	0.993601	-0.071271	2.27E+07	1.074586	1.000000	1.000000	0.000000	1.00E+09
0.05	0.679706	1.010904	0.991680	-0.106456	2.22E+05	1.151448	0.945013	1.000000	0.000000	1.00E+09
0.1	0.635927	1.037980	0.984796	-0.182620	4.40E+03	0.974222	0.950274	1.000000	0.000000	1.00E+09
0.2	0.651637	1.043100	0.984107	-0.207141	2.31E+03	1.084848	1.101550	1.000000	0.000000	1.00E+09
0.3	0.707216	1.065147	0.983422	-0.222960	1.65E+03	1.205896	1.166359	1.000000	0.000000	1.00E+09
0.4	0.755898	1.097644	0.982712	-0.236174	1.28E+03	1.093478	1.334035	1.000000	0.000000	1.00E+09
1	0.915893	1.367623	0.978436	-0.263900	8.15E+02	0.924116	0.974715	1.000000	0.000000	1.00E+09
2	0.608779	1.000000	0.974376	-0.242967	1.10E+03	1.238186	1.000000	1.000000	0.000000	1.00E+09

	Campbell & Bozorgnia (2008)					Chiou & Youngs (2008)				
T [s]	α_1	α_2	β_1	β_2	R_{max}	α_1	α_2	β_1	β_2	R_{max}
0.01	0.847179	1.094261	1.000000	0.000000	1.00E+09	2.462946	1.000000	0.944935	-0.458418	1.57E+02
0.02	0.881357	1.100586	1.000000	0.000000	1.00E+09	2.873730	1.000000	0.946856	-0.372663	2.54E+02
0.03	0.934893	1.114376	1.000000	0.000000	1.00E+09	3.109735	1.000000	0.966292	-0.248344	9.79E+02
0.05	0.976058	1.135405	1.000000	0.000000	1.00E+09	2.969316	1.000000	0.959155	-0.402534	2.17E+02
0.1	0.932945	1.141482	0.977278	-0.130765	3.52E+04	2.695695	1.000000	0.930247	-0.772189	6.67E+01
0.2	0.870681	1.181271	0.979148	-0.147509	1.53E+04	2.584716	1.000000	0.931449	-0.809059	6.32E+01
0.3	0.912008	1.289225	0.981219	-0.142015	2.00E+04	2.614341	1.000000	0.932936	-0.801818	6.40E+01
0.4	0.899165	1.326194	0.982502	-0.145844	1.69E+04	2.750116	1.000000	0.930586	-0.824968	6.18E+01
1	0.949262	1.221818	0.975229	-0.202856	2.45E+03	1.966745	1.000000	0.939658	-0.583454	1.00E+02
2	0.835687	1.000000	0.965445	-0.220424	1.60E+03	1.671214	1.000000	0.931415	-0.473294	1.43E+02

	Akkar & Bommer (2010)					Akkar & Cagnan (2010)				
T [s]	α_1	α_2	β_1	β_2	R_{max}	α_1	α_2	β_1	β_2	R_{max}
0.01	0.956934	0.949129	0.992409	-0.258327	9.32E+02	2.098964	1.000000	0.985549	-0.499646	1.44E+02
0.02	1.090919	1.000000	0.994584	-0.253021	1.02E+03	1.913122	1.000000	0.990459	-0.335515	3.83E+02
0.03	1.164927	1.000000	0.998788	-0.230673	1.52E+03	1.851248	1.000000	0.997570	-0.236164	1.37E+03
0.05	1.134080	1.040216	0.995602	-0.321814	4.41E+02	1.689890	1.000000	0.995553	-0.333705	3.95E+02
0.1	1.093536	0.986668	0.988564	-0.425342	2.04E+02	1.204350	1.157951	0.987542	-0.431630	1.97E+02
0.2	1.068203	1.007264	0.988710	-0.334035	3.86E+02	1.759524	1.071974	0.978784	-0.546911	1.20E+02
0.3	1.369695	0.988071	0.987967	-0.400250	2.36E+02	4.937988	1.000000	0.951557	-1.213879	4.38E+01
0.4	1.710275	1.062132	0.984888	-0.499538	1.44E+02	1.000000	1.000000	-0.142956	0.000000	1.99E+01
1	1.000000	1.000000	0.000000	0.000000	1.00E+09	-5.048030	1.000000	1.000000	0.000000	1.99E+01
2	7.299540	1.000000	0.881761	-1.575579	3.50E+01	-3.254365	1.000000	1.044931	0.593817	1.00E+09

	Zhao et al. (2006)				
T [s]	α_1	α_2	β_1	β_2	R_{max}
0.01	1.182482	1.313722	1.000000	0.000000	1.00E+09
0.02	1.217249	1.326714	1.000000	0.000000	1.00E+09
0.03	1.267071	1.340177	1.000000	0.000000	1.00E+09
0.05	1.288501	1.347281	1.000000	0.000000	1.00E+09
0.1	1.150978	1.265212	1.000000	0.000000	1.00E+09
0.2	1.268576	1.476775	1.000000	0.000000	1.00E+09
0.3	1.310229	1.625552	1.000000	0.000000	1.00E+09
0.4	1.308962	1.679158	1.000000	0.000000	1.00E+09
1	1.113543	1.465133	1.000000	0.000000	1.00E+09
2	0.718525	1.000000	1.000000	0.000000	1.00E+09

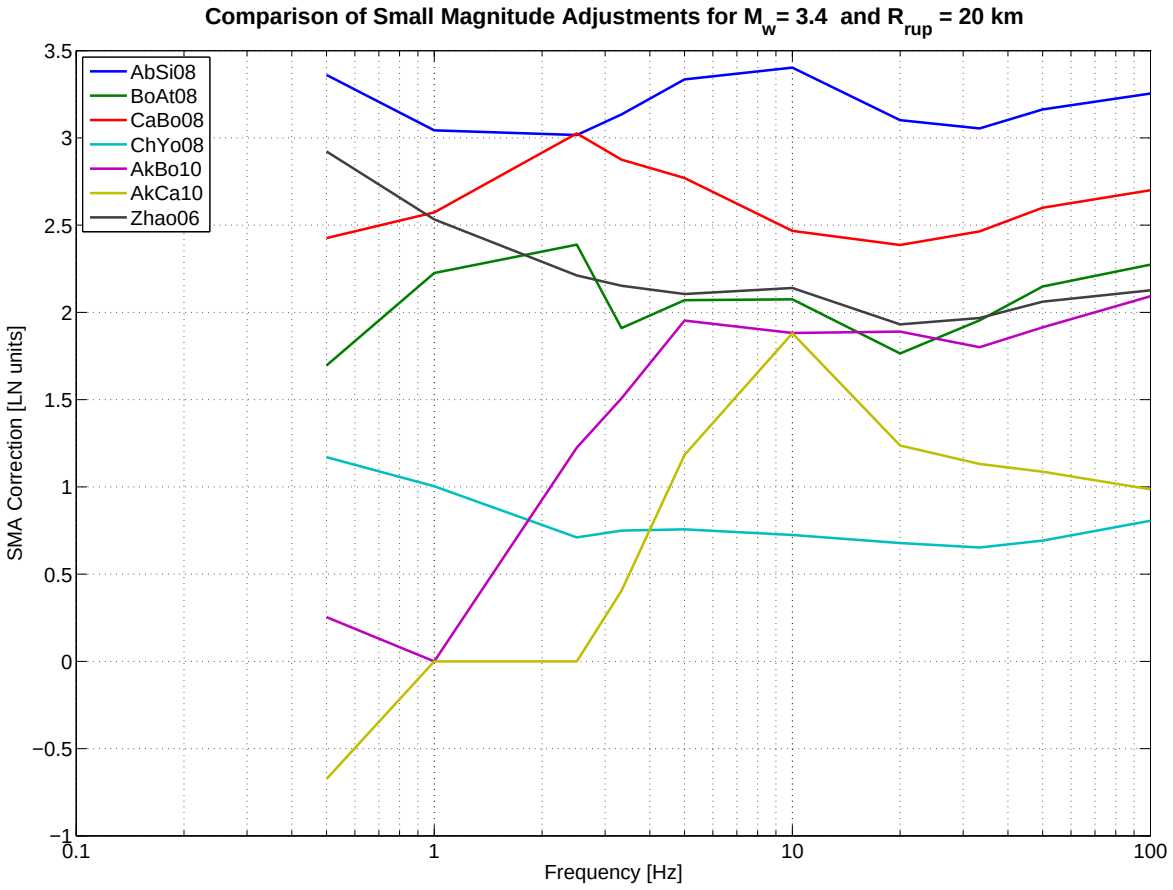

Figure III-2.12: Comparison of the resulting small magnitude adjustments functions as function of frequency for M=3.4 and R=20 km.

2.4 Aleatory Variability for the Horizontal Component

Section 6.7 in Part I, provides the final τ and ϕ models used for the PRP, which supersede the model of Rodriguez-Marek and Cotton [2011] (equations 4.1, 4.2 and table 5.3 and 5.4 in EXT-TB-1058) and Rodriguez-Marek [2012] (EXT-TN-1225). In Table III-2.15 the different weights for the aleatory variability logic tree branches are shown. The selected values for the ϕ_{SS} uncertainty are given in the second column at the bottom. The generic σ logic tree is represented in Figure I-9.2.

Table III-2.15: Weights and parameters assigned to the aleatory variability.

Model	Branch / Value for $\sigma(\phi_{SS})$	Weight
τ Model	Global	0.20
	Original GMPE	0.80
τ Uncert.	+0.1	0.20
	0	0.60
	-0.1	0.20
ϕ_{SS}	Model 1 (Constant)	0.80
	Model 2 (Distance Dependent)	-
	Model 3 (Dist. and Mag. Dependent)	0.20
ϕ_{SS} Uncert.	$-1.6 \cdot \sigma(\phi_{SS})$	0.20
	$0 \cdot \sigma(\phi_{SS})$	0.60
	$+1.6 \cdot \sigma(\phi_{SS})$	0.20
$\sigma(\phi_{SS})$	0.08	1.00

2.5 Maximum Ground Motion

Table III-2.16 shows that no frequency dependent weights are assigned to the horizontal maximum ground motion logic tree (see generic Figure I-9.3). The weights assigned to the six scaling factors for the six branches are given in Table III-2.17.

Table III-2.16: Weights for the horizontal maximum ground motion model.

Model	Frequency [Hz]								
	0.5	1	2.5	5	10	20	33.3	50	100
R-dependent	-	-	-	-	-	-	-	-	-
R-independent	1.00	1.00	1.00	1.00	1.00	1.00	1.00	1.00	1.00

The vertical maximum ground motion model is the same as the horizontal (see Figure I-9.3). Thus, the same weights and scale factors apply for the vertical hazard.

Based on the hazard feedback, which showed very little impact of the maximum ground motion truncation for rock, the project has decided to trim the maximum ground motion

Table III-2.17: Weights for the scaling factors for the maximum ground motion model (both horizontal and vertical).

Model	Scale Factors [LN units]					
	7.50	12.59	21.14	35.48	59.57	100
R-dependent	-	-	-	-	-	-
R-independent	-	1.00	-	-	-	-

branches for the practical implementation. Thus, the hazard will be computed based on untruncated ground motions for rock.

2.6 V/H Ratio

Table III-2.18 shows the weights of the candidate V/H models. No NPP site specific weights were assigned. This implies for the site of Gösgen to use the "shallow" case defined by the ratio based on the merged profiles 4-5 (see TP3-ASW-1004). The basic logic tree for the V/H models can be found in Figure I-9.4.

Table III-2.18: Weights for median V/H models.

Model	Weight
Bommer et al. (2011)	-
Campbell and Bozorgnia (2003)	0.30
Gülerce and Abrahamson (2011)	0.40
Edwards et al. (2011) with correction above 7 Hz	0.075
Edwards et al. (2011) without correction above 7 Hz	0.075
US West Median	0.15
US East Median	-

2.7 Aleatory Variability for the Vertical Component

The additional aleatory variability to be added to the median V/H models is shown in Table III-2.19 (see Figure I-9.2 for the generic logic tree).

Table III-2.19: Additional vertical variability (σ_{VADD} in LN units).

Frequency [Hz]								
0.5	1	2.5	5	10	20	33.3	50	100
0.06	0.06	0.13	0.14	0.18	0.20	0.20	0.17	0.14

Figure III-2.13 shows the additional aleatory variability for the vertical component over frequency.

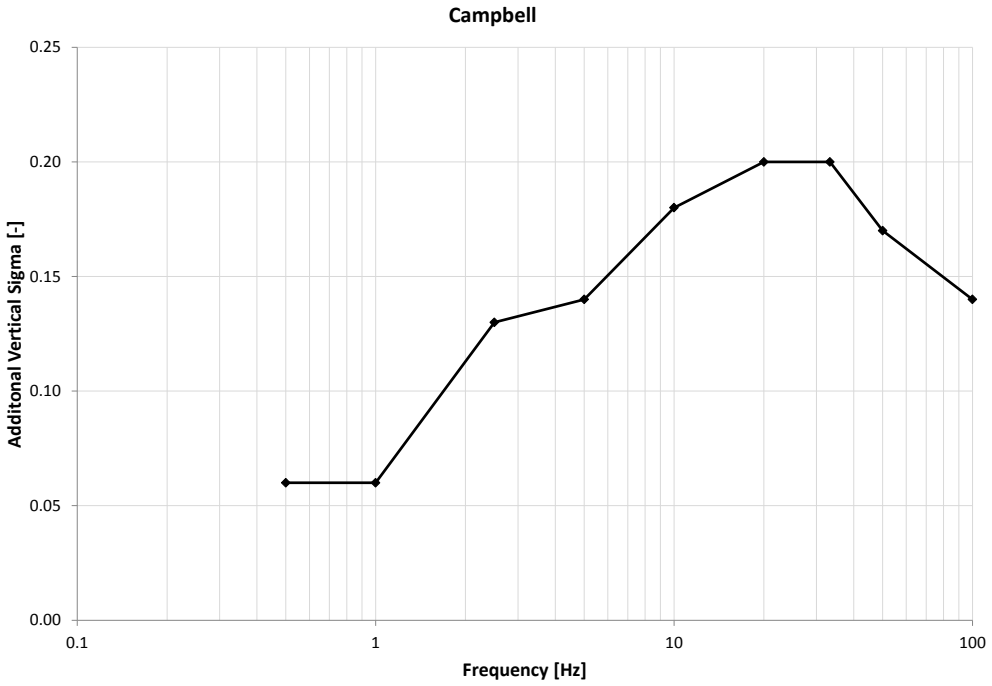

Figure III-2.13: Additional aleatory variability for the vertical component.

2.8 Implementation of Hazard Logic Tree

The total number of logic tree branches amounts to 1080 (see Figure III-2.1). Each individual combination of zonation alternatives and source parameters in each individual SP1 source has to be combined with these 1080 alternative ground motion models. Among other such measures, the project decided to reduce the huge number of combinations and thus, the CPU time necessary to obtain the rock hazard results by removing the maximum ground motion truncation from the SP2 models. This section documents the effect of this project management decision.

For the hazard computation we used one of the four SP1 Expert Group models, EG1c, with its entire complexity. We performed the calculation for one site only, Beznau, as we know the effect of the maximum ground motion truncation to be largely site independent and for 5 Hz spectral acceleration as the effect of the maximum ground motion truncation has been shown to be the highest for this frequency (see TP4-RF-1441). Figure III-2.14 shows the comparison for the mean hazard and four fractiles.

This conversion of the original "scientific logic tree" to a dealable "hazard logic tree" has been introduced in the framework of the PRP in order to allow for efficient computation without tradeoffs for the overall model in key elements of the initial logic tree.

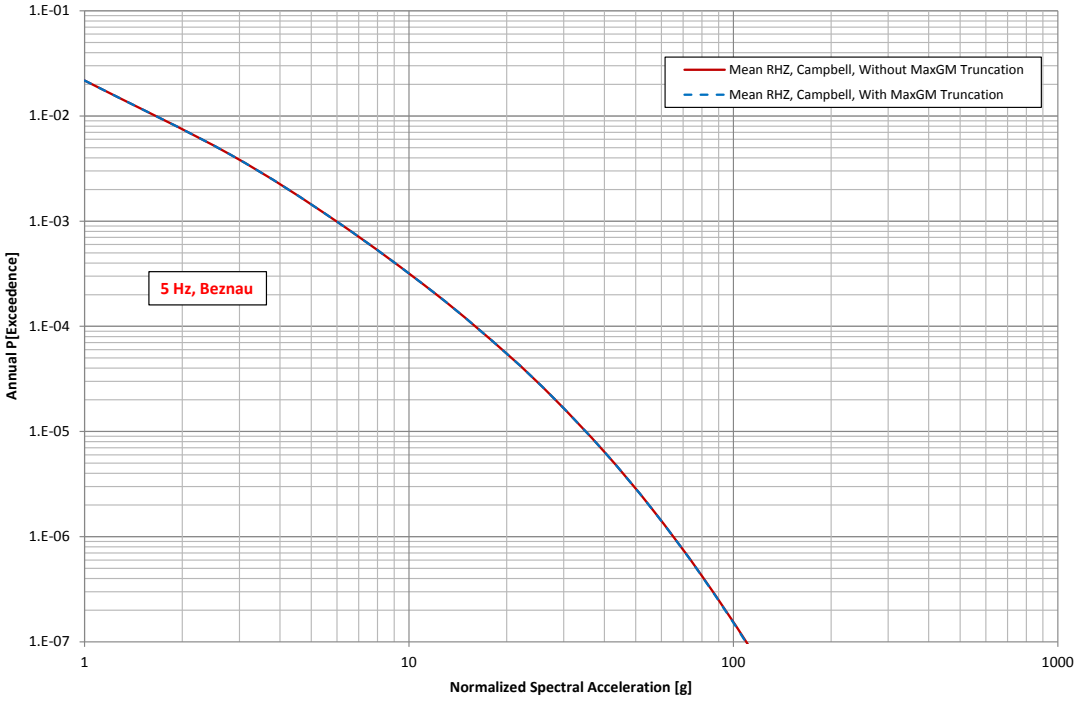

Figure III-2.14: Effect of the removal of the maximum ground motion truncation in the logic tree on the rock hazard for Beznau.

Chapter 3

Appendix to EG1-HID-1009

The procedure to retrieve the discrete 5-point distributions for the $V_S - \kappa$ corrections is visualized by means of 3 figure types:

- XY graph showing all correction function versus frequency with curve colors indicating the curve weights (see example Figure III-3.1)
- Plot of the probability distributions (cumulative weights) of $V_S - \kappa$ corrections at the 9 PRP frequencies (see example Figure III-3.2)
- Corresponding plot of the probability density of $V_S\kappa$ at the 9 analysis frequencies (see example Figure III-3.3)

which are attached as an electronic appendix to this HID and contains folders/files (or ZIP files), which correspond to the above listed figure types. Figures within above folders are provided as individual PNG and/or EPS files, where the individual files are named according to the convention and example as follows:
<expert>_<site>_<gmpe>_<figure-type>.<graphic-format>
Campbell_Beznau_AbSi08_fig1.png

A direct link to files containing a compilation of all figures per site is given here:

- Open external file: $V_S - \kappa$ correction functions for Beznau and associated cumulative probability functions and probability density functions.
- Open external file: $V_S - \kappa$ correction functions for Gösgen and associated cumulative probability functions and probability density functions.
- Open external file: $V_S - \kappa$ correction functions for Leibstadt and associated cumulative probability functions and probability density functions.
- Open external file: $V_S - \kappa$ correction functions for Mühleberg and associated cumulative probability functions and probability density functions.

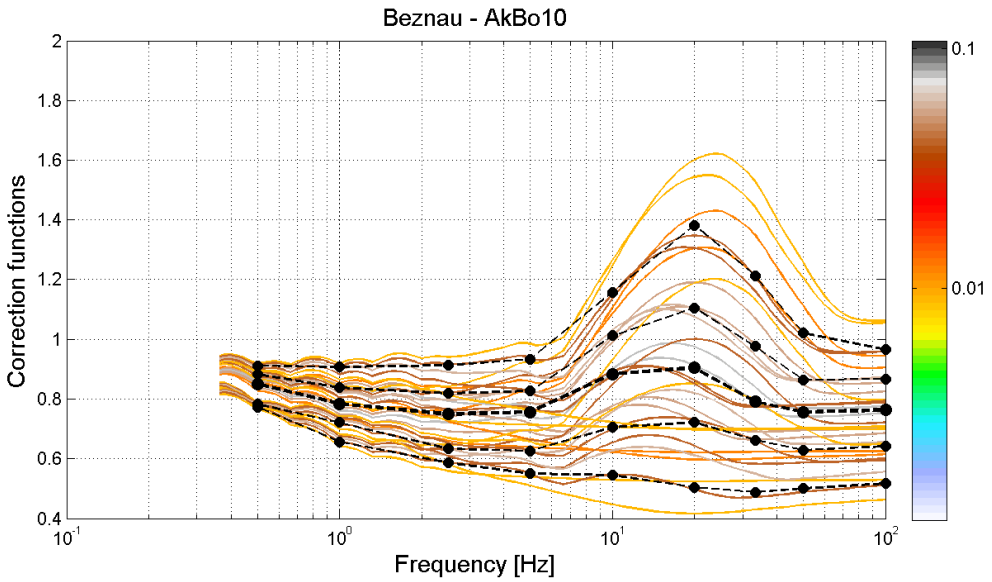

Figure III-3.1: Evaluated $V_S - \kappa$ correction functions for Akkar & Bommer (2010) at the site of Beznau and the final 5 discrete correction functions in black dashed lines. The weights of the individual correction functions are color coded according to the scale on the right.

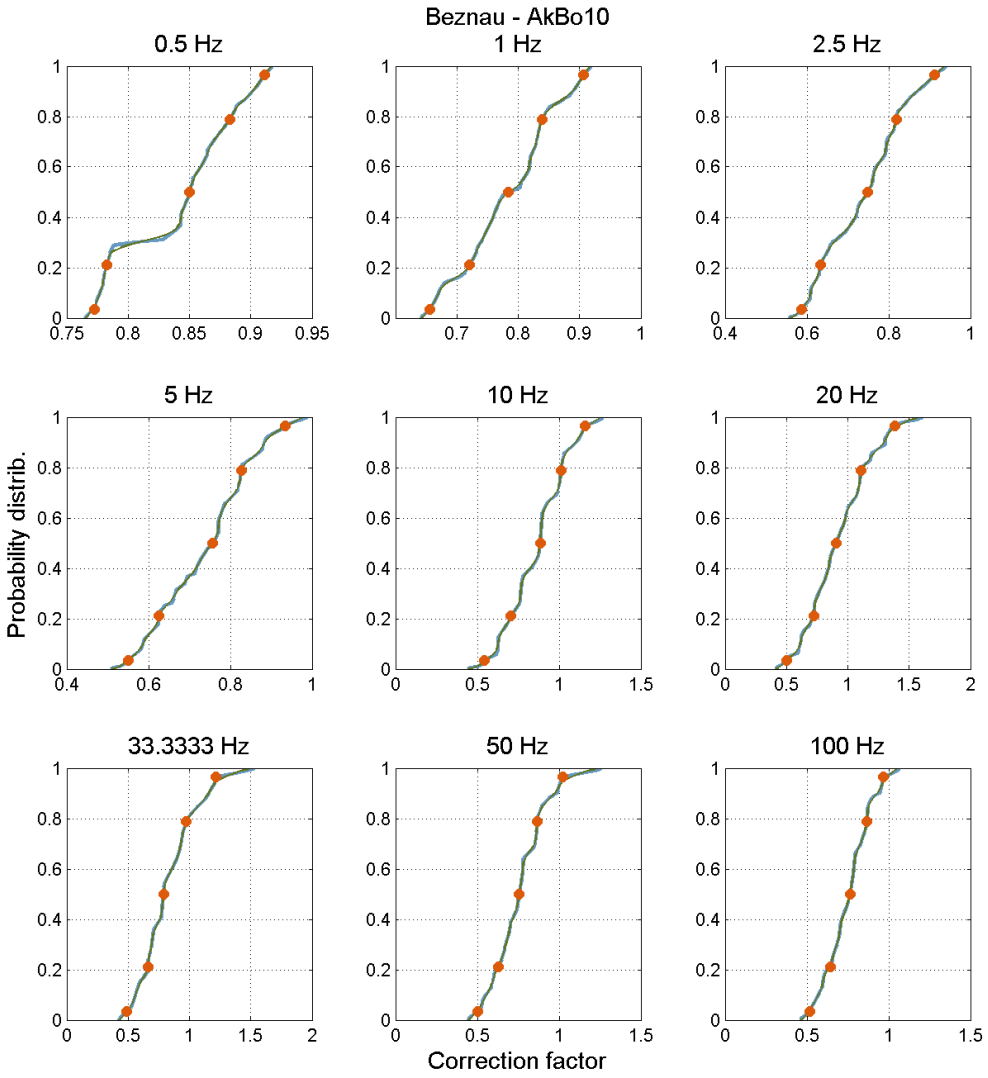

Figure III-3.2: Probability distributions (cumulative weights) of $V_S - \kappa$ corrections at the 9 PRP frequencies for Akkar & Bommer (2010) at the site of Beznau. The blue line represents the data by means of 105 fractiles. The thin green line is a smoothed version of above blue line (just for display, not used for further processing). The orange dots are the 3.4893, 21.1702, 50, 78.8298 and 96.5107 % percentiles used for the 5-point distribution.

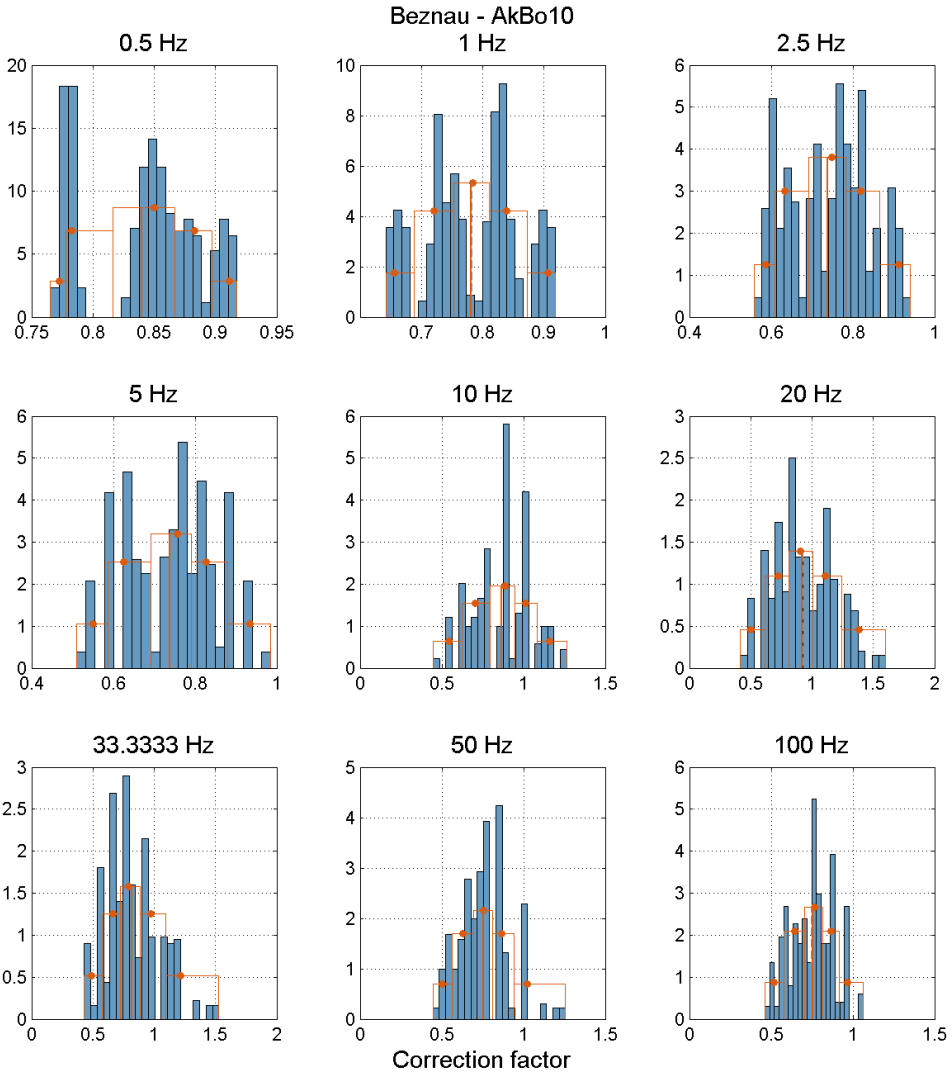

Figure III-3.3: Probability density functions of $V_S - \kappa$ corrections at the 9 PRP frequencies for Akkar & Bommer (2010) at the site of Beznau. The blue bars represent the weighted histogram of the data partitioned into 21 bins. The orange dots are the corresponding discrete 5 distribution points for the 3.4893, 21.1702, 50, 78.8298 and 96.5107 % percentiles, as in Figure III-3.2. The corresponding probabilities/weights are for the given discretization: 0.10108, 0.24429, 0.30926, 0.24429, 0.10108. The thin red and thin dashed blue line in the middle show the mean value of the data and the approximation with the 5-point distribution, respectively. Note that in the case of the thin dashed blue and red line being identical, only the red line is seen as it is on top of the blue line.

Chapter 4

QA-Certificate EG2-QC-1061

QA Certificate	PEGASOS REFINEMENT PROJECT
EG2-QC-1061	

Hazard Input Document (HID)

Expert group:	**EG2**	***HID designation:***	**EG2-HID-1010**
Expert:	K. W. Campbell	***Expert Model (EXM)***	EG2-EXM-1010

HID parameterisation of Expert Model:

TFI: N. A. Abrahamson ***Hazard Input Specialist of TFI-team:*** Ph. Roth

HID based on Elicitation Documents: ☒ EG2-ES-1019

HID based on Exp. Assessments (EXA): ☒ EG2-EXA-1017 to 1030

Remarks on the HID model parameterisation in terms of hazard computation input:

The undersigned Hazard Input Specialist confirms that this HID includes all required (subproject specific) input information for hazard computations. No further interpretations of this input will be required and no simplifications except Algorithmic Pinching according to paragraph 2.9 of the QA-Guidelines will be applied to convert this HID into hazard software Input Files.

Signature: P. Roth

HID acceptance by the Expert / Expert Group:

Date of HID review by the Expert / Expert group: 20.11.2013

HID accepted: ☒ ***HID not accepted:*** ☐

Reasons for non-acceptance of HID / Recommendations:

The undersigned Expert(s) accept(s) the parameterisation proposed in this HID as a faithful and adequate representation of his/their Expert Model. He/they confirm(s) that this HID is free of errors and agree(s) to its use as hazard computation input.

Signature Expert 1 / Expert: Kenneth W. Campbell

Signature Expert 2:

Signature Expert 3:

Part IV

Assessments of F. Cotton

Chapter 1

Evaluation Summary (EG2-ES-1020) of F. Cotton

1.1 Introduction

The present document comprises Fabrice Cotton evaluation summary as SP2 expert in the Pegasos Refinement Project. The model is based on a single and common master ground-motion logic tree [Abrahamson 2012a]. The present report describe my individual weights and justifications for the weights.

The present evaluation summary is resulting from extensive evaluations and discussions performed throughout the PRP, providing the underlying reasoning for the final models and weights. During this evaluation process the complete set of data, models, and methods proposed by the larger technical community that are relevant to the hazard analysis have been considered. The integration of the available information into the proposed models and weights are further- more aimed so as to represent the centre, body, and range of the technically defensible interpretations that the larger informed technical community would have if they were to conduct the study [Kammerer and Ake 2012].

The structure of this evaluation summary follow the structure of the master ground-motion logic tree report.

1.2 Logic tree for the Horizontal Component:Median

1.2.1 Background and State of the Art

Ground-motion prediction epistemic uncertainty is high in Switzerland:

- Swiss seismotectonic conditions include the Alps, the Rhine Graben and the Swiss Foreland, with the first one being more plate boundary related, the latter more intraplate related, and the second one somewhere in between (Fig. IV-1.1);
- Several works (e.g. Bakun and McGarr [2002]) have shown that intraplate ("stable") continental regions are very diverse.

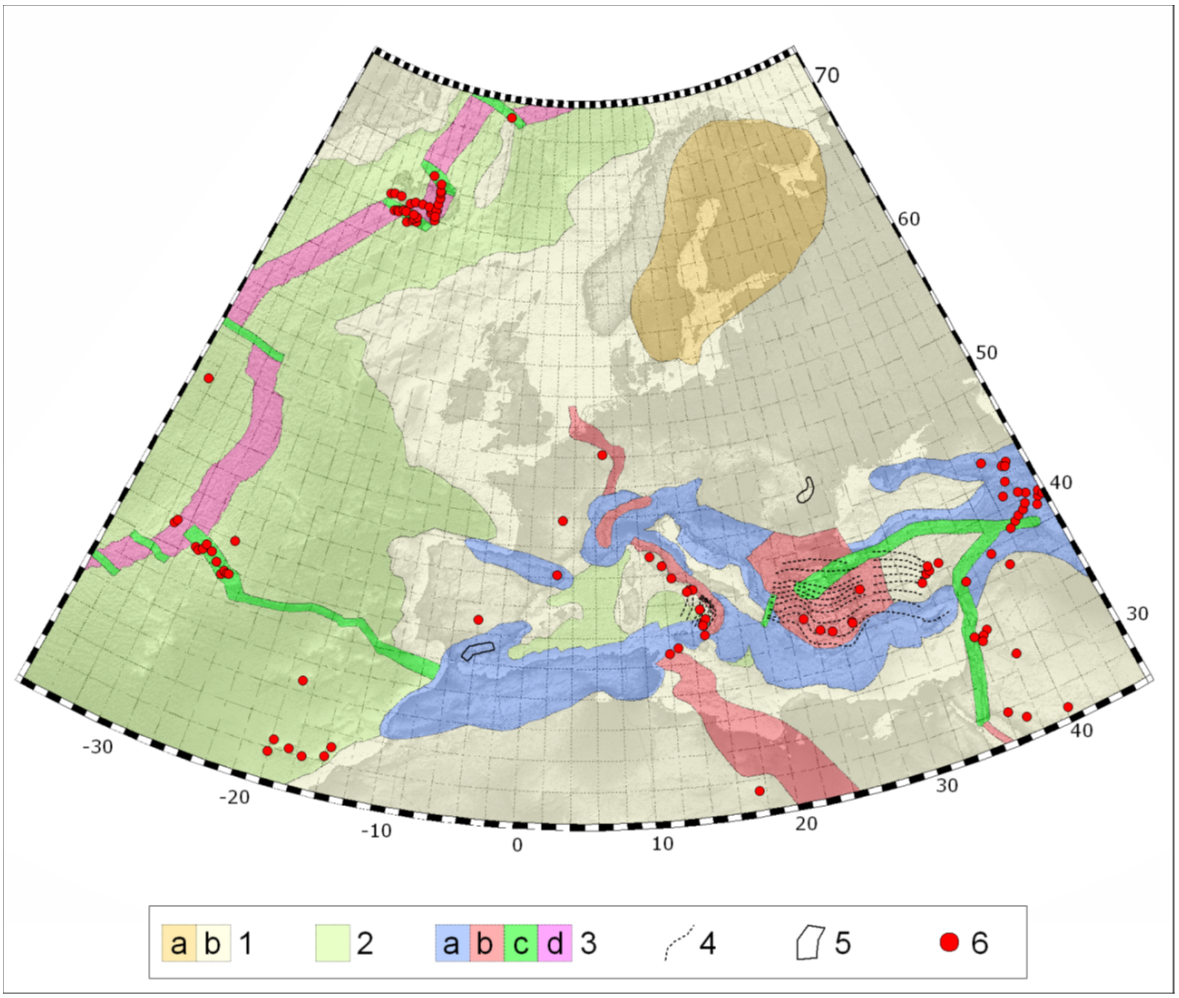

1. SCR, shield (a) and continental crust (b)
2. oceanic crust
3. ASCR, compression-dominated areas (a), extension-dominated areas (b), transforms (c), and mid oceanic ridges (d)
4. subduction zones shown by contours at 50 km depth interval of the dipping slab
5. areas of deep-focus non-subduction earthquakes
6. active volcanoes and other thermal/magmatic features.

Figure IV-1.1: Seismotectonic map of Europe [Delavaud et al. 2012b]. The map shows the complexity of the swiss tectonic context.

Since the PEGASOS Project, our understanding of ground-motion prediction has however been improved :

- PEGASOS experience (Saint Die earthquake analysis, regional quality factors, stress drops, kappa) shows that WUS and European active regions models are not inconsistent with Swiss Foreland observations. These results suggest that global models developed with the most recent projects like NGA are not irrelevant for Switzerland.

- Recent studies have shown that several ground-motions parameters (attenuation in first 70 km, magnitude scaling for $M5.5 - M7.0$) are similar for most regions (Figure IV-1.2).

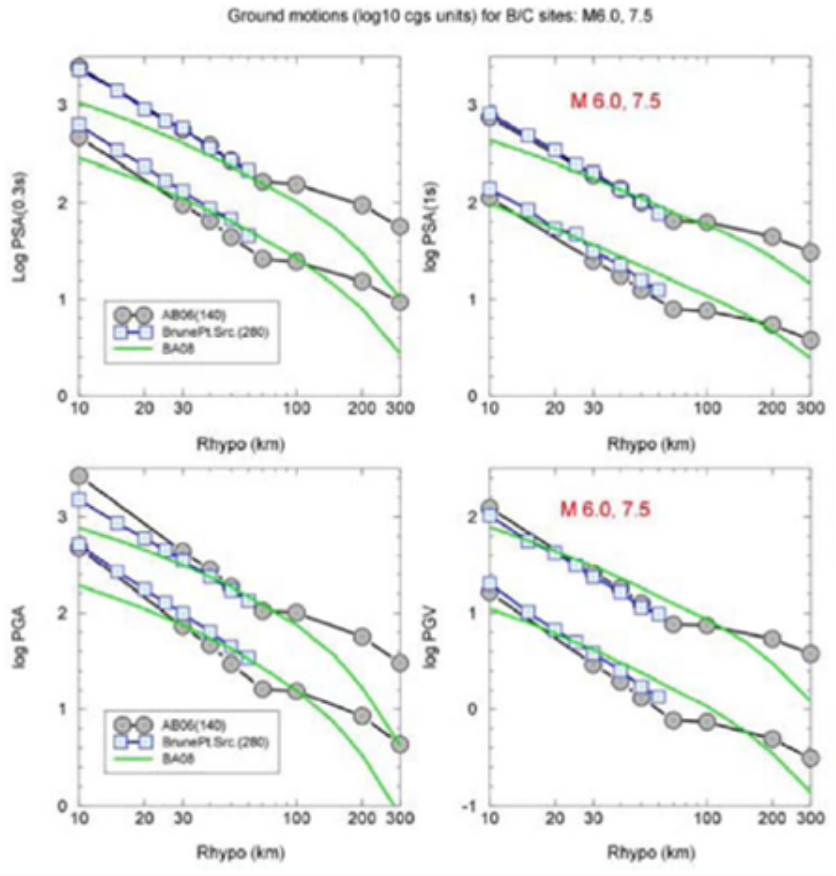

Figure IV-1.2: California and ENA ground-motions are similar for $R < 60km$ and $T < 3s$. The largest differences are observed beyond the "Moho Bounce" transition [Atkinson and Assatourians 2010].

Epistemic uncertainty related to ground-motion decays regional variations

Frankel et al. [1990] have shown that the geometrical decay is highly sensitive to the crustal velocity structure. Significant regional variations of ground-motions are then expected in Switzerland due to the crustal structure heterogeneity.

The data-analysis do confirm such variability of the ground-motion decay: the Swiss foreland model is characterized by a high decay compared to the values found in the Alpine area.

In my opinion, the variation explains, on the first order, the discrepancy between the Foreland, the Alpine and global ground-motion models as shown on Figure IV-1.3. This figure and the analysis performed in Renault [2012a] (PMT-TN-1232) show that the difference between the Swiss Foreland model and global models are, on the first order, explained by these geometrical spreading differences.

Years of additional data will be needed to confirm this Foreland specificity (which is based only on few observations as shown on Figure IV-1.4: such large epistemic uncertainty has to be taken into account within the logic tree.

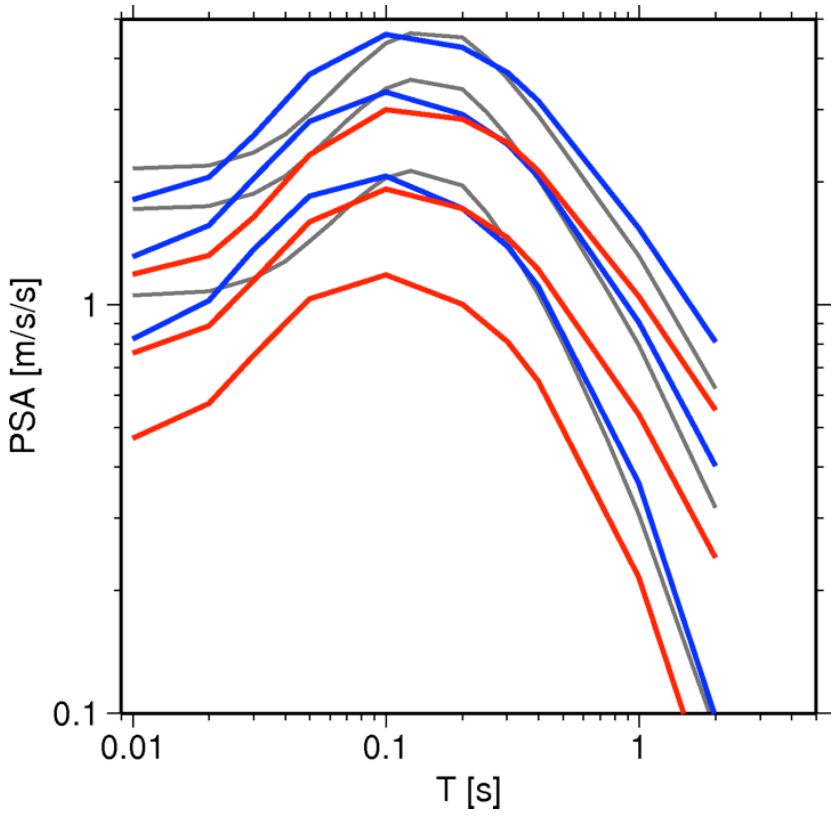

Figure IV-1.3: Comparison of the stochastic models (Alpine and Foreland, R=16km) and the Chiou and Youngs [2008a] model for events of M_W 5.5, 6.5 and 7.5 (courtesy of Edwards [2012a]).

1.2.2 Logic Tree Structure

There are two possible strategies to cover the epistemic uncertainties of ground-motion evaluations: the use of several models (strategy used during the PEGASOS Project) or the use of one or two models with scale factors to capture the range of other GMPEs.

The use of several models (PEGASOS Project strategy) has shown several weaknesses:

- some of the models are not calibrated for large magnitude and short distances,
- the $V_{S30} - \kappa$ corrections is difficult to apply for some models,
- some of the models are calibrated on similar datasets and are not independent.

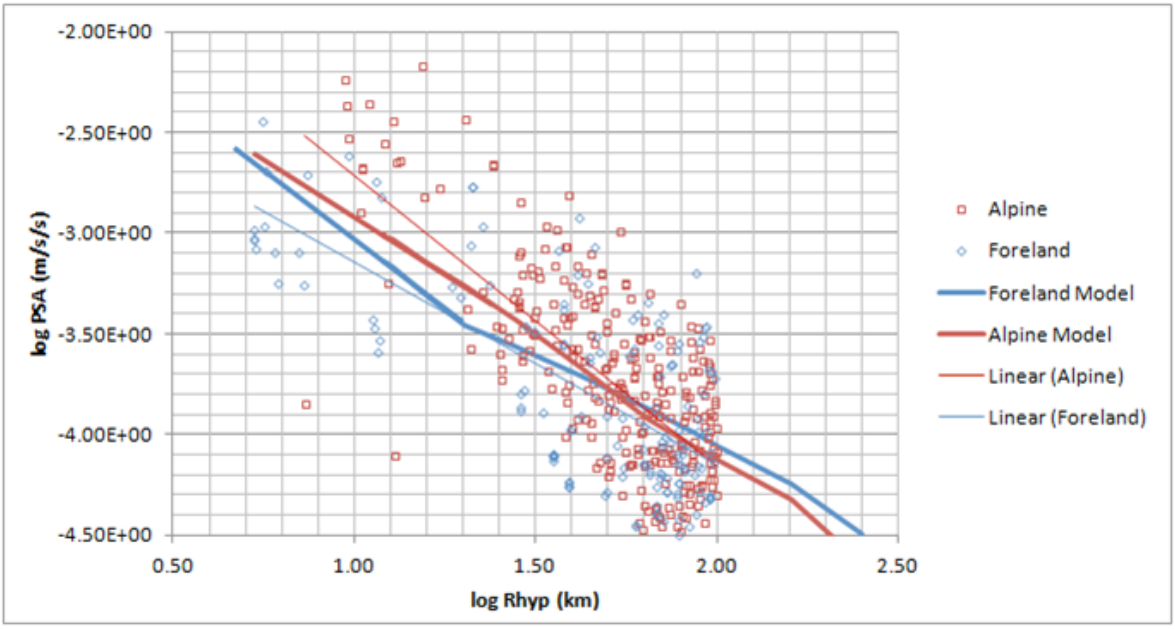

Figure IV-1.4: Ground-motion decay (data and model) for the Foreland and Alpine swiss models (courtesy of Ben Edwards,Edwards [2012a] SED, 2012).

I have then chosen to use a new strategy: my logic tree is based on two ("backbone") models with scale factors to capture the range of other GMPEs (for M, R range for which they are valid). These two models are based on independent datasets.

The first chosen model is the Abrahamson and Silva [2008] model. This model has the following strengths:

- the model is based on a large dataset,
- the functional form is complete,
- empirical $\kappa - V_{S30}$ adjustments are available and have been analyzed carefully during the PRP meetings,
- its decay is similar to the decay observed in western active Europe and the Alpine part of Switzerland.

The second chosen model is the Swiss Foreland model. This model has the following strengths:

- it is of considerable importance to include a relation that is developed specifically for Swiss Foreland conditions,
- the new model can be given a sufficient scientific credibility given the extensive work and improvements performed these last three years,
- the models decay is based on the results found for this area.

1.2.3 Logic Tree Weights

The weights given to the two models are equal in order to take into account the epistemic uncertainty (particularly the epistemic uncertainty related to ground-motion decay).

Weighting of Abrahamson & Silva (2008) 08 branches

Weights:
The weights are first based on the analysis which compare the PRP GMPEs with scaled versions of the Abrahamson and Silva [2008] model. The chosen factors (natural logarithm) are: -1.0, -0.75, -0.5, -0.25, 0.25, 0.5. (In May 2012, when the first comparison was made, the factor of 0.75 was also used.)

The resulting models are named: "AbSi08(-1.0)", "AbSi08(-0.75)", "AbSi08(-0.5)", "AbSi08(-0.25)", "AbSi08(0.25)", and "AbSi08(0.5)" in the following.

These comparisons show that :

- The "AbSi08(-1.0)" model is lower than other empirical models at all distances;
- the "AbSi08(0.25)" model is giving larger ground-motions than almost all other corrected GMPEs predictions. This model is close to the Toro [2002] model for a few cases (e.g. large magnitude) and is giving lower results than other GMPEs predictions only at short distances (<10 km), large magnitude (M=7.5) and for the Atkinson [2006] model. Such overestimation should however not be taking into account since the Atkinson [2006] is not constrained for such scenarios;
- The mean value of the Abrahamson & Silva (2008) is larger than most of the predictions of SP2 GMPEs (Fig. IV-1.7). For most frequencies and distances, this model is also giving larger values than the Chiou and Youngs [2008b] and Akkar and Bommer [2010] models. These two models have recently shown the best fit to European data [Beauval et al. 2012; Delavaud et al. 2012a] and are, in my opinion, close to the center of the distribution of potential ground-motions in active crustal Europe. This suggests that the center of the ground-motion distribution should be lower than the mean value of the Abrahamson & Silva (2008) model.
- The median value of the Abrahamson & Silva (2008) is lower than some of the predictions of SP2 GMPEs (Fig. IV-1.5) for short distances (R<10 km), large earthquakes (e.g M=7.5) and low frequencies (e.g 1 Hz)

Regional Differnces:
Interestingly, the regional differences observed recently show factors between -1.0 and 0.5 (Tab. IV-1.1). These regional variations of the scaling factors give an upper bound of the range that has to be used to cover the epistemic uncertainty in a limited area like Switzerland.

Testing:
The analysis of testing results (new testing, July 2012, 1 s and 3 s tests) performed by N. Kühn shows that the mean value of the Abrahamson & Silva (2008) model is overestimating Swiss Intensity data (figureIV-1.6). This is another point suggesting that the center of the predicted Ground-Motion distribution should be lower than the mean value of the Abrahamson & Silva (2008) model. The distance range up to 100 km is considered to be more important in this testing analysis (at larger distance intensities (III and IV values) are poorly constrained for historical events. I have also chosen not to use PGA in the Intensity testing (PGA seems not

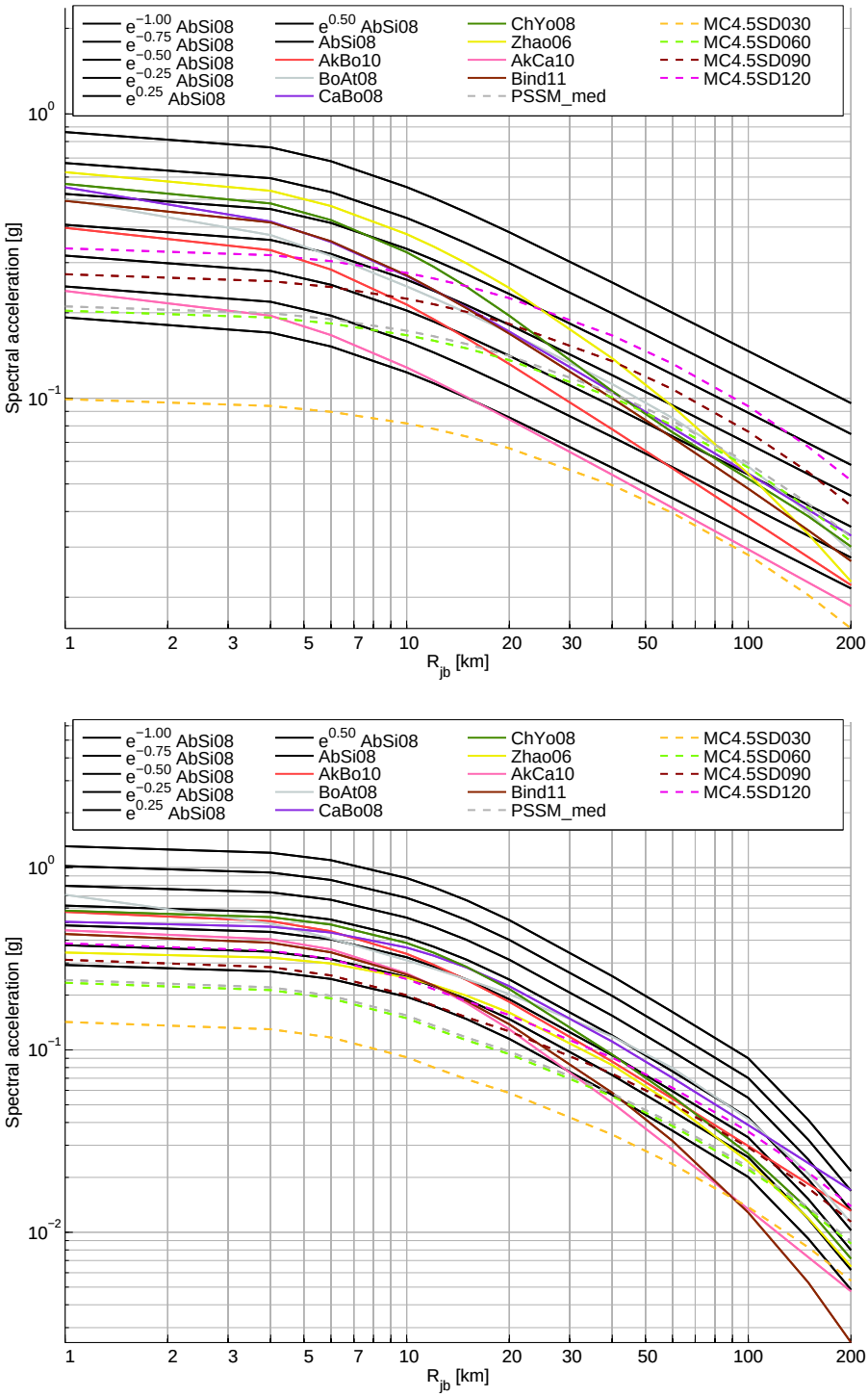

Figure IV-1.5: Comparison of the PRP GMPEs with the Abrahamson and Silva [2008] model for $M7.5$ at 1 Hz (top) and $M6$ at 5 Hz (bottom) with scaling factors of -1, -0.75, -0.5, -0.25, 0.25, and 0.5. Note: The plots are based on a comparison with $V_S - \kappa$ corrected GMPEs at the site Mühleberg. The correction functions of D. Fäh have been used in this example.

Table IV-1.1: Regional differences (LN scale) compared to the Abrahamson & Silva (2008) model [Abrahamson 2012c]. Note: The values reported from China are significantly large than for the other regions and need to be revisited.

Region	T=0.2 [s] (±SE)	T=1.0 [s]
California	-0.05 to 0.05	-0.05 to 0.05
Japan	0.10 to 0.35	-0.50 to 0.10
Italy	-0.40 to 0.05	-0.10 to 0.25
Taiwan	0.00 to 0.30	-0.10 to 0.30
Middle East	-0.15 to 0.30	-0.45 to 0.05
New Zealand	0.10 to 0.15	0.10 to 0.15
China (Wenchuan)	0.4 to 0.5	-1.2 to -1.0
Range for W. Europe?	-0.40 to 0.35	-0.50 to 0.30

to be very well correlated to larger intensity values, D. Fäh personal communication) and high frequencies are affected by possible soil-structure interaction.

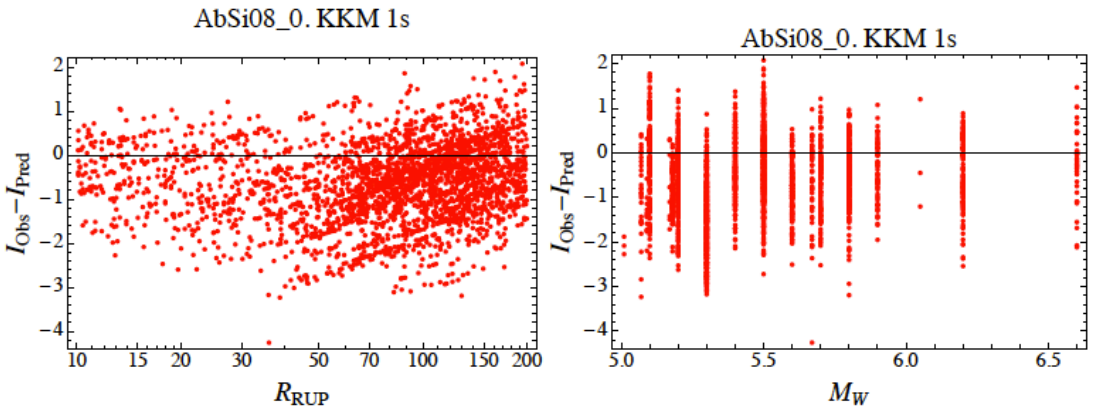

(a) a

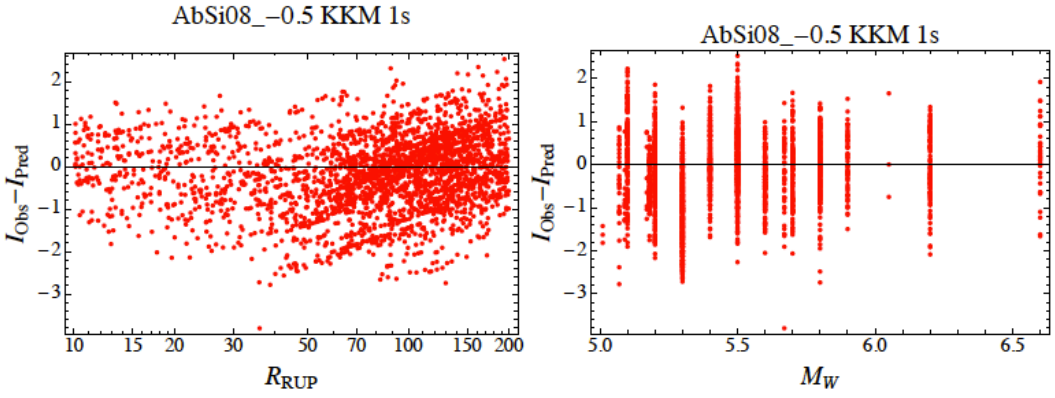

(b) b

Figure IV-1.6: Residual between observed intensities and predicted Intensities based on the Abrahamson and Silva Abrahamson and Silva [2008] -0.5 model (1 s, Correction for 1100 m/s, Mühleberg site).

The chosen weights (table IV-1.2) are then considering that the center of the ground-motion predictions is lower than the mean value of the Abrahamson and Silva [2008] model and is close to "AbSi08(-0.5)" and "AbSi08(-0.25)". "AbSi(0.0)" and "AbSi08(-0.75)" are capturing the range of the epistemic uncertainty. A broad distribution is chosen because the same factors are used for all frequencies.

Table IV-1.2: Weights of the Abrahamson and Silva scaled model branches.

Scaling factors (LN)	0	-0.25	-0.5	-0.75
Weights	0.1	0.4	0.4	0.1

Weighting of the Swiss models branches

The weights given on the various $Mc - \Delta\sigma$ swiss models are first based on the analysis of testing results performed by Kühn [2011a] (EXT-TB-1086). Intensity data are considered as not reliable at distances larger than 100 km (see above).

These results suggest that the models using Mc=4.5 show a slightly better fit to the observed Intensity data than the models using Mc=5.5 (Figure IV-1.7).

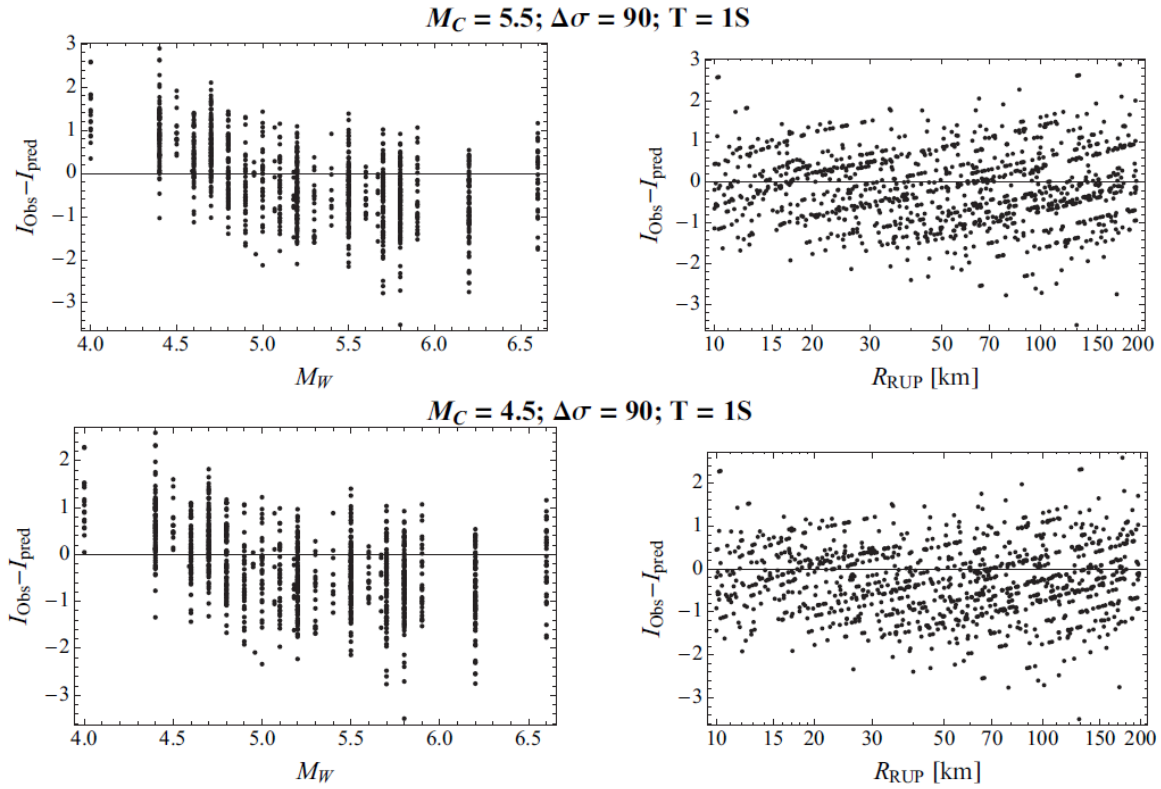

Figure IV-1.7: Residual between observed intensities and predicted Intensities based on the Swiss Model (Mc=4.5 compared to Mc=5.5, T=1 s, stress drop equal to 90 bar).

Additional comparison with the mixture model derived by N. Kühn have been provided in November 2012 (TFI-RF-1447).

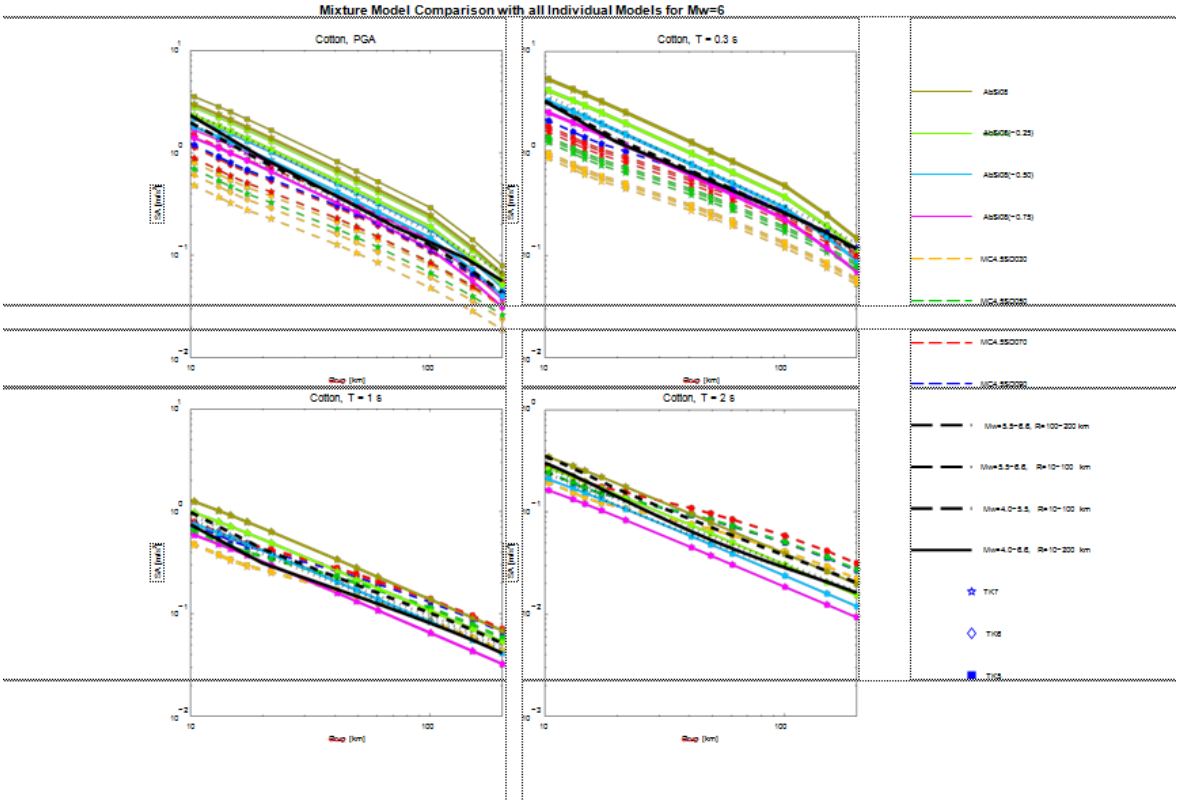

Figure IV-1.8: Comparison of the selected models with mixture models calibrated on Intensities (TFI-RF-1447).

These comparisons show the following points :

- Depending on periods, the best fit to the mixture model calibrated on Intensity data are observed for different stress drops values of the PSSM model ($\Delta\sigma$=50 bar for T=1 s, $\Delta\sigma$=90 bar for T=0.3 s);

- the AbSi08 model and the stochastic models have different distance decay and magnitude scaling properties. As discussed before, the AS08 model is, in my opinion, representative to the motion expected in active Europe and the alpine region. The Swiss stochastic models are more foreland specific. These models are given lower values than the AS08 scaled models because of a higher geometrical spreading decay in the near-field. The use of these two type of models help to capture the epistemic uncertainties of the center of expected ground-motions and the epistemic uncertainty related to the distance decay and magnitude scaling;

- Mixture models are calibrated using data from both alpine and foreland areas. These mixture models are then not expected to fit either the stochastic or the AS08 scaled models but rather to be close to the center of the distribution of the selected models (which is confirmed by Figure IV-1.8);

- The range covered by the two types of model is based on considerations related to observed average stress drop variations. The range covered by the two different models should then be roughly similar.

Edwards and Fäh [2012a], later published as Edwards and Fäh [2013a], have analyzed the ground-motions of the European Strong Motion database and found a mean stress drop value of 74 bar (equation 6) and 89 bar (equation 7). This study is really useful since the method used and the stress drop definition are consistent with the one used to derived the Swiss stochastic model. Source studies show a large stress drop variability and large values are shown for some earthquakes. The standard deviation of European stress drops found by Edwards and Fäh [2012a] is equal to 43 bar (equation 6). However, as discussed by Cotton et al. [2013], uncertainty in stress drop is dominated by uncertainty in the corner frequency and stress drop, determined by source studies like the Edwards and Fäh [2012a] study, has greater uncertainty than that implied by the ground-motion data. Moreover, the stress drop variability is also taken into account by the between-event variability. The stress drop variabilities found by Cotton et al. [2013] and Edwards and Fäh [2012a] are then upper bounds of the regional variations of the mean stress drop. In order to avoid a double counting we then should consider here only potential regional variations of the mean stress drop not taken into account by the between-event variability.These regional variations are difficult to evaluate but they should not lead to variations of ground-motions larger than the one shown by GMPEs derived in different regions.

I then have chosen not to include extreme values (30, 240 and 480 bar) within the median ground-motion logic tree. A chosen range of 80 bar gives about the same range of variations than the range of variations chosen for the scaled AbSi08 models.

The chosen weights (see Table IV-1.3) are then considering that the center of the ground-motion predictions is around 70 bar and that values of 40 and 120 bars are capturing the range of the epistemic uncertainty. A broad distribution is used because the same factors are used for all frequencies.

Table IV-1.3: Weights of the Swiss model branches (Mc is chosen equal to 4.5).

Stress drop [bar]	40	70	90	120
Weights	0.1	0.4	0.4	0.1

Center and range calibrations

Table IV-1.4 summarizes the methods used to calibrate the center and range of the median value of the horizontal component.

Table IV-1.4: Methods used to calibrate the center and the range of models weights.

Calibration	Methods	Results
Center (AbSi08 scaled models)	Comparison with the Swiss mixture model at 1 Hz (EXT-SUP-1078, Figure IV-1.6)	AbSi08(-0.25) to AbSi08(-0.5)
	Data testing (European strong-motions, [Beauval et al. 2012; Delavaud et al. 2012a])	Abrahamson & Silva (2008) is giving larger values than the Chiou & Youngs (2008) and Akkar & Bommer (2010) models which have recently shown the best fit to European data [Beauval et al. 2012; Delavaud et al. 2012a])
Center (PSSM)	Comparison with the Swiss mixture model at 1 Hz (EXT-SUP-1078, Fig. IV-1.8)	60-90 bar
	Average stress drop of European major earthquakes [Edwards 2012a]	Two models with mean values of 74 and 89 bar
Range (AbSi08 scaled models)	Capture of the variations shown by PRP selected models (Figure IV-1.3)	AbSi08(0.0) to AbSi08(-0.75)
	Analysis of regional variations (Figure IV-1.4)	A range of 0.80-0.75 is found for western Europe
Range (PSSM)	Range similar to the range of AbSi08 scaled models The stress drop variability found by Cotton et al. [2013] is about 0.5 (LN scale). This number is considered as an upper bound of the epistemic uncertainty of the average stress drop.	40-120 bar

$V_{S30} - \kappa$ corrections of the Abrahamson & Silva (2008) model

Host region properties:

1. In my case, the only adjusted GMPE is the model of Abrahamson and Silva [2008]. In order to evaluate the κ values associated to this model, I have chosen not to use the peak frequency methods since these methods are leading to:

   - different κ for the NGA models,
   - high κ values (higher than my experience with the data, much higher than empirical results);
   - values that could be controlled by the a priori shape of the GMPEs functional form (which is not totally data-driven).

   Methods using the empirical $V_{S30}\kappa$ relationship and κ RVT based FAS are given an equal weight of 0.5.

2. The κ obtained for the NGA models by the IRVT based FAS do not depend on the chosen V_{S30} (e.g. the values obtained for the Abrahamson and Silva [2008] model are almost the same for V_{S30}=620 m/s, V_{S30}=800 m/s or V_{S30}=1000 m/s). In my opinion, this point is showing that the rock high-frequency shape of this GMPE is mainly controlled by stiff soil/soft rock data. Due to the lack of hard rock data in the NGA dataset, the GMPEs high frequency shape is not calibrated for hard-rock. I then suggest to use a V_{S30}=620 m/s on the RVT based FAS branch which is leading to a value of κ=0.041. The obtained value (V_{S30}=620 m/s) is κ=0.04. This value is close to the value found using the empirical $V_{S30} - \kappa$ relationship of Silva et al. [1998].

3. I have chosen a US generic profile which is more adapted to an NGA model than the Swiss velocity model.

Target region properties:

Which dataset (site-specific / Swiss/ World)?

3 Main strategies are available to obtain the target κ:

- direct analysis of NPP sites records,
- analysis of κ values obtained on Swiss stations,
- of κ values obtained worldwide.

The physical basis of κ are not fully understood. Part of κ is quite certainly due to the upper crust attenuation and/or source effects (e.g. figure 9 from Ktenidou and Van Houtte [2013]) which favors the use of site specific records or (if site specific records are note available) the use of regional models of κ.

Correlation of κ with V_{S30} ?

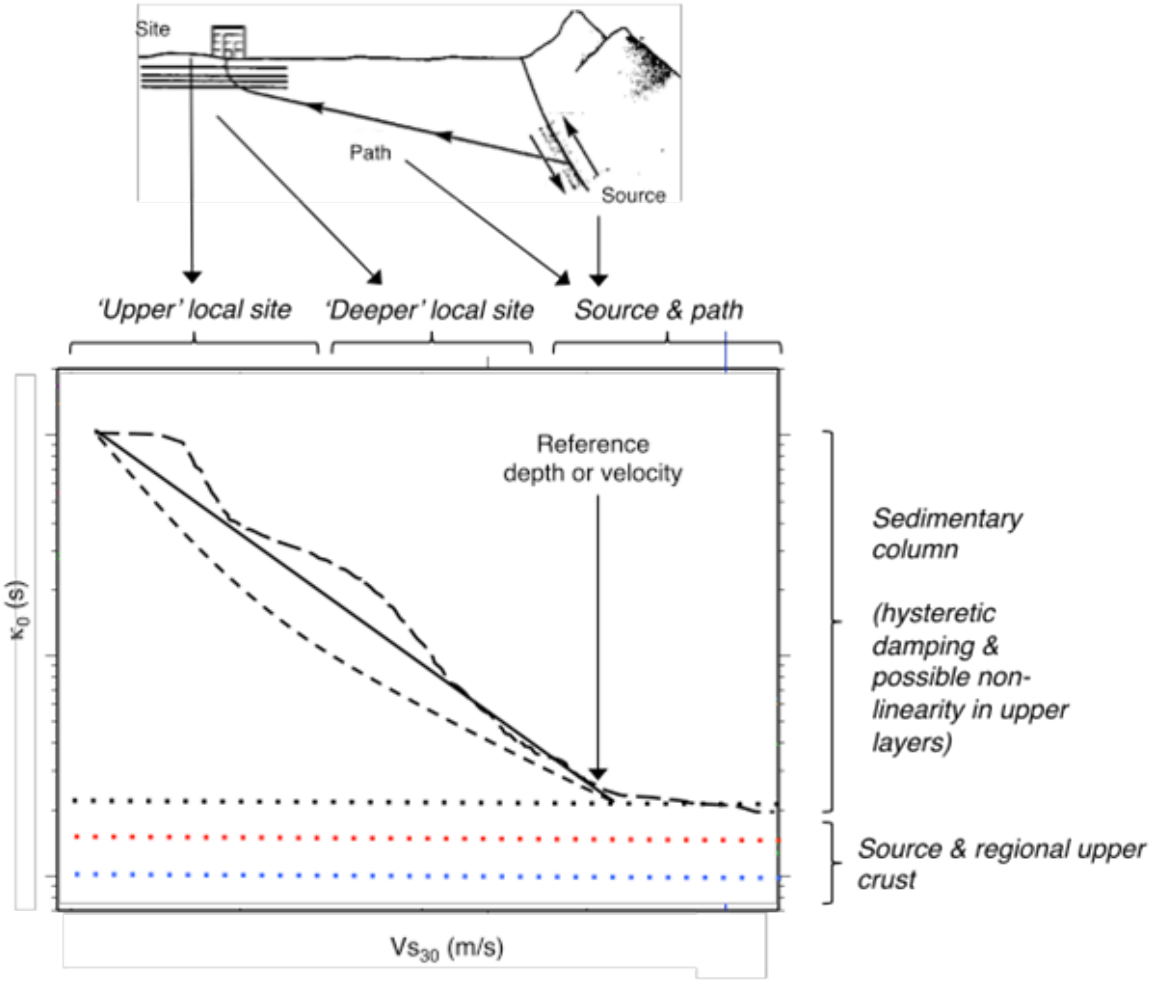

Figure IV-1.9: Example illustration of the possible regionalization of $\kappa_0 - V_S$ correlations and description of the underlying model. Regardless of the possible functional form (solid and dashed lines), an asymptotic κ_0 value for very high V_{S30}, which will depend on the source and regional upper crust (dotted lines) is suggested by Ktenidou and Van Houtte [2013]. Cartoon on top indicating source, path and site components adapted from Kramer, 1996.

From a physical point of view [Ktenidou and Van Houtte 2013] and as shown by Figure IV-1.10 target κ values should follow an asymptote for high V_{S30} values. One of the most intriguing questions is what is the "asymptotic" value of κ for very hard rock sites and what it depends on. To elucidate this issue we would need to acquire more data at hard sites, and kappa should be measured in a consistent way at frequency ranges as high as possible. Ktenidou and Van Houtte [2013] also suggest that it may be possible that different $\kappa - V_{S30}$ correlations might hold for different regions, and the high-V_{S30} asymptote κ values might in fact be a regional characteristic. For that reason, chosen target kappa values follow an asymptote and the minimum values are chosen for the largest V_{S30} sites.

Target κ for the host to target adjustment of the Swiss stochastic model.

Kappa is not only, a physical value but is dependent both on the approach chosen to obtain it and the method used to perform the host-to-target adjustments [Ktenidou and Van Houtte 2013]. The values computed by Edwards et al. [2010] (TP2-TB-1024) are obtained fitting the

full spectrum. Kappa is then correlated with other parameters and has to be preferred (for consistency reasons) for the host-to-target adjustments of the Swiss Stochastic Model.

As discussed above, κ values should follow an asymptote for high V_{S30} values which favors the log-log relationships of Edwards [2012b] (TP2-TN-1236). Part of κ is quite certainly due to the upper crust attenuation and/or source effects which favors the use of regional models of κ (since site-specific records are still missing) and relationships based on Swiss data only (R <50 km, see Edwards [2012b] (TP2-TN-1236), table 10).

The minimum Swiss station values (figure 6 of report Edwards [2012b] (TP2-TN-1236)) are around 0.003 s. The minimum potential κ value may also be evaluated assuming reasonable value of Q in the upper Swiss crust and no added attenuation due to the upper layers. Such minimum value has been evaluated by SED (D. Fäh, personal communication, September 2013 meeting) and is close to 0.005 s (this value is consistent with the minimum observed value).

The largest κ value (hard-rock conditions) observed on the eight hard rock site stations (AIGLE) is equal to 0.014 s. The upper bound of κ may also be based on the rock attenuation characteristics suggested recently by the Swiss Seismological Service [Poggi et al. 2012] (TP2-TB-1090). The obtained values (mean value of 0.22 for Gösgen) are larger than the one described above and have to be considered as upper bounds of possibilities. The mean κ value of the eight hard-rock Swiss site stations is equal to 0.007 s. This value is lower than the generic PSSM κ value (obtained with softer rock stations) which also confirms that κ values are decreasing when V_{S30} is increasing. Uncertainties are higher for low κ values for two reasons:

- κ values measured at the surface may overestimate the values at depth because of high frequencies shallow site response and lower lithostatic pressure,
- low κ values are difficult to measure because of instrumentation high pass filters [Laurendeau et al. 2013].

This uncertainty analysis motivates the use of a larger ratio (factor of 1.6) between branch 2 and branch 1 κ values than the ratio (factor of 1.4) between branch 3 and branch 2 κ values.

κ for the host to target adjustment of the Abrahamson & Silva (2008) model. Host κ estimation of the AbSi08 GMPE has been found trough the IRVT FAS approach which does not take into account the amplitude of the spectrum. κ are measured on the high-frequency part of the records spectra which show a clear decay.

For this reason, I favor the use of κ found using the classical Anderson and Hough [1984] methodology (use of records showing a clear decay, calibration on the high frequency slope of the spectra)

The central value of the κ obtained with these approaches (see e.g. TFI-RF-1457) are consistent between the recent analysis of B. Edwards and O. Ktenidou. These values show the expected asymptotic shape described on Figure IV-1.10 with larger values for lower V_{S30} sites. The largest κ value (hard-rock conditions) observed on the eight hard rock site stations is equal to 0.034 s. The lowest κ value (hard-rock conditions) observed on the eight hard rock site stations is equal to 0.018 s. A target κ value of 0.026 s explains the residuals.

The variations between the different scenarios and authors are used to evaluate the range of κ values for each site.

As explained above, the uncertainty analysis motivates the use of a larger ratio (factor of 1.6) between branch 2 and branch 1 κ values than the ratio (factor of 1.4) between branch 3 and branch 2 κ values.

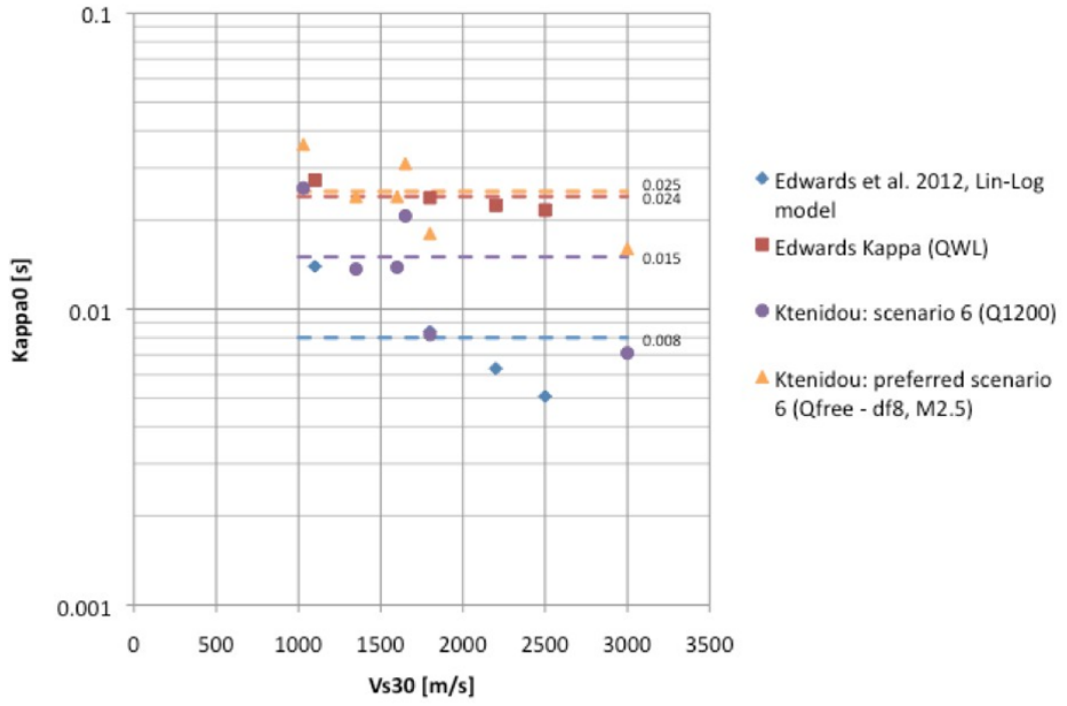

Figure IV-1.10: Kappa values based on slope at high frequency for Switzerland (TFI-RF-1457).

Mühleberg (V_{S30}=1100 m/s):

The events recorded at NPP Mühleberg were not of high enough quality to be of use in this analysis of Edwards et al. [2010] (TP2-TB-1024, page 94). No additional records have been evaluated recently.

My estimation (center) is based on the log-log κ values (R <50 km, log-log) for rock Swiss sites (host to target adjustment of PSSM) and on the values found by the preferred scenario of O. Ktenidou (host to target adjustment of AbSi08):

- κ = 0.016 s (host to target adjustment of PSSM),
- κ = 0.027 s (host to target adjustment of the AbSi08 model).

I suggest to capture the range of the target κ by a 3 branches logic tree with:

- a lower value of κ = 0.010 s and a larger κ value of 0.022 s (host to target adjustment of PSSM),

- a lower value of $\kappa = 0.017$ s and a larger κ value of 0.038 s (host to target adjustment of AbSi08).

Beznau, V_{S30}=1800 m/s:

At the nuclear power plant (NPP) located in Beznau there are two free-field instruments in use. Edwards [Biro and Renault 2012b] (PMT-TN-1244) reports a value of 0.023 s (surface) and 0.023 s (borehole). These values are similar to the one obtained by O. Ktenidou (0.025 s).

These instruments are however located on or within a layer with a rather low V_{S30} (476 m/s) far from the bedrock velocity (1800 m/s). I then will not consider these site-specific measures.

My estimation (center) is based on the log-log κ values (R <50 km, log-log) for rock Swiss sites (host to target adjustment of PSSM) and on the values found by the preferred scenario of O. Ktenidou (host to target adjustment of AbSi08):

- $\kappa = 0.011$ s (host to target adjustment of PSSM)
- $\kappa = 0.024$ s (host to target adjustment of the AbSi08 model)

I suggest to capture the range of the target κ by a 3 branches logic tree with:

- a lower value of $\kappa = 0.007$ s and a larger κ value of 0.015 s (host to target adjustment of PSSM),
- a lower value of $\kappa = 0.015$ s and a larger κ value of 0.034 s (host to target adjustment of AbSi08).

Leibstadt (V_{S30}=2200 m/s):

The events recorded at NPP Leibstadt were not of high enough quality to be of use in this analysis (TP2-TB-1024, page 94). No additional records have been analyzed recently.

My estimation (center) is based on the log-log κ values (R <50 km, log-log) for rock Swiss sites (host to target adjustment of PSSM) and on the values found by the preferred scenario of O. Ktenidou (host to target adjustment of AbSi08).

My estimation (center) is the average κ for rock Swiss sites :

- $\kappa = 0.010$ s (host to target adjustment of PSSM),
- $\kappa = 0.022$ s (host to target adjustment of the AbSi08 model).

I suggest to capture the range of the target κ by a 3 branches logic tree with:

- a lower value of $\kappa = 0.006$ s and a larger κ value of 0.014 s (host to target adjustment of PSSM),
- a lower value of $\kappa = 0.014$ s and a larger κ value of 0.031 s (host to target adjustment of AbSi08).

Gösgen (V_{S30}=2200 m/s):

Three events have recorded at the Gösgen NPP (borehole). The obtained values [Biro and Renault 2012b] (PMT-TN-1244) are between 0.011 s and 0.020 s (average = 0.014 s). O. Ktenidou has obtained a value of 0.017 s. Both values are consistent with the range of values expected from Swiss rock sites and assumed for the other plants. There will be some effect of the down-going waves that may reduce the κ but these effects are difficult to evaluate.

My estimation (center) is based on the log-log κ values (R <50 km, log-log) for rock Swiss sites (host to target adjustment of PSSM) and on the values found by the preferred scenario of O. Ktenidou (host to target adjustment of AbSi08):

- κ = 0.008 s (host to target adjustment of PSSM),
- κ = 0.020 s (host to target adjustment of the AbSi08 model).

I suggest to capture the range of the target κ by a 3 branches logic tree with:

- a lower value of κ = 0.005 s and a larger κ value of 0.011 s (host to target adjustment of PSSM),
- a lower value of κ = 0.0125 s and a larger κ value of 0.028 s (host to target adjustment of AbSi08 model).

Table IV-1.5: PSSM κ of the target NPP sites for the host-to-target adjustment. The values are based on the log-log κ values (R <30 km, log-log) for rock Swiss sites [Edwards 2012b] (TP2-TN-1236).

NPP V_{S30} [m/s]	κ, branch 1 weight: 0.2	κ, branch 2 weight: 0.6	κ branch 3 weight: 0.2
1000 m/s, Mühleberg	0.010	0.016	0.022
1800 m/s, Beznau	0.007	0.011	0.015
2200 m/s, Leibstadt	0.006	0.010	0.014
2500 m/s, Gösgen	0.005	0.008	0.011

Table IV-1.6: GMPE κ of the target NPP sites.

NPP V_{S30} [m/s]	κ, branch 1 weight: 0.2	κ, branch 2 weight: 0.6	κ branch 3 weight: 0.2
1000 m/s, Mühleberg	0.017	0.027	0.038
1800 m/s, Beznau	0.015	0.024	0.034
2200 m/s, Leibstadt	0.014	0.022	0.031
2500 m/s, Gösgen	0.0125	0.020	0.028

$V_S - \kappa$ correction method (Abrahamson & Silva (2008) 08 empirical model):

These methods have been developed recently. Most of them have not been reviewed and published in international papers. The main weakness of the HEM method is due to the fact that the κ correction is applied in the all frequency range which is not consistent with the way to derive host κ values (IRVT FAS approach).

The κ correction method of Scherbaum et al. [2011] is not defended anymore by the author and will not be published. I then have chosen to finally discard this method.

The empirical method is not calibrated for κ values lower than 0.010 s and this method is leading to large $V_{S30} - \kappa$ adjustments factors which have not been confirmed by the the residuals of SED hard rock station observations and $V_S - \kappa$ corrected GMPE/PSSM predictions (PMT-SUP-1084).

The FAS scaling with RVT is given a weight of one since this method is reasonably well justified and evaluated even if it is not fully documented and peer reviewed.

1.3 Logic Tree for the Horizontal Component: Aleatory Variability

1.3.1 Between-event variability

The between event variability depends on regions and datasets. Since my median logic tree is using only two models, I then use the frequency dependent model to take into account this epistemic uncertainty.

1.3.2 Within-event variability

The within-event variability is magnitude AND distance dependent. I therefore suggest not to use the distance dependent model.

However, this magnitude-distance dependency is not completely understood and data calibrated. I suggest to give a larger weight (0.7) to the constant model which seems more robust.

The within-event single station sigma depends on the number of records. The trend in the PRP data is consistent with what is expected from simple statistical error appears to extrapolate to a constant value that would represent the true station-to-station variability. Following the results obtained in Rodriguez-Marek [2012] (EXT-TN-1255), I suggest to use a value of 0.08 for all periods.

1.4 Logic Tree for the Horizontal Component: Maximum Ground-Motion

My understanding is that constructive interference of waves are the main explanation of upper bounds. Such constructive interference can occur both at short and long distances. This may explain the lack of distance-dependency and the fact that the some largest motions are observed at large distances.

I have then chosen to use only the branch 2 of the upper bound logic-tree (no distance decay and motion anchored to the BA08 median at 1 km R_{JB} distance).

For each period and each magnitude range (5-6, 6-7, 7-8) I have analyzed the number of standard deviation ($\sigma = 0.57$) of the BA08 model (anchored at 1 km) needed to cover the observed ground-motions for the all distance range (see reports M5p5V_CandidatesValuesSummary.pdf, M5p5H_CandidatesValuesSummary.pdf, M6p5V_CandidatesValuesSummary.pdf, M6p5H_CandidatesValuesSummary.pdf, M7p5V_CandidatesValuesSummary.pdf, M7p5H_CandidatesValuesSummary.pdf)

Table IV-1.7: Number of standard deviation (sigma=0.57) of the BA08 model (anchored at 1km) needed to cover the observed ground-motions (Horizontal motion).

Period [s]	0.01	0.02	0.03	0.05	0.10	0.2	0.4	1	2
$M = 7 - 8$	4	4	4	4	3.5	3	3	3.5	4
$M = 6 - 7$	4	3.5	3.5	3.5	3	3	3	3	3.5
$M = 5 - 6$	4.5	3.5	3.5	3.5	3.5	3.5	4	5	

Table IV-1.8: Number of standard deviation ($\sigma = 0.57$) of the BA08 model (anchored at 1 km) needed to cover the observed ground-motions (Vertical motion).

Period [s]	0.01	0.02	0.03	0.05	0.10	0.2	0.4	1	2
$M = 7 - 8$	3.5	3.5	3.5	3.5	3.5	2.5	2.5	2.5	2.5
$M = 6 - 7$	4	4	4	4	4	3	3	3	4
$M = 5 - 6$	5	5	5	5	5	4	4	5	5.5

This analysis does not show significant differences of observed upper bounds among different periods and there is no physical explanations to explain potential differences. There is also no significant differences of observed upper bounds for vertical and horizontal ground-motions and there is no physical explanations to explain potential differences.

I then have chosen, the same logic tree for vertical and horizontal motions. The highest weight (0.6) is given to the scale factor equal to 35 (5.35 equivalent σ of 0.57). Weights of 0.2 are given to the scale factors of 21 (5.35 equivalent σ of 0.57) and 60 (7.17 equivalent σ of 0.57).

1.5 Logic Tree for the Vertical Component: V/H Ratio

The ratio of vertical to horizontal damped pseudo-spectral acceleration (PSA) can be predicted by empirical relations based on V_{S30}, magnitude and distance (e.g. Bozorgnia and Campbell [2004] and Gülerce and Abrahamson [2011] and Bommer et al. [2011]) or alternatively relations based primary on quater-wavelength profiles like in Edwards et al. [2011a].

A general observation can be made by comparing the V/H spectra [Edwards and Fäh 2011a] (EXT-TN-1217) observed on various Japanese or Swiss hard rock sites: at the low-moderate κ sites, the spectra do not show the peak at 10-2 0Hz exhibited in the empirical V/H relations.

The model of Edwards and Fäh [2011a] model then seem better calibrated for hard rock sites. Moreover these models are site-specific: the predictive equation can be used for reconstructing the expected V/ H ratio given each NPP site shear-wave velocity profile. However, Edwards and Fäh [2011a] have been calibrating their model on data until 7 Hz and they propose two different models at higher frequencies. According to the discussions of the last PRP working

meeting (January 2013), no arguments are yet available to prefer one of the SED models and the main weakness of these models may be their lack of robustness (the fact that the models may be improved and modified in a near future).

The median US-West V/H model is not site-specific but this model is robust: this model is calibrated on a large database and future earthquake records will not challenge it.

The median US-East V/H models is not site-specific and is less robust than the median US-West V/H model. However this model is calibrated on hard rock sites and do not show the peak at 10-20 Hz.

Some of these models show large differences and the epistemic uncertainty of V/H ratio on very hard rock (e.g. Gösgen) is then high. In order to capture the range of these ratios I have then chosen to select and weight equally the models of Edwards and Fäh [2011a] (high frequency adjusted), Edwards and Fäh [2011a] (non-adjusted), Gülerce and Abrahamson [2011] and both the median US-West V/H model and US-East V/H model.

1.6 Aleatory Variability of V/H Ratios

Method 1 is rather complex and I'm not sure that the values obtained for the correlations are robust. Some physical reasons explain why the variability on the vertical motions should be larger than the variability on the horizontal motion (as found by method 2).

I then have chosen to give a lower weight to method 1 compared to method 2.

I have chosen to give an equal weighting to the different branched of these two methods.

Chapter 2

Hazard Input Document for F. Cotton (EG2-HID-1011)

Written by the PMT, SP4 and TFI

This document describes the implementation and parametrization of Fabrice Cotton's expert model EG2-EXM-1011, as described in the evaluation summary EG2-ES-1020 (see Chapter 1) and delivered on 07.02.2013, with an update for the target κ estimates on 12.11.2013. The purpose of this document is to translate the expert's evaluation of ground motion into an input usable by the hazard software. For PRP a consensus master logic tree for the median, the aleatory variability, the maximum and the V/H ratio of the ground motion was developed by the SP2 experts and is described in part I. The basic elements of those trees and models are not repeated here. This document only summarizes the parameters and model weights assigned by the expert F. Cotton. By this the master logic tree becomes expert specific and reflects the individual evaluations.

2.1 Model Implementation

Based on the evaluation summary, the logic trees for the median horizontal ground motion, the vertical/horizontal ratio, the maximum ground motion and the aleatory variability of the horizontal and vertical component were implemented. The key elements in the model are given below. Figure IV-2.1 shows the logic tree. The first level in the logic tree, "Model Category" is not explicitly specified by the expert but is used by SP4 to allow for an easier treatment of those subsequent global variables (or logic tree levels) like "Vs-Kappa", which are dependent on whether a GMPE or a PSSM model is considered. The logic tree has in total 1728 branches.

2.2 Median Horizontal Ground Motion

One of the ten candidate models by SP2 get non-zero weights in F. Cotton's model. The selected Abrahamson & Silva (2008) model is used in four versions with scaling factors (0,

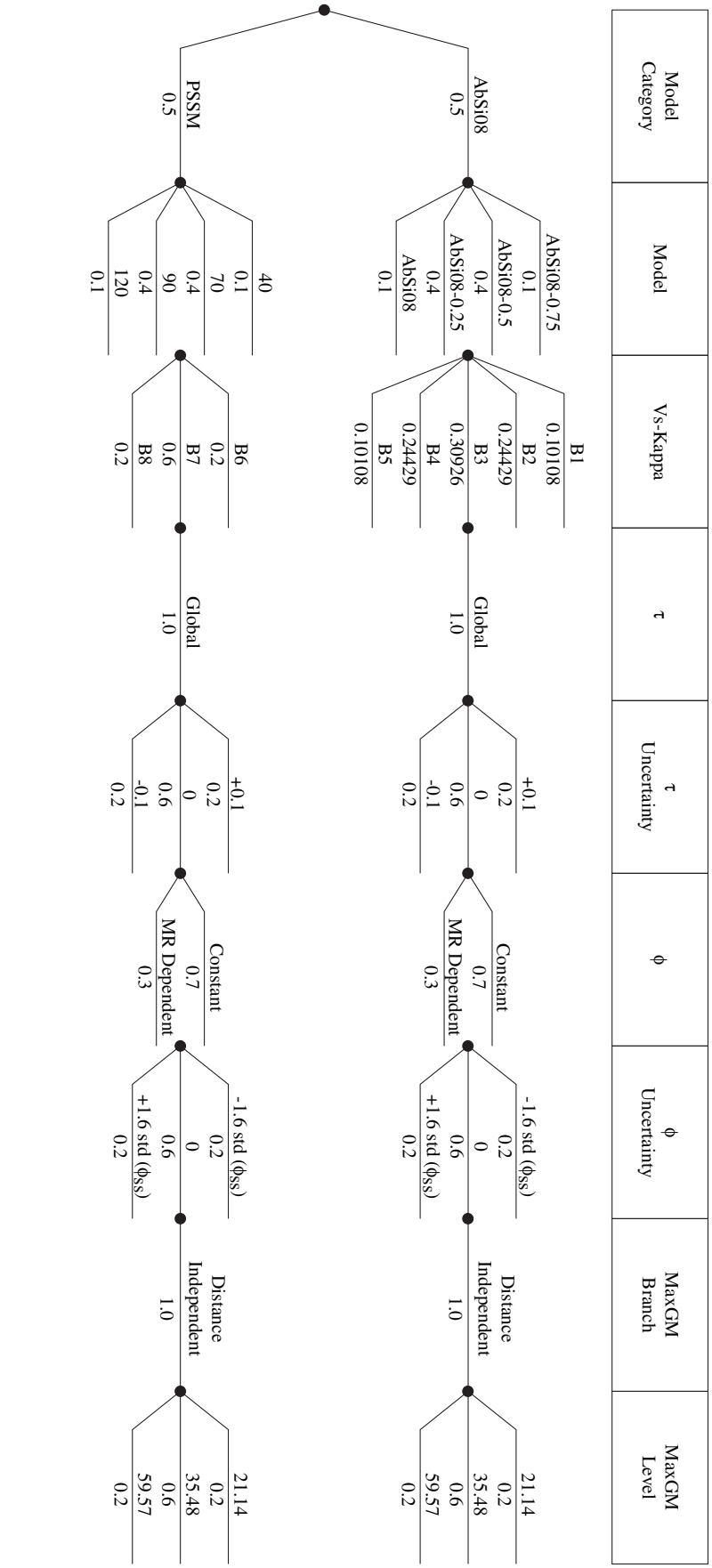

Figure IV-2.1: Logic tree for the horizontal ground motion.

-0.25, -0.50, -0.75) in LN space. Practically, the scaling of the model is introduced through multiplication of the exponent of the given scaling factors with the $V_S - \kappa$ corrections (see Figure IV-2.11). The empirical GMPE gets a total weight of 50% and the Swiss stochastic model a total weight of 50%. For the parametrized Swiss stochastic model (PSSM) the versions with a M_C=4.5 and stress drop values of 40, 70, 90 and 120 bars have been selected.

Table IV-2.1: Weights assigned to the GMPEs.

GMPE	Abbrv.	Weight	Sub-Model	Weight by category
Abrahamson & Silva (2008)	AbSi08	0.50	AbSi08	0.10
Boore & Atkinson (2008)	BoAt08	-	$e^{-0.25}$ · AbSi08	0.40
Campbell & Bozorgnia (2008)	CaBo08	-	$e^{-0.50}$ · AbSi08	0.40
Chiou & Youngs (2008)	ChYo08	-	$e^{-0.75}$ · AbSi08	0.10
Atkinson & Boore (2006)	AtBo06	-	-	
Toro et al. (2002)	Toro02	-	-	
Akkar & Bommer (2010)	AkBo10	-	-	
Akkar & Cagnan (2010)	AkCa10	-	-	
Bindi et al. (2011)	Bind11	-	-	
Zhao et al. (2006)	Zhao06	-	-	
PSSM30		-		-
PSSM40		0.05		0.10
PSSM60		-		-
PSSM70		0.20		0.40
PSSM90		0.20		0.40
PSSM120		0.05		0.10
Sum GMPE		0.50		1.00
Sum PSSM		0.50		1.00

Table IV-2.2 specifies the reference shear wave velocity ($V_{S30,rock}$) to be used for the NGA model. The host-to-target correction is applied to this reference model to account for the hard rock conditions at the Swiss NPP sites.

For the depth to sediment layer with V_S=1.0 km/s and 2.5 km/s at the site, the sediment thickness is defined as the depth to a material (bedrock) with a given shear-wave velocity or greater, starting at the top of the rock, as defined in the site response and not the ground surface. For AbSi08 and ChYo08 the parameter $Z_{1.0}$=0 m for rock sites, as the reference $V_{S,30}$ values of all four NPP sites is greater than 1000 m/s after application of the $V_S - \kappa$ corrections. For CaBo08 $Z_{2.5}$=0.800 km, based on assumed generic conditions of the Swiss region. The GMPE is evaluated with respect to the generic rock condition of 620 m/s and the value for $Z_{2.5}$ needs to be consistent, as the host-to-target correction towards the Swiss conditions (based on a full V_S profile) is applied afterwards.

Table IV-2.2: GMPE specific reference shear wave velocity.

GMPE	Ref. V_{S30} [m/s]
AbSi08	620

2.3 Host-to-target Correction

2.3.1 Host-to-target Correction

The host and target κ values were evaluated according to the PRP reports EXT-TB-1087 [Al Atik and Abrahamson 2012a] and EXT-TN-1233 [Al Atik and Abrahamson 2012b], where the average of different evaluated scenarios is taken. The scenarios are based on M=5, 6, 7 and R_{JB}=5, 10 , 20 km with an average depth of 12 km (which is consistent with the average depth in Switzerland).

The expert specific target κ values are summarized together with their weights in Table IV-2.3. The Figure I-3.10 depicts the generic logic tree which was developed in the course of the PRP and Figure II-2.2 shows the expert specific version. The finally selected parameters and weights are summarized in Table IV-2.4. Applying the given combinations leads to 24 discrete correction functions. The resulting 5-point distribution of $V_S - \kappa$ corrections for the used GMPE is reported in Tables IV-2.5 to IV-2.8. As the resulting distribution is not a known distribution, the evaluated 5 point distribution is based on the approach of Miller and Rice [1983] with the 0.034893, 0.211702, 0.50, 0.788298 and 0.965107 fractiles. The corresponding probabilities/weights for this given discretization are: 0.10108, 0.24429, 0.30926, 0.24429, 0.10108. Tables IV-2.9 and IV-2.10 have the correction functions to be applied to the different versions of the parameterized Swiss stochastic model, depending on the defined target κ per site. The scaling of the response spectrum depends on the shape of the Fourier spectrum. Changes in the frequency content of the Fourier spectrum due to different stress drops leads to differences in the $V_S - \kappa$ scale factors for different stress drops. The Tables IV-2.9 and IV-2.10 illustrate the small numerical differences, but the figures show almost no visible difference between the stress drops.

Table IV-2.3: Target Kappa values for GMPE and PSSM with weights.

	Weight	Mühleberg κ_0 [s]	Beznau κ_0 [s]	Leibstadt κ_0 [s]	Gösgen κ_0 [s]
GMPE					
TK5	0.20	0.017	0.015	0.014	0.0125
TK6	0.60	0.027	0.024	0.022	0.020
TK7	0.20	0.038	0.034	0.031	0.028
PSSM					
TK5	0.20	0.010	0.007	0.006	0.005
TK6	0.60	0.016	0.011	0.010	0.008
TK7	0.20	0.022	0.015	0.014	0.011

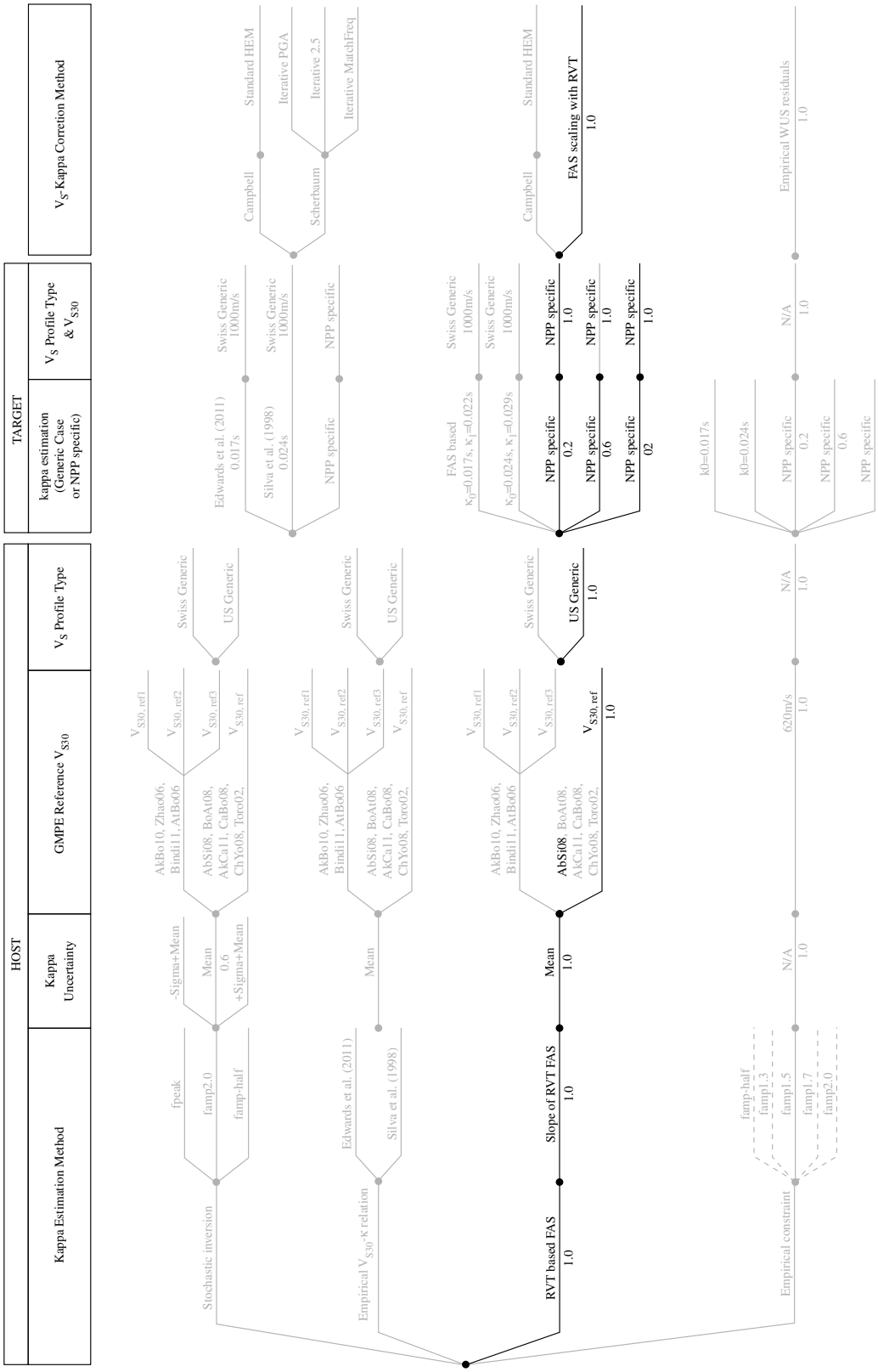

Figure IV-2.2: Logic tree for the evaluation of $V_S - \kappa$ scaling for GMPEs.

Table IV-2.4: Overview of parameters and weights assigned to the $Vs - \kappa$ logic tree for the NGA model.

Estimation Method emethod	**wt.**	**Host** hkest & emethod	κ hostk	**wt.**	**GMPE** AbSi08	**HostVS** vs30est	**wt.**	**Profile** vstypestr	**wt.**	**TargetVS** (npp) targetp	**Target** target TK	**Targ.** κ_0	**Targ.** κ_1 targetk	**wt.**	**Correction Method** cmethod	**wt.**
iRVT	1.00	kBE6	0.0472	1.00	AbSi08	620	1.00	US	1.00	KKB1800	TK5	0.015	0.020	0.20	FAS scaling with iRVT	1.00
											TK6	0.024	0.029	0.60		
											TK7	0.034	0.039	0.20		
										KKG2500	TK5	0.0125	0.017	0.20		
											TK6	0.020	0.025	0.60		
											TK7	0.028	0.033	0.20		
										KKL2200	TK5	0.014	0.019	0.20		
											TK6	0.022	0.027	0.60		
											TK7	0.031	0.036	0.20		
										KKM1100	TK5	0.017	0.022	0.20		
											TK6	0.027	0.032	0.60		
											TK7	0.038	0.043	0.20		

Table IV-2.5: Frequency dependent resulting $V_S - \kappa$ correction 5-point distributions for used GMPEs at Beznau.

GMPE	Frequency [Hz]									Weight
	0.5	1	2.5	5	10	20	33.3	50	100	
AbSi08	0.7795	0.7297	0.6460	0.6202	0.6314	0.6190	0.5716	0.5794	0.5893	0.1011
	0.7834	0.7364	0.6607	0.6482	0.6868	0.7053	0.6252	0.6132	0.6205	0.2443
	0.7936	0.7535	0.6987	0.7205	0.8299	0.9281	0.7635	0.7006	0.7007	0.3093
	0.8032	0.7693	0.7357	0.7964	1.0045	1.2982	1.1126	0.9244	0.8287	0.2443
	0.8069	0.7754	0.7500	0.8258	1.0722	1.4416	1.2479	1.0111	0.8783	0.1011

Table IV-2.6: Frequency dependent resulting $V_S - \kappa$ correction 5-point distributions for used GMPEs at Gösgen.

GMPE	Frequency [Hz]									Weight
	0.5	1	2.5	5	10	20	33.3	50	100	
AbSi08	0.7952	0.7416	0.6224	0.5944	0.6363	0.6705	0.5741	0.5643	0.5722	0.1011
	0.7983	0.7469	0.6336	0.6155	0.6802	0.7492	0.6357	0.5994	0.5992	0.2443
	0.8061	0.7606	0.6626	0.6701	0.7934	0.9523	0.7946	0.6899	0.6690	0.3093
	0.8137	0.7736	0.6916	0.7281	0.9299	1.2683	1.1291	0.9260	0.7849	0.2443
	0.8166	0.7786	0.7028	0.7506	0.9827	1.3907	1.2588	1.0175	0.8298	0.1011

Table IV-2.7: Frequency dependent resulting $V_S - \kappa$ correction 5-point distributions for used GMPEs at Leibstadt.

GMPE	Frequency [Hz]									Weight
	0.5	1	2.5	5	10	20	33.3	50	100	
AbSi08	0.7615	0.7015	0.6107	0.5896	0.6181	0.6262	0.5518	0.5541	0.5630	0.1011
	0.7648	0.7072	0.6231	0.6134	0.6667	0.7075	0.6090	0.5871	0.5914	0.2443
	0.7735	0.7219	0.6553	0.6748	0.7919	0.9175	0.7566	0.6725	0.6647	0.3093
	0.7815	0.7352	0.6860	0.7375	0.9382	1.2412	1.0783	0.8880	0.7786	0.2443
	0.7847	0.7404	0.6980	0.7618	0.9949	1.3666	1.2030	0.9714	0.8228	0.1011

Table IV-2.8: Frequency dependent resulting $V_S - \kappa$ correction 5-point distributions for used GMPEs at Mühleberg.

GMPE	Frequency [Hz]									Weight
	0.5	1	2.5	5	10	20	33.3	50	100	
AbSi08	1.0256	1.0367	0.8738	0.7865	0.7528	0.7249	0.7240	0.7380	0.7529	0.1011
	1.0314	1.0470	0.8957	0.8254	0.8240	0.8225	0.7752	0.7774	0.7910	0.2443
	1.0464	1.0738	0.9521	0.9261	1.0078	1.0744	0.9073	0.8792	0.8894	0.3093
	1.0607	1.0988	1.0081	1.0344	1.2418	1.5264	1.2931	1.1127	1.0444	0.2443
	1.0662	1.1085	1.0298	1.0764	1.3324	1.7016	1.4426	1.2032	1.1045	0.1011

Table IV-2.9: Frequency dependent $V_S - \kappa$ correction for PSSMs at the sites Beznau and Gösgen.

	Beznau			Gösgen		
Weight	0.20	0.60	0.20	0.20	0.60	0.20
Freq. [Hz]	B6 (TK5)	B7 (TK6)	B8 (TK7)	B6 (TK5)	B7 (TK6)	B8 (TK7)
Mc4.5 SD40						
0.5	0.8406	0.8352	0.8298	0.9001	0.8962	0.8921
1	0.7824	0.7726	0.7629	0.7790	0.7719	0.7647
2.5	0.8056	0.7808	0.7569	0.6925	0.6766	0.6610
5	0.8822	0.8300	0.7810	0.7544	0.7206	0.6885
10	1.0212	0.9068	0.8063	0.8985	0.8215	0.7517
20	1.3117	1.0478	0.8442	1.2220	1.0294	0.8709
33.33	1.6217	1.1624	0.8659	1.6101	1.2369	0.9676
50	1.6681	1.1311	0.8486	1.7471	1.2483	0.9441
100	1.2706	0.9701	0.8132	1.3040	0.9789	0.8128
Mc4.5 SD70						
0.5	0.8396	0.8338	0.8281	0.8967	0.8926	0.8883
1	0.7822	0.7723	0.7625	0.7776	0.7705	0.7634
2.5	0.8057	0.7809	0.7569	0.6924	0.6765	0.6609
5	0.8825	0.8301	0.7811	0.7545	0.7206	0.6885
10	1.0218	0.9071	0.8064	0.8990	0.8217	0.7518
20	1.3131	1.0485	0.8446	1.2234	1.0303	0.8713
33.33	1.6266	1.1651	0.8665	1.6151	1.2398	0.9696
50	1.6766	1.1349	0.8493	1.7570	1.2537	0.9468
100	1.2774	0.9729	0.8140	1.3123	0.9828	0.8145
Mc4.5 SD90						
0.5	0.8392	0.8332	0.8273	0.8950	0.8907	0.8864
1	0.7820	0.7721	0.7623	0.7770	0.7699	0.7627
2.5	0.8058	0.7809	0.7569	0.6925	0.6765	0.6609
5	0.8826	0.8302	0.7811	0.7546	0.7207	0.6885
10	1.0220	0.9072	0.8064	0.8991	0.8219	0.7519
20	1.3139	1.0489	0.8444	1.2241	1.0310	0.8716
33.33	1.6288	1.1660	0.8668	1.6174	1.2413	0.9701
50	1.6811	1.1370	0.8498	1.7621	1.2567	0.9482
100	1.2806	0.9743	0.8142	1.3163	0.9846	0.8152
Mc4.5 SD120						
0.5	0.8388	0.8325	0.8263	0.8931	0.8886	0.8841
1	0.7820	0.7719	0.7621	0.7762	0.7691	0.7619
2.5	0.8058	0.7810	0.7569	0.6925	0.6764	0.6608
5	0.8828	0.8303	0.7811	0.7546	0.7207	0.6884
10	1.0222	0.9073	0.8065	0.8993	0.8220	0.7519
20	1.3150	1.0497	0.8447	1.2252	1.0315	0.8722
33.33	1.6319	1.1677	0.8673	1.6207	1.2438	0.9713
50	1.6865	1.1393	0.8504	1.7683	1.2601	0.9500
100	1.2849	0.9760	0.8147	1.3215	0.9872	0.8162

Table IV-2.10: Frequency dependent $V_S - \kappa$ correction for PSSMs at the sites Leibstadt and Mühleberg.

	Leibstadt			Mühleberg		
Weight	0.20	0.60	0.20	0.20	0.60	0.20
Freq. [Hz]	B6 (TK5)	B7 (TK6)	B8 (TK7)	B6 (TK5)	B7 (TK6)	B8 (TK7)
Mc4.5 SD40						
0.5	0.8132	0.8081	0.8030	1.31399	1.30163	1.28929
1	0.7298	0.7207	0.7117	1.25257	1.22917	1.20615
2.5	0.7285	0.7061	0.6846	1.00714	0.96148	0.91821
5	0.8002	0.7527	0.7083	1.07592	0.98237	0.89749
10	0.9394	0.8339	0.7413	1.16626	0.97843	0.82412
20	1.2411	0.9897	0.7958	1.40905	1.02089	0.75858
33.33	1.5822	1.1253	0.8304	1.60719	1.03815	0.74257
50	1.6690	1.1043	0.8095	1.57814	1.02997	0.79258
100	1.2506	0.9184	0.7580	1.31753	1.01298	0.84895
Mc4.5 SD70						
0.5	0.8114	0.8059	0.8006	1.31067	1.29785	1.28501
1	0.7293	0.7201	0.7111	1.25107	1.22788	1.20477
2.5	0.7286	0.7062	0.6845	1.00678	0.96114	0.91764
5	0.8004	0.7529	0.7084	1.07598	0.98218	0.89724
10	0.9399	0.8342	0.7414	1.16644	0.97830	0.82360
20	1.2426	0.9906	0.7960	1.40996	1.02076	0.75743
33.33	1.5871	1.1277	0.8310	1.61047	1.03782	0.73990
50	1.6783	1.1085	0.8106	1.58362	1.02970	0.78904
100	1.2580	0.9214	0.7588	1.32104	1.01221	0.84596
Mc4.5 SD90						
0.5	0.8106	0.8049	0.7994	1.30894	1.29583	1.28269
1	0.7291	0.7200	0.7108	1.25050	1.22704	1.20408
2.5	0.7286	0.7062	0.6845	1.00667	0.96098	0.91742
5	0.8005	0.7529	0.7084	1.07602	0.98214	0.89705
10	0.9402	0.8343	0.7414	1.16654	0.97817	0.82334
20	1.2432	0.9910	0.7962	1.41038	1.02046	0.75673
33.33	1.5893	1.1292	0.8314	1.61250	1.03776	0.73857
50	1.6828	1.1106	0.8113	1.58644	1.02964	0.78745
100	1.2616	0.9228	0.7591	1.32253	1.01167	0.84435
Mc4.5 SD120						
0.5	0.8097	0.8038	0.7980	1.30688	1.29328	1.27978
1	0.7288	0.7196	0.7105	1.24948	1.22618	1.20304
2.5	0.7287	0.7062	0.6845	1.00657	0.96073	0.91716
5	0.8006	0.7530	0.7084	1.07607	0.98205	0.89685
10	0.9403	0.8344	0.7415	1.16663	0.97806	0.82296
20	1.2443	0.9916	0.7964	1.41133	1.02054	0.75617
33.33	1.5926	1.1307	0.8320	1.61441	1.03776	0.73708
50	1.6885	1.1132	0.8120	1.58986	1.02961	0.78544
100	1.2663	0.9246	0.7596	1.32478	1.01130	0.84265

Figures IV-2.3 to IV-2.6 show the five discrete correction functions versus frequency for the GMPE per site. Figures with all individual correction functions resulting from all combinations and color coded by their weight can be found in the appendix to the HID (Chapter 3). Furthermore, the individual histograms, selected 5-point distributions and a theoretically fitted distribution are also shown in the appendix. Figures IV-2.7 to IV-2.10 shows the different $V_S - \kappa$ corrections to be applied to the generic parameterized Swiss stochastic model in order to be applicable for the given site specific NPP conditions.

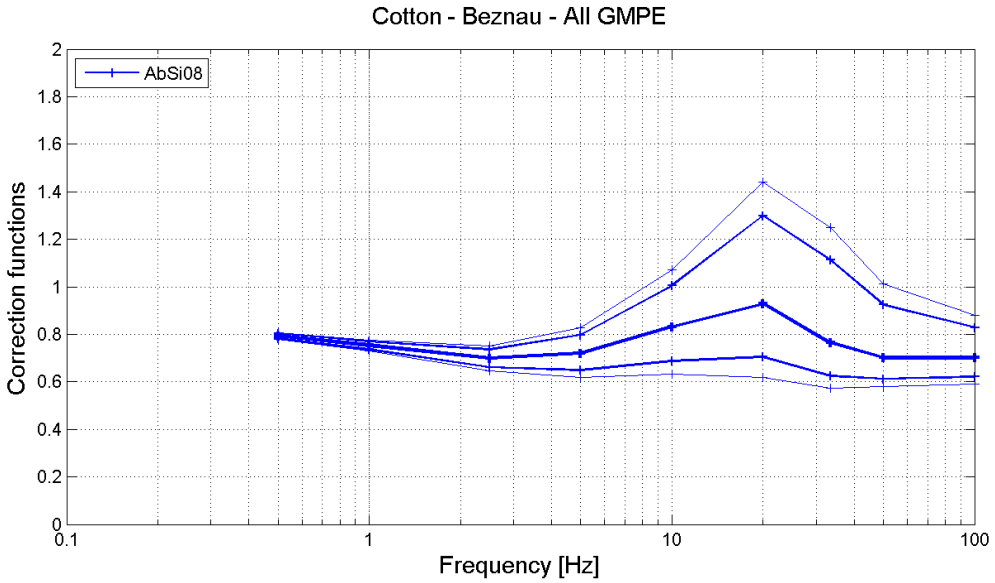

Figure IV-2.3: $V_S - \kappa$ corrections to be applied to the GMPE for Beznau.

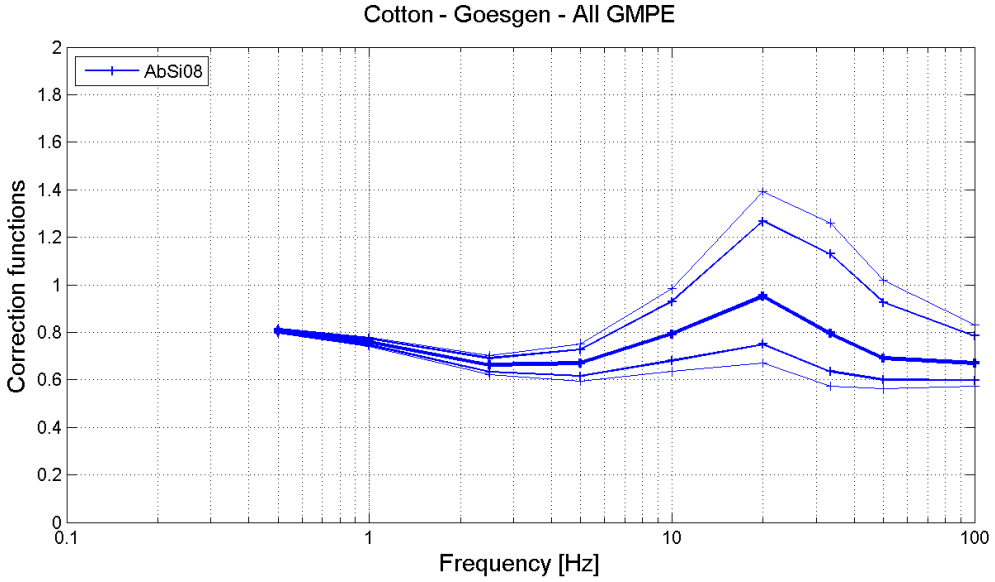

Figure IV-2.4: $V_S - \kappa$ corrections to be applied to the GMPE for Gösgen.

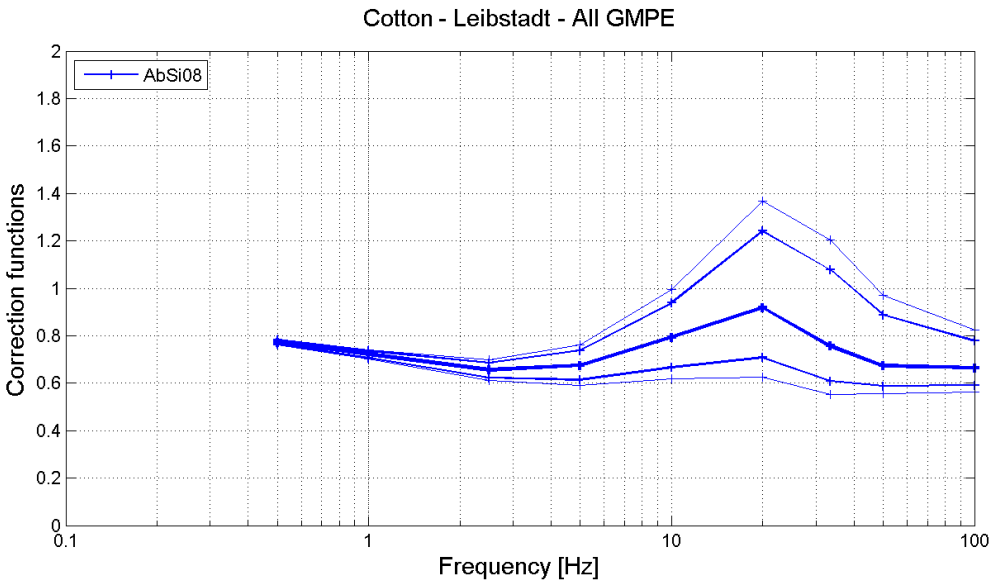

Figure IV-2.5: $V_S - \kappa$ corrections to be applied to the GMPE for Leibstadt.

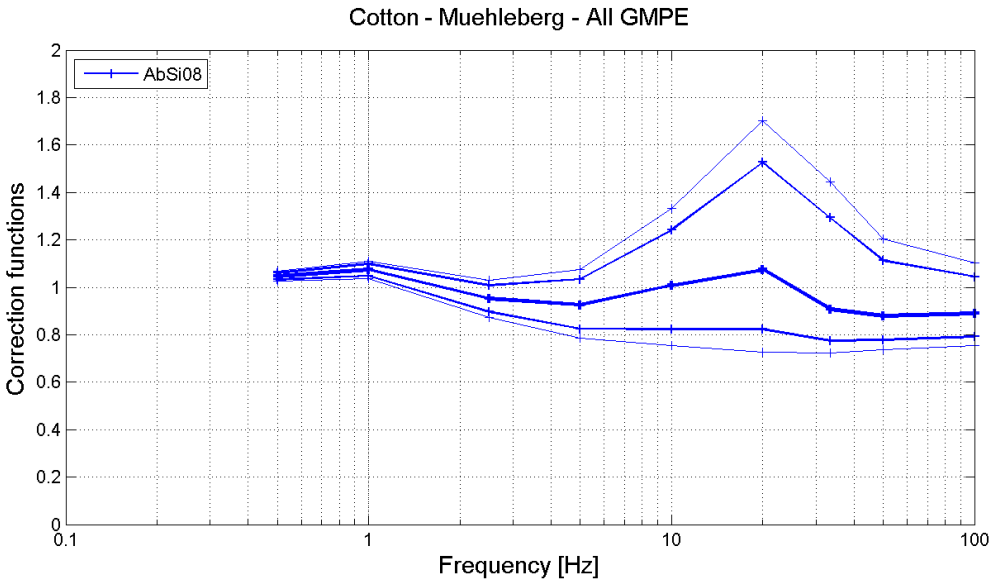

Figure IV-2.6: $V_S - \kappa$ corrections to be applied to the GMPE for Mühleberg.

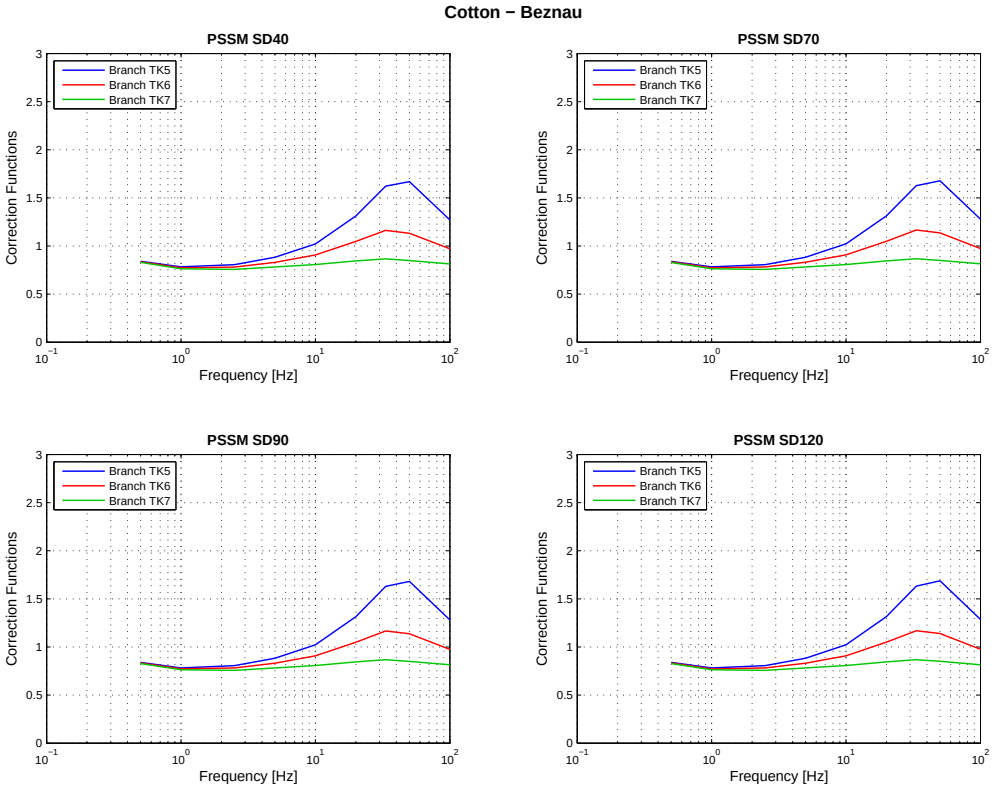

Figure IV-2.7: $V_S - \kappa$ corrections to be applied to the PSSMs for Beznau.

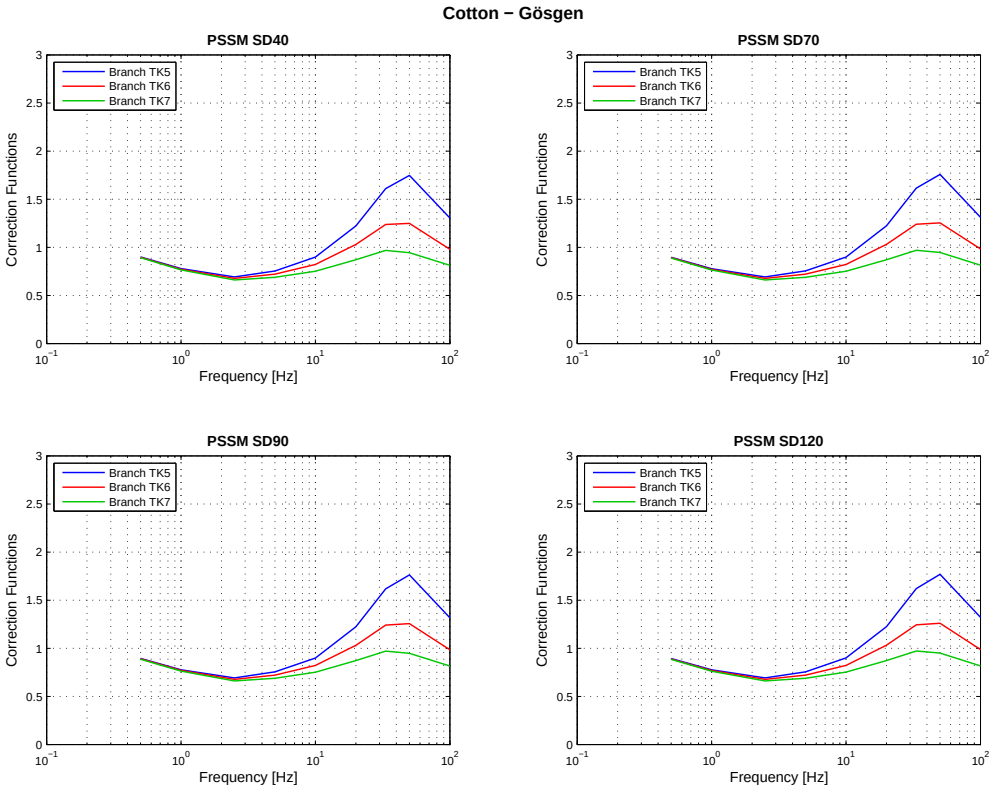

Figure IV-2.8: $V_S - \kappa$ corrections to be applied to the PSSMs for Gösgen.

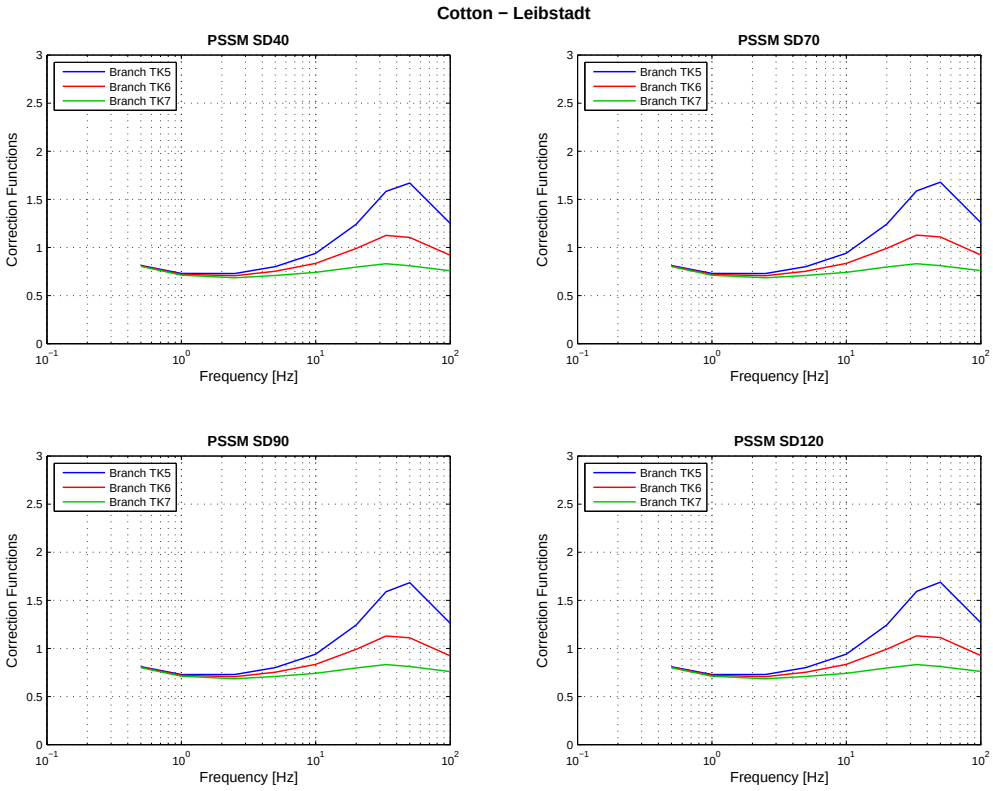

Figure IV-2.9: $V_S - \kappa$ corrections to be applied to the PSSMs for Leibstadt.

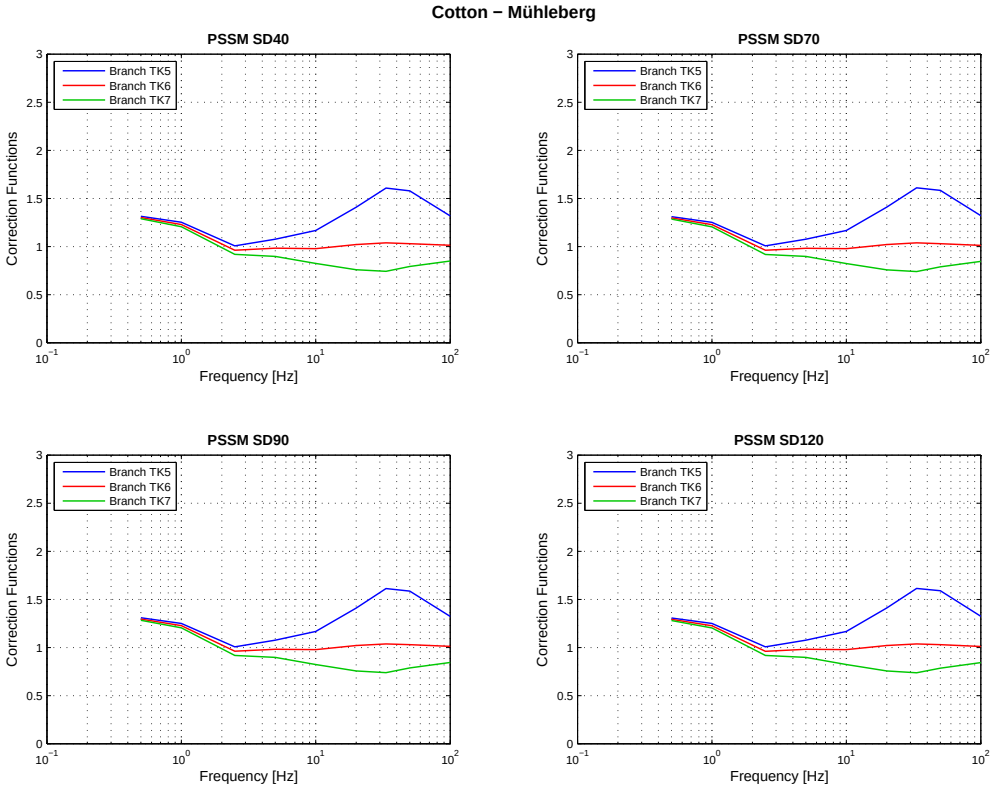

Figure IV-2.10: $V_S - \kappa$ corrections to be applied to the PSSMs for Mühleberg.

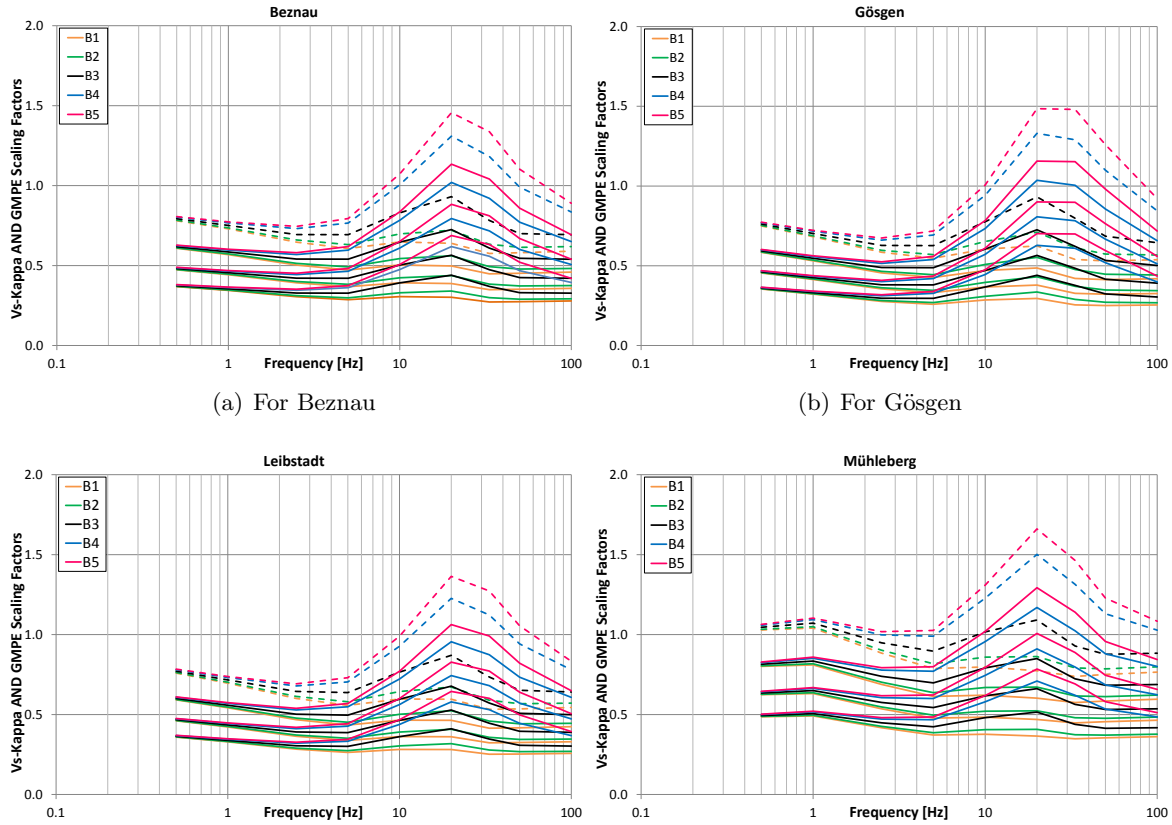

(a) For Beznau

(b) For Gösgen

(c) For Leibstadt

(d) For Mühleberg

Figure IV-2.11: Combined $V_S - \kappa$ corrections and scaling factors for the AbSi08 model for the resulting 5-point distribution (color-coded as B1 to B5). The dashed lines show the unscaled AbSi08 model with its five corrections and the solid lines represent the three scaled versions with factors of -0.25, -0.50 and -0.75, respectively.

2.3.2 Small Magnitude Adjustments

For the evaluation of the GMPE specific small magnitude adjustments only the median $V_S - \kappa$ correction factors of all the provided 5-point distributions are used, as it was decided that the small magnitude adjustments will only be developed for the average case and not for each individual correction function (PMT-TN-1238). Thus, the small magnitude adjustments are the same for all experts, but repeated here in Table IV-2.11 for the sake of completeness and illustrated in Figure IV-2.12 and IV-2.13.

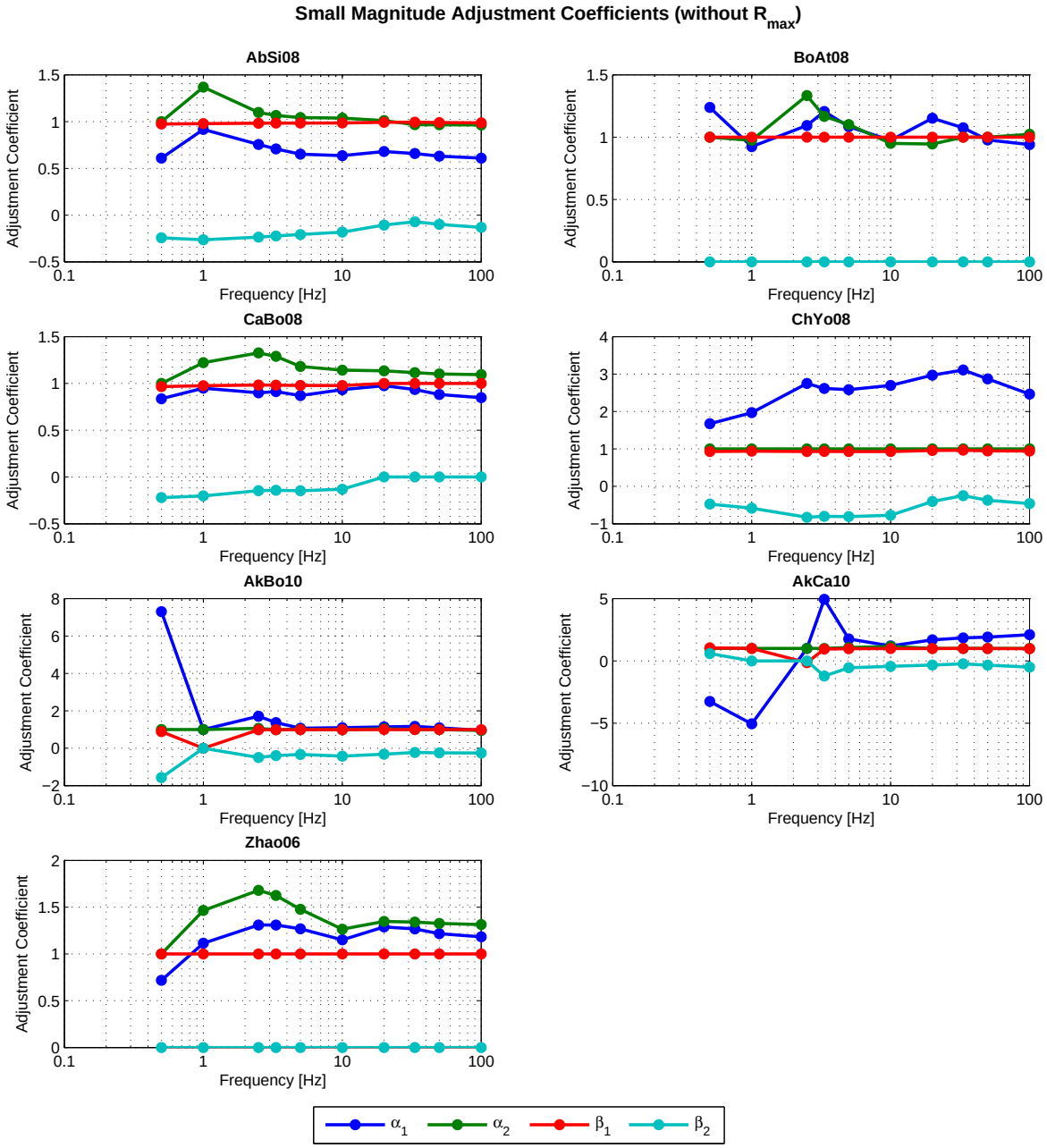

Figure IV-2.12: Small magnitude adjustments coefficients as function of frequency for the all GMPEs.

Table IV-2.11: Small magnitude adjustments coefficients.

	Abrahamson & Silva (2008)					Boore & Atkinson (2008)				
T [s]	α_1	α_2	β_1	β_2	R_{max}	α_1	α_2	β_1	β_2	R_{max}
0.01	0.609036	0.964257	0.986605	-0.131781	3.57E+04	0.940502	1.022616	1.000000	0.000000	1.00E+09
0.02	0.629604	0.965329	0.988756	-0.099660	4.07E+05	0.977300	1.000000	1.000000	0.000000	1.00E+09
0.03	0.657761	0.967357	0.993601	-0.071271	2.27E+07	1.074586	1.000000	1.000000	0.000000	1.00E+09
0.05	0.679706	1.010904	0.991680	-0.106456	2.22E+05	1.151448	0.945013	1.000000	0.000000	1.00E+09
0.1	0.635927	1.037980	0.984796	-0.182620	4.40E+03	0.974222	0.950274	1.000000	0.000000	1.00E+09
0.2	0.651637	1.043100	0.984107	-0.207141	2.31E+03	1.084848	1.101550	1.000000	0.000000	1.00E+09
0.3	0.707216	1.065147	0.983422	-0.222960	1.65E+03	1.205896	1.166359	1.000000	0.000000	1.00E+09
0.4	0.755898	1.097644	0.982712	-0.236174	1.28E+03	1.093478	1.334035	1.000000	0.000000	1.00E+09
1	0.915893	1.367623	0.978436	-0.263900	8.15E+02	0.924116	0.974715	1.000000	0.000000	1.00E+09
2	0.608779	1.000000	0.974376	-0.242967	1.10E+03	1.238186	1.000000	1.000000	0.000000	1.00E+09

	Campbell & Bozorgnia (2008)					Chiou & Youngs (2008)				
T [s]	α_1	α_2	β_1	β_2	R_{max}	α_1	α_2	β_1	β_2	R_{max}
0.01	0.847179	1.094261	1.000000	0.000000	1.00E+09	2.462946	1.000000	0.944935	-0.458418	1.57E+02
0.02	0.881357	1.100586	1.000000	0.000000	1.00E+09	2.873730	1.000000	0.946856	-0.372663	2.54E+02
0.03	0.934893	1.114376	1.000000	0.000000	1.00E+09	3.109735	1.000000	0.966292	-0.248344	9.79E+02
0.05	0.976058	1.135405	1.000000	0.000000	1.00E+09	2.969316	1.000000	0.959155	-0.402534	2.17E+02
0.1	0.932945	1.141482	0.977278	-0.130765	3.52E+04	2.695695	1.000000	0.930247	-0.772189	6.67E+01
0.2	0.870681	1.181271	0.979148	-0.147509	1.53E+04	2.584716	1.000000	0.931449	-0.809059	6.32E+01
0.3	0.912008	1.289225	0.981219	-0.142015	2.00E+04	2.614341	1.000000	0.932936	-0.801818	6.40E+01
0.4	0.899165	1.326194	0.982502	-0.145844	1.69E+04	2.750116	1.000000	0.930586	-0.824968	6.18E+01
1	0.949262	1.221818	0.975229	-0.202856	2.45E+03	1.966745	1.000000	0.939658	-0.583454	1.00E+02
2	0.835687	1.000000	0.965445	-0.220424	1.60E+03	1.671214	1.000000	0.931415	-0.473294	1.43E+02

	Akkar & Bommer (2010)					Akkar & Cagnan (2010)				
T [s]	α_1	α_2	β_1	β_2	R_{max}	α_1	α_2	β_1	β_2	R_{max}
0.01	0.956934	0.949129	0.992409	-0.258327	9.32E+02	2.098964	1.000000	0.985549	-0.499646	1.44E+02
0.02	1.090919	1.000000	0.994584	-0.253021	1.02E+03	1.913122	1.000000	0.990459	-0.335515	3.83E+02
0.03	1.164927	1.000000	0.998788	-0.230673	1.52E+03	1.851248	1.000000	0.997570	-0.236164	1.37E+03
0.05	1.134080	1.040216	0.995602	-0.321814	4.41E+02	1.689890	1.000000	0.995553	-0.333705	3.95E+02
0.1	1.093536	0.986668	0.988564	-0.425342	2.04E+02	1.204350	1.157951	0.987542	-0.431630	1.97E+02
0.2	1.068203	1.007264	0.988710	-0.334035	3.86E+02	1.759524	1.071974	0.978784	-0.546911	1.20E+02
0.3	1.369695	0.988071	0.987967	-0.400250	2.36E+02	4.937988	1.000000	0.951557	-1.213879	4.38E+01
0.4	1.710275	1.062132	0.984888	-0.499538	1.44E+02	1.000000	1.000000	-0.142956	0.000000	1.99E+01
1	1.000000	1.000000	0.000000	0.000000	1.00E+09	-5.048030	1.000000	1.000000	0.000000	1.99E+01
2	7.299540	1.000000	0.881761	-1.575579	3.50E+01	-3.254365	1.000000	1.044931	0.593817	1.00E+09

	Zhao et al. (2006)				
T [s]	α_1	α_2	β_1	β_2	R_{max}
0.01	1.182482	1.313722	1.000000	0.000000	1.00E+09
0.02	1.217249	1.326714	1.000000	0.000000	1.00E+09
0.03	1.267071	1.340177	1.000000	0.000000	1.00E+09
0.05	1.288501	1.347281	1.000000	0.000000	1.00E+09
0.1	1.150978	1.265212	1.000000	0.000000	1.00E+09
0.2	1.268576	1.476775	1.000000	0.000000	1.00E+09
0.3	1.310229	1.625552	1.000000	0.000000	1.00E+09
0.4	1.308962	1.679158	1.000000	0.000000	1.00E+09
1	1.113543	1.465133	1.000000	0.000000	1.00E+09
2	0.718525	1.000000	1.000000	0.000000	1.00E+09

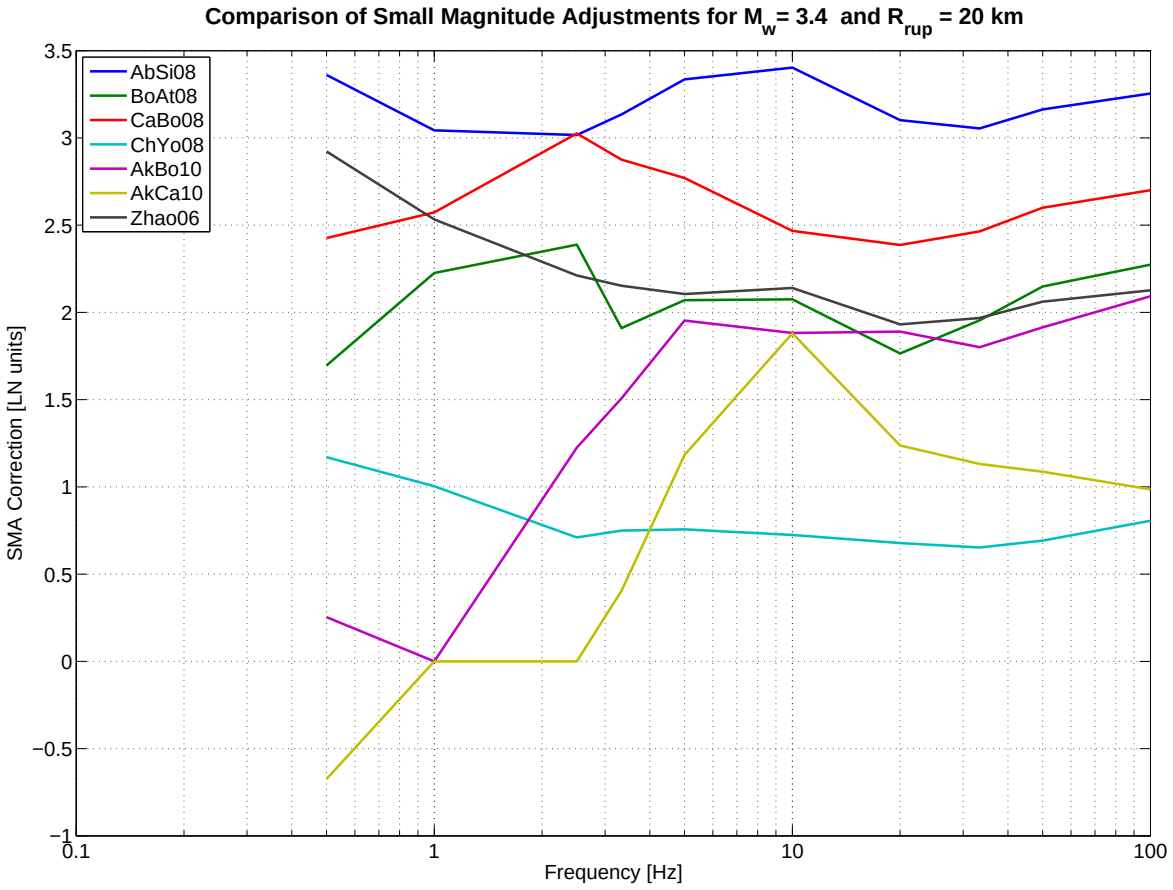

Figure IV-2.13: Comparison of the resulting small magnitude adjustments functions as function of frequency for M=3.4 and R=20 km.

2.4 Aleatory Variability for the Horizontal Component

Section 6.7 in Part I, provides the final τ and ϕ models used for the PRP, which supersede the model of Rodriguez-Marek and Cotton [2011] (equations 4.1, 4.2 and table 5.3 and 5.4 in EXT-TB-1058) and Rodriguez-Marek [2012] (EXT-TN-1225). In Table IV-2.12 the different weights for the aleatory variability logic tree branches are shown. The selected values for the ϕ_{SS} uncertainty are given in the second column at the bottom. The generic σ logic tree is represented in Figure I-9.2.

Table IV-2.12: Weights and parameters assigned to the aleatory variability.

Model	Branch / Value for $\sigma(\phi_{SS})$	Weight
τ Model	Global	1.00
	Original GMPE	-
τ Uncert.	+0.1	0.20
	0	0.60
	-0.1	0.20
ϕ_{SS}	Model 1 (Constant)	0.70
	Model 2 (Distance Dependent)	-
	Model 3 (Dist. and Mag. Dependent)	0.30
ϕ_{SS} Uncert.	$-1.6 \cdot \sigma(\phi_{SS})$	0.20
	$0 \cdot \sigma(\phi_{SS})$	0.60
	$+1.6 \cdot \sigma(\phi_{SS})$	0.20
$\sigma(\phi_{SS})$	0.08	1.00

2.5 Maximum Ground Motion

Table IV-2.13 shows that no frequency dependent weights are assigned to the horizontal maximum ground motion logic tree (see generic Figure I-9.3). The weights assigned to the six scaling factors for the six branches are given in Table IV-2.14.

Table IV-2.13: Weights for the horizontal maximum ground motion model.

Model	Frequency [Hz]								
	0.5	1	2.5	5	10	20	33.3	50	100
R-dependent	-	-	-	-	-	-	-	-	-
R-independent	1.00	1.00	1.00	1.00	1.00	1.00	1.00	1.00	1.00

The vertical maximum ground motion model is the same as the horizontal (see Figure I-9.3). Thus, the same weights and scale factors apply for the vertical hazard.

Based on the hazard feedback, which showed very little impact of the maximum ground motion truncation for rock, the project has decided to trim the maximum ground motion

Table IV-2.14: Weights for the scaling factors for the maximum ground motion model (both horizontal and vertical).

Model	Scale Factors [LN units]					
	7.50	12.59	21.14	35.48	59.57	100
R-dependent	-	-	-	-	-	-
R-independent	0	0	0.20	0.60	0.20	0

branches for the practical implementation. Thus, the hazard will be computed based on untruncated ground motions for rock.

2.6 V/H Ratio

Table IV-2.15 shows the weights of the candidate V/H models. No NPP site specific weights were assigned. This implies for the site of Gösgen to use the "shallow" case defined by the ratio based on the merged profiles 4-5 (see TP3-ASW-1004). The basic logic tree for the V/H models can be found in Figure I-9.4.

Table IV-2.15: Weights for median V/H models.

Model	Weight
Bommer et al. (2011)	-
Campbell and Bozorgnia (2003)	-
Gülerce and Abrahamson (2011)	0.20
Edwards et al. (2011) without correction above 7 Hz	0.20
Edwards et al. (2011) with correction above 7 Hz	0.20
US West Median	0.20
US East Median	0.20

2.7 Aleatory Variability for the Vertical Component

The additional aleatory variability to be added to the median V/H models is shown in Table IV-2.16 (see Figure I-9.2 for the generic logic tree). For the missing values of method 2, values have been provided to fill the table. The missing values for 2.5 and 5 Hz were obtained through linear interpolation in the log(frequency) $-\sigma_{VADD}$ space. In the case of the values marked with 0* the only model left was used, which leads to the discontinuities shown in the figure below.

Table IV-2.16: Additional vertical variability (σ_{VADD} in LN units).

Frequency [Hz]								
0.5	1	2.5	5	10	20	33.3	50	100
0.141	0.118	0.176*	0.219*	0.263	0.314	0.312	0.242	0.229

* Based on interpolated values. σ_{VADD} values of zero are discarded in the weighted average.

Figure IV-2.14 shows the additional aleatory variability for the vertical component over frequency.

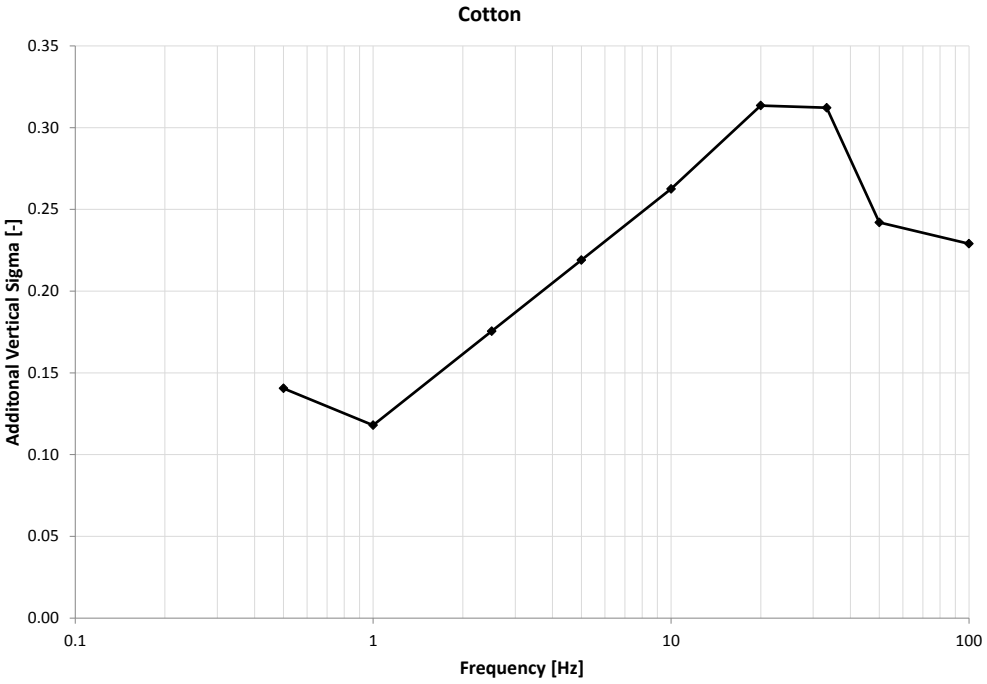

Figure IV-2.14: Additional aleatory variability for the vertical component.

2.8 Implementation of Hazard Logic Tree

The total number of logic tree branches amounts to 1728 (see Figure IV-2.1). Each individual combination of zonation alternatives and source parameters in each individual SP1 source has to be combined with these 1728 alternative ground motion models. Among other such measures, the project decided to reduce the huge number of combinations and thus, the CPU time necessary to obtain the rock hazard results by removing the maximum ground motion truncation from the SP2 models. This section documents the effect of this project management decision.

For the hazard computation we used one of the four SP1 Expert Group models, EG1c, with its entire complexity. We performed the calculation for one site only, Beznau, as we know the effect of the maximum ground motion truncation to be largely site independent and for 5 Hz spectral acceleration as the effect of the maximum ground motion truncation has been shown to be the highest for this frequency (see TP4-RF-1441). Figure IV-2.15 shows the comparison for the mean hazard and four fractiles.

This conversion of the original "scientific logic tree" to a dealable "hazard logic tree" has been introduced in the framework of the PRP in order to allow for efficient computation without tradeoffs for the overall model in key elements of the initial logic tree.

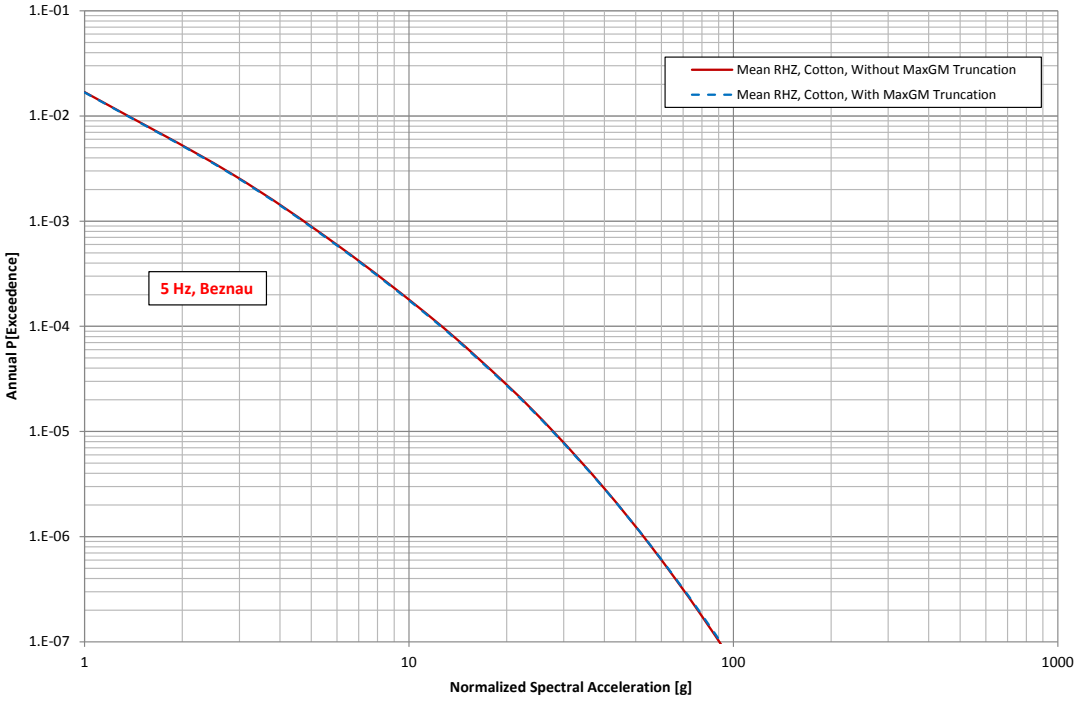

Figure IV-2.15: Effect of the removal of the maximum ground motion truncation in the logic tree on the rock hazard for Beznau.

Chapter 3

Appendix to EG1-HID-1011

The procedure to retrieve the discrete 5-point distributions for the $V_S - \kappa$ corrections is visualized by means of 3 figure types:

- XY graph showing all correction function versus frequency with curve colors indicating the curve weights (see example Figure IV-3.1)
- Plot of the probability distributions (cumulative weights) of $V_S - \kappa$ corrections at the 9 PRP frequencies (see example Figure IV-3.2)
- Corresponding plot of the probability density of $V_S\kappa$ at the 9 analysis frequencies (see example Figure IV-3.3)

which are attached as an electronic appendix to this HID and contains folders/files (or ZIP files), which correspond to the above listed figure types. Figures within above folders are provided as individual PNG and/or EPS files, where the individual files are named according to the convention and example as follows:
<expert>_<site>_<gmpe>_<figure-type>.<graphic-format>
`Cotton_Beznau_AbSi08_fig1.png`

A direct link to files containing a compilation of all figures per site is given here:

- Open external file: $V_S - \kappa$ correction functions for Beznau and associated cumulative probability functions and probability density functions.
- Open external file: $V_S - \kappa$ correction functions for Gösgen and associated cumulative probability functions and probability density functions.
- Open external file: $V_S - \kappa$ correction functions for Leibstadt and associated cumulative probability functions and probability density functions.
- Open external file: $V_S - \kappa$ correction functions for Mühleberg and associated cumulative probability functions and probability density functions.

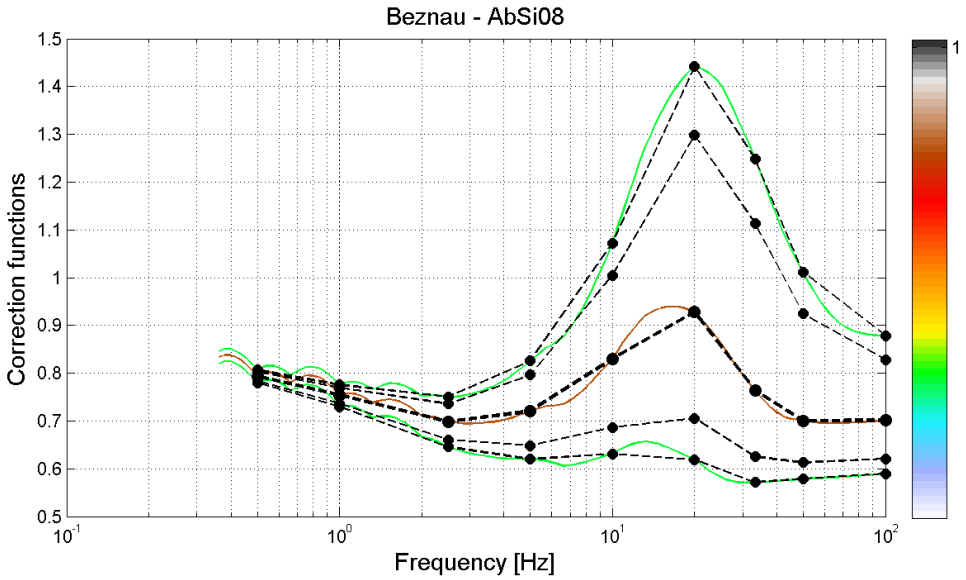

Figure IV-3.1: Evaluated $V_S - \kappa$ correction functions for Abrahamson & Silva (2008) at the site of Beznau and the final 5 discrete correction functions in black dashed lines. The weights of the individual correction functions are color coded according to the scale on the right.

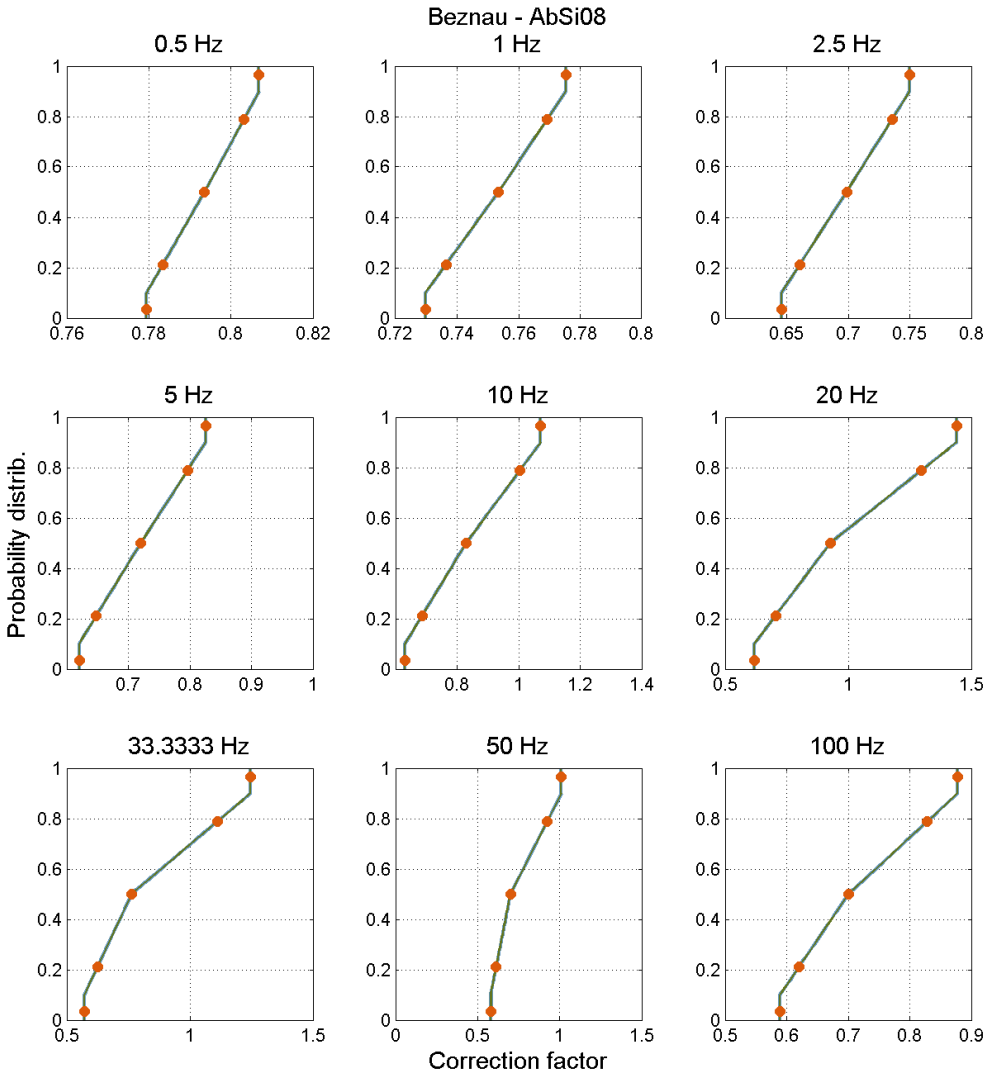

Figure IV-3.2: Probability distributions (cumulative weights) of $V_S - \kappa$ corrections at the 9 PRP frequencies for Abrahamson & Silva (2008) at the site of Beznau. The blue line represents the data by means of 105 fractiles. The thin green line is a smoothed version of above blue line (just for display, not used for further processing). The orange dots are the 3.4893, 21.1702, 50, 78.8298 and 96.5107 % percentiles used for the 5-point distribution.

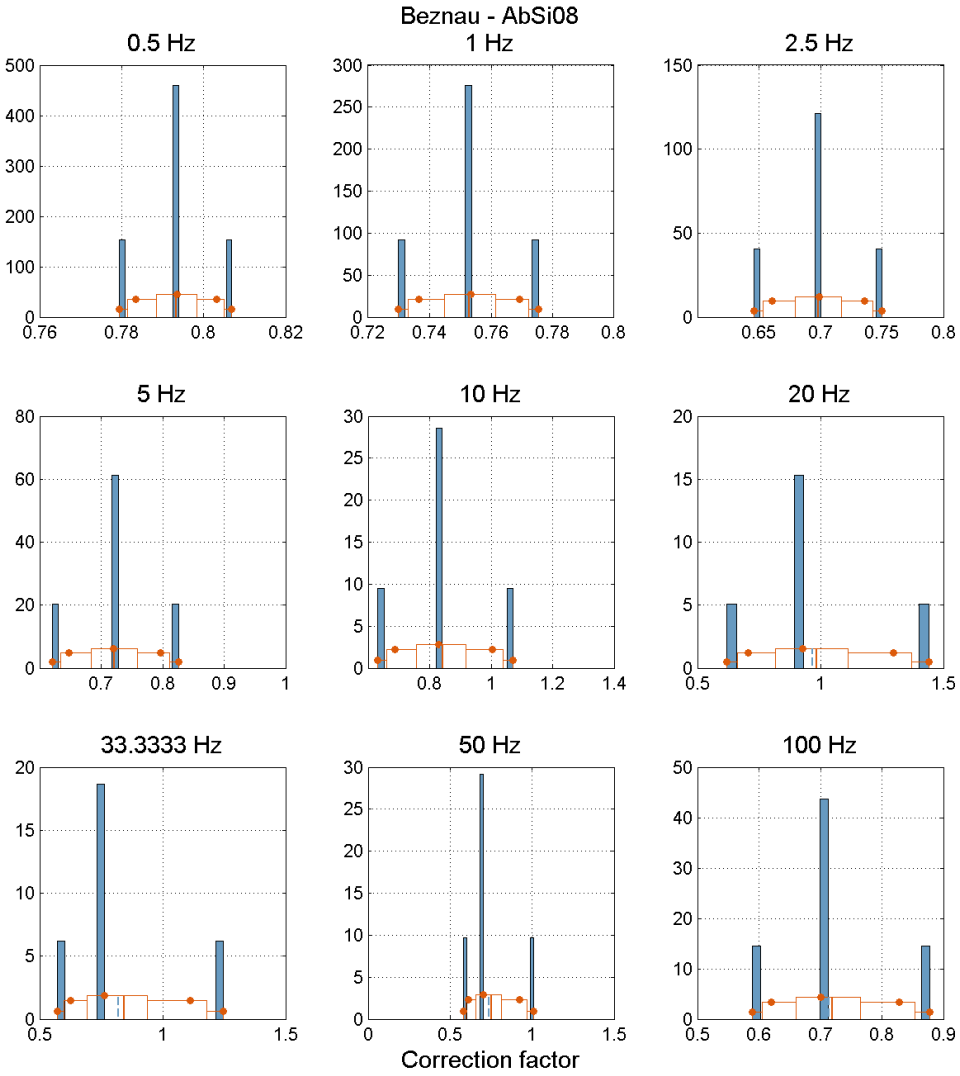

Figure IV-3.3: Probability density functions of $V_S - \kappa$ corrections at the 9 PRP frequencies for Abrahamson & Silva (2008) at the site of Beznau. The blue bars represent the weighted histogram of the data partitioned into 21 bins. The orange dots are the corresponding discrete 5 distribution points for the 3.4893, 21.1702, 50, 78.8298 and 96.5107 % percentiles, as in Figure IV-3.2. The corresponding probabilities/weights are for the given discretization: 0.10108, 0.24429, 0.30926, 0.24429, 0.10108. The thin red and thin dashed blue line in the middle show the mean value of the data and the approximation with the 5-point distribution, respectively. Note that in the case of the thin dashed blue and red line being identical, only the red line is seen as it is on top of the blue line.

Chapter 4

QA-Certificate EG2-QC-1062

QA Certificate	PEGASOS REFINEMENT PROJECT
EG2-QC-1062	

Hazard Input Document (HID)

Expert group:	**EG2**	***HID designation:***	**EG2-HID-1011**
Expert:	F. Cotton	***Expert Model (EXM)***	EG2-EXM-1011

HID parameterisation of Expert Model:

TFI: N. A. Abrahamson ***Hazard Input Specialist of TFI-team:*** Ph. Roth

HID based on Elicitation Documents: ☒ EG2-ES-1020

HID based on Exp. Assessments (EXA): ☒ EG2-EXA-1017 to 1031

Remarks on the HID model parameterisation in terms of hazard computation input:

The undersigned Hazard Input Specialist confirms that this HID includes all required (subproject specific) input information for hazard computations. No further interpretations of this input will be required and no simplifications except Algorithmic Pinching according to paragraph 2.9 of the QA-Guidelines will be applied to convert this HID into hazard software Input Files.

Signature:

HID acceptance by the Expert / Expert Group:

Date of HID review by the Expert / Expert group: 20.11.2013

HID accepted: ☒ ***HID not accepted:*** ☐

Reasons for non-acceptance of HID / Recommendations:

The undersigned Expert(s) accept(s) the parameterisation proposed in this HID as a faithful and adequate representation of his/their Expert Model. He/they confirm(s) that this HID is free of errors and agree(s) to its use as hazard computation input.

Signature Expert 1 / Expert: F. Cotton

Signature Expert 2:

Signature Expert 3:

Part V

Assessments of D. Fäh

Chapter 1

Evaluation Summary (EG2-ES-1021) of D. Fäh

This evaluation summary is the result of evaluations and discussions performed throughout the PRP, and provides the underlying reasoning for the selection of final models and weights. During this evaluation process, different sets of data, models, and methods proposed by the technical community have been considered. The integration of the available information into the proposed models and weights are furthermore aimed so as to represent the centre, body, and range of a technically defensible interpretation.

1.1 Assignment of Weights to the Proposed GMPEs

The selected ground motion prediction equations (GMPEs) of the GMP group and the extension of the Swiss stochastic model are given in Table V-1.1. These models are proposed in the PRP procedure to assess ground motion at given moment magnitude and distance. The equations originally proposed by SP2 are published in Abrahamson and Silva [2008](AbSi08), Akkar and Bommer [2010] (AkBo10), Atkinson [2006] (AtBo06), Boore and Atkinson [2008] (BoAt08), Campbell and Bozorgnia [2008] (CaBo08), Chiou and Youngs [2008b] (ChYo08), Toro et al. [1997] (Toroal), Zhao et al. [2006] (Zhaoal), and are hereinafter named according to the authors. The extension of the Swiss stochastic model refers here to the best models in terms of the scaling parameters Mc, different stress drops, and Reff that explain the Swiss intensity data as well as recorded ground motion on rock sites. During the SP2 workshop in August 2011, additional models were included for consideration in the logic tree. While Atkinson and Boore [2011] and Chiou et al. [2010] correspond to updates of their models, the GMPE proposed by Faccioli et al. [2010] was dropped by the TFI due to its magnitude scaling behavior above Mw 7.0. The models by Campbell [2003] and Pezeshk et al. [2011] are full hybrid models derived for stable continental regions. These two models apply the standard $V_S - \kappa$ adjustment that suffers from the drawback that it introduces a large bias at high frequency, as independently outlined by K. Campbell and F. Scherbaum during the SP2 workshop in August 2011. Such host-to-target adjusted models should, therefore not be readjusted to the NPP conditions because the existing bias would be propagated into the

ground motion at high frequency. Without further considerations, these two hybrid methods are excluded. Finally, two additional regional models were included in the logic tree for evaluation because these recent models meet the condition defined by SP2 for evaluation in the PRP process: these are the empirical models of Akkar and Cagnan [2010] (AkCa10) and Bindi et al. [2011] (Bial11).

In principle, the selected GMPEs are all considered to be valid for use in the PRP procedure. However, none of the models represents the true and only correct ground motion prediction equation. They are simply a projection of available data into a model. The appropriateness of the model varies with frequency, magnitude and distance, and is different for each GMPE. The tectonic setting is not taken into account in the assessment of weights. It seems unclear whether the Swiss region can be classed as active or stable continental. Despite many experts considering it to be stable continental, the derived stress drops in the extended Swiss stochastic model and the observations with instrumental data clearly indicate an active condition. As outlined further on, no weight is given to models from the stable continental regions due to several reasons that are explained later in this report.

For all empirical GMPEs the most reliable reference velocity profiles needs to be defined. The profiles are described in the logic tree and model overview [Abrahamson 2012a] (TP2-TB-1081). For the NGA models, the reference profile selected for implementation in the logic tree is the profile with the lowest value of 620 m/s for V_{S30} (labeled "Ref1" in Abrahamson [2012a], TP2-TB-1081) where the bulk of data is expected. An important issue for this selection refers to the κ that does not scale with V_{S30}, causing an inconsistent value for the reference profiles with V_{S30} of 800 m/s and 1000 m/s in the NGA models. For the GMPEs that use soil classes, V_{S30} is not a model parameter and must be estimated. For these GMPEs, the profile "Ref2" (Abrahamson [2012a], TP2-TB-1081) is always taken, which for the Zhaoal class I model is a V_{S30} of 700 m/s, and for the AkBo10 rock class model is a V_{S30} of 800 m/s. The models AkCa11 and Bial11 were given zero weight as outlined below and, therefore, do not need a selection of the V_S reference.

The same logic tree is used for all NPP sites. The original GMPEs are adjusted to V_{S30} and κ for rock at the NPP site, according to the alternative candidate procedures identified by the SP2 group. Each GMPE is assumed to have its own range of host κ values. The following issues are discussed in the following, and influence the selection of the weights:

- Metadata, overlapping datasets, proximity of GMPEs;
- Declared validity range, number of data points, extrapolation properties;
- Testing with Swiss intensity data from large historical events;
- Comparison with observations on rock.

We first discuss empirical GMPEs, then simulation based relations and compare the GMPEs to rock ground-motion from a Japanese dataset. The final part of Chapter 1.1 provides the weights to the GMPEs to be used in the logic tree. The main question is how to weight limited data in simulation-based GMPEs to constrain stress drop in relation to few or no data with V_{S30} >1000 m/s in the empirical GMPEs. Expert judgments are, therefore, important throughout the evaluation and weighting process.

Table V-1.1: Used ground motion prediction equations (GMPEs) and validity range declared by the authors.

GMPE	Declared Mw Range	Declared Distance Range [km]	Declared Period Range [s]	Method	Site
AbSi08	5.0-8.5	0.06-200	0.01-10	Em	Continuous O
AkBo10	5.0-7.6	0-100	0.00-3	Em	3 classes E
AtBo06	3.5-8.0	10*-1000	0.025-5	Sim	V_{S30}
BoAt08	5.0-8.0	0-200	0.01-10	Em	Continuous O
CaBo08	4.0-8.0	0-200	0.01-10	Em	Continuous O
ChYo08	4.0-8.0	0-200	0.01-10	Em	Continuous O
Toroal	5.0-8.0	10*-1000	0.03-2	Sim	1 Rock
Zhaoal	5.0-8.3	0-300	0.05-5	Em	5 classes O-M
Extension of the Swiss stoch. model	3.0-7.5?	10-200	0.01-2	Sim	Ref. Rock

Yellow color: unconstrained at high magnitude (above 7.6), large distance (>100 km), or unavailable frequencies as declared by the authors (inter- or extrapolation needed).
Em: Empirical GMPEs
Sim: Simulation-based GMPEs with a fitted functional form and limited data used for their derivation (models in green color)
M: V_S measured / O: V_S often measured / E: V_S often estimated

* As stated in Atkinson [2006]: "In reality, the attenuation behaviour inside 10 km is not known, and this is a source of uncertainty in the simulations at close distances." The same probably goes for Toro et al. [1997].

1.1.1 Weights Assigned to Empirical GMPEs

All empirical GMPEs are derived from few or no data with V_{S30} >1000 m/s. SP2, however, has the task of estimating the ground motion on non-weathered rock with shear-wave velocity as high as 2500 m/s. From V/H ratios, it seems to me that the NGA models and AkBo10 still include some site effects at frequencies in the range ~3-10 Hz caused by shallow unconsolidated layers.

The empirical models of AkCa10 and Bial11 mostly result in lower ground motion when compared to the other empirical GMPEs derived from datasets including worldwide data. It might be that these GMPEs are less affected by shallow surface structures, or this difference might indicate that regional differences in attenuation affect GMPEs. The AkCa10 model, however, shows unwanted behavior at magnitudes larger than magnitude 7.0. This model will, therefore, not be included in my logic tree. Moreover, the τ model of AkCa10 is characterized by very high values, considered to be outside the range of empirical GMPEs. Finally, another

argument is to not include two empirical models from the same author in the logic tree. The Bial11 model does not behave well at large magnitude (above 7.0). Furthermore, The Bial11 model has a stronger attenuation than observed in Switzerland, as well as problems related with the τ model. The model is therefore excluded from my logic tree. This reduces the number of empirical GMPEs to six.

Meta-Data

The available meta-data related to the waveforms, used to develop the GMPEs, are evaluated. While meta-data was part of the initial selection criteria of the GMPEs, this part attempts to evaluate the relative difference in quality of meta-data. This evaluation is qualitative and given according to available meta-data related to moment magnitude determination, and meta-data describing the site of the seismic stations.

The following subjective scheme is applied where high numbers relate to high quality:

1. Origin of used moment magnitudes:
    a) M_W without documentation: 1
    b) M_W with documentation but from conversions: 3
    c) Original M_W with documentation: 4
2. Instrument and housing information:
    a) Not available: 1
    b) Mostly available: 2
    c) Available: 3
3. Instrument response and related issues
    a) Including analogue data: 1
    b) Only digital data: 2
4. Site Information:
    a) Not documented: 1
    b) Documented: 2
        i. Model uses site classes
            A. E: V_S often estimated: 2
            B. O: V_S often measured: 3
            C. M: V_S measured: 4
        ii. Model based on V_{S30}
            A. E: V_S often estimated: 2
            B. O: V_S often measured: 4
            C. M: V_S measured: 5

The assessment of the eight GMPEs is given in Table V-1.2, and is only partly based on the declaration by the authors. Quality of the meta-data and total weight of the empirical GMPEs is similar, except for model AkBo10. From Figure V-1.1, it is eminent that the quality of V_{S30} values might be strongly influenced by the fact that V_{S30} values were often estimated from surface geology rather than from measurements of the V_S profile.

Table V-1.2: Used ground motion prediction equations (GMPEs) and qualitative rating of available meta-data. Simulation based methods are not considered and are discussed in the text.

GMPE	1 Origin of M_W	2 Instrument Housing	3 Analog/ Digital	4 Site	Total Weight
AbSi08	4	2	1	2	9
AkBo10	1	1	1	1	4
AtBo06	N/A	N/A	N/A	N/A	N/A
BoAt08	4	2	1	2	9
CaBo08	4	2	1	2	9
ChYo08	4	2	1	2	9
Toroal	N/A	N/A	N/A	N/A	N/A
Zhaoal	4	2	2	4	12
Swiss stoch. model	3	3	2	4	12

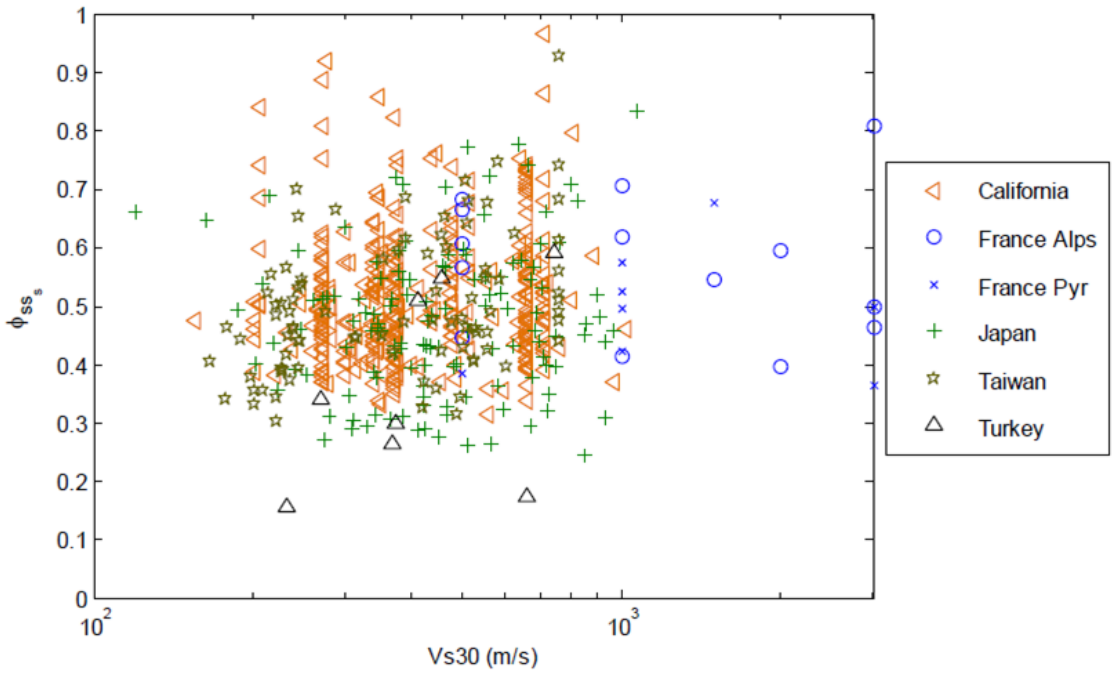

Figure V-1.1: Dependence of the single-station standard deviation on V_{S30} for PGA (From Rodriguez-Marek and Cotton [2011], EXT-TB-1058). The apparent vertical alignment of data points indicate V_{S30} values derived from geology.

Overlapping Datasets / Proximity of Ground-Motion Models

The four regional NGA models used are sub-selections of the same dataset (differing mainly by use or non-use of aftershocks). Most models (including AkBo10) do include aftershocks. AbSi08 and ChYo08 included aftershocks records, but treated them separately in the regressions and also in the calculation of σ. Two of the NGA models (BoAt08, CaBo08) excluded aftershock records from their datasets. This had a particular effect on the τ values for the models. For this reason, the NGA datasets are not strictly the same, and the projection into a model is not the same. For these reasons, the four NGA models are kept in the logic tree.

The PRP report TP2-TB-1015 prepared by [Douglas 2009a] for SP2 provides estimates of the number of commonly used waveforms and serves as an additional source of information (Table 3.2, page 23 in Douglas [2009a]). The Zhaoal and AkBo10 models can be considered to be quite independent from the NGA models and from one another as well. The method proposed by Scherbaum et al. [2010] to estimate the proximity of ground-motion models is not used because it difficult to weight this information.

Corrections for Style of Faulting

The corrections for the style-of-faulting that were implemented are documented in the description of the master ground motion logic tree in PRP report TP2-TB-1081 [Abrahamson 2012a]. The only model that will be considered in my logic tree that needs this correction is the Zhaoal model. Such adjustments need to be considered for this model when assigning the weights. However the influence of the final weight assignment was only minor.

Attenuation Properties from Testing with Intensity Attenuation

The testing procedure using intensity data points (PRP reports EXT-TB-1086 [Kühn 2011a] and TP2-TB-1078 [Kühn 2011d], SP2/WS8 presentation TP2-RF-1370) provides information related to the combination of GMPEs needed (in terms of mixture models) to explain the observed intensities of historical earthquakes (TP2-WAF-1010). It provides an assessment of the performance of the GMPEs in the magnitude range 4.5-6. However, we have to take into account that the macroseismic data are not covering the centre, body and range of all possible realisations. In addition, stress drop cannot be independently resolved from the historical events because M_W was estimated from the same dataset that is now used for testing. High stress drop results in higher M_W for a historical event. Therefore, it is not possible to test the stress drop of Swiss earthquakes with this procedure. Finally, all the assessments depend strongly on the selected magnitude and distance ranges of the events.

The intensity offset applied in the testing (γ value) is related to the assessed soil reference for the macroseismic data. The reference V_{S30} was estimated as 600 m/s, with a resulting correction $\gamma = -0.38$ when referred to V_{S30} of 1000 m/s. A reference V_{S30} of 500 m/s for the macroseismic intensities would explain an additional 0.1-0.2 intensity-units difference. Uncertainty is also due to the difference between EMS as used in Switzerland and MCS as used in Italy, and its influence on the ground-motion intensity relation described in Faenza and Michelini [2010] (EXT-TB-1030), which was applied in the testing procedure. Such uncertainties related to the γ value do not allow us to use this information for an assessment of the V_{S30} reference of the individual GMPEs. The distance range up to 100 km is considered

to be more important in the testing, because at larger distance the intensity range 3-4 is dominant. These intensities are difficult to distinguish, particularly for the historical events. Also the main interest is in the larger intensities and hazard is dominated by distances less than 100 km. I choose not to use PGA in the testing, because, from experience, PGA seems not to be very well correlated to larger intensity values [Kästli and Fäh 2006]. Moreover, high frequencies are affected by possible soil-structure interaction, site κ and data filtering effects. Focusing on the results from testing without PGA, a mixture model including the extended Swiss stochastic model, a combination of NGA models (with preference to "ChYo08", then "BoAt08", "CaBo08" and "AbSi08") and, to a smaller extent, the "Zhaoal" model are required to explain the intensity data for events below magnitude 5.5. The empirical model of "AkBo10" and the ENA simulation based methods ("AtBo06", "Toroal") are not needed to explain the intensity data in this magnitude distance range. When other distance and magnitude ranges were tested ([Kühn 2011d] (TP2-TB-1078), SP2/WS8 presentation TP2-RF-1370), similar results are found: a mixture model including the extended Swiss stochastic model, a combination of NGA models (preference to "AbSi08" and "ChYo08", then "BoAt08" and "CaBo08") and, to a smaller extent, the "Zhaoal" model is required to explain the intensity data. The empirical model "AkBo10" and the ENA simulation based methods ("AtBo06", "Toroal") are again not needed to explain the intensity data for this test.

The results of the intensity attenuation testing depend on the prior given to the model. For very similar GMPEs, only one model is selected because the other is not needed. The influence on weights was carefully tested using different initial priors (PRP reports TP2-TB-1078 [Kühn 2011d] and EXT-TB-1086 [Kühn 2011a]), and to allow adjustment of weights relative to each other. All empirical models are kept when given a large initial prior in the assessment summarized in TP2-TB-1078, which indicates that they can all explain the observed intensity data to some extent. The two ENA simulation based models show the tendency to be quickly pushed out, which indicates that they are not explaining the intensity data well. Giving a strong prior with different precision to the individual GMPEs, and restricting to 10-100km distance range, it can be seen that, for the magnitude range 4-5.5, the "ChYo08" and "BoAt08" models, in combination with the Swiss stochastic model with $Mc = 4.5$ and stress drop of 60 bars, are the models that explain the intensity data best (see EXT-TB-1086 [Kühn 2011a]). For the magnitude range above 5.5, other combinations are the preferred models, specifically "AtBo06" and "AkCa10" that are not used in my logic tree. However, fewer intensity data are available in this magnitude range.

The testing allowed the assessment of the magnitude and distance dependence offset of each GMPE. Here only the empirical GMPEs are considered and compared to the preferred extended Swiss stochastic model (zmc4.5sd60). The Swiss model appears similar to NGA models at larger M, but is different at M=4 due to more complicated geometrical spreading in the Swiss model. By comparing the distance dependence and the magnitude dependence in the relevant magnitude range $M_W = 4.5 - 6$ only (Figure V-1.2), the "AbSi08" is different from the other empirical models in the sense that on average, it has the largest deviation from the Swiss intensity data. The comparison of the distance dependence of the empirical models revealed qualitatively that the model "BoAt08" has the decay with distance most similar to the observations, followed by the "Zhaoal" and "CaBo08" models, then by the "ChYo08" and "AkBo10" models.

In summary, some NGA models together with the extended Swiss stochastic model performed

best in this testing for the most relevant range in magnitude and distance of events with available intensity data. This justifies higher weight assigned to the NGA models. For the Swiss stochastic model, this performance was expected due to the use of intensity data for the scaling to larger magnitudes.

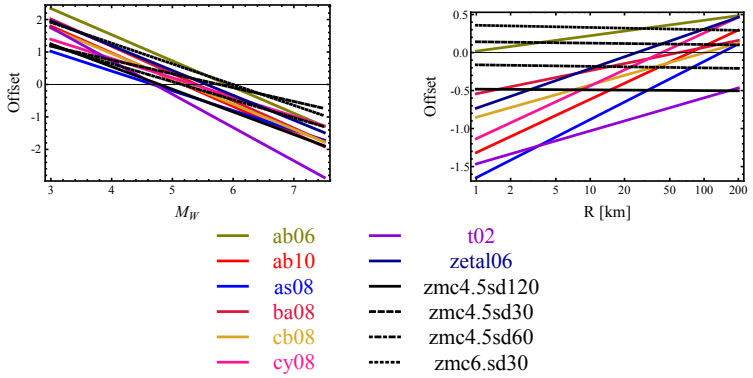

Figure V-1.2: Magnitude and distance dependent offset of each GMPE to the observed intensity data (taken from SP2/WS8 presentation TP2-RF-1370).

Data Coverage for Different Distance and Magnitude Bins

Three moment magnitude ranges are defined [4.0-5.5], [5.5-7.5], and [7.5-8.0], as well as three distance ranges [0-10 km], [10-100 km], and [100-200 km]. The assessment of the logic tree so far is mostly related the moment magnitude range [5.5-7.5], and distance range [10-100 km]. None of the proposed models is well constrained at large magnitude and short distance. No change in weight is assumed for the periods for which interpolation or extrapolation was necessary. The reliability of the GMPEs is different for different distance - magnitude bins. The degree of reliability is accounted for by introducing penalties (the minus signs in Table V-1.3) that are considered when assigning the final weights to the GMPEs. High reliability can be assumed only for the distance-range and period-range declared to be valid by the authors. Moreover, the number of waveforms in each magnitude distance bin was checked using PRP report TP2-RF-1114 [Toro et al. 1997] and compared to the other GMPEs, in order to verify the statement of the authors. The qualitatively assessed reliability is summarized in Table V-1.3 for the defined magnitude distance bins.

1.1.2 Weights Assigned to Simulation Based GMPEs

Simulation-based GMPEs with a fitted functional form (”AtBo06”, ”Toroal”, Swiss stochastic model) were all derived from limited ground motion data. Therefore, there is the question how to weight limited data in simulation based GMPEs in relation to few or no data with V_{S30} >1000 m/s in the empirical GMPEs.

For both the ”AtBo06” and ”Toroal” models, the meta-data criteria are not applicable, because they are calibrated with small events from Eastern North America (ENA) to adjust the parameters of the stochastic model. Both models introduce high values for the stress drop and generally result in ground motions much larger than obtained with the other models (e.g. for ”AtBo06” only in the near-field). Initially a model with high stress drop was kept. The high stress drop used in ”AtBo06” is compensated with high geometrical spreading in the

Table V-1.3: Qualitative assessment of data coverage for different magnitude and distance bins.

GMPE	Mw [4.0-5.5] [0-10 km]	Mw [4.0-5.5] [10-100 km]	Mw [4.0-5.5] [100-200 km]
Abrahamson and Silva (2008)	-	-	-
Akkar and Bommer (2010)	-	-	-
Atkinson and Boore (2006)	NA	NA	NA
Boore and Atkinson (2008)	-	-	-
Campbell and Bozorgnia (2008)	-*		
Chiou and Youngs (2008)	-*		
Toro et al. (1997)	NA	NA	NA
Zhao et al. (2006)	-	-	-
Swiss stochastic model	-		

GMPE	Mw [5.5-7.5] [0-10 km]	Mw [5.0-7.5] [10-100 km]	Mw [5.5-7.5] [100-200 km]
Abrahamson and Silva (2008)			
Akkar and Bommer (2010)			-
Atkinson and Boore (2006)	NA	NA	NA
Boore and Atkinson (2008)			
Campbell and Bozorgnia (2008)			
Chiou and Youngs (2008)			
Toro et al. (1997)	NA	NA	NA
Zhao et al. (2006)	-*		
Swiss stochastic model	-	-	-

GMPE	Mw [7.5-8.0] [0-10 km]	Mw [7.5-8.0] [10-100 km]	Mw [7.5-8.0] [100-200 km]
Abrahamson and Silva (2008)			
Akkar and Bommer (2010)	-	-	-
Atkinson and Boore (2006)	NA	NA	NA
Boore and Atkinson (2008)			
Campbell and Bozorgnia (2008)			
Chiou and Youngs (2008)			
Toro et al. (1997)	NA	NA	NA
Zhao et al. (2006)	-*		
Swiss stochastic model	-	-	-

[-] Outside validity range declared by authors
[-*] From the comparison of the used datasets

distance range up to 70 km. The "AtBo06" model, in general, provides spectral shapes far different to those observed, and is, therefore, not included in the logic tree. A zero weight is, therefore, assigned to this branch.

The "Toroal" model was initially considered as a possible model with a low weight. The stress drop used in model "Toroal" has not yet been observed in Switzerland, but it is also not outside the range of possible stress drops. There are few regional data above $M_W = 4.5$, from which a number of events show difference between M_l and M_W, an indication of higher stress drop than in the available dataset for Switzerland. The most prominent is the St. Dié event with stress drop around 50-80 bars which, however, is close to the stress drop of the extended Swiss stochastic model ($M_c = 4.5$, stress drop 60 bars), but is not reaching stress drop values in the "Toroal" model. If the large historical earthquakes in Switzerland, for which no ground motion recordings but only intensity data exists, would have had large stress drops, this would have been projected into the M_W estimate. High stress drop of an event would have increased the M_W estimated from intensity data. This effect would have biased any earthquake statistics with a tendency of decreasing the b-value in the Gutenberg-Richter relation. As long as the SP1 models use stress drops around 60 bars, this effect of large stress drop on M_W would then at least partly compensate.

The comparison between the GMPEs and recorded rock motion shows that the "Toroal" model provides spectral values that are systematically too high (see chapter 1.3 and PRP report EXT-TN-1165 [Al Atik and Renault 2011]). The reason is the geometrical spreading term which leads to much higher ground motion than the 120 bars model of the Swiss stochastic model. Finally, the testing with intensity data showed (PRP report TP2-TB-1078) that also with a high prior weight in the mixture model, the "Toroal" model was pushed out, and, therefore, cannot explain the observed intensity data. For all these reasons, the "Toroal" model is not considered and is, therefore, given a zero weight in the logic tree.

The extrapolated Swiss model is somewhat similar to the ENA models. However, the calibration at larger magnitude for the Swiss stochastic model (PRP report TP2-TB-1024 Edwards et al. [2010]) was done using the intensity attenuation model (PRP Report TP2-TB-1052 [Edwards and Fäh 2010]) that was derived for PRP and used to calibrate historical earthquakes for the earthquake catalogue of Switzerland ECOS'09 [SED 2010] (PRP Report TP1-TB-1022, Appendix D). In the following, the "best" Swiss models refer to the $M_c = 4.5$ and stress drops of 60 or 90 bars as described in PRP report TP2-TB-1024 [Edwards et al. 2010], based on the extension version of the Swiss stochastic point source model.

The extrapolated Swiss stochastic model was parametrized using point source approximation Chiou [2011] (EXT-TB-1066) while allowing for different M_c values and stress drops allowing for further adjustments. For application in the hazard analysis, the point source model requires a conversion from the closest distance to the effective point source distance (R_{EFF}) to account for the source geometry. Two candidate conversions methods are proposed in PRP report TFI-TN-1148 [Abrahamson 2011a]. Method 1 is simulation based (TP2-TB-1052 Edwards and Fäh [2010]) and defines the effective point source distance, R_{EFF}, as the distance that, over numerous random simulations of a finite fault with unknown hypocenter, leads to the same attenuation as would be experienced by the RMS summation of unique ray-paths from the discretized finite fault. The fault geometry and orientation need to be selected. Normal and strike-slip faults with average dips of 53 and 79 degrees, respectively, are selected. The

Wells and Coppersmith [1994] model was used to estimate the fault dimensions for a given magnitude (above M=5) and slip type. For events with magnitude less than 5, the diameter of the fault is used, assuming a circular rupture. An average stress drop of 50 bars is used to be consistent with stress drops of earthquakes in the "Wells and Coppersmith" database. A simple parametrization led to the following equation (PRP report TP2-TB-1081 [Abrahamson 2012a] and EXT-TN-1205 [Al Atik 2011d]):

$$R_{EFF}[km] = R_{RUP}[km] + e^{-1.60+(M-3)} \tag{V-1.1}$$

This equation is implemented in the hazard computation as method 1 and can use the SP1 hypocenter depth distribution (Figure V-1.3). A test performed [Edwards and Fäh 2011b] (EXT-TN-1210) indicated that this equation is not significantly frequency dependent.

The SP1 model for the distribution of sources was applied in a hazard sensitivity test, comparing the different methods for R_{EFF} (TP2-RF-1374). A large number of scenarios were therefore simulated with method 1 and the SP1 source depth model, and averaged. This averaging resulted to an average source asperity depth of about 12 km assuming that the asperity corresponds to the hypocentre (Figure V-1.4).

Model 2 for R_{EFF} uses an empirical calibration by Atkinson and Silva [2000]. They developed a point-source stochastic model for California. They calibrated the point source parameters by fitting the ground motions from large earthquakes in California that had inverted slip models. As part of this calibration, they found that the effective point source distance was the Joyner-Boore distance with a fictitious depth given by the depth of the largest asperity:

$$R_{EFF} = \sqrt{R_{JB}^2 + H_{ASP}^2} \tag{V-1.2}$$

For application in a hazard analysis, the depth of the largest asperity is not known. A value of H_{ASP}=8 km was found to be suitable for California (Comment by N. Abrahamson during SP2/WS8 on May 12, 2011). However, for the hazard computations, the distribution of the SP1 experts should be used.

The testing of the extended Swiss stochastic model for its behavior at larger magnitudes above M_W of 4.5, using model 1 for R_{EFF} (TP2-TB-1078) indicates that the best model proposed with $M_c = 4.5$ and stress drop of 60 bars is compatible with the intensity data for M_W values larger than 4.5. This result is expected due to the use of the intensity attenuation model in its derivation. A stress drop of 90 bars provides a good fit to intensity data as well.

The rock reference of the macroseismic attenuation model was not measured and was estimated (V_{S30}=600 m/s) so that an average reduction of 0.38 intensity units is to be applied when referenced to V_{S30} of 1000 m/s. The testing showed that the best correction might be slightly larger (γ in between -0.41 to -0.52 depending if PGA is used or not used; SP2/WS8 presentation TP-RF-1370). For the testing, the following assumptions were used to define R_{JB} or R_{RUP} (originally defined in TP2-TN-1115) with H=Focal depth (assumed equal to 10 km), $Width$=Width of fault, estimated using $10^{(-1.14+0.35*M_W)}$ (from Dave Boore's program to evaluate NGA models), Z_{TOR}=Depth to top of rupture, estimated using $\max(0.0, H - 0.5 Width \sin(45 \cdot \pi/180))$ assuming a 45 degree fault and hypocentre half way down fault), R=source-to-site distance (R_{JB} for models using Joyner-Boore distance and R_{RUP} for models using rupture distance). This results in equivalent asperity depths H_{ASP} between 10 and 11 km for M_W between 5.0 and 6.0 when relating R_{EFF} based on R_{RUP} with R_{EFF} based on

R_{JB}. Moving the focal depth H to shallower depths would reduce the average asperity depth as well as the best γ values. However, such considerations are only indicative of the direction of the change due to the uncertainty of the reference V_{S30} of the macroseismic data.

The Swiss stochastic model cannot be independently tested using the intensity data. As new earthquake data are recorded, it can be tested in the future. It has a number of issues that need to be carefully considered when assigning the weights:

1. It extrapolates beyond the observed data,
2. There might be trade-offs between model parameters, and
3. The spectral shape might be a problem: It might have been better to use a two-corner frequency model instead of the single-corner frequency model (not sufficiently complex source model),
4. The high geometrical spreading in the Swiss Foreland is based on few data and finally
5. The "best" extrapolated Swiss stochastic model was obtained for $M_c = 4.5$ and stress drop of 60 bars, while a good fit to intensity data can also be obtained for 90 bars stress drop.

The Swiss stochastic model has lower spectral values than all other GMPEs. In PRP report TP2-TB-1081 [Abrahamson 2012a], the different GMPEs are compared (Figure V-1.5). For the Swiss stochastic model, an asperity depth of 12 km was used. This results in large differences and very low values when comparing with the other GMPEs that are characterized by more shallow average asperity depths (e.g. NGA model have source depth around 8 km or even shallower) The comparisons (Figure V-1.5) are therefore somewhat misleading, and such comparison need to be considered before final assignment of weights.

The "best" extrapolated Swiss model (Mc=4.5, stress drop =60 bars) is based on the average rock velocity profile (V_{S30} of about 1000 m/s) and crustal amplification derived in the Dec. 2009 version of the Swiss stochastic model [Edwards et al. 2009]. This choice was made in order not to repeat the work for the $V_S - \kappa$ corrections of the GMPE for testing. This selection of the old version of the reference rock profile and the crustal amplification might have an impact on the selection of the best M_c value and stress drop for use in the logic tree, mostly due to the difference in crustal amplification. The difference in crustal amplification is shown Figure V-1.6.

This needs further consideration because it might have an influence on the selection of the best stress drop. By repeating the calibration procedure of the extended Swiss stochastic model as described in PRP report TP2-TB-1024 [Edwards et al. 2010] by using the new version of the point source stochastic model (slightly higher reference velocity profile and lower crustal amplification), we end up with a best stress drop of around 80bars when using the originally defined correction to the intensity data 0.38. When we select the intensity correction slightly higher 0.47 due to the V_{S30} the reference rock (V_{S30} of about 1100 m/s), then the best model has again a stress drop of 60 bars. The intensity correction of 0.47 is based on the factor in Figure V-1.6 which is between 1.04 at high frequency corresponding to 0.04 intensity units difference and 1.1 at intermediate frequencies which corresponds to about 0.09 intensity units correction between the two reference rock profiles.

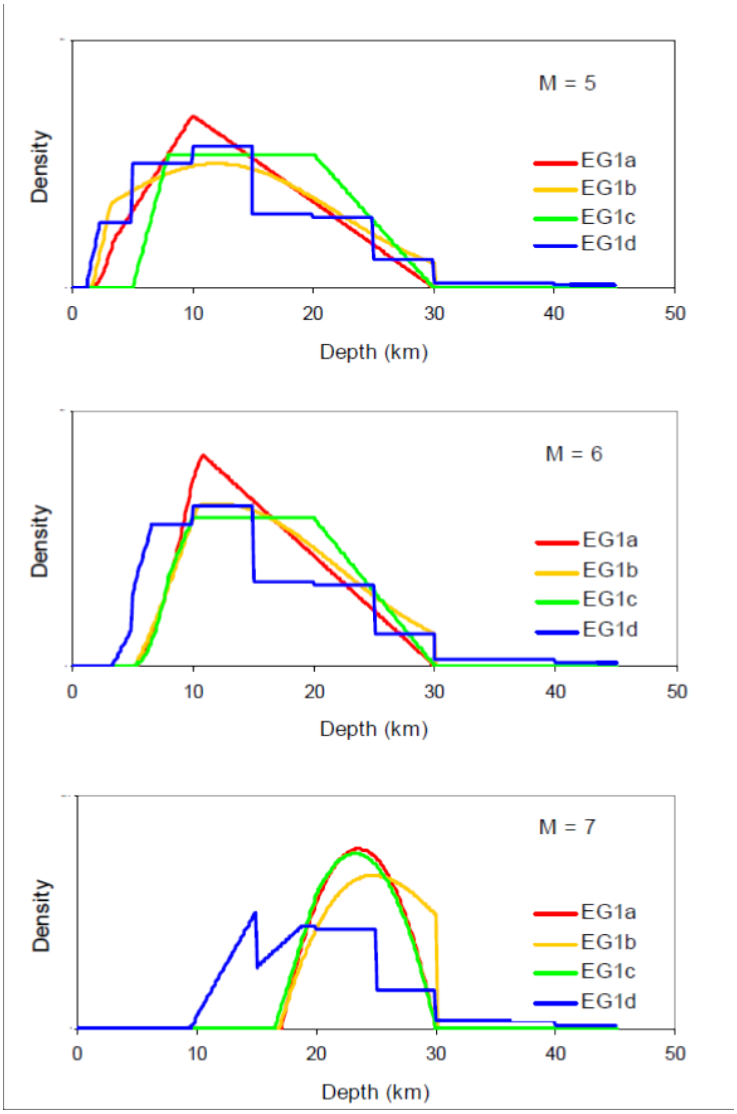

Figure V-1.3: Proposed SP1 models in PEGASOS for the hypocenter depth distribution used in the hazard computation. From this distribution, faults with finite size are generated in the hazard computation.

In conclusion, the Swiss stochastic model cannot be independently tested. The "best" extrapolated Swiss stochastic model was obtained for $Mc = 4.5$ and stress drop of 60 bars, while a good fit to intensity data can also be obtained for 90 bars stress drop. Due to the uncertainties in the calibration of the Swiss stochastic model, lower stress drop (30 bars) and higher stress drop (120 bars) cannot be excluded.

1.1.3 Comparison with Recorded Ground Motion on Rock

Comparisons of the Swiss stochastic model and different GMPEs with observed ground motion on stiff soils and rock were performed. This is done by using data from the Japanese network (Kik-net) using only sites with "reliable" V_S profiles [Poggi et al. 2013]. The GMPEs have the small-magnitude adjustment applied, but no $V_S - \kappa$ correction. The quarter-wavelength approach is selected to characterize the measured velocity profiles at the station sites. For a number of frequencies, the quarter-wavelength velocity with zero residual for

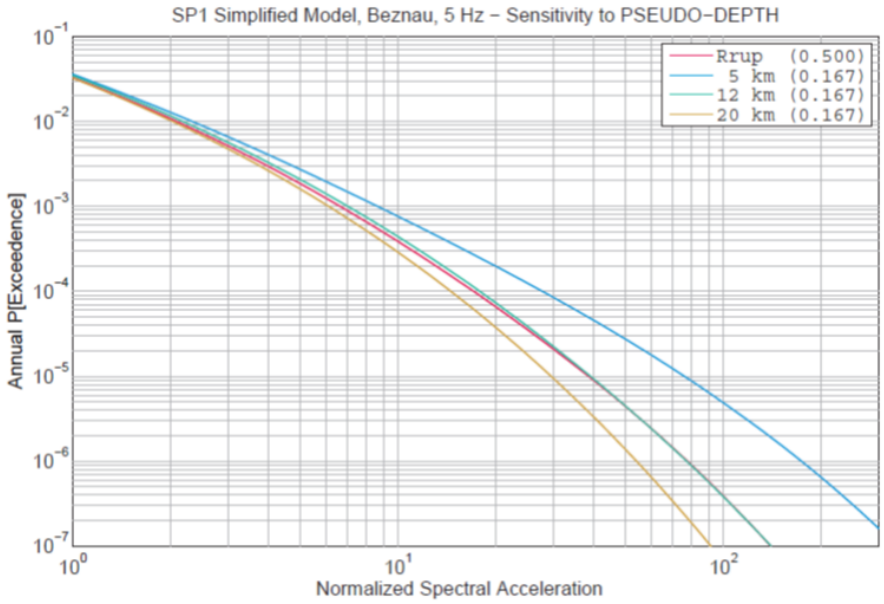

Figure V-1.4: Hazard sensitivity to R_{EFF} (from TP2-RF-1374). Averaging over scenarios defined by SP1 (using method 1 for R_{EFF}) and introducing the simplified parameterization for R_{RUP}, compared to assumptions of different asperity depth using method 2 for define R_{EFF} (from TP2-RF-1374).

each GMPE is determined. This provides some information on the GMPEs reference quarter-wavelength velocity profile and the GMPEs V_{S30} as shown in Figures V-1.7(a) to V-1.7(g). Four magnitude-distance ranges are selected:

- M_W 5-6, distances between 20 and 50 km;
- M_W 4.5-7.3, distances between 20 and 100 km;
- M_W 4.5-7.3, distances between 20 and 50 km; and
- M_W 5.5-6.5, distances between 20 and 50 km.

This consideration remains qualitative due to possible regional differences between Japan and other areas in terms of stress drop and event parameters. However, this assessment can be used to validate Ref1 and Ref2 models for the $V_S - \kappa$ adjustment in models "Zhaoal" and "AkBo10" as well as to validate the 620 m/s reference in the NGA models. Moreover, it can also be used to assess the scaling of the Swiss stochastic model.

The different data selections lead to different zero-crossings for the residuals (see Figure V-1.7). This indicates the influence of the other parameters, such as attenuation and stress drop. However, the range of different values and the crossing with the V_{S30} line in Figures V-1.7(a) to V-1.7(g) can be considered as indicative of the possible range of V_{S30}. The crossing of the zero residual curve with the V_{S30} line for the "Zhaoal" model (Figure V-1.7(a)) is between Ref1 (500 m/s) and just above Ref2 (700 m/s) with an average of around 700m/s. For the "AkBo10" model (Figure V-1.7(b)), the crossing of the zero residual curve is in the range of 500-700 m/s, which is close to Ref1 (600m/s). For the "best" Swiss stochastic model (60 bar stress drop) the crossing is around 800 m/s or higher (Figure V-1.7(c)), which might be used

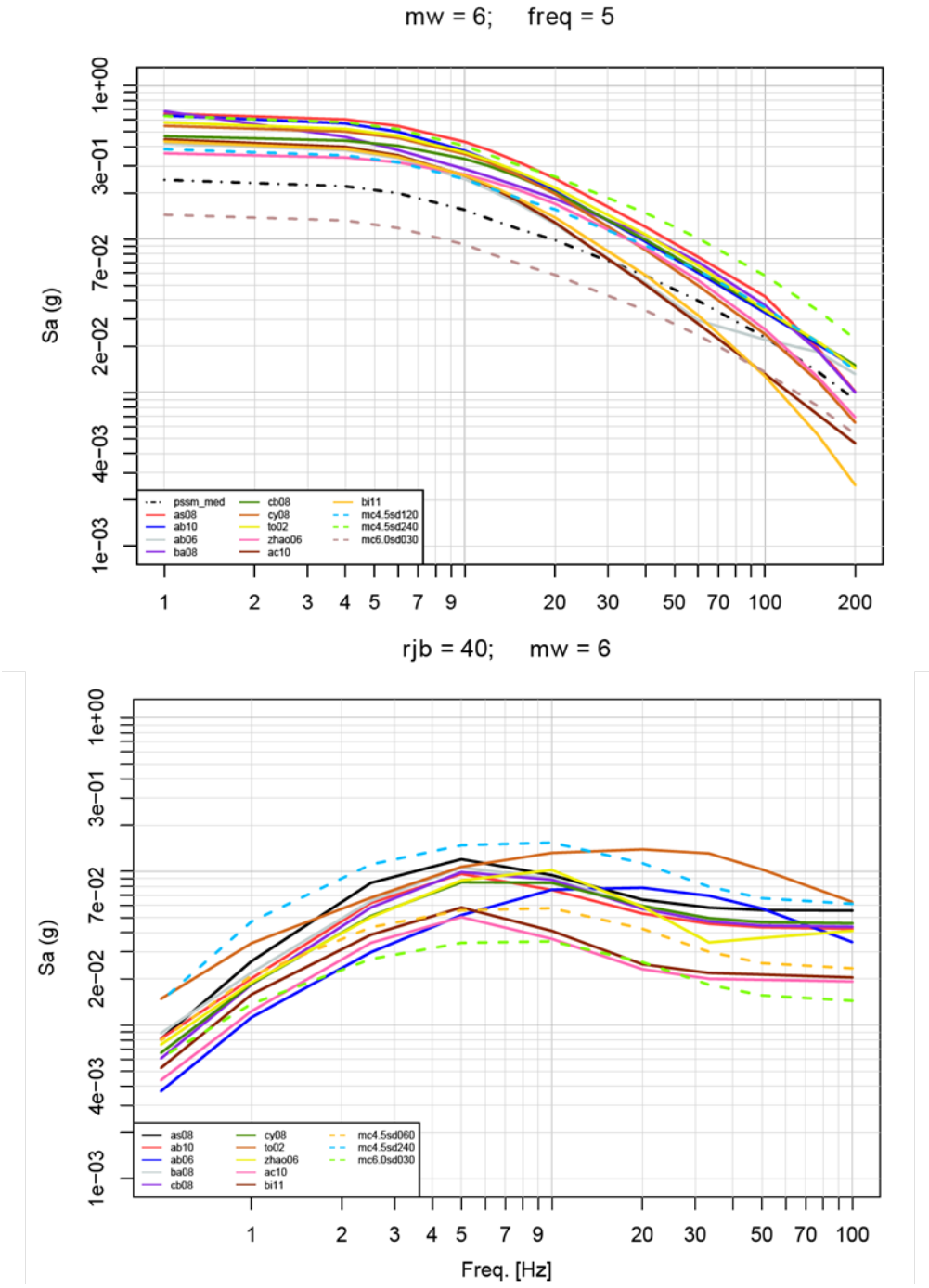

Figure V-1.5: Comparison of spectra obtained with different GMPEs with the extended Swiss model for different M_c and stress drop (SD) (from PRP report TP2-TB-1081 [Abrahamson 2012a]). The plots of the median GMPEs shown here are based on the original "as published" models without $V_S - \kappa$ correction. For the extended Swiss stochastic model $_{EFF}$ is defined with an asperity depth of 12 km, leading to large differences when compared to the other GMPEs.

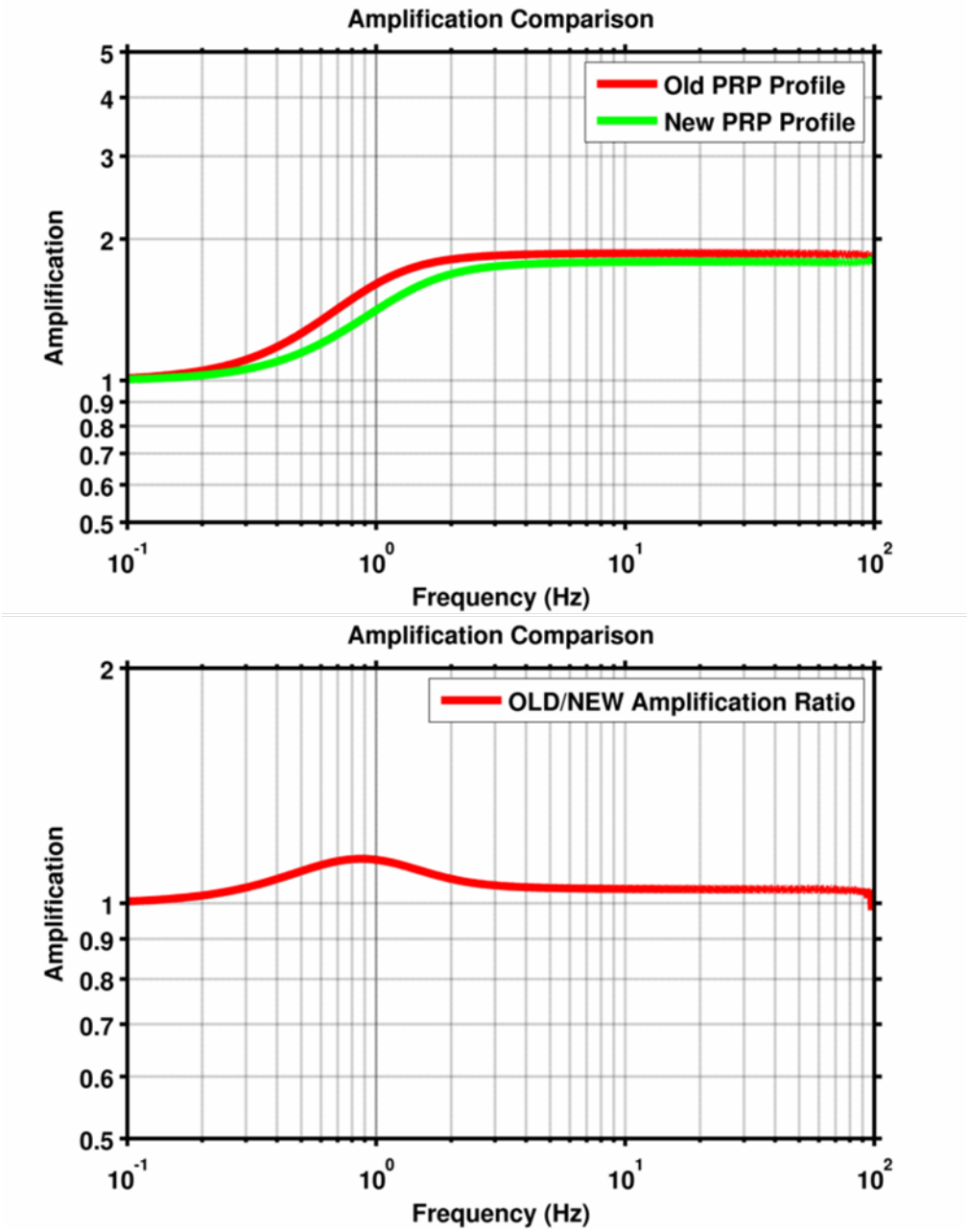

Figure V-1.6: Comparison between crustal amplification of the old stochastic model (Dec. 2009 version [Edwards et al. 2009]) with the final (new) stochastic model (PRP report TP2-TB-1024 Edwards et al. [2010]).

to argue for a lower stress drop to be used in the Swiss stochastic model. For the NGA models (Figures V-1.7(d) to V-1.7(g)), the zero residual curves crossing with the V_{S30} curve tends to be below the assumed reference velocity of 620 m/s, typically in the range 400-600 m/s.

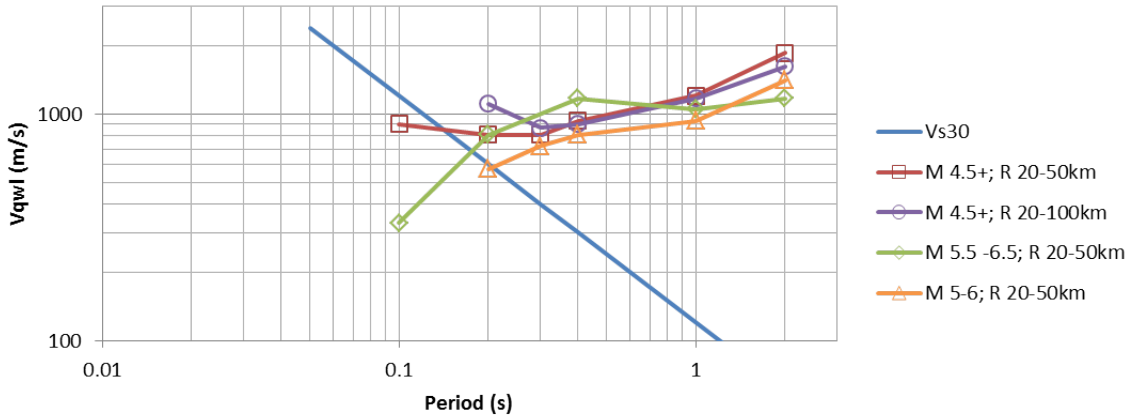

(a) Residual of the "Zhaoal" GMPE.

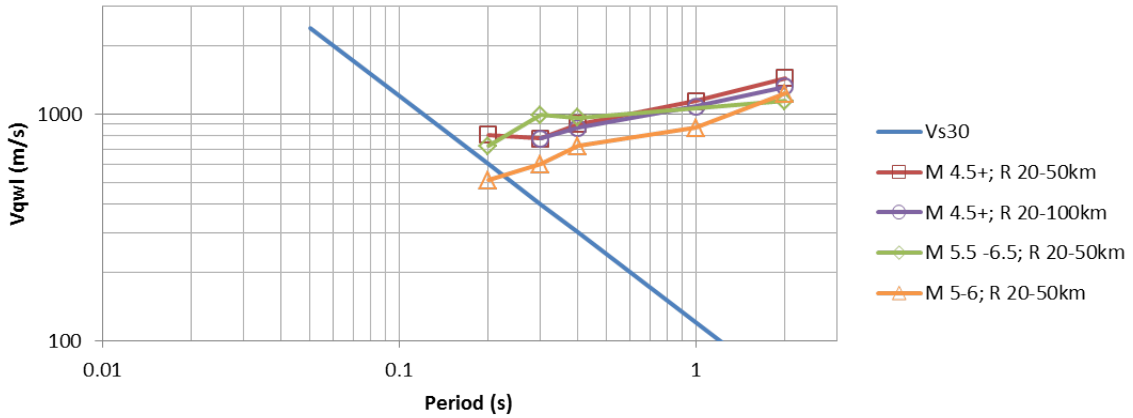

(b) Residual of the "AkBo10" GMPE.

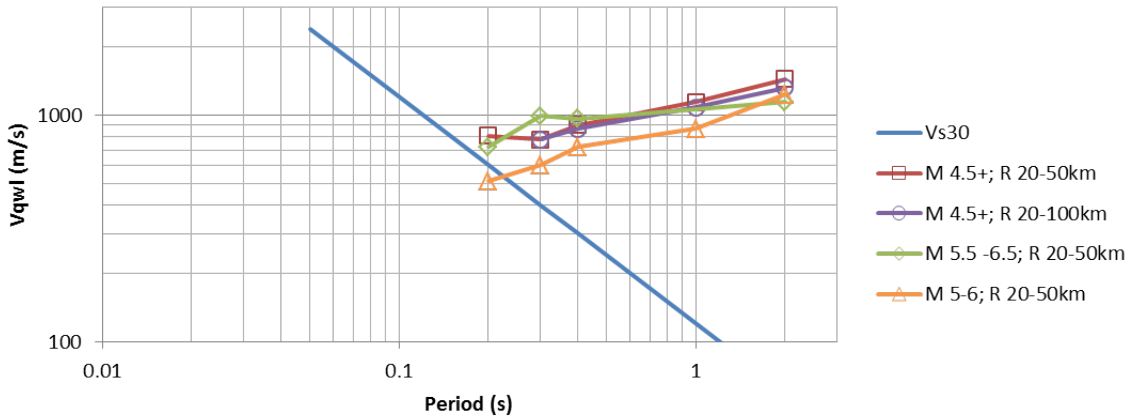

(c) Residual of the 60 bar PSSM GMPE.

Figure V-1.7: Comparison between the V_{S30} line and the quarter-wavelength velocity line with zero residual of the GMPEs to the selected ground motion data from the Kik-net.

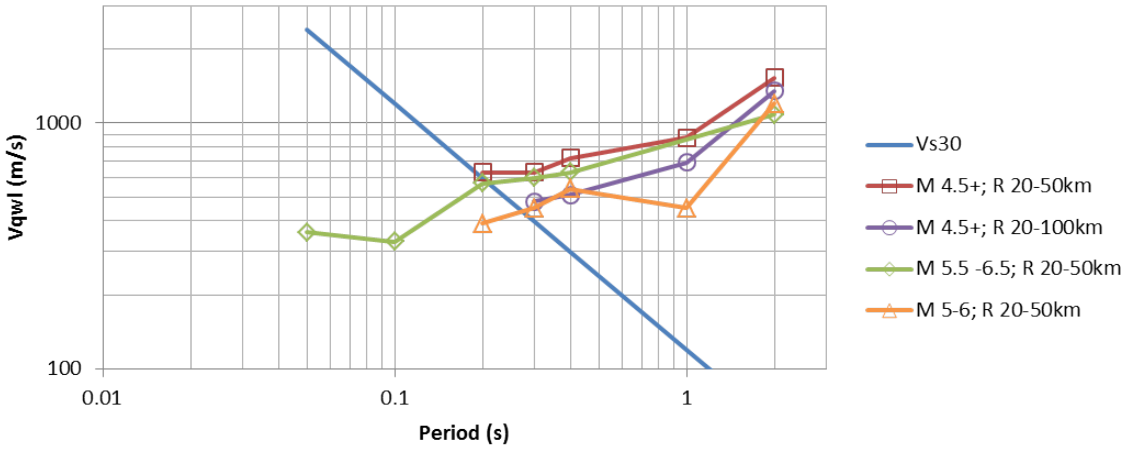

(d) Residual of the "AbSi08" GMPE.

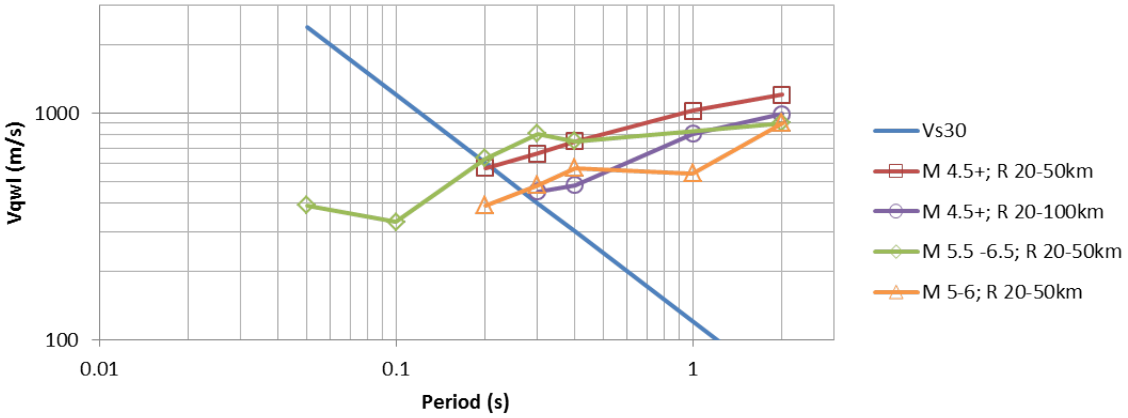

(e) Residual of the "BoAt08" GMPE.

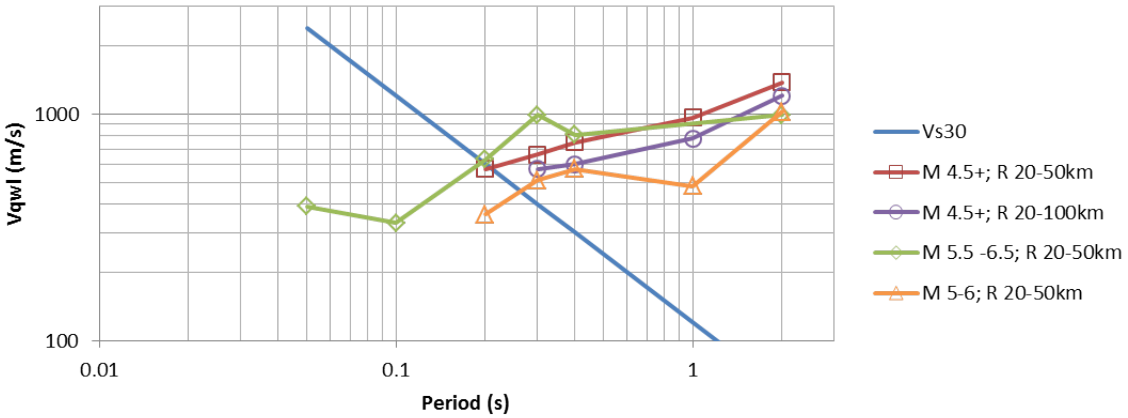

(f) Residual of the "CaBo08" GMPE.

Figure V-1.7: Continued: Comparison between the V_{S30} line and the quarter-wavelength velocity line with zero residual of the GMPEs to the selected ground motion data from the Kik-net.

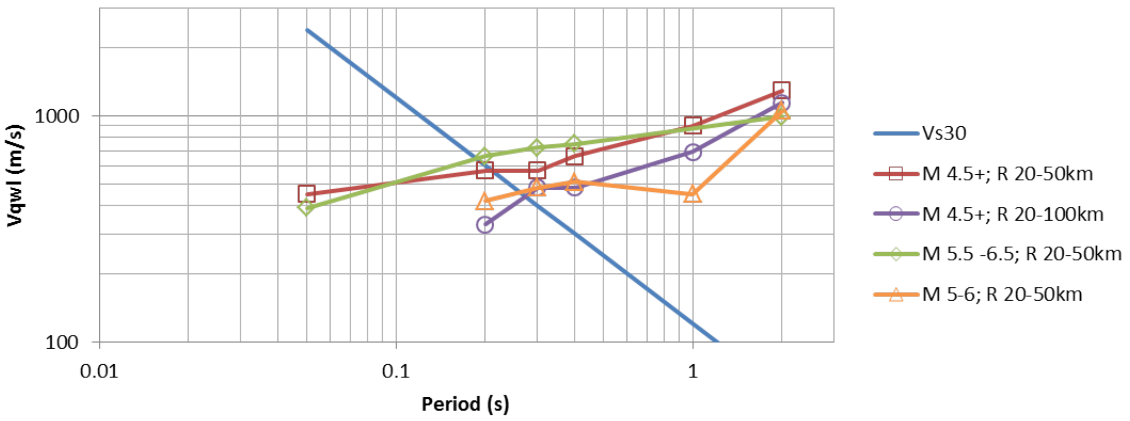

(g) Residual of the "ChYo08" GMPE.

Figure V-1.7: [
Comparison between the V_{S30} line and the quarter-wavelength velocity line.]Continued: Comparison between the V_{S30} line and the quarter-wavelength velocity line with zero residual of the GMPEs to the selected ground motion data from the Kik-net.

1.1.4 Testing the Swiss Stochastic Model with Strong Motion Data

The Swiss stochastic ground-motion prediction model was tested using European and Japanese strong motion data. For the Swiss stochastic model, the stress-parameter (62.5 bar) was calibrated through comparison of the stochastic model simulations with the macroseismic intensity model used to determine M_W of large historical earthquakes in Switzerland.

The first case was the investigation of the source properties of large magnitude events ($5 < M < 7.6$) which have occurred in Europe and the Middle East [Edwards and Fäh 2012a, 2013a]. In this investigation, it was found that the scaling adopted in the Swiss stochastic model, which was designed to be consistent with historical- and macro-seismicity, is consistent with the spread of observations of such large earthquakes. The resulting stress-parameters were found to be magnitude- and depth-independent, with average values of 74 or 88 bar depending on whether inverted or database M_W values were used. It was also found that the use of the effective distance metric (R_{EFF}) is useful for including near-source geometrical effects of finite sources.

The strong-motion database from the Japanese KiK-Net seismic network was used in the second test [Edwards et al. 2012] (TP2-TB-1091). First a reference rock profile for Japan was determined, along with corresponding amplification functions [Poggi et al. 2012] (TP2-TB-1090). The amplification functions were used to deconvolve the site response from the recordings, leaving rock-referenced ground-motion. Finally the stochastic ground-motion model for Switzerland was compared to the rock-referenced strong ground-motion data, by adjusting the Swiss stochastic model to the rock reference of the Japanese data. In order to investigate the stress-parameter scaling of the Swiss model, the mean bias in residuals (for distances up to 50 km) was compared using differing values (30 bar, 62.5 bar, 90 bar and 120 bar). The mean bias in the residuals using the different models shows that the 62.5 bar and 90 bar models perform very well against the Japanese strong-motion data: for f >1 Hz generally the 62.5 bar model is *slightly* below the mean of the data, while the 90 bar model is *slightly* above the data mean. The 30 bar model tends to under-predict the data while the 120 bar model tends to over-predict the data. For frequencies around 1 Hz the 62.5 bar and 90 bar stress drop both over-predict the data. Such low ground motion at 1 Hz however seems to be a specific characteristic of Japanese data, and is present also in the Zhaoal model. This Swiss stochastic model at frequencies around 1 Hz might be explained by the influence of the Molasse basin, or might be due to the source model used, with one corner frequency only.

1.1.5 Final Weights Assigned to GMPEs

This is the summary of the discussion in Chapter 1.1. Table V-1.4 provides a qualitative ranking of the different GMPEs for the discussed properties. The ranking is given in terms of the advantages (+) and weaknesses (−) of the different GPMEs relative to each other. Based in the total ranking the weights for the GMPEs are assigned, and are also given in Table V-1.4. Limited data in the simulation-based GMPE to constrain stress drop is weighted slightly lower (weight 0.40) than the empirical GMPEs derived from large datasets however with only few or no data with V_{S30} >1000 m/s (weight 0.60).

The reason for assigning this difference in weight is the large number of recordings used for deriving empirical GMPEs in the magnitude range 6 to 7. The NGA models in total are weighted with 0.35, the Japanese model with 0.20, the European model with 0.05, and

the ENA models with 0. Models from active regions are therefore given all weight (NGA, Japan), no weight to stable continental regions (ENA). The "ChYo08" model gets the highest weight from the NGA models, and this model is also recognized for its good performance (e.g. Delavaud et al. [2012a]). All four NGA models are kept in order to account for epistemic uncertainty in the magnitude-distance range not well covered by data, taking into account both the NGA models that include aftershocks and those that do not. Because the different NGA models perform differently in the different magnitude and distance range, it can be assumed that the distribution is not skewed. The European model is kept to take into account the opinion of a broader informed community. In the magnitude distance range with a large number of observations the average of "ChYo08" and "Zhaoal" is considered the centre with the other GMPEs with small weights defining the range of empirical GMPEs.

The extended Swiss stochastic model is fully compatible with the earthquake catalogue, the observed intensity data, and average properties of the crust. The "best" extended Swiss stochastic models assumes low stress drop in the range of 60-90 bars and this is not explicitly defined as a high stress drop model compatible with stable continental areas. High stress drop would, however, increase M_W of the historical events and would, therefore, enter in the hazard computation through the earthquakes statistics. The advantage of the Swiss stochastic model is the definition of a reference rock profile that goes with the relation.

To cover the Center, Body and Range in the scaling with intensity data, the following stress drop models are used in the logic tree with the given weights:

- Stress drop 40 bars: weight 0.01
- Stress drop 60 bars: weight 0.20
- Stress drop 90 bars: weight 0.16
- Stress drop 120 bars: weight 0.03

The "best" Swiss stochastic model is given the highest weight. The range covers the range of stress drops discussed in Section 1.1.2 and 1.1.4 and is based on the comparison with observations in Europe and Japan.

1.2 Host-to-target $V_S - \kappa$ Adjustments of the GMPEs to the NPP Rock Condition

A correction needs to be applied to the GMPEs in order to adjust the equations to the high $V_S - velocity$ and low κ values expected at the NPP-sites' rock conditions below the surface sediments. This correction has the largest effects at high frequencies, in the part of the GMPE spectra for which the developers probably did not pay much attention to the scaling. Moreover, spectra derived from the GMPEs for rock conditions might be affected by shallow soil resonances and damping, that were not identified as such due to the site parameterization using V_{S30}, or due to an insufficient resolution of the V_S-measurements (e.g. down-hole methods tend to have problems in the shallow soil part). From the logic-tree results of the host-to-target $V_S - \kappa$ adjustment a 5-point distribution is defined for each GMPE such that the distribution is not sensitive to the tails of the distribution. All correction factors

Table V-1.4: Proposed weights of the GMPEs for the logic tree based on a qualitative rating of the different properties of the proposed GMPEs.

GMPE	1 Meta-Data	2 Overlapping Datasets	3 Intensities & Testing	5 Constrain to ground motion data	6 Rock motion $V_{S,ref}$	Total Rating	Weight
AbSi08		– –	+			–	0.05
AkBo10[2)]	–	+	–	–		– –	0.05
BoAt08[2)]		– –	+			–	0.05
CaBo08[2)]		– –		+		–	0.05
ChYo08		– –	++	+		+	0.20
Zhaoal[3)]	+[1)]	+		–	+	++[1)]	0.20
PSSM	+	+	++	– –	+	+++	0.40

[1)] "Zhaoal" has good metadata that are however not used to their full potential. Other points taken into account:
[2)] "CaBo08", "AkBo10" and "BoAt08" have a low τ model when compared to Switzerland,
[3)] "Zhaoal" model needs a style-of-faulting correction.

were manually checked to exclude cases for which the correction method was not stable. The resulting distribution is not a log-normal distribution.

1.2.1 κ Estimation Method

The main issue is the question how much resonance effects remain in the GMPEs after $V_S - \kappa$ correction, because the QWL amplification correction does not account for resonances but only the "smooth" changes in the V_S profile. For the NGA models, the reference profile is that with the lowest value of 620 m/s for V_{S30} (also referred to as profile Ref1) where the bulk of data is expected (see also discussion in Section 1.1.3). An important observation related to this selection refers to the κ that does not scale with V_{S30}, causing an inconsistent κ to be obtained for the reference profiles Ref2 (V_{S30} of 800 m/s) and Ref3 (V_{S30} of 1000 m/s) in the NGA models. For the GMPEs that use site classes, V_{S30} is not a parameter of the model and the profile Ref2 is always taken, which for the "Zhaoal" class I model has an estimated V_{S30} of 700 m/s, and for the "AkBo10" rock class model which has an estimated V_{S30} of 800 m/s. When applying the $V_S - \kappa$ correction procedure for these two models, a lower V_{S30} ("Zhaoal" 500 m/s, "AkBo" 600 m/s) is also used, without changing the soil class and the κ of velocity profile Ref2.

There are four alternative methods used for the estimation of the host GMPE κ, given by four branches in the logic tree.

The first method (stochastic inversion) uses the correlation between κ and the frequency at which the GMPE reaches its peak spectral acceleration value (f_{peak}). The $f_{peak} - \kappa$ correlation is based on the point source stochastic model. The quantity f_{peak}, even if probably also affected by resonances of shallow layers, is a potential candidate for estimating κ with $f_{peak} - \kappa$ relationships. The standard deviation of the relation is included, simulating a normal distribution (with weights 0.2, 0.6, 0.2). This $f_{peak} - \kappa$ correlation method provided more stable results (e.g. between NGA models that basically use the same dataset) than the other

correlations that are based on the high-frequency slope of the spectrum. It might be that these other correlations were affected by the aforementioned problems in the high frequency spectral shapes of the GMPEs. Therefore, zero weight is given to branches $f_{amp2.0}$ and $f_{amp-half}$.

- Branch f_{peak}: weight 1.0 (with simulation of a normal distribution 0.2, 0.6, 0.2)
- Branch $f_{amp2.0}$: weight 0
- Branch $f_{amp-half}$: weight 0

The second method uses the empirical correlation between κ_0 and V_{S30}. Three alternative empirical correlations are considered, the Silva et al. [1998] relation, and two relations from Edwards and Fäh [2012a] (corrected 2011 relations), a lin-log and a log-log relation. These empirical relations are valid candidates for the definition of the κ of each GMPE. The standard deviation of the correlation is very high. Therefore, the standard deviation is not included in the logic tree, because it would require that this effect is taken away from the single-station sigma discussed below. The Silva et al. [1998] equation, and Edwards and Fäh [2012a] lin-log relation (for consistency with other work in SP3) and log-log relation are weighted as follows:

- Silva et al. (1998) relation: weight 0.6
- Edwards and Fäh (2012) lin-log relation: weight 0.3
- Edwards and Fäh (2012) log-log relation: weight 0.1
- Branches for mean-sigma and mean+sigma: weight 0

Slightly more weight is given to Silva's relation due to the smaller number of data points used in Edwards and Fäh [2012a]. Moreover the Silva relation has been confirmed by Van Houtte et al. [2011].

The third method uses the IRVT method to estimate κ_1 for each GMPE. The application of IRVT for different V_{S30} values shows that the GMPEs do not account properly for the change in κ. Therefore, the derived κ values for all GMPEs are only valid for the V_{S30} of the bulk of data used to derive the GMPE, as outlined before. The values are similar to the values estimated from the $f_{peak} - \kappa$ correlation.

Finally, the fourth method (Empirical constraint) uses the correlation between κ_1 and the highest frequency at which the normalized spectral shapes exceeds a specified value (1.3, 1.5, 1.7, or 2.0). The values tend to depend on the selected limited dataset, in our case the NGA dataset that might be characterized by shallow site effects. For these reasons, this empirical method is not used. Other limitations of this analysis include the use of κ versus f_{amp} relationships to estimate κ. The use of these relationships might result in recordings at the same station having very different κ values.

Due to the problems related to empirical GMPEs, epistemic uncertainty is considerable. In the logic tree, the results from IRVT are generally very similar to method 1 and the relation of Silva et al. [1998]. In order to balance between low κ values from the Edwards and Fäh [2012a] relation that are taken into account in the branch "empirical relation" (weight 0.5) and high κ values in the other relations (total weight 0.5), the following weights are assigned (see also Figure V-1.8 and discussion in the figure caption):

- Branch "Stochastic inversion": weight 0.1
- Branch "Empirical relation": weight 0.5
- Branch "RVT based FAS": weight 0.4
- Branch "Empirical constraint": weight 0.

The method IRVT is considered to be more stable (weight 0.4) than the iterative method used in the branch "Stochastic inversion" (weight 0.1).

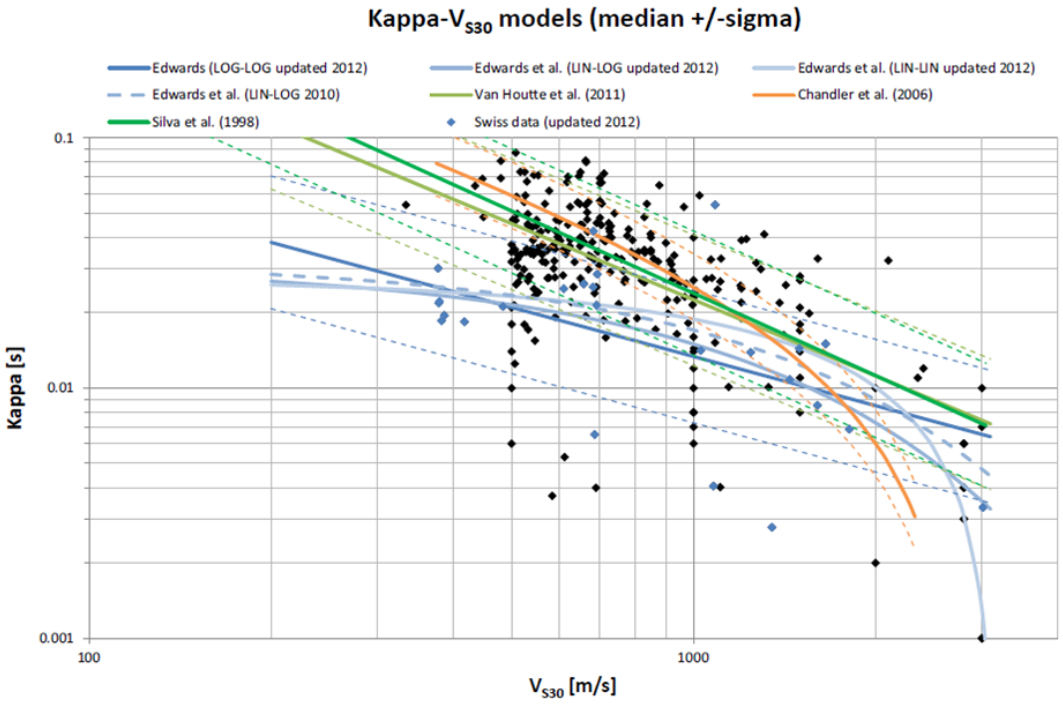

Figure V-1.8: Models for and observations of $V_S - \kappa$ pairs (from PRP report TP2-TB-1081 [Abrahamson 2012a]). Many of the profiles (e.g. Japanese data) were measured with downhole methods that in some cases do not resolve the first layer and therefore might give V_{S30} values that are slightly too high. If this is assumed to be correct then a number of points in reality should be shifted more to the left.

1.2.2 V_S Profile Type of the Host Region and Reference V_{S30}

For the NGA models only the reference profile Ref1 is considered, as discussed in Section 1.2.1 which corresponds to the profile in the range of V_{S30} where the bulk of data is expected to lie (V_{S30} of 620 m/s). The US generic profile is strongly related to the NGA models, and no weight is given to the Swiss profile.

For the "AkBo10" to my present knowledge, no detailed assessment of the velocity profile was performed for the host region. For this reason both profiles (Swiss Generic, US Generic) are kept as reasonable models with the same weight. The "Zhaoal" model refers to Japan. Ozel [1999] conclude that the near-surface velocity structure is complex with remarkable lateral velocity variations and with a high velocity gradient reaching high V_S velocities within the

first kilometer. This favors more the Swiss generic profile. All GMPEs could be affected by the properties of shallow sediments that are probably not accounted for in the V_{S30} estimate (e.g. shallow sediment layers (few meters thickness) with amplification and increased damping; biased measurements of V_S-profiles due to problems in resolving the structure close to the surface; V_{S30} estimates from geological information that might not take into consideration any layer of weathered material). In the logic tree, the Ref1 and Ref 2 models were therefore weighted for "AkBo10" and "Zhaoal", but the higher Ref3 values are excluded based on my judgement that the V_{S30} in reality tends to have lower values than indicated the Ref2 models. For the "Zhaoal" class I mode, Ref2 is 700 m/s, and is weighted higher than Ref1 based on the considerations in Section 1.1.3. For the "AkBo10" rock class model, Ref2 is 800 m/s and is given a lower weight based on the results of Section 1.1.3 and due the quality of metadata. For Ref1 we apply a lower V_{S30} in the $V_S - \kappa$ correction procedure for these two models ("Zhaoal" 500 m/s; "AkBo10" 600 m/s) without changing the soil class.

Finally, ENA models have zero weight in the logic tree and therefore need no assessment. The weights are as follow:

- NGA Ref1: weight to US Generic: 1.0
- NGA Ref1: weight to Swiss Generic: 0
- Zhaoal:
  - US Generic profile: weight 0.3
  - Swiss Generic profile: weight 0.7
  - Ref1 (without changing the soil class and the κ of Ref2): weight 0.2
  - Ref2: weight 0.8
  - Ref3: weight 0
- AkBo10:
  - US Generic profile: weight 0.5
  - Swiss Generic profile: weight 0.5
  - Ref1 (without changing the soil class and the κ of Ref2): weight 0.8
  - Ref2: weight 0.2
  - Ref3: weight 0

1.2.3 Target κ

The κ parameter is related to near surface attenuation. We can assume that the κ values for V_{S30} around 1000m/s are constrained within some variability. There are however only few data for rock conditions at higher V_S values. The κ values derived from recordings at great depth, even if the receivers are placed in hard rock, are affected by the anelastic damping of the overlying layers (see Ktenidou [2012] (EXT-RF-1443) for the range of κ values). In this project the near-surface condition needs to be assessed: we may expect that κ is decreasing

with increasing V_{S30} due to the expected dependence of κ on the shear-wave velocity of the rock material. Nevertheless, litho-static pressure is low near the surface, resulting in a large number of cracks which limits the decrease of κ values at high V_{S30}.

The target κ was evaluated in two steps. The first step considers a theoretical rock condition that would be expected at high litho-static pressure. For this I assume that extrapolation of the existing $V_{S30} - \kappa$ relations in the V_{S30} range, that is sparsely covered with data, is valid for the empirical GMPEs. This first step serves to test if the ground-motions from the two sets of relations (stochastic and GMPEs) converge through extrapolation of the κ values, whilst considering the κ uncertainty inherent within the GMPE. The extrapolation of κ for the stochastic model is done in the same manner, simply by application of the same $\Delta\kappa$ applied to the reference κ value at V_{S30} of 1000 m/s. If we take into consideration that the empirical GMPEs might be affected by shallow resonances, the convergence is expected solely for the ground motion at high frequency. The second step then accounts for the limit of κ for rock close to the surface. For site Gösgen, κ needs to be also assessed for a shallow rock depth, which implies that we have to consider the different proposed rock profiles.

For the evaluation of the target κ in step 1 the Silva et al. [1998] equation, and results in report TP2-TN-1236 [Edwards 2012b] combined with experience described in Edwards et al. [2011b]; Edwards and Fäh [2012a] are used to adjust the empirical GMPEs. All results obtained with the method based on full-spectrum fit, as applied for the derivation of the Swiss stochastic model, provide stable results and are used for the adjustment of the Swiss stochastic model. A full spectral fit to derive κ as performed in Edwards et al. [2011b] seems to be more reliable than fitting the slope of the high-frequency decay (e.g. Ktenidou [2012], EXT-RF-1443). However κ is also correlated with other parameters such a stress drop and Q, and this introduces uncertainty. Fitting the slope of the spectral decay on the other hand depends on the selection of the recordings, the frequency band in which the fitting is performed and also the possible correlation with stress drop and Q. The resulting κ values from the different methods therefore lead to the observed large scatter with a tendency to higher κ values for methods that only fit the spectrum at high frequency. This is due to the selection of the frequency range of the down-going part of the spectrum. A full spectral fit therefore often leads to lower κ values than fitting the slope of the high frequency decay.

High weight for estimation of the κ of the empirical GMPEs is given to the FAS method in TP2-TN-1236 [Edwards 2012b] using an average value obtained with the global dataset (R<50 km, V_S >600 m/s and 800 m/s, lin-log and log-log relations) and the results from the Swiss data only (R<50 km, all V_S values, lin-log and log-log relations). The values obtained by fitting the average near-source response spectrum (PSA method) are first considered to be an upper bound because κ values from PSA are generally larger than fitting the Fourier spectral shape. Moreover there might be an unwanted influence from the fact that the shape of the response spectrum at high frequency is strongly influenced by the energy at lower frequency. The PSA derived κ values cover the range of possible values, but the smallest weight is given to these higher κ values. Together with the values in Silva et al. [1998], these models define the range of the κ estimates. The following weights are assigned:

- Silva et al. [1998] relation: weight 0.25
- Edwards [2012b] (TP2-TN-1236) relations: weight 0.75

The weights of the relations in Edwards [2012b] (TP2-TN-1236) and Silva et al. [1998], and related average κ values from the data selections given above, are given in Table V-1.5:

Table V-1.5: Weights of the relations in Edwards [2012b] (TP2-TN-1236) and related average κ values.

Method	Weight	V_{S30} 1000 m/s	V_{S30} 1100 m/s	V_{S30} 1800 m/s	V_{S30} 2200 m/s	V_{S30} 2500 m/s
1. FAS, all data	0.25	0.022	0.02	0.01	0.008	0.006
2. FAS, Swiss	0.30	0.017	0.016	0.013	0.011	0.010
3. PSA, all data	0.20	0.03	0.029	0.027	0.026	0.025
4. Silva et al. (1998)	0.25	0.024	0.021	0.0125	0.01	0.0087

These κ values are applied in step 1 to correct the GMPEs.

In the Swiss stochastic model the κ value is a parameter that might be correlated with the stress drop model and regional Q model. The average Q model however has been confirmed through an independent study [Allmann 2009] (TP2-TB-1023). In order to be consistent with the κ correction of the empirical relations, the same $\Delta\kappa$ values are applied to the Swiss stochastic model with the same weight. $\Delta\kappa$ is referenced to the κ at V_{S30} of 1000 m/s, which is always assumed to be defined for the stochastic model (Tab. V-1.6).

Table V-1.6: $\Delta\kappa$ for the different methods of Table V-1.5.

Method	Weight	V_{S30} 1000 m/s	V_{S30} 1100 m/s	V_{S30} 1800 m/s	V_{S30} 2200 m/s	V_{S30} 250 0m/s
1. FAS, all data	0.25	0	-0.002	-0.012	-0.014	-0.016
2. FAS, Swiss	0.30	0	-0.001	-0.004	-0.006	-0.007
3. PSA, all data	0.20	0	-0.001	-0.003	-0.004	-0.005
4. Silva et al. (1998)	0.25	0	-0.003	-0.0115	-0.014	-0.0153

The $\Delta\kappa$s, when applied to the reference at V_{S30}=1000 m/s lead to the following κ values for extrapolation of the stochastic model (Tab. V-1.7):

Table V-1.7: κ for extrapolation of the Swiss stochastic model.

Method	Weight	V_{S30} 1000 m/s	V_{S30} 1100 m/s	V_{S30} 1800 m/s	V_{S30} 2200 m/s	V_{S30} 2500 m/s
1. FAS, all data	0.25	0.017	0.015	0.005	0.003	0.001
2. FAS, Swiss	0.30	0.017	0.016	0.013	0.011	0.010
3. PSA, all data	0.20	0.017	0.016	0.014	0.013	0.012
4. Silva et al. (1998)	0.25	0.017	0.014	0.0055	0.003	0.0017

Surprisingly, by using these κ models, the result of the empirical GMPEs and the Swiss stochastic model converge at PGA for high V_{S30} (Figure V-1.9). However the values of κ are below the range that is reasonable for a rock at shallow depth. Results from report

PMT-SUP-1084 [Renault and Biro 2013] was not used due to the applied amplification corrections that were not referenced to the same velocity for the different sites.

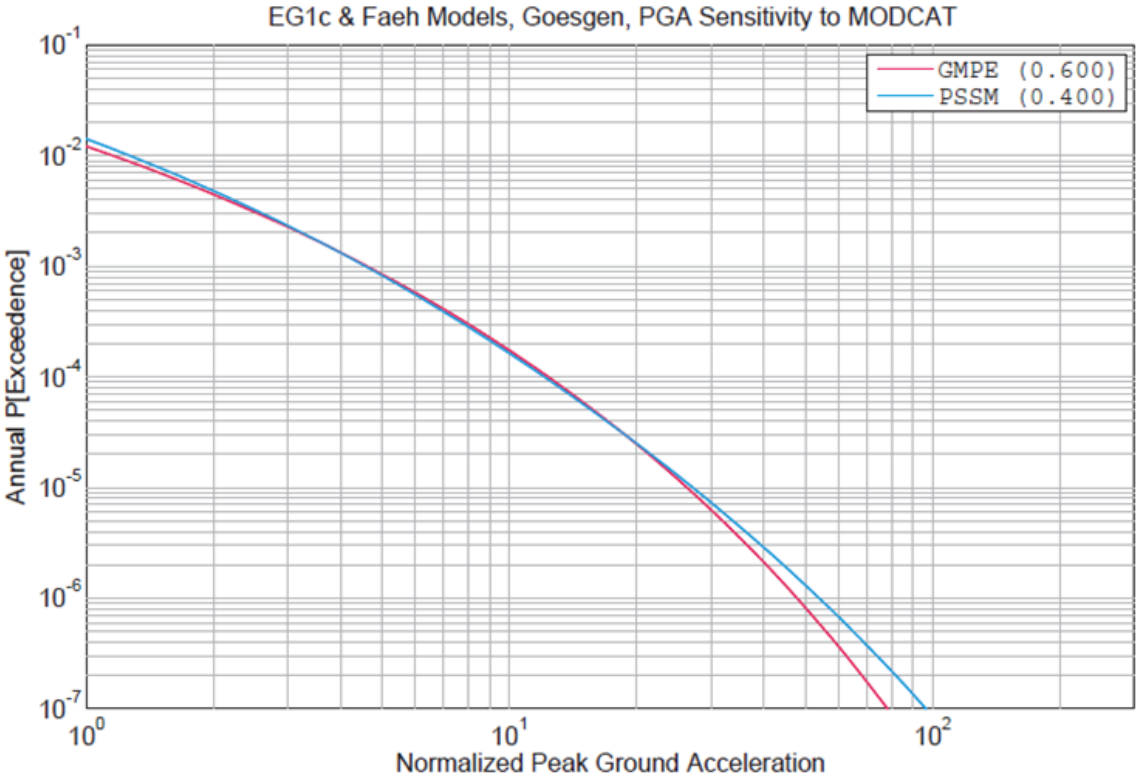

Figure V-1.9: Sensitivity of the hazard for site Gösgen relative to the two sets of relations. (Presentation of rock hazard feedback by P. Roth, SP2/WS11, 16.1.2003).

Step 2 now takes into account the physical limit of κ due to the low litho-static pressure in the near surface condition. This discussion now relates to the values in the Swiss stochastic model.

Using high-quality recordings of induced earthquakes in the city of Basel, Switzerland, Bethmann et al. [2012] studied the attenuation properties in the area. Attenuation of waves emitted from induced earthquakes in the frequency range of 10-130 Hz decreases with depth: Qs is around 40-60 for depths between 500 and 2700 m, and Qs about 85 at depths of 1.2-2.7 km. They obtain similar values of Q for estimates of attenuation in the time and frequency domain. They also observe that Qp is similar to Qs. The results are confirmed when comparing the Q values to the study of Abercrombie [1998] that also infer similar Q values in geologically different environments. Their typical values of both P wave and S wave total Q (Qp and Qs, respectively) in the upper 100 m are very low, around 10 in the frequency range of a few Hz to a few tens of Hz. They also appear to be almost independent of rock type. Abercrombie [1998] summarizes experiments that encompass a wide range of rock types, but find relatively small differences in Q values in the upper few hundred metres. In the upper 500 m typical values are Qp<50 and Qs<30. This depth range probably includes a layer of weathered rock.

We therefore assess reasonable ranges and limits for κ, assuming Q to be constant in a thick layer close to the surface. We can explore values for κ taking into account a reasonable limit

of an average Qs, and a range for Qs in the upper 500 and 1000 m, using a lower bound for V_{S500} and the values for V_{S500} and V_{S1000} from the profiles.

Table V-1.8: κ values for the NPP sites depending on Q.

Method	Ref. κ	KKM	KKB	KKL	KKG1	KKG2
$V_{S500} = V_{S30}$:						
Qs=30	0.017	0.015	0.009	0.008	0.007	0.007
V_{S500} from profile:						
Qs=20	0.014	0.018	0.01	0.009	0.016	0.01
Qs=30	0.009	0.012	0.007	0.006	0.011	0.007
Qs=40	0.007	0.009	0.005	0.005	0.008	0.005
V_{S1000} from profile:						
Qs=40	0.011	0.014	0.009	0.009	0.013	0.009
Qs=60	0.008	0.009	0.006	0.006	0.009	0.006
Qs=100	0.005	0.006	0.004	0.003	0.005	0.004
Mean	0.010	0.012	0.007	0.007	0.010	0.007

The κ values from step 1 for the Swiss stochastic model are modified taking into account the κ obtained by assuming first V_{S30} V_{S500} which has a similar effect as assuming a Q value lower than 30 and the V_{S500} values from the profiles. These values are used to modify method 1 for the Swiss stochastic model. Method 2 is kept from step 1 of our assessment. For method 3 we take into account the work of Poggi et al. [2012] (see values in TP2-TB-1090) on Japanese data to define a new model for the upper limit for the κ of the empirical GMPEs. For method 4 of the Swiss stochastic model, the average κ values are taken from the assessment of κ assuming the different Q values and shear wave velocities (all values in the table above). In order to cover possible lower values of κ a fifth set of κ values is proposed based on the values for V_{S500} and Qs=40.

The $\Delta\kappa$ values are again kept the same between the sites for the two sets of ground motion relations, by balancing the weights of the higher and lower κ values. For the empirical GMPEs the κ values given in Table V-1.9 are finally used. After review of the resulting correction functions and spectral shapes of the corrected GMPEs, it was obvious that the target κ is not allowed to be larger than the host κ. In such cases the target κ is taken equal to the host κ.

Table V-1.9: κ values for empirical GMPEs.

Method	Weight	KKM	KKB	KKL	KKG
1	0.25	0.020	0.014	0.013	0.012
FAS, Swiss	0.30	0.016	0.013	0.011	0.010
TP2-TB-1090	0.20	0.027	0.024	0.022	0.022
4	0.20	0.019	0.014	0.014	0.015
5	0.05	0.013	0.009	0.009	0.009

For the Swiss stochastic model the κ values given in Table V-1.10 are used:

Table V-1.10: κ values for the Swiss stochastic model.

Method	Weight	KKM	KKB	KKL	KKG
1	0.25	0.015	0.009	0.008	0.007
FAS, Swiss	0.30	0.016	0.013	0.011	0.01
3	0.20	0.017	0.014	0.012	0.012
4	0.20	0.012	0.007	0.007	0.008
5	0.05	0.009	0.005	0.005	0.005

The κ estimates from the NPP sites (Biro and Renault [2012b] (PMT-TN-1244) and Ktenidou [2012] (EXT-RF-1443) are consistent with the range of values provided in the logic tree, when taking into account the possible influence of the surface sediment in the recordings at depth and possibly lower Vs at the instrument location than in the target site-specific SP2 rock V_{S30}.

1.2.4 $V_S - \kappa$ Adjustment Method

Initially, the $V_S - \kappa$ correction was to be computed only using the stochastic model. A key problem for the $V_S - \kappa$ adjustments is that spectral shapes of empirical models are different from the shapes of equivalent stochastic models. This might be due to the aforementioned effects of shallow structures (resonances at high frequency) or maybe too simplistic parametrization of the stochastic models. Different methods were proposed to correct for V_{S30} and κ.

The "standard hybrid empirical method" (HEM) can lead to unstable results. This instability of the method is due to the fact that for response spectra no simple ratios can be applied at high frequencies (as it is the case for the Fourier spectra). This method, therefore, often leads to high values in the amplifications, and rather unrealistic $V_S - \kappa$ corrections. For this reason, the HEM method is not used.

The iterative method of develpped by Scherbaum [Kühn 2011c] (EXT-SUP-1051) corrects empirical spectra directly, and relies on stochastic simulations to correct the PGA value. Because the iterative correction is not unique, three different iterative correction procedures are proposed in the technical note EXT-SUP-1051. Presently, it is not possible to validate these methods against each other. They are used for the $V_S - \kappa$ correction of the GMPE with equal weight, even if it seems that small changes in κ can lead to large changes in the shape of the spectrum. Finally, the IRVT method documented in [Al Atik et al. 2013; Al Atik and Abrahamson 2012a] (EXT-TB-1087) is an alternative to the iterative $V_{S30} - \kappa$ corrections, even if some concerns were raised that the method might not be valid at high frequencies. But the questionable validity at high frequencies seems not to influence the scaling factor. The IRVT method is, therefore, also used in the logic tree. It cannot be applied the branch "Empirical relations" because it requires the κ to be consistent with the shape of the inverted FAS.

The following weights are therefore assigned:

- Branch "stochastic inversion": weight 0.1
  - Branch "HEM": weight 0

  - Branch "Scherbaum": weight 1.0, with each of the 3 sub-branches having weights of 0.333

- Branch "Empirical relation": weight 0.5
  - Branch "HEM": weight 0
  - Branch "Scherbaum": weight 1.0, with each of the 3 sub-branches having weight 0.333
  - Branch "FAS scaling with IRVT": weight 0

- Branch "RVT based FAS": weight 0.4
  - Branch "HEM": weight 0
  - Branch "FAS scaling with IRVT": weight 1.0

The reasons for the weights of the main branches are explained in Section 1.2.1.

1.3 Logic Tree for Upper Ground Motion for Horizontal and Vertical

The maximum ground motion logic tree is applied to define the level of ground motion with zero chance of higher values. Extreme values occur at all distances, magnitudes and site conditions [Strasser and Zulu 2010] (report EXT-TB-1067, and data TP2-WAF-1012). For this reason, the proposed logic tree has two branches, Branch 1 with a distance decay anchored to the Boore & Atkinson (2008) "BA08" median , and Branch 2 with no distance decay anchored to the "BA08" median at 10 km R_{JB} distance. The data show that high values occur at all distances, which might reflect a sampling problem so that the number of near-source recordings is still insufficient. The second branch is non-physical because it does not reflect geometrical spreading and anelastic attenuation. Therefore zero weight is given to this branch. Since SP2 is providing ground motion estimates for rock at V_{S30} larger than 1000 m/s (at the base rock of each NPP), only observed data were used for the evaluation of maximum ground motion that are recorded on either site class A or site class B from data collected and analyzed in TP2-WAF-1012. Additionally, the results from numerical modeling performed during the PEGASOS Project were also taken into account. The branch with factor 7.5 (equivalent σ of 3.54) was reached by a considerable number of recordings and is, therefore, given zero weight. The next higher level is exceeded by only few recordings. However, these occurrences might reflect special conditions not achievable at the NPP sites due to the hard rock conditions. The larger factors obtain some weight because we might not have seen the largest ground motions. Using this information, the following weights are assigned:

- Branch 1 (distance decay): Weight 1.0

  Factor 7.5: weight 0

  Factor 12.6: weight 0.1

  Factor 21.1: weight 0.5

Factor 35.5: weight 0.3

Factor 59.6: weight 0.1

Factor 100: weight 0

- Branch 2 (no distance decay): weight 0

For the vertical component a similar distribution of extreme ground motion is observed, and the same model as for the horizontal is therefore applied.

1.4 Logic Tree for the Aleatory Variability σ

Assessment of uncertainties of σ is very important and includes the within-event single station residuals Φ_{SS} and the between-event variability (τ model). Models for Φ_{SS} and τ are proposed in PRP report EXT-TB-1058 [Rodriguez-Marek and Cotton 2011], and are summarized and discussed below.

1.4.1 Models for the Between-event Variability τ

Between-event variability, τ of the Swiss dataset is consistent with the larger values of the NGA models that take into account aftershocks. This could be due to the fact that the Swiss data are mainly controlled by small magnitude earthquakes and/or to the fact that the Swiss datasets are mixing data from two tectonic regimes (Alps and Foreland). Between-event variability, τ decreases when magnitude increases. This could be due to a higher stress drop variability of small earthquakes or increased uncertainty in magnitude determination (e.g. Moss [2009]). The logic tree for the between-event uncertainty is based on two models: a period dependent average model (τ-Model 1) and a model based on the original GMPEs between-event variability (τ-Model 2). The period dependent model has been obtained by calculating the mean value of the between-event variability over a selection of models.

τ varies from dataset to dataset, and should have the effects of magnitude uncertainty removed. The magnitude uncertainty in the different GMPEs is difficult to assess, and varies between 0.05 and 0.2 magnitude units, whereas older and smaller events have generally larger uncertainties. Dataset differences are probably more important than magnitude error uncertainty: some of the models also removed the magnitude uncertainty from the τ model, some do not.

As long as the τ model provided with the GMPE has reasonable shape (Fig. V-1.10), only the τ-Model 2 should be taken into account in the logic tree, because the value of τ depends on the dataset, e.g. the tectonic regime(s), the use of aftershocks, the magnitude distribution in the dataset and the magnitude uncertainties. Therefore model 2 is selected as the only branch of the logic tree for almost all GMPEs, with the reasoning that τ is strongly related to the particular GMPE. There are, however, models with large jumps in τ from one period to the next: "AkBo10" (that is used in the proposed logic tree), in addition to others with the same problem but not used here. The origin of these jumps is unknown and might be due to noise in the data, issues related to the applied filters, or the number of small events in the dataset. In this case the global average is preferred. The selected weights for the GMPEs are therefore as follows:

- All GMPEs except "AkBo10":

τ-Model 1: with weight 0

τ-Model 2: with weight 1.0

- For "AkBo10":

τ-Model 1: with weight 1.0

τ-Model 2: with weight 0

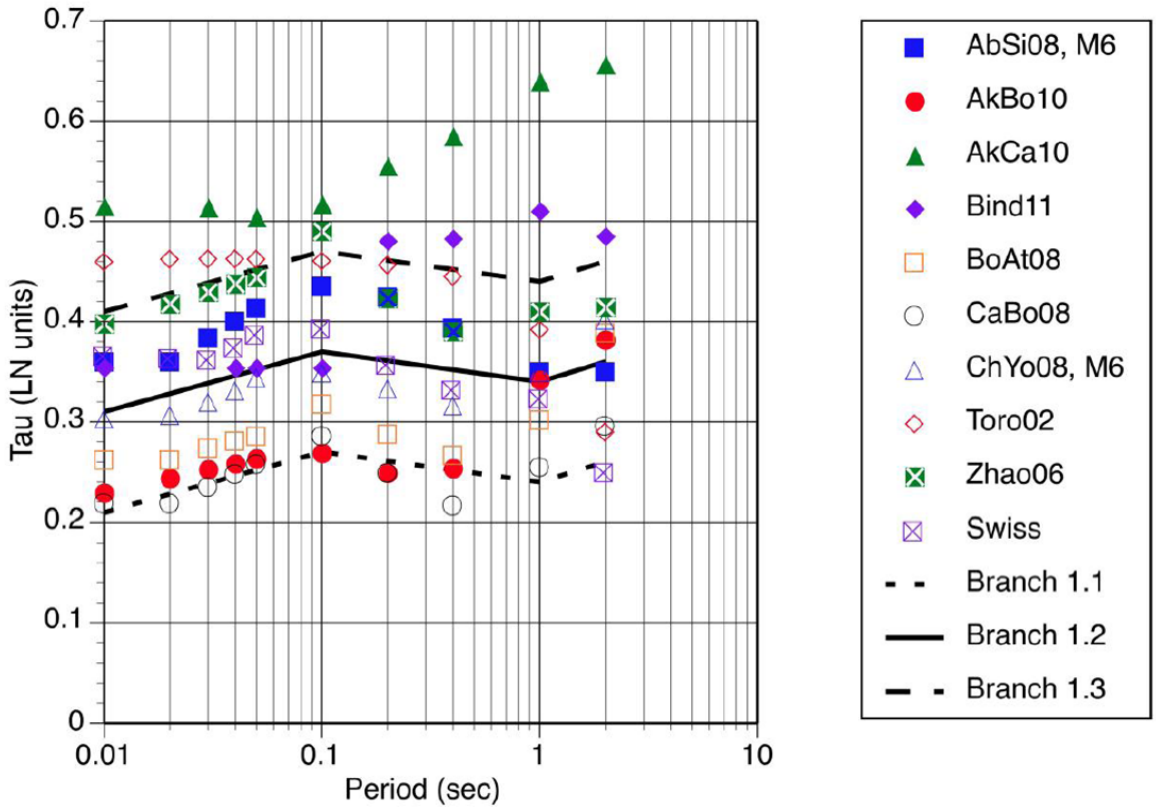

Figure V-1.10: Comparison of proposed τ-Model 1 to between-event standard deviations calculated for the different datasets. τ values for the GMPEs are also shown [Rodriguez-Marek and Cotton 2011].

1.4.2 Models for the Within-event Single Station Residuals Φ_{SS}

Three different models are considered for Φ_{SS}: Φ_{SS}-Model 1 with a constant Φ_{SS}; Φ-Model 2 with a distance-dependent Φ_{SS}, and Φ_{SS}-Model 3 with a magnitude- and distance-dependent Φ_{SS}. Of these three models, I consider the magnitude-distance dependence of Φ_{SS} to be the most physical model, and it seems to be evident from the analyzed data. For small magnitudes, there is a clear increase in the values of Φ_{SS} at very short distances. For intermediate magnitudes ($5.5 < M < 7$), the trend of higher Φ_{SS} at short distances is not observed for the California data, and for large magnitudes, no apparent trend is visible. Shallow events produce different ground motion (surface waves) than deep events (S-wave), and this might be a reason of the effect that can be seen for the smaller magnitudes Φ_{SS}.

This disappears for larger events around magnitude 6, because energy is released in the entire depth range.

A reason for keeping Model 2, with a distance-dependent Φ_{SS}, could be that from numerical modeling of near-source ground motion, there is evidence for larger variability [Ripperger et al. 2008]. However, Model 2 largely over-predicts the Φ_{SS} values for large magnitudes and short distances, and is, therefore, not kept in the logic tree. Model 1 is kept in the logic tree due to limited data in some bins of Model 3, especially for large magnitude and short distances. Model 3 is given higher weight than Model 1 because it is the more physical model. Due to these reasons, the following weights are given to the three models:

- Φ_{SS}-Model 1: weight 0.3
- Φ_{SS}-Model 2: weight 0
- Φ_{SS}-Model 3: weight 0.7

There is some evidence for regional dependence of site-corrected within-event residuals and the data from all regions were used together to develop these models. The values for all the regions are similar to those from Switzerland. Site-corrected Φ_{SS} for California were, however, slightly higher, the values from Turkish data slightly lower than data from Taiwan, Japan and Switzerland. Φ_{SS} varies with period. For larger periods the values for Φ_{SS} are smaller, indicating less influence of site effect variability. Sites in deep basins and complex geology are included in the statistics, whereas our assessment needs to consider NPP rock sites that are not complex. The main question to answer is if Φ_{SS} at the NPP rock sites are different from the world-wide average. It has been observed that Φ_{SS} for receivers at depth are slightly lower than at the surface [Rodriguez-Marek et al. 2011] with about 0.01 difference around 0.2s to 0.02-0.03 difference around 1s period. These borehole sites, however, are still influenced by the soil response induced by shallow layers above the sensor at depth (reflected waves, effects from resonances, surface waves, etc.). An observation of smaller Φ_{SS} at depth would somewhat justify a reduction of the Φ_{SS} at rock sites. Observed Φ_{SS} of rock sites in Switzerland are not different from the Φ_{SS} of other sites (PRP report TP2-TB-1024 [Edwards et al. 2010]), however, there might still be an effect of the surface layers and topography. On one hand, no general dependence of the single-station standard deviation on V_{S30} was outlined in PRP report EXT-TB-1058 (see figure 4.2 in Rodriguez-Marek and Cotton [2011]). While, on the other hand, an analysis using V_{S30} as used in the two previously mentioned studies is probably inadequate, because V_{S30} is not directly related to the portion of the structure seen by a wave at given period.

The standard deviation of Φ_{SS} computed from other regions is similar to that of Switzerland [Rodriguez-Marek 2012] (EXT-TN-1225). This statement is conditioned on the fact that the comparison is done with relatively few data. The standard deviation for Φ_{SS} is taken from the values derived for the largest number of records per site (larger than 20 in table 4.6 in PRP report EXT-TB-1058). The $\sigma(\Phi_{SS})$ is decreasing with the number of records, whereas Φ_{SS} does not. The range between $\Phi_{SS,max}$ and $\Phi_{SS,min}$ is, however, changing with an increasing number of records. The decrease of $\sigma(\Phi_{SS})$ might also be affected by a large number of recorded aftershocks within a limited azimuth of the particular station. The proposed value for the standard deviation is strictly applicable only to Model 1. The lack of data, however,

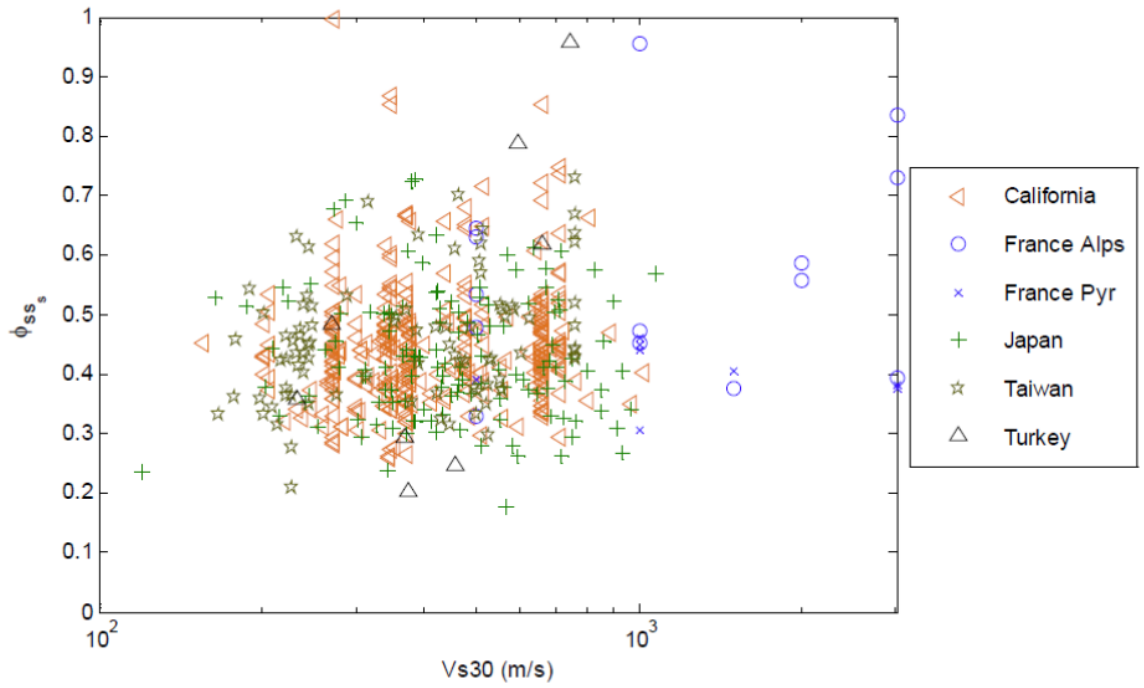

Figure V-1.11: Dependence of the single-station standard deviation on V_{S30} for T=1.0 s (Figure 4.3 in PRP report EXT-TB-1058). From this plot we recognize that the data from California are clustering at specific V_{S30} values probably due to a V_{S30} assigned by site geology.

precludes an equally robust estimate of this variability for Model 3. Therefore, the proposed values of Model 1 are also applied to Model 3 as proposed in EXT-TN-1225 [Rodriguez-Marek 2012]. Theoretically, the values should be even smaller.

We can expect that Φ_{SS} values for rock sites without topographic effects should be lower than the world-wide average, and Φ_{SS} derived at 3 s period could be used as a possible anchor value for such Φ_{SS} (0.41 at 3 s period versus 0.46-47 at periods in the range 0.1-0.5 s, using Model 1 for Φ_{SS}). Due to the lack of recordings on hard rock sites without low-velocity surface layers, such a hypothesis is difficult to be verified. The standard deviation of Model 1 for Φ_{SS} is in the range 0.08-0.10 when using more than 15 recordings per site for the analysis. This normal distribution for rock sites without strong site effects would be expected to be narrower, because, again, very special sites in deep basins and complex geology are included in the world-wide statistic, whereas the considered NPP rock sites are not complex. Again, an anchor value could be the derived standard deviation at 3s period of 0.07 when using more than 20 recordings per site for the analysis.

In order to account for the fact that the statistics might be influenced by sites with strong and highly variable site effects and its possible influence on Φ_{SS} and Φ_{SS} uncertainty, the Φ_{SS} uncertainty branch is weighted asymmetrically. An asymmetric distribution shifts the mean Φ_{SS} to lower values.

In order to assess rock sites for having lower Φ_{SS} I use the concept of the quarter wave-length representation of the structure, $V_{S_{QWL}}$. A quarter-wavelength representation of the velocity profile is more representative than V_{S30}, and it was so far not investigated. Such analysis

was performed in this evaluation process, using the Japanese sites reported in EXT-TB-1058 by relating $V_{S_{QWL}}$ of each profile with Φ_{SS} for different periods. The result is shown in Figure V-1.12. It becomes evident that Φ_{SS} is weakly varying with V_SQWL values in the Japanese dataset. The world-wide dataset provides similar trends for Φ_{SS} as the average for the Japanese dataset, as shown in Figure V-1.13. We can see a trend (skewness) in the $V_{S_{QWL}}$ dependence in Japanese data (Figure V-1.12): lower Φ_{SS} for small $V_{S_{QWL}}$ (maybe due to the effect of damping), large values in the intermediate velocity range, and again smaller values for Φ_{SS} for $V_{S_{QWL}}$ above 1500 m/s. Lower values for Φ_{SS} at rock sites, are, therefore, supported by the Japanese data, as well as by the results presented in figure 8 of Rodriguez-Marek et al. [2011] (see Figure V-1.13). The value of Φ_{SS} is consistently lower, both at surface and borehole, for V_{S30} higher than 900 m/s (with the exception of the surface PGA). The authors also notice that, in general, sites with higher V_{S30} have lower site-to-site variability. This, however, is not considered here, because site-to-site variability was removed from total σ.

It seems evident that Φ_{SS} is reduced at high V_{S30}, even though as reported in Rodriguez-Marek [2012] (EXT-TN-1225) high V_{S30} sites have a lower azimuth standard deviation, hence, they might have recorded preferentially a single-path standard deviation. In order to account for a reduced Φ_{SS} at high V_{S30}, a skewed distribution for the epistemic uncertainty in Φ_{SS} is modeled by the following three branches:

- Branch 1 with weight 0.4 : Mean(Φ_{SS}) -1.6 $\sigma(\Phi_{SS})$
- Branch 2 with weight 0.6 : Mean(Φ_{SS})
- Branch 3 with weight 0.0 : Mean(Φ_{SS}) +1.6 $\sigma(\Phi_{SS})$

For the standard deviation $\sigma(\Phi_{SS})$, the following 3 values are selected: 0.07, 0.10 and 0.13. The value 0.07 is derived from the standard deviation at 3s period when using more than 20 recordings, the value 0.10 is an upper limit of the derived standard deviation when using more than 15 recordings, and the value 0.13 from the range of derived standard deviation when using more than 10 recordings.

Applying these values with the skewed distribution for the epistemic uncertainty of Φ_{SS}, the mean of Φ_{SS} is shifted in the range -0.045 (for 0.07) to -0.083 (for 0.13) which are target values that can be justified from the data shown in Figures V-1.12 and V-1.13. A lower weight is applied for std(Φ_{SS}) of 0.13, because it is the bound that can be seen in the observations. The following weights are applied:

- $\sigma(\Phi_{SS})$ is 0.07: weight 0.4
- $\sigma(\Phi_{SS})$ is 0.10: weight 0.4
- $\sigma(\Phi_{SS})$ is 0.13: weight 0.2

There is lack of data in the V_{S30} range of the NPPs rock condition, and the proposed model for Φ_{SS} cannot be better constrained.

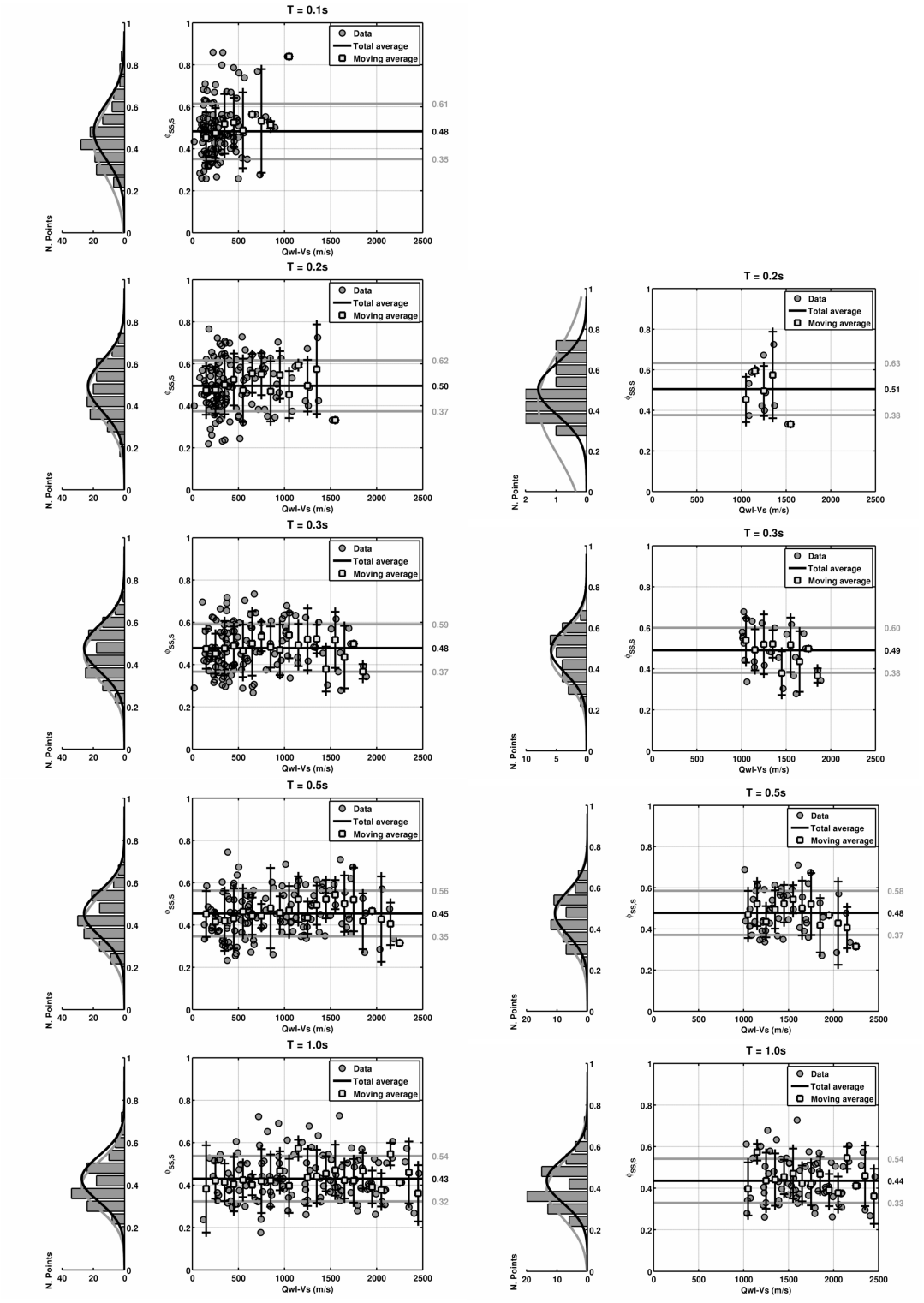

Figure V-1.12: Dependence of Φ_{SS} on $V_{S_{QWL}}$ for different periods, for the Japanese sites analyzed in Rodriguez-Marek and Cotton [2011] (EXT-TB-1058), using different ranges of the $V_{S_{QWL}}$. The black curve to the left of each subplot is a Gaussian obtained directly from the mean and standard deviation, computed from the whole ensemble of data. The gray curve is a Gaussian obtained indirectly by polynomial fit of the histogram, and depends on the number of bins used to create the histogram, but it useful to qualitatively assess the "skewness" of the distribution itself.

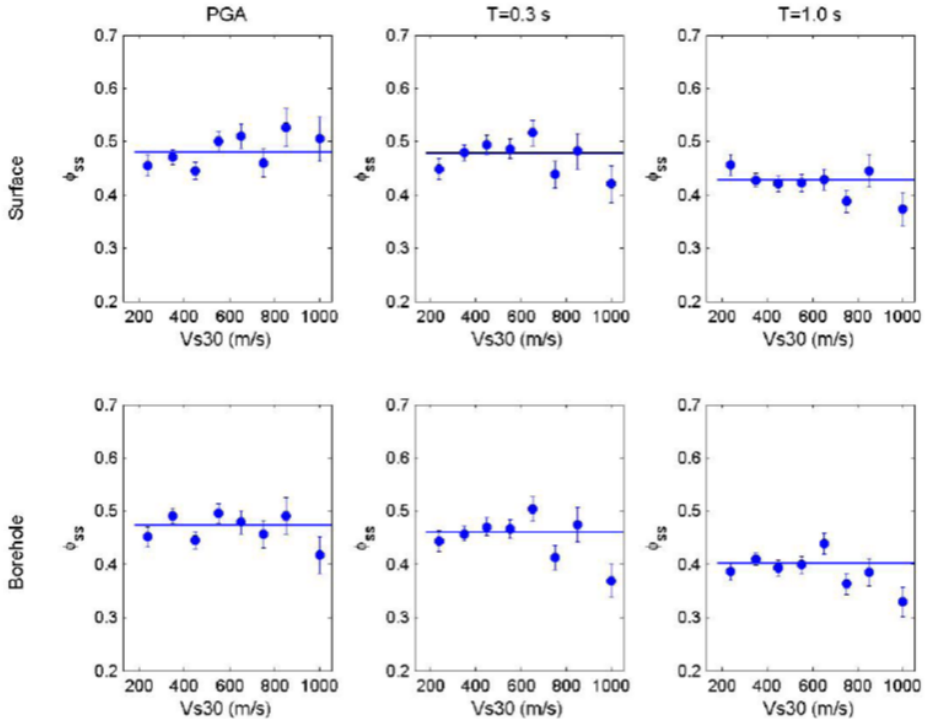

Figure 8: Variation of ϕ_{ss} with Vs30. Vs30 bins are 100 m/s wide. The last bin groups all stations with Vs30 higher than 900 m/s. The solid line is the average ϕ_{ss}, and the error bars represent a one standard deviation range of the estimated standard deviation.

Figure V-1.13: Corresponds to Figure 8 taken from Rodriguez-Marek et al. [2011] indicating a reduction of Φ_{SS} at larger V_{S30} ("banana shape").

1.5 Weight on V/H Spectral Ratios

All empirical V/H GMPEs, except the SED model, are derived from few or no data with V_{S30} >1000 m/s. V/H reported in NUREG 6728 are related to code-type spectra and are not used as an alternative model in the logic tree. There is a V/H peak at high frequency in the models produced using theGülerce and Abrahamson [2010] ("GüAb10"), Campbell and Bozorgnia [2003], and the Bommer et al. [2011] methods. It is, however, unclear what the reason might be for this peak. This still might be a trace from the trough in H/V that is observed in the case of sites characterized by sediment or weathered rock layers over compact rock [Edwards and Fäh 2011a] (EXT-TN-1217). From the limited analysis of some Swiss sites, the report concludes that the V/H curve is somewhat linked to the κ value of the site, with the higher κ site's V/H shape more closely matching the model of Bommer et al. [2011]. Rather than an explicit relation between V/H and κ, this is probably due to the correlation of κ with site-type: with sites having a layer with soil or weathered material being inclined to have high κ values, and showing a peak in V/H (related to the characteristic of the thin surface layer), and "real" rock or high velocity sites more often showing lower κ values and not

having peaks in V/H. On average, Swiss and Japanese sites do not follow the shape generally exhibited in the empirical V/H relations, with no consistent peak in V/H present at 10-20 Hz. Looking at individual sites, we sometimes observe a peak in the V/H, but its location is inconsistent and more likely to be related to resonance phenomena (and, therefore, to a thin shallow surface layer). The empirical relations, therefore, represent an average over different sites, whereas the rock model of Edwards et al. [2011b] represents an average rock scenario with low-velocity layer at the surface. Differences in the Japanese and Swiss rock sites were evident in the high frequency part, as detailed in Edwards et al. [2011b]. The PRP rock V/H model adopted was an average of these two regions, as the differences could not be accounted for in the site description (velocity profile).

Because average κ values in NGA models and "AkBo10" model are high, we might expect only low energy in the high frequency part of the ground motion and V/H is, therefore, very unstable. Both models are to be applied with caution to sites with very high V_{S30} as is required for the rock at NPP sites. Because metadata for the "Bommer et al." model are not as good as for the "GüAb11" relation or the SED model, zero weight is given. The same is true for the Campbell and Bozorgnia [2003] model because it is also very unspecific to V_{S30} adjustment and also zero weight is assigned. The SED model is able to adjust V/H to the high V_S values. However, this model is an empirical model based on Japanese data that are all filtered at 30 Hz, with a number of sites that are characterized by a surface layer with reduced V_S velocity. The site conditions defined for the NPPs, on the other hand, have very high V_S velocities (no surface layer with reduced velocity). Such rock conditions are very theoretical, and are rarely found in empirical V/H relations as well as in almost all station sites of seismic networks. From this observation it is, therefore, straightforward to define a theoretical model that goes with a theoretical V/H ratio without the correction above 7 Hz introduced in the Edwards et al. [2011b] relation. For such a model, the V/H is, therefore, only dependent on the quarter wave-length velocity of the profiles, and only the profile defines the frequency dependence of V/H.

Data from rock sites in Eastern-US analyzed within PRP [Biro and Renault 2012a] (PMT-TN-1257) show a similar behavior than the corrected SED relation for higher V_{S30} of the rock. Hard rock sites without significant surface weathering have been analyzed by Siddiqqi and Atkinson [2002]. Qualitative comparison between the published H/V ratios from Fourier spectra at these hard rock sites supports the SED model at low frequency and also indicates good agreement with the model without the correction above 7 Hz. The SED models are given a higher weight (total 0.7), because they are site specific, whereas not sufficient observed data are yet available to select only one of the SED models. However, if we assume the same composition of the wavefield at low and high frequency, then the uncorrected SED model is expected. But we may also consider more P-wave contribution at high frequency, and then the corrected SED relation might be preferred. However the higher the V_S30 value of the profile is, the larger is the incidence angle of the P-waves at the surface. For these reasons a lower weight is assigned to the corrected SED relation, and the uncorrected SED relation is preferred. The Eastern-US rock observation and "GüAb10" are kept with lower weight (total 0.3) to cover the range of possible models and uncertainties in the Vs profiles. The following weights are therefore applied in the logic tree of KKM, KKL and KKB:

- SED model [Edwards et al. 2011b] without the correction above 7 Hz: weight 0.5

- SED model [Edwards et al. 2011b] with the correction above 7 Hz: weight 0.2
- Eastern-US rock observations [Biro and Renault 2012a]: weight 0.2
- Gülerce and Abrahamson [2010] V/H model: weight 0.1

For site KKG three rock profiles were proposed by SP3 and weights are assigned as follows:

- SED model [Edwards et al. 2011b] without the correction above 7 Hz (Profile P4): weight 0.3
- SED model [Edwards et al. 2011b] with the correction above 7 Hz (Profile P4): weight 0.2
- SED model [Edwards et al. 2011b] without the correction above 7 Hz (Profile P1): weight 0.1
- SED model [Edwards et al. 2011b] without the correction above 7 Hz (Profile P2): weight 0.1
- Eastern-US rock observations [Biro and Renault 2012a]: weight 0.2
- Gülerce and Abrahamson [2010] V/H model for the rock profile with steeper gradient: weight 0.1

In the past, it was recognized that κ for the vertical motion is smaller than the one for the horizontal motion (e.g. Silva and Darragh [2012], EXT-TB-1089). This was related to the larger contribution of P-wave energy at higher frequency on the vertical, due to less attenuated P-waves and S-wave to P-wave conversions. On the one hand, this observation is generally related to sites with V_{S30} around 1000 m/s [Silva and Darragh 2012] or lower, with an observed difference in κ by a factor of about two. On the other hand, the study of Douglas et al. [2010] showed that the estimates for κ for the vertical component are only slightly smaller than for the horizontal component. Moreover, analysis and discussion in Silva and Darragh [2012] did point out the likely mechanisms for similarity of the peak frequency for horizontal and vertical response spectra being at close rupture distance and for the few examples with very hard rock condition. These observations support the SED models that do not lead to significant shifts in the peak between the vertical and horizontal components for rock sites. Moreover there is also no candidate model for rock available that would shift the peak in the vertical spectrum. Due to the limited data, it is not possible to resolve the conditions under which rock site vertical response spectra is expected to have a peak at a higher frequency than horizontal spectra.

1.5.1 Aleatory Part of V/H

For the aleatory part of the model, the difference in the vertical and horizontal variability can be added using two proposed approaches (TP2-TB-1081 [Abrahamson 2012a] and PMT-TN-1240 [Renault and Biro 2012]). Method 1 takes into account that the aleatory variability of the V/H ratio is correlated with the aleatory variability of the horizontal, which is included in the horizontal hazard. To estimate the vertical hazard, this correlation needs to be considered.

For this approach 1, four cases are computed based on different models for the horizontal component aleatory terms and the V/H aleatory terms. No technical base is presently available to set some preferences to these four cases.

For method 2, two GMPEs with both horizontal and vertical models are used to compute the model for the difference in the vertical and horizontal variability: the Abrahamson and Silva [1997] and Campbell and Bozorgnia [2003] models. These two models both show a significantly larger standard deviation on the vertical component than on the horizontal component in the high frequency range.

The disadvantage of both methods is that the values are probably affected the fact that these two models are based on broad range of site categories and so the standard deviations include a wide range of sites within each category. Real hard rock sites need to be considered in our assessment.

The increased standard deviation at high frequency on the vertical component can be explained by the results presented in Beresnev et al. [2002]. They investigated the ratio of S- to P-wave spectra of the vertical component to find which wave type predominantly contribute to the vertical motions, and, therefore, defines the response spectral value. The results show that S-waves dominated the vertical motions on rock and soils at frequencies up to about 10 Hz, above which the average contribution of P- and S-waves are about the same. This possible change in the dominant part of the waveform affects the aleatory uncertainty at frequencies around 10 Hz or at higher. Beresnev et al. [2002] found no significant differences in results by grouping the observations in different distance and acceleration groups.

Based on this consideration, the following additional aleatory uncertainty is derived by averaging the values obtained from method 1 and method 2 for frequencies larger or equal to 5 Hz:

Table V-1.11: Additional aleatory uncertainty for V/H.

Frequency [Hz]	0.5	1	2.5	5	10	20	33.3	50	100
σ_{Vadd} [ln units]	0	0	0	0.06	0.22	0.28	0.23	0.19	0.13

No uncertainty is given because uncertainty is already in the standard deviation (σ) for the horizontal.

1.6 Issues Related to the Center, Body and Range of the Proposed Model

The integration of the available information into the proposed models and weights are aimed so as to represent the center, body, and range of a technically defensible interpretation.

The main issue was to weight the simulation-based Swiss GMPE (with the limitation of restricted data available to constrain stress drop) in relation to the selected empirical GMPEs (with the limitation of few or no data with V_{S30} >1000 m/s). Expert judgment was, therefore, important throughout the evaluation and weighting process, to exclude models with obvious deficits. From the initially proposed 11 GMPEs only 7 are used in the logic tree as outlined in

the summary. The extended Swiss stochastic model is fully compatible with the earthquake catalog, the observed intensity data, and average properties of the crust. While the Swiss stochastic model has the clear advantage of being referenced to a velocity profile that was derived from measured V_S-profiles at seismic stations, empirical GMPEs often rely on meta-data and V_{S30} values of unknown quality. The empirical GMPEs used could therefore be affected by the properties of shallow sediments that are probably not accounted for in the V_{S30} estimate, and which cannot be removed from the equations. Moreover the reference velocities of some of the empirical GMPEs might be biased, as outlined in Section 1.1.3. Improved quality of meta-data in developments of GMPEs will be one of the key issues to address in the future. The Swiss stochastic model on the other hand has the disadvantages to extrapolate beyond the observed data. The high near-field geometrical spreading in the Swiss Foreland is presently based on few data only. With additional future recordings and increasing station density in the Swiss Foreland, this issue can be resolved. The collection of high-quality meta-data for seismic stations in Switzerland and the updating of the Swiss stochastic model therefore remain important issues.

In order to cover the range of possible models, the Swiss stochastic model is included with a range for stress drop based on comparison with observed strong ground-motion data. The selected empirical GMPEs are all included in the proposed model because none of the models represents the true and only correct ground motion prediction equation. They are simply a projection of available data into a model with some advantages and disadvantages which influenced the choice of their specific weight in the logic tree.

Recordings of strong earthquakes in the near-field and on hard rock conditions are still rare and meta-data (e.g. S-wave velocity profiles) often incomplete. Such data however would be required for a verification of the proposed models in this project. Therefore, it might be that with additional future observations the weighting of the different models could also change. This is particularly true for the V/H models and the κ estimates at hard-rock sites with high S-wave velocity. The $V_S - \kappa$ adjustment presently remains a scientific challenge including improved physical models for the high-frequency attenuation.

Chapter 2

Hazard Input Document for D. Fäh (EG2-HID-1012)

Written by the PMT, SP4 and TFI

This document describes the implementation and parametrization of Donat Fäh's expert model EG2-EXM-1012, as described in the evaluation summary EG2-ES-1021 (see Chapter 1) and delivered on 07.02.2013, with an update for the target κ estimates on 20.11.2013. The purpose of this document is to translate the expert's evaluation of ground motion into an input usable by the hazard software. For PRP a consensus master logic tree for the median, the aleatory variability, the maximum and the V/H ratio of the ground motion was developed by the SP2 experts and is described in part I. The basic elements of those trees and models are not repeated here. This document only summarizes the parameters and model weights assigned by the expert D. Fäh. By this the master logic tree becomes expert specific and reflects the individual evaluations.

2.1 Model Implementation

Based on the evaluation summary, the logic trees for the median horizontal ground motion, the vertical/horizontal ratio, the maximum ground motion and the aleatory variability of the horizontal and vertical component were implemented. The key elements in the model are given below. Figure V-2.1 shows the logic tree. The first level in the logic tree, "Model Category" is not explicitly specified by the expert but is used by SP4 to allow for an easier treatment of those subsequent global variables (or logic tree levels) like "Vs-Kappa", which are dependent on whether a GMPE or a PSSM model is considered. The logic tree has in total 1600 branches.

2.2 Median Horizontal Ground Motion

Six of the ten candidate models by SP2 get non-zero weights in D. Fäh's model. The empirical GMPEs have a total weight of 60% and the Swiss stochastic model a total weight of 40%. For

Figure V-2.1: Logic tree for the horizontal ground motion.

the parameterized Swiss stochastic model (PSSM) the versions with a M_C=4.5 and stress drop values of 40, 60, 90 and 120 bars have been selected.

Table V-2.1: Weights assigned to the GMPEs.

GMPE	Abbrv.	Weight	Weight by category
Abrahamson & Silva (2008)	AbSi08	0.05	0.0833
Boore & Atkinson (2008)	BoAt08	0.05	0.0833
Campbell & Bozorgnia (2008)	CaBo08	0.05	0.0833
Chiou & Youngs (2008)	ChYo08	0.20	0.3333
Atkinson & Boore (2006)	AtBo06	-	-
Toro et al. (2002)	Toro02	-	-
Akkar & Bommer (2010)	AkBo10	0.05	0.0833
Akkar & Cagnan (2010)	AkCa10	-	-
Bindi et al. (2011)	Bind11	-	-
Zhao et al. (2006)	Zhao06	0.20	0.3333
PSSM30		-	-
PSSM40		0.01	0.025
PSSM60		0.20	0.50
PSSM90		0.16	0.40
PSSM120		0.03	0.075
Sum GMPE		0.60	1.00
Sum PSSM		0.40	1.00

Table V-2.2 specifies the reference shear wave velocity ($V_{S30,rock}$) to be used for the NGA models and the site category for the models which have only a category, respectively. The host-to-target correction is applied to those reference models to account for the hard rock conditions at the Swiss NPP sites.

For the depth to sediment layer with V_S=1.0 km/s and 2.5 km/s at the site, the sediment thickness is defined as the depth to a material (bedrock) with a given shear-wave velocity or greater, starting at the top of the rock, as defined in the site response and not the ground surface. For AbSi08 and ChYo08 the parameter $Z_{1.0}$=0 m for rock sites, as the reference $V_{S,30}$ values of all four NPP sites is greater than 1000 m/s after application of the $V_S - \kappa$ corrections. For CaBo08 $Z_{2.5}$=0.800 km, based on assumed generic conditions of the Swiss region. The GMPE is evaluated with respect to the generic rock condition of 620 m/s and the value for $Z_{2.5}$ needs to be consistent, as the host-to-target correction towards the Swiss conditions (based on a full V_S profile) is applied afterwards.

Table V-2.2: GMPE specific reference shear wave velocity or site category.

GMPE	Ref. V_{S30} [m/s]
AbSi08, BoAt08, CaBo08, ChYo08	620
AkBo10	Rock Cat. (=800)
Zhao06	Rock Cat. (=700)

2.3 Host-to-target Correction

2.3.1 Host-to-target Correction

The host and target κ values were evaluated according to the PRP reports EXT-TB-1087 [Al Atik and Abrahamson 2012a] and EXT-SUP-1051 (also TP2-ASW-1010), where the average of different evaluated scenarios is taken. The scenarios are based on M=5, 6, 7 and R_{JB}=5, 10 , 20 km with an average depth of 12 km (which is consistent with the average depth in Switzerland).

The expert specific target κ values are summarized together with their weights in Table V-2.3. The Figure I-3.10 depicts the generic logic tree which was developed in the course of the PRP and Figure II-2.2 shows the expert specific version. The finally selected parameters and weights are summarized in Tables V-2.4 to V-2.6. Applying the given combinations leads to 3876 discrete correction functions. The resulting 5-point distribution of $V_S - \kappa$ corrections for each of the used GMPEs is reported in Tables V-2.7 to V-2.10. As the resulting distribution is not a known distribution, the evaluated 5 point distribution is based on the approach of Miller and Rice [1983] with the 0.034893, 0.211702, 0.50, 0.788298 and 0.965107 fractiles. The corresponding probabilities/weights for this given discretization are: 0.10108, 0.24429, 0.30926, 0.24429, 0.10108. Tables V-2.11 and V-2.12 have the correction functions to be applied to the different versions of the parameterized Swiss stochastic model, depending on the defined target κ per site. The scaling of the response spectrum depends on the shape of the Fourier spectrum. Changes in the frequency content of the Fourier spectrum due to different stress drops leads to differences in the $V_S - \kappa$ scale factors for different stress drops. The Tables V-2.11 and V-2.12 illustrate the small numerical differences, but the figures show almost no visible difference between the stress drops.

After review of the resulting correction functions and spectral shapes of the corrected GMPES, D. Fäh decided in November 2013 that the target κ is not allowed to be larger than the host κ. Thus, not allowing for a negative $\delta\kappa$ (0 <! Host κ - Target κ). In such cases the target κ is taken equal to the host κ.

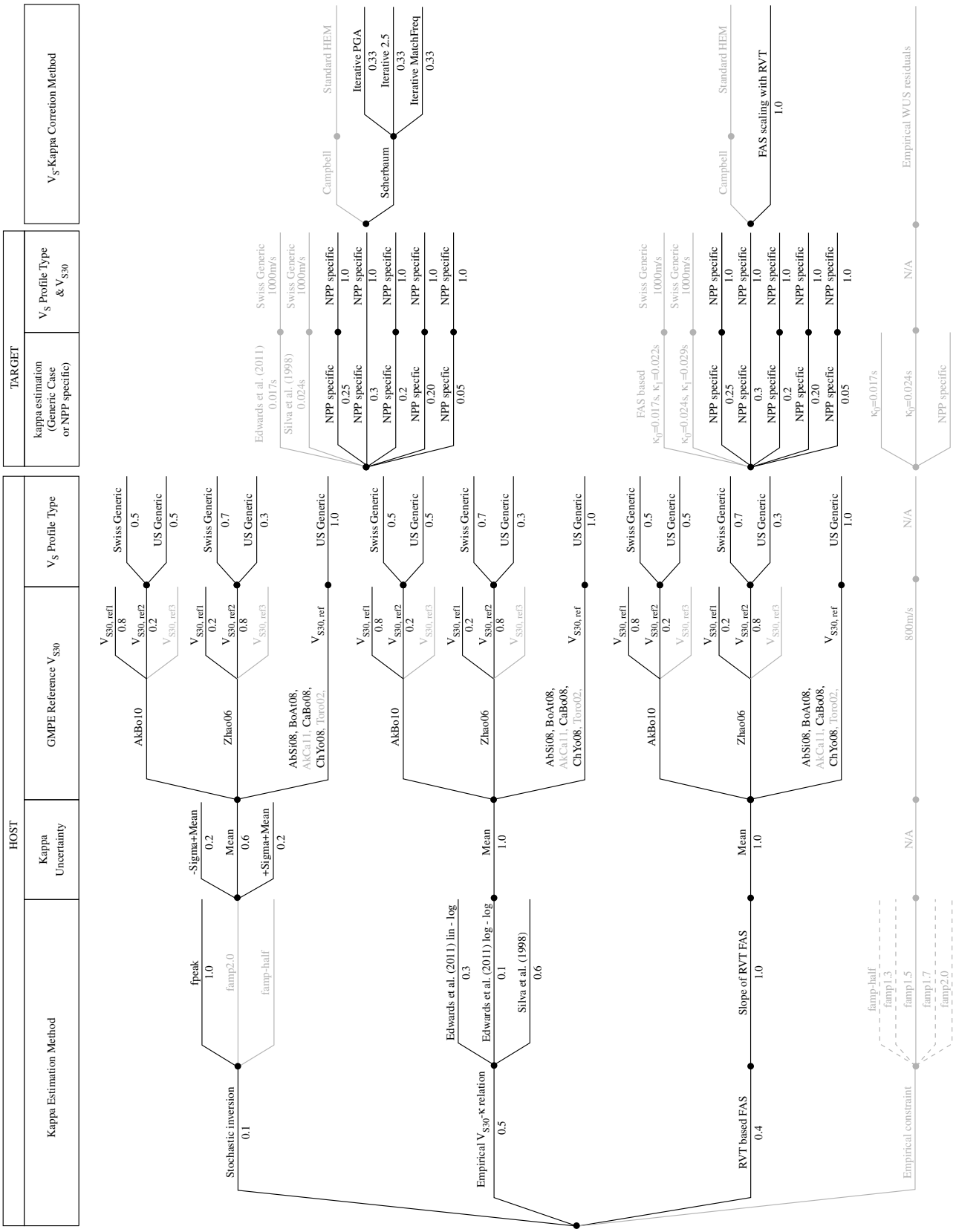

Figure V-2.2: Logic tree for the evaluation of $V_S - \kappa$ scaling for GMPEs.

Table V-2.3: Target κ values for GMPE and PSSM with weights.

	Weight	Mühleberg κ_0 [s]	Beznau κ_0 [s]	Leibstadt κ_0 [s]	Gösgen κ_0 [s]
GMPE					
TK5	0.25	0.020	0.014	0.013	0.012
TK6	0.30	0.016	0.013	0.011	0.010
TK7	0.20	0.027	0.024	0.022	0.022
TK8	0.20	0.019	0.014	0.014	0.015
TK9	0.05	0.013	0.009	0.009	0.009
PSSM					
TK5	0.25	0.015	0.009	0.008	0.007
TK6	0.30	0.016	0.013	0.011	0.010
TK7	0.20	0.017	0.014	0.012	0.012
TK8	0.20	0.012	0.007	0.007	0.008
TK9	0.05	0.009	0.005	0.005	0.005

Table V-2.4: Overview of parameters and weights assigned to the $V_S - \kappa$ logic tree for the NGA models.

Estimation Method	**wt.**	**Host**			**GMPE**	**HostVS**	**wt.**	**Profile**	**wt.**	**TargetVS**	**Target**				**Correction Method**	**wt.**
emethod		hkest & emethod	hostk	**Host κ**	**wt.**	vs30est	**wt.**	vstypestr		(npp) targetp	target TK	**Targ. κ_0**	**Targ. κ_1**	targetk		cmethod	
Stoch. Inv. fpeak	0.10	kLB1	0.0480	0.20	AbSi08	620	1.00	US	1.00	KKB1800	TK5	0.014	0.018	0.25		Iterative PGA	0.33
Stoch. Inv. fpeak		kBE1	0.0639	0.60							TK6	0.013	0.017	0.30		Iterative 2.5	0.33
Stoch. Inv. fpeak		kUB1	0.0799	0.20							TK7	0.024	0.028	0.20		Iterative MatchFreq.	0.33
Emp. Edw. Lin-Log	0.15	kBE4	0.0197	1.00							TK8	0.014	0.018	0.20		FAS scaling with iRVT	1.00
Emp. Edw. Log-Log	0.05	kBE7	0.0183	1.00							TK9	0.009	0.013	0.05			
Emp. Silva	0.30	kBE5	0.0401	1.00						KKG2500	TK5	0.012	0.016	0.25			
iRVT	0.40	kBE6	0.0414	1.00							TK6	0.010	0.014	0.30			
Stoch. Inv. fpeak	0.10	kLB1	0.0412	0.20	BoAt08	620	1.00	US	1.00		TK7	0.022	0.026	0.20			
Stoch. Inv. fpeak		kBE1	0.0511	0.60							TK8	0.015	0.019	0.20			
Stoch. Inv. fpeak		kUB1	0.0611	0.20							TK9	0.009	0.013	0.05			
Emp. Edw. Lin-Log	0.15	kBE4	0.0197	1.00						KKL2200	TK5	0.013	0.017	0.25			
Emp. Edw. Log-Log	0.05	kBE7	0.0183	1.00							TK6	0.011	0.015	0.30			
Emp. Silva	0.30	kBE5	0.0401	1.00							TK7	0.022	0.026	0.20			
iRVT	0.40	kBE6	0.04042	1.00							TK8	0.014	0.018	0.20			
Stoch. Inv. fpeak	0.10	kLB1	0.0476	0.20	CaBo08	620	1.00	US	1.00		TK9	0.009	0.013	0.05			
Stoch. Inv. fpeak		kBE1	0.0518	0.60						KKM1100	TK5	0.020	0.024	0.25			
Stoch. Inv. fpeak		kUB1	0.0560	0.20							TK6	0.016	0.020	0.30			
Emp. Edw. Lin-Log	0.15	kBE4	0.0197	1.00							TK7	0.027	0.031	0.20			
Emp. Edw. Log-Log	0.05	kBE7	0.0183	1.00							TK8	0.019	0.023	0.20			
Emp. Silva	0.30	kBE5	0.0401	1.00							TK9	0.013	0.017	0.05			
iRVT	0.40	kBE6	0.0413	1.00													
Stoch. Inv. fpeak	0.10	kLB1	0.0430	0.20	ChYo08	620	1.00	US	1.00								
Stoch. Inv. fpeak		kBE1	0.0452	0.60													
Stoch. Inv. fpeak		kUB1	0.0473	0.20													
Emp. Edw. Lin-Log	0.15	kBE4	0.0197	1.00													
Emp. Edw. Log-Log	0.05	kBE7	0.0183	1.00													
Emp. Silva	0.30	kBE5	0.0401	1.00													
iRVT	0.40	kBE6	0.0374	1.00													

Table V-2.5: Overview of parameters and weights assigned to the $V_S - \kappa$ logic tree for the Akkar & Bommer (2010) model.

Estimation Method emethod	**wt.**		**Host** **Host κ** hostk	**wt.**	**GMPE**	**HostVS** vs30est	**wt.**	**Profile** vstypestr	**wt.**	**TargetVS** (npp) targetp		**Target** **Targ. κ_0**	**Targ. κ_1** targetk	**wt.**	**Correction Method** cmethod	**wt.**
		hkest & emethod									target TK					
Stoch. Inv. fpeak	0.10	kLB1	0.0394	0.20	AkBo10	600	0.80	CH	0.50	KKB1800	TK5	0.014	0.018	0.25	Iterative PGA	0.33
Stoch. Inv. fpeak		kBE1	0.0540	0.60							TK6	0.013	0.017	0.30	Iterative 2.5	0.33
Stoch. Inv. fpeak		kUB1	0.0686	0.20							TK7	0.024	0.028	0.20	Iterative MatchFreq.	0.33
Emp. Edw. Lin-Log	0.15	kBE4	0.0200	1.00							TK8	0.014	0.018	0.20	FAS scaling with iRVT	1.00
Emp. Edw. Log-Log	0.05	kBE7	0.0187	1.00							TK9	0.009	0.013	0.05		
Emp. Silva	0.30	kBE5	0.0415	1.00						KKG2500	TK5	0.012	0.016	0.25		
iRVT	0.40	kBE6	0.0290	1.00							TK6	0.010	0.014	0.30		
Stoch. Inv. fpeak	0.10	kLB1	0.0491	0.20	AkBo10	600	0.80	US	0.50		TK7	0.022	0.0262	0.20		
Stoch. Inv. fpeak		kBE1	0.0649	0.60							TK8	0.015	0.0192	0.20		
Stoch. Inv. fpeak		kUB1	0.0807	0.20							TK9	0.009	0.0132	0.05		
Emp. Edw. Lin-Log	0.15	kBE4	0.0200	1.00						KKL2200	TK5	0.013	0.0171	0.25		
Emp. Edw. Log-Log	0.05	kBE7	0.0187	1.00							TK6	0.011	0.0151	0.30		
Emp. Silva	0.30	kBE5	0.0415	1.00							TK7	0.022	0.0261	0.20		
iRVT	0.40	kBE6	0.0346	1.00							TK8	0.014	0.0181	0.20		
Stoch. Inv. fpeak	0.10	kLB1	0.0368	0.20	AkBo10	800	0.20	CH	0.50		TK9	0.009	0.0131	0.05		
Stoch. Inv. fpeak		kBE1	0.0485	0.60						KKM1100	TK5	0.020	0.0245	0.25		
Stoch. Inv. fpeak		kUB1	0.0601	0.20							TK6	0.016	0.0205	0.30		
Emp. Edw. Lin-Log	0.15	kBE4	0.0173	1.00							TK7	0.027	0.0315	0.20		
Emp. Edw. Log-Log	0.05	kBE7	0.0155	1.00							TK8	0.019	0.0235	0.20		
Emp. Silva	0.30	kBE5	0.0303	1.00							TK9	0.013	0.0175	0.05		
iRVT	0.40	kBE6	0.0290	1.00												
Stoch. Inv. fpeak	0.10	kLB1	0.0412	0.20	AkBo10	800	0.20	US	0.50							
Stoch. Inv. fpeak		kBE1	0.0534	0.60												
Stoch. Inv. fpeak		kUB1	0.0656	1.00												
Emp. Edw. Lin-Log	0.15	kBE4	0.0173	1.00												
Emp. Edw. Log-Log	0.05	kBE7	0.0155	1.00												
Emp. Silva	0.30	kBE5	0.0303	1.00												
iRVT	0.40	kBE6	0.0314	1.00												

Table V-2.6: Overview of parameters and weights assigned to the $V_S - \kappa$ logic tree for the Zhao et al. (2006) model.

Estimation Method	**wt.**	**Host**		**GMPE**	**HostVS**	**wt.**	**Profile**	**wt.**	**TargetVS**	**Target**				**Correction Method**	**wt.**
emethod		hkest & emethod	hostk	κ wt.	vs30est		vstypestr		(npp) targetp	target TK	**Targ.** κ_0	**Targ.** κ_1	**wt.**	cmethod	
Stoch. Inv. fpeak	0.10	kLB1	0.0729	0.20 Zhao06	500	0.20	US	0.30	KKB1800	TK5	0.014	0.0178	0.25	Iterative PGA	0.33
Stoch. Inv. fpeak	0.10	kBE1	0.0885	0.60						TK6	0.013	0.0168	0.30	Iterative 2.5	0.33
Stoch. Inv. fpeak	0.10	kUB1	0.1041	0.20						TK7	0.024	0.0278	0.20	Iterative MatchFreq.	0.33
Emp. Edw. Lin-Log	0.15	kBE4	0.0215	1.00						TK8	0.014	0.0178	0.20	FAS scaling with iRVT	1.00
Emp. Edw. Log-Log	0.05	kBE7	0.0210	1.00						TK9	0.009	0.0128	0.05		
Emp. Silva	0.30	kBE5	0.0507	1.00					KKG2500	TK5	0.012	0.0162	0.25		
iRVT	0.40	kBE6	0.0322	1.00						TK6	0.010	0.0142	0.30		
Stoch. Inv. fpeak	0.10	kLB1	0.0461	0.20 Zhao06	500	0.20	CH	0.70		TK7	0.022	0.0262	0.20		
Stoch. Inv. fpeak	0.10	kBE1	0.0523	0.60						TK8	0.015	0.0192	0.20		
Stoch. Inv. fpeak	0.10	kUB1	0.0586	0.20						TK9	0.009	0.0132	0.05		
Emp. Edw. Lin-Log	0.15	kBE4	0.0215	1.00					KKL2200	TK5	0.013	0.0171	0.25		
Emp. Edw. Log-Log	0.05	kBE7	0.0210	1.00						TK6	0.011	0.0151	0.30		
Emp. Silva	0.30	kBE5	0.0507	1.00						TK7	0.022	0.0261	0.20		
iRVT	0.40	kBE6	0.0329	1.00						TK8	0.014	0.0181	0.20		
Stoch. Inv. fpeak	0.10	kLB1	0.0343	0.20 Zhao06	700	0.80	US	0.30		TK9	0.009	0.0131	0.05		
Stoch. Inv. fpeak	0.10	kBE1	0.0360	0.60					KKM1100	TK5	0.020	0.0245	0.25		
Stoch. Inv. fpeak	0.10	kUB1	0.0377	0.20						TK6	0.016	0.0205	0.30		
Emp. Edw. Lin-Log	0.15	kBE4	0.0186	1.00						TK7	0.027	0.0315	0.20		
Emp. Edw. Log-Log	0.05	kBE7	0.0169	1.00						TK8	0.019	0.0235	0.20		
Emp. Silva	0.30	kBE5	0.0351	1.00						TK9	0.013	0.0175	0.05		
iRVT	0.40	kBE6	0.0353	1.00											
Stoch. Inv. fpeak	0.10	kLB1	0.0295	0.20 Zhao06	700	0.80	CH	0.70							
Stoch. Inv. fpeak	0.10	kBE1	0.0310	0.60											
Stoch. Inv. fpeak	0.10	kUB1	0.0326	0.20											
Emp. Edw. Lin-Log	0.15	kBE4	0.0186	1.00											
Emp. Edw. Log-Log	0.05	kBE7	0.0169	1.00											
Emp. Silva	0.30	kBE5	0.0351	1.00											
iRVT	0.40	kBE6	0.0326	1.00											

Table V-2.7: Frequency dependent resulting $V_S - \kappa$ correction 5-point distributions for used GMPEs at Beznau.

GMPE	Frequency [Hz]									Weight
	0.5	1	2.5	5	10	20	33.3	50	100	
AbSi08	0.7777	0.7127	0.6044	0.5344	0.4774	0.5117	0.5243	0.5280	0.5273	0.1011
	0.7917	0.7496	0.6857	0.6986	0.6862	0.6649	0.6547	0.6601	0.6621	0.2443
	0.8087	0.7760	0.7476	0.8304	0.8827	0.9397	0.8573	0.8504	0.8480	0.3093
	0.8112	0.7798	0.7608	0.8488	1.1157	1.5196	1.3404	1.1366	0.9423	0.2443
	0.8425	0.8364	0.9017	1.2082	1.3336	1.6109	1.6823	1.5985	1.4559	0.1011
BoAt08	0.7777	0.7127	0.6044	0.5427	0.4604	0.4845	0.5044	0.5180	0.5224	0.1011
	0.7914	0.7379	0.6592	0.6449	0.6749	0.6963	0.6569	0.6307	0.6356	0.2443
	0.8017	0.7626	0.7172	0.7584	0.9038	0.9109	0.9109	0.9109	0.8137	0.3093
	0.8102	0.7735	0.7446	0.8174	0.9295	1.2385	1.1410	1.0050	0.9093	0.2443
	0.8254	0.8029	0.8142	0.9851	1.1494	1.3419	1.4195	1.3761	1.2657	0.1011
CaBo08	0.7777	0.7127	0.6044	0.5427	0.4494	0.4802	0.5048	0.5212	0.5242	0.1011
	0.7876	0.7347	0.6529	0.6329	0.6520	0.7246	0.6567	0.6294	0.6303	0.2443
	0.7997	0.7594	0.7103	0.7453	0.8775	0.9257	0.9263	0.9265	0.8100	0.3093
	0.8102	0.7735	0.7417	0.8174	0.9138	1.1786	1.1439	1.0021	0.9196	0.2443
	0.8265	0.8050	0.8195	0.9978	1.1663	1.3071	1.4213	1.3588	1.2669	0.1011
ChYo08	0.7777	0.7127	0.6044	0.5427	0.4986	0.4989	0.4952	0.4906	0.4881	0.1011
	0.7847	0.7257	0.6322	0.5939	0.5863	0.5863	0.5854	0.5854	0.5854	0.2443
	0.7902	0.7429	0.6730	0.6707	0.7248	0.8426	0.8078	0.7264	0.6654	0.3093
	0.8102	0.7735	0.7417	0.8174	0.8952	0.9029	0.8921	0.8926	0.8915	0.2443
	0.8180	0.7885	0.7781	0.8995	1.3859	2.2415	2.0875	1.7617	1.4330	0.1011
AkBo10	0.7728	0.6532	0.5810	0.5459	0.4584	0.4845	0.4872	0.4956	0.5117	0.1011
	0.7818	0.6776	0.6140	0.6039	0.6478	0.6602	0.6294	0.6329	0.6311	0.2443
	0.7932	0.7292	0.6663	0.6995	0.8421	0.8740	0.8414	0.8244	0.7580	0.3093
	0.8359	0.7670	0.7345	0.8334	0.9359	1.0977	1.0729	0.9500	0.9269	0.2443
	0.8678	0.8478	0.8666	1.1283	1.3755	1.4328	1.4705	1.4210	1.4276	0.1011
Zhao06	0.7501	0.6120	0.5091	0.4103	0.4019	0.4845	0.4931	0.4617	0.4534	0.1011
	0.8050	0.6934	0.6341	0.6383	0.6796	0.7008	0.6888	0.6768	0.6783	0.2443
	0.8195	0.7260	0.6972	0.7673	0.9093	1.0510	1.0516	0.9607	0.8779	0.3093
	0.8335	0.7790	0.7273	0.8267	1.0774	1.2744	1.2327	1.1109	1.1093	0.2443
	0.8476	0.8227	0.8017	0.8758	1.1763	1.4470	1.3541	1.2812	1.2014	0.1011

Table V-2.8: Frequency dependent resulting $V_S - \kappa$ correction 5-point distributions for used GMPEs at Gösgen.

GMPE	Frequency [Hz]									Weight
	0.5	1	2.5	5	10	20	33.3	50	100	
AbSi08	0.7471	0.6596	0.5295	0.4584	0.4095	0.4350	0.4450	0.4503	0.4500	0.1011
	0.7686	0.6981	0.6102	0.6149	0.6051	0.6055	0.6182	0.6181	0.6181	0.2443
	0.7845	0.7272	0.6706	0.7215	0.7531	0.8677	0.7554	0.7636	0.7559	0.3093
	0.8172	0.7804	0.7141	0.7781	1.0038	1.4271	1.3084	1.1413	0.9270	0.2443
	0.8214	0.7869	0.8088	1.0803	1.1226	1.6042	1.5657	1.3500	1.2671	0.1011
BoAt08	0.7471	0.6596	0.5295	0.4630	0.3927	0.4133	0.4315	0.4423	0.4455	0.1011
	0.7686	0.6981	0.6102	0.5603	0.5839	0.6127	0.6285	0.5838	0.5852	0.2443
	0.7836	0.7256	0.6601	0.6844	0.7790	0.8203	0.8201	0.7684	0.7467	0.3093
	0.8144	0.7652	0.6764	0.7195	0.8656	1.1639	1.1065	1.0520	0.8320	0.2443
	0.8169	0.7720	0.7295	0.8789	1.0279	1.2935	1.2945	1.1680	1.1869	0.1011
CaBo08	0.7471	0.6596	0.5295	0.4630	0.3710	0.4019	0.4270	0.4438	0.4469	0.1011
	0.7686	0.6981	0.6102	0.5568	0.5767	0.6397	0.6170	0.5835	0.5799	0.2443
	0.7842	0.7267	0.6601	0.6782	0.7871	0.8335	0.8257	0.7890	0.7498	0.3093
	0.8110	0.7606	0.6719	0.7220	0.8334	1.0946	1.0932	1.0496	0.8248	0.2443
	0.8143	0.7680	0.7305	0.8812	1.0450	1.2684	1.2924	1.1673	1.1983	0.1011
ChYo08	0.7471	0.6596	0.5295	0.4630	0.4232	0.4235	0.4180	0.4214	0.4201	0.1011
	0.7686	0.6981	0.5768	0.5269	0.5238	0.5169	0.5169	0.5169	0.5169	0.2443
	0.7833	0.7240	0.6272	0.6149	0.6438	0.7433	0.7064	0.6837	0.6395	0.3093
	0.8003	0.7440	0.6601	0.7195	0.7925	0.8715	0.8922	0.7920	0.7863	0.2443
	0.8039	0.7501	0.6898	0.7857	1.2196	1.9996	1.9013	1.5896	1.3043	0.1011
AkBo10	0.7456	0.6058	0.5090	0.4613	0.3909	0.4229	0.4422	0.4467	0.4497	0.1011
	0.7721	0.6550	0.5694	0.5399	0.5673	0.5960	0.5573	0.5580	0.5463	0.2443
	0.7913	0.6901	0.6153	0.6257	0.7159	0.7857	0.7750	0.7301	0.6877	0.3093
	0.8081	0.7422	0.6653	0.7316	0.8359	1.0223	1.0016	0.9519	0.8159	0.2443
	0.8679	0.8321	0.7715	0.9932	1.2079	1.2545	1.2759	1.2732	1.2867	0.1011
Zhao06	0.7258	0.6034	0.4716	0.3627	0.3476	0.3902	0.4655	0.4391	0.4104	0.1011
	0.7734	0.6470	0.5643	0.5614	0.6097	0.6441	0.6243	0.6115	0.6115	0.2443
	0.8020	0.6881	0.6319	0.6758	0.7874	0.9211	0.9120	0.8210	0.7631	0.3093
	0.8316	0.7348	0.6622	0.7276	0.9286	1.1270	1.1458	1.0581	0.9378	0.2443
	0.8523	0.8139	0.7258	0.7788	1.0865	1.4313	1.4423	1.1964	1.1697	0.1011

Table V-2.9: Frequency dependent resulting $V_S - \kappa$ correction 5-point distributions for used GMPEs at Leibstadt.

GMPE	Frequency [Hz]									Weight
	0.5	1	2.5	5	10	20	33.3	50	100	
AbSi08	0.7586	0.6791	0.5569	0.4863	0.4344	0.4655	0.4804	0.4838	0.4832	0.1011
	0.7721	0.7188	0.6418	0.6538	0.6437	0.6258	0.6479	0.6576	0.6576	0.2443
	0.7869	0.7400	0.6946	0.7586	0.8005	0.9233	0.7911	0.8075	0.8055	0.3093
	0.7918	0.7465	0.7124	0.7918	1.0752	1.4421	1.2942	1.1736	0.9267	0.2443
	0.8244	0.8020	0.8440	1.1307	1.2128	1.6264	1.5906	1.4388	1.3513	0.1011
BoAt08	0.7586	0.6791	0.5569	0.4922	0.4176	0.4394	0.4607	0.4746	0.4797	0.1011
	0.7725	0.7046	0.6110	0.5910	0.6204	0.6544	0.6480	0.6031	0.6035	0.2443
	0.7825	0.7297	0.6694	0.7033	0.8217	0.8572	0.8571	0.8459	0.7617	0.3093
	0.7916	0.7395	0.6889	0.7533	0.8876	1.1753	1.1034	1.0398	0.8490	0.2443
	0.8076	0.7698	0.7616	0.9208	1.0700	1.3133	1.3065	1.2417	1.2159	0.1011
CaBo08	0.7586	0.6791	0.5569	0.4922	0.3951	0.4277	0.4541	0.4719	0.4751	0.1011
	0.7701	0.7034	0.6089	0.5874	0.6129	0.6822	0.6507	0.6028	0.5977	0.2443
	0.7805	0.7264	0.6630	0.6912	0.8081	0.8715	0.9498	0.8556	0.7976	0.3093
	0.7917	0.7397	0.6895	0.7547	0.8569	1.1101	1.1000	1.0314	0.8950	0.2443
	0.8084	0.7713	0.7653	0.9298	1.0926	1.2316	1.3261	1.2169	1.1898	0.1011
ChYo08	0.7586	0.6791	0.5569	0.4922	0.4509	0.4512	0.4503	0.4470	0.4453	0.1011
	0.7673	0.6947	0.5894	0.5514	0.5455	0.5440	0.5451	0.5466	0.5470	0.2443
	0.7709	0.7117	0.6305	0.6267	0.6864	0.7819	0.7529	0.6808	0.6392	0.3093
	0.7916	0.7394	0.6888	0.7531	0.8413	0.8951	0.9095	0.8325	0.8121	0.2443
	0.7994	0.7541	0.7234	0.8307	1.2918	2.1330	1.9506	1.6408	1.3367	0.1011
AkBo10	0.7544	0.6225	0.5353	0.4951	0.4166	0.4475	0.4693	0.4680	0.4765	0.1011
	0.7637	0.6496	0.5747	0.5651	0.6113	0.6194	0.5841	0.5848	0.5763	0.2443
	0.7762	0.6980	0.6238	0.6532	0.7740	0.8156	0.8111	0.7460	0.7091	0.3093
	0.8167	0.7345	0.6888	0.7669	0.8686	1.0328	1.0308	0.9322	0.8583	0.2443
	0.8479	0.8105	0.8050	1.0395	1.2840	1.3176	1.3368	1.3375	1.3461	0.1011
Zhao06	0.7322	0.5869	0.4749	0.3747	0.3651	0.4394	0.4778	0.4472	0.4250	0.1011
	0.7853	0.6629	0.5889	0.5880	0.6317	0.6676	0.6592	0.6424	0.6302	0.2443
	0.8007	0.6939	0.6489	0.7077	0.8440	0.9718	0.9816	0.9195	0.8091	0.3093
	0.8155	0.7453	0.6808	0.7616	0.9961	1.2024	1.1751	1.0710	1.0172	0.2443
	0.8290	0.7881	0.7503	0.8151	1.1266	1.4228	1.4278	1.1980	1.1808	0.1011

Table V-2.10: Frequency dependent resulting $V_S - \kappa$ correction 5-point distributions for used GMPEs at Mühleberg.

GMPE	Frequency [Hz]									Weight
	0.5	1	2.5	5	10	20	33.3	50	100	
AbSi08	1.0228	1.0311	0.8407	0.7195	0.6186	0.6326	0.6530	0.6634	0.6633	0.1011
	1.0441	1.0597	0.9315	0.8921	0.8737	0.8347	0.8275	0.8073	0.8070	0.2443
	1.0588	1.0982	0.9991	1.0204	1.0667	1.0781	1.1041	1.0528	1.0226	0.3093
	1.0677	1.1121	1.0318	1.0839	1.3482	1.5438	1.3961	1.2567	1.1396	0.2443
	1.1028	1.1987	1.2250	1.5427	1.5880	1.9416	1.8631	1.6950	1.6950	0.1011
BoAt08	1.0228	1.0311	0.8407	0.7265	0.6030	0.6099	0.6291	0.6449	0.6496	0.1011
	1.0358	1.0505	0.8919	0.8164	0.8098	0.8601	0.7937	0.7936	0.8043	0.2443
	1.0513	1.0804	0.9685	0.9492	1.0335	1.1307	1.0527	0.9770	0.9534	0.3093
	1.0577	1.1017	1.0012	1.0295	1.1275	1.2931	1.2998	1.1306	1.1152	0.2443
	1.0804	1.1505	1.1055	1.2563	1.4069	1.6029	1.5633	1.4733	1.4779	0.1011
CaBo08	1.0228	1.0311	0.8407	0.7265	0.5785	0.6183	0.6519	0.6764	0.6806	0.1011
	1.0344	1.0460	0.8889	0.8114	0.7940	0.8441	0.7935	0.7937	0.8034	0.2443
	1.0487	1.0744	0.9562	0.9334	1.0117	1.0689	1.0424	0.9945	0.9856	0.3093
	1.0573	1.1017	0.9970	1.0131	1.1135	1.3246	1.2585	1.1245	1.0648	0.2443
	1.0815	1.1527	1.1108	1.2685	1.4389	1.5701	1.5439	1.4512	1.4512	0.1011
ChYo08	1.0228	1.0232	0.8407	0.7265	0.6509	0.5989	0.5859	0.5854	0.5837	0.1011
	1.0263	1.0380	0.8547	0.7510	0.6732	0.6628	0.6808	0.6914	0.7010	0.2443
	1.0398	1.0573	0.9147	0.8569	0.8683	0.9061	0.8948	0.8478	0.8376	0.3093
	1.0573	1.1017	0.9920	1.0115	1.0672	1.0717	1.0650	1.0444	1.0444	0.2443
	1.0677	1.1235	1.0418	1.1158	1.2348	1.2752	1.3465	1.3732	1.3800	0.1011
AkBo10	1.0149	0.9274	0.7787	0.6226	0.5169	0.5858	0.6112	0.6328	0.6402	0.1011
	1.0224	0.9638	0.8341	0.7711	0.7631	0.7652	0.7489	0.7309	0.7491	0.2443
	1.0384	1.0358	0.9058	0.8964	0.9629	1.0053	0.9413	0.9064	0.8885	0.3093
	1.0960	1.0937	0.9987	1.0309	1.1181	1.2319	1.1483	1.1287	1.1183	0.2443
	1.1325	1.2066	1.1598	1.3962	1.6611	1.6792	1.6935	1.6983	1.6966	0.1011
Zhao06	0.9782	0.8772	0.7063	0.5219	0.4755	0.5229	0.5821	0.5767	0.5631	0.1011
	1.0588	0.9942	0.8520	0.8055	0.7688	0.7903	0.7984	0.7984	0.7984	0.2443
	1.0747	1.0274	0.9363	0.9446	1.0467	1.1677	1.1083	0.9949	0.9936	0.3093
	1.0910	1.1139	0.9881	1.0274	1.2054	1.3467	1.3166	1.2257	1.2222	0.2443
	1.1083	1.1765	1.0855	1.1183	1.4007	1.5741	1.4936	1.4223	1.4006	0.1011

Table V-2.11: Frequency dependent $V_S - \kappa$ correction for PSSMs at the sites Beznau and Gösgen.

	Beznau					Gösgen				
Weight	0.25	0.30	0.20	0.20	0.05	0.25	0.30	0.20	0.20	0.05
Freq. [Hz]	B6 (TK5)	B7 (TK6)	B8 (TK7)	B9 (TK8)	B10 (TK9)	B6 (TK5)	B7 (TK6)	B8 (TK7)	B9 (TK8)	B10 (TK9)
Mc4.5 SD40										
0.5	0.8380	0.8325	0.8311	0.8406	0.8433	0.8975	0.8935	0.8908	0.8962	0.9001
1	0.7775	0.7678	0.7653	0.7824	0.7873	0.7742	0.7671	0.7624	0.7719	0.7790
2.5	0.7931	0.7687	0.7628	0.8056	0.8182	0.6818	0.6662	0.6559	0.6766	0.6925
5	0.8556	0.8051	0.7929	0.8822	0.9098	0.7317	0.6990	0.6781	0.7206	0.7544
10	0.9622	0.8549	0.8301	1.0212	1.0844	0.8463	0.7742	0.7299	0.8215	0.8985
20	1.1711	0.9395	0.8903	1.3117	1.4716	1.0895	0.9203	0.8246	1.0294	1.2220
33.33	1.3671	0.9979	0.9286	1.6217	1.9383	1.3478	1.0476	0.8959	1.2369	1.6101
50	1.3560	0.9682	0.9039	1.6681	2.1021	1.3879	1.0294	0.8716	1.2483	1.7471
100	1.0912	0.8817	0.8455	1.2706	1.5644	1.0610	0.8585	0.7739	0.9789	1.3040
Mc4.5 SD60										
0.5	0.8371	0.8314	0.8299	0.8400	0.8427	0.8949	0.8908	0.8880	0.8936	0.8976
1	0.7774	0.7676	0.7651	0.7823	0.7872	0.7733	0.7662	0.7615	0.7710	0.7781
2.5	0.7931	0.7688	0.7628	0.8057	0.8184	0.6818	0.6661	0.6558	0.6765	0.6925
5	0.8558	0.8051	0.7930	0.8824	0.9100	0.7317	0.6990	0.6781	0.7207	0.7545
10	0.9624	0.8550	0.8302	1.0216	1.0848	0.8465	0.7743	0.7299	0.8217	0.8988
20	1.1720	0.9397	0.8905	1.3126	1.4728	1.0902	0.9208	0.8248	1.0300	1.2230
33.33	1.3695	0.9989	0.9290	1.6250	1.9428	1.3504	1.0490	0.8969	1.2388	1.6137
50	1.3601	0.9701	0.9050	1.6742	2.1107	1.3928	1.0319	0.8730	1.2522	1.7542
100	1.0943	0.8829	0.8463	1.2755	1.5720	1.0647	0.8602	0.7746	0.9816	1.3099
Mc4.5 SD90										
0.5	0.8362	0.8302	0.8287	0.8392	0.8422	0.8921	0.8878	0.8849	0.8907	0.8950
1	0.7771	0.7672	0.7648	0.7820	0.7871	0.7723	0.7651	0.7604	0.7699	0.7770
2.5	0.7932	0.7688	0.7628	0.8058	0.8185	0.6817	0.6660	0.6557	0.6765	0.6925
5	0.8560	0.8053	0.7931	0.8826	0.9102	0.7318	0.6990	0.6780	0.7207	0.7546
10	0.9627	0.8552	0.8304	1.0220	1.0852	0.8468	0.7744	0.7300	0.8219	0.8991
20	1.1731	0.9400	0.8907	1.3139	1.4743	1.0912	0.9212	0.8251	1.0310	1.2241
33.33	1.3724	1.0001	0.9298	1.6288	1.9476	1.3534	1.0512	0.8977	1.2413	1.6174
50	1.3649	0.9716	0.9061	1.6811	2.1205	1.3982	1.0348	0.8744	1.2567	1.7621
100	1.0977	0.8840	0.8471	1.2806	1.5803	1.0685	0.8618	0.7753	0.9846	1.3163
Mc4.5 SD120										
0.5	0.8357	0.8294	0.8278	0.8388	0.8420	0.8901	0.8856	0.8827	0.8886	0.8931
1	0.7770	0.7671	0.7646	0.7820	0.7869	0.7715	0.7643	0.7596	0.7691	0.7762
2.5	0.7933	0.7688	0.7629	0.8058	0.8186	0.6817	0.6659	0.6556	0.6764	0.6925
5	0.8561	0.8053	0.7931	0.8828	0.9103	0.7318	0.6990	0.6780	0.7207	0.7546
10	0.9630	0.8552	0.8304	1.0222	1.0855	0.8470	0.7745	0.7300	0.8220	0.8993
20	1.1736	0.9406	0.8911	1.3150	1.4758	1.0919	0.9218	0.8257	1.0315	1.2252
33.33	1.3747	1.0011	0.9306	1.6319	1.9518	1.3559	1.0524	0.8987	1.2438	1.6207
50	1.3686	0.9729	0.9072	1.6865	2.1281	1.4025	1.0370	0.8760	1.2601	1.7683
100	1.1008	0.8850	0.8478	1.2849	1.5869	1.0717	0.8633	0.7760	0.9872	1.3215

Table V-2.12: Frequency dependent $V_S - \kappa$ correction for PSSMs at the sites Leibstadt and Mühleberg.

	Leibstadt					Mühleberg				
Weight	0.25	0.30	0.20	0.20	0.05	0.25	0.30	0.20	0.20	0.05
Freq. [Hz]	B6 (TK5)	B7 (TK6)	B8 (TK7)	B9 (TK8)	B10 (TK9)	B6 (TK5)	B7 (TK6)	B8 (TK7)	B9 (TK8)	B10 (TK9)
Mc4.5 SD40										
0.5	0.8107	0.8069	0.8055	0.8120	0.8145	1.3037	1.3016	1.2995	1.3099	1.3160
1	0.7253	0.7185	0.7162	0.7275	0.7320	1.2331	1.2292	1.2253	1.2446	1.2563
2.5	0.7172	0.7007	0.6953	0.7228	0.7342	0.9690	0.9615	0.9542	0.9916	1.0149
5	0.7760	0.7414	0.7302	0.7881	0.8126	0.9973	0.9824	0.9676	1.0437	1.0925
10	0.8850	0.8096	0.7861	0.9118	0.9680	1.0073	0.9784	0.9506	1.0995	1.2012
20	1.1073	0.9365	0.8865	1.1721	1.3149	1.0755	1.0209	0.9697	1.2624	1.4897
33.33	1.3292	1.0389	0.9616	1.4488	1.7312	1.1089	1.0381	0.9747	1.3746	1.7441
50	1.3405	1.0122	0.9338	1.4913	1.8787	1.0909	1.0300	0.9775	1.3367	1.7319
100	1.0484	0.8692	0.8270	1.1371	1.3993	1.0495	1.0130	0.9798	1.1879	1.4006
Mc4.5 SD60										
0.5	0.8092	0.8052	0.8038	0.8106	0.8131	1.3011	1.2990	1.2969	1.3074	1.3137
1	0.7249	0.7181	0.7159	0.7272	0.7318	1.2322	1.2284	1.2245	1.2439	1.2556
2.5	0.7173	0.7007	0.6953	0.7229	0.7342	0.9688	0.9613	0.9539	0.9914	1.0148
5	0.7762	0.7414	0.7302	0.7881	0.8127	0.9972	0.9822	0.9675	1.0437	1.0926
10	0.8852	0.8098	0.7862	0.9120	0.9685	1.0072	0.9784	0.9504	1.0996	1.2015
20	1.1081	0.9369	0.8869	1.1729	1.3160	1.0755	1.0207	0.9694	1.2628	1.4906
33.33	1.3314	1.0404	0.9629	1.4515	1.7351	1.1090	1.0378	0.9741	1.3763	1.7469
50	1.3450	1.0145	0.9355	1.4966	1.8863	1.0910	1.0299	0.9768	1.3388	1.7369
100	1.0517	0.8708	0.8281	1.1413	1.4060	1.0492	1.0124	0.9788	1.1890	1.4039
Mc4.5 SD90										
0.5	0.8077	0.8035	0.8021	0.8091	0.8119	1.2980	1.2958	1.2936	1.3045	1.3111
1	0.7245	0.7176	0.7153	0.7268	0.7314	1.2309	1.2270	1.2232	1.2426	1.2544
2.5	0.7173	0.7007	0.6953	0.7230	0.7344	0.9684	0.9610	0.9536	0.9911	1.0146
5	0.7763	0.7415	0.7303	0.7883	0.8129	0.9971	0.9821	0.9674	1.0437	1.0927
10	0.8855	0.8100	0.7864	0.9123	0.9688	1.0071	0.9782	0.9503	1.0996	1.2016
20	1.1092	0.9373	0.8872	1.1741	1.3172	1.0754	1.0205	0.9693	1.2632	1.4919
33.33	1.3342	1.0420	0.9639	1.4549	1.7392	1.1093	1.0378	0.9736	1.3775	1.7501
50	1.3500	1.0172	0.9376	1.5028	1.8950	1.0912	1.0296	0.9760	1.3412	1.7424
100	1.0553	0.8725	0.8294	1.1459	1.4132	1.0490	1.0117	0.9778	1.1901	1.4074
Mc4.5 SD120										
0.5	0.8068	0.8024	0.8009	0.8082	0.8111	1.2955	1.2933	1.2911	1.3024	1.3091
1	0.7242	0.7173	0.7151	0.7266	0.7311	1.2300	1.2262	1.2223	1.2417	1.2534
2.5	0.7173	0.7007	0.6953	0.7230	0.7344	0.9682	0.9607	0.9533	0.9910	1.0144
5	0.7764	0.7416	0.7303	0.7884	0.8131	0.9971	0.9821	0.9673	1.0437	1.0927
10	0.8857	0.8100	0.7864	0.9125	0.9691	1.0070	0.9781	0.9501	1.0996	1.2017
20	1.1098	0.9380	0.8879	1.1748	1.3185	1.0757	1.0205	0.9691	1.2642	1.4925
33.33	1.3370	1.0434	0.9651	1.4576	1.7429	1.1096	1.0378	0.9734	1.3789	1.7529
50	1.3541	1.0192	0.9394	1.5075	1.9017	1.0914	1.0296	0.9753	1.3433	1.7468
100	1.0583	0.8739	0.8305	1.1496	1.4191	1.0489	1.0113	0.9772	1.1913	1.4105

Figures V-2.3 to V-2.6 show the five discrete correction functions versus frequency for all GMPEs per site. Figures with all individual correction functions resulting from all combinations and color coded by their weight can be found in the appendix to the HID (Chapter 3). Furthermore, the individual histograms, selected 5-point distributions and a theoretically fitted distribution are also shown in the appendix. Figures V-2.7 to V-2.10 shows the different $V_S - \kappa$ corrections to be applied to the generic parameterized Swiss stochastic model in order to be applicable for the given site specific NPP conditions.

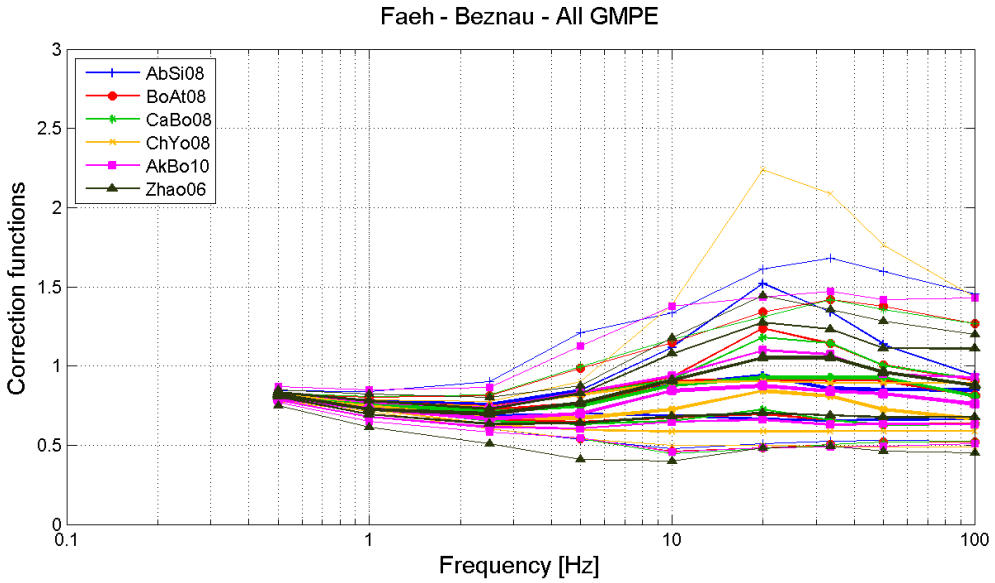

Figure V-2.3: $V_S - \kappa$ corrections to be applied to the GMPEs for Beznau.

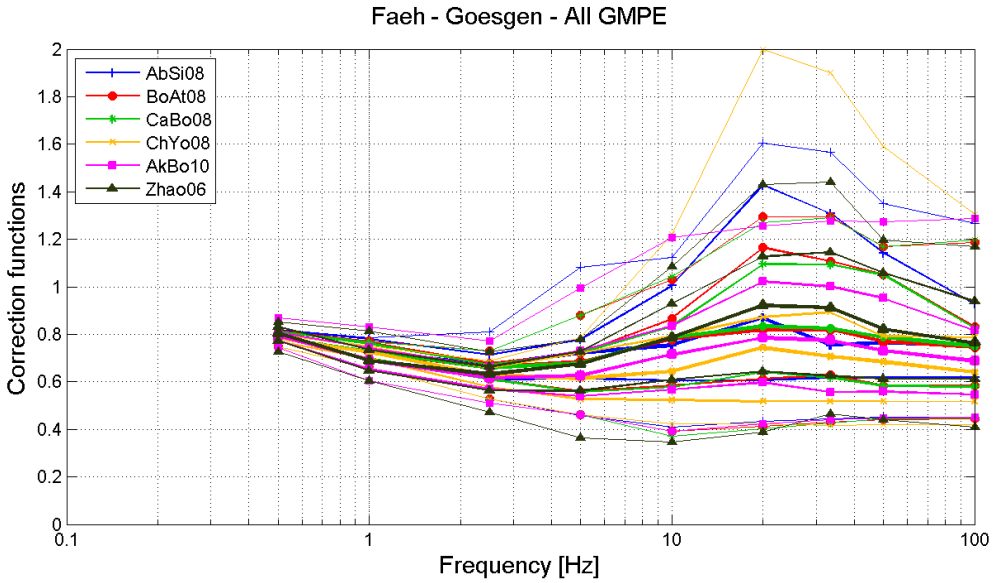

Figure V-2.4: $V_S - \kappa$ corrections to be applied to the GMPEs for Gösgen.

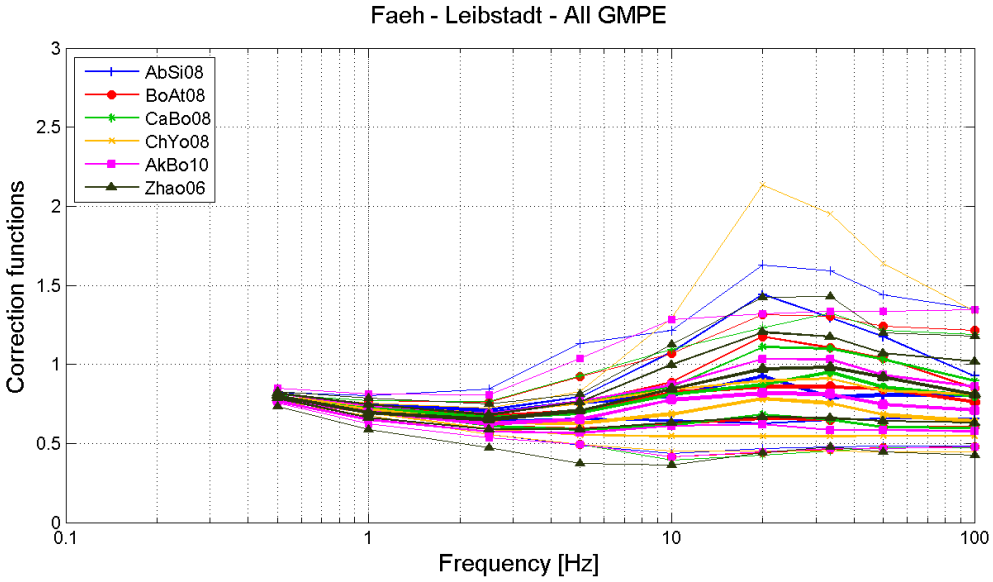

Figure V-2.5: $V_S - \kappa$ corrections to be applied to the GMPEs for Leibstadt.

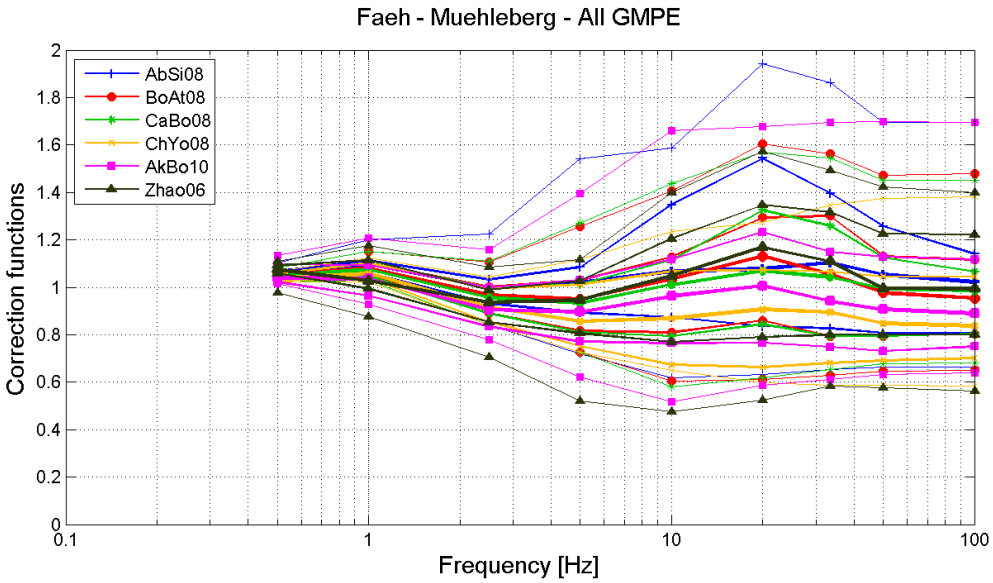

Figure V-2.6: $V_S - \kappa$ corrections to be applied to the GMPEs for Mühleberg.

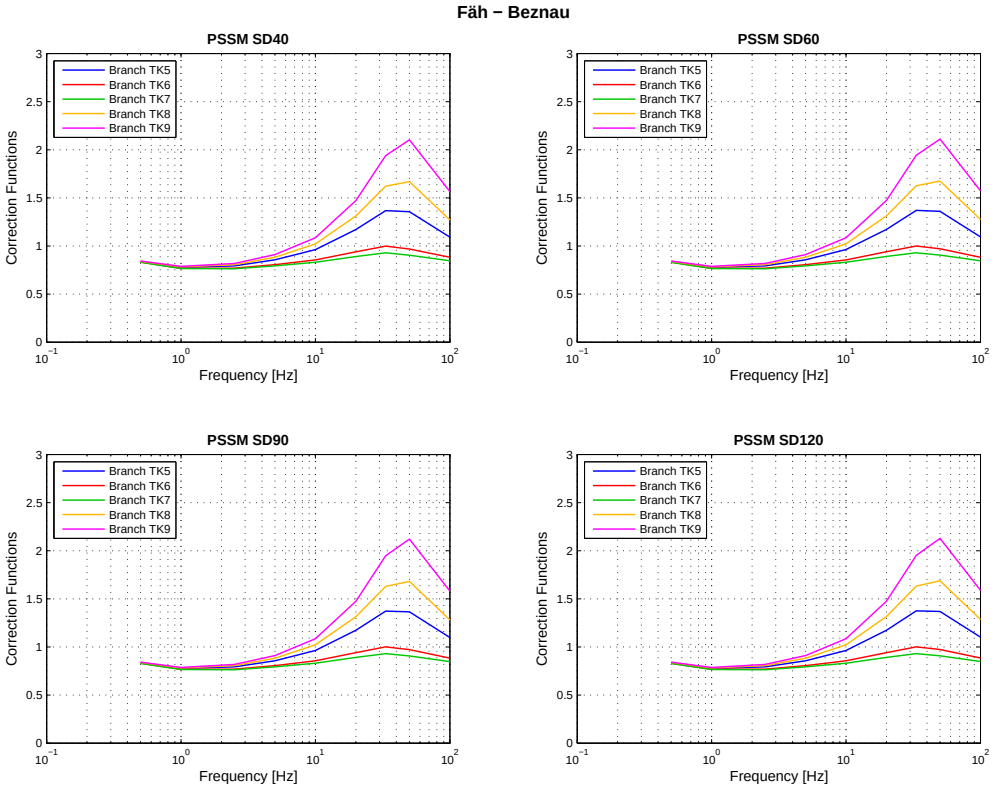

Figure V-2.7: $V_S - \kappa$ corrections to be applied to the PSSMs for Beznau.

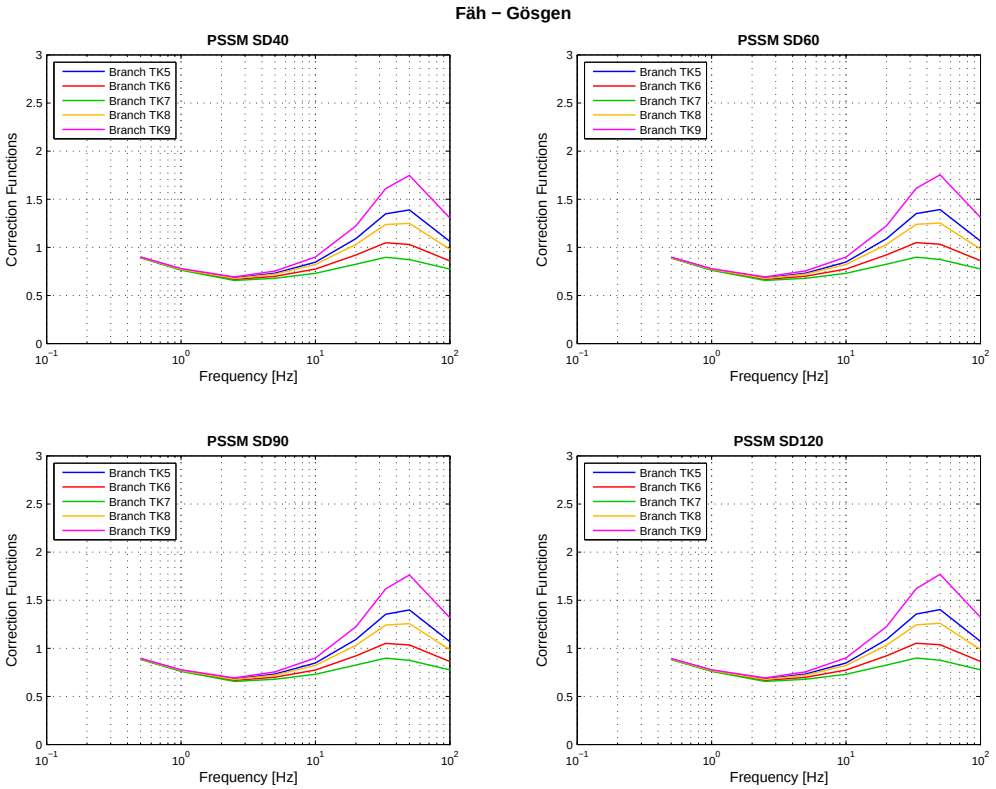

Figure V-2.8: $V_S - \kappa$ corrections to be applied to the PSSMs for Gösgen.

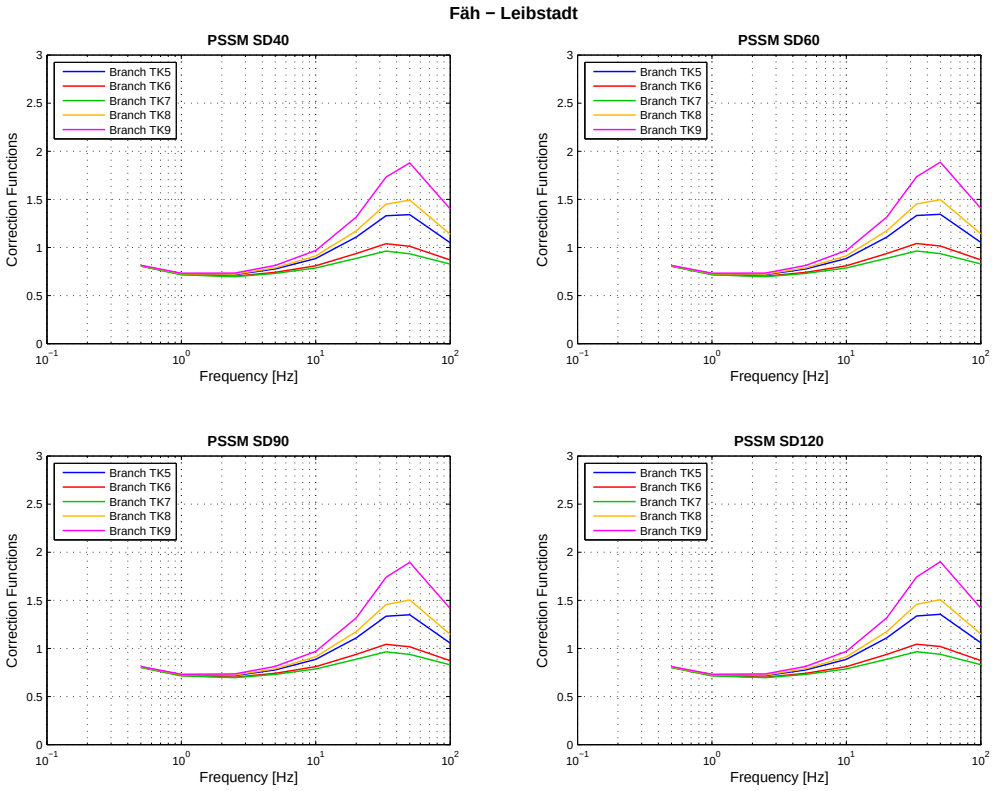

Figure V-2.9: $V_S - \kappa$ corrections to be applied to the PSSMs for Leibstadt.

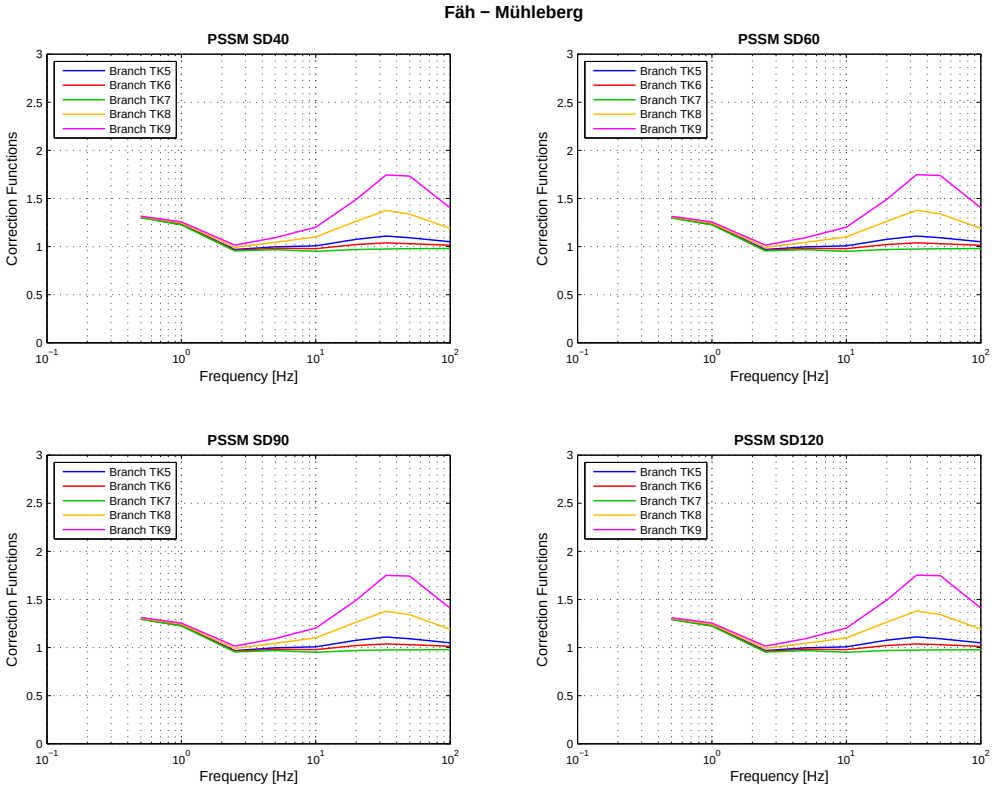

Figure V-2.10: $V_S - \kappa$ corrections to be applied to the PSSMs for Mühleberg.

2.3.2 Small Magnitude Adjustments

For the evaluation of the GMPE specific small magnitude adjustments only the median $V_S - \kappa$ correction factors of all the provided 5-point distributions are used, as it was decided that the small magnitude adjustments will only be developed for the average case and not for each individual correction function (PMT-TN-1238). Thus, the small magnitude adjustments are the same for all experts, but repeated here in Table V-2.13 for the sake of completeness and illustrated in Figure V-2.11 and V-2.12.

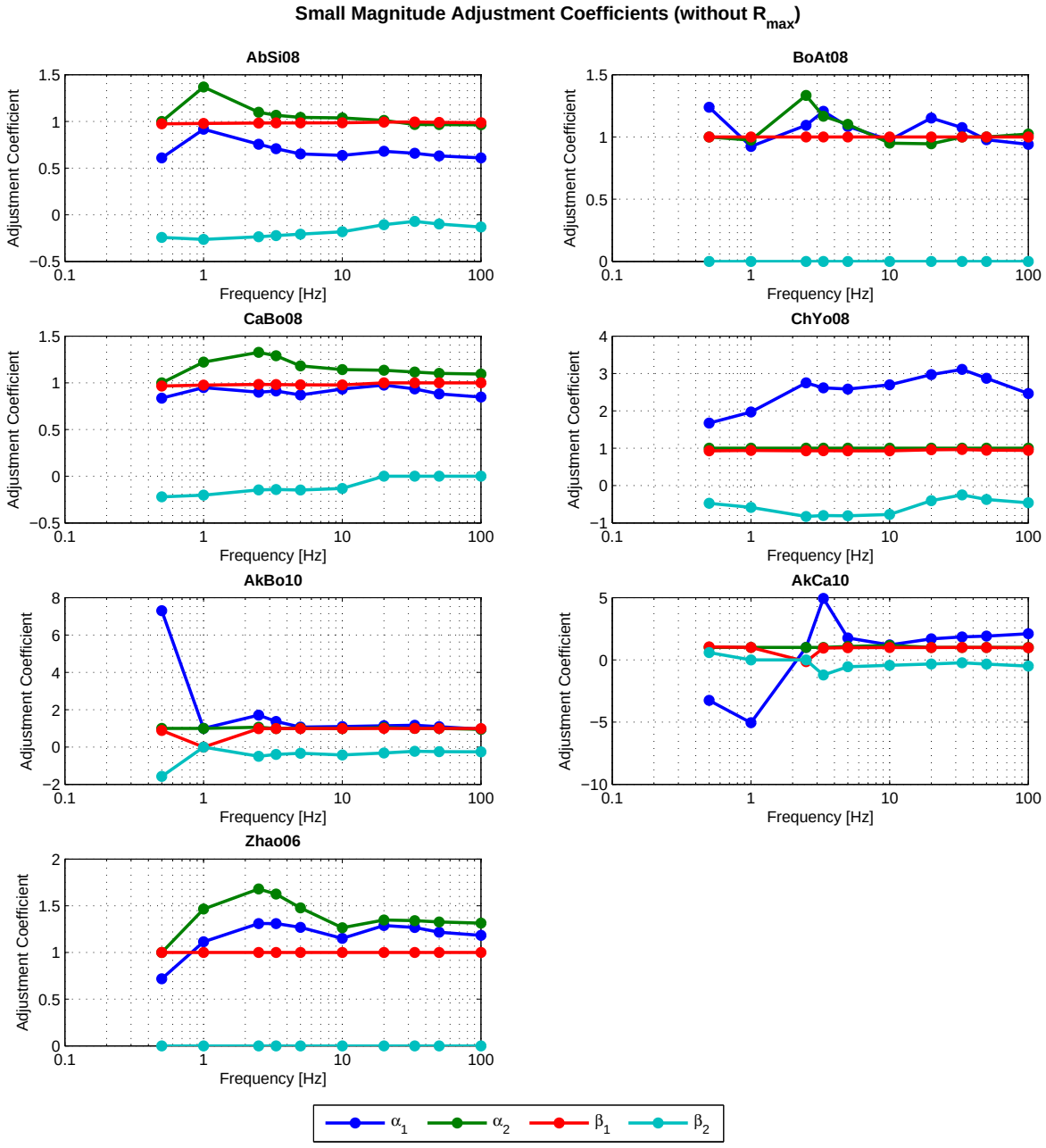

Figure V-2.11: Small magnitude adjustments coefficients as function of frequency for the all GMPEs.

Table V-2.13: Small magnitude adjustments coefficients.

	Abrahamson & Silva (2008)					Boore & Atkinson (2008)				
T [s]	α_1	α_2	β_1	β_2	R_{max}	α_1	α_2	β_1	β_2	R_{max}
0.01	0.609036	0.964257	0.986605	-0.131781	3.57E+04	0.940502	1.022616	1.000000	0.000000	1.00E+09
0.02	0.629604	0.965329	0.988756	-0.099660	4.07E+05	0.977300	1.000000	1.000000	0.000000	1.00E+09
0.03	0.657761	0.967357	0.993601	-0.071271	2.27E+07	1.074586	1.000000	1.000000	0.000000	1.00E+09
0.05	0.679706	1.010904	0.991680	-0.106456	2.22E+05	1.151448	0.945013	1.000000	0.000000	1.00E+09
0.1	0.635927	1.037980	0.984796	-0.182620	4.40E+03	0.974222	0.950274	1.000000	0.000000	1.00E+09
0.2	0.651637	1.043100	0.984107	-0.207141	2.31E+03	1.084848	1.101550	1.000000	0.000000	1.00E+09
0.3	0.707216	1.065147	0.983422	-0.222960	1.65E+03	1.205896	1.166359	1.000000	0.000000	1.00E+09
0.4	0.755898	1.097644	0.982712	-0.236174	1.28E+03	1.093478	1.334035	1.000000	0.000000	1.00E+09
1	0.915893	1.367623	0.978436	-0.263900	8.15E+02	0.924116	0.974715	1.000000	0.000000	1.00E+09
2	0.608779	1.000000	0.974376	-0.242967	1.10E+03	1.238186	1.000000	1.000000	0.000000	1.00E+09

	Campbell & Bozorgnia (2008)					Chiou & Youngs (2008)				
T [s]	α_1	α_2	β_1	β_2	R_{max}	α_1	α_2	β_1	β_2	R_{max}
0.01	0.847179	1.094261	1.000000	0.000000	1.00E+09	2.462946	1.000000	0.944935	-0.458418	1.57E+02
0.02	0.881357	1.100586	1.000000	0.000000	1.00E+09	2.873730	1.000000	0.946856	-0.372663	2.54E+02
0.03	0.934893	1.114376	1.000000	0.000000	1.00E+09	3.109735	1.000000	0.966292	-0.248344	9.79E+02
0.05	0.976058	1.135405	1.000000	0.000000	1.00E+09	2.969316	1.000000	0.959155	-0.402534	2.17E+02
0.1	0.932945	1.141482	0.977278	-0.130765	3.52E+04	2.695695	1.000000	0.930247	-0.772189	6.67E+01
0.2	0.870681	1.181271	0.979148	-0.147509	1.53E+04	2.584716	1.000000	0.931449	-0.809059	6.32E+01
0.3	0.912008	1.289225	0.981219	-0.142015	2.00E+04	2.614341	1.000000	0.932936	-0.801818	6.40E+01
0.4	0.899165	1.326194	0.982502	-0.145844	1.69E+04	2.750116	1.000000	0.930586	-0.824968	6.18E+01
1	0.949262	1.221818	0.975229	-0.202856	2.45E+03	1.966745	1.000000	0.939658	-0.583454	1.00E+02
2	0.835687	1.000000	0.965445	-0.220424	1.60E+03	1.671214	1.000000	0.931415	-0.473294	1.43E+02

	Akkar & Bommer (2010)					Akkar & Cagnan (2010)				
T [s]	α_1	α_2	β_1	β_2	R_{max}	α_1	α_2	β_1	β_2	R_{max}
0.01	0.956934	0.949129	0.992409	-0.258327	9.32E+02	2.098964	1.000000	0.985549	-0.499646	1.44E+02
0.02	1.090919	1.000000	0.994584	-0.253021	1.02E+03	1.913122	1.000000	0.990459	-0.335515	3.83E+02
0.03	1.164927	1.000000	0.998788	-0.230673	1.52E+03	1.851248	1.000000	0.997570	-0.236164	1.37E+03
0.05	1.134080	1.040216	0.995602	-0.321814	4.41E+02	1.689890	1.000000	0.995553	-0.333705	3.95E+02
0.1	1.093536	0.986668	0.988564	-0.425342	2.04E+02	1.204350	1.157951	0.987542	-0.431630	1.97E+02
0.2	1.068203	1.007264	0.988710	-0.334035	3.86E+02	1.759524	1.071974	0.978784	-0.546911	1.20E+02
0.3	1.369695	0.988071	0.987967	-0.400250	2.36E+02	4.937988	1.000000	0.951557	-1.213879	4.38E+01
0.4	1.710275	1.062132	0.984888	-0.499538	1.44E+02	1.000000	1.000000	-0.142956	0.000000	1.99E+01
1	1.000000	1.000000	0.000000	0.000000	1.00E+09	-5.048030	1.000000	1.000000	0.000000	1.99E+01
2	7.299540	1.000000	0.881761	-1.575579	3.50E+01	-3.254365	1.000000	1.044931	0.593817	1.00E+09

	Zhao et al. (2006)				
T [s]	α_1	α_2	β_1	β_2	R_{max}
0.01	1.182482	1.313722	1.000000	0.000000	1.00E+09
0.02	1.217249	1.326714	1.000000	0.000000	1.00E+09
0.03	1.267071	1.340177	1.000000	0.000000	1.00E+09
0.05	1.288501	1.347281	1.000000	0.000000	1.00E+09
0.1	1.150978	1.265212	1.000000	0.000000	1.00E+09
0.2	1.268576	1.476775	1.000000	0.000000	1.00E+09
0.3	1.310229	1.625552	1.000000	0.000000	1.00E+09
0.4	1.308962	1.679158	1.000000	0.000000	1.00E+09
1	1.113543	1.465133	1.000000	0.000000	1.00E+09
2	0.718525	1.000000	1.000000	0.000000	1.00E+09

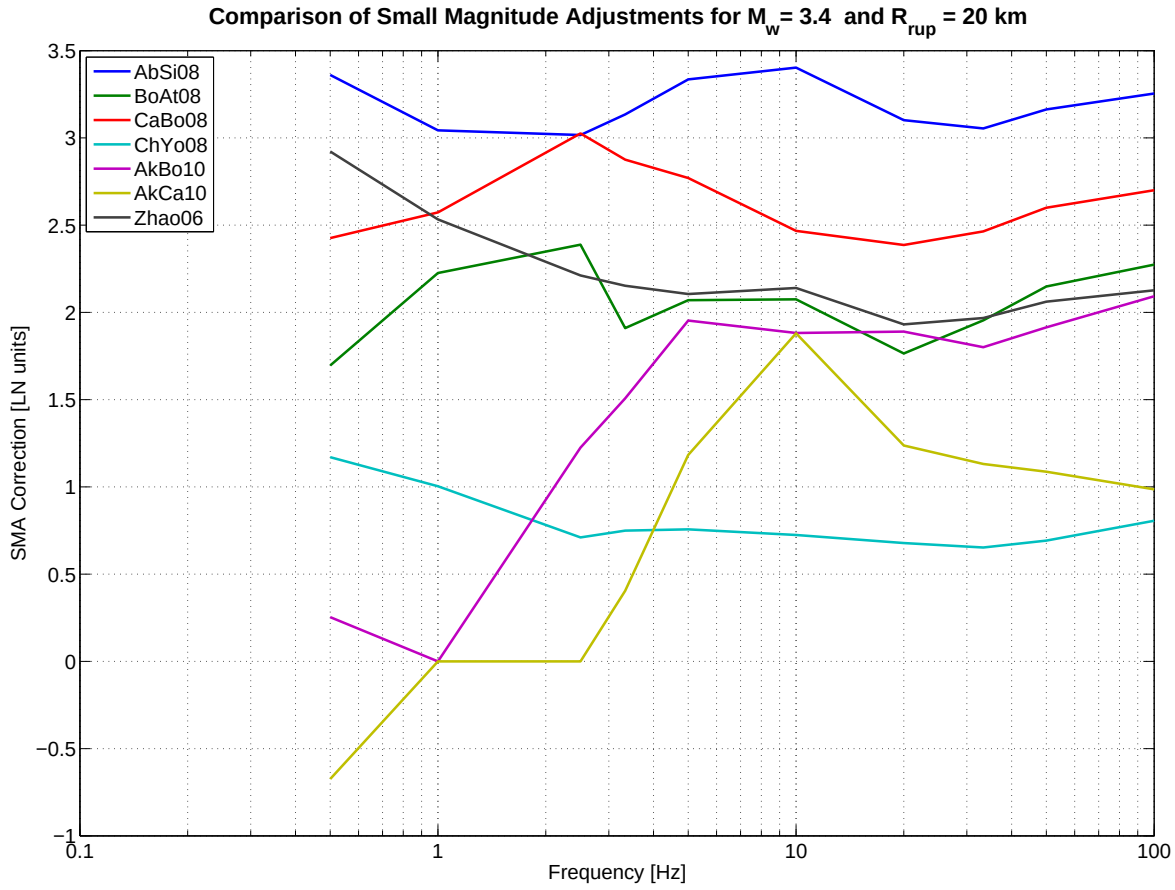

Figure V-2.12: Comparison of the resulting small magnitude adjustments functions as function of frequency for M=3.4 and R=20 km.

2.4 Aleatory Variability for the Horizontal Component

Section 6.7 in Part I, provides the final τ and ϕ models used for the PRP, which supersede the model of Rodriguez-Marek and Cotton [2011] (equations 4.1, 4.2 and table 5.3 and 5.4 in EXT-TB-1058() and Rodriguez-Marek [2012] (EXT-TN-1225). In Table V-2.14 the different weights for the aleatory variability logic tree branches are shown. The selected values for the ϕ_{SS} uncertainty are given in the second column at the bottom. The generic σ logic tree is represented in Figure I-9.2.

Table V-2.14: Weights and parameters assigned to the aleatory variability.

(a) For all GMPEs except AkBo10

Model	Branch / Value for $\sigma(\phi_{SS})$	Weight
τ Model	Global	-
	Original GMPE	1.00
τ Uncert.	"Zero"	1.00
ϕ_{SS}	Model 1 (Constant)	0.30
	Model 2 (Distance Dep.)	-
	Model 3 (Dist. & Mag. Dep.)	0.70
ϕ_{SS} Uncert.	$-1.6 \cdot \sigma(\phi_{SS})$	0.40
	$0 \cdot \sigma(\phi_{SS})$	0.60
	$+1.6 \cdot \sigma(\phi_{SS})$	0.00
$\sigma(\phi_{SS})$	0.07	0.40
	0.10	0.40
	0.13	0.20

(b) For AkBo10

Model	Branch / Value for $\sigma(\phi_{SS})$	Weight
τ Model	Global	1.00
	Original GMPE	-
τ Uncert.	"Zero"	1.00
ϕ_{SS}	Model 1 (Constant)	0.30
	Model 2 (Distance Dep.)	-
	Model 3 (Dist. & Mag. Dep.)	0.70
ϕ_{SS} Uncert.	$-1.6 \cdot \sigma(\phi_{SS})$	0.40
	$0 \cdot \sigma(\phi_{SS})$	0.60
	$+1.6 \cdot \sigma(\phi_{SS})$	0.00
$\sigma(\phi_{SS})$	0.07	0.40
	0.10	0.40
	0.13	0.20

2.5 Maximum Ground Motion

Table V-2.15 shows that no frequency dependent weights are assigned to the horizontal maximum ground motion logic tree (see generic Figure I-9.3). The weights assigned to the six scaling factors for the six branches are given in Table V-2.16.

Table V-2.15: Weights for the horizontal maximum ground motion model.

Model	Frequency [Hz]								
	0.5	1	2.5	5	10	20	33.3	50	100
R-dependent	1.00	1.00	1.00	1.00	1.00	1.00	1.00	1.00	1.00
R-independent	-	-	-	-	-	-	-	-	-

The vertical maximum ground motion model is the same as the horizontal (see Figure I-9.3). Thus, the same weights and scale factors apply for the vertical hazard.

Based on the hazard feedback, which showed very little impact of the maximum ground motion truncation for rock, the project has decided to trim the maximum ground motion branches for the practical implementation. Thus, the hazard will be computed based on untruncated ground motions for rock.

Table V-2.16: Weights for the scaling factors for the maximum ground motion model (both horizontal and vertical).

Model	Scale Factors [LN units]					
	7.50	12.59	21.14	35.48	59.57	100
R-dependent	0	0.10	0.50	0.30	0.10	0
R-independent	-	-	-	-	-	-

2.6 V/H Ratio

Tables V-2.17 and V-2.18 show the weights of the candidate V/H models. The weights and models are NPP specific and KKG is assigned differently (using only the "shallow" case - see TP3-ASW-1004). The basic logic tree for the V/H models can be found in Figure I-9.4.

Table V-2.17: Weights for median V/H models for KKB, KKM, KKL.

Model	Weight
Bommer et al. (2011)	-
Campbell and Bozorgnia (2003)	-
Gülerce and Abrahamson (2011)	0.10
Edwards et al. (2011) with correction above 7 Hz	0.20
Edwards et al. (2011) without correction above 7 Hz	0.50
US West Median	-
US East Median	0.20

Table V-2.18: Weights for median V/H models for KKG.

Model (with the profiles defined by SP3)	Weight
Akkar et al. (2011)	-
Campbell and Bozorgnia (2003)	-
Gülerce and Abrahamson (2011)	0.10
Edwards et al. (2011) with correction above 7 Hz (Profile P4-5)	0.20
Edwards et al. (2011) without correction above 7 Hz (Profile P4-5)	0.30
Edwards et al. (2011) without correction above 7 Hz (Profile P1)	0.10
Edwards et al. (2011) without correction above 7 Hz (Profile P2)	0.10
US West Median	-
US East Median	0.20

2.7 Aleatory Variability for the Vertical Component

The additional aleatory variability to be added to the median V/H models is shown in Table V-2.19 (see Figure I-9.2 for the generic logic tree).

Figure V-2.13 shows the additional aleatory variability for the vertical component over frequency.

Table V-2.19: Additional vertical variability (σ_{VADD} in LN units).

Frequency [Hz]								
0.5	1	2.5	5	10	20	33.3	50	100
0.0	0.0	0.0	0.06	0.22	0.28	0.23	0.19	0.13

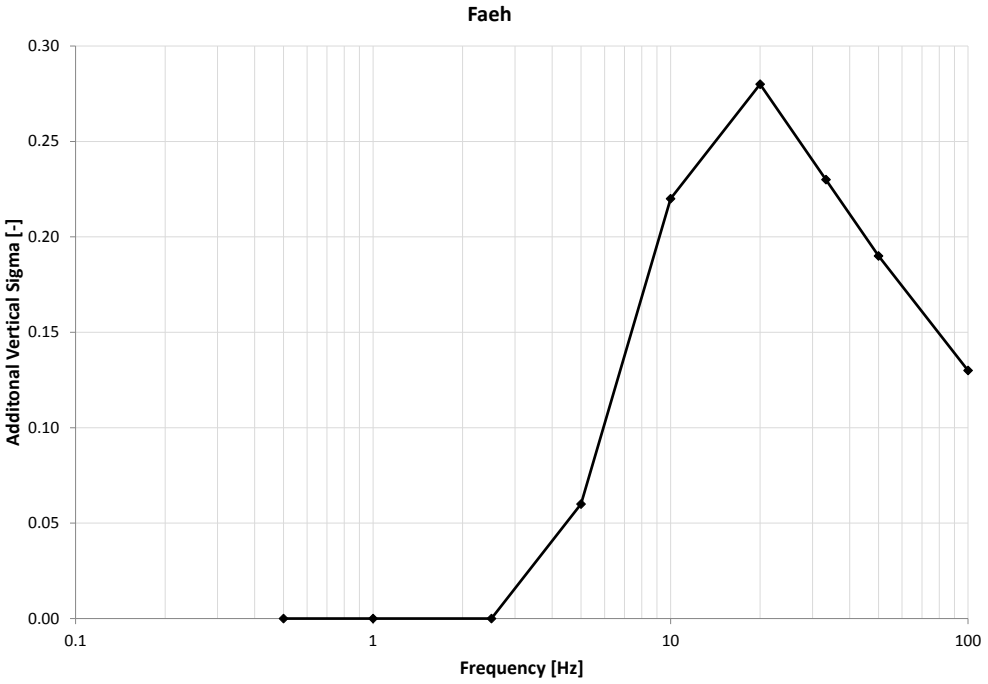

Figure V-2.13: Additional aleatory variability for the vertical component.

2.8 Implementation of Hazard Logic Tree

The total number of logic tree branches amounts to 1600 (see Figure V-2.1). Each individual combination of zonation alternatives and source parameters in each individual SP1 source has to be combined with these 1600 alternative ground motion models. Among other such measures, the project decided to reduce the huge number of combinations and thus, the CPU time necessary to obtain the rock hazard results by removing the maximum ground motion truncation from the SP2 models. This section documents the effect of this project management decision.

For the hazard computation we used one of the four SP1 Expert Group models, EG1c, with its entire complexity. We performed the calculation for one site only, Beznau, as we know the effect of the maximum ground motion truncation to be largely site independent and for 5 Hz spectral acceleration as the effect of the maximum ground motion truncation has been shown to be the highest for this frequency (see TP4-RF-1441). Figure V-2.14 shows the comparison for the mean hazard and four fractiles.

This conversion of the original "scientific logic tree" to a dealable "hazard logic tree" has been introduced in the framework of the PRP in order to allow for efficient computation without

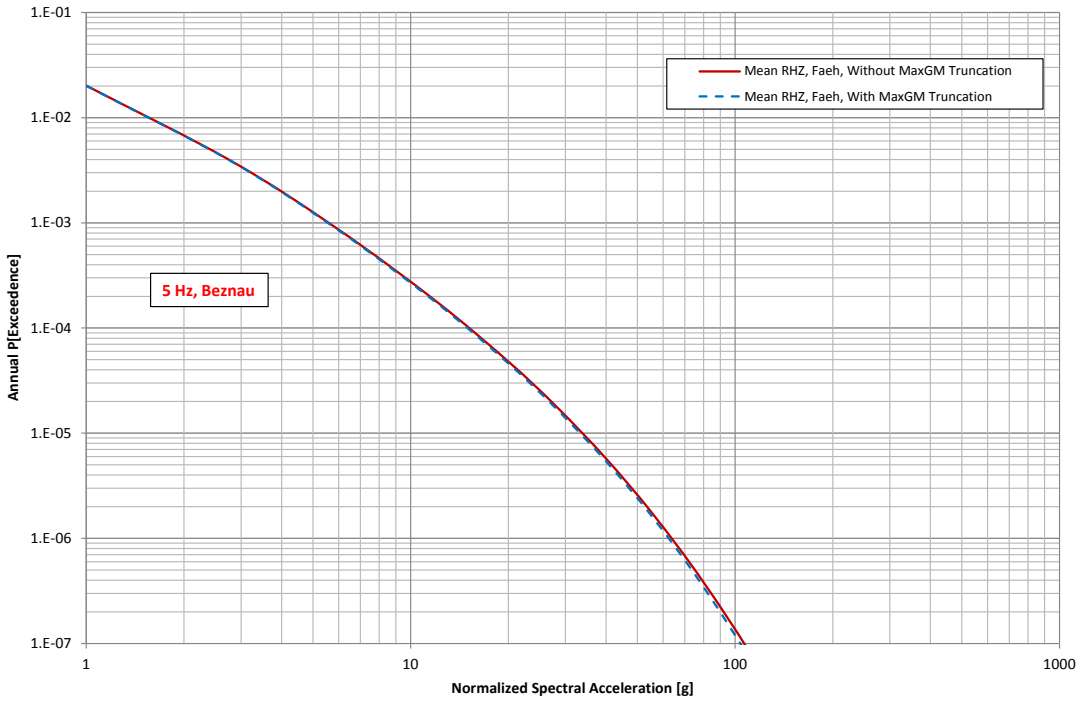

Figure V-2.14: Effect of the removal of the maximum ground motion truncation in the logic tree on the rock hazard for Beznau.

tradeoffs for the overall model in key elements of the initial logic tree.

Chapter 3

Appendix to EG1-HID-1012

The procedure to retrieve the discrete 5-point distributions for the $V_S - \kappa$ corrections is visualized by means of 3 figure types:

- XY graph showing all correction function versus frequency with curve colors indicating the curve weights (see example Figure V-3.1)
- Plot of the probability distributions (cumulative weights) of $V_S - \kappa$ corrections at the 9 PRP frequencies (see example Figure V-3.2)
- Corresponding plot of the probability density of $V_S - \kappa$ at the 9 analysis frequencies (see example Figure V-3.3)

which are attached as an electronic appendix to this HID and contains folders/files (or ZIP files), which correspond to the above listed figure types. Figures within above folders are provided as individual PNG and/or EPS files, where the individual files are named according to the convention and example as follows:
<expert>_<site>_<gmpe>_<figure-type>.<graphic-format>
`Faeh_Beznau_AbSi08_fig1.png`

A direct link to files containing a compilation of all figures per site is given here:

- Open external file: $V_S - \kappa$ correction functions for Beznau and associated cumulative probability functions and probability density functions.
- Open external file: $V_S - \kappa$ correction functions for Gösgen and associated cumulative probability functions and probability density functions.
- Open external file: $V_S - \kappa$ correction functions for Leibstadt and associated cumulative probability functions and probability density functions.
- Open external file: $V_S - \kappa$ correction functions for Mühleberg and associated cumulative probability functions and probability density functions.

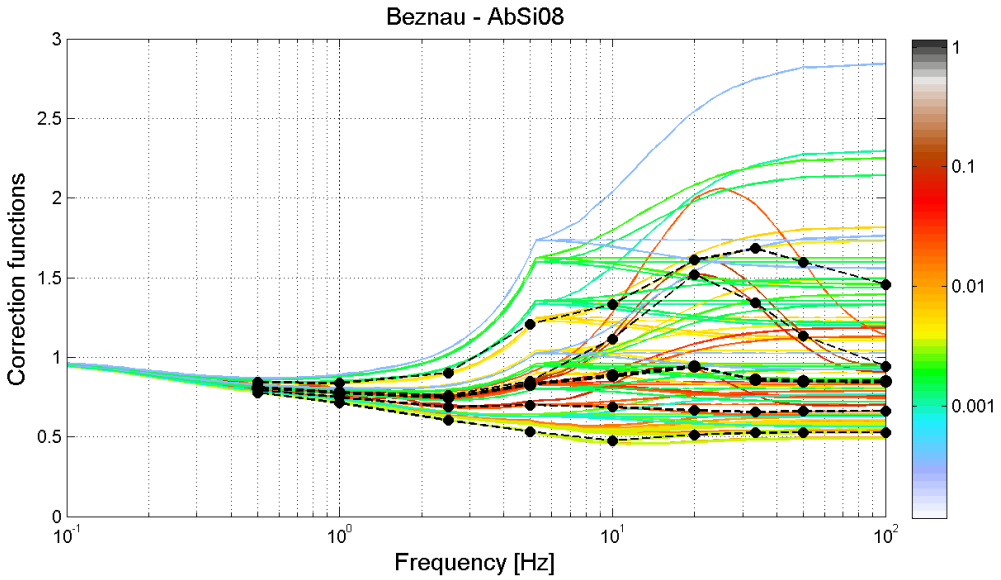

Figure V-3.1: Evaluated $V_S - \kappa$ correction functions for Abrahamson & Silva (2008) at the site of Beznau and the final 5 discrete correction functions in black dashed lines. The weights of the individual correction functions are color coded according to the scale on the right.

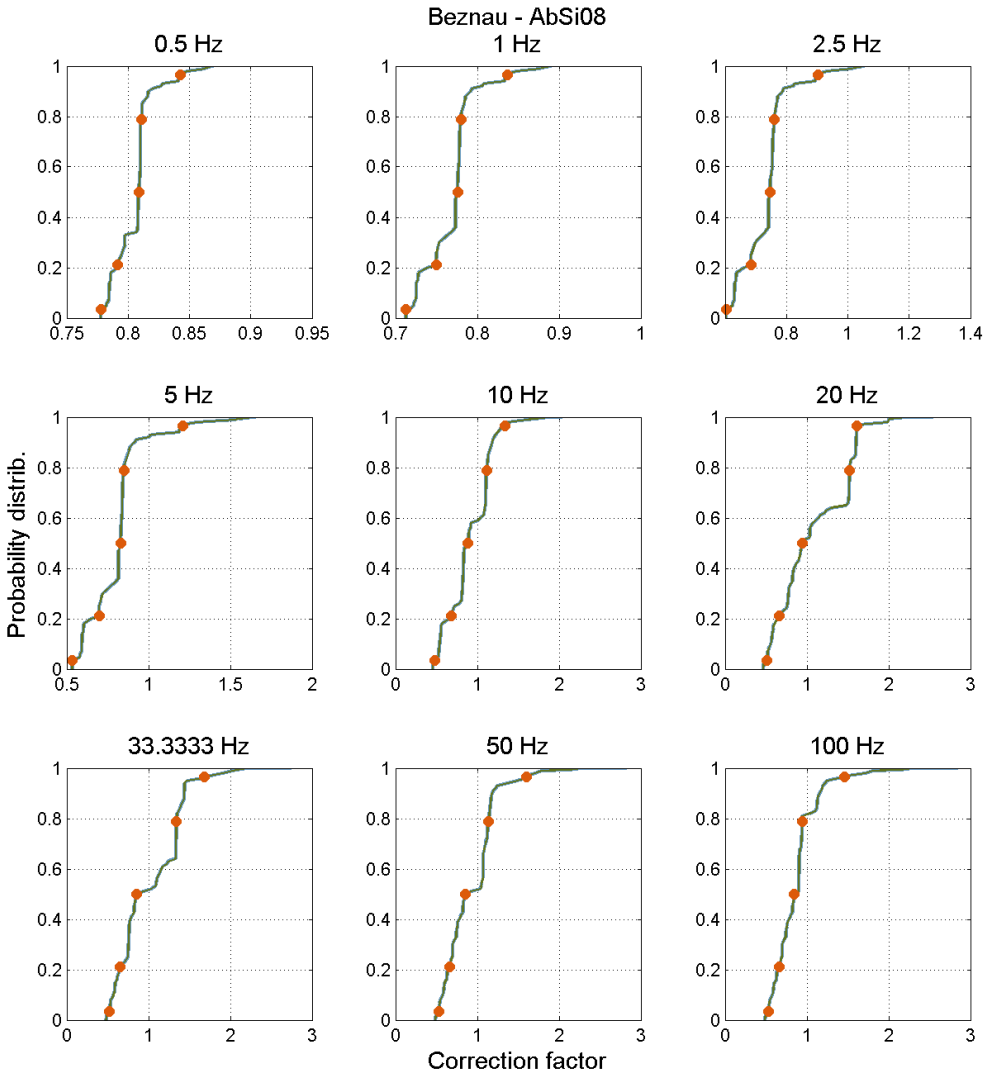

Figure V-3.2: Probability distributions (cumulative weights) of $V_S - \kappa$ corrections at the 9 PRP frequencies for Abrahamson & Silva (2008) at the site of Beznau. The blue line represents the data by means of 105 fractiles. The thin green line is a smoothed version of above blue line (just for display, not used for further processing). The orange dots are the 3.4893, 21.1702, 50, 78.8298 and 96.5107 % percentiles used for the 5-point distribution.

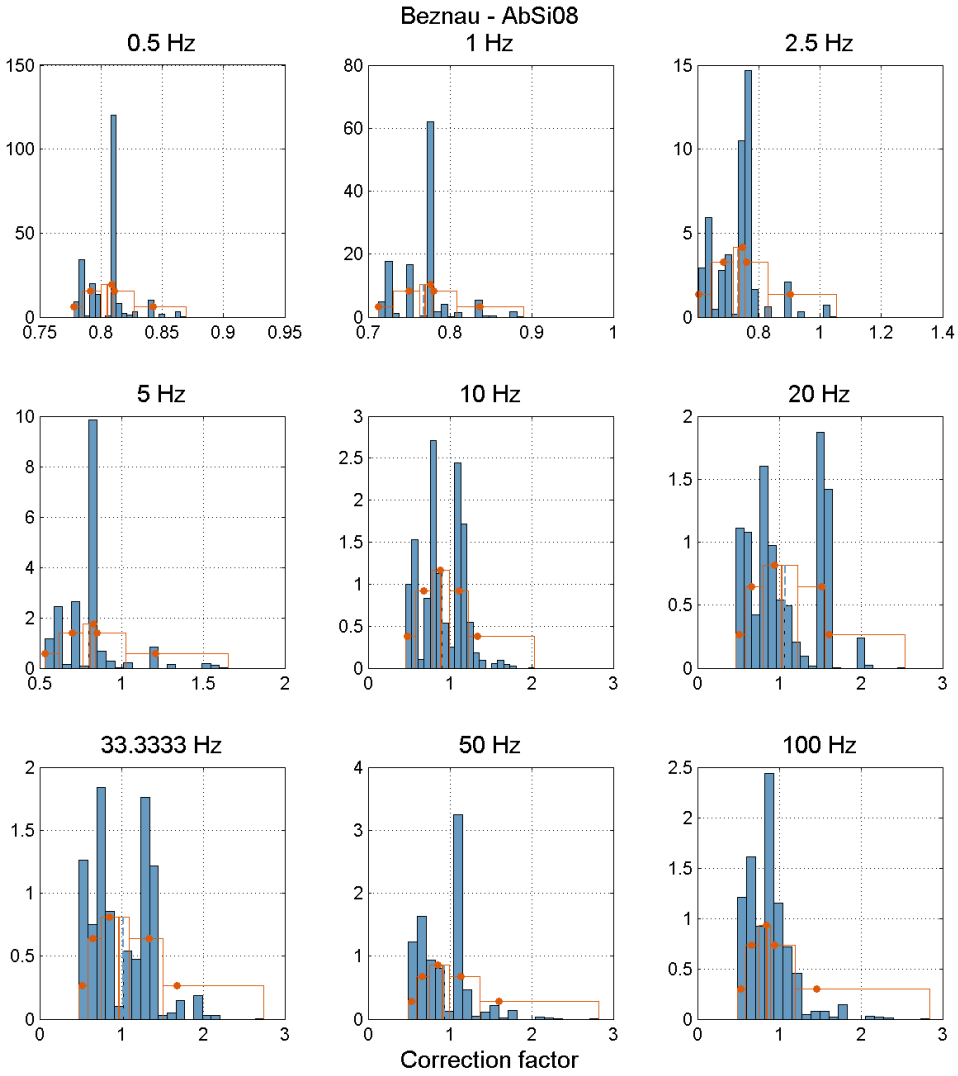

Figure V-3.3: Probability density functions of $V_S - \kappa$ corrections at the 9 PRP frequencies for Abrahamson & Silva (2008) at the site of Beznau. The blue bars represent the weighted histogram of the data partitioned into 21 bins. The orange dots are the corresponding discrete 5 distribution points for the 3.4893, 21.1702, 50, 78.8298 and 96.5107 % percentiles, as in Figure V-3.2. The corresponding probabilities/weights are for the given discretization: 0.10108, 0.24429, 0.30926, 0.24429, 0.10108. The thin red and thin dashed blue line in the middle show the mean value of the data and the approximation with the 5-point distribution, respectively. Note that in the case of the thin dashed blue and red line being identical, only the red line is seen as it is on top of the blue line.

Chapter 4

QA-Certificate EG2-QC-1063

QA Certificate	PEGASOS REFINEMENT PROJECT
EG2-QC-1063	

Hazard Input Document (HID)

Expert group:	**EG2**	***HID designation:***	**EG2-HID-1012**
Expert:	D. Fäh	***Expert Model (EXM)***	EG2-EXM-1012

HID parameterisation of Expert Model:

TFI: N. A. Abrahamson ***Hazard Input Specialist of TFI-team:*** Ph. Roth

HID based on Elicitation Documents: ☒ EG2-ES-1021

HID based on Exp. Assessments (EXA): ☒ EG2-EXA-1017 to 1032

Remarks on the HID model parameterisation in terms of hazard computation input:

The undersigned Hazard Input Specialist confirms that this HID includes all required (subproject specific) input information for hazard computations. No further interpretations of this input will be required and no simplifications except Algorithmic Pinching according to paragraph 2.9 of the QA-Guidelines will be applied to convert this HID into hazard software Input Files.

Signature:

HID acceptance by the Expert / Expert Group:

Date of HID review by the Expert / Expert group: 20.11.2013

HID accepted: ☒ ***HID not accepted:*** ☐

Reasons for non-acceptance of HID / Recommendations:

The undersigned Expert(s) accept(s) the parameterisation proposed in this HID as a faithful and adequate representation of his/their Expert Model. He/they confirm(s) that this HID is free of errors and agree(s) to its use as hazard computation input.

Signature Expert 1 / Expert:

Signature Expert 2:

Signature Expert 3:

Bibliography

Abercrombie 1998 Abercrombie, R.E.: A summary of attenuation measurements from borehole recordings of earthquakes: the 10Hz transition problem,. In: *Pure appl. Geophys.* 153 (1998), p. 475–487. [cited at p. 350]

Abrahamson 2011a Abrahamson, N.: Effective point source distance model (Reff) for the parameterized extrapolated Swiss stochastic GMM / prepared for PRP - PEGASOS Refinement Project. 2011 (TFI-TN-1148). – Technical Note. SP2 [cited at p. 12, 201, 332]

Abrahamson 2011b Abrahamson, N.: Proposal for new approach to develop Vs-Kapa corrections / prepared for PRP - PEGASOS Refinement Project. 2011 (TFI-RF-1368). – Reference Publication. SP2 [cited at p. 126, 130, 131]

Abrahamson 2011c Abrahamson, N.: Vs-Kappa Correction of GMPE's - Introduction / prepared for PRP - PEGASOS Refinement Project. 2011 (TFI-RF-1409). – Reference Publication. SP2 [cited at p. 126, 130, 131]

Abrahamson 2012a Abrahamson, N.: Master Ground Motion Logic Tree / prepared for PRP - PEGASOS Refinement Project. 2012 (TP2-TB-1081). – Technical Report. SP2 [cited at p. 93, 94, 96, 113, 114, 115, 132, 134, 138, 141, 181, 271, 324, 325, 328, 333, 334, 337, 346, 362]

Abrahamson 2012b Abrahamson, N.: Web-Elicitation Meeting with Hilmar Bungum / prepared for PRP - PEGASOS Refinement Project. 2012. – Technical Report. SP2 [cited at p. 115, 119, 121]

Abrahamson and PMT 2012 Abrahamson, N. ; PMT: PRP SP2 Web-Meeting, discussion of NPP specific kappa / prepared for PRP - PEGASOS Refinement Project. 2012 (TFI-RF-1444). – Reference Publication. SP2 [cited at p. 122, 123, 127]

Abrahamson and Silva 2008 Abrahamson, N. ; Silva, W.: Summary of the Abrahamson and Silva NGA Ground-Motion Relations. In: *Earthquake Spectra* 24 (2008), February, No. 1, p. 67–97. http://dx.doi.org/10.1193/1.2924360. – TP2-RF-1114. – DOI 10.1193/1.2924360 [cited at p. 57, 61, 62, 63, 141, 189, 190, 229, 275, 276, 277, 278, 279, 283, 323, 425]

Abrahamson 2013a Abrahamson, N. A.: Evaluation of Vs-Kappa Scaling for Swiss Stations based on the NGA-West2 GMPEs and PRP NGA-West1 GMPEs / prepared for PRP - PEGASOS Refinement Project. 2013 (TFI-TN-1272). – Technical Report. Revision c, Ver.8 [cited at p. 128]

Abrahamson et al. 2008 Abrahamson, N. A. ; Atkinson, G. ; Boore, D. ; Bozorgnia, Y. ; Campbell, K. ; Chiou, B. ; Idriss, I. M. ; Silva, W. ; Youngs, B.: Comparisons of the NGA Ground-Motion Relations. In: *Earthquake Spectra* 24 (2008), February, No. 1, p. 45–66. http://dx.doi.org/10.1193/1.2924363. – DOI 10.1193/1.2924363 [cited at p. 190]

Abrahamson and Silva 1997 Abrahamson, N. A. ; Silva, W. J.: Empirical Response Spectral Attenuation Relations for Shallow Crustal Earthquakes. In: *Seismological Research Letters* 68 (1) (1997), p. 94–127 [cited at p. 77, 141, 362]

Abrahamson and SP2 Experts 2013 Abrahamson, N. A. ; SP2 Experts: SP2 - Ground Motion Characterisation - Evaluation Summaries and Hazard Input Documents / prepared for PRP - PEGASOS Refinement Project. 2013. – Technical Report. SP2 [cited at p. 181, 182]

Abrahamson 2012c Abrahamson, N.A.: *Empirical Ground Motion Prediction Models applied to Western Europe: Characterization of Epistemic Uncertainties and Extension to Small Magnitudes.* SIGMA Workshop No2 , Paris, France, February 1-3 2012. – Presentation [cited at p. 278]

Abrahamson 2013b Abrahamson, N.A.: Intensity Testing & Key Parameter Uncertainties for Hazard / prepared for PRP - PEGASOS Refinement Project. 2013 (TFI-RF-1450). – Reference Publication. SP2 [cited at p. 131, 140]

Abrahamson and Wooddell 2009 Abrahamson, N.A. ; Wooddell, K.: Evaluation of Evidence for Inhibition of Very Strong Ground Motions in the Abrahamson and Silva NGA Ground Motion Model. (2009) [cited at p. 81]

Aghabarati and Tehranizadeh 2009a Aghabarati, H. ; Tehranizadeh, M.: Near-source ground motion attenuation relationship for PGA and PSA of the vertical and horizontal components. In: *Bull. Earthquake Eng.* 7 (2009), April-May, p. 609–635. http://dx.doi.org/DOI10.1007/s10518-009-9114-9. – DOI DOI 10.1007/s10518–009–9114–9 [cited at p. 8]

Aghabarati and Tehranizadeh 2009b Aghabarati, H. ; Tehranizadeh, M.: Prediction of Vertical Peak Ground Acceleration and Vertical Acceleration Response Spectra from Shallow Crustal Earthquakes. In: *Journal of Applied Sciences* 9 (2009), No. 6, p. 1153–1158 [cited at p. 8]

Akkar and Bommer 2007 Akkar, S. ; Bommer, J. J.: Empirical Prediction Equations for Peak Ground Velocity Derived from Strong-Motion Records from Europe and the Middle East. In: *Bulletin of the Seismological Society of America* 97 (2007), April, No. 2, p. 511–530. http://dx.doi.org/10.1785/0120060141. – DOI 10.1785/0120060141 [cited at p. 6, 183]

Akkar and Bommer 2010 Akkar, S. ; Bommer, J. J.: Empirical Equations for the Prediction of PGA, PGV and Spectral Accelerations in Europe, the Mediterranean Region and the Middle East. In: *Seismological Research Letters* 81 (2010), No. 2, p. 195–206. – Electronic Supplement of Table 1 available: Akkar-Bommer SRL 2010 AB10 PanEuropeanGMPE coeffs.csv [cited at p. 6, 16, 37, 38, 39, 72, 74, 183, 232, 233, 235, 276, 323]

Akkar and Cagnan 2010 Akkar, S. ; Cagnan, Z.: A Local Ground-Motion Predictive Model for Turkey, and Its Comparison with Other Regional and Global Ground-Motion Models. In: *Bulletin of the Seismological Society of America* 100 (2010), November, No. 6, p. 2978–2995. http://dx.doi.org/doi:10.1785/0120090367. – DOI doi: 10.1785/0120090367 [cited at p. 8, 16, 183, 324]

Al Atik 2010a Al Atik, L.: Comparison of the PRP GMPEs and Swiss Stochastic Model with Different Stress Drop and Geometrical Spreading Parameters / prepared for PRP - PEGASOS Refinement Project. 2010 (TP2-TB-1059). – Technical Report. SP2 [cited at p. 40]

Al Atik 2010b Al Atik, L.: Comparison Plots of the Alternative Methods for Extension of Ground Motion Prediction Equations to Small Magnitude / prepared for PRP - PEGASOS Refinement Project. 2010 (TP2-TN-1112). – Technical Note. SP2 [cited at p. 40]

Al Atik 2010c Al Atik, L.: Summary of between-event standard deviation models of the 8 PRP ground motion prediction equations / prepared for PRP - PEGASOS Refinement Project. 2010 (TP2-TN-1122.). – PRP Technical Note [cited at p. 63]

Al Atik 2010d Al Atik, L.: Variability of the Swiss Small Magnitude Ground Motion Models / prepared for PRP - PEGASOS Refinement Project. 2010 (TP2-TB-1037). – Technical Report. SP2 [cited at p. 57]

Al Atik 2011a Al Atik, L.: Comparison of the Proposed PRP Single-Station Standard Deviation / prepared for PRP - PEGASOS Refinement Project. 2011 (EXT-TB-1076). – Technical Report. SP2 [cited at p. 61, 62]

Al Atik 2011b Al Atik, L.: Kappa Evaluation for PRP GMPEs, Swiss NPP Sites and SED Network Sites / prepared for PRP - PEGASOS Refinement Project. 2011 (EXT-TN-1150). – Technical Note. SP2 [cited at p. 17, 113, 115, 218, 220]

Al Atik 2011c Al Atik, L.: Sensitivity of Effective Point-Source Distance Conversion to Dip Angle / prepared for PRP - PEGASOS Refinement Project. 2011 (EXT-TN-1205). – Technical Note. SP2 [cited at p. 12]

Al Atik 2011d Al Atik, L.: Sensitivity of Effective Point-Source Distance Conversion to Dip Angle / prepared for PRP - PEGASOS Refinement Project. 2011 (EXT-TN-1205). – Technical Note. SP2 [cited at p. 333]

Al Atik 2011e Al Atik, L.: Summary of Methology for Kappa-fpeak Evaluation / prepared for PRP - PEGASOS Refinement Project. 2011 (EXT-TN-1164). – Technical Note. SP2 [cited at p. 17]

Al Atik 2011f Al Atik, L.: Vs-Kappa Correction Factors for the PRP-Selected Ground-Motion Prediction Equations to Generic Swiss Conditions / prepared for PRP - PEGASOS Refinement Project. 2011 (EXT-TN-1173). – Technical Note. SP2 [cited at p. 13]

Al Atik and Abrahamson 2010a Al Atik, L. ; Abrahamson, N.: Alternative Method for Extension of Empirical Ground Motion Prediction Equations to Small Magnitudes / prepared for PRP - PEGASOS Refinement Project. 2010 (TP2-TB-1038). – Technical Report. SP2 [cited at p. 40, 41]

Al Atik and Abrahamson 2012a Al Atik, L. ; Abrahamson, N.: Vs-Kappa Scaling using IRVT Approach / prepared for PRP - PEGASOS Refinement Project. 2012 (EXT-TB-1087, Ver. 2). – Technical Report. SP2 [cited at p. 19, 27, 113, 114, 148, 209, 210, 240, 296, 352, 368]

Al Atik et al. 2010 Al Atik, L. ; Abrahamson, N. ; Bommer, J.J. ; Scherbaum, F. ; Cotton, F. ; Kühn, N.: The Variability of Ground-Motion Prediction Models and Its Components. In: *Seismological Research Letters* 81 (2010), October, No. 5, p. 794–801. http://dx.doi.org/10.1785/gssrl.81.5.794. – DOI 10.1785/gssrl.81.5.794 [cited at p. 55, 231]

Al Atik and Abrahamson 2010b Al Atik, L. ; Abrahamson, N.A.: *Evaluation of the Use of Generalized Pareto Distribution to Constrain Uncertainty in Peak Ground Accelerations.* Presentation Slides, October, 7 2010. – EXT-RF-1271 [cited at p. 81]

Al Atik and Abrahamson 2011 Al Atik, L. ; Abrahamson, N.A.: Comparison of the Updated NGA-West Dataset to Ground Motion Predictions of the Abrahamson and Silva (2008) Model / prepared for PRP - PEGASOS Refinement Project. 2011 (EXT-TN-1166). – Technical Note. SP2 [cited at p. 10]

Al Atik and Abrahamson 2012b Al Atik, L. ; Abrahamson, N.A.: Kappa Scaling Using Empirical Ground Motion Data / prepared for PRP - PEGASOS Refinement Project. 2012 (EXT-TN-1233, EXT-TB-1233). – Technical Note. SP2 [cited at p. 11, 21, 28, 29, 113, 114, 148, 210, 224, 240, 296]

Al Atik et al. 2013 Al Atik, L. ; Kottke, A. ; Abrahamson, N. ; Hollenback, J.: Kappa Scaling of Ground Motion Prediction Equations Using IRVT Approach. In: *Bulletin of the Seismollogical Society of America* 104 (2013), February, No. 1, p. 336–346. http://dx.doi.org/10.1785/0120120200. – submitted in June 2012. – DOI 10.1785/0120120200 [cited at p. 27, 114, 209, 352]

Al Atik and Renault 2011 Al Atik, L. ; Renault, P.: Comparison of PRP GMPEs with observations on hard rock conditions / prepared for PRP - PEGASOS Refinement Project. 2011 (EXT-TN-1165). – Technical Note. SP2 [cited at p. 332]

Al Atik and Youngs 2013 Al Atik, L. ; Youngs, R.R.: Epistemic Uncertainty for NGA-West2 Models / Pacific Earthquake Engineering Research Center (PEER). 2013 (PEER 2013/11). – Technical Report. PEER NGA-WEST 2 [cited at p. 128]

Allmann 2009 Allmann, B.: SED Workpackage 2: Source Studies / SED, prepared for PRP - PEGASOS Refinement Project. 2009 (TP2-TB-1023). – Technical Report. SP2 [cited at p. 349]

Ancheta et al. 2013 Ancheta, T.D. ; Darragh, R. B. ; Stewart, J.P. ; Seyhan, E. ; Silva, W. J. ; Chiou, B.S.J. ; Wooddell, K.E. ; Graves, R.W. ; Kottke, A.R. ; Boore, D.B. ; Kishida, T. ; Donahue, J.L.: PEER NGA-West2 Database / Pacific Earthquake Engineering Research Center (PEER). 2013 (PEER 2013/03). – Technical Report. PEER NGA-WEST 2 [cited at p. 10]

Anderson 2008 Anderson, J.: Exceptional ground accelerations and velocities caused by earthquakes / Pegasos Refinement Projekt. 2008 (ORD-FY 06-022). – Technical Report [cited at p. 81]

Anderson 2010 Anderson, J. G.: Source and Site Characteristics of Earthquakes that have caused Exceptional Ground Accelerations and Velocities. In: *Bulletin of the Seismological Society of America* (2010), p. 1–36 [cited at p. 81]

Anderson and Hough 1984 Anderson, J. G. ; Hough, S. E.: A model for the shape of the Fourier amplitude spectrum of acceleration at high frequencies. In: *Bull. Seismmol. Soc. Am.* 74 (1984), p. 1969–1993. – SP2 [cited at p. 116, 127, 204, 209, 211, 212, 213, 217, 219, 285, 424]

Atkinson and Assatourians 2010 Atkinson, G. ; Assatourians, K.: Attenuation and Source Characteristics of the 23 June 2010 M 5.0 Val-des-Bois, Quebec, Earthquake,. In: *Seismological Research Letters* 81 (2010), p. 849–860. http://dx.doi.org/doi:10.1785/gssrl.81.5.849. – DOI doi:10.1785/gssrl.81.5.849 [cited at p. 273]

Atkinson and Beresnev 1997 Atkinson, G. ; Beresnev, I. A.: Dont' call it stress drop. In: *Seismological Research Letters* 68 (1997), No. 1, p. 3–4. – SP2 [cited at p. 104]

Atkinson 2006 Atkinson, G. M.: Single-Station Sigma. In: *Bulletin of the Seismological Society of America* 96 (2006), April, No. 2, p. 446–455. http://dx.doi.org/10.1785/0120050137. – DOI 10.1785/0120050137 [cited at p. 16, 37, 63, 276, 323, 324]

Atkinson 2008 Atkinson, G. M.: Ground-Motion Prediction Equations for Eastern North America from a Referenced Empirical Approach: Implications for Epistemic Uncertainty. In: *Bulletin of the Seismological Society of America* 98 (2008), p. 1304–1318. http://dx.doi.org/10.1785/0120070199. – TP2-RF-1114. – DOI 10.1785/0120070199 [cited at p. 7]

Atkinson and Boore 2011 Atkinson, G. M. ; Boore, D. M.: Modifications to Existing Ground-Motion Prediction Equations in Light of New Data. In: *Bulletin of the Seismological Society of America* 101 (2011), June, No. 3, p. pp. 1121–1135. http://dx.doi.org/doi:10.1785/0120100270. – DOI doi: 10.1785/0120100270 [cited at p. 8, 323]

Atkinson and Silva 2000 Atkinson, G.M. ; Silva, W.: Stochastic Modeling of California Ground Motions. In: *Bulletin of the Seismological Society of America* 90 (2000), No. 2, p. 255–274 [cited at p. 11, 13, 333]

Bakun and McGarr 2002 Bakun, W.H. ; McGarr, A.: Differences in attenuation among the stable continental régions,. In: *Geophysical Research Letters,* (2002). http://dx.doi.org/doi:10.1029/2002GL015457. – SP2. – DOI doi:10.1029/2002GL015457 [cited at p. 271]

Baltay and Hanks 2013 Baltay, A. ; Hanks, T.: Magnitude Dependence of Swiss Strong Motion Data in Comparison to NGA-West2 Data Magnitude dependence of PGA and PGV in NGA-West2 data: Parameterization of the model for use by NGA-developers / USGS, prepared for PRP - PEGASOS Refinement Project. Menlo Park, CA, February 15 2013 (EXT-TN-1262). – Technical Note. Revised version of 02.11.2012 [cited at p. 110, 112, 211, 212, 213, 214, 215, 216]

Beauval et al. 2012 Beauval, C. ; Tasan, H. ; Laurendeau, A. ; Delavaud, E. ; F., Cotton ; Scherbaum, F. ; Guéguen, P. ; Kühn, N. ; Allen, T.: On the Testing of Ground-Motion Prediction Equations against Small-Magnitude Data. In: *Bulletin of the Seismological Society of America* 102 (2012), No. 102, p. 1994–2007. http://dx.doi.org/10.1785/0120110271. – SP2. – DOI 10.1785/0120110271 [cited at p. 276, 282]

Beresnev et al. 2002 Beresnev, I. A. ; Nightengale, A. M. ; Silva, W. J.: Properties of Vertical Ground Motions. In: *Bulletin of the Seismological Society of America* 92 (2002), December, No. 8, p. 3152–3164. – TP2-RF-1438 [cited at p. 79, 362, 363]

Bethmann et al. 2012 Bethmann, F. ; Deichmann, N. ; Mai, P.: Seismic wave attenuation from borehole and surface records in the top 2.5 km beneath the city of Basel, Switzerland. In: *Geophys. J. Int.* 190 (2012), p. 1257?1270 [cited at p. 350]

Bindi et al. 2011 Bindi, D. ; Pacor, F. ; Luzi, L. ; Puglia, R. ; Massa, M. ; Ameri, G. ; Paolucci, R.: Ground motion prediction equations derived from the Italian strong motion database. In: *Bull. Earthquake Eng* 9 (2011), p. 1899–1920. http://dx.doi.org/DOI10.1007/s10518-011-9313-z. – SP2. – DOI DOI 10.1007/s10518–011–9313–z [cited at p. 8, 15, 16, 183, 324]

Biro 2012 Biro, Y.: Comparison of Christchurch and Virginia Mineral earthquakes with GMPE's. PMT-SUP-1063 / swissnuclear, prepared for PRP - PEGASOS Refinement Project. 2012 (PMT-SUP-1063). – Support Comoutations. SP2 [cited at p. 9, 133]

Biro and Renault 2012a Biro, Y. ; Renault, P.: Comparison of Empirical V/H Relations with V/H of the US-East, US-West Databases and KKG Borehole Recordings. / swissnuclear, prepared for PRP - PEGASOS Refinement Project. 2012 (PMT-TN-1257). – Technical Note [cited at p. 72, 233, 361, 362]

Biro and Renault 2012b Biro, Y. ; Renault, P.: Re-evaluation of Kappa from new (2009-2012) and existing recordings from NPP's and the SED station LLS / swissnuclear, prepared for PRP - PEGASOS Refinement Project. 2012 (PMT-TN-1244). – Technical Note. SP2 [cited at p. 33, 116, 122, 123, 127, 217, 218, 219, 220, 287, 351]

Boatwright et al. 2001 Boatwright, J. ; Thywissen, K. ; Seekins, L.C.: Correlation of ground motion and intensity for the 17 January 1994 Northridge, California, earthquake. In: *Bulletin of the Seismological Society of America,* 91 (2001), p. 739?752 [cited at p. 186]

Bommer and Stafford 2010a Bommer, J. ; Stafford, P.: Extension of Selected Ground-Motion Prediction Equations to Small Magnitudes / Imperial College Consultants Ltd., prepared for PRP - PEGASOS Refinement Project. 2010 (TP2-TB-1039, Ver. 2.3). – Technical Report. SP2 [cited at p. 5, 16, 38, 39, 40, 41]

Bommer et al. 2011 Bommer, J. J. ; Akkar, S. ; Kale, O.: A Model for Vertical-to-Horizontal Response Spectral Ratios for Europe and the Middle East. In: *Bulletin of the Seismological Society of America* 101 (2011), No. 4, p. 1783–1806. http://dx.doi.org/10.1785/0120100285. – EXT-RF-1336. – DOI 10.1785/0120100285 [cited at p. 72, 74, 76, 139, 140, 290, 358, 360]

Bommer et al. 2003 Bommer, J. J. ; Douglas, J. ; Strasser, F. O.: Style-of-faulting in ground-motion prediction equations. In: *Bulletin of Earthquake Engineering* 1 (2) (2003), No. 1 ISSN: 1570-761X, p. 171–203. – SP2 [cited at p. 16, 113]

Bommer et al. 2009 Bommer, J. J. ; Stafford, P.J. ; Alarcón, J. E.: Empirical Equations for the Prediction of the Significant, Bracketed, and Uniform Duration of Earthquake Ground Motion. In: *Bulletin of the Seismological Society of America* 99 (2009), December, No. 6, p. 3217–3233. http://dx.doi.org/10.1785/0120080298. – DOI 10.1785/0120080298 [cited at p. 132]

Bommer 2011 Bommer, J.J.: Using real earthquake accelerograms for dynamic analysis of nuclear facilities: Defining spectral targets, selecting records and adjusting for consistency. In: *Transactions, SMiRT 21, New Delhi, India*, 2011, p. 1–8 [cited at p. 138, 141]

Bommer and Akkar 2010a Bommer, J.J. ; Akkar, S.: Models for the Prediction of V/H Ratios of Response Spectra, SP2,-SP3-SP4 Interface Workshop / Imperial College Consultants Ltd., prepared for PRP - PEGASOS Refinement Project. 2010 (TP2-RF-1261). – Presentation Slides. SP2 [cited at p. 138]

Bommer and Akkar 2010b Bommer, J.J. ; Akkar, S.: Models for the V/H (vertical to horizontal) Ratios of Spectral Response Ordinates and their Associated Variability / Imperial College Consultants Ltd., prepared for PRP - PEGASOS Refinement Project. 2010 (TP2-TB-1061). – Technical Report. SP2 [cited at p. 138]

Bommer and Stafford 2010b Bommer, J.J. ; Stafford, P.: Extrapolation of Selected and Adjusted GMPE's to Fit Swiss Ground Motion to Small Magnitudes SP2 Workshop WS4 / prepared for PRP - PEGASOS Refinement Project. 2010 (TP2-RF-1195). – Presentation Slides. SP2 [cited at p. 132]

Boore and Atkinson 2008 Boore, D. M. ; Atkinson, G. M.: Ground-Motion Prediction Equations for the Average Horizontal Component of PGA, PGV, and 5%-Damped PSA at Spectral Periods between 0.01 s and 10.0 s. In: *Earthquake Spectra* 24 (2008), February, No. 1, p. 99–138. http://dx.doi.org/10.1193/1.2830434. – TP2-RF-1114. – DOI 10.1193/1.2830434 [cited at p. 7, 8, 83, 142, 323]

Boore and Joyner 1997 Boore, D. M. ; Joyner, W. B.: Site Amplifications for Generic Rock Sites. In: *Bulletin of the Seismological Society of America* 87 (1997), April, No. 2, p. 327–341 [cited at p. 21, 26]

Bozorgnia et al. 2012 Bozorgnia, Y. ; Abrahamson, N.A. ; Campbell, K. W. ; Rowshandel, B. ; Shantz, T.: NGA-West2: A comprehensive research program to update ground motion prediction equations for shallow crustal earthquakes in active tectonic regions. In: *Proceedings of the 15th World Conference on Earthquake Engineering.* Lisbon, Portugal, Sep. 24-28 2012 [cited at p. 211]

Bozorgnia and Campbell 2004 Bozorgnia, Y. ; Campbell, K.W.: The vertical-to-horizontal spectral ratio and tentative procedures for developing simplified V/H and vertical design spectra. In: *Journal of Earthquake Engineering* 4 (2004), No. 4, p. 539–561.. – SP3 [cited at p. 233, 290]

Brune 1970 Brune, J.: Tectonic stress and the spectra of seismic shear waves. In: *Journal of Geophysical Research* 75 (1970), p. 4997–5009 [cited at p. 204]

Brune 1971 Brune, J: Correction: Tectonic stress and the spectra of seismic shear waves. In: *Journal of Geophysical Research* 76 (1971), p. 5002 [cited at p. 204]

Bungum 2010a Bungum, H.: Initial Upper Bounds Model, SP2-WS5 / prepared for PRP - PEGASOS Refinement Project. 2010 (TP2-RF-1243). – Presentation Slides. SP2 [cited at p. 141]

Bungum 2010b Bungum, H.: Response to questions raised at the 27. August 2010 Working Meeting / prepared for PRP - PEGASOS Refinement Project. 2010 (TP2-TN-1144). – Technical Note. SP2 [cited at p. 83]

Bungum 2010c Bungum, H.: SP2 Upper Bounds Model, SP2-WS6 / prepared for PRP - PEGASOS Refinement Project. 2010 (TP2-RF-1260). – Presentation Slides. SP2 [cited at p. 141, 143]

Bungum 2010d Bungum, H.: SP2 Upper Bounds Weights, SP2-WS6 / prepared for PRP - PEGASOS Refinement Project. 2010 (TP2-RF-1267). – Presentation Slides. SP2 [cited at p. 142]

Bungum 2010e Bungum, H.: Updated Bounds Model, SP2 Working Meeting / prepared for PRP - PEGASOS Refinement Project. 2010 (TP2-RF-1253). – Presentation Slides. SP2 [cited at p. 141]

Bungum 2010f Bungum, H.: Upper Bounds - Existing approaches, new information, SP2-WS4 / prepared for PRP - PEGASOS Refinement Project. 2010 (TP2-RF-1192). – Presentation Slides. SP2 [cited at p. 141]

Campbell 2003 Campbell, K. W.: Prediction of Strong Ground Motion Using the Hybrid Empirical Method and Its Use in the Development of Ground-Motion (Attenuation) Relations in Eastern North America. In: *Bulletin of the Seismological Society of America* 93 (2003), June, No. 3, p. 1012–1033 [cited at p. 25, 113, 138, 323]

Campbell 2013 Campbell, K. W.: An evaluation of eastern North American ground motion models developed using the hybrid empirical method. In: *Bulletin of the Seismological Society of America* in press. (2013). – SP2 [cited at p. 224]

Campbell and Bozorgnia 2008 Campbell, K. W. ; Bozorgnia, Y.: NGA Ground Motion Model for the Geometric Mean Horizontal Component of PGA, PGV, PGD and 5% Damped Linear Elastic Response Spectra for Periods Ranging from 0.01 to 10 s. In: *Earthquake Spectra* 24 (2008), February, No. 1, p. 139–171. http://dx.doi.org/10.1193/1.2857546. – TP2-RF-1114. – DOI 10.1193/1.2857546 [cited at p. 63, 189, 323]

Campbell and Bozorgnia 2013 Campbell, K. W. ; Bozorgnia, Y.: NGA-West2 Campbell-Bozorgnia Ground Motion Model for the Horizontal Components of PGA, PGV, and 5%-Damped Elastic Pseudo-Acceleration Response Spectra for Periods Ranging from 0.01 to 10 sec / Pacific Earthquake Engineering Research Center (PEER). 2013 (PEER 2013/06). – Technical Report. PEER NGA-WEST 2 [cited at p. 189]

Campbell et al. 2013 Campbell, K. W. ; Hashash, Y. M. A. ; Kim, B. ; Kottke, A.R. ; Rathje, E.M. ; Silva, W.J. ; Stewart, J. P.: Reference rock site condition for central and eastern North America, Part II - Attenuation (Kappa) definition / Pacific Earthquake Engineering Research Center, University of California, Berkeley, CA. 2013 (in press.). – Technical Report. SP2 [cited at p. 223]

Campbell and Bozorgnia 2003 Campbell, K.W. ; Bozorgnia, Y.: Updated Near-Source Ground Motion (Attenuation) Relations for the Horizontal and Vertical Components of Peak Ground Acceleration and Acceleration Response Spectra. In: *Bulletin of the Seismological Society of America* 93 (2003), No. 1, p. 314–331 [cited at p. 72, 77, 138, 141, 230, 232, 233, 235, 358, 361, 362]

Campbell et al. 2003 Campbell, R. ; Hardy, G. ; Ravindra, M.: Trial Plant Review of an American Nuclear Society External Event Probabilistic Risk Assessment Standard / EPRI. 300 Commerce Drive, Suite 200, Irvine, CA 92602, September 2003 (1009074). – EPRI report [cited at p. 7, 25, 139, 140]

Carminati et al. 2009 Carminati, E. ; Cuffaro, M. ; Doglioni, C.: Cenozoic uplift of Europe. In: *Tectonics* 28 (2009), No. TC4016, p. 1–16. http://dx.doi.org/10.1029/2009TC002472. – DOI 10.1029/2009TC002472 [cited at p. 188]

Cauzzi and Faccioli 2008 Cauzzi, C. ; Faccioli, E.: Broadband (0.05 to 20 s) prediction of displacement response spectra based on worldwide digital records. In: *Journal of Seismology* 12 (2008), p. 453–475. http://dx.doi.org/10.1007/s10950-008-9098-y. – TP2-RF-1114. – DOI 10.1007/s10950–008–9098–y [cited at p. 8]

Chandler et al. 2006 Chandler, A. M. ; Lam, N. T. K. ; Tsang, H. H.: Near-surface attenuation modelling based on rock shear-wave velocity profile. In: *Soil Dynamics and Earthquake Engineering* 26 (2006), p. 1004–1014. http://dx.doi.org/10.1016/j.soildyn.2006.02.010. – DOI 10.1016/j.soildyn.2006.02.010 [cited at p. 121]

Chiou 2011 Chiou, B.: Parameterization of the Simulated Data from Swiss Stochastic Ground Motion Model / prepared for PRP - PEGASOS Refinement Project. 2011 (EXT-TB-1066). – Technical Report. SP2 [cited at p. 332]

Chiou et al. 2010 Chiou, B. ; Youngs, R. ; Abrahamson, N. ; Addo, K.: Ground-Motion Attenuation Model for Small-To-Moderate Shallow Crustal Earthquakes in California and Its Implications on Regionalization of Ground-Motion Prediction Models. In: *Earthquake Spectra Earthquake Engineering Research Institute* 26 (2010), November, No. 4, p. pages 907–926. http://dx.doi.org/DOI:10.1193/1.3479930. – DOI DOI: 10.1193/1.3479930 [cited at p. 7, 37, 189, 190, 323]

Chiou and Youngs 2008a Chiou, B. S.-J. ; Youngs, R. R.: NGA Model for Average Horizontal Component of Peak Ground Motion and Response Spectra / Pacific Earthquake Engineering Research Center (PEER). Pacific Engineering Research Center, College of Engineering, University of California, Berkeley, November 2008 (PEER 2008/09). – Technical Report. TP2-RF-1114 [cited at p. 274]

Chiou and Youngs 2008b Chiou, B. S.-J. ; Youngs, R. R.: An NGA Model for the Average Horizontal Component of Peak Ground Motion and Response Spectra. In: *Earthquake Spectra* 24 (2008), February, No. 1, p. 173–215. http://dx.doi.org/10.1193/1.2894832. – TP2-RF-1114. – DOI 10.1193/1.2894832 [cited at p. 8, 12, 190, 229, 276, 323]

Cotton and Abrahamson 2010 Cotton, F. ; Abrahamson, N.N.: Single-Station Sigma Project and Task Guidelines / prepared for PRP - PEGASOS Refinement Project. 2010 (TP2-TN-1080). – Technical Note. SP2 [cited at p. 56, 227]

Cotton et al. 2013 Cotton, F. ; Archuleta, R. ; Causse, M.: What is sigma of stress drop? In: *Seismological Research Letter* 84 (2013), July-August, No. 1, p. 42–48. http://dx.doi.org/10.1785/0220120087. – DOI 10.1785/0220120087 [cited at p. 281, 282]

Cotton et al. 2006 Cotton, F. ; Scherbaum, F. ; Bommer, J. J. ; Bungum, H.: Criteria for selecting and adjusting ground-motion models for specific target regions: Application to Central Europe and rock sites. In: *Journal of Seismology* 10 (2006), p. 137–156. http://dx.doi.org/10.1007/s10950-005-9006-7. – DOI 10.1007/s10950–005–9006–7 [cited at p. 5]

Delavaud et al. 2012a Delavaud, E. ; Cotton, F. ; Akkar, S. ; Scherbaum, F. ; Danciu, L. ; Beauval, C. ; Drouet, S. ; Douglas, J. ; Basili, R. ; Abdullah, M. ; Sandikkaya, M. ; Segou, M. ; Faccioli, E. ; Theodoulidis, N.: Toward a Ground-Motion Logic Tree for Probabilistic Seismic Hazard Assessment in Europe. In: *Journal of Seismology* 16 (2012), February, 22, p. 451–473. http://dx.doi.org/10.1007/s10950-012-9281-z. – SHARE. – DOI 10.1007/s10950–012–9281–z [cited at p. 188, 196, 276, 282, 343]

Delavaud et al. 2012b Delavaud, E. ; Scherbaum, F. ; Kühn, N. ; Allen, T.: Testing the Global Applicability of Ground-Motion Prediction Equations for Active Shallow Crustal Regions. In: *Bulletin of the Seismollogical Society of America* 102 (2012), April, No. 2, p. 707–721. http://dx.doi.org/10.1785/0120110113. – SHARE. – DOI 10.1785/0120110113 [cited at p. 272]

Douglas 2007 Douglas, J.: On the regional dependence of earthquake response spectra. In: *ISET Journal of Earthquake Technology* 44 (2007), No. 1, p. 71–99 [cited at p. 189, 190]

Douglas 2009a Douglas, J.: Pre-selection of ground motion models for the PEGASOS Refinement Project (PRP) / BRGM, prepared for PRP - PEGASOS Refinement Project. 2009 (TP2-TB-1015). – Technical Report. SP2 [cited at p. 6, 8, 97, 182, 183, 188, 328]

Douglas 2009b Douglas, J.: Testing the applicability of various ground-motion-intensity relations for the PEGASOS Refinement / BRGM, prepared for PRP - PEGASOS Refinement Project. 2009 (TP2-TB-1018). – Technical Report. SP2 [cited at p. 186]

Douglas 2011a Douglas, J.: Addendum to 'Pre-selection of ground-motion models for the PEGASOS Refinement Project (PRP)' / BRGM, prepared for PRP - PEGASOS Refinement Project. 2011 (EXT-TN-1200). – Technical Note. SP2 [cited at p. 8, 182, 183, 188]

Douglas 2011b Douglas, J.: Ground-motion prediction equations 1964-2010 / Pacific Earthquake Engineering Research Center (PEER). Pacific Earthquake Engineering Research Center, College of Engineering, University of California, Berkeley, April 2011 (PEER 2011/102). – Technical Report. (also published as Final Report BRGM/RP-59356-FR by BRGM) [cited at p. 6, 190]

Douglas et al. 2010 Douglas, J. ; Gehl, P. ; Bonilla, L.F. ; Gélis, C.: A Kappa Model for Mainland France. In: *Pure and Applied Geophysics* 167 (2010), April, 20, p. 1303–1315. http://dx.doi.org/10.1007/s00024-010-0146-5. – DOI 10.1007/s00024–010–0146–5 [cited at p. 116, 119, 120, 362]

Drouet et al. 2010 Drouet, S. ; Cotton, F. ; Gueguen, P.: VS30, kappa, regional attenuation and Mw from accelerograms: application to magnitude 3-5 French earthquakes. In: *Geophys. J. Int. Seismology* 182 (2010), April, p. 880–898. http://dx.doi.org/doi:10.1111/j.1365-246X.2010.04626.x. – SHARE. – DOI doi: 10.1111/j.1365–246X.2010.04626.x [cited at p. 116, 119, 120, 125]

Edwards 2012a Edwards, B.: Revised Vs30-Kappa models / SED, prepared for PRP - PEGASOS Refinement Project. ETHZ, January 2012 (TP2-TN-1236). – Technical Note. Personal Communication [cited at p. 32, 274, 275, 282]

Edwards 2012b Edwards, B.: Site Specific Kappa / SED, prepared for PRP - PEGASOS Refinement Project. ETHZ, April, 10 (updated 13, June 2012) 2012 (TP2-TN-1236). – Technical Note. SP2 [cited at p. 33, 113, 116, 117, 119, 122, 123, 127, 130, 285, 288, 348, 349]

Edwards 2013 Edwards, B.: Note on the Parameter Correlation in the Swiss Stochastic Model / SED, prepared for PRP - PEGASOS Refinement Project. 2013 (EXT-TN-1261). – Technical Note. SP2 [cited at p. 33, 131]

Edwards and Fäh 2010 Edwards, B. ; Fäh, D.: Extrapolation of Swiss Stochastic Ground Motion Model / SED, prepared for PRP - PEGASOS Refinement Project. 2010 (TP2-TB-1052). – Technical Report. SP2 [cited at p. 11, 12, 200, 201, 202, 211, 217, 332]

Edwards and Fäh 2011a Edwards, B. ; Fäh, D.: Note on the Relation of Kappa to V/H in Swiss/Japanese Data / SED, prepared for PRP - PEGASOS Refinement Project. 2011 (EXT-TN-1217). – Technical Note. SP2 [cited at p. 290, 291, 358]

Edwards and Fäh 2011b Edwards, B. ; Fäh, D.: Sensitivity of REFF Simulations / SED, prepared for PRP - PEGASOS Refinement Project. 2011 (EXT-TN-1210). – Technical Note. SP2 [cited at p. 333]

Edwards and Fäh 2012a Edwards, B. ; Fäh, D.: Measurements of Stress Parameter and Site Attenuation from Recordings of Large Earthquakes in Europe and the Middle East. In: *Submitted to Geophysical Journal International* submitted (2012) [cited at p. 33, 281, 342, 345, 348]

Edwards and Fäh 2012b Edwards, B. ; Fäh, D.: Site Specific Kappa (SP2/ WS10 09 - 11. May 2012) / SED, prepared for PRP - PEGASOS Refinement Project. ETHZ, May 2012 (EXT-RF-1451). – Presentation Slides. SP2 [cited at p. 118, 119]

Edwards and Fäh 2013a Edwards, B. ; Fäh, D.: Measurements of stress parameter and site attenuation from recordings of moderate to large earthquakes in Europe and the Middle East. In: *Geophysical Journal International* 194 (2013), May 8, No. 2, 1190-1202. http://dx.doi.org/10.1093/gji/ggt158. – DOI 10.1093/gji/ggt158 [cited at p. 33, 281, 342]

Edwards and Fäh 2013b Edwards, B. ; Fäh, D.: A Stochastic Ground-Motion Model for Switzerland. In: *Bulletin of the Seismological Society of America* 103 (2013), No. 1, p. 78–98. http://dx.doi.org/10.1785/0120110231. – DOI 10.1785/0120110231 [cited at p. 110, 124, 125]

Edwards et al. 2009 Edwards, B. ; Fäh, D. ; Allmann, B. ; Poggi, V.: Stochastic Ground Motion Model for Switzerland (Revision) / SED, prepared for PRP - Pegasos Refinement Project. 2009 (TP2-TB-1024). – Technical Report. SP2 [cited at p. 34, 96, 334, 338]

Edwards et al. 2010 Edwards, B. ; Fäh, D. ; Allmann, B. ; Poggi, V.: Stochastic Ground Motion Model for Switzerland / SED, prepared for PRP - PEGASOS Refinement Project. 2010 (TP2-TB-1024). – Technical Report. SP2 [cited at p. 11, 33, 34, 63, 96, 116, 131, 185, 200, 201, 202, 210, 212, 213, 217, 218, 219, 220, 222, 284, 286, 332, 334, 338, 356]

Edwards et al. 2011a Edwards, B. ; Fäh, D. ; Giardini, D.: Attenuation of seismic shear wave energy in Switzerland. In: *Geophysical Journal International* 185 (2011), February, 11, No. 2, p. 967–984. http://dx.doi.org/10.1111/j.1365-246X.2011.04987.x. – SP2. – DOI 10.1111/j.1365–246X.2011.04987.x [cited at p. 74, 113, 116, 123, 124, 125, 138, 232, 233, 234, 235, 290]

Edwards et al. 2013a Edwards, B. ; Michel, C. ; Poggi, V. ; Fäh, D.: Determination of Site Amplification from Regional Seismicity: Application to the Swiss National Seismic Networks. In: *Seismological Research Letters* 84 (2013), July/ August, No. 4, p. 611–621. http://dx.doi.org/10.1785/0220120176. – Online Material: Supplemental figures and tables.. – DOI 10.1785/0220120176 [cited at p. 201, 221]

Edwards et al. 2011b Edwards, B. ; Poggi, V ; Fäh, D.: A Predictive Equation for the Vertical-to-Horizontal Ratio of Ground-Motion at Rock Sites based on Shear Wave Velocity

Profiles from Japan to Switzerland. In: *Bulletin of Seismological Society of America* 101 (2011), No. 6, p. 2998–3019. http://dx.doi.org/10.1785/0120110023. – TP2-TB-1065, SP3+ SP2. – DOI 10.1785/0120110023 [cited at p. 18, 72, 138, 139, 140, 232, 233, 234, 235, 348, 360, 361, 422]

Edwards et al. 2012 Edwards, B. ; Poggi, V. ; Fäh, D.: Comparison of Japanese Strong Ground-Motion Recordings with the Swiss Stochastic Model / SED, prepared for PRP - PEGASOS Refinement Project. Version: December 19 2012. http://dx.doi.org/10.1785/0120110231. 2012 (TP2-TB-1091). – Technical Report. – Electronic Resource. – 78–98 S. SP2 [cited at p. 202, 203, 204, 206, 218, 342]

Edwards et al. 2013b Edwards, B. ; Poggi, V. ; Fäh, D.: European and Japanese Strong-Motion Data in the Context of the Swiss Stochastic Model / SED, prepared for PRP - PEGASOS Refinement Project. 2013 (TP2-RF-1453). – Presentation Slides. SP2 [cited at p. 124]

Faccioli et al. 2010 Faccioli, E. ; Villani, M. ; Vanini, M. ; Cauzzi, C.: Mapping Seismic Hazard for the Needs of Displacement-Based Design: The Case of Italy. In: *Advances in Performance-Based Earthquake Engineering,* (2010). http://dx.doi.org/DOI10.1007/978-90-481-8746-1-1. – DOI DOI 10.1007/978–90–481–8746–1–1 [cited at p. 323]

Faenza 2010 Faenza, L.: Addendum Report IGNV / INGV, prepared for PRP - PEGASOS Refinement Project. 2010 (EXT-TB-1031). – Technical Report. SP2 [cited at p. 186, 201]

Faenza and Michelini 2010 Faenza, L. ; Michelini, A.: Regression Analysis of MCS Intensity and ground motion spectral accelerations, SA, in Italy / INGV, prepared for PRP - PEGASOS Refinement Project. 2010 (EXT-TB-1030). – Technical Report. SP2 [cited at p. 328]

Faenza and Michelini 2011 Faenza, L. ; Michelini, A.: Regression analysis of MCS Intensity and ground motion spectral accelerations (SAs) in Italy. In: *Geophysical Journal International* 186 (2011), September, No. 3, p. 1415–1430. http://dx.doi.org/10.1111/j.1365-246X.2011.05125.x. – DOI 10.1111/j.1365–246X.2011.05125.x [cited at p. 103, 186, 201]

Fäh et al. 2011 Fäh, D. ; Giardini, D. ; Kästli, P. ; Deichmann, N. ; Gisler, M. ; Schwarz-Zanetti, G. ; Alvarez-Rubio, S. ; Sellami, S. ; Edwards, B. ; Allmann, B. ; Bethmann, F. ; Wössner, J. ; Gassner-Stamm, G. ; Fritsche, S. ; Eberhard, D.: ECOS-09: Earthquake catalogue of Switzerland, Release 2011, report and database, public catalogue, 17.4.2011, Report SED/RISK/R/001/20110417 / SED Swiss Seismological Service, ETH, Zurich, Switzerland. 2011. – Technical Report [cited at p. 185]

Fäh et al. 2009a Fäh, D. ; Gisler, M. ; Jaggi, B. ; Kästli, P. ; Lutz, T. ; Masciadri, V. ; Matt, C. ; Mayer-Rosa, D. ; Rippmann, D. ; Schwarz-Zanetti, G. ; Tauber, J. ; Wenk, T.: The 1356 Basel earthquake: an interdisciplinary revision. In: *Geophysical Journal International* 178 (2009), July, No. 1, p. 351–374. http://dx.doi.org/10.1111/j.1365-246X.2009.04130.x. – DOI 10.1111/j.1365–246X.2009.04130.x [cited at p. 185]

Fäh et al. 2009b Fäh, D. ; Kästli, P. ; Alvarez, S. ; Poggi, V.: Intensity data from the MECOS database / Swiss Seismological Service, ETH, Zurich, Switzerland, prepared fpr PRP Pegasos Refinement Project. 2009 (Report SED/PRP/R/012/20100607). – Technical Report [cited at p. 185, 201]

Frankel et al. 1990 Frankel, A. ; McGarr, A. ; Bicknell, J. ; Mori, L. ; Cranswick, E.: Attenuation of high-frequency shear waves in the crust: Measurements from New York state, South Africa and southern California, ,. In: *J. Geophys. Res.* 95(B11) (1990), p. 17441–17457.. – SP2 [cited at p. 273]

Giardini and Wössner 2013 Giardini, D. ; Wössner, J.: *SHARE - Seismic Hazard Harmonization in Europe*. Version: 2013. URL http://www.share-eu.org/. – Online–Ressource, Last checked: July 2013 [cited at p. 7]

Gülerce and Abrahamson 2010 Gülerce, Z. ; Abrahamson, N. A.: Vector-Valued Probabilistic Seismic Hazard Assessment for the Effects of Vertical Ground Motions on the Seismic Response of Highway Bridges. In: *Earthquake Spectra, Earthquake Engineering Research Institute* 26 (2010), November, No. 4, p. 999–1016. http://dx.doi.org/DOI:10.1193/1.3464548. – DOI DOI: 10.1193/1.3464548 [cited at p. 72, 74, 138, 232, 233, 235, 358, 361, 362]

Gülerce and Abrahamson 2011 Gülerce, Z. ; Abrahamson, N.N.: Site-Specific Design Spectra for Vertical Ground Motion. In: *Earthquake Spectra* 27 (2011), January, 13, No. 4, p. 1023–1047. http://dx.doi.org/http://dx.doi.org/10.1193/1.3651317. – SP3 + SP2. – DOI http://dx.doi.org/10.1193/1.3651317 [cited at p. 76, 138, 139, 140, 141, 290, 291]

Goulet et al. 2014 Goulet, C. A. ; Kishida, T. ; Ancheta, T. D. ; Cramer, C. H. ; Darragh, R. B. ; Silva, W. J. ; Hashash, Y. M. ; Harmon, J. ; Stewart, J. P. ; Wooddell, K. E. ; Youngs, R. R.: PEER NGA-East Database / PEER Center, University of California, Berkeley. Version: October 2014. URL http://peer.berkeley.edu/ngaeast/ (2014/17). – Technical Report. – Electronic Resource [cited at p. 28]

Hanks 1982 Hanks, T. C.: fmax. In: *Bulletin of the Seismological Society of America* 72 (1982), December, No. No. 6A, p. 1867–1879 [cited at p. 211]

Hashash et al. 2013 Hashash, Y. M. A. ; Kottke, A. R. ; Campbell, K.K. W. ; Stewart, J. P. ; Kim, B. ; Moss, C. ; Nikolaou, S. ; Rathje, E.M. ; Silva, W.J.: Reference rock site condition for central and eastern North America, Transactions. In: *SMiRT 22 Transactions*. San Francisco, CA, August 18-23 2013 [cited at p. 223]

HSK 2004 HSK: HSK-RT Final Report: Review Approach and Comments on "Probabilistic Seismic Hazard Analysis for Swiss Nuclear Power Plant Sites (PEGASOS Projekt) - Final Report" / Hauptabteilung für die Sicherheit der Kernanlagen. 5232 Villigen-HSK, December, 3 2004 (HSK-AN-5364). – Review Report [cited at p. 182]

Huyse et al. 2010 Huyse, L. ; Chen, R. ; Stamatakos, J. A.: Application of Generalized Pareto Distribution to Constrain Uncertainty in Peak Ground Accelerations. In: *Bulletin of the Seismological Society of America* 100 (2010), February, No. 1, p. 87–101. http://dx.doi.org/10.1785/0120080265. – DOI 10.1785/0120080265 [cited at p. 81]

Kammerer and Ake 2012 Kammerer, A. M. ; Ake, J. P.: *Practical Implementation Guidelines for SSHAC Level 3 and 4 Hazard Studies (Rev.1)*. URL http://pbadupws.nrc.gov/docs/ML1211/ML12118A445.pdf. Version: Manuscript Completed: May 2011 Date Published: February 2012 Date Revision: April 2012 2012 [cited at p. 93, 182, 271]

Kastrup et al. 2004 Kastrup, U. ; Zoback, M. L. ; Deichmann, N. ; Evans, K. F. ; Giardini, D. ; Michael, A. J.: Stress field variations in the Swiss Alps and the northern Alpine foreland derived from inversion of fault plane solutions. In: *Journal of Geophysical Research* 109 (2004), No. B01402, p. B01402. http://dx.doi.org/10.1029/2003JB002550,2004. – DOI 10.1029/2003JB002550, 2004 [cited at p. 188]

Kühn 2011a Kühn, N.: Testing of empirical ground motion prediction equations and the Swiss stochastic model using Swiss intensity data / Universität Potsdam, prepared for PRP - PEGASOS Refinement Project. 2011 (EXT-TB-1086). – Technical Report. SP2 [cited at p. 103, 104, 183, 185, 186, 187, 279, 328, 329]

Kühn 2011b Kühn, N.: Update of SOM analysis for the PRP GMPE's, EXT-SUP-1050 / Universität Potsdam, prepared for PRP - PEGASOS Refinement Project. 2011 (EXT-SUP-1050). – Support Computations. SP2 [cited at p. 98, 99, 100, 183, 184]

Kühn 2012 Kühn, N.: Comparison of Self-Organizing Maps / Universität Potsdam, prepared for PRP - PEGASOS Refinement Project. 2012 (EXT-TN-1222). – Technical Note. SP2 [cited at p. 101]

Kühn and Renault 2012 Kühn, N. ; Renault, Ph.: Mixture Model Comparison / Universität Potsdam, prepared for PRP - PEGASOS Refinement Project. 2012 (EXT-SUP-1078). – Technical Report. SP2 [cited at p. 103, 104, 111]

Kühn 2011c Kühn, N. M.: Short Summary of Vs-Kappa correction factors / Universität Potsdam, prepared for PRP - PEGASOS Refinement Project. 2011 (EXT-SUP-1051). – Technical Note. SP2 [cited at p. 352]

Kühn 2011d Kühn, N. M.: Testing of Empirical Ground Motion Prediction Equations and the Swiss Stochastic Model using Swiss Intensity Data / Universität Potsdam, prepared for PRP - PEGASOS Refinement Project. 2011 (TP2-TB-1078). – Technical Report. SP2 [cited at p. 328, 329]

Kästli and Fäh 2006 Kästli, P. ; Fäh, D.: Rapid Estimation of Macroseismic Effects and Shake maps combining Macroseismic and Instrumental Data. In: *1st ECEES - First European Conference on Earthquake Engineering and Seismology (a joint event of the 13th ECEE & 30th General Assembly of the ESC)*. Genève, 2006. – CD ROM [cited at p. 185, 186, 205, 329]

Ktenidou et al. 2014 Ktenidou, O. ; Cotton, F. ; Abrahamson, N. ; Anderson, J.: Taxonomy of kappa: A review of definitions and estimation approaches targeted to applications. In: *Seismological Research Letter* 85 (2014), January/February, No. 1, p. 135–146. http://dx.doi.org/10.1785/0220130027. – DOI 10.1785/0220130027 [cited at p. 33]

Ktenidou 2012 Ktenidou, O.-J.: (Re)estimation of kappa for selected stations in Switzerland / Université de Grenoble/CNRS, prepared for PRP - PEGASOS Refinement Project. 2012 (EXT-RF-1443). – Presentation Slides. Presented at the SP2 workshop WS10/SP2 [cited at p. 33, 126, 127, 128, 129, 347, 348, 351]

Ktenidou et al. 2012a Ktenidou, O.-J. ; Cotton, F. ; Chaljub, E. ; Drouet, S. ; Theodoulidis, N. ; Arnaouti, S.: Estimation of kappa (k) for a sedimentary basin in Greece (EUROSEISTEST) - Correlation to site characterisation parameters. In: *15 WCEE - World Conference of Earthquake Engineering*. Lisboa, Portugal, September 24-28 2012 [cited at p. 33, 121, 122, 123, 126, 219]

Ktenidou et al. 2012b Ktenidou, O.-J. ; Cotton, F. ; Drouet, S. ; Theodoulidis, N. ; Chaljub, E.: Kappa (k): Estimates, origins, and correlation to site characterization parameters / AGU Fall Meeting. 2012. – Poster [cited at p. 219]

Ktenidou et al. 2012c Ktenidou, O.-J. ; Gélis, C. ; Bonilla, L.-F.: A Study on the Variability of Kappa (k) in a Borehole: Implications on the Computation Method Used. In: *Bulletin of the Seismollogical Society of America* 103 (2012), March, No. 2a, p. 1048–1068. http://dx.doi.org/10.1785/0120120093. – DOI 10.1785/0120120093 [cited at p. 33, 140, 219, 223]

Ktenidou and Van Houtte 2013 Ktenidou, O.-J. ; Van Houtte, C.: (Re)estimation of kappa for selected rock and hard rock SED stations in Switzerland / Université de Grenoble/CNRS, prepared for PRP - PEGASOS Refinement Project. 2013 (TP2-RF-1455 EXT-RF-1448). – Presentation Slides. SP2 workshop WS11/SP2 [cited at p. 33, 123, 124, 125, 126, 219, 222, 283, 284, 423]

Ktenidou et al. 2013 Ktenidou, O.-J. ; Van Houtte, C. ; Cotton, F. ; Abrahamson, N.: Kappa0 (k0) estimates for hard rock SED stations in Switzerland using a high-frequency approach. In: *AGU Fall Meeting*, 2013. – Poster Presentation [cited at p. 33]

Laurendeau and Cotton 2012 Laurendeau, A. ; Cotton, F.: Analysis of Kappa-fpeak relationships, TP2-TN-1224 / prepared for PRP - PEGASOS Refinement Project. 2012 (TP2-TN-1224). – Techical Note. SP2 [cited at p. 113]

Laurendeau et al. 2013 Laurendeau, A. ; Cotton, F. ; Ktenidou, O. ; Bonilla, F. ; Hollender, F.: Rock and Stiff-Soil Site Amplification: Dependency on VS30 and Kappa0. In: *Bulletin of the Seismollogical Society of America* 103 (2013), December, No. 6, p. 3131–3148. http://dx.doi.org/doi:10.1785/0120130020. – DOI doi: 10.1785/0120130020 [cited at p. 285]

McGuire et al. 2001 McGuire, R. K. ; Silva, W.J. ; Costantino, C.J.: *Technical Basis for Revision of Regulatory Guidance on Design Ground Motions: Hazard- and Risk-consistent Ground Motion Spectra Guidelines*. U.S. Nuclear Regulatory Commission, Office of Nuclear Regulatory Research, Washington, DC 20555-0001, 2001 [cited at p. 72]

Miller and Rice 1983 Miller, A. C. ; Rice, T. R.: Discrete Approximations of Probability Distributions. In: *The Institute of Management Science* 29 (1983), March, No. 3, p. 352–362 [cited at p. 148, 240, 296, 368]

Moss 2009 Moss, R.E.S.: Reduced uncertainty of ground motion prediction equations through Bayesian variance analysis / Pacific Earthquake Engineering Research Center, College of Engineering, University of California, Berkeley, USA. 2009 (PEER Report 2009/105). – Technical Report. SP2 [cited at p. 354]

Musson et al. 2010 Musson, R. M. W. ; Grünthal, G. ; Stucchi, M.: The comparison of macroseismic intensity scales. In: *Journal of Seismology* 14 (2010), No. 2, p. 413–428 [cited at p. 186]

NAGRA 2004 NAGRA: Probabilistic Seismic Hazards Analysis for Swiss Nuclear Power Plant Sites (PEGASOS Project) / prepared for Unterausschuss Kernenergie der Überlandwerke (UAK). 2004. – final report [cited at p. 182]

Ozel 1999 Ozel, O. et. a.: Crustal structure of central Japan and its petrological implications. In: *Geophys. J. Int. Seismology* 138 (1999), p. 257–274 [cited at p. 346]

PEER Center 2013 PEER Center, Berkeley: *NGA-West2*. Version: 2013. URL http://peer.berkeley.edu/ngawest2/. – Online–Ressource [cited at p. 9]

Pezeshk et al. 2011 Pezeshk, S. ; ZANDieh, A. ; Tavakoli, B.: Hybrid Empirical Ground-Motion Prediction Equations for Eastern North America Using NGA Models and Updated Seismological Parameters. In: *Bulletin of the Seismological Society of America* 101 (2011), August, No. 4, p. pp. 1859–1870. http://dx.doi.org/doi:10.1785/0120100144. – DOI doi: 10.1785/0120100144 [cited at p. 7, 323]

Pitarka et al. 2002 Pitarka, A. ; Somerville, P. ; Collins, N.: Numerical Simulations for Evaluation of Median and Upper Limit Ground Motions in Switzerland / URS Corporation, prepared for the PEGASOS project. 2002 (EXT-TN-0277). – Technical Report [cited at p. 81]

Poggi et al. 2011 Poggi, V. ; Edwards, B. ; Fäh, D.: Derivation of a Reference Shear-Wave Velocity Model from Empirical Site Amplification. In: *Bulletin of the Seismological Society of America* 101 (2011), February, No. 1, p. 258–274. http://dx.doi.org/10.1785/0120100060. – DOI 10.1785/0120100060 [cited at p. 221]

Poggi et al. 2012 Poggi, V. ; Edwards, B. ; Fäh, D.: Empirical estimation of kappa from rock velocity profiles at the Swiss NPP sites / SED, prepared for PRP - PEGASOS Refinement Project. 2012 (TP2-TB-1090). – Technical Report. SP2 [cited at p. 33, 221, 285, 342, 351]

Poggi et al. 2013 Poggi, V. ; Edwards, B. ; Fäh, D.: Reference S-wave velocity profile and attenuation models for ground-motion prediction equations: Application to Japan. In: *Bulletin of the Seismological Society of America* 103 (2013), No. 5, p. 2645–2656. http://dx.doi.org/10.1785/0120120362. – DOI 10.1785/0120120362 [cited at p. 221, 335]

Poggi and Fäh 2013 Poggi, V. ; Fäh, D.: Calibration of a reference profile for host-to-target correction of ground motion models / SED, prepared for PRP - PEGASOS Refinement Project. ETHZ, October 7 2013 (TP2-TN-1279). – Technical Note [cited at p. 130]

Priolo et al. 2002 Priolo, E. ; Vuan, A. ; Klinc, P. ; Laurenzano, G.: Estimation of the Ground Motion Upper Limit in Switzerland: EXWIM Numerical Simulations (and supplement) / OGS - Istituto Nazionale di Oceanografia e di Geofisica Sperimentale, prepared for the PEGASOS project. Trieste, 2002 (EXT-TN-0278, EXT-TN-0303). – Technical Report (Ver.4) [cited at p. 81]

Rathje et al. 2005 Rathje, E.M. ; Kottke, A. R. ; Ozbey, M. C.: Using inverse random vibration theory to develop input Fourier Amplitude Spectra for use in Site Resoponse. In: *16th International Conference on Soil Mechanics and Geotechnical Engineering: TC4*. Osaka, Japan : Earthquake Geotechnical Engineering Satellite Conference, Osaka, Japan, September 2005, p. 160–166. – SP2 [cited at p. 114, 209]

Renault 2010 Renault, P.: Single-Station Sigma Project - Task Guidelines / swissnuclear, prepared for PRP - PEGASOS Refinement Project. 2010 (TP2-TN-1106). – Technical Note. SP2 (Rev. 2 after Workshop in July 2010) [cited at p. 57]

Renault 2012a Renault, P.: Comparison of empirical and stochastic model for the same region / swissnuclear, prepared for PRP - PEGASOS Refinement Project. 2012 (PMT-TN-1232). – Technical Note. SP2 [cited at p. 274]

Renault 2012b Renault, P.: Overview of available kappa estimates for Switzerland as constraints for NPP specific kappa values / swissnuclear, prepared for PRP - PEGASOS Refinement Project. 2012 (PMT-TN-1221). – Technical Note. SP2 [cited at p. 116, 119, 140]

Renault and Biro 2012 Renault, P. ; Biro, Y.: Explanations and overview of the SP2 logic tree values for the additional vertical variability (provided for hazard feedback computations in April 2012) / swissnuclear, prepared for PRP - PEGASOS Refinement Project. 2012 (PMT-TN-1240). – Technical Note. SP3 [cited at p. 235, 362]

Renault and Biro 2013 Renault, P. ; Biro, Y.: Residuals for estimation centering of Vs-Kappa corrections.PMT-SUP-1084 / swissnuclear, prepared for PRP - PEGASOS Refinement Project. 2013 (PMT-SUP-1084). – Technical Report [cited at p. 127, 128, 129, 130, 349]

Renault et al. 2010 Renault, P. ; Heuberger, S. ; Abrahamson, N. A.: PEGASOS Refinement Project: An improved PSHA for Swiss nuclear power plants. In: *14th European Conference on Earthquake Engineering - 30. August to 3. September 2010, Ohrid, Republic of Macedonia*, 2010 [cited at p. 227]

Renault and Kuhlmann 2012 Renault, P. ; Kuhlmann, U.: GMPE-PSSM comparison plotting tool / prepared for PRP - PEGASOS Refinement Project. 2012 (RDZ-ASW-1005). – Techncal Note Version 5. SP2 [cited at p. 43]

Renault 2011 Renault, Ph.: Compilation of most relevant SP2 documents for K. Campbell / swissnuclear, prepared for PRP - PEGASOS Refinement Project. 2011 (PMT-AN-1116). – Administration Note Final v. 2, [cited at p. 182]

Rhoades et al. 2008 Rhoades, D. A. ; Zhao, J. X. ; McVerry, G. H.: A Simple Test for Inhibition of Very Strong Shaking in Ground-Motion Models. In: *Bulletin of the Seismological Society of America* 98 (2008), No. 1, p. 448–453. http://dx.doi.org/10.1785/0120070133. – DOI 10.1785/0120070133 [cited at p. 81]

Ripperger et al. 2008 Ripperger, J. ; Mai, P. M. ; Ampuero, J.-P.: Variability of Near-Field Ground Motion from Dynamic Earthquake Rupture Simulations. In: *Bulletin of the Seismological Society of America* 98 (2008), June, No. 3, p. 1207–1228. http://dx.doi.org/10.1785/0120070076. – DOI 10.1785/0120070076 [cited at p. 355]

Rodriguez-Marek 2012 Rodriguez-Marek, A.: Addendum to "Single Station Sigma", EXT-TN-1225 / prepared for PRP - PEGASOS Refinement Project. 2012 (EXT-TN-1225). – Technical Note. SP2 (Rev.1, 31 January) [cited at p. 57, 64, 65, 135, 137, 167, 228, 230, 258, 289, 310, 356, 358, 386]

Rodriguez-Marek and Cotton 2011 Rodriguez-Marek, A. ; Cotton, F.: Final Report: Single Station Sigma Project / prepared for PRP - PEGASOS Refinement Project. 2011 (EXT-TB-1058). – Technical Report. SP2 (Ver.7.1, 29 July) [cited at p. 57, 58, 59, 60, 63, 64, 65, 135, 136, 167, 228, 229, 230, 231, 258, 310, 327, 354, 355, 356, 359, 386]

Rodriguez-Marek et al. 2011 Rodriguez-Marek, A. ; Montalva, G. A. ; Cotton, F. ; Bonilla, F.: Analysis of Single-Station standard deviation using the KiK-net Data. In: *Bulletin of the Seismological Society of America* 101 (2011), June, No. 3, p. 1242–1258. http://dx.doi.org/10.1785/0120100252. – DOI 10.1785/0120100252 [cited at p. 64, 135, 231, 356, 358, 360, 427]

Roth 2010a Roth, P.: Extraction of the Five Largest Events per SP1 Expert Group Source Zone in ECOS02 & ECOS09 / Interoil, prepared for PRP - PEGASOS Refinement Project. 2010 (TP1-TN-1065). – Technical Note. SP1 [cited at p. 142]

Roth 2010b Roth, P.: Plant Specific Adjustment of the SP2 GMPE and Merging with SP3 Soil Profiles / prepared for PRP - PEGASOS Refinement Project. 2010 (EXT-TN-1110). – Technical Note. SP2 [cited at p. 140]

Roth 2011 Roth, P.: Hazard Sensitivity to Maximum Ground Motion Truncation; Follow-up computations, SP2 Working Meeting 24. Jan. 2011 / Interoil, prepared for PRP - PEGASOS Refinement Project. 2011 (TP4-RF-1305). – Referenece Publication. SP2 [cited at p. 142]

Roth 2012 Roth, P.: Derivation of mean magnitudes and mean distances for the vertical hazard / INTEROIL E&P SWITZERLAND AG, prepared for PRP - PEGASOS Refinement Project. 2012 (TP4-TN-1255). – Technical Note [cited at p. 187, 189]

Sabetta et al. 2005 Sabetta, F. ; Lucantonia, A. ; Bungum, H. ; Bommer, J.J.: Sensitivity of PSHA results to ground motion prediction relations and logic-tree weights. In: *Soil Dynamics and Earthquake Engineering* 25 (2005), p. 317–329. – SP2 [cited at p. 102]

Scherbaum 2010 Scherbaum, F.: Determination of Vs-Kappa correction factors & Appendix / prepared for PRP - PEGASOS Refinement Project. 2010 (TP2-TB-1036). – Technical Report. SP2 (New appendix to report after WM on 03.07.2010) [cited at p. 17, 183, 207, 209]

Scherbaum 2011a Scherbaum, F.: Current state of new Vs-kappa correction approach / prepared for PRP - PEGASOS Refinement Project. 2011 (TP2-RF-1397). – Technical Report. SP2 [cited at p. 224]

Scherbaum 2011b SCHERBAUM, F.: Some ideas for a Vs-kappa correction approach (material for the web-conference on June 23, 2011) / prepared for PRP - PEGASOS Refinement Project. 2011 (TP2-RF-1379). – Technical Report. SP2 [cited at p. 224]

Scherbaum and Kühn 2011 SCHERBAUM, F. ; KÜHN, N. M.: Logic tree branch weights and probabilities: Summing up to one is not enough. In: *Earthqake Spectra, OPINION PAPER* 27 (2011), No. 4, p. 1237–1251. – SP2 [cited at p. 102]

Scherbaum et al. 2010 SCHERBAUM, F. ; KÜHN, N. M. ; OHRNBERGER, M. ; KOEHLER, A.: Exploring the Proximity of Ground-Motion Models using High-Dimensional Visualization Techniques. In: *Earthquake Spectra* 26 (2010), p. 1117–1138 [cited at p. 97, 183, 184, 185, 209, 328]

Scherbaum et al. 2011 SCHERBAUM, F. ; SEIF, S. ; KÜHN, N.M.: Vs-Kappa correction, Workshop SP2/WS9 / Universität Potsdam, prepared for PRP - PEGASOS Refinement Project. 2011 (TP2-RF-1367). – Reference Publication. SP2 [cited at p. 113, 114, 289]

SED 2010 SED: SED ECOS-09: Earthquake Catalogue of Switzerland, Release 2009 / ETH Report, Swiss Seismological Service, prepared for PRP - PEGASOS Refinement Project. 2010 (TP1-TB-1022). – Technical Report. SP1 [cited at p. 332]

SED 2011 SED: SED ECOS-09: Earthquake Catalogie of Switzerland, release 2010 / ETH Report, Swiss Seismological Service, prepared for PRP - PEGASOS Refinement Project. 2011 (SED/PRP/R/008/20100331). – not public catalogue [cited at p. 185]

Selverstone 2005 SELVERSTONE, J.: Are the Alps collapsing? In: *Annual Reviews of Earth and Planetary Science* 33 (2005), p. 113–132 [cited at p. 188]

Siddiqqi and Atkinson 2002 SIDDIQQI, J. ; ATKINSON, G. M.: Ground-Motion Amplification at Rock Sites across Canada as Determined from the Horizontal-to-Vertical Component Ratio. In: *Bulletin of the Seismological Society of America* 92 (2002), March, No. 2, p. 877–884 [cited at p. 361]

Silva and Darragh 2012 SILVA, W. ; DARRAGH, R.: Assessment of kappa for vertical and horizontal motions at rock sites using spectral shapes / Pacific Engineering and Analysis, prepared for PRP - PEGASOS Refinement Project. 2012 (EXT-TB-1089). – Technical Report. SP2 [cited at p. 121, 127, 233, 362]

Silva et al. 1998 SILVA, W. ; DARRAGH, R. ; GREGOR, N. ; MARTIN, G. ; ABRAHAMSON, N. ; KIRCHER, C.: Reassessment of site coefficients and near-fault factors for building code provisions / Pacific Engineering and Analysis. Version: 1998. URL http://www.pacificengineering.org/rpts_page2.shtml (Program Element: II; 98-HQ-GR-1010). – Technical Report. – Electronic Resource [cited at p. 18, 19, 33, 113, 117, 119, 120, 121, 126, 131, 283, 345, 348, 423]

Silva 2008 SILVA, W.J.: Site Response Simulations for the NGA project / Pacific Earthquake Engineering Research Center (PEER). 2008. – Technical Report. Manuscript [cited at p. 125]

Sinclair et al. 1991 SINCLAIR, H. D. ; COAKLEY, B.J. ; ALLEN, P.A. ; WATTS, A.B.: Simulation of foreland basin stratigraphy using a diffusion model of mountain belt uplift and erosion: An example from the central Alps, Switzerland. In: *Tectonics* 10 (1991), p. 599–620 [cited at p. 188]

Spiegelhalter and Rice 2009 SPIEGELHALTER, D. ; RICE, K.: Scholarpedia. 4 (2009), p. 5230 [cited at p. 185]

Stafford and Bommer 2010 STAFFORD, P. ; BOMMER, J.J.: The problem of selected GMPE's that do not provide coefficients at all PEGASOS response frequencies Workshop SP2/ WS5 / Imperial College Consultants Ltd., prepared for PRP - PEGASOS Refinement Project. 2010 (TP2-RF-1234). – Reference Publication. SP2 [cited at p. 113]

Stafford et al. 2008 Stafford, P. J. ; Strasser, F. O. ; Bommer, J. J.: An Evaluation of the Applicability of the NGA Models to Ground-Motion Prediction in the Euro-Mediterranean Region. In: *Bulletin of Earthquake Engineering* 6 (2008), May, No. 2, p. 149–177. http://dx.doi.org/10.1007/s10518-007-9053-2. – DOI 10.1007/s10518–007–9053–2 [cited at p. 97, 103]

Stafford 2011 Stafford, P.J.: Procedure for Small-Magnitude Extensions of GMPE's / Imperial College Consultants Ltd., prepared for PRP - PEGASOS Refinement Project. 2011 (EXT-TN-1180, Ver.3). – Technical Note. SP2 [cited at p. 132]

Stafford 2012 Stafford, P.J.: Small-Magnitude extensions for Akkar & Cagnan (2010) and Bindi et. al. (2011), Amendment to report TP2-TB-10180 / Imperial College Consultants Ltd., prepared for PRP - PEGASOS Refinement Project. 2012 (EXT-TN-1180, Ver.4). – Technical Note. SP2 [cited at p. 132]

Stewart et al. 2012 Stewart, J. P. ; Lanzo, G. ; Pagliaroli, A. ; Scasserra, G. ; Di Capua, G. ; Peppoloni, S. ; Darragh, R. ; Gregor, N.: Ground motion recordings from the MW 6.3 2009 L'Aquila earthquake in Italy and their engineering implications. In: *Earthquake Spectra* 28 (2012), p. 317–345 [cited at p. 190]

Strasser and Bommer 2009 Strasser, F.O. ; Bommer, J.J.: Strong Ground-Motions: Have we seen the worst? In: *Bulletin of the Seismological Society of America* 99 (2009), No. 5, p. 2613–2637. http://dx.doi.org/10.1785/0120080300. – Manuscript Draft. – DOI 10.1785/0120080300 [cited at p. 81]

Strasser and Zulu 2010 Strasser, F.O. ; Zulu, S.: Determination of empirical Maximum Ground Motions for PRP / CGS, prepared for PRP - PEGASOS Refinement Project. 2010 (EXT-TB-1067 CGS Report Number: 2010 - 0177). – Technical Report. SP2 + SP3 [cited at p. 82, 84, 85, 86, 141, 353]

swissnuclear 2011 swissnuclear: PEGASOS Refinement Project plan, V. 4.2 / swissnuclear, prepared for PRP - PEGASOS Refinement Project. 4600 Olten, Switzerland, April 7 2011 (PMT-TB-1012). – Technical Report. 44 pp. and 2 Appendices [cited at p. 182]

Toro 2002 Toro, G. R.: Modifications of the Toro et al. (1997) Attenuation Equations for Large Magnitudes and Short Distances / Risk Engineering, Inc., prepared for PRP - PEGASOS Refinement Project. 2002 (TP2-RF-1114). – Technical Report. SP2 [cited at p. 16, 63, 276]

Toro et al. 1997 Toro, G. R. ; Abrahamson, N. A. ; Schneider, J. F.: Model of strong ground motions from earthquakes in central and eastern north america: best estimates and uncertainities. In: *Seismological Research Letters* 68 (1997), January/February, No. 1, p. 41–57 [cited at p. 16, 323, 324, 330]

Van Houtte et al. 2011 Van Houtte, C. ; Drouet, S. ; Cotton, F.: Analysis of the origins of kappa to compute hard rock to rock adjustment factors for GMPEs. In: *Bulletin of Seismological Society of America* 101 (2011), December, No. 6, p. 2926–2941. http://dx.doi.org/10.1785/0120100345. – DOI 10.1785/0120100345 [cited at p. 19, 116, 117, 121, 125, 126, 219, 345]

Wells and Coppersmith 1994 Wells, D. L. ; Coppersmith, K. J.: New Empirical Relationships among Magnitude, Rupture Length, Rupture Width, Rupture Area, and Surface Displacement. In: *Bulletin of the Seismological Society of America* 84 (1994), August, No. 4, p. 974–1002 [cited at p. 12, 332]

Zhao et al. 2006 Zhao, J. X. ; Zhang, J. ; Asano, A. ; Ohno, Y. ; Oouchi, T. ; Takahashi, T. ; Ogawa, H. ; Irikura, K. ; Thio, H. K. ; Somerville, P. G. ; Fukushima, Y. ; Y.,

Fukushima: Attenuation relations of strong Ground-Motion in Japan using site classification based on predominant Period. In: *Bulletin of the Seismological Society of America* 96 (2006), No. 3, p. 898–913. http://dx.doi.org/10.1785/0120050122. – TP2-RF-1114. – DOI 10.1785/0120050122 [cited at p. 7, 16, 323]

Appendices

Appendix A

Hazard Feedback for SP2

The development and finalization of the HIDs were preceded by provision of hazard feedback plots for each SP2 expert. The different feedback plots are attached as electronic supplement to this report.

List of Figures

List of Tables